frontiers | Research Topics

Effector functions of therapeutic antibodies

Edited by
Peter Boross, Matthias Peipp and Falk Nimmerjahn

Published in
Frontiers in Immunology

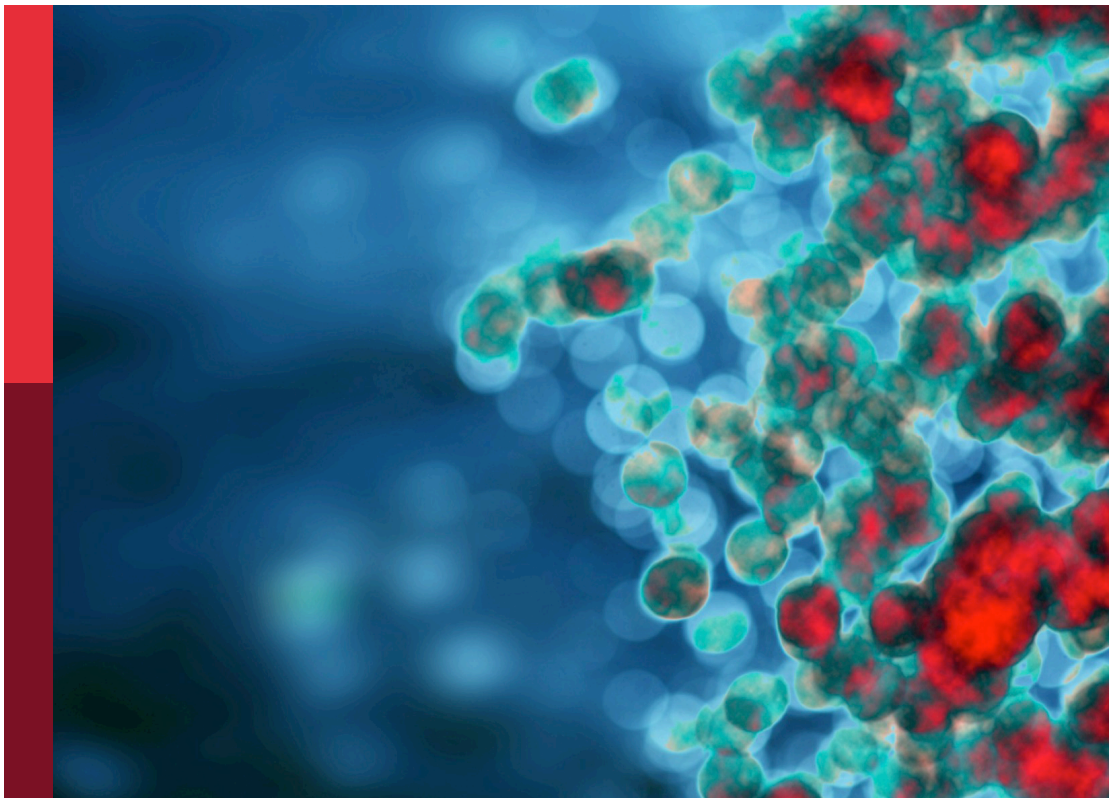

ISSN 1664-8714
ISBN 978-2-83251-472-6
DOI 10.3389/978-2-83251-472-6

About Frontiers

Frontiers is more than just an open access publisher of scholarly articles: it is a pioneering approach to the world of academia, radically improving the way scholarly research is managed. The grand vision of Frontiers is a world where all people have an equal opportunity to seek, share and generate knowledge. Frontiers provides immediate and permanent online open access to all its publications, but this alone is not enough to realize our grand goals.

Frontiers journal series

The Frontiers journal series is a multi-tier and interdisciplinary set of open-access, online journals, promising a paradigm shift from the current review, selection and dissemination processes in academic publishing. All Frontiers journals are driven by researchers for researchers; therefore, they constitute a service to the scholarly community. At the same time, the *Frontiers journal series* operates on a revolutionary invention, the tiered publishing system, initially addressing specific communities of scholars, and gradually climbing up to broader public understanding, thus serving the interests of the lay society, too.

Dedication to quality

Each Frontiers article is a landmark of the highest quality, thanks to genuinely collaborative interactions between authors and review editors, who include some of the world's best academicians. Research must be certified by peers before entering a stream of knowledge that may eventually reach the public - and shape society; therefore, Frontiers only applies the most rigorous and unbiased reviews. Frontiers revolutionizes research publishing by freely delivering the most outstanding research, evaluated with no bias from both the academic and social point of view. By applying the most advanced information technologies, Frontiers is catapulting scholarly publishing into a new generation.

What are Frontiers Research Topics?

Frontiers Research Topics are very popular trademarks of the *Frontiers journals series*: they are collections of at least ten articles, all centered on a particular subject. With their unique mix of varied contributions from Original Research to Review Articles, Frontiers Research Topics unify the most influential researchers, the latest key findings and historical advances in a hot research area.

Find out more on how to host your own Frontiers Research Topic or contribute to one as an author by contacting the Frontiers editorial office: frontiersin.org/about/contact

Effector functions of therapeutic antibodies

Topic editors
Peter Boross — Genmab, Netherlands
Matthias Peipp – University Medical Center Schleswig-Holstein, Germany
Falk Nimmerjahn — University of Erlangen Nuremberg, Germany

Citation
Boross, P., Peipp, M., Nimmerjahn, F., eds. (2023). *Effector functions of therapeutic antibodies*. Lausanne: Frontiers Media SA. doi: 10.3389/978-2-83251-472-6

PB is an employee and holds warrants and shares at Genmab B.V. a company that is investigating the application of Antibody effector functions for drug therapy.

The remaining authors declare that the research was conducted in the absence of any commercial or financial relationships that could be construed as a potential conflict of interest.

Table of contents

frontiers | Frontiers in Immunology

TYPE Editorial
PUBLISHED 12 January 2023
DOI 10.3389/fimmu.2022.1126966

OPEN ACCESS

EDITED AND REVIEWED BY
Harry W Schroeder,
University of Alabama at Birmingham,
United States

*CORRESPONDENCE
Peter Boross
peterboross@gmail.com

SPECIALTY SECTION
This article was submitted to
B Cell Biology,
a section of the journal
Frontiers in Immunology

RECEIVED 18 December 2022
ACCEPTED 21 December 2022
PUBLISHED 12 January 2023

CITATION
Boross P, Peipp M and Nimmerjahn F (2023) Editorial: Effector functions of therapeutic antibodies.
Front. Immunol. 13:1126966.
doi: 10.3389/fimmu.2022.1126966

Editorial: Effector functions of therapeutic antibodies

Peter Boross[1]*, Matthias Peipp[2] and Falk Nimmerjahn[3]

[1]Genmab BV, Utrecht, Netherlands, [2]Stem Cell Transplantation and Immunotherapy, Division of Antibody-Based Immunotherapy, Department of Medicine II, Christian Albrechts University Kiel and University Medical Center Schleswig-Holstein, Kiel, Germany, [3]Department of Biology, Institute of Genetics, University of Erlangen-Nürnberg, Erlangen, Germany

KEYWORDS

antibodies, glycosylation, IgA, effector functions, Fc receptors, complement, checkpoint

Editorial on the Research Topic
Effector functions of therapeutic antibodies

Therapeutic antibodies are broadly used in both oncology and autoimmune indications. Currently there are more than hundred antibodies approved by the FDA and many more are in development. Therapeutic antibodies of the human IgG1 subclass with an unmodified Fc portion are increasingly being replaced with engineered antibodies or novel antibody formats. In order to improve the therapeutic index of antibodies, the Fc portion of IgG can be protein- or glyco-engineered (1). Other IgG subclasses or antibody isotypes are also being explored. These modifications are aimed at altering the natural interactions with immune effector functions, such as Fc receptors or the complement system to ultimately improve the efficacy and safety of therapeutic antibodies.

The effector functions induced by the IgG Fc domain of therapeutic antibodies are characterized by complex interactions *in vivo*. The type and magnitude of these interactions depend on a number of factors. However it is not well understood how *in vitro* results, and pre-clinical *in vivo* studies, translate into clinical efficacy and safety. In *in vitro* assays, IgG effector functions are often studied in isolation and the effector functions in pre-clinical mouse models differ from those available in humans. Therefore bridging data from these different model systems is important to enable the use of preclinical results to predict clinical efficacy.

This Research Topic collates eleven articles focusing on the role of the IgG Fc domain for the effector functions of antibodies and highlights different strategies to alter IgG Fc to modify wanted and unwanted biological effects.

In addition to immune checkpoints on adaptive immune cells, targeting similar checkpoints on myeloid cells are also being explored. Chan et al. provides a comprehensive overview of the most prominent example of these, the CD47-SIRPα axis, and describes other potential myeloid checkpoints that could be explored to enhance immunotherapy. IgA is being explored as an alternative isotype instead of IgG for anti-cancer antibodies. As IgA antibodies predominantly engage Polymorphonuclear Leukocytes (PMNs) as effector cells, the authors also discuss the potential advantage of

combining IgA antibody therapy with myeloid checkpoint blockade. Baumann et al. show *in vitro* anti-tumor activity with an IgA2 version of the anti-CD38 antibody daratumumab (Dara) in *in vitro* antibody-dependent cell-mediated cytotoxicity (ADCC) and ADCP assays. The activity of the IgA Dara variant could be further boosted by the inhibition of myeloid checkpoints CD47-SIRPα axis.

Zeller et al. analyzed whether dual checkpoint inhibition of the CD47-SIRPα and HLAI/LILRB1 axes in combination with CD20-directed antibodies is a suitable approach to further boost antibody-dependent cellular phagocytosis (ADCP) of lymphoma cells. Analysis of lymphoma cell lines revealed that the ratio of CD20 to HLA class I cell surface molecules determined the sensitivity to ADCP by the combination of rituximab and CD47 antibody. LILRB1 blockade promoted serial engulfment of lymphoma cells and potentiated ADCP but required CD47 co-blockade and the presence of the CD20 antibody. These data provide first *in vitro* evidence that dual checkpoint blockade of CD47 and LILRB1 may be promising to improve antibody therapy of lymphoma patients through enhancing ADCP by macrophages.

Agonistic antibodies that engage co-stimulatory receptors, such as anti-CD40 antibodies, have great promise but their clinical use is complicated by the small therapeutic window. The challenge is to separate the mechanisms that lead to anti-tumor response from those that result in unwanted toxicity. Salomon and Dahan provide an overview of the next generation of anti-CD40 antibodies. These strategies may include Fc engineering for enhanced FcγRIIB binding, intratumoral administration but also the use of bispecific antibodies to restrict CD40 agonism exclusively at the tumor site or specifically to dendritic cells.

For a number of agonistic therapeutic antibodies the IgG Fc part has been shown to be important for therapeutic activity but also play a role in the induction of unwanted side effects. Some of these antibodies are of the IgG4 isotype which is expected to have mild interactions with human FcγRs. Using a deglycosylated version of urelumab, an anti-CD137 antibody, Reitinger et al. showed that abrogating residual FcγR interactions by glycan removal maintains T cell stimulatory activity while ameliorating toxicity. These results suggest that glyco-engineering of IgG4 is an interesting strategy to explore. Furthermore, their data highlights the importance of dosing in order to separate beneficial effects from toxic side effects.

Protein engineering of the IgG Fc is an attractive strategy to enhance or to ameliorate IgG effector functions. Gehlert et al. used the anti-CD19 antibody tafasitamab in which the Fc domain has been modified by two mutations (S239D/I332E) that result in enhanced ADCP and ADCC. The authors have introduced a third mutation, E345K that improves Fc-Fc interactions and increases hexamer formation on the cell membrane resulting in improved complement activation. This mutation was functional, and resulted in improved Complement-dependent Cytotoxicity (CDC) when effector functions were studied in isolation. Importantly, however, in whole blood assays when all effector functions were available, stronger complement activation negatively impacted FcR engagement, highlighting the need for experimental systems where all effector functions can be studies simultaneously.

IgG1 contains one N-linked glycosylation site (Asn-297) and the glycan structure on the IgG has profound functional effects. In particular the presence of core fucose is of high importance, as antibodies with low core fucose are able to trigger stronger FcγR-mediated effector functions. Golay et al. provided a comprehensive overview of the literature on the biological effects of the IgG core fucosylation both in the context of therapeutic antibodies where it can be explored to modulate antibody effector functions and in physiological polyclonal IgG response.

IgG antibodies lacking the penultimate fucose residue are well known to bind with increased affinity to FcγRIIIa. Hatfield et al. now show that in afucosylated sugar moieties galactose residues play an important role in this enhanced binding. By using an enzymatic transglycosylation approach allowing addition of add defined sugar moieties to IgG, they demonstrate that galactosylation at the α6 but not the α3 antennae was responsible for this enhanced binding. The authors further validate their finding by demonstrating that these IgG glycovariants have an enhanced ADCC activity.

In addition to the impact of the sugar moiety attached to the Fc-domain of antibodies it is well established that glycosylation of FcγRs may also impact the IgG-FcγR interaction. For example a specific sugar moiety in FcγRIIIa is critical for detecting IgG glycovariants with low fucose with higher affinity (2). It remained unclear, however, which sugar residues in IgG or FcγRIIIa associated sugar domains have a major impact on this interaction. Van Coillie et al. addressed this important question by generating well-defined libraries of IgG and FcγRIIIa glycosylation variants and demonstrate that afucosylated IgG1 has the highest affinity for oligomannose containing sugar moieties attached to the Asn162 site on FcγRIIIa. Of note, this FcγRIIIa glycovariant seems to be present predominantly on NK cells and much less on monocytes.

Antibodies have become an essential therapeutic tool to treat autoimmune diseases. Thus, antibodies in the form of cytotoxic or immunomodulatory antibodies have become part of established or experimental treatments. Mariottini et al. discuss which antibody-based treatment options are available for patients with multiple sclerosis (MS) and which antibody-dependent effector mechanisms contribute to the therapeutic effect. In addition, they include an in depth comparison of antibody-based versus other treatment options, such as autologous hematopoietic stem cell transplantation.

de Vor et al. studied the potential of monoclonal antibodies against S. epidermidis to induce phagocytic killing by human neutrophils. Different mAbs recognizing Staphylococcal surface components were characterized. To study the immune-activating potential of selected clones, bacteria were opsonized with mAbs in the presence or absence of complement. Activation of the complement system was essential to induce efficient phagocytosis of S. epidermidis. Similar to the study of Gehlert et al. in the context of cancer, complement activation and phagocytic killing of S. epidermidis could be enhanced by Fc-mutations that improve IgG1 hexamerization on cellular surfaces. The authors were able to show that mAbs could greatly enhance phagocytosis of S. epidermidis in neonatal plasma and provide insights that are crucial for optimizing anti-S. epidermidis mAbs as prophylactic agents for neonatal Central line associated bloodstream infections (CLABSI).

Taken together, a collection of original papers, Reviews and Perspective published in this Research Topic highlight recent insights and extend our understanding of the effector functions of human antibodies. We hope that the new insights will contribute to the better understanding of antibody biology and help translate this knowledge into even more effective therapeutic interventions.

Author contributions

All three Guest-Editors of this Research Topic; PB, FN and MP contributed to the preparation to the present Editorial article. All authors contributed to the article and approved the submitted version.

Funding

Funding was provided by the German Research Foundation (TRR305-B02, CRC1181-A07, CRC1526-A07 to F.N.)

Conflict of interest

PB is an employee and holds warrants and shares at Genmab B.V. a company that is investigating the application of Antibody effector functions for drug therapy.

The remaining authors declare that the research was conducted in the absence of any commercial or financial relationships that could be construed as a potential conflict of interest.

Publisher's note

References

1. Liu R, Oldham RJ, Teal E, Beers SA, Cragg MS. Fc-engineering for modulated effector functions-improving antibodies for cancer treatment. *Antibodies (Basel) 9* (2020) 7;9(4):64. doi: 10.3390/antib9040064

2. Ferrara C, Grau S, Jager C, Sondermann P, Brunker P, Waldhauer I, et al. Unique carbohydrate-carbohydrate interactions are required for high affinity binding between FcgammaRIII and antibodies lacking core fucose. *Proc Natl Acad Sci U.S.A.* (2011) 108:12669–74. doi: 10.1073/pnas.1108455108

frontiers | Frontiers in Immunology

REVIEW
published: 30 June 2022
doi: 10.3389/fimmu.2022.929895

Role of Fc Core Fucosylation in the Effector Function of IgG1 Antibodies

Josée Golay[1*], *Alain E. Andrea*[2†] *and Irene Cattaneo*[1†]

[1] Center of Cellular Therapy "G. Lanzani", Division of Hematology, Azienda Socio Sanitaria Territoriale Papa Giovanni XXIII, Bergamo, Italy, [2] Laboratoire de Biochimie et Thérapies Moléculaires, Faculté de Pharmacie, Université Saint Joseph de Beyrouth, Beirut, Lebanon

The presence of fucose on IgG1 Asn-297 N-linked glycan is the modification of the human IgG1 Fc structure with the most significant impact on FcγRIII affinity. It also significantly enhances the efficacy of antibody dependent cellular cytotoxicity (ADCC) by natural killer (NK) cells *in vitro*, induced by IgG1 therapeutic monoclonal antibodies (mAbs). The effect of afucosylation on ADCC or antibody dependent phagocytosis (ADCP) mediated by macrophages or polymorphonuclear neutrophils (PMN) is less clear. Evidence for enhanced efficacy of afucosylated therapeutic mAbs *in vivo* has also been reported. This has led to the development of several therapeutic antibodies with low Fc core fucose to treat cancer and inflammatory diseases, seven of which have already been approved for clinical use. More recently, the regulation of IgG Fc core fucosylation has been shown to take place naturally during the B-cell immune response: A decrease in α-1,6 fucose has been observed in polyclonal, antigen-specific IgG1 antibodies which are generated during alloimmunization of pregnant women by fetal erythrocyte or platelet antigens and following infection by some enveloped viruses and parasites. Low IgG1 Fc core fucose on antigen-specific polyclonal IgG1 has been linked to disease severity in several cases, such as SARS-CoV 2 and Dengue virus infection and during alloimmunization, highlighting the *in vivo* significance of this phenomenon. This review aims to summarize the current knowledge about human IgG1 Fc core fucosylation and its regulation and function *in vivo*, in the context of both therapeutic antibodies and the natural immune response. The parallels in these two areas are informative about the mechanisms and *in vivo* effects of Fc core fucosylation, and may allow to further exploit the desired properties of this modification in different clinical contexts.

Keywords: therapeutic antibodies, IgG, N-glycan, fucosylation, ADCC, NK cells, virus, humoral response

OPEN ACCESS

Edited by:
Peter Boross, Genmab, Netherlands

Reviewed by:
Kutty Selva Nandakumar, Karolinska Institutet (KI), Sweden
Gestur Vidarsson, Sanquin Research, Netherlands
Mattias Collin, Lund University, Sweden

***Correspondence:**
Josée Golay
jgolay59@gmail.com

[†]*These authors have contributed equally to this work*

Specialty section:
This article was submitted to B Cell Biology, a section of the journal Frontiers in Immunology

Received: *27 April 2022*
Accepted: *03 June 2022*
Published: *30 June 2022*

Citation:
Golay J, Andrea AE and Cattaneo I (2022) Role of Fc Core Fucosylation in the Effector Function of IgG1 Antibodies. Front. Immunol. 13:929895. doi: 10.3389/fimmu.2022.929895

INTRODUCTION

IgGs are among the most abundant proteins in the circulation (700-1600 mg/dl in healthy adults), and specific IgGs are induced in response to infection, endogenous or allogeneic challenges, or by vaccination. Different IgG subclasses are found in man, which are very similar structurally but have distinct functions due to their differential binding to FcγRs, complement components as well as other

proteins. About 60% of plasma IgG is IgG1, 32% IgG2 and 4% each IgG3 and IgG4 in humans (1). IgGs are glycoproteins and their glycosylation pattern can change during time, due to age, diseases or environmental factors (2, 3).

Therapeutic monoclonal antibodies (mAbs) have emerged as an important therapeutic option in cancer since the approval in 1997 of the anti-CD20 antibody rituximab for the treatment of B-non Hodgkin's lymphoma (B-NHL). Since then, antibodies directed against different antigens expressed by cancer, immune cells or infectious agents have been developed to treat a variety of diseases. Indeed, so far, over 130 antibodies have been approved by the US and EU Drug Agencies, with 45% for oncological disorders, 27% for immune- or inflammation-related conditions and the rest for infectious or other diseases (4).

Most unconjugated therapeutic mAbs are IgG1 or in some cases IgG4 or IgG2. This is because the human IgG1 Fc moiety interacts efficiently with activating FcγRs (FcγRI, IIA, IIC, IIIA and IIIB), expressed on the surface of immune cells (1, 5). This interaction leads to antibody-dependent cellular cytotoxicity (ADCC) by NK cells (mostly *via* FcγRIIIA, CD16A) (6, 7), antibody dependent phagocytosis (ADCP) by macrophages (mostly through FcγRI, CD64 and to some extent FcγRIIA, CD32A) (8–12) and ADCC/ADCP by polymorphonuclear neutrophils (PMN)(mostly *via* FcγRIIA, CD32A) (13–15). IgG1 also interacts with FcγRIIIB (CD16B), a GPI-linked molecules lacking activating domain, highly expressed by PMN and involved in PMN mediated ADCC and ADCP, but whose role may be either activating or inhibiting, perhaps depending on stimulus (13–16). Immune cell activation *via* FcγRs also induces the release of cytokines and chemokines that may cooperate in eliminating the target cells but also induce unwanted side-effects (17). Finally the Fc region of human IgG1 can bind to the first component of the complement cascade C1q and activate the classical pathway of complement which may lead to cell lysis and death through complement dependent cytotoxicity (CDC), as well as phagocytosis by macrophages and PMN through complement receptors on these cells (18). Therefore, many therapeutic antibodies against cancer cells or other targets are of the IgG1 isotype to allow activation of a panoply of immune-mediated mechanisms, many of which rely on FcγRs.

When the activation of the immune system is not desired, for example when a therapeutic antibody is required only to neutralize the antigen, such as a growth factor or checkpoint inhibitor, then the human IgG4 or IgG2 subclasses are often chosen, because they do not interact efficiently with FcγRs or with C1q. The more recent human IgG4 formats include a mutation in Fc (S228A) to avoid Fab arm exchange, a natural phenomenon that leads to IgG4 instability (19).

Over the last 10-15 years, various modifications of antibody structures have been introduced to increase the efficacy of therapeutic mAbs *in vitro* and *in vivo*: these include extensively modified Abs with additional effector functions, such as bispecific antibodies (bsAbs), antibody-drug conjugates (ADCs) and fusion proteins carrying for example cytokines (17, 20). Less dramatic modifications of therapeutic mAbs include the introduction of point mutations in the Fc domain, as well as modification of Fc N-linked glycans that modulate IgG binding to FcγRs and therefore enhance or abolish Fc mediated immune activation (ADCC, ADCP and/or CDC) (17, 20).

In this paper, we will summarize the knowledge gained about the role of IgG1 N-glycan core fucosylation in the *in vitro* and *in vivo* functions of IgG1 antibodies. Ig isotypes or subclasses other than IgG1 bear N-glycans, but less is known about the role of core Fc fucosylation in their case and these will not be further discussed here. Interestingly, the studies on the role of Fc core fucose in therapeutic IgG1 mAbs has facilitated the detection and understanding of the significance of this modification, observed during the polyclonal IgG1 response to some infectious agents, alloimmunization and in some autoimmune conditions. The knowledge on these aspects will therefore also be summarized and discussed.

THE IGG N-LINKED GLYCANS

Human IgGs are glycosylated proteins with a complex and variable glycosylation pattern. An important and extensively studied N-glycosylation site is present at conserved Asparagine 297 (Asn 297) in the CH2 domain, that interacts with FcγRs. 20-30% of IgGs also bear N-glycans on Fab arms (21). Although there are reports of functional effects of different Fab N-glycosylation patterns in some antibodies (22), these are likely to be mostly antibody specific (23). Detailed structural studies of several commercial therapeutic mAbs has revealed that although Fab interacts with FcγRIIIA and stabilizes the Fc-FcγRIIIA binding, Fab fucosylation has a limited effect on the affinity of IgG for FcγRIIIA (23, 24). The modulation of Fab fucosylation will therefore not be further discussed here.

The IgG Asn 297 N-glycans show a high degree of microheterogeneity, and they can be grouped in oligomannose, hybrid or complex type, the latter being the most abundant (about 90%) in IgG, either circulating or produced by cell lines *in vitro* (25) (**Figure 1A**). The presence of Fc N-glycan induces in general a more open structure compared to aglycosylated IgG, favors binding to activating FcγRs and promotes antibody stability *in vitro* and *in vivo* (1, 26). The complex type N-glycosylation itself shows microheterogeneity: whereas it always contains a heptaglycan biantennary core structure (four GlcNAc and three mannose residues), the core can bear an additional bisecting GlcNAc (in about 10% of IgGs), and 1 or 2 galactose residues (in 35% and 15% of IgG, respectively) and 1-2 terminal N-acetylneuraminic acid (sialic acid, SA), on 10-15% of IgGs (**Figure 1B**). Finally, an α-1,6 fucose residue (core fucose) is present in 90% of complex type IgG N-glycans (**Figure 1B**). Interestingly the presence of bisecting GlcNAc inhibits α-1,6 core fucosylation due to steric hindrance and therefore IgGs generally contain either a bisecting GlcNAc or a core fucose residue, although some IgGs may have both bisecting GlcNAc and fucose (2, 27–29). IgGs are composed of least 30 glycovariants, to which specific abbreviations have been assigned: G0 (no Gal residue), G1 (1 Gal), G2 (2 Gals), F (fucose) etc (**Figure 1B**) (2, 27–29).

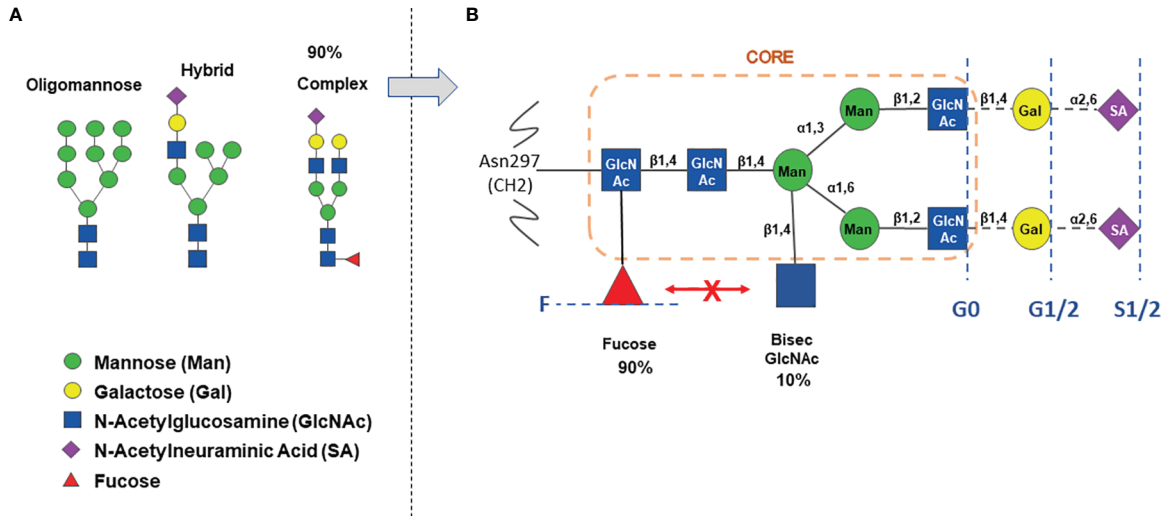

FIGURE 1 | The IgG Asn-297 N-glycan heterogeneity. Panel **(A)** major types of N-glycosylation observed in IgG. Panel **(B)** detail of complex type glycosylation with percentage of circulating IgG containing either fucose or bisecting N-Acetylglucosamine. The orange circle indicates the core structure. The blue broken lines and text indicate the heterogeneity of complex N-glycans, carrying either no Gal (G0), 1-2 Gal (G1/2), 1-2 Sialic acids (S1/2), with (F) or without core α-1,6-fucose.

THE BIOSYNTHESIS OF HUMAN IGG N-LINKED GLYCANS

N-glycosylation is a multi-step enzyme-mediated biochemical process. IgG N-glycan biosynthesis starts in the endoplasmic reticulum with the addition of a pyrophosphate-dolichol precursor (Dol-P, Glc3Man9GlcNAc2) to the Asn 297 N-glycosylation site of IgG. This structure is then trimmed by glucosidases and mannosidases, as the process moves to the Golgi, leading to the formation of high mannose, hybrid and the complex types N-glycans (26, 30–33). The main enzymatic reactions taking place in the Golgi are summarized in **Figure 2**. The stable overexpression or reduction/inhibition of some of these enzymes in antibody producing cell lines have been used to modify IgG glycan composition and perform structure-function studies of N-glycan microheterogeneity ((31); and see below). The structure of N-linked and other IgG glycans and glycosylation pathways have already been extensively reviewed by others (30, 32, 34, 35) and we refer the readers to these more complete descriptions of the process.

The enzymatic pathways for GDP-fucose biosynthesis and Fc core fucosylation are shown in **Figure 3** (26, 30, 36). L-Fucose (6-deoxy-L-galactose) is a monosaccharide obtained by glycoprotein degradation or diet. In the salvage pathway, L-fucose is phosphorylated in the cytosol to fucose-1-phosphate by fucokinase (FUK), and then converted to GDP-fucose by GDP-fucose-pyrophosphorylase (GDPP), an essential substrate for the fucosylation of proteins (**Figure 3**). Alternatively, and most commonly, *de novo* GDP-fucose is synthesized from GDP-mannose by GDP-mannose 4,6 dehydratase (GMD) and then GDP-4-keto 6-deoxymannose 3,5-epimerase-4-reductase (FX) (**Figure 3**). GDP-fucose is transported to the ER *via* the SLC35C1 and SLC35C2 transporters and used by several fucosyltransferases (FUT) in the Golgi to fucosylate glycoproteins. There are 11 different FUTs, but only FUT 8 catalyzes IgG Fc core fucosylation *via* an α-1,6 linkage (**Figure 3**). As mentioned above, the presence of bisected GlcNAc inhibits the addition of core α-1,6 fucose (26, 30, 36).

These pathways show that there are multiple steps where a modulation of fucosylation can take place including the supply of diet fucose (36). The mechanisms of IgG Fc glycosylation regulation in B cells in healthy individuals and in disease are however still little understood.

STRATEGIES TO GENERATE THERAPEUTIC IGG1 WITH LOW LEVELS OF FUCOSE LEVELS

In the last 10-15 years, removal of IgGs Fc core fucose has been shown to be an important method to enhance ADCC by therapeutic IgG1 mAbs (37–39). Based on the knowledge of the pathways of N-glycan fucosylation described above, several strategies have been used to generate therapeutic IgGs with low or no fucose [reviewed by Pereira et al. (40)]. These are briefly summarized below:

i. The selection of cell lines that naturally have low FUT8 enzyme, such as the Y2B/0 rat cell line (38).

ii. The creation of FUT8 knock out cell lines such as CHO FUT8$^{-/-}$ (41, 42). These produce antibodies completely lacking fucose, but may have a low growth rate unless specifically adapted.

iii. The selection of natural cell lines with defects in other enzymes involved in fucosylation, such as Lec 13, which has defective GDP mannose 4,6 dehydratase (GMD) which converts

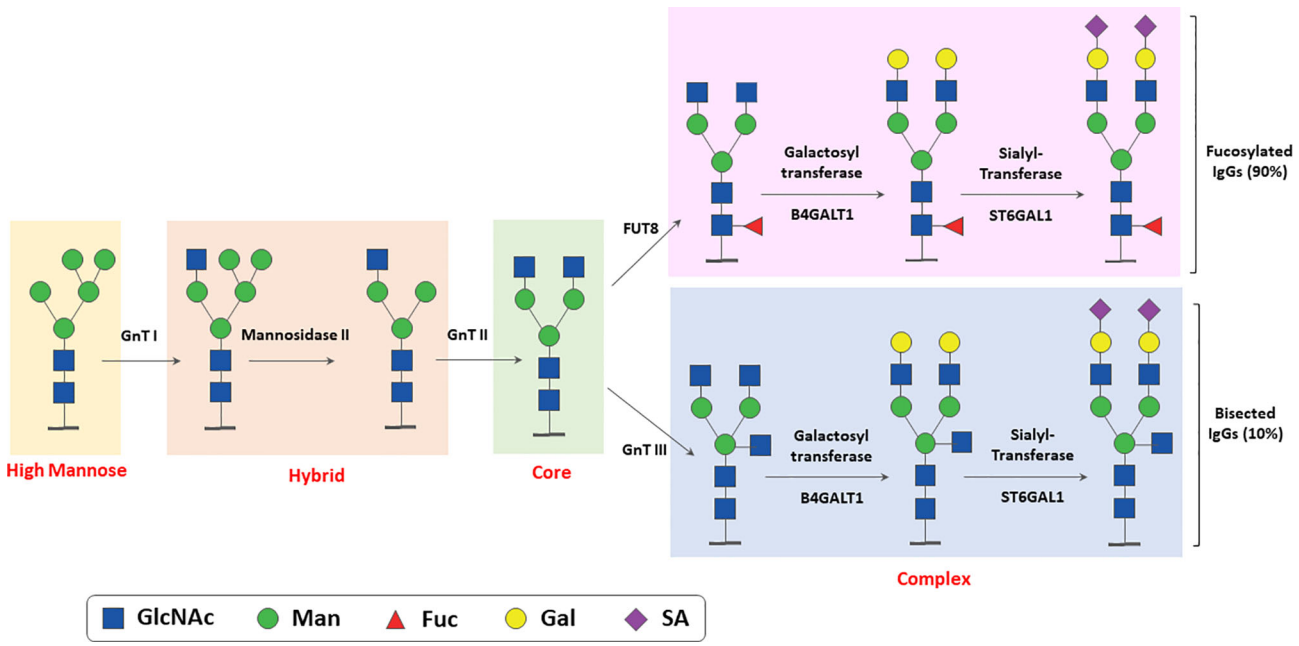

FIGURE 2 | Simplified scheme of enzymatic reactions involved in N-linked glycosylation of IgG. The major glycosylation steps and enzymes involved in N- linked glycosylation of IgGs taking place in ER and Golgi are shown. GnT, N-Acetyl glucosamine transferase; FUT, Fucosyl transferase; Man, Mannose; Gal, Galactose; GlcNAcm N-acetylglucosamine; SA, sialic acid (N-Acetylneuraminic Acid).

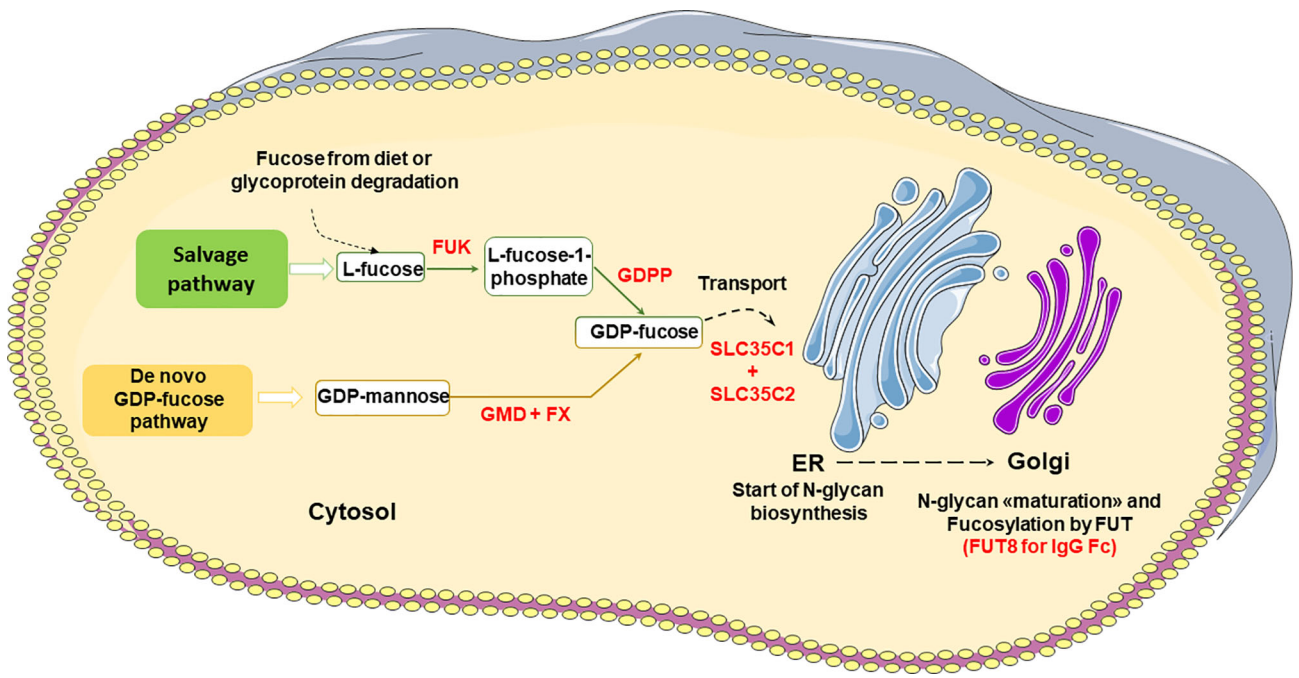

FIGURE 3 | Major pathways of GDP-fucose biosynthesis and IgG Fc core fucosylation. FUK, Fucose Kinase; GDPP, GDP-fucose-pyrophosphorylase; GMD, GDP-mannose 4,6 dehydratase; FX, GDP-4-keto 6-deoxymannose 3,5-epimerase-4-reductase; FUT, Fucosyltransferase.

GDP mannose to GDP-fucose, the substrate for N-glycan core fucosylation (**Figure 3**) (37, 43).

iv. The creation of engineered cell lines lacking GMD, GDP-L-fucose synthase (FX) and/or the GDP-fucose transporter SCL35C1 (**Figure 3**) (44, 45). For example, the $FX^{-/-}$ and $GMD^{-/-}$ CHOZN® cell clones produced IgG1 antibody with core fucosylation reduced to 6-8% or 1-3%, respectively. The $FX^{-/-}$ clones also showed some aberrant glycan forms suggesting the $GMD^{-/-}$ CHOZN® cell line may be the best choice (44).

v. Another strategy is to engineer CHO clones with higher β-1,4-N-acetylglucoseaminyl-transferase III (GnTIII), best with a Golgi localization domain (2, 31, 46, 47). GnTIII catalyzes the transfer of GlcNAc to a core mannose residue in N-linked oligosaccharides *via* a β-1,4 linkage, which results in the formation of a bisected sugar chain. The bisection GlcNAc inhibits the transfer of fucose by FUT8, so that GnTIII overexpressing cells produce antibodies with lower levels of core fucose.

vi. Another modality is to use non-mammalian cells such as plant or insect cells that are engineered to synthesize human-type N-glycans, to reduce potential immunogenicity, but lack core fucosylation capacity (48).

vii. Cells can be treated with inhibitors of FUT8 such as 2F-Peracetyl-Fucose (49) or anti-FUT8 antibody (50).

viii. Finally, antibodies can also be enzymatically modified *in vitro* by treatment with glycosidase and glycosynthase enzymes. This is somewhat more complex since it requires antibody deglycosylation followed by a controlled glycosylation (51, 52).

The major strategies based on engineered mammalian cell lines are listed in **Table 1**.

It is worth noting that, depending on the system used, the amount of fucose may vary from 0% for cell lines lacking FUT8 enzyme to 10-30% for the those with reduced FUT8 or other enzymatic modifications (**Table 1**). Also, different production cell lines and systems may lead to antibodies with different N-glycan profiles, not only regarding fucose residues. These may in turn affect function of antibodies since carbohydrates other than fucose, for example galactose or sialic acid may affect CDC or inflammation, respectively, among others (33, 53). A more detailed description of the role of galactosylation and sialic acid is beyond the scope of this review.

FUNCTIONAL CONSEQUENCES OF LOW CORE FUCOSE ON IGG1 ASN 297 N-GLYCAN

Binding to FcγRIIIA and FcγRIIIB

Human, humanized or chimeric IgG1 antibodies lacking fucose on the Asn N-glycan bind with 10-100 fold higher affinity to human FcγRIIIA and FcγRIIIB (CD16B) (37, 54, 55). Structural studies have shown an increased carbohydrate-carbohydrate interaction between the N-glycans of FcγRIIIA and Fc, explaining the higher affinity of afucosylated IgG1 (56, 57).

NK Cells and ADCC

Since FcγRIIIA is the major activating receptor on NK cells and mediates ADCC, the net result of increased binding to FcγRIIIA is a significant enhancement of ADCC by afucosylated IgG1 antibodies with respect to their fully fucosylated counterpart (2-40 fold, also depending on galactosylation) (37–39) (**Table 2**). In addition, FcγRIIIA has relatively low-medium affinity for IgG so that ADCC is inhibited by excess IgG in plasma. In contrast, ADCC induced by afucosylated IgG1, which has a significantly higher affinity for FcγRIIIA, is not significantly inhibited by plasma IgG. Thus afucosylated anti-CD20 antibody may be more effective in inducing ADCC in whole blood by 2 mechanisms: 1) higher affinity for FcγRIIIA and 2) significantly reduced inhibition by serum IgG (99). Afucosylated IgG1 has also been reported to induce greater FcγRIIIA downmodulation from the NK cell surface, a phenomenon which takes place *via* shedding of the extracellular domain by the ADAM 17 metalloproteinase and may participate in the serial target cell killing by NK cells (100).

Phagocytosis by Macrophages

FcγRIIIA is expressed by monocytes/macrophages, particularly M2 and red pulp macrophages as well as microglial cells. However, macrophages also express the activating FcγRI and FcγRIIA, and FcγRI is thought to be the major mediator of phagocytosis of IgG1 opsonized targets (10, 11, 101). Therefore, afucosylated therapeutic mAbs, despite binding with higher affinity to FcγRIIIA, are not generally reported to significantly enhance phagocytosis, at least *in vitro* (10, 11, 102). There is some evidence that phagocytosis of targets opsonized with anti-

TABLE 1 | Examples of cell lines and strategies developed for low fucose antibody production.

Cell line or system	Enzyme defect	Approximate Fc core fucosylation level (normal is >90%)	References
Lec 13 (CHO mutant)	Defective GMD	10%	(37, 43)
YB2/0 (rat)	Low FUT 8	9-30%	(38)
CHO $FUT8^{-/-}$ (e.g. Potelligent®)	FUT8 KO	0%	(41, 42)
CHO $GMD^{-/-}GFT^{-/-}$	GMD+SLC35C1 KO	0%	(45)
CHO $FX^{-/-}$	FX KO	6-8%	(44)
CHO $GMD^{-/-}$	GMD KO	1-3%	(44)
CHO $GnTIII^{+++}$ (e.g. GlycomAbs®)	GnTIII overexpression	10-15%	(46, 47)

FUT, Fucosyltransferase; GMD, GDP-mannose 4,6 dehydratase; FX, GDP-4-keto 6-deoxymannose 3,5-epimerase-4-reductase; GnTIII, N-acetylglucosamine transferases III; SLC35C1, GDP-fucose transporter; KO, knock out.

CD20 by liver Kupfer cells *in vivo* is enhanced by the afucosylated mAb (103), but this point still needs to be further investigated and confirmed. In the context of polyclonal alloimmune anti-HPA1a IgG1 antibodies (see below), increased phagocytosis of target platelets *in vitro* by both monocytes (*via* FcγRIIIA) and PMN (*via* FcγRIIIB) has been reported (104).

ADCC by γδ T Cells

FcγRIIIA is also expressed by γδ T cells and these can mediate ADCC in presence of IgG1 antibodies (105, 106). There are reports of increased ADCC by γδ T cells in presence of low fucose anti-CD20 mAb obinutuzumab compared to rituximab (58, 107). γδ T cells represent <5% of T cells in the circulation of healthy individuals; they are also localized in non-lymphoid tissues and constitute the majority of immune cells in some epithelia (108). The role of γδ T cells in the response to IgG1 antibody *in vivo* is not well understood.

ADCC and Trogocytosis by PMN

IgG1 with low Fc core fucose also binds more strongly than fucosylated antibody to FcγRIIIB, which has >97% sequence identity with FcγRIIIA in its extracellular IgG binding domain (14, 15, 55). FcγRIIIB is a GPI-linked receptor lacking activating module (ITAM), is expressed only by PMN and at high levels on these cells (5, 55, 109). Low fucose anti-CD20 therapeutic

TABLE 2 | Selected therapeutic antibodies with low or no fucose, approved by FDA/EU or in clinical development.

Antibody name (code)	Antigen	Antibody isotype	Method of defucosylation	% fucose	Diseases	Major findings	references
1.1. Approved antibodies (FDA/EU)							
Obinutuzumab (GA101)	CD20	Humanized IgG1	CHO overexpressing GnTIII (GlycoMAb)	About 15%	B-NHL	Higher ADCC by NK and γδ Tells, more effective than RTX *in vivo* in some mice models or in primates	(47, 55, 58–62) (63)
						Phase III in CLL compared to RTX in combination with CLb	(64)
						Phase III studies with different chemotherapy regimen in CLL and compared to RTX	(65)
						Phase III studies in diff chemo combinations compared to RTX in untreated FL.	(66)
Mogamulizumab (KW-7061)	CCR4	Humanized IgG1	CHO FUT8 $^{-/-}$ (Potelligent)	0%	Cutaneous T cell lymphoma	Equivalent ADCC by afucosylated mAb, but with 10-fold lower antigen expression on target compared to fucosylated mAb	(67, 68)
Inebilizumab (MEDI 551)	CD19	Humanized IgG1	CHO FUT8 $^{-/-}$ (Potelligent)	0%	Neuromyelitis optica	Increased ADCC *in vitro*. Depletes B cells more effectively than fucosylated antibody in hCD19 transgenic mice (PB, spleen and BM)	(69–72)
Benralizumab (MEDI-563)	IL-5Rα	Humanized IgG1	CHO FUT8 $^{-/-}$ (Potelligent)	0%	Severe asthma with eosinophilia	Increased ADCC *in vitro*. Efficacy in depleting eosinophil in non-human primates and in clinical Phase III studies	(73–75)
Margetuximab (MGAH22)	HER2	Chimeric IgG1	CHO FUT8 $^{-/-}$ Also mutation in Fc to decreased CD32B binding	0%	Advanced metastatic HER2^{+++} breast cancer	Increased ADCC. *In vivo* increased activity in hFcγRIII+ mice. Phase III trial in breast cancer compared to trastuzumab	(76, 77)
Belantamab vedotin (GSK2857916)	BCMA	IgG1-MMAF ADC	CHO FUT8 $^{-/-}$	0%	Multiple myeloma	Increased ADCC of naked mAbs. Phase II ORR 31%. 72% survival at 6 months	(78)
Amivantamab (JNJ-61186372)	EGFRxMET	Humanized bispecificIgG1	Low fucose producing cell line	<10%	Non-small cell lung cancer (NSCLC)	Increased ADCC, not ADCP compared to high fucose variant. Phase III NSCLC	(79)
1.2. Selected antibodies in clinical studies							
Ublituximab (Emab-6)	CD20	Chimeric IgG1	YB2/0	24%	CLL, B-NHL, multiple sclerosis, neuromyelitis optica	High ADCC and ADCP (not compared with fully fucosylated antibodies). Phase I and II trials in B-NHL, CLL and autoimmune diseases + neuromyelitis optica. Phase III in CLL with or w/o ibrutinib (ORR 85% vs 65%)	(80–82)
Tomuzotuximab (cetuGEX)	EGFR	Humanized IgG1 (cetuximab seq)	Glyco Express System®	0%	Advanced carcinoma	Increased ADCC *in vitro*, Phase I study	
						Phase II study comparing CetuGEX with cetuximab combined with chemo: no difference observed	(83)
Imgatuzumab GA201 (RG7160)	EGFR	Humanized rat IgG1 (ICR62)	CHO stably expressing GnTIII (GlycomAb)	15%	Carcinoma	Increased ADCC *in vitro*. Higher efficacy in mouse models (SCID beige or SCID hFcγRIIIA tg) also in combination with chemotherapy	(84)
						Phase I study in EGF^{+++} solid tumors	(85) (86)

(Continued)

TABLE 2 | Continued

Antibody name (code)	Antigen	Antibody isotype	Method of defucosylation	% fucose	Diseases	Major findings	references
						Open label study in advanced CRC. Decrease NK post treatment in PB	
						Enhanced ADCC *in vitro*	(87)
						Favorable combination of GA201 and chemo *in vitro* and in carcinoma models in SCID mice	(88)
						Open label study of GA201 vs cetuximab in head & neck squamous carcinoma (N=44). Greater decrease in NK in PB and greater cytokine release with GA201 vs CTX. No difference in clinical response.	(89)
KHK4083	OX40	Human IgG1	FUT8 $^{-/-}$Potelligent	0%	Ulcerative colitis	Phase I	(90)
Tragex	HER2	Humanized IgG1	Glyco Express system® (FUT8-/-)		HER2+++ tumors	Increased ADCC *in vitro*. Enhanced activity *in vivo* in hFcγRIIIA tg mice. Phase I in HER2^{+++} solid tumors	(37, 91–94)
Cusatuzumab (JNJ-74494550, ARGX-110)	CD70	Humanized IgG1	CHO FUT8 ko (Potelligent)	0%	Hematological and solid cancers	Phase I study	(95, 96)
Bemarituzumab (AMG 522)	FGFR2b	Humanized IgG1	CHO FUT8	0%	Gastric cancer FGFR2b^{+++}	Increased ADCC *in vitro*. Efficacy *in vivo* in mouse sc SCID model. Recruitment of NK and T cells into tumor.	(97, 98)

ADCC, Antibody dependent cellular cytotoxicity; ADCP, Antibody dependent cellular phagocytosis; BM, Bone marrow; B-NHL, B-Non Hodgkin's lymphoma; CLb, chlorambucil; CLL, Chronic lymphocytic leukemia; CR, Complete response; EGFR, Epidermal growth factor receptor; FL, follicular lymphoma; PB, Peripheral blood; NSCLC, Non-small cell lung cancer; ORR, Overall response rate; RTX, Rituximab; SCID, Severe combined immunodeficient.

antibody obinutuzumab was shown to activate PMN more effectively than rituximab, which is ≥90% fucosylated, initially suggesting that enhanced FcγRIIIB binding was responsible for this effect (55). However, subsequent experiments performed with PMN isolated from a rare FcγRIIIB null donor, as well as the observation that PMN may express very low levels of FcγRIIIA, indicated that PMN activation by afucosylated anti-CD20 antibodies may be mediated by FcγRIIIA, FcγRIIIB, or both, depending on conditions (110). The presence of low levels of FcγRIIIA on resting or activated PMN however still needs to be confirmed. The activation of PMN by anti-CD20 antibodies does not induce ADCC or phagocytosis, but only trogocytosis and cytokine production (55, 110). Interestingly other antibodies, such as anti-EGFR antibodies do mediate ADCC of tumor targets by PMN, but this function strictly requires FcγRIIA (15). Furthermore, PMN and FcγRIIA mediated ADCC is inhibited by FcγRIIIB (111, 112). Indeed, ADCC by PMN is diminished in the presence of afucosylated anti-EGFR, because the latter binds more strongly to FcγRIIIB, which is highly abundant on PMN and is thought to compete with FcγRIIA. Therefore, at least in this context, FcγRIIIB may act as a decoy receptor (111, 112). It remains to be established whether and how the level of fucosylation of other antibodies, for example those directed against microbes, affect PMN functions.

Cytokine Release by Immune Cells

Several studies indicate that afucosylated IgG1 antibodies induce a more rapid and intense cytokine release by NK cells, monocytes/macrophages, PMN and/or γδ T cells compared to their fully fucosylated counterparts. Induced cytokines include IFN-γ, MCP1, IL-6, TNF, MIP1αβ, Rantes, IL-8 (55, 100, 107, 113–115). The level of cytokines induced *in vitro* is however generally quite low and the significance of such release *in vivo* is not fully clear. Nonetheless, the more frequent or severe immediate reaction syndrome observed in patients treated with obinutuzumab compared to rituximab indicates that increased cytokine release, particularly IL-6 and IFN-γ by afucosylated antibodies may be relevant *in vivo* (64, 116, 117). Cytokine release should therefore be carefully studied during the pre-clinical and clinical development of afucosylated antibodies.

The functional effects of IgG1 Fc core afucosylation are summarized in **Figure 4**.

EVIDENCE THAT AFUCOSYLATION ENHANCES THE EFFICACY OF THERAPEUTIC MABS *IN VIVO* IN ANIMAL MODELS

Studying the role of Fc core fucosylation using small animal models is complicated by the fact that mice express different set of FcγRs compared to humans (5, 118–120). The more recently discovered mouse FcγRIV molecule has been shown several years ago to be the murine ortholog of human FcγRIIIA and to be an important mediator of human IgG1 efficacy in mice. Afucosylated human IgG1 binds with higher affinity also murine FcγRIV (121). This suggests that, despite species differences, human IgG1 therapeutic antibodies can be tested in mice, at least for some aspects of their functions. However, because of differences in FcγR expression pattern in mice, humanized mice or human FcγRIIIA transgenic mice may be used more appropriately. Nonetheless one should bear in mind that mice do not have the equivalent of FcγRIIIB, which therefore makes this species not completely adequate to test the role of PMN in antibody efficacy *in vivo*, unless fully humanized models are used

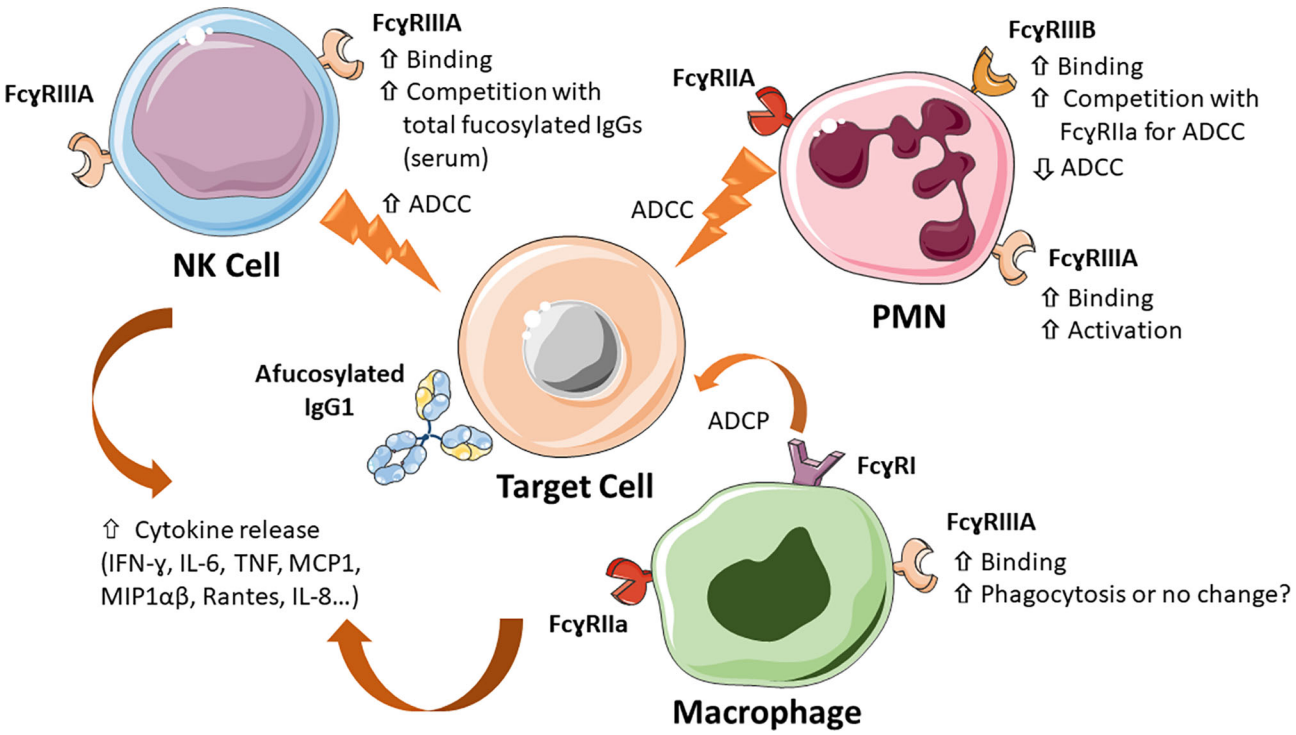

FIGURE 4 | Major mechanisms of action of Fc core afucosylated IgG1 antibodies. IgG1 antibodies lacking Fc core α-1,6-fucose show a 10-100 fold increased binding to FcγRIIIA and FcγRIIIB on the indicated immune cells (NK, monocytes/macrophages and PMN), which results in increased ADCC by NK cells, enhanced competition with plasma IgGs, increased PMN activation, increased inhibition of FcγRIIA-mediated ADCC by PMN, induced by some antibodies (e.g. anti-EGFR mAbs). The effect of monocyte/macrophage induced ADCP is less clear. Low Fc core fucose can also increase release of cytokines, such as IL-6, TNF-α and IL-8, both *in vitro* and *in vivo*.

(119). Despite these caveats, it is worth noting that afucosylated or low fucose anti-cancer mAbs have consistently been shown to control tumor growth more efficiently than their fully fucosylated parent molecules in mice (69, 84, 92, 122), as well as macaque, the latter having a more similar pattern of FcγRs to humans (123). These results have led to an increased attention to the N-glycan profile of therapeutic mAbs (124), as well as the development of new afucosylated therapeutic antibodies in a variety of clinical contexts. These are discussed below.

ANTI-CANCER MABS WITH LOW CORE FUCOSE IN THE CLINIC

Many antibodies with no or low Fc core fucose have entered pre-clinical or clinical development to treat different diseases. Seven such antibodies have been approved so far by FDA/EMA (**Table 2**). They include one bispecific and one ADC, the others being unconjugated IgG1 antibodies. Five are approved for cancer therapy and two for immune/inflammatory diseases. Many other antibodies are in clinical trial (**Table 2, part 2**) or in pre-clinical development (47, 55, 58–79). In all cases, a significantly enhanced ADCC activity by NK cells has been shown *in vitro* and, in some, more effective target depleting activity *in vivo* in mice or non-human primates, as discussed above (**Table 2**).

It is obviously difficult to evaluate whether removal of Fc core fucose significantly increases the efficacy of therapeutic anti-cancer mAbs in patients without performing phase III comparative studies of parent and afucosylated counterpart, studies that are rarely performed. Glycoengineered anti-CD20 antibody obinutuzumab was the first therapeutic antibody with low fucose to be approved in 2013 for the treatment of B-cell neoplasia. It has been extensively compared with rituximab *in vitro* and in clinical trials in Phase III studies in chronic lymphocytic leukemia and B-NHL, usually in combination with chemotherapy. Obinutuzumab has shown either enhanced activity or, in some cases, non-inferior activity to rituximab depending on disease contexts and treatment protocols (64, 116, 125). However, these two anti-CD20 antibodies differ from each other in aspects other than level of core fucosylation. They differ in epitope recognition, binding mode to CD20, and to some extent mechanisms of action (125). Rituximab induces higher CDC whereas obinutuzumab induces homotypic adhesion and direct cell death, in addition to the higher ADCC due to low fucose (62, 102, 126). It is therefore difficult to clearly identify the mechanism of higher efficacy of obinutuzumab in some disease contexts, compared to rituximab.

Another way to understand whether FcγRIIIA binding affinity (and therefore the degree of IgG1 core fucosylation) is important for antibody efficacy is to study the response of patients carrying different FcγRIIIA variants, in particular the 158V (high affinity) and 158F polymorphism (lower affinity). The studies of rituximab activity in follicular lymphoma patients treated with rituximab as single agent and the correlation between clinical response and the FcγRIIIA-158V carriers suggested that FcγRIIIA and ADCC by NK cells are important for the *in vivo* efficacy of this antibody (127). Similar data have been obtained in HER2 overexpressing breast cancer patients treated with trastuzumab (128). Nonetheless, for both rituximab and trastuzumab, these data have not been confirmed in all clinical contexts, perhaps also due to the fact that these therapeutic mAbs are generally used in combination with chemotherapy, which itself may modulate cell-mediated mechanisms (9, 129). Thus, both FcγRIIIA-dependent and independent mechanisms are likely to be important for anti-cancer IgG1 efficacy and these may vary in different clinical and therapeutic conditions.

Importantly, defucosylation has been shown not to alter significantly FcRn binding or pharmacokinetics *in vivo*, encouraging the development of afucosylated antibodies for clinical use (30).

To summarize, the fact that afucosylated IgG1 have consistently shown higher FcγRIIIA binding and ADCC *in vitro* as well as often a greater efficacy *in vivo* in animal models without significant changes in antibody pharmacokinetics *in vivo* (69, 92) has led many groups to design and generate afucosylated therapeutic IgG1 mAbs or BsAb, as well as ADCs.

MODULATION OF IGG FUCOSYLATION IN PHYSIOLOGICAL STATES AND DISEASE

Physiological Modulation of Fc N-Glycan Fucosylation

The glycosylation pattern of IgGs has been shown to be modulated during life. Children starting to produce their own IgGs show higher N-glycan core fucose levels, which decrease during childhood (130, 131). In adults, the levels of IgG fucosylation is quite stable in absence of pathology or interventions, but quite variable between individuals (ranging from 1.3 to 19.3% afucosylation), presumably due to hereditary as well as environmental factors (29).

How changes during pregnancy or aging are brought about is not clear. During pregnancy, chorionic gonadotropin (hCG) has been shown to promote the development of IL-10 producing B cells which are associated with production of highly core fucosylated IgG (132). The B cell response to infections that induce afucosylated IgGs probably explains the increased afucosylation during childhood (see below), but the mechanisms are unclear. Recently the spleen has been suggested to be an important site of fucosylation regulation: IgG1-Fc core fucosylation was observed to be increased in trauma splenectomized healthy individuals as well as in spherocytosis or immune thrombocytopenia (ITP) patients that were splenectomized, compared to non-splenectomized controls (133). There are several possible explanations for this observation: 1) The spleen may be a site of afucosylated IgG generation. Indeed in ITP, the spleen is also a source of anti-platelets IgGs which are highly afucosylated compared to total IgGs. 2) The spleen removes preferentially immune complexes containing afucosylated IgGs *via* FcγRIIIA positive myeloid cells, so that splenectomy induces a change in the ratio of fucosylated/afucosylated IgGs (133). Further investigation of these possible mechanisms is warranted.

Several gene array analyses correlating IgG N-glycan traits with genome-wide polymorphic variants have allowed to identify gene pathways involved in N-glycome regulation, several of which were confirmed in more than one study (134–140). Some of the genes identified are glycosyltransferases, most significantly FUT8, B4GALT1 and MGAT3 (the latter encoding the GnTIII enzyme)(**Figure 2**), as well as transcription factors known or suspected to regulate these genes, such as RUNX1, RUNX3, IKZ1, IKZ3, IRF1, SMARCB1, TBX21O and HFN1 (138). Others are novel genes with no known role in glycosylation (135). With specific regard to fucosylation, FUT8 itself, the fucosidase FUCA2 and transcription factors regulating FUT8, most notably IKZF1, have been implicated in several studies (135, 137, 141). Altogether these results suggest that the expression level, localization and perhaps substrate availability of glycosylation enzymes define IgG glycosylation patterns. Clearly, further work will be required to fully identify the pathways involved and their role in the physiological regulation of IgG Fc N-glycan composition and core fucosylation in B cells.

Since N-glycosylation and core fucosylation take place in the ER and Golgi (**Figures 2** and **3**), the physiological state, pH, ionic and redox of ER and Golgi can also affect glycosylation (142, 143). Indeed some studies have evidenced the role of ER stress in modifying protein glycosylation patterns (144). In particular in B cells, the mutation or deletion of the ER protein Jagn1 leads to ER stress, reduced IgG core fucosylation and increased sialylation, indicating that afucosylated IgG1 may be induced during ER stress (145).

Interestingly many loci identified to play a role in regulating the glycosylation pattern of IgGs and other plasma proteins are also associated with autoimmune and inflammatory diseases (135, 137). The specific role of IgG Fc core fucosylation in these pathological conditions is discussed below.

IgG1 Fc Core Fucosylation in Alloimmunity

The fact that IgG Fc core fucosylation is physiologically modulated was first observed in the context of alloimmunization, frequently occurring during pregnancy, and mostly involving red blood cells (RBC) and platelets. Rhesus D antigen alloimmunization during pregnancy and delivery of a RhD^+ fetus by a RhD negative mother has been in the past the most common cause of hemolytic disease of the fetus and newborn (HDFN), occurring in sensitized mothers who had given birth to a previous RhD^+ baby. The disease is due to anti-RhD IgG antibodies crossing the placenta and destroying the

RhD^+ RBC in the reticuloendothelial system of the fetus and newborn, causing severe fetal anemia and hydrops fetalis in severe cases. Before the advent of prophylaxis of RhD negative women with anti-RhD immunoglobulin, which prevents alloimmunization, HDFN affected 150 per 100 000 births and 10% of perinatal deaths in the Caucasian population. Analysis of IgG glycosylation in alloimmunized pregnant mothers has revealed a variable decrease in IgG1 Fc core fucosylation (even down to 12%), whereas the total IgG remained highly fucosylated, as in healthy individuals (>90%). Furthermore, the level of anti-RhD Fc core fucosylation correlated significantly with FcγRIIIA-mediated ADCC and with low fetal-neonatal hemoglobin levels (146).

A later *in vitro* study investigated the functional activity of monoclonal anti-RhD antibodies of different subclasses (IgG1, 2, 3 or 4), bearing either low (usually <30%) or high (>90%) Fc core fucose levels (147). Whereas reduced fucosylation increased FcγRIIIA binding of all IgG subclasses, only defucosylated IgG1 and IgG3 showed a 12- and 7-fold increase in ADCC by NK cells, respectively, presumably due to the fact that IgG2 and IgG4 are poor binders of FcγRIIIA (147). Afucosylation of the anti-RhD mAbs did not enhance *in vitro* phagocytosis of RBC by GM-CSF (M1) or M-CSF (M2) induced macrophages, reminiscent of what has been most often observed with anti-tumor antibodies (see above). Another study of an anti-RhD mAb with low core fucose showed a higher RBC clearance capacity *in vivo* in mice, compared to highly fucosylated antibody (148).

These data altogether show that IgG Fc core fucosylation is likely to be an important pathological feature in HDFN with diagnostic potential, and that a significant mechanism of the disease may be RBC destruction by NK cells (149), in addition to ADCP by the reticuloendothelial system.

RBC alloantigens other than Rhesus D (c, E, Kell) can induce an antibody response and HDFN. The level of defucosylation of anti-Kell, but not anti-c or anti-E, was shown to correlate with severe fetal anemia. These data suggest that the antigens shape the type of response (150).

Alloimmunization of mothers by fetal platelets can also occur during birth or pregnancy, leading to the generation of antibodies directed against polymorphic human platelet antigens (HPAs), the phagocytosis of opsonized platelets in fetal spleen and liver and the development of fetal and neonatal alloimmune thrombocytopenia (FNAIT), a rare but potentially fatal diseases of the fetus and newborn (151). FNAIT can also occur during first pregnancy of incompatible mothers and can have severe consequences, including intracranial hemorrhage. In 80% of FNAIT cases, the targeted antigen is human platelet antigen-1a (HPA-1a), i.e. a polymorphic epitope of the β3 integrin (152). The HPA-1a antigen is presented to maternal T and B cells in combination with the HLA DRB3*01:01 molecule and leads to production of anti-platelets, mostly IgG1 antibodies (151, 153). Several groups have shown that pregnant women have decreased, although variable, IgG1 Fc core fucosylation, which is specific for anti-HPA-1a as opposed to total IgG. Low core fucose on anti-platelet antibodies appeared to increase phagocytosis by monocytes and PMN (104). Reduced anti-HPA-1a Fc core fucosylation as well as antibody levels correlated with decreased neonatal platelet counts and increased disease severity in FNAIT patients (104, 152, 154). Interestingly, low fucosylation of anti-HPA antibodies was observed in patients with FNAIT but not in those with refractory thrombocytopenia following platelet transfusion, indicating that the level of fucosylation is antigen dependent and/or related to the immune milieu defined by pregnancy (104).

IgG1 Fc Core Fucosylation in Autoimmune and Inflammatory Diseases

The IgG Fc N-glycosylation pattern of total or antigen specific IgGs has also been investigated in several autoimmune and inflammatory diseases, including rheumatoid arthritis (RA), systemic lupus erythematosus (SLE), multiple sclerosis (MS), autoimmune thyroid diseases, inflammatory bowel diseases (ICB), chronic obstructive pulmonary disease (COPD), ulcerative colitis (UC), etc. In these clinical contexts the greatest changes have been observed in galactosylation and sialylation, which in some cases such as in RA correlate with disease activity (155, 156). Fc core fucosylation has been observed to be modulated in only few autoimmune diseases, with an increase observed in RA, juvenile idiopathic arthritis and Crohn's diseases and a decrease in SLE, MS, and Lambert-Eaton myasthenic syndrome, immune thrombocytopenia (ITP) and either increase or decrease in different thyroid autoimmune diseases (157–159). It is worth noting that in this context, total IgGs rather than antigen-specific IgG have generally been analyzed. The pathological significance of these results is still unclear, except that low galactosylation and sialylation as well as high fucosylation of IgGs have been associated with a pro-inflammatory state (160). Several reviews of the state of the art regarding Fc N-glycosylation in autoimmune and inflammatory diseases has been published recently and we suggest the reader to consult these articles for further details on the subject (157, 161–163).

Interestingly, intravenous immunoglobulins (IVIGs) are extensively used as an immunomodulatory agent to treat autoimmune and inflammatory diseases. One mechanism of action of IVIGs is thought to be through competition with pathogenic IgG for Fcγ receptors on immune cells. A very recent report analyzed the functional effects of different IVIGs glycoforms (i.e. IVIGs carrying 2 galactose, 2 sialic acids or no galactose, with or without α-1,6-fucose). Galactosylated and afucosylated IVIGs [$(G2)_2$] had the highest affinity for FcγRIIIA. The greatest effect was given by fucose removal as expected, but presence of 2 Gal residues increased affinity still further. Interestingly, $(G2)_2$ IVIGs were also most potent in blocking ADCC *in vitro* and in reducing inflammation and serum IL-6 levels in a collagen antibody-induced arthritis model in mice (164). These data confirm that the anti-inflammatory activity of IVIGs is in part mediated *via* blockade of FcγRIIIA by their galactosylated, non-fucosylated IgG component, at least in some clinical settings (165). They also corroborate the immunomodulatory capacity of Fc N-glycan composition in health and disease, particularly regarding core α-

1,6-fucose and galactose. Finally, they suggest that modified IVIGs [$(G2)_2$] may be a more effective immunomodulatory agent than unmodified IVIGs. This hypothesis will need to be verified.

IgG1 Core Fucosylation During the Humoral Response to Infectious Agents

Evidence for an important role of antibodies in the control viral or parasitic infections has gained strength over the last decade. IgG1 antibodies in infection, just like for anti-cancer mAbs, can act through a variety of mechanisms: *via* Fab they can neutralize viruses and parasites by blocking cellular entry and the replication cycle; through Fc they induce complement activation and phagocytosis by macrophages or PMN of opsonized immune complexes, clearing the infectious agent, as well as activate ADCC by NK cells which will destroy infected cells (166–170). Fab- and Fc-mediated activities probably synergize with each other, at least in some cases, although some antibodies under some circumstances can also enhance infection probably by facilitating the entry of the virus into FcγR positive target cells, a phenomenon called antibody dependent enhancement (ADE). This has been particularly well described following secondary infection by a different Dengue virus serotype (166, 167, 171–173).

The role of the different FcγRs and immune cells in protection from viral or parasitic diseases is not fully established, also because establishing suitable models is particularly challenging. Nonetheless FcγRs as well monocytes and macrophages have been implicated as important effectors in controlling viral diseases caused by Influenza A virus, SARS-CoV and SARS-CoV-2 viruses, Chikunguya virus, West Nile virus and Yellow Fever virus (166, 170, 172, 174). Less frequently a role of NK cells or NKT cells has been demonstrated (166).

Interestingly, recent technical improvements in dissecting glycan structures have allowed to demonstrate that during natural antibody responses to viral or parasitic infections, there may be in some cases a decreased Fc core fucosylation of antigen-specific IgGs. **Table 3** lists the major examples of this phenomenon and indicates the levels of afucosylation and duration that has been reported (whenever known). IgG1 antibodies against cytomegalovirus (CMV) (175) or against the plasmodium falciparum erythrocyte membrane antigen 1 (pfEMP1), a parasite antigen expressed on infected erythrocytes (183), show the highest levels of afucosylation following infection (median 30-75%), although this was highly variable between individuals. The effect appeared to be quite stable during time, perhaps due to continuous stimulation and/or formation of long-lived plasma cells secreting these afucosylated antibodies (175, 183). Other infectious agents, such as SARS-CoV-2 virus (175–179, 184), Dengue virus (180–182), Hepatitis B virus and Mump virus (175), induce lower (median 12-18%), although significant, levels of afucosylated antigen-specific IgG1s (**Table 3**). Worth noting is that afucosylation has been demonstrated to be specific for the IgG1s that recognize the viral or parasite membrane antigen and has not been observed in total circulating IgG1 or IgGs. The mechanism involved is not yet clear. Nonetheless, present evidence suggests that antigens presented in the context of host cell membranes may induce specific Fc core afucosylation. Indeed, infection by enveloped viruses or by plasmodium falciparum decreases Fc core fucosylation of IgGs induced by membrane associated antigens, whereas vaccination with the soluble antigens from the same microorganisms does not (175, 183).

A recent paper investigating total plasma IgG N-glycosylation patterns in patients with asymptomatic filariasis (MF^+) or with chronic disease (CP), compared to non-infected local control donors showed that CP patients had higher N-glycan heterogeneity. Afucosylation was highest in the CP group and lowest in MF^+ group compared to controls. Other changes in glycosylation were observed, which may also have affected the immune and inflammatory state of the patients (185). Further studies will be required to investigate N-glycosylation pattern also on antigen-specific IgGs in the context of filariasis.

An important question is the functional effect of an increased level of antibody afucosylation during viral or parasitic infections and whether modulation of Fc core fucosylation is important for the control of the infecting microorganisms. This is obviously a difficult question to answer, also because afucosylation may be accompanied by other modifications in glycan structure and because glycosylation of other proteins could also be modified during infection (175, 186). Fc core fucosylation also affects the B

TABLE 3 | Examples of modulation of Fc core fucosylation of antigen-specific IgGs in infectious diseases.

Antigen	Afucosylation level	% afucosylation (median)	IgG involved	Time frame	Clinical significance of afucosylation	ref
CMV	Low	35%	IgG1	Stable over time	Not known	(175)
SARS-CoV-2 Spike	Fast upon sero-conversion	12-18%	IgG1	Reversible	Correlates with ARDS, IL-6 and CRP levels, correlates with IL6 induction by macrophages *in vitro*	(175–179)
Dengue E and NS1 proteins	Induced by infection (1° and 2°)	12-18%	IgG1	Stable over time	Correlates with disease severity; correlates with low platelets and RBC	(180–182)
HIV-1	low	12%	IgG1	Stable over time	Unknown	(175)
HBV	Low	16%	IgG1	–	Unknown	(175)
Mumps virus	Low	12%	IgG1	–	Unknown	(175)
Plasmodium falciparum EMP1	High	30-75%	IgG1	Stable w/o antigen boost, further decreases with multiple exposure	Induces higher degranulation of $Fc\gamma RIIIA^+$ cell line *ex vivo*	(183)

ARDS, Acute Respiratory Distress Syndrome; CRP, C Reactive Protein; CMV, cytomegalovirus.

cell receptor assembly (BCR) and BCR signaling (32). There is however some evidence that Fc core afucosylation may help in the control of infection, since the humoral response, ADCC and NK cells can play a role on the control of viral spread (187–190). Nonetheless afucosylation may also lead to major side effects, through pro-inflammatory mediators released by FcγRIII expressing immune cells (see paragraph 5.5). Indeed, a correlation has been observed in some studies between degree of Fc core afucosylation and acute respiratory syndrome (ARDS) and inflammatory markers following SARS-CoV-2 virus infection (175, 177). Pongracz et al. confirmed decreased core fucosylation of anti-Spike protein in Covid-19 hospitalized patients, but could not observe a difference between those recovered or not in intensive care unit (178). Nor did they observe a negative correlation with inflammatory markers. In another study, degree of core afucosylation appeared to correlate with younger age of hospitalized patients (179). Recent work suggests that antibody titers, modifications of the IgG1 N-glycome profile other than afucosylation and FcγRs other than FcγIIIA, such as FcγIIA, may contribute to Covid-19 disease severity (177–179, 191, 192), which would be in line with the complexity of the immune response. Clearly much work still needs to be done to fully define the factors contributing to SARS-CoV-2 infection control and ARDS.

During secondary infection with Dengue virus, the degree of Fc core afucosylation correlated with disease severity and with low platelets and RBCs (180–182).

DISCUSSION

Afucosylation of Asn-297 N-glycan of human IgG1 is the glycan modification with the highest impact on the effector functions of therapeutic IgG1 antibodies, notably a 10-100 fold increase in affinity for human FcγRIIIA and 2-40 fold increased ADCC by NK cells. The effect of Fc core afucosylation on phagocytosis by macrophages is less clear and may depend on context, because these cells express several other activating FcγRs that participate in the process of phagocytosis, in addition to FcγRIIIA. Afucosylation of IgG1 also enhances its binding affinity to human FcγRIIIB, a major receptor on PMN. The functional effect of this on the PMN response to therapeutic antibodies is not well understood, since many data suggest that FcγRIIIB is an activating receptor for PMN, whereas others suggest that it may act as a decoy receptor in some circumstances.

The strong enhancement of ADCC by Fc core afucosylated IgG1 antibodies has led to the development of many novel therapeutic antibodies, with the idea that enhancing their activity *in vivo*. How much more effective these antibodies are *in vivo* in the clinic, compared to their fully fucosylated counterparts is still not completely clear. Despite these uncertainties, given that animal models suggest greater efficacy of therapeutic mAbs with lower Fc core fucosylation and that afucosylation does not significantly affect the pharmacokinetics of antibodies, this modification is frequently used as a method to try and enhance the efficacy of therapeutic IgG1 mAbs. Removal of fucose can also be combined with point mutations of IgG1 antibodies to further enhance their immune-mediated mechanisms of action (193).

Novel data have accumulated showing an increase in IgG1 Fc core afucosylation during the polyclonal antibody response to infections by some enveloped viruses and parasites and during alloimmunization by RBC or platelets in pregnancy. The correlation between disease severity in alloimmunization points to a more effective removal of target cells by the core afucosylated antibodies, mediated by NK cells and/or the mononuclear phagocyte system. In the case of infectious diseases, a decreased in core fucose in IgG1 antibodies directed against membrane-associated antigens has been demonstrated in several cases. A correlation with disease severity is suggested in some cases, such as SARS-CoV-2 infection, in which the modified N-glycome may indeed induce higher immune cells activation and inflammatory cytokine release. This observation is interesting in view of the more severe or frequent cytokine release syndrome reported with some therapeutic anti-tumor afucosylated antibodies compared to fucosylated antibodies, indicating that similar mechanisms may play a role in these phenomena.

These results emphasize the strong parallelism between the activities of therapeutic IgG1 mAbs and polyclonal IgGs naturally induced in health and disease. Still much remains to be investigated and clarified about the *in vivo* role of Fc core fucosylation, not only of IgG1 but also other Ig isotypes. Further studies on the physiological mechanisms of regulation of IgG core fucosylation in B cells *in vivo* is another exciting area of research, that may allow in the future to control pharmacologically this phenomenon in different pathological conditions.

AUTHOR CONTRIBUTIONS

JG took the lead in writing the manuscript. AA and IC have critically revised the manuscript, designed and completed the figures and tables. All authors contributed to the article and approved the submitted version.

FUNDING

This work was supported by Fondazione Cariplo (Covid-Bank project). IC was supported by AIRC 5x1000 (Project n. 21147).

REFERENCES

1. Vidarsson G, Dekkers G, Rispens T. IgG Subclasses and Allotypes: From Structure to Effector Functions. *Front Immunol* (2014) 5:520. doi: 10.3389/fimmu.2014.00520
2. Pezer M, Pezer M. Immunoglobulin G Glycosylation in Diseases. In: *Antibody Glycosylation*, vol. 112. . Cham: Springer International Publishing (2021). doi: 10.1007/978-3-030-76912-3_13
3. Gudelj I, Lauc G, Pezer M. Immunoglobulin G Glycosylation in Aging and Diseases. *Cell Immunol* (2018) 333:65–79. doi: 10.1016/j.cellimm.2018.07.009

4. Kaplon H, Chenoweth A, Crescioli S, Reichert JM. Antibodies to Watch in 2022. *mAbs* (2022) 14(1):2014296. doi: 10.1080/19420862.2021.2014296
5. Bruhns P, Iannascoli B, England P, Mancardi DA, Fernandez N, Jorieux S, et al. Specificity and Affinity of Human Fcgamma Receptors and Their Polymorphic Variants for Human IgG Subclasses. *Blood* (2009) 113 (16):3716–25. doi: 10.1182/blood-2008-09-179754
6. Weiner GJ. Rituximab: Mechanism of Action. *Semin Hematol* (2010) 47 (2):115–23. doi: 10.1053/j.seminhematol.2010.01.011
7. Cartron G, Watier H, Golay J, Solal-Celigny P. From the Bench to the Bedside: Ways to Improve Rituximab Efficacy. *Blood* (2004) 104(9):2635 –42. doi: 10.1182/blood-2004-03-1110
8. Hussain K, Cragg MS, Beers SA. Remodeling the Tumor Myeloid Landscape to Enhance Antitumor Antibody Immunotherapies. *Cancers* (2021) 13 (19):4904. doi: 10.3390/cancers13194904
9. Musolino A, Gradishar WJ, Rugo HS, Nordstrom JL, Rock EP, Arnaldez F, et al. Role of Fcγ Receptors in HER2-Targeted Breast Cancer Therapy. *J Immunother Cancer* (2022) 10(1):e003171. doi: 10.1136/jitc-2021-003171
10. Gordan S, Albert H, Danzer H, Lux A, Biburger M, Nimmerjahn F. The Immunological Organ Environment Dictates the Molecular and Cellular Pathways of Cytotoxic Antibody Activity. *Cell Rep* (2019) 29(10):3033–46.e4. doi: 10.1016/j.celrep.2019.10.111
11. Nagelkerke SQ, Bruggeman CW, den Haan JMM, Mul EPJ, van den Berg TK, van Bruggen R, et al. Red Pulp Macrophages in the Human Spleen are a Distinct Cell Population With a Unique Expression of Fc-γ Receptors. *Blood Adv* (2018) 2(8):941–53. doi: 10.1182/bloodadvances.2017015008
12. Wiener E, Abeyakoon O, Benchetrit G, Lyall M, Keler T, Rodeck CH. Anti-HPA-1a-Mediated Platelet Phagocytosis by Monocytes *In Vitro* and its Inhibition by Fc Gamma Receptor (FcgammaR) Reactive Reagents. *Eur J Haematol* (2003) 70(2):67–74. doi: 10.1034/j.1600-0609.2003.00025.x
13. Golay J, Valgardsdottir R, Musaraj G, Giupponi D, Spinelli O, Introna M. Human Neutrophils Express Low Levels of Fcγriiia, Which Plays a Role in PMN Activation. *Blood* (2019) 133(13):1395–405. doi: 10.1182/blood-2018-07-864538
14. Wang Y, Jönsson F. Expression, Role, and Regulation of Neutrophil Fcγ Receptors. *Front Immunol* (2019) 10:1958. doi: 10.3389/fimmu.2019.01958
15. Derer S, Glorius P, Schlaeth M, Lohse S, Klausz K, Muchhal U, et al. Increasing Fcγriia Affinity of an Fcγriii-Optimized Anti-EGFR Antibody Restores Neutrophil-Mediated Cytotoxicity. *mAbs* (2014) 6(2):409–21. doi: 10.4161/mabs.27457
16. Unkeless JC, Shen Z, Lin CW, DeBeus E. Function of Human Fc Gamma RIIA and Fc Gamma RIIIB. *Semin Immunol* (1995) 7(1):37–44. doi: 10.1016/1044-5323(95)90006-3
17. Bournazos S, Ravetch JV. Diversification of IgG Effector Functions. *Int Immunol* (2017) 29(7):303–10. doi: 10.1093/intimm/dxx025
18. Golay J, Taylor RP. The Role of Complement in the Mechanism of Action of Therapeutic Anti-Cancer Mabs. *Antibodies* (2020) 9(4):58. doi: 10.3390/antib9040058
19. Aalberse RC, Stapel SO, Schuurman J, Rispens T. Immunoglobulin G4: An Odd Antibody. *Clin Exp Allergy* (2009) 39(4):469–77. doi: 10.1111/j.1365-2222.2009.03207.x
20. Carter PJ, Lazar GA. Next Generation Antibody Drugs: Pursuit of the « High-Hanging Fruit ». *Nat Rev Drug Discovery* (2018) 17(3):197–223. doi: 10.1038/nrd.2017.227
21. Bondt A, Rombouts Y, Selman MHJ, Hensbergen PJ, Reiding KR, Hazes JMW, et al. Immunoglobulin G (IgG) Fab Glycosylation Analysis Using a New Mass Spectrometric High-Throughput Profiling Method Reveals Pregnancy-Associated Changes. *Mol Cell Proteomics* (2014) 13(11):3029 –39. doi: 10.1074/mcp.M114.039537
22. Giddens JP, Lomino JV, DiLillo DJ, Ravetch JV, Wang L-X. Site-Selective Chemoenzymatic Glycoengineering of Fab and Fc Glycans of a Therapeutic Antibody. *Proc Natl Acad Sci U S A* (2018) 115(47):12023–7. doi: 10.1073/pnas.1812833115
23. Yamaguchi Y, Wakaizumi N, Irisa M, Maruno T, Shimada M, Shintani K, et al. The Fab Portion of Immunoglobulin G has Sites in the CL Domain That Interact With Fc Gamma Receptor IIIa. *mAbs* (2022) 14(1):2038531. doi: 10.1080/19420862.2022.2038531
24. Yogo R, Yamaguchi Y, Watanabe H, Yagi H, Satoh T, Nakanishi M, et al. The Fab Portion of Immunoglobulin G Contributes to its Binding to Fcγ Receptor III. *Sci Rep* (2019) 9(1):11957. doi: 10.1038/s41598-019-48323-w
25. Zhang Z, Shah B, Richardson J. Impact of Fc N-Glycan Sialylation on IgG Structure. *mAbs* (2019) 11(8):1381–90. doi: 10.1080/19420862.2019.1655377
26. Li W, Zhu Z, Chen W, Feng Y, Dimitrov DS. Crystallizable Fragment Glycoengineering for Therapeutic Antibodies Development. *Front Immunol* (2017) 8:1554. doi: 10.3389/fimmu.2017.01554
27. Jefferis R. Glycosylation as a Strategy to Improve Antibody-Based Therapeutics. *Nat Rev Drug Discovery* (2009) 8(3):226–34. doi: 10.1038/nrd2804
28. Jefferis R. Glycosylation of Natural and Recombinant Antibody Molecules. *Adv Exp Med Biol* (2005) 564:143–8. doi: 10.1007/0-387-25515-X_26
29. Pucić M, Knezević A, Vidic J, Adamczyk B, Novokmet M, Polasek O, et al. High Throughput Isolation and Glycosylation Analysis of IgG-Variability and Heritability of the IgG Glycome in Three Isolated Human Populations. *Mol Cell Proteomics* (2011) 10(10):M111.010090. doi: 10.1074/mcp.M111.010090
30. Boune S, Hu P, Epstein AL, Khawli LA. Principles of N-Linked Glycosylation Variations of IgG-Based Therapeutics: Pharmacokinetic and Functional Considerations. *Antibodies* (2020) 9(2):22. doi: 10.3390/antib9020022
31. Popp O, Moser S, Zielonka J, Rüger P, Hansen S, Plöttner O. Development of a Pre-Glycoengineered CHO-K1 Host Cell Line for the Expression of Antibodies With Enhanced Fc Mediated Effector Function. *mAbs* (2018) 10(2):290–303. doi: 10.1080/19420862.2017.1405203
32. Sun Y, Li X, Wang T, Li W. Core Fucosylation Regulates the Function of Pre-BCR, BCR and IgG in Humoral Immunity. *Front Immunol* (2022) 13:844427. doi: 10.3389/fimmu.2022.844427
33. Wang Q, Wang T, Zhang R, Yang S, McFarland KS, Chung C-Y, et al. The Interplay of Protein Engineering and Glycoengineering to Fine-Tune Antibody Glycosylation and its Impact on Effector Functions. *Biotechnol Bioeng* (2022) 119(1):102–17. doi: 10.1002/bit.27953
34. Jefferis R. Glycosylation of Recombinant Antibody Therapeutics. *Biotechnol Prog* (2008) 21(1):11–6. doi: 10.1021/bp040016j
35. Zlatina K, Galuska SP. Immunoglobulin Glycosylation – An Unexploited Potential for Immunomodulatory Strategies in Farm Animals. *Front Immunol* (2021) 12:753294. doi: 10.3389/fimmu.2021.753294
36. Becker DJ, Lowe JB. Fucose: Biosynthesis and Biological Function in Mammals. *Glycobiology* (2003) 13(7):41R–53R. doi: 10.1093/glycob/cwg054
37. Shields RL, Lai J, Keck R, O'Connell LY, Hong K, Meng YG, et al. Lack of Fucose on Human IgG1 N-Linked Oligosaccharide Improves Binding to Human Fcγriii and Antibody-Dependent Cellular Toxicity. *J Biol Chem* (2002) 277(30):26733–40. doi: 10.1074/jbc.M202069200
38. Shinkawa T, Nakamura K, Yamane N, Shoji-Hosaka E, Kanda Y, Sakurada M, et al. The Absence of Fucose But Not the Presence of Galactose or Bisecting N-Acetylglucosamine of Human IgG1 Complex-Type Oligosaccharides Shows the Critical Role of Enhancing Antibody-Dependent Cellular Cytotoxicity*. *J Biol Chem* (2003) 278(5):3466–73. doi: 10.1074/jbc.M210665200
39. Umaña P, Jean-Mairet J, Moudry R, Amstutz H, Bailey JE. Engineered Glycoforms of an Antineuroblastoma IgG1 With Optimized Antibody-Dependent Cellular Cytotoxic Activity. *Nat Biotechnol* (1999) 17(2):176 –80. doi: 10.1038/6179
40. Pereira NA, Chan KF, Lin PC, Song Z. The « Less-is-More » in Therapeutic Antibodies: Afucosylated Anti-Cancer Antibodies With Enhanced Antibody-Dependent Cellular Cytotoxicity. *mAbs* (2018) 10(5):693–711. doi: 10.1080/19420862.2018.1466767
41. Yang G, Wang Q, Chen L, Betenbaugh MJ, Zhang H. Glycoproteomic Characterization of FUT8 Knock-Out CHO Cells Reveals Roles of FUT8 in the Glycosylation. *Front Chem* (2021) 9:755238. doi: 10.3389/fchem.2021.755238
42. Yuan Y, Zong H, Bai J, Han L, Wang L, Zhang X, et al. Bioprocess Development of a Stable FUT8-/–CHO Cell Line to Produce Defucosylated Anti-HER2 Antibody. *Bioprocess Biosyst Eng* (2019) 42 (8):1263–71. doi: 10.1007/s00449-019-02124-7

43. Ripka J, Adamany A, Stanley P. Two Chinese Hamster Ovary Glycosylation Mutants Affected in the Conversion of GDP-Mannose to GDP-Fucose. *Arch Biochem Biophys* (1986) 249(2):533–45. doi: 10.1016/0003-9861(86)90031-7
44. Liu W, Padmashali R, Monzon OQ, Lundberg D, Jin S, Dwyer B, et al. Generation of FX-/- and Gmds-/- CHOZN Host Cell Lines for the Production of Afucosylated Therapeutic Antibodies. *Biotechnol Prog* (2021) 37(1):e3061. doi: 10.1002/btpr.3061
45. Misaki R, Iwasaki M, Takechi H, Yamano-Adachi N, Ohashi T, Kajiura H, et al. Establishment of Serum-Free Adapted Chinese Hamster Ovary Cells With Double Knockout of GDP-Mannose-4,6-Dehydratase and GDP-Fucose Transporter. *Cytotechnology* (2022) 74(1):163–79. doi: 10.1007/s10616-021-00501-3
46. Davies J, Jiang L, Pan LZ, LaBarre MJ, Anderson D, Reff M. Expression of GnTIII in a Recombinant Anti-CD20 CHO Production Cell Line: Expression of Antibodies With Altered Glycoforms Leads to an Increase in ADCC Through Higher Affinity for FC Gamma RIII. *Biotechnol Bioeng* (2001) 74(4):288–94. doi: 10.1002/bit.1119
47. Ferrara C, Brünker P, Suter T, Moser S, Püntener U, Umaña P. Modulation of Therapeutic Antibody Effector Functions by Glycosylation Engineering: Influence of Golgi Enzyme Localization Domain and Co-Expression of Heterologous Beta1, 4-N-Acetylglucosaminyltransferase III and Golgi Alpha-Mannosidase II. *Biotechnol Bioeng* (2006) 93(5):851–61. doi: 10.1002/bit.20777
48. Beck A, Reichert JM. Marketing Approval of Mogamulizumab. *mAbs* (2012) 4(4):419–25. doi: 10.4161/mabs.20996
49. Okeley NM, Alley SC, Anderson ME, Boursalian TE, Burke PJ, Emmerton KM, et al. Development of Orally Active Inhibitors of Protein and Cellular Fucosylation. *Proc Natl Acad Sci U S A* (2013) 110(14):5404–9. doi: 10.1073/pnas.1222263110
50. Joubert S, Guimond J, Perret S, Malenfant F, Elahi SM, Marcil A, et al. Production of Afucosylated Antibodies in CHO Cells by Coexpression of an Anti-FUT8 Intrabody. *Biotechnol Bioeng* (2022). doi: 10.1002/bit.28127
51. Li C, Li T, Wang L-X. Chemoenzymatic Defucosylation of Therapeutic Antibodies for Enhanced Effector Functions Using Bacterial α-Fucosidases. *Methods Mol Biol* (2018) 1827:367–80. doi: 10.1007/978-1-4939-8648-4_19
52. Giddens JP, Wang L-X. Chemoenzymatic Glyco-Engineering of Monoclonal Antibodies. *Methods Mol Biol* (2015) 1321:375–87. doi: 10.1007/978-1-4939-2760-9_25
53. Wang TT, Ravetch JV. Functional Diversification of IgGs Through Fc Glycosylation. *J Clin Invest* (2019) 129(9):3492–8. doi: 10.1172/JCI130029
54. Subedi GP, Barb AW. The Immunoglobulin G1 N-Glycan Composition Affects Binding to Each Low Affinity Fc γ Receptor. *mAbs* (2016) 8(8):1512–24. doi: 10.1080/19420862.2016.1218586
55. Golay J, Da Roit F, Bologna L, Ferrara C, Leusen JH, Rambaldi A, et al. Glycoengineered CD20 Antibody Obinutuzumab Activates Neutrophils and Mediates Phagocytosis Through CD16B More Efficiently Than Rituximab. *Blood* (2013) 122(20):3482–91. doi: 10.1182/blood-2013-05-504043
56. Ferrara C, Stuart F, Sondermann P, Brünker P, Umaña P. The Carbohydrate at FcgammaRIIIa Asn-162. An Element Required for High Affinity Binding to non-Fucosylated IgG Glycoforms. *J Biol Chem* (2006) 281(8):5032–6. doi: 10.1074/jbc.M510171200
57. Ferrara C, Grau S, Jäger C, Sondermann P, Brünker P, Waldhauer I, et al. Unique Carbohydrate-Carbohydrate Interactions are Required for High Affinity Binding Between FcgammaRIII and Antibodies Lacking Core Fucose. *Proc Natl Acad Sci U S A* (2011) 108(31):12669–74. doi: 10.1073/pnas.1108455108
58. Hoeres T, Pretscher D, Holzmann E, Smetak M, Birkmann J, Triebel J, et al. Improving Immunotherapy Against B-Cell Malignancies Using γδ T-Cell-Specific Stimulation and Therapeutic Monoclonal Antibodies. *J Immunother* (2019) 42(9):331–44. doi: 10.1097/CJI.0000000000000289
59. Chu Y, Awasthi A, Lee S, Edani D, Yin C, Hochberg J, et al. Obinutuzumab (GA101) vs. Rituximab Significantly Enhances Cell Death, Antibody-Dependent Cytotoxicity and Improves Overall Survival Against CD20+ Primary Mediastinal B-Cell Lymphoma (PMBL) in a Xenograft NOD-Scid IL2Rgnull (NSG) Mouse Model: A Potential Targeted Agent in the Treatment of PMBL. *Oncotarget* (2020) 11(32):3035–47. doi: 10.18632/oncotarget.27691
60. Decaup E, Rossi C, Gravelle P, Laurent C, Bordenave J, Tosolini M, et al. A Tridimensional Model for NK Cell-Mediated ADCC of Follicular Lymphoma. *Front Immunol* (2019) 10:1943. doi: 10.3389/fimmu.2019.01943
61. Herter S, Birk MC, Klein C, Gerdes C, Umana P, Bacac M. Glycoengineering of Therapeutic Antibodies Enhances Monocyte/Macrophage-Mediated Phagocytosis and Cytotoxicity. *J Immunol* (2014) 192(5):2252–60. doi: 10.4049/jimmunol.1301249
62. Mössner E, Brünker P, Moser S, Püntener U, Schmidt C, Herter S, et al. Increasing the Efficacy of CD20 Antibody Therapy Through the Engineering of a New Type II Anti-CD20 Antibody With Enhanced Direct and Immune Effector Cell-Mediated B-Cell Cytotoxicity. *Blood* (2010) 115(22):4393–402. doi: 10.1182/blood-2009-06-225979
63. Herter S, Herting F, Muth G, van Puijenbroek E, Schlothauer T, Ferrara C, et al. GA101 P329GLALA, a Variant of Obinutuzumab With Abolished ADCC, ADCP and CDC Function But Retained Cell Death Induction, is as Efficient as Rituximab in B-Cell Depletion and Antitumor Activity. *Haematologica* (2018) 103(2):e78–81. doi: 10.3324/haematol.2017.178996
64. Goede V, Fischer K, Busch R, Engelke A, Eichhorst B, Wendtner CM, et al. Obinutuzumab Plus Chlorambucil in Patients With CLL and Coexisting Conditions. *N Engl J Med* (2014) 370(12):1101–10. doi: 10.1056/NEJMoa1313984
65. Stilgenbauer S, Bosch F, Ilhan O, Kisro J, Mahé B, Mikuskova E, et al. Safety and Efficacy of Obinutuzumab Alone or With Chemotherapy in Previously Untreated or Relapsed/Refractory Chronic Lymphocytic Leukaemia Patients: Final Analysis of the Phase IIIb GREEN Study. *Br J Haematol* (2021) 193(2):325–38. doi: 10.1111/bjh.17326
66. Hiddemann W, Barbui AM, Canales MA, Cannell PK, Collins GP, Dürig J, et al. Immunochemotherapy With Obinutuzumab or Rituximab for Previously Untreated Follicular Lymphoma in the GALLIUM Study: Influence of Chemotherapy on Efficacy and Safety. *J Clin Oncol* (2018) 36(23):2395–404. doi: 10.1200/JCO.2017.76.8960
67. Ishii T, Ishida T, Utsunomiya A, Inagaki A, Yano H, Komatsu H, et al. Defucosylated Humanized Anti-CCR4 Monoclonal Antibody KW-0761 as a Novel Immunotherapeutic Agent for Adult T-Cell Leukemia/Lymphoma. *Clin Cancer Res* (2010) 16(5):1520–31. doi: 10.1158/1078-0432.CCR-09-2697
68. Niwa R, Sakurada M, Kobayashi Y, Uehara A, Matsushima K, Ueda R, et al. Enhanced Natural Killer Cell Binding and Activation by Low-Fucose IgG1 Antibody Results in Potent Antibody-Dependent Cellular Cytotoxicity Induction at Lower Antigen Density. *Clin Cancer Res* (2005) 11(6):2327–36. doi: 10.1158/1078-0432.CCR-04-2263
69. Gallagher S, Turman S, Yusuf I, Akhgar A, Wu Y, Roskos LK, et al. Pharmacological Profile of MEDI-551, a Novel Anti-CD19 Antibody, in Human CD19 Transgenic Mice. *Int Immunopharmacol* (2016) 36:205–12. doi: 10.1016/j.intimp.2016.04.035
70. Frampton JE. Inebilizumab: First Approval. *Drugs* (2020) 80(12):1259–64. doi: 10.1007/s40265-020-01370-4
71. Herbst R, Wang Y, Gallagher S, Mittereder N, Kuta E, Damschroder M, et al. B-Cell Depletion *In Vitro* and *In Vivo* With an Afucosylated Anti-CD19 Antibody. *J Pharmacol Exp Ther* (2010) 335(1):213–22. doi: 10.1124/jpet.110.168062
72. Rensel M, Zabeti A, Mealy MA, Cimbora D, She D, Drappa J, et al. Long-Term Efficacy and Safety of Inebilizumab in Neuromyelitis Optica Spectrum Disorder: Analysis of Aquaporin-4-Immunoglobulin G-Seropositive Participants Taking Inebilizumab for ≧4 Years in the N-MOmentum Trial. *Mult Scler* (2022) 28(6):925–32. doi: 10.1177/13524585211047223
73. FitzGerald JM, Bleecker ER, Nair P, Korn S, Ohta K, Lommatzsch M, et al. Benralizumab, an Anti-Interleukin-5 Receptor α Monoclonal Antibody, as Add-on Treatment for Patients With Severe, Uncontrolled, Eosinophilic Asthma (CALIMA): A Randomised, Double-Blind, Placebo-Controlled Phase 3 Trial. *Lancet* (2016) 388(10056):2128–41. doi: 10.1016/S0140-6736(16)31322-8
74. Ghazi A, Trikha A, Calhoun WJ. Benralizumab–a Humanized mAb to IL-5rα With Enhanced Antibody-Dependent Cell-Mediated Cytotoxicity–a Novel Approach for the Treatment of Asthma. *Expert Opin Biol Ther* (2012) 12(1):113–8. doi: 10.1517/14712598.2012.642359
75. Kolbeck R, Kozhich A, Koike M, Peng L, Andersson CK, Damschroder MM, et al. MEDI-563, a Humanized Anti-IL-5 Receptor Alpha mAb With

Enhanced Antibody-Dependent Cell-Mediated Cytotoxicity Function. *J Allergy Clin Immunol* (2010) 125(6):1344–53.e2. doi: 10.1016/j.jaci.2010.04.004

76. Nordstrom JL, Gorlatov S, Zhang W, Yang Y, Huang L, Burke S, et al. Anti-Tumor Activity and Toxicokinetics Analysis of MGAH22, an Anti-HER2 Monoclonal Antibody With Enhanced Fcγ Receptor Binding Properties. *Breast Cancer Res* (2011) 13(6):R123. doi: 10.1186/bcr3069
77. Rugo HS, Im S-A, Cardoso F, Cortés J, Curigliano G, Musolino A, et al. Efficacy of Margetuximab vs Trastuzumab in Patients With Pretreated ERBB2-Positive Advanced Breast Cancer: A Phase 3 Randomized Clinical Trial. *JAMA Oncol* (2021) 7(4):573–84. doi: 10.1001/jamaoncol.2020.7932
78. Tai Y-T, Mayes PA, Acharya C, Zhong MY, Cea M, Cagnetta A, et al. Novel Anti–B-Cell Maturation Antigen Antibody-Drug Conjugate (GSK2857916) Selectively Induces Killing of Multiple Myeloma. *Blood* (2014) 123(20):3128–38. doi: 10.1182/blood-2013-10-535088
79. Grugan KD, Dorn K, Jarantow SW, Bushey BS, Pardinas JR, Laquerre S, et al. Fc-Mediated Activity of EGFR X C-Met Bispecific Antibody JNJ-61186372 Enhanced Killing of Lung Cancer Cells. *mAbs* (2017) 9(1):114–26. doi: 10.1080/19420862.2016.1249079
80. Church AK, VanDerMeid KR, Baig NA, Baran AM, Witzig TE, Nowakowski GS, et al. Anti-CD20 Monoclonal Antibody-Dependent Phagocytosis of Chronic Lymphocytic Leukaemia Cells by Autologous Macrophages. *Clin Exp Immunol* (2015) 183(1):90–101. doi: 10.1111/cei.12697
81. de Romeuf C, Dutertre C-A, Le Garff-Tavernier M, Fournier N, Gaucher C, Glacet A, et al. Chronic Lymphocytic Leukaemia Cells are Efficiently Killed by an Anti-CD20 Monoclonal Antibody Selected for Improved Engagement of FcgammaRIIIA/Cd16. *Br J Haematol* (2008) 140(6):635–43. doi: 10.1111/j.1365-2141.2007.06974.x
82. Klein C, Jamois C, Nielsen T. Anti-CD20 Treatment for B-Cell Malignancies: Current Status and Future Directions. *Expert Opin Biol Ther* (2021) 21(2):161–81. doi: 10.1080/14712598.2020.1822318
83. Klinghammer K, Fayette J, Kawecki A, Dietz A, Schafhausen P, Folprecht G, et al. A Randomized Phase II Study Comparing the Efficacy and Safety of the Glyco-Optimized Anti-EGFR Antibody Tomuzotuximab Against Cetuximab in Patients With Recurrent and/or Metastatic Squamous Cell Cancer of the Head and Neck - the RESGEX Study. *ESMO Open* (2021) 6(5):100242. doi: 10.1016/j.esmoop.2021.100242
84. Gerdes CA, Nicolini VG, Herter S, van Puijenbroek E, Lang S, Roemmele M, et al. GA201 (RG7160): A Novel, Humanized, Glycoengineered Anti-EGFR Antibody With Enhanced ADCC and Superior *In Vivo* Efficacy Compared With Cetuximab. *Clin Cancer Res* (2013) 19(5):1126–38. doi: 10.1158/1078-0432.CCR-12-0989
85. Paz-Ares LG, Gomez-Roca C, Delord J-P, Cervantes A, Markman B, Corral J, et al. Phase I Pharmacokinetic and Pharmacodynamic Dose-Escalation Study of RG7160 (GA201), the First Glycoengineered Monoclonal Antibody Against the Epidermal Growth Factor Receptor, in Patients With Advanced Solid Tumors. *J Clin Oncol* (2011) 29(28):3783–90. doi: 10.1200/JCO.2011.34.8888
86. Delord J-P, Tabernero J, García-Carbonero R, Cervantes A, Gomez-Roca C, Bergé Y, et al. Open-Label, Multicentre Expansion Cohort to Evaluate Imgatuzumab in Pre-Treated Patients With KRAS-Mutant Advanced Colorectal Carcinoma. *Eur J Cancer* (2014) 50(3):496–505. doi: 10.1016/j.ejca.2013.10.015
87. Oppenheim DE, Spreafico R, Etuk A, Malone D, Amofah E, Peña-Murillo C, et al. Glyco-Engineered Anti-EGFR mAb Elicits ADCC by NK Cells From Colorectal Cancer Patients Irrespective of Chemotherapy. *Br J Cancer* (2014) 110(5):1221–7. doi: 10.1038/bjc.2014.35
88. Gonzalez-Nicolini V, Herter S, Lang S, Waldhauer I, Bacac M, Roemmele M, et al. Premedication and Chemotherapy Agents do Not Impair Imgatuzumab (GA201)-Mediated Antibody-Dependent Cellular Cytotoxicity and Combination Therapies Enhance Efficacy. *Clin Cancer Res* (2016) 22(10):2453–61. doi: 10.1158/1078-0432.CCR-14-2579
89. Temam S, Spicer J, Farzaneh F, Soria JC, Oppenheim D, McGurk M, et al. An Exploratory, Open-Label, Randomized, Multicenter Study to Investigate the Pharmacodynamics of a Glycoengineered Antibody (Imgatuzumab) and Cetuximab in Patients With Operable Head and Neck Squamous Cell Carcinoma. *Ann Oncol* (2017) 28(11):2827–35. doi: 10.1093/annonc/mdx489
90. Furihata K, Ishiguro Y, Yoshimura N, Ito H, Katsushima S, Kaneko E, et al. A Phase 1 Study of KHK4083: A Single-Blind, Randomized, Placebo-Controlled Single-Ascending-Dose Study in Healthy Adults and an Open-Label Multiple-Dose Study in Patients With Ulcerative Colitis. *Clin Pharmacol Drug Dev* (2021) 10(8):870–83. doi: 10.1002/cpdd.918
91. Fiedler W, Stoeger H, Perotti A, Gastl G, Weidmann J, Dietrich B, et al. Phase I Study of TrasGEX, a Glyco-Optimised Anti-HER2 Monoclonal Antibody, in Patients With HER2-Positive Solid Tumours. *ESMO Open* (2018) 3(4):e000381. doi: 10.1136/esmoopen-2018-000381
92. Junttila TT, Parsons K, Olsson C, Lu Y, Xin Y, Theriault J, et al. Superior *In Vivo* Efficacy of Afucosylated Trastuzumab in the Treatment of HER2-Amplified Breast Cancer. *Cancer Res* (2010) 70(11):4481–9. doi: 10.1158/0008-5472.CAN-09-3704
93. Suzuki E, Niwa R, Saji S, Muta M, Hirose M, Iida S, et al. A Nonfucosylated Anti-HER2 Antibody Augments Antibody-Dependent Cellular Cytotoxicity in Breast Cancer Patients. *Clin Cancer Res* (2007) 13(6):1875–82. doi: 10.1158/1078-0432.CCR-06-1335
94. Nakajima T, Okayama H, Ashizawa M, Noda M, Aoto K, Saito M, et al. Augmentation of Antibody-Dependent Cellular Cytotoxicity With Defucosylated Monoclonal Antibodies in Patients With GI-Tract Cancer. *Oncol Lett* (2018) 15(2):2604–10. doi: 10.3892/ol.2017.7556
95. De Meulenaere A, Vermassen T, Creytens D, De Keukeleire S, Delahaye T, Deron P, et al. An Open-Label, Nonrandomized, Phase Ib Feasibility Study of Cusatuzumab in Patients With Nasopharyngeal Carcinoma. *Clin Transl Sci* (2021) 14(6):2300–13. doi: 10.1111/cts.13089
96. Leupin N, Zinzani PL, Morschhauser F, Dalle S, Maerevoet M, Michot J-M, et al. Cusatuzumab for Treatment of CD70-Positive Relapsed or Refractory Cutaneous T-Cell Lymphoma. *Cancer* (2022) 128(5):1004–14. doi: 10.1002/cncr.34005
97. Xiang H, Chan AG, Ahene A, Bellovin DI, Deng R, Hsu AW, et al. Preclinical Characterization of Bemarituzumab, an Anti-FGFR2b Antibody for the Treatment of Cancer. *mAbs* (2021) 13(1):1981202. doi: 10.1080/19420862.2021.1981202
98. Catenacci DVT, Rasco D, Lee J, Rha SY, Lee K-W, Bang YJ, et al. Phase I Escalation and Expansion Study of Bemarituzumab (FPA144) in Patients With Advanced Solid Tumors and FGFR2b-Selected Gastroesophageal Adenocarcinoma. *J Clin Oncol* (2020) 38(21):2418–26. doi: 10.1200/JCO.19.01834
99. Iida S, Kuni-Kamochi R, Mori K, Misaka H, Inoue M, Okazaki A, et al. Two Mechanisms of the Enhanced Antibody-Dependent Cellular Cytotoxicity (ADCC) Efficacy of non-Fucosylated Therapeutic Antibodies in Human Blood. *BMC Cancer* (2009) 9:58. doi: 10.1186/1471-2407-9-58
100. Karampatzakis A, Brož P, Rey C, Önfelt B, Cruz De Matos GDS, Rycroft D, et al. Antibody Afucosylation Augments CD16-Mediated Serial Killing and Ifnγ Secretion by Human Natural Killer Cells. *Front Immunol* (2021) 12:641521. doi: 10.3389/fimmu.2021.641521
101. Leidi M, Gotti E, Bologna L, Miranda E, Rimoldi M, Sica A, et al. M2 Macrophages Phagocytose Rituximab-Opsonized Leukemic Targets More Efficiently Than M1 Cells *In Vitro*. *J Immunol* (2009) 182(7):4415–22. doi: 10.4049/jimmunol.0713732
102. Bologna L, Gotti E, Manganini M, Rambaldi A, Intermesoli T, Introna M, et al. Mechanism of Action of Type II, Glycoengineered, Anti-CD20 Monoclonal Antibody GA101 in B-Chronic Lymphocytic Leukemia Whole Blood Assays in Comparison With Rituximab and Alemtuzumab. *J Immunol* (2011) 186(6):3762–9. doi: 10.4049/jimmunol.1000303
103. Grandjean CL, Montalvao F, Celli S, Michonneau D, Breart B, Garcia Z, et al. Intravital Imaging Reveals Improved Kupffer Cell-Mediated Phagocytosis as a Mode of Action of Glycoengineered Anti-CD20 Antibodies. *Sci Rep* (2016) 6(1):34382. doi: 10.1038/srep34382
104. Kapur R, Kustiawan I, Vestrheim A, Koeleman CAM, Visser R, Einarsdottir HK, et al. A Prominent Lack of IgG1-Fc Fucosylation of Platelet Alloantibodies in Pregnancy. *Blood* (2014) 123(4):471–80. doi: 10.1182/blood-2013-09-527978
105. Oberg HH, Kellner C, Gonnermann D, Sebens S, Bauerschlag D, Gramatzki M, et al. Tribody [(HER2)2xCD16] Is More Effective Than Trastuzumab in Enhancing γδ T Cell and Natural Killer Cell Cytotoxicity Against HER2-Expressing Cancer Cells. *Front Immunol* (2018) 9:814. doi: 10.3389/fimmu.2018.00814

106. Gertner-Dardenne J, Bonnafous C, Bezombes C, Capietto A-H, Scaglione V, Ingoure S, et al. Bromohydrin Pyrophosphate Enhances Antibody-Dependent Cell-Mediated Cytotoxicity Induced by Therapeutic Antibodies. *Blood* (2009) 113(20):4875–84. doi: 10.1182/blood-2008-08-172296
107. Braza MS, Klein B, Fiol G, Rossi J-F. γδ T-Cell Killing of Primary Follicular Lymphoma Cells is Dramatically Potentiated by GA101, a Type II Glycoengineered Anti-CD20 Monoclonal Antibody. *Haematologica* (2011) 96(3):400–7. doi: 10.3324/haematol.2010.029520
108. Shiromizu CM, Jancic CC. γδ T Lymphocytes: An Effector Cell in Autoimmunity and Infection. *Front Immunol* (2018) 9:2389. doi: 10.3389/fimmu.2018.02389
109. Shibata-Koyama M, Iida S, Misaka H, Mori K, Yano K, Shitara K, et al. Nonfucosylated Rituximab Potentiates Human Neutrophil Phagocytosis Through its High Binding for FcgammaRIIIb and MHC Class II Expression on the Phagocytotic Neutrophils. *Exp Hematol* (2009) 37 (3):309–21. doi: 10.1016/j.exphem.2008.11.006
110. Valgardsdottir R, Cattaneo I, Klein C, Introna M, Figliuzzi M, Golay J. Human Neutrophils Mediate Trogocytosis Rather Than Phagocytosis of CLL B Cells Opsonized With Anti-CD20 Antibodies. *Blood* (2017) 129(19):2636–44. doi: 10.1182/blood-2016-08-735605
111. Peipp M, Lammerts van Bueren JJ, Schneider-Merck T, Bleeker WWK, Dechant M, Beyer T, et al. Antibody Fucosylation Differentially Impacts Cytotoxicity Mediated by NK and PMN Effector Cells. *Blood* (2008) 112 (6):2390–9. doi: 10.1182/blood-2008-03-144600
112. Treffers LW, van Houdt M, Bruggeman CW, Heineke MH, Zhao XW, van der Heijden J, et al. Fcγriiib Restricts Antibody-Dependent Destruction of Cancer Cells by Human Neutrophils. *Front Immunol* (2018) 9:3124. doi: 10.3389/fimmu.2018.03124
113. Kircheis R, Halanek N, Koller I, Jost W, Schuster M, Gorr G, et al. Correlation of ADCC Activity With Cytokine Release Induced by the Stably Expressed, Glyco-Engineered Humanized Lewis Y-Specific Monoclonal Antibody MB314. *mAbs* (2012) 4(4):532–41. doi: 10.4161/mabs.20577
114. Capuano C, Pighi C, Molfetta R, Paolini R, Battella S, Palmieri G, et al. Obinutuzumab-Mediated High-Affinity Ligation of Fcγriiia/CD16 Primes NK Cells for Ifnγ Production. *Oncoimmunology* (2017) 6(3):e1290037. doi: 10.1080/2162402X.2017.1290037
115. Romeo V, Gierke S, Edgar KA, Liu SD. Effects of PI3K Inhibition on Afucosylated Antibody-Driven Fcγriiia Events and Phospho-S6 Activity in NK Cells. *J Immunol* (2019) 203(1):137–47. doi: 10.4049/jimmunol.1801418
116. Sehn LH, Martelli M, Trněný M, Liu W, Bolen CR, Knapp A, et al. A Randomized, Open-Label, Phase III Study of Obinutuzumab or Rituximab Plus CHOP in Patients With Previously Untreated Diffuse Large B-Cell Lymphoma: Final Analysis of GOYA. *J Hematol Oncol* (2020) 13(1):71. doi: 10.1186/s13045-020-00900-7
117. Marcus R, Davies A, Ando K, Klapper W, Opat S, Owen C, et al. Obinutuzumab for the First-Line Treatment of Follicular Lymphoma. *N Engl J Med* (2017) 377(14):1331–44. doi: 10.1056/NEJMoa1614598
118. Crowley AR, Ackerman ME. Mind the Gap: How Interspecies Variability in IgG and Its Receptors May Complicate Comparisons of Human and Non-Human Primate Effector Function. *Front Immunol* (2019) 10:697. doi: 10.3389/fimmu.2019.00697
119. Nimmerjahn F, Ravetch JV. Fcgamma Receptors: Old Friends and New Family Members. *Immunity* (2006) 24(1):19–28. doi: 10.1016/j.immuni.2005.11.010
120. Wang Y, Krémer V, Iannascoli B, Goff OR-L, Mancardi DA, Ramke L, et al. Specificity of Mouse and Human Fcgamma Receptors and Their Polymorphic Variants for IgG Subclasses of Different Species. *Eur J Immunol* (2022) 52(5):753–9. doi: 10.1002/eji.202149766
121. Dekkers G, Bentlage AEH, Plomp R, Visser R, Koeleman CAM, Beentjes A, et al. Conserved Fcγr- Glycan Discriminates Between Fucosylated and Afucosylated IgG in Humans and Mice. *Mol Immunol* (2018) 94:54–60. doi: 10.1016/j.molimm.2017.12.006
122. Braster R, Bögels M, Benonisson H, Wuhrer M, Plomp R, Bentlage AEH, et al. Afucosylated IgG Targets Fcγriv for Enhanced Tumor Therapy in Mice. *Cancers* (2021) 13(10):2372. doi: 10.3390/cancers13102372
123. Crowley AR, Osei-Owusu NY, Dekkers G, Gao W, Wuhrer M, Magnani DM, et al. Biophysical Evaluation of Rhesus Macaque Fc Gamma Receptors Reveals Similar IgG Fc Glycoform Preferences to Human Receptors. *Front Immunol* (2021) 12:754710. doi: 10.3389/fimmu.2021.754710
124. Kaur H. Characterization of Glycosylation in Monoclonal Antibodies and its Importance in Therapeutic Antibody Development. *Crit Rev Biotechnol* (2021) 41(2):300–15. doi: 10.1080/07388551.2020.1869684
125. Tobinai K, Klein C, Oya N, Fingerle-Rowson G. A Review of Obinutuzumab (GA101), a Novel Type II Anti-CD20 Monoclonal Antibody, for the Treatment of Patients With B-Cell Malignancies. *Adv Ther* (2017) 34 (2):324–56. doi: 10.1007/s12325-016-0451-1
126. Alduaij W, Ivanov A, Honeychurch J, Cheadle EJ, Potluri S, Lim SH, et al. Novel Type II Anti-CD20 Monoclonal Antibody (GA101) Evokes Homotypic Adhesion and Actin-Dependent, Lysosome-Mediated Cell Death in B-Cell Malignancies. *Blood* (2011) 117(17):4519–29. doi: 10.1182/blood-2010-07-296913
127. Cartron G, Dacheux L, Salles G, Solal-Celigny P, Bardos P, Colombat P, et al. Therapeutic Activity of Humanized Anti-CD20 Monoclonal Antibody and Polymorphism in IgG Fc Receptor FcgammaRIIIa Gene. *Blood* (2002) 99 (3):754–8. doi: 10.1182/blood.v99.3.754
128. Musolino A, Naldi N, Bortesi B, Pezzuolo D, Capelletti M, Missale G, et al. Immunoglobulin G Fragment C Receptor Polymorphisms and Clinical Efficacy of Trastuzumab-Based Therapy in Patients With HER-2/Neu-Positive Metastatic Breast Cancer. *J Clin Oncol* (2008) 26(11):1789–96. doi: 10.1200/JCO.2007.14.8957
129. Roca L, Diéras V, Roché H, Lappartient E, Kerbrat P, Cany L, et al. Correlation of HER2, FCGR2A, and FCGR3A Gene Polymorphisms With Trastuzumab Related Cardiac Toxicity and Efficacy in a Subgroup of Patients From UNICANCER-PACS 04 Trial. *Breast Cancer Res Treat* (2013) 139 (3):789–800. doi: 10.1007/s10549-013-2587-x
130. de Haan N, Reiding KR, Driessen G, van der Burg M, Wuhrer M. Changes in Healthy Human IgG Fc-Glycosylation After Birth and During Early Childhood. *J Proteome Res* (2016) 15(6):1853–61. doi: 10.1021/acs.jproteome.6b00038
131. Pucic M, Muzinic A, Novokmet M, Skledar M, Pivac N, Lauc G, et al. Changes in Plasma and IgG N-Glycome During Childhood and Adolescence. *Glycobiology* (2012) 22(7):975–82. doi: 10.1093/glycob/cws062
132. Fettke F, Schumacher A, Canellada A, Toledo N, Bekeredjian-Ding I, Bondt A, et al. Maternal and Fetal Mechanisms of B Cell Regulation During Pregnancy: Human Chorionic Gonadotropin Stimulates B Cells to Produce IL-10 While Alpha-Fetoprotein Drives Them Into Apoptosis. *Front Immunol* (2016) 7:495. doi: 10.3389/fimmu.2016.00495
133. Wojcik I, Schmidt DE, de Neef LA, Rab MAE, Meek B, de Weerdt O, et al. A Functional Spleen Contributes to Afucosylated IgG in Humans. *Sci Rep* (2021) 11(1):24045. doi: 10.1038/s41598-021-03196-w
134. Huffman JE, Knezevic A, Vitart V, Kattla J, Adamczyk B, Novokmet M, et al. Polymorphisms in B3GAT1, SLC9A9 and MGAT5 are Associated With Variation Within the Human Plasma N-Glycome of 3533 European Adults. *Hum Mol Genet* (2011) 20(24):5000–11. doi: 10.1093/hmg/ddr414
135. Klarić L, Tsepilov YA, Stanton CM, Mangino M, Sikka TT, Esko T, et al. Glycosylation of Immunoglobulin G is Regulated by a Large Network of Genes Pleiotropic With Inflammatory Diseases. *Sci Adv* (2020) 6(8):eaax0301. doi: 10.1126/sciadv.aax0301
136. Landini A, Trbojević-Akmačić I, Navarro P, Tsepilov YA, Sharapov SZ, Vučković F, et al. Genetic Regulation of Post-Translational Modification of Two Distinct Proteins. *Nat Commun* (2022) 13(1):1586. doi: 10.1038/s41467-022-29189-5
137. Lauc G, Huffman JE, Pučić M, Zgaga L, Adamczyk B, Mužinić A, et al. Loci Associated With N-Glycosylation of Human Immunoglobulin G Show Pleiotropy With Autoimmune Diseases and Haematological Cancers. *PLoS Genet* (2013) 9(1):e1003225. doi: 10.1371/journal.pgen.1003225
138. Sharapov SZ, Tsepilov YA, Klaric L, Mangino M, Thareja G, Shadrina AS, et al. Defining the Genetic Control of Human Blood Plasma N-Glycome Using Genome-Wide Association Study. *Hum Mol Genet* (2019) 28(12):2062–77. doi: 10.1093/hmg/ddz054
139. Shen X, Klarić L, Sharapov S, Mangino M, Ning Z, Wu D, et al. Multivariate Discovery and Replication of Five Novel Loci Associated With

Immunoglobulin G N-Glycosylation. *Nat Commun* (2017) 8(1):447. doi: 10.1038/s41467-017-00453-3
140. Wahl A, van den Akker E, Klaric L, Štambuk J, Benedetti E, Plomp R, et al. Genome-Wide Association Study on Immunoglobulin G Glycosylation Patterns. *Front Immunol* (2018) 9:277. doi: 10.3389/fimmu.2018.00277
141. Matsumoto K, Shimizu C, Arao T, Andoh M, Katsumata N, Kohno T, et al. Identification of Predictive Biomarkers for Response to Trastuzumab Using Plasma FUCA Activity and N-Glycan Identified by MALDI-TOF-Ms. *J Proteome Res* (2009) 8(2):457–62. doi: 10.1021/pr800655p
142. Ackerman ME, Crispin M, Yu X, Baruah K, Boesch AW, Harvey DJ, et al. Natural Variation in Fc Glycosylation of HIV-Specific Antibodies Impacts Antiviral Activity. *J Clin Invest* (2013) 123(5):2183–92. doi: 10.1172/JCI65708
143. Viinikangas T, Khosrowabadi E, Kellokumpu S. N-Glycan Biosynthesis: Basic Principles and Factors Affecting Its Outcome. *Exp Suppl 2012* (2021) 112:237–57. doi: 10.1007/978-3-030-76912-3_7
144. Wong MY, Chen K, Antonopoulos A, Kasper BT, Dewal MB, Taylor RJ, et al. XBP1s Activation can Globally Remodel N-Glycan Structure Distribution Patterns. *Proc Natl Acad Sci U S A* (2018) 115(43):E10089–98. doi: 10.1073/pnas.1805425115
145. Hagelkruys A, Wirnsberger G, Stadlmann J, Wöhner M, Horrer M, Vilagos B, et al. A Crucial Role for Jagunal Homolog 1 in Humoral Immunity and Antibody Glycosylation in Mice and Humans. *J Exp Med* (2021) 218(1): e20200559. doi: 10.1084/jem.20200559
146. Kapur R, Della Valle L, Sonneveld M, Hipgrave Ederveen A, Visser R, Ligthart P, et al. Low Anti-RhD IgG-Fc-Fucosylation in Pregnancy: A New Variable Predicting Severity in Haemolytic Disease of the Fetus and Newborn. *Br J Haematol* (2014) 166(6):936–45. doi: 10.1111/bjh.12965
147. Bruggeman CW, Dekkers G, Bentlage AEH, Treffers LW, Nagelkerke SQ, Lissenberg-Thunnissen S, et al. Enhanced Effector Functions Due to Antibody Defucosylation Depend on the Effector Cell Fcγ Receptor Profile. *J Immunol* (2017) 199(1):204–11. doi: 10.4049/jimmunol.1700116
148. Sibéril S, de Romeuf C, Bihoreau N, Fernandez N, Meterreau J-L, Regenman A, et al. Selection of a Human Anti-RhD Monoclonal Antibody for Therapeutic Use: Impact of IgG Glycosylation on Activating and Inhibitory Fc Gamma R Functions. *Clin Immunol* (2006) 118(2–3):170–9. doi: 10.1016/j.clim.2005.10.008
149. Oepkes D, van Kamp IL, Simon MJ, Mesman J, Overbeeke MA, Kanhai HH. Clinical Value of an Antibody-Dependent Cell-Mediated Cytotoxicity Assay in the Management of Rh D Alloimmunization. *Am J Obstet Gynecol* (2001) 184(5):1015–20. doi: 10.1067/mob.2001.112970
150. Sonneveld ME, Koelewijn J, de Haas M, Admiraal J, Plomp R, Koeleman CAM, et al. Antigen Specificity Determines Anti-Red Blood Cell IgG-Fc Alloantibody Glycosylation and Thereby Severity of Haemolytic Disease of the Fetus and Newborn. *Br J Haematol* (2017) 176(4):651–60. doi: 10.1111/bjh.14438
151. Brojer E, Husebekk A, Dębska M, Uhrynowska M, Guz K, Orzińska A, et al. Fetal/Neonatal Alloimmune Thrombocytopenia: Pathogenesis, Diagnostics and Prevention. *Arch Immunol Ther Exp (Warsz)* (2016) 64(4):279–90. doi: 10.1007/s00005-015-0371-9
152. Wuhrer M, Porcelijn L, Kapur R, Koeleman CAM, Deelder AM, de Haas M, et al. Regulated Glycosylation Patterns of IgG During Alloimmune Responses Against Human Platelet Antigens. *J Proteome Res* (2009) 8 (2):450–6. doi: 10.1021/pr800651j
153. Kjeldsen-Kragh J, Bengtsson J. Fetal and Neonatal Alloimmune Thrombocytopenia-New Prospects for Fetal Risk Assessment of HPA-1a-Negative Pregnant Women. *Transfus Med Rev* (2020) 34(4):270–6. doi: 10.1016/j.tmrv.2020.09.004
154. Sonneveld ME, Natunen S, Sainio S, Koeleman CAM, Holst S, Dekkers G, et al. Glycosylation Pattern of Anti-Platelet IgG is Stable During Pregnancy and Predicts Clinical Outcome in Alloimmune Thrombocytopenia. *Br J Haematol* (2016) 174(2):310–20. doi: 10.1111/bjh.14053
155. Ercan A, Cui J, Chatterton DEW, Deane KD, Hazen MM, Brintnell W, et al. Aberrant IgG Galactosylation Precedes Disease Onset, Correlates With Disease Activity, and is Prevalent in Autoantibodies in Rheumatoid Arthritis. *Arthritis Rheum* (2010) 62(8):2239–48. doi: 10.1002/art.27533
156. Huang C, Liu Y, Wu H, Sun D, Li Y. Characterization of IgG Glycosylation in Rheumatoid Arthritis Patients by MALDI-TOF-MSn and Capillary Electrophoresis. *Anal Bioanal Chem* (2017) 409(15):3731–9. doi: 10.1007/s00216-017-0302-1
157. Flevaris K, Kontoravdi C. Immunoglobulin G N-Glycan Biomarkers for Autoimmune Diseases: Current State and a Glycoinformatics Perspective. *Int J Mol Sci* (2022) 23(9):5180. doi: 10.3390/ijms23095180
158. Martin TC, Šimurina M, Ząbczyńska M, Martinic Kavur M, Rydlewska M, Pezer M, et al. Decreased Immunoglobulin G Core Fucosylation, A Player in Antibody-Dependent Cell-Mediated Cytotoxicity, is Associated With Autoimmune Thyroid Diseases. *Mol Cell Proteomics* (2020) 19(5):774–92. doi: 10.1074/mcp.RA119.001860
159. Wang W, Xu X, Huang C, Gao C. N-Glycan Profiling Alterations of Serum and Immunoglobulin G in Immune Thrombocytopenia. *J Clin Lab Anal* (2022) 36(2):e24201. doi: 10.1002/jcla.24201
160. Plomp R, Ruhaak LR, Uh H-W, Reiding KR, Selman M, Houwing-Duistermaat JJ, et al. Subclass-Specific IgG Glycosylation is Associated With Markers of Inflammation and Metabolic Health. *Sci Rep* (2017) 7 (1):12325. doi: 10.1038/s41598-017-12495-0
161. Alter G, Ottenhoff THM, Joosten SA. Antibody Glycosylation in Inflammation, Disease and Vaccination. *Semin Immunol* (2018) 39:102–10. doi: 10.1016/j.smim.2018.05.003
162. Dekkers G, Rispens T, Vidarsson G. Novel Concepts of Altered Immunoglobulin G Galactosylation in Autoimmune Diseases. *Front Immunol* (2018) 9:553. doi: 10.3389/fimmu.2018.00553
163. Seeling M, Brückner C, Nimmerjahn F. Differential Antibody Glycosylation in Autoimmunity: Sweet Biomarker or Modulator of Disease Activity? *Nat Rev Rheumatol* (2017) 13(10):621–30. doi: 10.1038/nrrheum.2017.146
164. Mimura Y, Mimura-Kimura Y, Saldova R, Rudd PM, Jefferis R. Enhanced Immunomodulatory Effect of Intravenous Immunoglobulin by Fc Galactosylation and Nonfucosylation. *Front Immunol* (2022) 13:818382. doi: 10.3389/fimmu.2022.818382
165. Schwab I, Nimmerjahn F. Intravenous Immunoglobulin Therapy: How Does IgG Modulate the Immune System? *Nat Rev Immunol* (2013) 13(3):176–89. doi: 10.1038/nri3401
166. Keeler SP, Fox JM. Requirement of Fc-Fc Gamma Receptor Interaction for Antibody-Based Protection Against Emerging Virus Infections. *Viruses* (2021) 13(6):1037. doi: 10.3390/v13061037
167. Khandia R, Munjal A, Dhama K, Karthik K, Tiwari R, Malik YS, et al. Modulation of Dengue/Zika Virus Pathogenicity by Antibody-Dependent Enhancement and Strategies to Protect Against Enhancement in Zika Virus Infection. *Front Immunol* (2018) 9:597. doi: 10.3389/fimmu.2018.00597
168. Sicca F, Neppelenbroek S, Huckriede A. Effector Mechanisms of Influenza-Specific Antibodies: Neutralization and Beyond. *Expert Rev Vaccines* (2018) 17(9):785–95. doi: 10.1080/14760584.2018.1516553
169. Bournazos S, Ravetch JV. Anti-Retroviral Antibody Fcγr-Mediated Effector Functions. *Immunol Rev* (2017) 275(1):285–95. doi: 10.1111/imr.12482
170. Bernard NF, Kiani Z, Tremblay-McLean A, Kant SA, Leeks CE, Dupuy FP. Natural Killer (NK) Cell Education Differentially Influences HIV Antibody-Dependent NK Cell Activation and Antibody-Dependent Cellular Cytotoxicity. *Front Immunol* (2017) 8:1033. doi: 10.3389/fimmu.2017.01033
171. Balsitis SJ, Williams KL, Lachica R, Flores D, Kyle JL, Mehlhop E, et al. Lethal Antibody Enhancement of Dengue Disease in Mice is Prevented by Fc Modification. *PLoS Pathog* (2010) 6(2):e1000790. doi: 10.1371/journal.ppat.1000790
172. Bournazos S, Gupta A, Ravetch JV. The Role of IgG Fc Receptors in Antibody-Dependent Enhancement. *Nat Rev Immunol* (2020) 20(10):633–43. doi: 10.1038/s41577-020-00410-0
173. Halstead SB, Mahalingam S, Marovich MA, Ubol S, Mosser DM. Intrinsic Antibody-Dependent Enhancement of Microbial Infection in Macrophages: Disease Regulation by Immune Complexes. *Lancet Infect Dis* (2010) 10 (10):712–22. doi: 10.1016/S1473-3099(10)70166-3
174. Nanaware N, Banerjee A, Mullick Bagchi S, Bagchi P, Mukherjee A. Dengue Virus Infection: A Tale of Viral Exploitations and Host Responses. *Viruses* (2021) 13(10):1967. doi: 10.3390/v13101967
175. Larsen MD, de Graaf EL, Sonneveld ME, Plomp HR, Nouta J, Hoepel W, et al. Afucosylated IgG Characterizes Enveloped Viral Responses and Correlates With COVID-19 Severity. *Science* (2021) 371(6532):eabc8378. doi: 10.1126/science.abc8378

176. Chakraborty S, Gonzalez J, Edwards K, Mallajosyula V, Buzzanco AS, Sherwood R, et al. Proinflammatory IgG Fc Structures in Patients With Severe COVID-19. *Nat Immunol* (2021) 22(1):67–73. doi: 10.1038/s41590-020-00828-7
177. Hoepel W, Chen H-J, Geyer CE, Allahverdiyeva S, Manz XD, de Taeye SW, et al. High Titers and Low Fucosylation of Early Human Anti–SARS-CoV-2 IgG Promote Inflammation by Alveolar Macrophages. *Sci Transl Med* (2021) 13(596):eabf8654. doi: 10.1126/scitranslmed.abf8654
178. Pongracz T, Nouta J, Wang W, van Meijgaarden KE, Linty F, Vidarsson G, et al. Immunoglobulin G1 Fc Glycosylation as an Early Hallmark of Severe COVID-19. *EBioMedicine* (2022) 78:103957. doi: 10.1016/j.ebiom.2022.103957
179. Schwedler C, Grzeski M, Kappert K, Rust J, Heymann G, Hoppe B, et al. Coronavirus Disease 2019-Related Alterations of Total and Anti-Spike IgG Glycosylation in Relation to Age and Anti-Spike IgG Titer. *Front Microbiol* (2022) 13:775186. doi: 10.3389/fmicb.2022.775186
180. Bournazos S, Vo HTM, Duong V, Auerswald H, Ly S, Sakuntabhai A, et al. Antibody Fucosylation Predicts Disease Severity in Secondary Dengue Infection. *Science* (2021) 372(6546):1102–5. doi: 10.1126/science.abc7303
181. Thulin NK, Brewer RC, Sherwood R, Bournazos S, Edwards KG, Ramadoss NS, et al. Maternal Anti-Dengue IgG Fucosylation Predicts Susceptibility to Dengue Disease in Infants. *Cell Rep* (2020) 31(6):107642. doi: 10.1016/j.celrep.2020.107642
182. Wang TT, Sewatanon J, Memoli MJ, Wrammert J, Bournazos S, Bhaumik SK, et al. IgG Antibodies to Dengue Enhanced for Fcγriiia Binding Determine Disease Severity. *Science* (2017) 355(6323):395–8. doi: 10.1126/science.aai8128
183. Larsen MD, Lopez-Perez M, Dickson EK, Ampomah P, Tuikue Ndam N, Nouta J, et al. Afucosylated Plasmodium Falciparum-Specific IgG is Induced by Infection But Not by Subunit Vaccination. *Nat Commun* (2021) 12(1):5838. doi: 10.1038/s41467-021-26118-w
184. Chakraborty S, Gonzalez JC, Sievers BL, Mallajosyula V, Chakraborty S, Dubey M, et al. Early non-Neutralizing, Afucosylated Antibody Responses are Associated With COVID-19 Severity. *Sci Transl Med* (2022) 14(635):eabm7853. doi: 10.1126/scitranslmed.abm7853
185. Adjobimey T, Hoerauf A. Distinct N-Linked Immunoglobulin G Glycosylation Patterns Are Associated With Chronic Pathology and Asymptomatic Infections in Human Lymphatic Filariasis. *Front Immunol* (2022) 13:790895. doi: 10.3389/fimmu.2022.790895
186. Gutiérrez-Huante K, Salinas-Marín R, Mora-Montes HM, Gonzalez RA, Martínez-Duncker I. Human Adenovirus Type 5 Increases Host Cell Fucosylation and Modifies Ley Antigen Expression. *Glycobiology* (2019) 29(6):469–78. doi: 10.1093/glycob/cwz017
187. Sun Y, Zhou J, Jiang Y. Negative Regulation and Protective Function of Natural Killer Cells in HIV Infection: Two Sides of a Coin. *Front Immunol* (2022) 13:842831. doi: 10.3389/fimmu.2022.842831
188. Cao J, Wang L, Yu C, Wang K, Wang W, Yan J, et al. Development of an Antibody-Dependent Cellular Cytotoxicity Reporter Assay for Measuring Anti-Middle East Respiratory Syndrome Antibody Bioactivity. *Sci Rep* (2020) 10(1):16615. doi: 10.1038/s41598-020-73960-x
189. Oswald WB, Geisbert TW, Davis KJ, Geisbert JB, Sullivan NJ, Jahrling PB, et al. Neutralizing Antibody Fails to Impact the Course of Ebola Virus Infection in Monkeys. *PLoS Pathog* (2007) 3(1):e9. doi: 10.1371/journal.ppat.0030009
190. Liu Q, Fan C, Li Q, Zhou S, Huang W, Wang L, et al. Antibody-Dependent-Cellular-Cytotoxicity-Inducing Antibodies Significantly Affect the Post-Exposure Treatment of Ebola Virus Infection. *Sci Rep* (2017) 7:45552. doi: 10.1038/srep45552
191. Hou H, Yang H, Liu P, Huang C, Wang M, Li Y, et al. Profile of Immunoglobulin G N-Glycome in COVID-19 Patients: A Case-Control Study. *Front Immunol* (2021) 12:748566. doi: 10.3389/fimmu.2021.748566
192. Reis CA, Tauber R, Blanchard V. Glycosylation is a Key in SARS-CoV-2 Infection. *J Mol Med Berl Ger* (2021) 99(8):1023–31. doi: 10.1007/s00109-021-02092-0
193. Roßkopf S, Eichholz KM, Winterberg D, Diemer KJ, Lutz S, Münnich IA, et al. Enhancing CDC and ADCC of CD19 Antibodies by Combining Fc Protein-Engineering With Fc Glyco-Engineering. *Antibodies* (2020) 9(4):63. doi: 10.3390/antib9040063

Conflict of Interest: The authors declare that the research was conducted in the absence of any commercial or financial relationships that could be construed as a potential conflict of interest.

Publisher's Note: All claims expressed in this article are solely those of the authors and do not necessarily represent those of their affiliated organizations, or those of the publisher, the editors and the reviewers. Any product that may be evaluated in this article, or claim that may be made by its manufacturer, is not guaranteed or endorsed by the publisher.

frontiers | Frontiers in Immunology

REVIEW
published: 05 July 2022
doi: 10.3389/fimmu.2022.932155

Targeting Myeloid Checkpoint Molecules in Combination With Antibody Therapy: A Novel Anti-Cancer Strategy With IgA Antibodies?

Chilam Chan[1], *Marta Lustig*[2], *Niklas Baumann*[2], *Thomas Valerius*[2], *Geert van Tetering*[1†] *and Jeanette H. W. Leusen*[1*†]

[1] Center for Translational Immunology, University Medical Center Utrecht, Utrecht, Netherlands, [2] Division of Stem Cell Transplantation and Immunotherapy, Department of Medicine II, Christian Albrechts University Kiel and University Medical Center Schleswig-Holstein, Kiel, Germany

OPEN ACCESS

Edited by:
Peter Boross,
Genmab, Netherlands

Reviewed by:
Markus Biburger,
Friedrich-Alexander-University Erlangen-Nürnberg, Germany
Stephen Andrew Beers,
University of Southampton, United Kingdom

***Correspondence:**
Jeanette H. W. Leusen
jleusen@umcutrecht.nl

[†]These authors have contributed equally to this work

Specialty section:
This article was submitted to B Cell Biology, a section of the journal Frontiers in Immunology

Received: 29 April 2022
Accepted: 07 June 2022
Published: 05 July 2022

Citation:
Chan C, Lustig M, Baumann N, Valerius T, van Tetering G and Leusen JHW (2022) Targeting Myeloid Checkpoint Molecules in Combination With Antibody Therapy: A Novel Anti-Cancer Strategy With IgA Antibodies? Front. Immunol. 13:932155. doi: 10.3389/fimmu.2022.932155

Immunotherapy with therapeutic antibodies has shown a lack of durable responses in some patients due to resistance mechanisms. Checkpoint molecules expressed by tumor cells have a deleterious impact on clinical responses to therapeutic antibodies. Myeloid checkpoints, which negatively regulate macrophage and neutrophil anti-tumor responses, are a novel type of checkpoint molecule. Myeloid checkpoint inhibition is currently being studied in combination with IgG-based immunotherapy. In contrast, the combination with IgA-based treatment has received minimal attention. IgA antibodies have been demonstrated to more effectively attract and activate neutrophils than their IgG counterparts. Therefore, myeloid checkpoint inhibition could be an interesting addition to IgA treatment and has the potential to significantly enhance IgA therapy.

Keywords: IgA, myeloid checkpoints, neutrophils (PMNs), cancer immonotherapy, immune checkpoint, antibodies, CD47-SIRPalpha axis, macrophages

INTRODUCTION

For many patients, cancer is a devastating disease that is caused by an unfavorable imbalance between the immune system and the tumor. Many current cancer immunotherapies attempt to restore this balance by boosting the patient's immune system through strategies such as monoclonal antibodies (mAb), adoptive T-cell transfer, or therapeutic vaccines. mAbs are an established therapeutic tool due to their well-documented clinical activity in many different tumor types and indications. Following the approval of rituximab in 1997 for the treatment of B-cell lymphoma, many others, including trastuzumab (approved in 1998 for HER2 overexpressing breast cancer) and cetuximab (approved in 2009 for colorectal cancers) were developed (1). However, over recent years it has become apparent that clinical responses to therapeutic antibodies are often critically affected by the balance of immunostimulatory signals – typically mediated by immunoreceptor tyrosine-

based activation motifs (ITAM)-containing Fc receptors (but also other molecules) – and immunoinhibitory signals mediated by a plethora of different ITIM-containing molecules (2). The term immune checkpoint blockade refers to the interference of these interactions between immunoinhibitory molecules and their ligands (3).

Identifying and blocking checkpoint molecules on T cells has evolved as a successful strategy for cancer treatment. For example, the discovery of cytotoxic T-lymphocyte-associated protein 4 (CTLA-4) and programmed cell death protein 1 (PD-1)/programmed death-ligand 1 (PD-L1) accelerated the field's progress. Antibodies that inhibit these checkpoints, thereby preventing inhibitory signals from suppressing T cells, have been shown to improve anti-tumor responses. After the discovery of these checkpoint molecules, in 2011, the FDA approved ipilimumab, an anti-CTLA-4 blocking antibody, for patients with metastatic melanoma (4). Pembrolizumab and nivolumab, both PD-1 blocking antibodies approved for the same indication, followed in 2014 (4). Later the FDA approved atezolizumab and avelumab, both antibodies against PD-L1 (5). In the following years, the list of indications for these antibodies quickly expanded to many different tumor entities (6). However, tumor types with typically low response rates were also observed, which stimulated research into the mechanisms of antibody response and resistance (7).

Today's inhibitory checkpoint landscape extends beyond T cells and adaptive immunity. Antibody-mediated phagocytosis of cancer cells is a primary anti-tumor response mediated by macrophages in innate immunity (8). Genome-wide CRISPR screens have identified critical regulators of macrophage-mediated antibody-dependent cellular phagocytosis (ADCP) of tumor cells. The well-known CD47 anti-phagocytic factor and genes associated with protein sialylation are among the top hits. Moreover, a novel gene, adipocyte plasma membrane-associated protein (APMAP), traditionally associated with white adipose tissue differentiation but not previously associated with phagocytosis, was discovered to strongly desensitize tumor cells to ADCP (9). Such regulators are overexpressed on cancer cells to evade immune surveillance by myeloid immune cells. For example, the binding of CD47 to signal regulatory protein α (SIRPα) on macrophages reduces their anti-tumor response, which can be restored by blocking this interaction (10). Interestingly, SIRPα and other myeloid regulators are often also expressed on neutrophils, which are the most abundant immune cell in the circulation and are also found in many tumor cell infiltrates (11).

Meanwhile, several CD47-SIRPα directed treatments are being studied in combination with tumor-directed monoclonal antibodies, which are of the human IgG1 isotype (12). While IgG1 antibodies have been found to activate neutrophils, IgA antibodies have been shown to be significantly more effective. IgA-mediated antibody-dependent cellular cytotoxicity (ADCC) by neutrophils outperforms IgG-mediated ADCC using this cell subset, and when combined with CD47 blockade, the anti-tumor capacity can be greatly increased using IgA antibodies (13, 14).

Although IgA has been proven to be particularly effective in activating neutrophils, the numerous regulators overexpressed on tumor cells indicate that antibody-driven cytotoxicity alone is insufficient to battle cancer, and that antibody therapy should be combined with checkpoint inhibition to be effective (9). This review summarizes myeloid checkpoint molecules and proposes a novel combination strategy involving therapeutic IgA antibodies.

MYELOID IMMUNE CHECKPOINT MOLECULES

Traditional therapeutic antibodies, such as rituximab and trastuzumab, generally rely on Fc receptor expression on effector cells to induce cytotoxic effects such as cellular activation, cytotoxicity, and phagocytosis of antibody-opsonized tumor targets (15). The primary innate myeloid population driving the anti-tumor response, likely by phagocytosis, was proposed to be IgG-complex crosslinking to FcγRIIIa on macrophages (16). Crosslinking of the IgG-complex induced phosphorylation of the ITAM tyrosine residues and led to downstream regulation of actin polymerization and activation of phagocytosis (17). Just like the inhibitory Fc gamma receptor FcγRIIb, myeloid checkpoint molecules contain immunoreceptor tyrosine-based inhibitory motifs (ITIM) with tyrosine residues that, when phosphorylated, initiate downstream signaling that suppresses phagocytosis by counteracting ITAM signaling (18).

Weissman's lab discovered the first myeloid checkpoint molecule, the CD47-SIRPα interaction, in 2009 (19). Following that, researchers have been looking for alternative myeloid checkpoints. To date, ITIM bearing sialic acid-binding immunoglobulin-like lectins (Siglecs) expressed on myeloid cells have been discovered to bind to tumor cell ligands and inhibit immune responses in a manner similar to the CD47-SIRPα interaction. Moreover, leukocyte immunoglobulin-like receptor subfamily B (LILRB) receptors 1 and 2 on myeloid cells, were discovered to bind β2 microglobulin (B2M) exerting a similar inhibitory response in myeloid cells. The role of these myeloid checkpoint molecules (**Figure 1**) in cancer immunotherapy will be further examined.

CD47-SIRPA AXIS

One of the most studied myeloid checkpoints is the CD47-SIRPα axis. The ligand CD47, which is overexpressed on the tumor, has an Ig-like domain in its extracellular region as well as five transmembrane domains. It is ubiquitously expressed in healthy tissues, including platelets and erythrocytes, and can bind to integrins, thrombospondin-1, and signal regulatory proteins, the most relevant of which is SIRPα, since other signal regulatory proteins, such as SIRPβ and SIRPγ, bind with minimal affinity to CD47, if at all (20).

Because of its demonstrated role in immunotherapy resistance, CD47-SIRPα has received a lot of attention (21). SIRPα is a plasma membrane protein that is expressed on myeloid cells such as macrophages, granulocytes, some

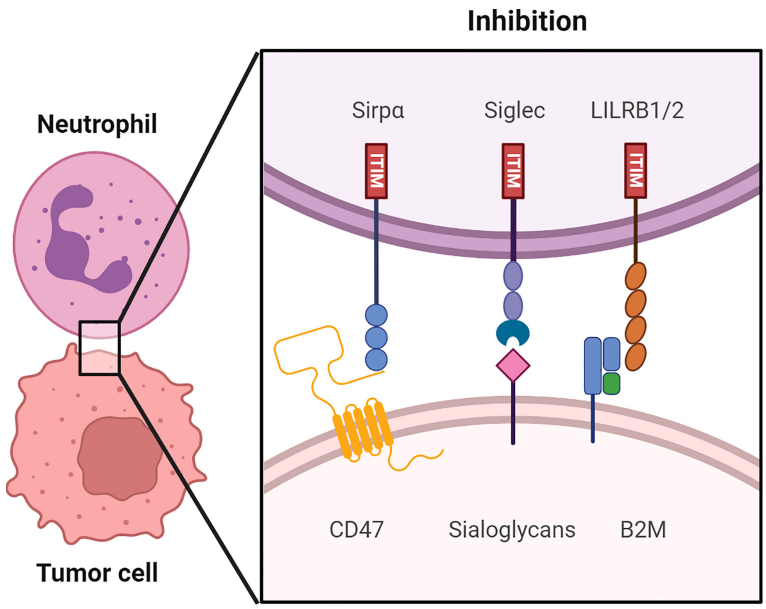

FIGURE 1 | An overview of putative immune checkpoints molecules regulating myeloid cell function in human tumor microenvironments (TME). Receptor-ligand interaction including the CD47-SIRPα axis, sialoglycans-Siglec axis and HLA1 (B2M)-LILRB 1/2 axis in the immune synapse between the myeloid cells, such as neutrophils and macrophages and the tumor cells. Src family kinases phosphorylate the ITIM upon binding of checkpoint molecules to their respective receptors. The following recruitment and activation of SHP-1 and SHP-2 suppresses the anti-tumor immune responses. Consequently, tumor cells are able to evade immune surveillance.

dendritic cell subsets, and neurons (22). SIRPα was also found to be overexpressed on natural killer (NK) cells after IL-2 activation (23). In its extracellular region, the protein has three Ig-like domains, where the NH2 terminal V-set domain is a critical CD47 interaction site (24). Furthermore, two ITIMs are present in its intracellular regions, which are phosphorylated by Src family kinases upon interaction with CD47. Subsequently, Src homology region 2 domain-containing phosphatase-1 (SHP-1) and SHP-2 are recruited and activated. These phosphatases prevent the assembly of myosin IIA at the immunological synapse, preventing phagocytosis or trogoptosis (25).

In a physiological setting, the CD47-SIRPα interaction is a critical mediator of hematopoietic cell homeostasis, most notably in erythrocytes and platelets. Healthy cells are protected from phagocytes by high CD47 expression, whereas senescent cells have low CD47 expression and are quickly cleared (20). Furthermore, recent research has discovered that functional CD47-SIRPα interaction is crucial for the survival of T-and NK cells in a steady state condition (26).

Tumor Cells Redirect the Immune System by up Regulating CD47 Expression

In both solid tumors and hematological malignancies, such as ovarian cancer, breast cancer, multiple myeloma and Non-Hodgkin lymphoma (NHL), elevated CD47 expression is associated with a poor prognosis (19, 27–35). Several mechanisms have been proposed to explain regulation of CD47 expression in cancer cells (**Figure 2**).

Transcriptional CD47 super enhancers were found in tumor cells with a high level of CD47 expression. Moreover, additional research discovered the presence of a functional enhancer E7 upstream of the CD47 gene, with increased activity correlating with CD47 overexpression in a number of cancer cell lines. Two other enhancers, E5 at a downstream CD47 gene-associated super enhancer and E3.2 within an upstream CD47 gene-associated super enhancer, were discovered in some but not all cancer cell lines, indicating that CD47 regulation may be tumor specific (36).

While on the protein level, numerous cytokines secreted by tumor-associated macrophages (TAMs) contribute to immune evasion. Tumor necrosis factor alpha (TNF-α) promotes translocation of nuclear factor kappa-light-chain-enhancer of activated B cells (NFκB) to the nucleus in tumor cells. It binds to E5 and possibly E7 at this site, allowing bromodomain-containing protein 4 (BRD4) to be recruited to the super enhancer site and promoting CD47 gene transcription (36, 37). Co-culture of TNF-α with cancer cells at concentrations up to 100 ng/ml resulted in a maximum fourfold increase in CD47 expression due to enhanced CD47 promotor activity. This could be reversed by using an anti-TNF-α antibody-to disrupt the TNF-α – TNF receptor interaction (36, 38). Similarly, interleukin-1β (IL-1β) was shown to activate NFκB and enhanced CD47 expression in cervical cancer cells (39).

Other cytokines, such as interleukin-6 (IL-6) and interferon gamma (IFN-γ), also increased CD47 expression by activating the signal transducer and activator of transcription 3 (STAT3) pathway (32). Co-culture with these cytokines at concentrations ranging from 20 ng/ml to 100 ng/ml decreased anti-tumor ADCP of various cancer cells as a direct result of increased CD47 expression (40).

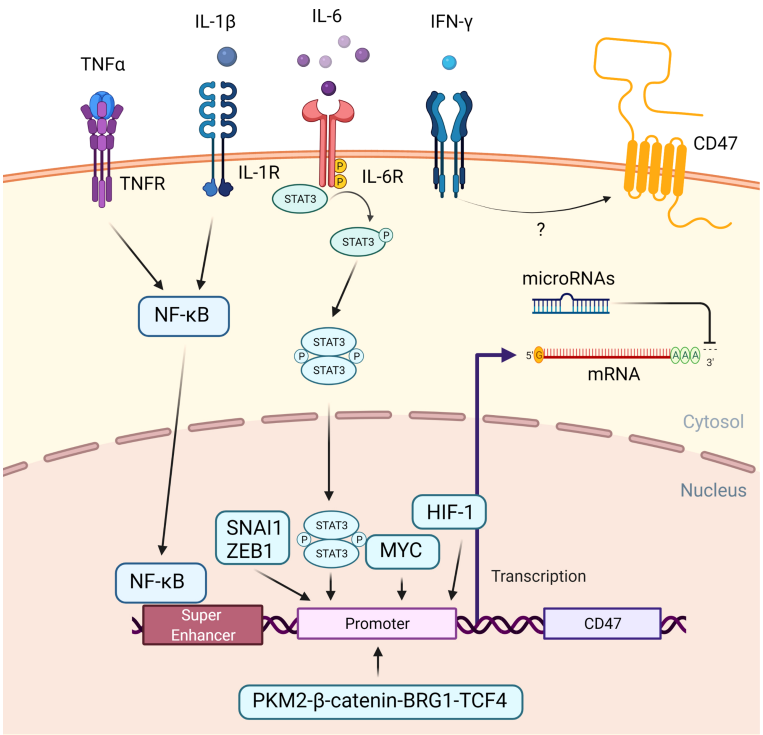

FIGURE 2 | Regulation of CD47 expression in cancer cells. An overview of the mechanisms that cause CD47 overexpression in cancer. When the TNF receptor and the IL-1 receptor are activated by extracellular TNF-α and IL-1, NFκB is recruited and translocated to the nucleus, where it binds to a super-enhancer to promote CD47 expression. Extracellular IL-6 induces STAT3 signaling. Phosphorylated STAT3 complex and other transcription factors, including SNAI1, ZEB1, MYC, HIF-1, PKM2-β-catenin-BRG1-TCF4 complex enhance CD47 expression by directly binding to the CD47 promotor. Extracellular IFN-γ increased the CD47 expression, albeit the exact mechanism is unknown. Subsequently, at a post-transcription level, microRNAs could bind to the 3' untranslated region of CD47 mRNA, causing translation to be disrupted.

In addition, several transcription factors bind to the CD47 promotor to increase CD47 transcription. MYC, a transcription factor involved in cell proliferation, differentiation, and apoptosis, was discovered to promote tumorigenesis *via* direct binding to the promotor of the checkpoint proteins CD47 and PD-L1 (41, 42). MYC inactivation in various tumor cells down-regulated cell surface expression of CD47 (41). Similarly, recruitment of Snail Family Transcriptional Repressor 1 (SNAI1), Zinc Finger E-Box Binding Homeobox 1(ZEB1), Hypoxia-inducible factor-1 (HIF-1), and the Pyruvate kinase isozymes M2 (PKM2)-β-catenin- Brahma-Related Gene-1 (BRG1)- Transcription Factor 4 (TCF4) complex to the CD47 promotor increased CD47 expression (43–45).

Finally, microRNAs could negatively regulate CD47 gene expression in cancer cells by degrading messenger RNA or limiting translation. Numerous microRNAs that bind to the CD47 3' UTR and inhibit its expression have been identified. MiR-133a, for example, is downregulated in esophageal squamous cell cancer (46, 47). In T cell acute lymphoblastic leukemia, miR-708 is downregulated and sustained CD47 expression (48, 49). Other miRNAs known to influence CD47 expression include miR-155 (50), miR-200a (51), miR-192 (52), and miR-340 (53), which all act post-transcriptionally on CD47 mRNA.

CD47 Ligation Impairs Anti-Tumor Response

The interaction between CD47 and SIRPα on macrophages inhibits phagocytosis, serving as a "don't eat me" signal, which may counteract pro-inflammatory responses mediated by cancer therapeutic antibodies, reducing therapeutic efficacy. Targeting this axis is hypothesized to disrupt the inhibitory signal, improving the efficacy of therapeutic cancer antibody candidates targeting tumor associated antigen (TAA), such as rituximab (31). Because CD47 is expressed in both hematological and solid tumors, it is a promising and broadly applicable therapeutic target. Although CD47-specific blocking antibodies are capable of improving macrophage-mediated ADCP and neutrophil-mediated ADCC, the mechanisms underlying CD47 targeted treatment are not restricted to these functions.

Some CD47 antibodies (**Table 1**) have been reported to induce tumor cell death *via* a caspase-independent mechanism (64). Apoptosis induced by CD47 ligation appears to be epitope-dependent, as demonstrated by anti-CD47 clones MABL (60) and CC2C6 (65), but not with clone B6H12 (19, 54).

Moreover, treatments using CD47 antibodies can promote adaptive T-cell immune responses. Anti-CD47 therapy administered intratumorally to colon adenocarcinoma tumor (MC38)-bearing syngeneic WT C57BL/6 mice decreased tumor

TABLE 1 | The characteristics of anti-human CD47/SIRPα antibodies and proteins.

Name	Target	Isotype	Origin	Status	REF
ADU-1805	SIRPα	IgG2	Humanized	Research	(54)
ALX148	CD47	Inactive Fc domain	Fusion protein	Phase 1/2/3	(55)
AO-176	CD47	IgG2	Humanized	Phase ½	(56)
B6H12	CD47	IgG1	Mouse	Research	(57)
B6H12.2	CD47	IgG1	Humanized	Research	(19)
BI 765063	SIRPα	IgG4	Humanized	Phase 1	NCT04653142 (58),
BRIC126	CD47	IgG2b	Mouse	Research	(59)
CC2C6	CD47	IgG1	Mouse	Research	(60)
CC-95251	SIRPα	IgG1	Humanized	Phase 1	NCT05168202
Hu5F9-G4	CD47	IgG4	Humanized	Phase I/2	(61)
MABL sc(Fv)2	CD47	Sc(Fv)2	Mouse	Research	(62)
MY-1	CD47	IgG2a	Rat	Research	(63)

growth, but no effect was observed in T cell-deficient nude mice. $CD8^+$ T cell depletion revealed that the therapeutic effect was mediated by cytotoxic T cells. Additionally, dendritic cells, but not macrophages isolated from the tumor microenvironment demonstrated increased cross-priming of the cytotoxic T cells (55, 56). The infiltration of $CD8^+$ dendritic cells into the spleens of colon carcinoma tumor (CT-26)-bearing mice was increased following treatment with ALX148, a high affinity anti-CD47 fusion protein with blocking capacities, Moreover the dendritic cells were more activated. Increased levels of splenic effector memory and central memory $CD4^+$ T cells, as well as increased numbers of central memory $CD8^+$ T cells, were observed in these mice (55). In a NHL model, CD47 mAb synergized with a CD19/CD3 bispecific T cell engagers (BiTE) and activated both macrophages and T cells. It was demonstrated that the CD47 mAb required macrophages, PBMCs, and possibly others for optimal tumor clearance, as validated by macrophage depletion using liposomal clodronate or NOD/SCID mice lacking human PBMCs (57). It has been proposed that the association between CD47 on tumor cells and thrombospondin-1 on T cells acts as an immunological checkpoint, impairing T cell activation and thereby decreasing antigen-dependent killing of tumor cells by $CD8^+$ T cells (58). Overall, inhibition of the CD47-SIRPα axis promotes tumor antigen cross-presentation to $CD8^+$ T cells by dendritic cells, boosting the adaptive response.

Blocking the CD47-SIRPα Axis Improves Macrophage-Mediated Phagocytosis

CD47 antibodies, such as the humanized B6H12 (often referred as B6H12.2) and BRIC126 (**Table 1**) have been shown to be effective in pre-clinical mouse models of acute myeloid leukemia (AML) (19), acute lymphoblastic leukemia (27), T-cell lymphoma (TCL) (54), and various solid tumors. After CD47 was blocked, TAMs in solid tumors could be converted to pro-phagocytic (59, 61). Interfering with the CD47-SIRPα interaction slowed tumor growth and prevented metastasis. Both B6H12.2 and BRIC126 are first generation CD47 antibodies that disrupt the CD47-SIRPα interaction while also triggering Fc-FcγR ADCC and ADCP, i.e. NK-mediated cell death, *via* an intact IgG Fc tail. Monotherapy in PDX and immunocompetent TCL mouse models using these antibodies was proven to be efficient in killing tumor cells due to their Fc effector properties, whereas antibodies with blocking properties need to be used in combination therapies (54).

Despite promising results in (pre)clinical studies, the field remains concerned about the clinical applicability of this approach. CD47 is expressed ubiquitously on somatic cells, including platelets and erythrocytes, which is of major concern for CD47 targeted therapy. Thrombocytopenia occurred spontaneously in CD47-deficient mice due to uncontrolled platelet phagocytosis. The CD47-SIRPα interaction was found to be directly involved in the regulation of macrophage uptake of CD47-negative platelets. Additionally, CD47-deficient mice develop anemia and die prematurely as a result of rapid erythrocyte clearance (62, 63, 66). As a result, CD47 must be targeted with caution. Blocking antibodies such as F(ab) fragments and Fc silent mAbs directed at CD47 were developed to overcome dose-limiting toxicity. Again, these blocking antibodies demonstrated that interrupting SIRPα signaling requires the presence a pro-phagocytic signal, as the blocking antibody alone had no effect on tumor suppression (19, 31, 67).

For example, Calreticulin and SLAMF7, are pro-phagocytic receptors that are found in a variety of malignancies but are minimally expressed on healthy cells. Calreticulin expression is increased in a range of cancers, including leukemias, bladder cancer, and ovarian cancer, whereas SLAMF7 expression is increased in predominantly hematopoietic tumor cells (68). When CD47 was blocked, Calreticulin overexpression resulted in an increase in macrophage phagocytic capability. Surprisingly, increased expression of SLAMF7 had no effect on macrophage phagocytosis (54, 68, 69). Disrupting the CD47-SIRPα downstream SHP-1 signaling in a melanoma mouse model by using mutant mice lacking the SIRPα cytoplasmic tail had no effect on tumor growth or metastasis. Tumor formation in these mice was, however, prevented when combined with an anti-gp75 antibody (28, 70). It is clear that, in addition to removing the 'brake', an activating cue, whether a therapeutic Fc-active antibody or another pro-phagocytic signal like calreticulin, is required for optimal immune response.

Multiple pro-phagocytic signals may be beneficial in the treatment of more advanced, resistant late-stage cancers. Blocking CD47 did, in fact, synergize with rituximab and improved macrophage-mediated phagocytosis in NHL

xenotransplant mouse models (31). In a pre-clinical model of $HER2^+$ breast cancer, a combination of a CD47 mAb and trastuzumab was also found to successfully augment macrophage-mediated phagocytosis (71).

The Development of Next-Generation Antibodies

The humanized anti-CD47 antibody developed by Arch Oncology, AO-176 (**Table 1**), has the distinctive property of displaying low affinity to normal healthy cells and negligible binding to erythrocytes and platelets. The differential binding was most likely caused by the antibody's binding epitope characteristics, which allows it to bind more potently to tumors in an acidic microenvironment (72, 73). Other novel strategies for reducing the on-target toxicity of CD47 targeting have been investigated. To reduce Fc-mediated effector functions, the humanized 5F9 (Hu5F9) antibody was placed on an IgG4 scaffold. Hu5F9-G4 inhibited the CD47-SIRPα interaction and induced phagocytosis of AML cell lines by macrophages. Furthermore, Hu5F9-G4 reduced NHL engraftment *in vivo*, but total tumor clearance was only achieved when combined with rituximab (74, 75). The on-target toxicity of these modified antibodies is significantly reduced. These agents, however, still face the issue of a large antibody sink and are restricted to combination therapies as they lack Fc-mediated effector functions.

ALX148 is a SIRPα-Fc protein engineered by fusing a modified SIRPα to an inert human IgG1 Fc portion, not capable of binding FcγR or C1q complement protein (55). Binding to the neonatal Fc receptor, on the other hand, was retained, which is beneficial for serum half-life. When compared to the WT SIRPα, it was found to have a 7000-fold higher affinity for human CD47. Because of the inert Fc portion on-target adverse reactions were reduced. *In vivo* anti-tumor responses were achieved in mantle cell lymphoma and gastric tumor models using obinutuzumab and trastuzumab, respectively. ALX148 promoted macrophage phagocytosis, induced dendritic cell activation, and promoted T cell activation in non-human primates with a favorable safety profile (55).

Another strategy to limit hematotoxicity are antibodies that target SIRPα. Several SIRPα antibodies are currently undergoing clinical trials or being researched, such as BI 765063 (NCT04653142), CC-95251 (NCT05168202), and ADU-1805 (76). These antibodies do not bind to erythrocytes and platelets and show similar efficacies *in vitro* as CD47 antibodies (76–78). However, validation in mouse models are difficult because of the human specificity. MY-1 a SIRPα antibody that binds to the NH2-terminal Ig-V–like domain of mouse SIRPα and thereby blocks the CD47/SIRPα interactions in mice. MY-1 showed no hematotoxicity in mice and improved ADCP and ADCC activity (14, 79). Moreover, the antibody also binds the extracellular region of mouse SIRPβ1 and promoted anti-tumor immunity independent of macrophage-mediated ADCP (80). SIRPβ1 lacks an ITIM motif and does not bind CD47 efficiently (81). It was found that ligation of MY-1 to SIRPβ1 promoted TNFα secretion by macrophages and suppressed tumor growth through activation of a DAP12-Syk- MAPK signaling pathway (80).

Small molecules are being investigated as a novel strategy for disrupting the CD47-SIRPα interaction. A haploid genetic screen revealed that the enzyme glutaminyl-peptide cyclotransferase-like protein (QPCTL) is required for the formation of pyroglutamate on CD47. QPCTL is an enzyme that catalyzes the conversion of N-terminal glutamine and glutamic acid residues to N-terminal pyroglutamate residues (82). The CD47 protein's N-terminal pyroglutamate is the primary binding site for SIRPα (24). SEN177, a QPCTL inhibitor, or QPCTL knockout abolished the binding of an anti-CD47 antibody (CC2C6) that recognizes the same recognition site as SIRPα (83). Pre-treatment of MDA-MB-468 and A431 cells with SEN177 for three days, decreased SIRPα-Fc binding dose dependently and enhanced antibody-dependent macrophage-mediated ADCP and neutrophil-mediated ADCC (84). Traditional CD47 antibodies also bind to CD47 on healthy cells, leading to a decrease in the antibody's bioavailability, also known as the antigen sink issue. Since pyroglutamate modification occurs early in the cell cycle, before reaching the cell surface, QPCTL inhibitors bypass the antigen sink problem and may not compete with physiological SIRPα (83). It has not been determined if tumor cells utilize the QPCTL enzyme to stabilize the CD47-SIRPα interaction. The QPCTL expression level did not correlate with the activation of phagocytosis in response to anti-CD47 antibodies (54).

Small molecules/peptides are an intriguing study target due to their favorable hematotoxicity profile. Both Pep-20 and RRx-001 are such small compounds that, when administered, disrupt the CD47-SIRP axis with minimal systemic toxicity (85, 86). More small molecules are likely to be discovered as a result of optimized high throughput screenings for the discovery of new CD47-SIRPα inhibitors (87, 88).

Furthermore, an anti-leishmanial drug, sodium stibogluconate, was found to improve neutrophil-mediated killing of B cell malignancies that were previously resistant to anti-CD20 IgG antibodies. The drug had no direct effect on the CD47-SIRPα axis, but was only effective when the CD47-SIRPα interaction was disrupted. Despite the fact that sodium stibogluconate inhibits the phosphatase SHP-1, the therapeutic effect was not entirely dependent on SHP-1 (89). This indicates that the CD47-SIRPα interaction is a key suppressor in the tumor microenvironment.

ALTERNATIVE MYELOID CHECKPOINTS

Sialoglycans and Siglecs

Many tumor cells, including colorectal, breast, ovarian, prostate, non-small cell lung cancer, and glioma, overexpress sialic acid sugar-containing glycans known as sialoglycans, which have emerged as important regulatory molecules in tumor development (90, 91).

The hypoxic tumor microenvironment, as well as the presence of oncogenic Ras, were proposed to support tumor

cell hypersialylation. The 2,6-sialyltransferase enzyme (ST6Gal-I) found downstream of Ras oncogene signaling is responsible for the addition of α2,6-sialic acid to termini N-glycans (92, 93). In breast cancers, the cyclooxygenase COX-2 can increase the α2,3-sialyltransferase enzyme (ST3Gal-I) expression (94). Moreover, both ST6Gal-I and ST3Gal-(I, III and IV) overexpression was associated with poor clinical outcome in different malignancies, including myeloid leukemia, hepatocellular carcinoma and bladder cancer (95–98).

By interacting with Siglecs, sialoglycans modulates immunological responses (99). Siglecs are a family of 14-transmembrane proteins that are expressed by the majority of immune cells. They are classified into two groups: those with a conserved structural motif (Siglec-1, -2, -4, and -15) and those related to Siglec-3 (Siglec-3, -5 to -11, -14, and -16). Each Siglec has an extracellular sialic acid-binding site that recognizes sialylated proteins to which it can bind.

The majority of human Siglecs have an intracellular ITIM that is phosphorylated in response to sialoglycan binding, which results in the recruitment of SHP1/2 phosphates that inhibit downstream activation pathways (100, 101). Among the ITIM-containing Siglecs expressed on neutrophils, tumors predominantly express sialoglycan ligands for Siglec-9 and to a lesser extent for Siglec-7 (90, 91). Siglec-9 recognizes both α2,3- and α2,6-linked sialic acids at low affinity, but not α2,8-linked sialic acids. Whereas, Siglec 7 preferentially binds α2,8-linked sialic acids (102–104).

The removal of sialic acids from tumor cells using sialidase impaired their interaction with Siglecs on immune cells. The interaction of sialic acid on the tumor cell and Siglec on the immune cell results in an inhibitory immunological response mediated by activation of ITIM signaling in the tumor microenvironment (105). Although the majority of Siglec ligands remain undiscovered, certain ligands have been identified.

HLA I-LILRB Axis

LILRB receptors, also known as ILT, LIR, or CD85, are type I transmembrane glycoproteins that have an extracellular Ig-like domain and intracellular ITIM motifs. They are expressed in human myeloid and lymphocyte cell populations. LILRB1 (ILT2, LIR-1, CD85j) and LILRB2 (ILT4, LIR-2, CD85d) are currently the best understood (106). Both receptors bind MHC class I (107), where LILRB1 only binds B2M-associated MHC class I heavy chains, while LILRB2 also binds B2M-free MHC class I heavy chains (108, 109). Both LILRB1 and LILRB2 seem to have a role in inhibiting phagocytosis by macrophages, albeit to a different extent. In one study, LILRB1, but not LILRB2, was found to inhibit macrophage-mediated phagocytosis. This could be due to the lower surface expression level of LILRB2 in macrophages (107, 110). In yet another study, LILRB2 ligation also decreased FcγR-dependent phagocytic capacity and ROS production (111).

These LILRB receptors were discovered to be active in tumor immune evasion due to their association with MHC class I. In humans the MHC Class I complex is made up of HLA α chains as well as the invariant B2M. MHC class I is ubiquitously expressed on nucleated cells and is responsible for presenting endogenous peptides to cytotoxic T cells (112). The peptide-binding cleft is formed by two membrane-distal domains (α1 and α2) that are non-covalently bound to two membrane-proximal domains (α3 and Beta 2 Microglobulin). Domains α1 and α2 interact with the T cell receptor of the cytotoxic T cell, while α3, which has a conserved Ig like domain, interacts with the CD8 co-receptor (112).

MHC Class I molecules are classified as either classical (HLA-A, B, and C) or non-classical (HLA-E,-G,-F). While LILRB1 and LILRB2 recognize the conserved α3 and B2M domains in most HLA haplotypes, HLA-G has emerged as an interesting binding partner due to its more restricted expression on tumor cells. HLA-G is mainly expressed on placental trophoblasts and thymic epithelial cells in healthy tissue and is best known for suppressing maternal immune responses (113). Tumor cells express HLA-G *de novo* to evade immune surveillance, similar to the immunosuppressive function seen in the placenta. High HLA-G expression has been found in a variety of cancers, including lung cancer (114), breast cancer (115, 116), colorectal cancer (117), gastric cancer (118), and esophageal squamous cell carcinoma (119). Furthermore, the presence of HLA-G on solid tumors has been related to poor prognosis (120). HLA-G is also expressed on hematological malignancies, although a connection between expression and tumor growth has not been established (121–124). Both LILRB1 and LILRB2 bind to HLA-G, however LILRB2 binds with a more α3 domain dominant hydrophobic interaction, confirming the B2M independency, suggesting a higher affinity association than LILRB1-HLA-G (113).

LILRB1 was discovered to interact with HLA class I and soluble HLA-G, and thereby reduce antibody-dependent NK cell induced cytotoxicity. By blocking this interaction, cetuximab-mediated ADCC was restored (120). Antibody-dependent cytotoxicity was also shown to be impaired in macrophage-mediated phagocytosis of tumor target cells (110). In this study, LILRB1 was shown to be more prevalent than LILRB2 in both healthy donor-derived macrophages and tumor-associated macrophages. These observations led to the assumption that LILRB1 is the primary mediator of MHC class I signaling in human macrophages (110).

Other LILRB members, LILRB3 (ILT5, LIR-3, CD85a), LILRB4 (ILT3, LIR-5, CD85k) and LILRB5 (LIR-8, CD85c) are orphan receptors with little information about their function (125). Since LILRB5 is not expressed on myeloid cells, it plays a minor, if any, role in myeloid immune regulation (125).

IGA ANTIBODIES

The majority of studies on the therapeutic relevance of myeloid checkpoint therapy have concentrated on macrophage-dependent phagocytosis. Myeloid checkpoints are typically not restricted to expression on macrophages and monocytes. Neutrophils, for example, account for the majority of white blood cells in circulation, making them an intriguing effector population. Ongoing clinical trials for CD47-targeted antibodies are focused on combining mAb IgG therapy with CD47 blocking, primarily aimed at the effect of macrophages. However, IgG antibodies can also activate neutrophils.

Neutrophils express two classical activating FcγRs, namely FcγRI (CD64) at less than 2000 molecules, and FcγRIIa (CD32a) at 30.000-60.000 molecules (126). The majority of IgG-induced neutrophil activation is mediated by FcγRIIa, the most prevalent FcγR in neutrophils (127, 128). Both IgG1 and IgG2 are able to induce neutrophil-mediated ADCC through FcγRIIA binding (129). Moreover, the FcγRIIA-H131 allotype has increased binding affinity to IgG1 and IgG2 compared to the FcγRIIA-R131 allotype, which was also reflected in the ADCC capacity (130). Engineered IgG antibody with a G236A substitution enhanced FcγRIIA binding and improved ADCC (131, 132).

Moreover, neutrophils express FcαRI (CD89) which can crosslink with IgA-complexes. Unexpectedly, IgA induced substantially more robust neutrophil activation than IgG with only about 10.000 molecules of FcαRI per neutrophil (133, 134). IgA elicited much stronger ITAM signaling compared to IgG, which was thought to be triggered due to the 1:2 stoichiometry, resulting in the activation of four ITAMs at once (**Figure 3**). (133, 135, 136) However, neutrophils also express the inhibitory receptor FcγRIIb (CD32b) and GPI-anchored FcγRIIIb (CD16b). The latter is expressed nearly 9-fold greater than FcγRIIa and lacks an active intracellular signaling domain, thereby scavenging away IgG and thus acts as a decoy receptor (137–139). FcγRIIIb does not bind IgA but competes for binding IgG with activating FcγRIIa, thereby reducing IgG Fc-FcγRIIa mediated ADCC potential (138).

IgA is the most abundant immunoglobulin produced in the human body, with a daily production rate of 66 mg/kg (140, 141).A significant amount of IgA is found on mucosal surfaces, mainly in dimeric or secretory form, where they play an important role in mucosal defense. However, IgA is also present in serum, with monomeric IgA being the second most abundant immunoglobin at 1-3 mg/ml (142). In humans two subclasses of IgA are found, IgA1 and IgA2 where the latter has two major allotypes, IgA2m(1) and IgA2m(2). Structural differences between IgA1 and IgA2 are primarily found in the elongated hinge region of IgA1, and higher number of N-glycosylation sites of IgA2. Both subclasses share a C-terminal tailpiece of 18 amino acids needed for dimerization. About 95 percent of IgAs in serum are monomeric, of which 90 percent being IgA1 and 10 percent being IgA2 (140, 143, 144).

Signaling Mediated by IgA Fc-FcαRI

IgA antibodies bind to FcαRI, a type 1 transmembrane receptor expressed on neutrophils, eosinophils, monocytes, macrophages, and some dendritic cell subsets (140, 145). IgA-complexes associate with a dimer FcR gamma chain containing two ITAMs, followed by tyrosine phosphorylation of the ITAMs. This then acts as a docking site for the tyrosine kinase Syk, which, when activated through calcium release, activates downstream targets such as PI3K, phospholipase C-γ and NADPH oxidase (146–148). Furthermore, ITAM activation enhances

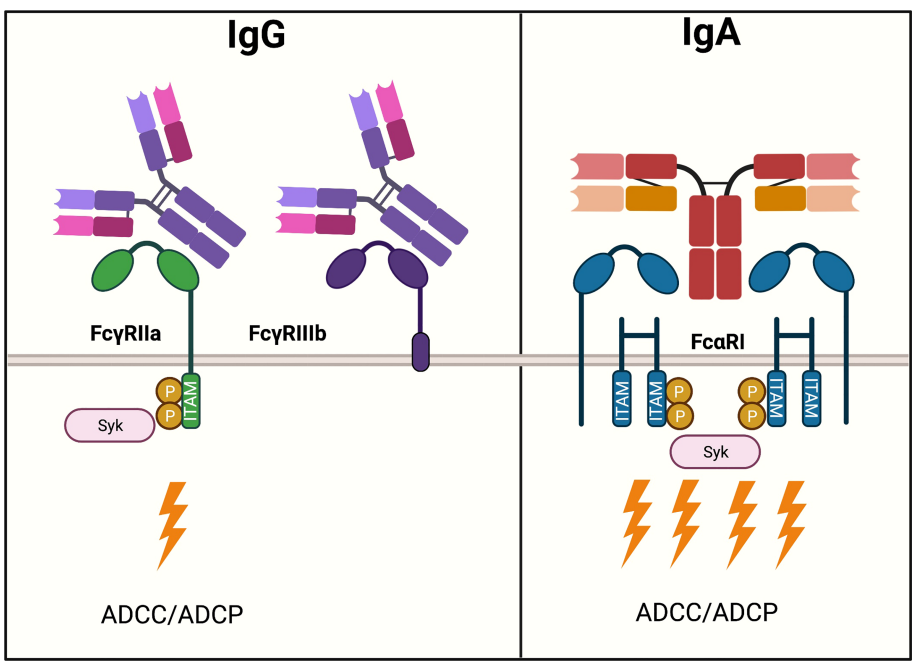

FIGURE 3 | IgG- and IgA-mediated activation of neutrophils. Neutrophils express various Fc receptors, the two most abundant of which, FcγRIIa and CD16b, are important in modulating activation upon IgG ligation. FcγRIIb is expressed nearly 9-fold greater than FcγRIIa. FcγRIIa is an activating receptor that binds to IgG in a 1:1 stoichiometry and signals *via* one ITAM motif. Downstream ITAM signaling activates effector functions such as ADCC. Moreover, neutrophils express FcγRIIb, which lacks an active intracellular signaling domain and functions as a scavenger receptor for IgG. IgA binds to FcαRI expressed on neutrophils, an activating Fc receptor in a 1:2 stoichiometry. A total of four ITAMs cause a strong activation of ADCC.

phagocytosis, oxidative burst, ADCC, and cytokine release (134, 144, 149). In soluble form, both IgA isotypes have low binding affinity to the FcαRI with a K_a of 10 (6) M^{-1}, but this is increased by 30-fold when IgA is immobilized (136, 140). Two domains on IgA, the CH2 and CH3 domains, have been identified as critical FcαRI binding sites (136).

Whereas ADCC by NK cells mediated by IgG induces apoptosis of target cells *via* perforin and granzymes, neutrophilic cytotoxicity is mediated by different mechanisms. Neutrophil mediated cytotoxicity is distinguished by an irregular neutrophil shape and a swarming effect towards the tumor cell (150). In attempting to phagocytose larger tumor cells, neutrophils adhere and spread around their target, a process previously known as frustrated phagocytosis (151). Recently, this mechanism of neutrophil-mediated effector function responsible for superior killing of cancer cells was identified as trogoptosis. It is a mechanism that involves active disruption of the cell plasma membrane which results in lytic cell death (152). The first lytic events were discovered to occur within 20 minutes, indicating that neutrophils are very efficient at IgA-mediated cell death (133).

IgA antibodies have been recombinantly engineered against a variety of targets, including CD20, EGFR, GD2 and HER2 (153–156). cetuximab IgA variants were developed and shown to block the EGFR ligand-binding domain, inhibit EGFR phosphorylation, and inhibit EGF-induced cell growth in the same way as IgG1 cetuximab (157, 158). When these IgG antibodies were converted to IgA antibodies, their Fab-mediated activities were unaffected (159, 160). Upon analyzing antibody-mediated cytotoxic functions, it was demonstrated that IgG1 antibodies primarily induced ADCC by peripheral blood mononuclear cells (PBMCs) and to a much lesser extent by polymorphonuclear leukocytes (PMNs). IgA variants, on the other hand, induced ADCC mainly by PMNs but not by PBMCs in an FcαRI-dependent manner (154). Furthermore, IgA appears to play a role in macrophage-mediated phagocytosis (161–164). However, when monocytes/macrophages were used as effector cells, the difference was less pronounced, indicating that PMNs are the most important effector cell population for IgA mediated killing. Indeed, at an E:T ratio as low as 5:1, IgA was able to induce PMN-mediated ADCC. In experiments with IgA2-EGFR complexed with A431 cells using whole leukocytes, mimicking physiological conditions, IgA2 outperformed IgG1 in ADCC (157–159). Myeloid cell numbers can be easily increased by GM-CSF and G-CSF and have been shown to improve IgA anti-tumor effects. However, it was not required for effective IgA mediated kill (153, 162, 165).

Although promising, preclinical studies with IgA therapeutic antibodies have been challenging for decades. One of the limitations include the short half-life of IgA compared to IgG. IgA lacks the binding site for the FcRn, resulting in a significantly shorter serum half-life. Additionally, hepatic clearance of exposed terminal galactose by the asialoglycoprotein receptor (ASGPR) reduces the half-life (166, 167). However, through extensive antibody engineering, the IgA antibody has been improved in producibility and stability (153, 154, 157–160). Moreover, *In vivo* studies have been limited by the absence of FcαRI in mice and the rapid clearance of IgA. Pre-clinical models to study IgA were developed by the generation of a functional hFcαRI transgenic mouse, described here (168).

The first demonstration of the anti-tumor response of IgA *in vivo* was shown in an EGFR model using FcαRI transgenic mice, using both IgA1 and IgA2 EGFR antibodies (162). The typical fast clearance of the IgA antibody was resolved by repetitive dosing to match the serum levels of IgG. Multiple doses of 50 μg IgA2 EGFR antibody restricted tumor growth in an A431 lung carcinoma SCID model in a FcαRI dependent manner (162). Furthermore, in A431 cell-based short-term intraperitoneal (i.p.) models, i.p. treatment with multiple doses of 50 μg IgA suppressed outgrowth while increasing macrophage and neutrophil influx. However, the anti-tumor response appears to be primarily Fab-dependent rather than ADCC-dependent. In a short term i.p. syngeneic C57BL/6 model with Ba/F3-EGFR cells IgA2 EGFR induced cytotoxicity, but it was primarily mediated by macrophages/monocytes (162). IgA2 induced a cytotoxic response that lasted longer than cetuximab in a long-term immunocompetent C57BL/6 model (162). An engineered variant of IgA2, termed IgA2.0, against EGFR inhibited outgrowth as well. IgA2.0 has improved pharmacokinetics and has been found to be beneficial in long-term *in vivo* models (153). IgA2.0, was more effective than IgA2 in the i.p. model, most likely due to its improved serum stability (153). Following that, other models produced demonstrated comparable results for other targets, including CD20 (13, 154), HER2 (155, 159) and GD2 (169). To summarize, IgA antibodies have demonstrated efficient anti-tumor responses in various tumor models expressing various tumor target antigens.

COMBINING MYELOID CHECKPOINT INHIBITION WITH IGA ANTIBODIES

The Role of Neutrophils in Myeloid Checkpoint Inhibition

Killing of target cells by an anti-CD47 mAb was reduced in the absence of macrophages, showing that macrophages mediate the majority of therapeutic effectiveness (170). However, because neutrophils play such a minor role in IgG immunotherapy, this effector population is often overlooked. Nevertheless, recent research has highlighted the importance of neutrophils in myeloid checkpoint inhibition. In a variety of neuroblastoma cell lines, knocking down CD47 or blocking SIRPα on neutrophils increased the neutrophil-mediated ADCC induced by dinutuximab (anti-GD2 antibody). Blocking the CD47-SIRPα interaction also increased ADCC capacity in primary patient-derived neuroblastoma spheroid cells as long as GD2 expression was sufficient, once again highlighting the relevance of combination therapy (**Figure 4**) (171, 172). Furthermore, anti-CD47 monoclonal antibodies were shown to work synergistically with trastuzumab to improve neutrophil ADCC against breast cancer cell lines (28, 152). Cetuximab-opsonized A431 cells, as

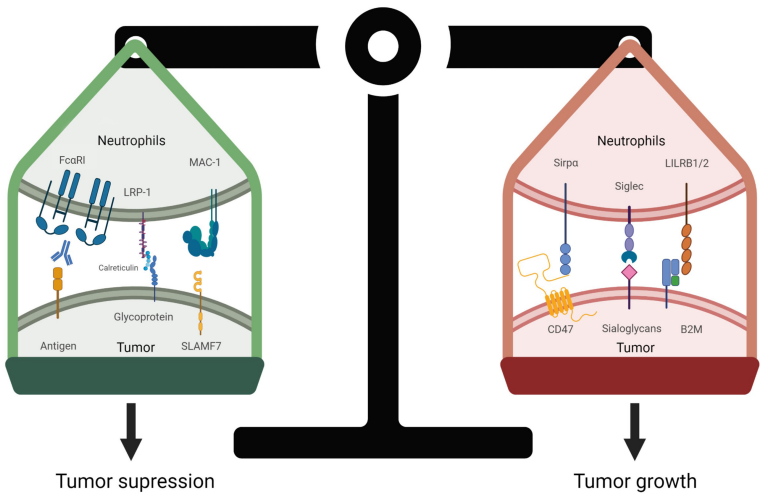

FIGURE 4 | Regulation of neutrophil-mediated tumor cell death. The balance of pro-phagocytic and anti-phagocytic signals determines the fate of the tumor cell. Pro-phagocytic signals are elicited by Fc receptor engagement to IgA-opsonized tumor cells, resulting in Fc activation and phosphorylation of downstream ITAM tyrosines. Calreticulin is tethered to the cell surface by membrane glycans and interacts with lipoprotein receptor-related protein 1 (LRP1) receptor expressed on neutrophils. Likewise, SLAMF7 (CD319) binds to macrophage-1 antigen (MAC-1, $\alpha_M\beta_2$), these interactions promote tumor cell killing by neutrophils. In contrast, overexpression of CD47 on tumor cells interact with SIRPα to inhibit neutrophil activation. Similarly, if expressed, the sialoglycans-Siglec axis, and HLA1 (B2M)-LILRB axis if expressed decrease immune responses, allowing tumor cells to evade immune surveillance.

well as trastuzumab-opsonized A431 cells, demonstrated enhanced neutrophil-dependent tumor killing in response to CD47-SIRPα inhibition (152, 173). The role of neutrophil killing in CD47 checkpoint inhibition was subsequently examined *in vivo*, where disruption of the CD47-SIRPα axis significantly reduced the metastatic load in the liver and was revealed to be dependent on neutrophil killing (152). When the CD47-SIRPα axis was blocked by an anti-human SIRPα antibody, KWAR23, not only macrophages but also neutrophils infiltrated the tumor in a human Burkitt's lymphoma xenograft. Neutrophil depletion resulted in tumor growth, suggesting that neutrophils, like macrophages, also play an anti-tumor role (174).

To support the role of granulocytes, in NHL models, the synergy between rituximab and anti-CD47 occurred independently of NK cells or complement (31). Furthermore, in melanoma, CD47 may protect NK cells from chronic inflammation, and CD47 deficiency resulted in splenic NK cell exhaustion (175). Since clinical IgG antibodies primarily act through NK cell-mediated ADCC of tumor cells and, to a lesser extent, interact with macrophages and neutrophils, it is debatable whether IgG-mediated tumor killing is the best strategy (176).

IgA Synergizes With CD47 Targeted Therapy

We hypothesize that the observed effects of myeloid cells upon CD47 blockade could be enhanced even further by the use of IgA antibodies, which primarily recruit neutrophils and macrophages thereby potentially benefiting the most from CD47-SIRPα targeted therapy.

Previous research has shown that targeting CD47-SIRPα in combination with IgA therapeutic antibodies is beneficial. *In vitro* studies showed improved IgA-mediated ADCC by PMNs upon disruption of the CD47-SIRPα interaction in SKBR3 and A431 cells, either by blocking SIRPα or knocking out CD47 in the tumor cell line. PMN-ADCC mediated by IgA2 trastuzumab and IgA2 cetuximab in CD47KO SKBR3 and CD47KO A431 cells, respectively, improved ADCC more than 10-fold when compared to IgG equivalents (14). The beneficial role of IgA in CD47 blocking therapy was translated into *in vivo* findings as well. In an A431 hFcαRI Tg xenograft mouse model, CD47 KO A431 cells were subcutaneously injected in one side of the flank and WT A431 cells in the other flank, and mice were treated with either IgA anti-EGFR, cetuximab or control. Only the IgA treated mice showed reduced tumor size for the CD47 KO tumor. Improved anti-tumor response was also observed in a shorter syngeneic i.p. Ba/F3-HER2 model, where consistent with previous data, IgA outperformed trastuzumab in the absence of CD47-SIRPα signaling. The CD47-SIRPα axis was disrupted at the neutrophil site using an anti-SIRPα blocking antibody (clone MY-1), demonstrating various strategies for disrupting the inhibitory interaction. In this model, IgA-HER2 was responsible for an enhanced influx of granulocytes to the tumor, whereas trastuzumab did not improve the influx of granulocytes (14). In a similar mouse model, but a different approach to interrupting the CD47-SIRPα signaling, QPCTL deficient Ba/F3-HER2 cells that lack pyroglutamate on CD47, were effectively killed by neutrophils directed to the tumor by IgA-HER2, in a similar fashion to CD47KO Ba/F3-HER2 cells (83). These studies consistently show that IgA synergizes with CD47 targeted therapy and outperforms IgG in a variety of tumor cell lines and targets in both short and long term mouse models.

The Immunosuppressive Function of Siglecs in Myeloid Cells

While the sialoglycan-siglec and HLA1 (B2M)-LILRB1/2 axis have rarely been explored in combination with IgA antibodies, they have been found to be ITIM-mediated, comparable to the CD47-SIRPα interaction. These alternative checkpoint receptors have been shown to inhibit FcγR-mediated IgG responses in monocytes and macrophages. Because of their expression on neutrophils and the inhibition mediated by ITIM signaling, these inhibitory receptors are likely to modulate FcαRI signaling in a similar fashion.

The immunosuppressive function of Siglecs in neutrophils has been well described for Siglec-9 in both bacterial infections and tumor immunology (177, 178). Accordingly, Siglec-9 agonists were reported to prevent neutrophil activation and NETosis in SARS-CoV-2, where NETosis is undesirable due to respiratory damage (179). In a tumor co-culture *in vitro* experiment, Siglec-9 ligation on neutrophils resulted in decreased activation as measured by ROS generation (90). Similarly, siglec-9 binding to glycophorin A on erythrocytes inhibited NET formation and ROS production (180). The activation of Siglec-9 suppresses both caspase-dependent and caspase-independent neutrophil-induced apoptosis of tumor cells (181).

Siglec-E (the mouse homolog of Siglec-9) expression allows for preclinical mouse studies. Siglec-E was reported to have an immunosuppressive effect on neutrophils in an acute inflammatory model. Ligation of Siglec-E reduced the influx of neutrophils, by inhibiting CD11b signaling (182). This inhibitory response was controlled by activation of NADPH oxidase and the production of ROS by Siglec-E (183). The inhibitory role of Siglec-9/Siglec-E was also verified in an *in vivo* MC38 tumor intravenous (i.v.) model, where Siglec-E knock out mice had decreased lung metastasis (90). Siglec-E is found on infiltrating neutrophils, macrophages and DCs in B16 and MC38 tumormodels (184). Furthermore, Siglec-9 is also expressed on macrophages and has been demonstrated to reduce TNFα secretion while increasing IL-10 production (185). Surprisingly, contrary to the immunosuppressive findings, Siglec-E knock out mice demonstrated increased M2 macrophage polarization in later stages of tumor growth, indicating that the stage of cancer should be considered when targeting Siglec-E/9 (90).

To generate a humanized immunocompetent mouse model, Siglec-E was knocked out and human Siglec-7 and -9 were introduced (184). B16 tumors were inoculated s.c. in this model to assess the antibody tumor response. When treated with the gp76 antibody, Siglec-E KO mice had less tumor outgrowth than Siglec-7^+/Siglec-9^+ Siglec-E KO mice, indicating that Siglec-7 and Siglec-9 decrease the antibody response (184). Although it is evident that tumor cell hypersialylation has an immunosuppressive function, little is known about the Siglec-ligands.

These ligands have been investigated as potential novel immunotherapy targets. Previously, it was discovered that Mucin 1 (MUC1) and MUC16, which are frequently overexpressed in adenocarcinomas, bind Siglec-9 (186, 187). MUC1 binding to Siglec-9 on macrophages induced calcium flux, which activated the MEK-ERK pathway. This resulted in the macrophages adopting an more immunosuppressive TAM phenotype (188). Similarly, MUC 16 is highly expressed in ovarian carcinoma where siglec-9 binding mediates inhibition of anti-tumor immune responses (187, 189).

Moreover, lectin galactoside-binding soluble 3 binding protein (LGALS3BP) or Mac-2 binding protein was recently found as a Siglec-9, -5 and -10 ligand. However, Siglec binding is likely not restricted to LGALS3BP and MUCs, and there may be additional unidentified ligands (186). Recombinant LGALS3BP inhibited both spontaneous and Lipopolysaccharides (LPS)-induced neutrophil ROS generation, indicating decreased neutrophil activation. Furthermore, when neutrophils were co-cultured with LGALS3BP knock out HT-29 tumor cells, neutrophil mediated apoptosis was higher than in WT HT-29 cells (190).

Siglec-7 is also expressed at low levels on neutrophils, but its immunosuppressive function is less well characterized. One of the Siglec-7 ligands was recently identified as GD2, which is overexpressed on neuroblastoma cells. By activating neutrophil-mediated ADCC and disrupting the Siglec-7-GD2 axis, GD2-targeted mAbs effectively induced killing of neuroblastoma cells (172).

The Immunosuppressive Function of LILRB in Neutrophils

LILRB expression on neutrophils seems to be phase dependent. Mainly LILRB2 is expressed on the cell surface of healthy peripheral neutrophils in a steady state condition. While there have been contradictory findings on the expression of LILRB1, proteomic analysis has verified LILRB1 expression on neutrophils (191). LILRB1 expression was increased in primed neutrophils, indicating that LILRB2 controls immune responses throughout the middle and late activation phases of the neutrophil lifecycle, avoiding overactivation (111).

In neutrophils, LILRB2 has shown to reduce neutrophil cytotoxicity. Both antibody-dependent phagocytic functions and neutrophil ROS production were inhibited by HLA-G interaction (111).

Despite the fact that LILRB3 and LILRB4 are orphan receptors, they remain interesting receptors to investigate in the context of myeloid cells. LILRB3 is expressed on neutrophils and suppresses the formation of ROS *via* FcαRI in infectious diseases. After one hour of incubation on an anti-LILRB3 or isotype control coated plate, neutrophils were activated *via* FcαRI crosslinking. In this study, ROS production was decreased when neutrophils were incubated in wells coated with anti-LILRB3. Following that, phagocytosis mediated by FcαRI was evaluated using IgA1-opsonized microparticles. The phagocytic uptake of microparticles was decreased in LILRB3-blocked neutrophils. Similarly, LILRB3 impaired IgA-mediated phagocytosis of bacteria (*S. capitis*) (192). Therefore, we should not limit our attention to LILRB1 and 2.

Moreover, crosslinking of a different family member LILRB4 using immobilized anti-LILRB4 monoclonal antibody, inhibited

FcγRI-dependent phagocytosis and TNFα production *via* monocytes through phosphatase recruitment (193, 194). Interestingly, LILRB4 expression was found on PMN- Myeloid derived suppressor cells (MDSCs) but not on PMNs obtained from healthy control donors in one study of 105 non-small cell lung cancer patients, and expression was found to be inversely related to patient survival (195). These findings suggest that LILRB4 may play a role in neutrophil suppressive progression.

STRATEGIES TO COMBINE IGA ANTIBODY TREATMENT WITH MYELOID CHECKPOINT INHIBITION

As a result of checkpoint-related advancements in the IgG field, we've acquired a number of ways for checkpoint inhibition in IgA treatment. Since comparable approaches may be used, the switch to IgA therapy is straightforward (**Figure 5**).

A straightforward strategy for proof-of-concept experiments is to knock out target genes of interest. In CD47 studies, tumor cells can be effectively knocked out, resulting in improved anti-tumor response (173). Similarly, essential enzymes in the sialic acid metabolism pathway can be knocked out to reduce sialylation of surface glycans on tumor cells. One of these enzymes is UDP-N-acetylglucosamine 2-epimerase/N-acetylmannosamine kinase (GNE) (196).

Antibodies that bind to checkpoint molecules and block their activity can also be considered to prevent the suppressive interaction. Several antibodies have been developed to interrupt the CD47-SIRPα axis, including anti-CD47 mAbs, anti-SIRPα mAbs, and SIRPα-Fc fusion proteins (**Table 1**). Moreover, anti-Siglec-7 antibody clone Z176, S7.7 and 1E8 have been successfully shown to bind Siglec-7 (90, 184). To target Siglec-9, antibody clone 191240, E10-286 and mAbA has been tested in several studies (177, 178, 184). Furthermore, antibodies against HLA Class I [clone W6/32 (110)], LILRB1 [clone GHI/75 (110) and BND-22 (197)] LILRB2 (clone 27D2) (197) have been shown to inhibit the immunosuppressive activities of the HLA/LILBR axis and enhanced anti-tumor activity.

Small molecules and enzymes provide a novel approach to checkpoint modulation. SEN177, a small molecule glutaminyl cyclase inhibitor, for example, has been found to interfere with QPCTL function and prevent pyroglutamate synthesis on CD47, interrupting binding of SIRPα to CD47 (83). RRx-001, an inhibitor of MYC downregulates CD47, while another small molecule Pep-20 targets CD47 to disrupt the interaction with SIRPα (85, 86). Sodium stibogluconate, albeit not directly targeting the CD47-SIRPα axis, synergized with CD47 blockade and improved anti-tumor response (89).

Furthermore, cleaving surface sialic acid residues with sialidase is a frequent method for modulating the sialoglycan/Siglec interaction (198). A different approach is to target sialyltransferases, which catalyze the conversion of sialic acid residues to oligosaccharide chains by using cytidine monophosphate N-acetylneuraminic acid (CMP-Neu5Ac) as the donor. Hypersialylation can be prevented by inhibiting the sialyltransferases (199).

Finally, several strategies are presented dependent on the intended target. Small molecules and antibodies with clinical promise have received increased attention throughout the years. The majority of treatments, however, have not been clinically studied and are still in the early stages of research.

Bispecific Approaches

Combination therapy with monovalent IgA antibodies and CD47 targeted antibodies has limitations, such as the antigen

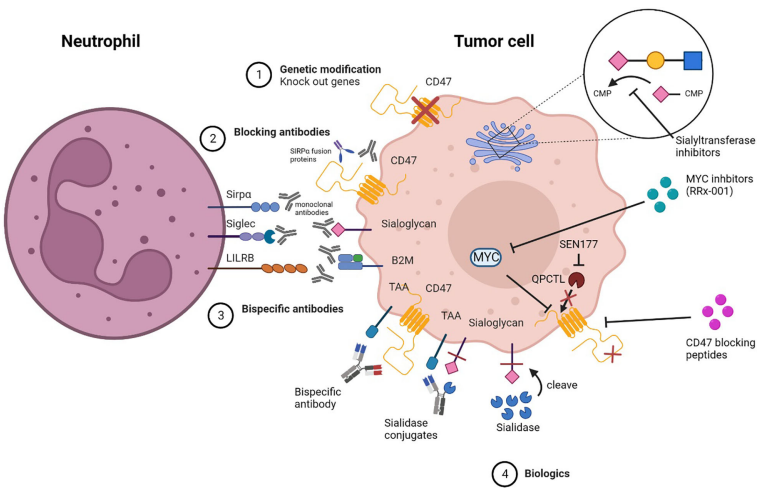

FIGURE 5 | Strategies for inhibiting myeloid checkpoints. 1) Genetic knock out of target genes involved in the inhibitory pathway. 2) Specific blocking of target checkpoint molecules with mAbs or soluble ligand-Fc fusion proteins to inhibit receptor binding and checkpoint axis activation. 3) Bispecific antibodies that target both TAA and checkpoint molecules simultaneously to avoid off-target side effects.4) Biologics that alter the structure of the target protein, preventing it from binding to the receptor, or that inhibit expression or block the target protein.

sink problem that traditional anti-CD47 antibodies suffer from (200). Similarly, combination therapy with novel checkpoint molecules will likely face the same challenge. Bispecific antibodies (bsAbs) have gained recognition as a novel format of antibody in recent years, and we believe they can potentially fill the gap left by anti-checkpoint and TAA-antibody combination therapies. Bispecific antibodies have a greater affinity for dual antigen-expressing cells than for single antigen-expressing cells, resulting in a more avid interaction.

The potential of bispecific TAA/CD47 targeting antibodies, have been demonstrated by several studies. The novel HuNb1-Ig4 antibody demonstrated a lower affinity for RBCs than the anti-CD47 antibody Hu5F9-G4. The affinity for RBC was reduced much further when developed into a bispecific antibody and linked to the C-terminus CH3 domain of rituximab. When compared to the combination treatment of rituximab and HuNb1-IgG4, the bispecific CD20/CD47 HuNb1-IgG4 significantly lowered tumor volume *in vivo* (201). However, it is unclear whether this rituximab modification will affect the ADCC capacity.

Another approach is the dual variable domain immunoglobulin (DVD-Ig)format to generate a CD20/CD47 bispecific antibody (202). Using an amino acid linker, the variable domain of one antibody was engineered on the N-terminal variable domain of the other antibody. The CD47 variable domain was placed in the inner position because steric hindrance was expected to reduce affinity. Indeed, the affinity of CD47 in the bispecific antibody format was reduced by 20-fold when compared to the affinity of CD47 mAb, whereas the affinity of CD20 appeared to be unaffected. When incubated with RBCs, the binding assay confirmed simultaneous binding to CD47 and CD20, as well as preferential binding to dual antigen-expressing cells. Furthermore, the bsAb was shown to increase phagocytosis in the same way that anti-CD47 mAb and rituximab combination therapy did. Additionally, in a subcutaneous Raji NSG mouse model, the CD20/CD47 DVD-Ig reduced tumor burden in a manner comparable to combination therapy (202).

Moreover, anti-CD47/CD19 (71) or anti-CD47/MSLN (72) antibodies were generated in the κλ body format, which has the human IgG1 isotype (203). They differ from conventional IgG1 in that they have two different light chains, one kappa and one lambda paired to the IgG1 heavy chain. The kappa light chain in the κλ body format targets CD47, while the lambda light chain targets either CD19 or MSLN. To prevent undesired binding from TAA-negative cells, the CD47 arm has a lower affinity. When tested, the κλ bsAbs demonstrated selective binding for dual antigen-expressing cells, tumor killing *in vitro*, and were superior to combination therapy with monovalent antibodies. *In vivo*, bsAbs inhibited tumor growth in the same way that the combination treatment did. These bsAbs were found to be at least as effective in mediating phagocytosis as the monovalent antibodies combined, with no undesired binding to erythrocytes or platelets, making them potential clinical candidates (204, 205).

Sialylation does not occur exclusively on the tumor's surface. To avoid unfavorable side effects, it is critical to selectively remove sialoglycans from tumor cells while leaving healthy cells undisturbed. However, targeting sialoglycans may involve a slightly different approach. Antibody-enzyme conjugates could provide a method for removing sialoglycans from tumor cells specifically. In one study, a trastuzumab-sialidase conjugate demonstrated specific sialic acid cleavage on HER2 positive SKBR3 cells and had no effect on the HER2 negative MDA-MB-468 cells. Furthermore, when compared to trastuzumab monotherapy, the trastuzumab-sialidase conjugate demonstrated increased NK-cell mediated ADCC against a variety of HER2 expressing cell lines, making this a promising tool for avoiding on-target side effects while maintaining improved anti-tumor capacities (105).

Glycoproteins and glycosaminoglycans are large proteins found in the glycocalyx of both tumor and immunological cells. Not surprisingly, the glycocalyx has been shown to inhibit phagocytosis through steric and electrostatic hindrance. As a result, removing this barrier and revealing tumor targets may improve tumor killing. The removal of mucins from tumor cells improved phagocytosis (206). Combination strategies, in which the glycocalyx of the tumor cell is first stripped, followed by targeting other checkpoint molecules in combination with IgA treatment, could be an effective and novel strategy.

CONCLUDING REMARKS

IgA antibodies are an emerging novel strategy for antibody therapeutics that, due to their unique mode of action, hold promise for use in tumors infiltrated by neutrophils. These tumors often have a poor prognosis with currently available therapies (207) – supporting the need for new approaches. Because myeloid cells are recruited, combining CD47-SIRPα checkpoint inhibition with IgA antibodies might be a good method for targeting resistant tumor cells. Similarly, we believe that blocking other myeloid checkpoint molecules addressed in this review could improve IgA-mediated tumor responses. Combining IgA treatment with checkpoint inhibitors such as those described in **Figure 5** is proposed.

Alternatively, a bsAb IgA antibody directed against a TAA and a checkpoint molecule could be used to circumvent some of the limitations of monovalent antibody-based combination therapy. We are confident that techniques comparable to those used to generate IgG-based bsAbs can be utilized to create novel IgA-based bsAbs as long as the modifications do not interfere with FcαRI signaling. However, the efficacy of such bsAbs is unclear and needs to be further investigated. These developments could improve current therapies that use identified myeloid checkpoint molecules, while also highlighting the potential of myeloid checkpoints to accelerate the discovery of more inhibitory molecules.

AUTHOR CONTRIBUTIONS

CC, GT, and JL contributed to the concept of the review. CC visualized and wrote the first draft of the review. All authors

contributed to manuscript revision, read, and approved the submitted version.

FUNDING

This work was supported by a grant of The Dutch Cancer Society (KWF Kankerbestrijding) - Project: 11944. ML and TV are supported by the Clinical Research Unit CATCH-ALL funded by the Deutsche Forschungsgemeinschaft - Project: 444949889.

ACKNOWLEDGMENTS

Illustrations were created with BioRender.com.

REFERENCES

1. Mullard A. FDA Approves 100th Monoclonal Antibody Product. *Nat Rev Drug Discovery* (2021) 20:491–5. doi: 10.1038/d41573-021-00079-7
2. Daëron M, Jaeger S, Du Pasquier L, Vivier E. Immunoreceptor Tyrosine-Based Inhibition Motifs: A Quest in the Past and Future. *Immunol Rev* (2008) 224:11–43. doi: 10.1111/j.1600-065X.2008.00666.x
3. Sharma P, Allison JP. The Future of Immune Checkpoint Therapy. *Science* (2015) 348:56–61. doi: 10.1126/science.aaa8172
4. Alexander W. The Checkpoint Immunotherapy Revolution: What Started as a Trickle Has Become a Flood, Despite Some Daunting Adverse Effects; New Drugs, Indications, and Combinations Continue to Emerge. *P T* (2016) 41:185–91.
5. Twomey JD, Zhang B. Cancer Immunotherapy Update: FDA-Approved Checkpoint Inhibitors and Companion Diagnostics. *AAPS J* (2021) 23:39. doi: 10.1208/s12248-021-00574-0
6. Nirschl CJ, Drake CG. Molecular Pathways: Coexpression of Immune Checkpoint Molecules: Signaling Pathways and Implications for Cancer Immunotherapy. *Clin Cancer Res* (2013) 19:4917–24. doi: 10.1158/1078-0432.CCR-12-1972
7. Chen DS, Mellman I. Elements of Cancer Immunity and the Cancer-Immune Set Point. *Nature* (2017) 541:321–30. doi: 10.1038/nature21349
8. Weiskopf K, Weissman IL. Macrophages are Critical Effectors of Antibody Therapies for Cancer. *MAbs* (2015) 7:303–10. doi: 10.1080/19420862.2015.1011450
9. Kamber RA, Nishiga Y, Morton B, Banuelos AM, Barkal AA, Vences-Catalán F, et al. Inter-Cellular CRISPR Screens Reveal Regulators of Cancer Cell Phagocytosis. *Nature* (2021) 597:549–54. doi: 10.1038/s41586-021-03879-4
10. Tian L, Lei A, Tan T, Zhu M, Zhang L, Mou H, et al. Macrophage-Based Combination Therapies as a New Strategy for Cancer Immunotherapy. *Kidney Dis* (2022) 8:26–43. doi: 10.1159/000518664
11. Ocana A, Nieto-Jiménez C, Pandiella A, Templeton AJ. Neutrophils in Cancer: Prognostic Role and Therapeutic Strategies. *Mol Cancer* (2017) 16:137. doi: 10.1186/s12943-017-0707-7
12. Sharma P, Siddiqui BA, Anandhan S, Yadav SS, Subudhi SK, Gao J, et al. The Next Decade of Immune Checkpoint Therapy. *Cancer Discovery* (2021) 11:838–57. doi: 10.1158/2159-8290.CD-20-1680
13. Evers M, Broeke TT, Jansen JHM, Nederend M, Hamdan F, Reiding KR, et al. Novel Chimerized IgA CD20 Antibodies: Improving Neutrophil Activation Against CD20-Positive Malignancies. *MAbs* (2020) 12:1795505. doi: 10.1080/19420862.2020.1795505
14. Treffers LW, Broeke TT, Rösner T, Jansen JHM, Houdt Mv Kahle S, Houdt MV, et al. IgA-Mediated Killing of Tumor Cells by Neutrophils is Enhanced by CD47–SIRPA Checkpoint Inhibition. *Cancer Immunol Res* (2020) 8:120–30. doi: 10.1158/2326-6066.CIR-19-0144
15. Scott AM, Wolchok JD, Old LJ. Antibody Therapy of Cancer. *Nat Rev Cancer* (2012) 12:278–87. doi: 10.1038/nrc3236
16. DiLillo DJ, Ravetch JV. Differential Fc-Receptor Engagement Drives an Anti-Tumor Vaccinal Effect. *Cell* (2015) 161:1035–45. doi: 10.1016/j.cell.2015.04.016
17. Bournazos S, Ravetch JV. Fcγ Receptor Pathways During Active and Passive Immunization. *Immunol Rev* (2015) 268:88–103. doi: 10.1111/imr.12343
18. Nakamura K, Smyth MJ. Myeloid Immunosuppression and Immune Checkpoints in the Tumor Microenvironment. *Cell Mol Immunol* (2020) 17:1–12. doi: 10.1038/s41423-019-0306-1
19. Majeti R, Chao MP, Alizadeh AA, Pang WW, Jaiswal S, Gibbs KD Jr, et al. CD47 Is an Adverse Prognostic Factor and Therapeutic Antibody Target on Human Acute Myeloid Leukemia Stem Cells. *Cell* (2009) 138:286–99. doi: 10.1016/j.cell.2009.05.045
20. Barclay AN, Van den Berg TK. The Interaction Between Signal Regulatory Protein Alpha (Sirpα) and CD47: Structure, Function, and Therapeutic Target. *Annu Rev Immunol* (2014) 32:25–50. doi: 10.1146/annurev-immunol-032713-120142
21. Yanagita T, Murata Y, Tanaka D, Motegi S-I, Arai E, Daniwijaya EW, et al. Anti-Sirpα Antibodies as a Potential New Tool for Cancer Immunotherapy. *JCI Insight* (2017) 2:e89140–0. doi: 10.1172/jci.insight.89140
22. Matozaki T, Murata Y, Okazawa H, Ohnishi H. Functions and Molecular Mechanisms of the CD47–Sirpα Signalling Pathway. *Trends Cell Biol* (2009) 19:72–80. doi: 10.1016/j.tcb.2008.12.001
23. Deuse T, Hu X, Agbor-Enoh S, Jang MK, Alawi M, Saygi C. The Sirpα-CD47 Immune Checkpoint in NK Cells. *J Exp Med* (2021) 218:e20200839. doi: 10.1084/jem.20200839
24. Hatherley D, Graham SC, Turner J, Harlos K, Stuart DI, Barclay AN, et al. Paired Receptor Specificity Explained by Structures of Signal Regulatory Proteins Alone and Complexed With CD47. *Mol Cell* (2008) 31:266–77. doi: 10.1016/j.molcel.2008.05.026
25. Tsai RK, Discher DE. Inhibition of 'Self' Engulfment Through Deactivation of Myosin-II at the Phagocytic Synapse Between Human Cells. *J Cell Biol* (2008) 180:989–1003. doi: 10.1083/jcb.200708043
26. Legrand N, Huntington ND, Nagasawa M, Bakker AQ, Schotte R, Strick-Marchand H, et al. Functional CD47/signal Regulatory Protein Alpha (SIRP (alpha)) Interaction is Required for Optimal Human T- and Natural Killer- (NK) Cell Homeostasis *In Vivo*. *Proc Natl Acad Sci USA* (2011) 108:13224–9. doi: 10.1073/pnas.1101398108
27. Chao MP, Alizadeh AA, Tang C, Jan M, Weissman-Tsukamoto R, Zhao F, et al. Therapeutic Antibody Targeting of CD47 Eliminates Human Acute Lymphoblastic Leukemia. *Cancer Res* (2011) 71:1374–84. doi: 10.1158/0008-5472.CAN-10-2238
28. Zhao XW, van Beek EM, Schornagel K, Van der Maaden H, Van Houdt M, Otten MA, et al. CD47-Signal Regulatory Protein-α (Sirpα) Interactions Form a Barrier for Antibody-Mediated Tumor Cell Destruction. *Proc Natl Acad Sci USA* (2011) 108:18342–7. doi: 10.1073/pnas.1106550108
29. Rendtlew Danielsen JM, Knudsen LM, Dahl IM, Lodahl M, Rasmussen T. Dysregulation of CD47 and the Ligands Thrombospondin 1 and 2 in Multiple Myeloma. *Br J Haematol* (2007) 138:756–60. doi: 10.1111/j.1365-2141.2007.06729.x
30. Willingham SB, Volkmer J-P, Gentles AJ, Sahoo D, Dalerba P, Mitra SS, et al. The CD47-Signal Regulatory Protein Alpha (SIRPa) Interaction is a Therapeutic Target for Human Solid Tumors. *Proc Natl Acad Sci USA* (2012) 109:6662–7. doi: 10.1073/pnas.1121623109
31. Chao MP, Alizadeh AA, Tang C, Myklebust JH, Varghese B, Gill S, et al. Anti-CD47 Antibody Synergizes With Rituximab to Promote Phagocytosis and Eradicate non-Hodgkin Lymphoma. *Cell* (2011) 142:699–713. doi: 10.1016/j.cell.2010.07.044
32. Chen J, Zheng D-X, Yu X-J, Sun H-W, Xu Y-T, Zhang Y-J, et al. Macrophages Induce CD47 Upregulation *via* IL-6 and Correlate With Poor Survival in Hepatocellular Carcinoma Patients. *Oncoimmunology* (2019) 8:e1652540. doi: 10.1080/2162402X.2019.1652540
33. Pai S, Bamodu OA, Lin Y-K, Lin C-S, Chu P-Y, Chien M-H, et al. CD47-Sirpα Signaling Induces Epithelial-Mesenchymal Transition and Cancer

Stemness and Links to a Poor Prognosis in Patients With Oral Squamous Cell Carcinoma. *Cells* (2019) 8:1658. doi: 10.3390/cells8121658
34. Yuan J, Shi X, Chen C, He H, Liu L, Wu J, et al. High Expression of CD47 in Triple Negative Breast Cancer is Associated With Epithelial-Mesenchymal Transition and Poor Prognosis. *Oncol Lett* (2019) 18:3249–55. doi: 10.3892/ol.2019.10618
35. Wang CL, Lin M-J, Hsu C-Y, Lin H-Y, Tsai H-P, Long C-Y, et al. CD47 Promotes Cell Growth and Motility in Epithelial Ovarian Cancer. *Biomed Pharmacother* (2019) 119:109105. doi: 10.1016/j.biopha.2019.109105
36. Betancur PA, Abraham BJ, Yiu YY, Willingham SB, Khameneh F, Zarnegar M, et al. A CD47-Associated Super-Enhancer Links Pro-Inflammatory Signalling to CD47 Upregulation in Breast Cancer. *Nat Commun* (2017) 8:14802. doi: 10.1038/ncomms14802
37. Zhang X, Wang Y, Fan J, Chen W, Luan J, Mei X, et al. Blocking CD47 Efficiently Potentiated Therapeutic Effects of Anti-Angiogenic Therapy in non-Small Cell Lung Cancer. *J Immunother Cancer* (2019) 7:1–11. doi: 10.1186/s40425-019-0812-9
38. Lo J, Lau EYT, Ching RHH, Cheng BYL, Ma MKF, Ng IOL, et al. Nuclear Factor Kappa B-Mediated CD47 Up-Regulation Promotes Sorafenib Resistance and its Blockade Synergizes the Effect of Sorafenib in Hepatocellular Carcinoma in Mice. *Hepatology* (2015) 62:534–45. doi: 10.1002/hep.27859
39. Liu F, Dai M, Xu Q, Zhu X, Zhou Y, Jiang S, et al. SRSF10-Mediated IL1RAP Alternative Splicing Regulates Cervical Cancer Oncogenesis *via* Mil1rap-NF-κb-CD47 Axis. *Oncogene* (2018) 37:2394–409. doi: 10.1038/s41388-017-0119-6
40. Sockolosky JT, Dougan M, Ingram JR, Ho CCM, Kauke MJ, Almo SC, et al. Durable Antitumor Responses to CD47 Blockade Require Adaptive Immune Stimulation. *Proc Natl Acad Sci USA* (2016) 113:E2646–54. doi: 10.1073/pnas.1604268113
41. Casey SC, Tong L, Li Y, Do R, Walz S, Fitzgerald KN, et al. MYC Regulates the Antitumor Immune Response Through CD47 and PD-L1. *Science* (2016) 352:227–31. doi: 10.1126/science.aac9935
42. Li W, Gupta SK, Han W, Kundson RA, Nelson S, Knutson D, et al. Targeting MYC Activity in Double-Hit Lymphoma With MYC and BCL2 and/or BCL6 Rearrangements With Epigenetic Bromodomain Inhibitors. *J Hematol Oncol* (2019) 12:1–13. doi: 10.1186/s13045-019-0761-2
43. Noman MZ, Van Moer K, Marani V, Gemmill RM, Tranchevent L-C, Azuaje F, et al. CD47 is a Direct Target of SNAI1 and ZEB1 and its Blockade Activates the Phagocytosis of Breast Cancer Cells Undergoing EMT. *Oncoimmunology* (2018) 7:1–9. doi: 10.1080/2162402X.2017.1345415
44. Zhang H, Lu H, Xiang L, Bullen JW, Zhang C, Samanta D, et al. HIF-1 Regulates CD47 Expression in Breast Cancer Cells to Promote Evasion of Phagocytosis and Maintenance of Cancer Stem Cells. *Proc Natl Acad Sci USA* (2015) 112:E6215–23. doi: 10.1073/pnas.1520032112
45. Gowda P, Patrick S, Singh A, Sheikh T, Sen E. Mutant Isocitrate Dehydrogenase 1 Disrupts PKM2-β-Catenin-BRG1 Transcriptional Network-Driven CD47 Expression. *Mol Cell Biol* (2018) 38:e00001–18. doi: 10.1128/MCB.00001-18
46. Suzuki S, Yokobori T, Tanaka N, Sakai M, Sano A, Inose T, et al. CD47 Expression Regulated by the miR-133a Tumor Suppressor is a Novel Prognostic Marker in Esophageal Squamous Cell Carcinoma. *Oncol Rep* (2012) 28:465–72. doi: 10.3892/or.2012.1831
47. Li H, Wang Y, Li YZ. MicroRNA-133a Suppresses the Proliferation, Migration, and Invasion of Laryngeal Carcinoma Cells by Targeting CD47. *Tumor Biol* (2016) 37:16103–13. doi: 10.1007/s13277-016-5451-x
48. Huang W, Wang W-T, Fang K, Chen Z-H, Sun Y-M, Han C, et al. MIR-708 Promotes Phagocytosis to Eradicate T-ALL Cells by Targeting CD47. *Mol Cancer* (2018) 17:12. doi: 10.1186/s12943-018-0768-2
49. Sun S, Hang T, Zhang B, Zhu L, Wu Y, Lv X , et al. MiRNA-708 Functions as a Tumor Suppressor in Colorectal Cancer by Targeting ZEB1 Through Akt/mTOR Signaling Pathway. *Am J Transl Res* (2019) 11(9): 5338–56. doi: 10.3892/ol.2017.6429.
50. Rastgoo N, Wu J, Liu A, Pourabdollah M, Atenafu EG, Reece D, et al. Targeting CD47/TNFAIP8 by miR-155 Overcomes Drug Resistance and Inhibits Tumor Growth Through Induction of Phagocytosis and Apoptosis in Multiple Myeloma. *Haematologica* (2020) 105(12):2813–23. doi: 10.3324/haematol.2019.227579
51. Zhao Y, Yu X, Tang H, Han R, Wang X, Wang J, et al. MicroRNA-200a Promotes Phagocytosis of Macrophages and Suppresses Cell Proliferation, Migration, and Invasion in Nasopharyngeal Carcinoma by Targeting Cd47. *BioMed Res Int* (2020) 2022:13. doi: 10.1155/2020/3723781
52. Yang SY, Choi SA, Lee JY, Park A-K, Wang K-C, Phi JH, et al. miR-192 Suppresses Leptomeningeal Dissemination of Medulloblastoma by Modulating Cell Proliferation and Anchoring Through the Regulation of DHFR, Integrins, and CD47. *Oncotarget* (2015) 6:43712–30. doi: 10.18632/oncotarget.6227
53. Xi Q, Zhang J, Yang G, Zhang L, Chen Y, Wang C, et al. Restoration of miR-340 Controls Pancreatic Cancer Cell CD47 Expression to Promote Macrophage Phagocytosis and Enhance Antitumor Immunity. *J Immunother Cancer* (2020) 8:e000253. doi: 10.1136/jitc-2019-000253
54. Jain S, Van Scoyk A, Morgan EA, Matthews A, Stevenson K, Newton G, et al. Targeted Inhibition of CD47-SIRPa Requires Fc-FcgR Interactions to Maximize Activity in T-Cell Lymphomas. *Blood* (2019) 134:1430–40. doi: 10.1182/blood.2019001744
55. Kauder SE, Kuo TC, Harrabi O, Chen A, Sangalang E, Doyle L, et al. ALX148 Blocks CD47 and Enhances Innate and Adaptive Antitumor Immunity With a Favorable Safety Profile. *PloS One* (2018) 13:e0201832. doi: 10.1371/journal.pone.0201832
56. Liu X, Pu Y, Cron K, Deng L, Kline J, Frazier WA, et al. CD47 Blockade Triggers T Cell-Mediated Destruction of Immunogenic Tumors. *Nat Med* (2015) 21:1209–15. doi: 10.1038/nm.3931
57. Xu L, Wang S, Li J, Li B. Cd47/Sirpα Blocking Enhances CD19/CD3-Bispecific T Cell Engager Antibody-Mediated Lysis of B Cell Malignancies. *Biochem Biophys Res Commun* (2019) 509:739–45. doi: 10.1016/j.bbrc.2018.12.175
58. Schwartz AL, Nath PR, Allgauer M, Lessey-Morillon EC, Sipes JM, Ridnour LA, et al. Antisense Targeting of CD47 Enhances Human Cytotoxic T-Cell Activity and Increases Survival of Mice Bearing B16 Melanoma When Combined With Anti-CTLA4 and Tumor Irradiation. *Cancer Immunol Immunother* (2019) 68:1805–17. doi: 10.1007/s00262-019-02397-7
59. Schürch CM, Roelli MA, Forster S, Wasmer M-H, Brühl F, Maire RS, et al. Targeting CD47 in Anaplastic Thyroid Carcinoma Enhances Tumor Phagocytosis by Macrophages and Is a Promising Therapeutic Strategy. *Thyroid* (2019) 29:979–92. doi: 10.1089/thy.2018.0555
60. Uno S, Kinoshita Y, Azuma Y, Tsunenari T, Yoshimura Y, Iida S, et al. Antitumor Activity of a Monoclonal Antibody Against CD47 in Xenograft Models of Human Leukemia. *Oncol Rep* (2007) 17:1189–94. doi: 10.3892/or.17.5.1189
61. Vaeteewoottacharn K, Kariya R, Pothipan P, Fujikawa S, Pairojkul C, Waraasawapati S, et al. Attenuation of CD47-Sirpα Signal in Cholangiocarcinoma Potentiates Tumor-Associated Macrophage-Mediated Phagocytosis and Suppresses Intrahepatic Metastasis. *Transl Oncol* (2019) 12:217–25. doi: 10.1016/j.tranon.2018.10.007
62. Olsson M, Bruhns P, Frazier WA, Ravetch JV, Oldenborg PA. Platelet Homeostasis is Regulated by Platelet Expression of CD47 Under Normal Conditions and in Passive Immune Thrombocytopenia. *Blood* (2005) 105:3577–82. doi: 10.1182/blood-2004-08-2980
63. Oldenborg PA, Gresham HD, Chen Y, Izui S, Lindberg FP. Lethal Autoimmune Hemolytic Anemia in CD47-Deficient Nonobese Diabetic (NOD) Mice. *Blood* (2002) 99:3500–4. doi: 10.1182/blood.V99.10.3500
64. Manna PP, Frazier WA. The Mechanism of CD47-Dependent Killing of T Cells: Heterotrimeric G I -Dependent Inhibition of Protein Kinase a. *J Immunol* (2003) 170:3544–53. doi: 10.4049/jimmunol.170.7.3544
65. Leclair P, Liu C-C, Monajemi M, Reid GS, Sly LM, Lim CJ, et al. CD47-Ligation Induced Cell Death in T-Acute Lymphoblastic Leukemia Article. *Cell Death Dis* (2018) 9:544. doi: 10.1038/s41419-018-0601-2
66. Sikic BI, Lakhani N, Patnaik A, Shah SA, Chandana SR, Rasco D, et al. First-In-Human, First-in-Class Phase I Trial of the Anti-CD47 Antibody Hu5F9-G4 in Patients With Advanced Cancers. *J Clin Oncol* (2019) 37:946–53. doi: 10.1200/JCO.18.02018
67. Petrova PS, Viller NN, Wong M, Pang X, Lin GHY, Dodge K, et al. TTI-621 (Sirpαfc): A CD47-Blocking Innate Immune Checkpoint Inhibitor With Broad Antitumor Activity and Minimal Erythrocyte Binding. *Clin Cancer Res* (2017) 23:1068–79. doi: 10.1158/1078-0432.CCR-16-1700

68. Chao MP, Jaiswal S, Weissman-Tsukamoto R, Alizadeh AA, Gentles AJ, Volkmer J, et al. Calreticulin is the Dominant Pro-Phagocytic Signal on Multiple Human Cancers and is Counterbalanced by CD47. *Sci Transl Med* (2010) 2(63):63ra94. doi: 10.1126/scitranslmed.3001375
69. Bouwstra R, van Meerten T, Bremer E. Does Cancer Cell-Expressed SLAMF7 Impact on CD47-Mediated Phagocytosis? *Mol Cell Oncol* (2019) 6:1–3. doi: 10.1080/23723556.2019.1600349
70. Yamao T, Noguchi T, Takeuchi O, Nishiyama U, Morita H, Hagiwara T, et al. Negative Regulation of Platelet Clearance and of the Macrophage Phagocytic Response by the Transmembrane Glycoprotein SHPS-1. *J Biol Chem* (2002) 277:39833–9. doi: 10.1074/jbc.M203287200
71. Tsao LC, Crosby EJ, Trotter TN, Agarwal P, Hwang B-J, Acharya C, et al. CD47 Blockade Augmentation of Trastuzumab Antitumor Efficacy Dependent on Antibody-Dependent Cellular Phagocytosis. *JCI Insight* (2019) 4:1–21. doi: 10.1172/jci.insight.131882
72. Puro RJ, Bouchlaka MN, Hiebsch RR, Capoccia BJ, Donio MJ, Manning PT, et al. Development of AO-176, a Next-Generation Humanized Anti-CD47 Antibody With Novel Anticancer Properties and Negligible Red Blood Cell Binding. *Mol Cancer Ther* (2020) 19:835–46. doi: 10.1158/1535-7163.MCT-19-1079
73. Richards J, Bouchlaka MN, Puro RJ, Capoccia BJ, Hiebsch RR, Donio MJ, et al. Highly Differentiated Anti-CD47 Antibody, AO-176, Potently Inhibits Hematologic Malignancies Alone and in Combination. *Blood* (2019) 134:1844–4. doi: 10.1182/blood-2019-126298
74. Liu J, Wang L, Zhao F, Tseng S, Narayanan C, Shura L, et al. Pre-Clinical Development of a Humanized Anti-CD47 Antibody With Anti-Cancer Therapeutic Potential. *PloS One* (2015) 10:1–23. doi: 10.1371/journal.pone.0137345
75. Gholamin S, Mitra SS, Feroze AH, Liu J, Kahn SA, Zhang M, et al. Disrupting the CD47-Sirpα Anti-Phagocytic Axis by a Humanized Anti-CD47 Antibody is an Efficacious Treatment for Malignant Pediatric Brain Tumors. *Sci Transl Med* (2017) 9:eaaf2968. doi: 10.1126/scitranslmed.aaf2968
76. Voets E, Paradé M, Hulsik DL, Spijkers S, Janssen W, Rens J, et al. Functional Characterization of the Selective Pan-Allele Anti-Sirpα Antibody ADU-1805 That Blocks the Sirpα-CD47 Innate Immune Checkpoint. *J Immunother Cancer* (2019) 7:340. doi: 10.1186/s40425-019-0772-0
77. Champiat S, Cassier PA, Kotecki N, Korakis I, Vinceneux A, Jungels C, et al. Safety, Pharmacokinetics, Efficacy, and Preliminary Biomarker Data of First-in-Class BI 765063, a Selective Sirpα Inhibitor: Results of Monotherapy Dose Escalation in Phase 1 Study in Patients With Advanced Solid Tumors. *J Clin Oncol* (2021) 39:2623. doi: 10.1200/JCO.2021.39.15_suppl.2623
78. Chan H, Trout C, Mikolon D, Adams P, Guzman R, Fenalti G, et al. Discovery and Preclinical Characterization of CC-95251, an Anti-Sirpα Antibody That Enhances Macrophage-Mediated Phagocytosis of Non-Hodgkin Lymphoma (NHL) Cells When Combined With Rituximab. *Blood* (2021) 138:2271. doi: 10.1182/blood-2021-147262
79. Murata Y, Tanaka D, Hazama D, Yanagita T, Saito Y, Kotani T, et al. Anti-Human Sirpα Antibody is a New Tool for Cancer Immunotherapy. *Cancer Sci* (2018) 109:1300–8. doi: 10.1111/cas.13548
80. Sakamoto M, Murata Y, Tanaka D, Kakuchi Y, Okamoto T, Hazama D, et al. Anticancer Efficacy of Monotherapy With Antibodies to Sirpα/Sirpβ1 Mediated by Induction of Antitumorigenic Macrophages. *Proc Natl Acad Sci USA* (2022) 119:1–10. doi: 10.1073/pnas.2109923118
81. Seiffert M, Brossart P, Cant C, Cella M, Colonna M, Brugger W, et al. Signal-Regulatory Protein α (Sirpα) But Not Sirpβ is Involved in T-Cell Activation, Binds to CD47 With High Affinity, and is Expressed on Immature CD34 +CD38–hematopoietic Cells. *Blood* (2001) 97:2741–9. doi: 10.1182/blood.V97.9.2741
82. Wu Z, Weng L, Zhang T, Tian H, Fang L, Teng H, et al. Identification of Glutaminyl Cyclase Isoenzyme isoQC as a Regulator of Sirpα-CD47 Axis. *Cell Res* (2019) 29:502–5. doi: 10.1038/s41422-019-0177-0
83. Logtenberg MEW, Jansen JHM, Raaben M, Toebes M, Franke K, Brandsma AM, et al. Glutaminyl Cyclase is an Enzymatic Modifier of the CD47- Sirpα Axis and a Target for Cancer Immunotherapy. *Nat Med* (2019) 25:612–9. doi: 10.1038/s41591-019-0356-z
84. Baumann N, Rösner T, Jansen JHM, Chan C, Eichholz KM, Klausz K, et al. Enhancement of EGFR Antibody Tumor Immunotherapy by Glutaminyl Cyclase Inhibition to Interfere With CD47/Sirpα Interactions. *Cancer Sci* (2021) 112:3029–40. doi: 10.1111/cas.14999
85. Wang H, Sun Y, Zhou X, Chen C, Jiao L, Li W, et al. Cd47/Sirpα Blocking Peptide Identification and Synergistic Effect With Irradiation for Cancer Immunotherapy. *J Immunother Cancer* (2020) 8:1–13. doi: 10.1136/jitc-2020-000905
86. Oronsky B, Cabrales P, Caroen S, Guo X, Scribner C, Oronsky A, et al. RRx-001, a Downregulator of the CD47- Sirpα Checkpoint Pathway, Does Not Cause Anemia or Thrombocytopenia. *Expert Opin Drug Metab Toxicol* (2021) 17:355–7. doi: 10.1080/17425255.2021.1876025
87. Miller TW, Amason JD, Garcin ED, Lamy L, Dranchak PK, Macarthur R, et al. Quantitative High-Throughput Screening Assays for the Discovery and Development of Sirpα-CD47 Interaction Inhibitors. *PloS One* (2019) 14: e0218897. doi: 10.1371/journal.pone.0218897
88. Yu W-B, Ye Z-H, Chen X, Shi J-J, Lu J-J. The Development of Small-Molecule Inhibitors Targeting CD47. *Drug Discovery Today* (2021) 26:561–8. doi: 10.1016/j.drudis.2020.11.003
89. van Rees DJ, Brinkhaus M, Klein B, Verkuijlen P, Tool ATJ, Schornagel K, et al. Sodium Stibogluconate and CD47-Sirpα Blockade Overcome Resistance of Anti-CD20-Opsonized B Cells to Neutrophil Killing. *Blood Adv* (2021) 6(7):2156–66. doi: 10.1182/bloodadvances.2021005367
90. Läubli H, Pearce OMT, Schwarz F, Siddiqui SS, Deng L, Stanczak MA, et al. Engagement of Myelomonocytic Siglecs by Tumor-Associated Ligands Modulates the Innate Immune Response to Cancer. *Proc Natl Acad Sci USA* (2014) 111:14211–6. doi: 10.1073/pnas.1409580111
91. Santegoets KCM, Gielen PR, Büll C, Schulte BM, Kers-Rebel ED, Küsters B, et al. Expression Profiling of Immune Inhibitory Siglecs and Their Ligands in Patients With Glioma. *Cancer Immunol Immunother* (2019) 68:937–49. doi: 10.1007/s00262-019-02332-w
92. Go S, Sato C, Yin J, Kannagi R, Kitajima K. Hypoxia-Enhanced Expression of Free Deaminoneuraminic Acid in Human Cancer Cells. *Biochem Biophys Res Commun* (2007) 357:537–42. doi: 10.1016/j.bbrc.2007.03.181
93. Seales EC, Jurado GA, Singhal A, Bellis SL. Ras Oncogene Directs Expression of a Differentially Sialylated, Functionally Altered β1 Integrin. *Oncogene* (2003) 22:7137–45. doi: 10.1038/sj.onc.1206834
94. Sproviero D, Julien S, Burford B, Taylor-Papadimitriou J, Burchell JM. Cyclooxygenase-2 Enzyme Induces the Expression of the -2,3-Sialyltransferase-3 (ST3Gal-I) in Breast Cancer. *J Biol Chem* (2012) 287:44490–7. doi: 10.1074/jbc.M112.425827
95. Zhou H, Li Y, Liu B, Shan Y, Li Y, Zhao L, et al. Downregulation of miR-224 and Let-7i Contribute to Cell Survival and Chemoresistance In Chronic Myeloid Leukemia Cells by Regulating ST3GAL IV Expression. *Gene* (2017) 626:106–18. doi: 10.1016/j.gene.2017.05.030
96. Wu H, Shi X-L, Zhang H-J, Song Q-J, Yang X-B, Hu W-D, et al. Overexpression of ST3Gal-I Promotes Migration and Invasion of HCCLM3 *In Vitro* and Poor Prognosis in Human Hepatocellular Carcinoma. *Onco Targets Ther* (2016) 9:2227–36. doi: 10.2147/OTT.S96510
97. Videira PA, Correia M, Malagolini N, Crespo HJ, Ligeiro D, Calais FM, et al. ST3Gal.I Sialyltransferase Relevance in Bladder Cancer Tissues and Cell Lines. *BMC Cancer* (2009) 9:357. doi: 10.1186/1471-2407-9-357
98. Pérez-Garay M, Arteta B, Llop E, Cobler L, Pagès L, Ortiz R, et al. α2,3-Sialyltransferase ST3Gal IV Promotes Migration and Metastasis in Pancreatic Adenocarcinoma Cells and Tends to be Highly Expressed in Pancreatic Adenocarcinoma Tissues. *Int J Biochem Cell Biol* (2013) 45:1748–57. doi: 10.1016/j.biocel.2013.05.015
99. Pillai S, Netravali IA, Cariappa A, Mattoo H. Siglecs and Immune Regulation. *Annu Rev Immunol* (2012) 30:357–92. doi: 10.1146/annurev-immunol-020711-075018
100. Macauley MS, Crocker PR, Paulson JC. Siglec-Mediated Regulation of Immune Cell Function in Disease. *Nat Rev Immunol* (2014) 14:653–66. doi: 10.1038/nri3737
101. Büll C, Heise T, Adema GJ, Boltje TJ. Sialic Acid Mimetics to Target the Sialic Acid – Siglec Axis. *Trends Biochem Sci* (2016) 41:519–31. doi: 10.1016/j.tibs.2016.03.007
102. Nicoll G, Ni J, Liu D, Klenerman P, Munday J, Dubock S, et al. Identification and Characterization of a Novel Siglec, Siglec-7, Expressed by Human Natural Killer Cells and Monocytes. *J Biol Chem* (1999) 274:34089–95. doi: 10.1074/jbc.274.48.34089

103. Angata T, Varki A. Cloning, Characterization, and Phylogenetic Analysis of Siglec-9, a New Member of the CD33-Related Group of Siglecs: Evidence for Co-Evolution With Sialic Acid Synthesis Pathways. *J Biol Chem* (2000) 275:22127–35. doi: 10.1074/jbc.M002775200
104. Zhang JQ, Nicoll G, Jones C, Crocker PR. Siglec-9, a Novel Sialic Acid Binding Member of the Immunoglobulin Superfamily Expressed Broadly on Human Blood Leukocytes. *J Biol Chem* (2000) 275:22121–6. doi: 10.1074/jbc.M002788200
105. Xiao H, Woods EC, Vukojicic P, Bertozzi CR. Precision Glycocalyx Editing as a Strategy for Cancer Immunotherapy. *Proc Natl Acad Sci USA* (2016) 113:10304–9. doi: 10.1073/pnas.1608069113
106. Zhang J, Mai S, Chen H-M, Kang K, Li XC, Chen S-H, et al. Leukocyte Immunoglobulin-Like Receptors in Human Diseases: An Overview of Their Distribution, Function, and Potential Application for Immunotherapies. *J Leukoc Biol* (2017) 102:351–60. doi: 10.1189/jlb.5MR1216-534R
107. Fanger NA, Cosman D, Peterson L, Braddy SC, Maliszewski CR, Borges L, et al. The MHC Class I Binding Proteins LIR-1 and LIR-2 Inhibit Fe Receptor-Mediated Signaling in Monocytes. *Eur J Immunol* (1998) 28:3423–34. doi: 10.1002/(SICI)1521-4141(199811)28:11<3423::AID-IMMU3423>3.0.CO;2-2
108. Jones DC, Kosmoliaptsis V, Apps R, Lapaque N, Smith I, Kono A, et al. HLA Class I Allelic Sequence and Conformation Regulate Leukocyte Ig-Like Receptor Binding. *J Immunol* (2011) 186:2990 LP – 2997. doi: 10.4049/jimmunol.1003078
109. Ryu M, Chen Y, Qi J, Liu J, Fan Z, Nam G, et al. LILRA3 Binds Both Classical and Non-Classical HLA Class I Molecules But With Reduced Affinities Compared to LILRB1/LILRB2: Structural Evidence. *PloS One* (2011) 6: e19245. doi: 10.1371/journal.pone.0019245
110. Barkal AA, Weiskopf K, Kao KS, Gordon SR, Rosental B, Yiu YY, et al. Engagement of MHC Class I by the Inhibitory Receptor LILRB1 Suppresses Macrophages and is a Target of Cancer Immunotherapy. *Nat Immunol* (2018) 19:76–84. doi: 10.1038/s41590-017-0004-z
111. Baudhuin J, Migraine J, Faivre V, Loumagne L, Lukaszewicz A-C, Payen D, et al. Exocytosis Acts as a Modulator of the ILT4-Mediated Inhibition of Neutrophil Functions. *Proc Natl Acad Sci USA* (2013) 110:17957–62. doi: 10.1073/pnas.1221535110
112. Sidney J, Peters B, Frahm N, Brander C, Sette A. HLA Class I Supertypes: A Revised and Updated Classification. *BMC Immunol* (2008) 9:1. doi: 10.1186/1471-2172-9-1
113. Shiroishi M, Kuroki K, Rasubala L, Tsumoto K, Kumagai I, Kurimoto E, et al. Structural Basis for Recognition of the Nonclassical MHC Molecule HLA-G by the Leukocyte Ig-Like Receptor B2 (LILRB2/LIR2/ILT4/CD85d). *Proc Natl Acad Sci USA* (2006) 103:16412–7. doi: 10.1073/pnas.0605228103
114. Yie S, Yang H, Ye S-R, Li K, Dong D-D, Lin X-M, et al. Expression of Human Leucocyte Antigen G (HLA-G) is Associated With Prognosis in non-Small Cell Lung Cancer. *Lung Cancer* (2007) 58:267–74. doi: 10.1016/j.lungcan.2007.06.011
115. He X, Dong DD, Yie S-M, Yang H, Cao M, Ye S-R, et al. HLA-G Expression in Human Breast Cancer: Implications for Diagnosis and Prognosis, and Effect on Allocytotoxic Lymphocyte Response After Hormone Treatment *In Vitro*. *Ann Surg Oncol* (2010) 17:1459–69. doi: 10.1245/s10434-009-0891-9
116. Lefebvre S, Antoine M, Uzan S, McMaster M, Dausset J, Carosella ED, et al. Specific Activation of the non-Classical Class I Histocompatibility HLA-G Antigen and Expression of the ILT2 Inhibitory Receptor in Human Breast Cancer. *J Pathol* (2002) 196:266–74. doi: 10.1002/path.1039
117. Guo Z-Y, LV Y-G, Wang L, Shi S-J, Yang F, Zheng G-X, et al. Predictive Value of HLA-G and HLA-E in the Prognosis of Colorectal Cancer Patients. *Cell Immunol* (2015) 293:10–6. doi: 10.1016/j.cellimm.2014.10.003
118. Yie S-M, Yang H, Ye S-R, Li K, Dong D-D, Lin X-M, et al. Expression of Human Leukocyte Antigen G (HLA-G) Correlates With Poor Prognosis in Gastric Carcinoma. *Ann Surg Oncol* (2007) 14:2721–9. doi: 10.1245/s10434-007-9464-y
119. Yie S-M, Yang H, Ye S-R, Li K, Dong D-D, Lin X-M, et al. Expression of HLA-G is Associated With Prognosis in Esophageal Squamous Cell Carcinoma. *Am J Clin Pathol* (2007) 128:1002–9. doi: 10.1309/JNCW1QLDFB6AM9WE
120. Ibrahim EC, Aractingi S, Allory Y, Borrini F, Dupuy A, Duvillard P, et al. Analysis of HLA Antigen Expression in Benign and Malignant Melanocytic Lesions Reveals That Upregulation of HLA-G Expression Correlates With Malignant Transformation, High Inflammatory Infiltration and HLA-A1 Genotype. *Int J Cancer* (2004) 108:243–50. doi: 10.1002/ijc.11456
121. Wang Y, Ye Z, Meng X-Q, Zheng S-S. Expression of HLA-G in Patients With Hepatocellular Carcinoma. *Hepatobil Pancreat Dis Int* (2011) 10:158–63. doi: 10.1016/S1499-3872(11)60025-8
122. Guo QY, Chen BG, Ruan YY, Lin A, Yan WH. HLA-G Expression is Irrelevant to Prognosis in Patients With Acute Myeloid Leukemia. *Leuk Res* (2011) 35:1350–4. doi: 10.1016/j.leukres.2011.05.036
123. Własiuk P, Tomczak W, Zając M, Dmoszyńska A, Giannopoulos K. Total Expression of HLA-G and TLR-9 in Chronic Lymphocytic Leukemia Patients. *Hum Immunol* (2013) 74:1592–7. doi: 10.1016/j.humimm.2013.08.277
124. PEREZ-CHACON G, Rosado S, Rebolleda N, Losada-Fernandez I, Vargas JA, Morado M, et al. Prognostic Irrelevance of HLA-G in B-Cell Chronic Lymphocytic Leukemia. *Int J Lab Hematol* (2009) 31:327–37. doi: 10.1111/j.1751-553X.2008.01030.x
125. Zhang Z, Hatano H, Shaw J, Nordkamp MO, Jiang G, Li D, et al. The Leukocyte Immunoglobulin-Like Receptor Family Member LILRB5 Binds to HLA-Class I Heavy Chains. *PloS One* (2015) 10:1–15. doi: 10.1371/journal.pone.0129063
126. Wang Y, Jönsson F. Expression, Role, and Regulation of Neutrophil Fcγ Receptors. *Front Immunol* (2019) 10:1–13. doi: 10.3389/fimmu.2019.01958
127. Kerst JM, van de Winkel JG, Evans AH, de Haas M, Slaper-Cortenbach IC, de Wit TP, et al. Granulocyte Colony-Stimulating Factor Induces Hfcγri (CD64 Antigen)- Positive Neutrophils *via* an Effect on Myeloid Precursor Cells. *Blood* (1993) 81:1457–64. doi: 10.1182/blood.V81.6.1457.1457
128. Treffers LW, Zhao XW, van der Heijden J, Nagelkerke SQ, van Rees DJ, Gonzalez P, et al. Genetic Variation of Human Neutrophil Fcγ Receptors and Sirpα in Antibody-Dependent Cellular Cytotoxicity Towards Cancer Cells. *Eur J Immunol* (2018) 48:344–54. doi: 10.1002/eji.201747215
129. Schneider-Merck T, van Bueren JJL, Berger S, Rossen K, van Berkel PHC, Derer S, et al. Human IgG2 Antibodies Against Epidermal Growth Factor Receptor Effectively Trigger Antibody-Dependent Cellular Cytotoxicity But, in Contrast to IgG1, Only by Cells of Myeloid Lineage. *J Immunol* (2010) 184:512–20. doi: 10.4049/jimmunol.0900847
130. van der Heijden J, Nagelkerke S, Zhao X, Geissler J, Rispens T, van den Berg TK, et al. Haplotypes of Fcγriia and Fcγriiib Polymorphic Variants Influence IgG-Mediated Responses in Neutrophils. *J Immunol* (2014) 192:2715–21. doi: 10.4049/jimmunol.1203570
131. Richards JO, Karki S, Lazar GA, Chen H, Dang W, Desjarlais JR, et al. Optimization of Antibody Binding to Fcγriia Enhances Macrophage Phagocytosis of Tumor Cells. *Mol Cancer Ther* (2008) 7:2517–27. doi: 10.1158/1535-7163.MCT-08-0201
132. Derer S, Glorius P, Schlaeth M, Lohse S, Klausz K, Muchhal U, et al. Increasing Fcaγriia Affinity of an Fcaγriii-Optimized Anti-EGFR Antibody Restores Neutrophil-Mediated Cytotoxicity. *MAbs* (2014) 6:409–21. doi: 10.4161/mabs.27457
133. Brandsma AM, Bondza S, Evers M, Koutstaal R, Nederend M, Jansen JHM, et al. Potent Fc Receptor Signaling by IgA Leads to Superior Killing of Cancer Cells by Neutrophils Compared to IgG. *Front Immunol* (2019) 10:704. doi: 10.3389/fimmu.2019.00704
134. van der Steen L, Tuk CW, Bakema JE, Kooij G, Reijerkerk A, Vidarsson G, et al. Immunoglobulin A: Fcαri Interactions Induce Neutrophil Migration Through Release of Leukotriene B4. *Gastroenterology* (2009) 137:2018–2029.e3. doi: 10.1053/j.gastro.2009.06.047
135. Herr AB, Ballister ER, Bjorkman PJ. Insights Into IgA-Mediated Immune Responses From the Crystal Structures of Human Fcαri and its Complex With IgA1-Fc. *Nature* (2003) 423:614–20. doi: 10.1038/nature01685
136. Wines BD, Sardjono CT, Trist HM, Lay C-S, Hogarth PM. The Interaction of Fcαri With IgA and Its Implications for Ligand Binding by Immunoreceptors of the Leukocyte Receptor Cluster. *J Immunol* (2001) 166:1781–9. doi: 10.4049/jimmunol.166.3.1781
137. Kerntke C, Nimmerjahn F, Biburger M. There Is (Scientific) Strength in Numbers: A Comprehensive Quantitation of Fc Gamma Receptor Numbers on Human and Murine Peripheral Blood Leukocytes. *Front Immunol* (2020) 11:1–17. doi: 10.3389/fimmu.2020.00118

138. Treffers LW, van Houdt M, Bruggeman CW, Heineke MH, Zhao XW, van der Heijden J, et al. Fcγriiib Restricts Antibody-Dependent Destruction of Cancer Cells by Human Neutrophils. *Front Immunol* (2019) 9. doi: 10.3389/fimmu.2018.03124
139. Peipp M, van Bueren JJL, Schneider-Merck T, Bleeker WWK, Dechant M, Beyer T, et al. Antibody Fucosylation Differentially Impacts Cytotoxicity Mediated by NK and PMN Effector Cells. *Blood* (2008) 112:2390–9. doi: 10.1182/blood-2008-03-144600
140. Leusen JHW. IgA as Therapeutic Antibody. *Mol Immunol* (2015) 68:35–9. doi: 10.1016/j.molimm.2015.09.005
141. Dechant M, Valerius T. IgA Antibodies for Cancer Therapy. *Crit Rev Oncol Hematol* (2001) 39:69–77. doi: 10.1016/S1040-8428(01)00105-6
142. Steffen U, Koeleman CA, Sokolova MV, Bang H, Kleyer A, Rech J, et al. IgA Subclasses Have Different Effector Functions Associated With Distinct Glycosylation Profiles. *Nat Commun* (2020) 11:120. doi: 10.1038/s41467-019-13992-8
143. Mestecky J, Russell MW, Jackson S, Brown TA. The Human IgA System: A Reassessment. *Clin Immunol Immunopathol* (1986) 40(1):105–14. doi: 10.1016/0090-1229(86)90073-5
144. van Tetering G, Evers M, Chan C, Stip M, Leusen J. Fc Engineering Strategies to Advance IgA Antibodies as Therapeutic Agents. *Antibodies* (2020) 9:70. doi: 10.3390/antib9040070
145. Bruhns P, Jönsson F. Mouse and Human FcR Effector Functions. *Immunol Rev* (2015) 268:25–51. doi: 10.1111/imr.12350
146. Bakema JE, de Haij S, den Hartog-Jager CF, Bakker J, Vidarsson G, van Egmond M, et al. Signaling Through Mutants of the IgA Receptor CD89 and Consequences for Fc Receptor γ-Chain Interaction. *J Immunol* (2006) 176:3603–10. doi: 10.4049/jimmunol.176.6.3603
147. Bakema JE, Van Egmond M. The Human Immunoglobulin A Fc Receptor Fcαri: A Multifaceted Regulator of Mucosal Immunity. *Mucosal Immunol* (2011) 4:612–24. doi: 10.1038/mi.2011.36
148. Lang ML, Kerr MA. Characterization of Fcαr-Triggered Ca2+ Signals: Role in Neutrophil NADPH Oxidase Activation. *Biochem Biophys Res Commun* (2000) 276:749–55. doi: 10.1006/bbrc.2000.3542
149. Ben Mkaddem S, Rossato E, Heming N, Monteiro RC. Anti-Inflammatory Role of the IgA Fc Receptor (CD89): From Autoimmunity to Therapeutic Perspectives. *Autoimmun Rev* (2013) 12:666–9. doi: 10.1016/j.autrev.2012.10.011
150. Lämmermann T, Afonso PV, Angermann BR, Wang JM, Kastenmüller W, Parent CA, et al. Neutrophil Swarms Require LTB4 and Integrins at Sites of Cell Death *in vivo*. *Nature* (2013) 498:371–5. doi: 10.1038/nature12175
151. Waldmannová E, Caisová V, Fáberová J, Sváčková P, Kovářová M, Sváčková D, et al. The Use of Zymosan A and Bacteria Anchored to Tumor Cells for Effective Cancer Immunotherapy: B16-F10 Murine Melanoma Model. *Int Immunopharmacol* (2016) 39:295–306. doi: 10.1016/j.intimp.2016.08.004
152. Matlung HL, Babes L, Zhao XW, van Houdt M, Treffers LW, van Rees DJ, et al. Neutrophils Kill Antibody-Opsonized Cancer Cells by Trogoptosis. *Cell Rep* (2018) 23:3946–3959.e6. doi: 10.1016/j.celrep.2018.05.082
153. Lohse S, Meyer S, Meulenbroek LAPM, Jansen JHM, Nederend M, Kretschmer A, et al. An Anti-EGFR IgA That Displays Improved Pharmacokinetics and Myeloid Effector Cell Engagement *In Vivo*. *Cancer Res* (2016) 76:403–17. doi: 10.1158/0008-5472.CAN-15-1232
154. Lohse S, Loew S, Kretschmer A, Jansen JHM, Meyer S, Broeke TT, et al. Effector Mechanisms of IgA Antibodies Against CD20 Include Recruitment of Myeloid Cells for Antibody-Dependent Cell-Mediated Cytotoxicity and Complement-Dependent Cytotoxicity. *Br J Haematol* (2018) 181:413–7. doi: 10.1111/bjh.14624
155. Meyer S, Nederend M, Jansen JHM, Reiding KR, Jacobino SR, Meeldijk J, et al. Improved *In Vivo* Anti-Tumor Effects of IgA-Her2 Antibodies Through Half-Life Extension and Serum Exposure Enhancement by FcRn Targeting. *MAbs* (2016) 8:87–98. doi: 10.1080/19420862.2015.1106658
156. Evers M, Stip M, Keller K, Willemen H, Nederend M, Jansen M, et al. Anti-GD2 IgA Kills Tumors by Neutrophils Without Antibody-Associated Pain in the Treatment of High-Risk Neuroblastoma. *J Immunother Cancer* (2021) 9 (10):e003163. doi: 10.1136/jitc-2021-003163
157. Dechant M, Beyer T, Schneider-Merck T, Weisner W, Peipp M, van de Winkel JGJ, et al. Effector Mechanisms of Recombinant IgA Antibodies Against Epidermal Growth Factor Receptor. *J Immunol* (2007) 179:2936–43. doi: 10.4049/jimmunol.179.5.2936
158. Lohse S, Brunke C, Derer S, Peipp M, Boross P, Kellner C, et al. Characterization of a Mutated IgA2 Antibody of the M(1) Allotype Against the Epidermal Growth Factor Receptor for the Recruitment of Monocytes and Macrophages. *J Biol Chem* (2012) 287:25139–50. doi: 10.1074/jbc.M112.353060
159. Rouwendal GJ, van der Lee MM, Meyer S, Reiding KR, Schouten J, de Roo G, et al. A Comparison of Anti-HER2 IgA and IgG1 *In Vivo* Efficacy is Facilitated by High N-Glycan Sialylation of the IgA. *MAbs* (2016) 8:74–86. doi: 10.1080/19420862.2015.1102812
160. Pascal V, Laffleur B, Debin A, Cuvillier A, van Egmond M, Drocourt D, et al. Anti-CD20 IgA can Protect Mice Against Lymphoma Development: Evaluation of the Direct Impact of IgA and Cytotoxic Effector Recruitment on CD20 Target Cells. *Haematologica* (2012) 97:1686–94. doi: 10.3324/haematol.2011.061408
161. Huls G, Heijnen IA, Cuomo E, van der Linden J, Boel E, van de Winkel JG, et al. Antitumor Immune Effector Mechanisms Recruited by Phage Display-Derived Fully Human IgG1 and IgA1 Monoclonal Antibodies. *Cancer Res* (1999) 59:5778–84.
162. Boross P, Lohse S, Nederend M, Jansen JHM, van Tetering G. IgA EGFR Antibodies Mediate Tumour Killing *In Vivo*. *EMBO Mol Med* (2013) 5:1213–26. doi: 10.1002/emmm.201201929
163. Braster R, O'Toole T, van Egmond M. Myeloid Cells as Effector Cells for Monoclonal Antibody Therapy of Cancer. *Methods* (2014) 65:28–37. doi: 10.1016/j.ymeth.2013.06.020
164. Van Egmond M, Hanneke Van Vuuren AJ, Van De Winkel JGJ. The Human Fc Receptor for IgA (Fcαri, CD89) on Transgenic Peritoneal Macrophages Triggers Phagocytosis and Tumor Cell Lysis. *Immunol Lett* (1999) 68:83–7. doi: 10.1016/S0165-2478(99)00034-6
165. Keler T, Wallace PK, Vitale LA, Russoniello C, Sundarapandiyan K, Graziano RF, et al. Differential Effect of Cytokine Treatment on Fcα Receptor I- and Fcγ Receptor I-Mediated Tumor Cytotoxicity by Monocyte-Derived Macrophages. *J Immunol* (2000) 164:5746–52. doi: 10.4049/jimmunol.164.11.5746
166. Stockert RJ, Kressner MS, Collins JC, Sternlieb I, Morell AG. IgA Interaction With the Asialoglycoprotein Receptor. *Proc Natl Acad Sci USA* (1982) 79:6229–31. doi: 10.1073/pnas.79.20.6229
167. Lombana TN, Rajan S, Zorn JA, Mandikian D, Chen EC, Estevez A, et al. Production, Characterization, and *In Vivo* Half-Life Extension of Polymeric IgA Molecules in Mice. *MAbs* (2019) 11:1122–38. doi: 10.1080/19420862.2019.1622940
168. Van Egmond M, van Vuuren AJ, Morton HC, van Spriel AB, Shen L, Hofhuis FM, et al. Human Immunoglobulin A Receptor (Fcαri, CD89) Function in Transgenic Mice Requires Both FCR γ Chain and CR3 (CD11b/Cd18). *Blood* (1999) 93:4387–94. doi: 10.1182/blood.V93.12.4387
169. Evers M, Stip M, Keller K, Willemen H, Nederend M, Jansen M, et al. Anti-GD2 IgA Kills Tumors by Neutrophils Without Antibody-Associated Pain in the Preclinical Treatment of High-Risk Neuroblastoma. *J Immunother Cancer* (2021) 9:e003163. doi: 10.1136/jitc-2021-003163
170. Sun J, Muz B, Alhallak K, Markovic M, Gurley S, Wang Z, et al. Targeting CD47 as a Novel Immunotherapy for Multiple Myeloma. *Cancers (Basel)* (2020) 12:305. doi: 10.3390/cancers12020305
171. Martínez-Sanz P, Hoogendijk AJ, Verkuijlen PJJH, Schornagel K, van Bruggen R, van den Berg TK, et al. CD47-Sirpα Checkpoint Inhibition Enhances Neutrophil-Mediated Killing of Dinutuximab-Opsonized Neuroblastoma Cells. *Cancers (Basel)* (2021) 13:4261. doi: 10.3390/cancers13174261
172. Theruvath J, Menard M, Smith BAH, Linde MH, Coles GL, Dalton GN, et al. Anti-GD2 Synergizes With CD47 Blockade to Mediate Tumor Eradication. *Nat Med* (2022). doi: 10.1038/s41591-021-01625-x
173. Rosner T, Kahle S, Montenegro F, Matlung HL, Jansen JHM, Evers M, et al. Immune Effector Functions of Human IgG2 Antibodies Against EGFR. *Mol Cancer Ther* (2019) 18:75–88. doi: 10.1158/1535-7163.MCT-18-0341
174. Ring NG, Herndler-Brandstetter D, Weiskopf K, Shan L, Volkmer J-P, George BM, et al. Anti-Sirpα Antibody Immunotherapy Enhances Neutrophil and Macrophage Antitumor Activity. *Proc Natl Acad Sci USA* (2017) 114:E10578–85. doi: 10.1073/pnas.1710877114

175. Nath PR, Pal-Nath D, Mandal A, Cam MC, Schwartz AL, Roberts DD. Natural Killer Cell Recruitment and Activation are Regulated by CD47 Expression in the Tumor Microenvironment. *Cancer Immunol Res* (2019) 7 (9):1547–61. doi: 10.1158/2326-6066.CIR-18-0367
176. Oldham RK, Dillman RO. Monoclonal Antibodies in Cancer Therapy: 25 Years of Progress. *J Clin Oncol* (2008) 26:1774–7. doi: 10.1200/JCO.2007.15.7438
177. Carlin AF, Uchiyama S, Chang Y-C, Lewis AL, Nizet V, Varki A, et al. Molecular Mimicry of Host Sialylated Glycans Allows a Bacterial Pathogen to Engage Neutrophil Siglec-9 and Dampen the Innate Immune Response. *Blood* (2009) 113:3333–6. doi: 10.1182/blood-2008-11-187302
178. Jandus C, Boligan KF, Chijioke O, Liu H, Dahlhaus M, Démoulins T, et al. Interactions Between Siglec-7/9 Receptors and Ligands Influence NK Cell-Dependent Tumor Immunosurveillance. *J Clin Invest* (2014) 124:1810–20. doi: 10.1172/JCI65899
179. Delaveris CS, Wilk AJ, Riley NM, Stark JC, Yang SS, Rogers AJ, et al. Synthetic Siglec-9 Agonists Inhibit Neutrophil Activation Associated With COVID-19. *ACS Cent Sci* (2021) 7:650–7. doi: 10.1021/acscentsci.0c01669
180. Lizcano A, Secundino I, Döhrmann S, Corriden R, Rohena C, Diaz S, et al. Erythrocyte Sialoglycoproteins Engage Siglec-9 on Neutrophils to Suppress Activation. *Blood* (2017) 129:3100–10. doi: 10.1182/blood-2016-11-751636
181. Von Gunten S, Yousefi S, Seitz M, Jakob SM, Schaffner T, Seger R, et al. Siglec-9 Transduces Apoptotic and Nonapoptotic Death Signals Into Neutrophils Depending on the Proinflammatory Cytokine Environment. *Blood* (2005) 106:1423–31. doi: 10.1182/blood-2004-10-4112
182. McMillan SJ, Sharma RS, McKenzie EJ, Richards HE, Zhang J, Prescott A, et al. Siglec-E is a Negative Regulator of Acute Pulmonary Neutrophil Inflammation and Suppresses CD11b β2-Integrin-Dependent Signaling. *Blood* (2013) 121:2084–94. doi: 10.1182/blood-2012-08-449983
183. McMillan SJ, Sharma RS, Richards HE, Hegde V, Crocker PR. Siglec-E Promotes β2-Integrin-Dependent NADPH Oxidase Activation to Suppress Neutrophil Recruitment to the Lung. *J Biol Chem* (2014) 289:20370–6. doi: 10.1074/jbc.M114.574624
184. Ibarlucea-Benitez I, Weitzenfeld P, Smith P, Ravetch JV. Siglecs-7/9 Function as Inhibitory Immune Checkpoints *In Vivo* and can be Targeted to Enhance Therapeutic Antitumor Immunity. *Proc Natl Acad Sci USA* (2021) 118:e2107424118. doi: 10.1073/pnas.2107424118
185. Ando M, Tu W, Nishijima K, Iijima S. Siglec-9 Enhances IL-10 Production in Macrophages *via* Tyrosine-Based Motifs. *Biochem Biophys Res Commun* (2008) 369:878–83. doi: 10.1016/j.bbrc.2008.02.111
186. Tanida S, Akita K, Ishida A, Mori Y, Toda M, Inoue M, et al. Binding of the Sialic Acid-Binding Lectin, Siglec-9, to the Membrane Mucin, MUC1, Induces Recruitment of β-Catenin and Subsequent Cell Growth. *J Biol Chem* (2013) 288:31842–52. doi: 10.1074/jbc.M113.471318
187. Belisle JA, Horibata S, Jennifer GAA, Petrie S, Kapur A, André S, et al. Identification of Siglec-9 as the Receptor for MUC16 on Human NK Cells, B Cells, and Monocytes. *Mol Cancer* (2010) 9:1–14. doi: 10.1186/1476-4598-9-118
188. Beatson R, Tajadura-Ortega V, Achkova D, Picco G, Tsourouktsoglou T-D, Klausing S, et al. The Mucin MUC1 Modulates the Tumor Immunological Microenvironment Through Engagement of the Lectin Siglec-9. *Nat Immunol* (2016) 17:1273–81. doi: 10.1038/ni.3552
189. Tyler C, Kapur A, Felder M, Belisle JA, Trautman C, Gubbels JAA, et al. The Mucin MUC16 (CA125) Binds to NK Cells and Monocytes From Peripheral Blood of Women With Healthy Pregnancy and Preeclampsia. *Am J Reprod Immunol* (2012) 68:28–37. doi: 10.1111/j.1600-0897.2012.01113.x
190. Läubli H, Alisson-Silva F, Stanczak MA, Siddiqui SS, Deng L, Verhagen A, et al. Lectin Galactoside-Binding Soluble 3 Binding Protein (LGALS3BP) is a Tumor-Associated Immunomodulatory Ligand for CD33-Related Siglecs. *J Biol Chem* (2014) 289:33481–91. doi: 10.1074/jbc.M114.593129
191. Lewis Marffy AL, McCarthy AJ. Leukocyte Immunoglobulin-Like Receptors (LILRs) on Human Neutrophils: Modulators of Infection and Immunity. *Front Immunol* (2020) 11. doi: 10.3389/fimmu.2020.00857
192. Zhao Y, van Woudenbergh E, Zhu J, Heck AJR, van Kessel KPM, de Haas CJC, et al. The Orphan Immune Receptor LILRB3 Modulates Fc Receptor–Mediated Functions of Neutrophils. *J Immunol* (2020) 204:954–66. doi: 10.4049/jimmunol.1900852
193. Park M, Raftery MJ, Thomas PS, Geczy CL, Bryant K, Tedla N, et al. Leukocyte Immunoglobulin-Like Receptor B4 Regulates Key Signalling Molecules Involved in Fcγri-Mediated Clathrin-Dependent Endocytosis and Phagocytosis. *Sci Rep* (2016) 6:1–11. doi: 10.1038/srep35085
194. Lu HK, Rentero C, Raftery MJ, Borges L, Bryant K, Tedla N, et al. Leukocyte Ig-Like Receptor B4 (LILRB4) is a Potent Inhibitor of Fcγri-Mediated Monocyte Activation *via* Dephosphorylation of Multiple Kinases. *J Biol Chem* (2009) 284:34839–48. doi: 10.1074/jbc.M109.035683
195. de Goeje PL, Bezemer K, Heuvers ME, Dingemans A-MC, Groen HJ, Smit EF, et al. Immunoglobulin-Like Transcript 3 is Expressed by Myeloid-Derived Suppressor Cells and Correlates With Survival in Patients With non-Small Cell Lung Cancer. *Oncoimmunology* (2015) 4:1–11. doi: 10.1080/2162402X.2015.1014242
196. Willems AP, Sun L, Schulz MA, Tian W, Ashikov A, van Scherpenzeel M, et al. Activity of N-Acylneuraminate-9-Phosphatase (NANP) is Not Essential for *De Novo* Sialic Acid Biosynthesis. *Biochim Biophys Acta Gen Subj* (2019) 1863:1471–9. doi: 10.1016/j.bbagen.2019.05.011
197. Mandel I, Haves D, Goldshtein I, Peretz T, Alishekevitz D, Sapir Y, et al. Abstract 3266: BND-22, a First-in-Class, Anti-ILT2 Monoclonal Antibody Inhibits the Immunosuppressive Effects of HLA-G and Enhances Anti-Tumor Activity of Immune Cells in Preclinical *In Vitro*, Ex Vivo, and *In Vivo* Models. *Cancer Res* (2020) 80:3266. doi: 10.1158/1538-7445.AM2020-3266
198. Barkal AA, Brewer RE, Markovic M, Kowarsky M, Barkal SA, Zaro BW, et al. CD24 Signalling Through Macrophage Siglec-10 is a Target for Cancer Immunotherapy. *Nature* (2019) 10:392–6. doi: 10.1038/s41586-019-1456-0
199. Rillahan CD, Antonopoulos A, Lefort CT, Sonon R, Azadi P, Ley K, et al. Global Metabolic Inhibitors of Sialyl- and Fucosyltransferases. *Nat Chem Biol* (2013) 8:661–8. doi: 10.1038/nchembio.999
200. Tzatzarakis E, Hissa B, Reissfelder C, Schölch S. The Overall Potential of CD47 in Cancer Immunotherapy: With a Focus on Gastrointestinal Tumors. *Expert Rev Anticancer Ther* (2019) 19:993–9. doi: 10.1080/14737140.2019.1689820
201. Ma L, Zhu M, Gai J, Li G, Chang Q, Qiao P, et al. Preclinical Development of a Novel CD47 Nanobody With Less Toxicity and Enhanced Anti-Cancer Therapeutic Potential. *J Nanobiotechnol* (2020) 18:1–15. doi: 10.1186/s12951-020-0571-2
202. Piccione EC, Juarez S, Liu J, Tseng S, Ryan CE, Narayanan C, et al. A Bispecific Antibody Targeting CD47 and CD20 Selectively Binds and Eliminates Dual Antigen Expressing Lymphoma Cells. *MAbs* (2015) 7:946–56. doi: 10.1080/19420862.2015.1062192
203. Fischer N, Elson G, Magistrelli G, Dheilly E, Fouque N, Laurendon A, et al. Exploiting Light Chains for the Scalable Generation and Platform Purification of Native Human Bispecific IgG. *Nat Commun* (2015) 6:1–12. doi: 10.1038/ncomms7113
204. Dheilly E, Dheilly E, Moine V, Broyer L, Salgado-Pires S, Johnson Z, et al. Selective Blockade of the Ubiquitous Checkpoint Receptor CD47 Is Enabled by Dual-Targeting Bispecific Antibodies. *Mol Ther* (2017) 25:523–33. doi: 10.1016/j.ymthe.2016.11.006
205. Hatterer E, Chauchet X, Richard F, Barba L, Moine V, Chatel L, et al. Targeting a Membrane-Proximal Epitope on Mesothelin Increases the Tumoricidal Activity of a Bispecific Antibody Blocking CD47 on Mesothelin-Positive Tumors. *MAbs* (2020) 12:1739408. doi: 10.1080/19420862.2020.1739408
206. Imbert PRC, Saric A, Pedram K, Bertozzi CR, Grinstein S, Freeman SA, et al. An Acquired and Endogenous Glycocalyx Forms a Bidirectional 'Don't Eat' and 'Don't Eat Me' Barrier to Phagocytosis. *Curr Biol* (2021) 31:77–89.e5. doi: 10.1016/j.cub.2020.09.082
207. Gentles AJ, Gentles AJ, Newman AM, Liu CL, Bratman SV, Feng W, et al. The Prognostic Landscape of Genes and Infiltrating Immune Cells Across Human Cancers. *Nat Med* (2015) 21:938–45. doi: 10.1038/nm.3909

Conflict of Interest: The authors declare that the research was conducted in the absence of any commercial or financial relationships that could be construed as a potential conflict of interest.

this article, or claim that may be made by its manufacturer, is not guaranteed or endorsed by the publisher.

GLOSSARY

ADCC	Antibody-dependent cellular cytotoxicity
ADCP	Antibody-dependent cellular phagocytosis
AML	Acute myeloid leukemia
APMAP	Adipocyte plasma membrane-associated protein
B2M	β2 microglobulin
BiTE	Bispecific T cell engager
BRD4	Bromodomain-containing protein 4
BRG1	Brahma-Related Gene-1
BsAb	Bispecific antibody
CD47	Cluster of differentiation 47
CTLA-4	Cytotoxic T-lymphocyte-associated protein 4
DVD-Ig	Dual variable domain immunoglobulin
GNE	UDP-N-acetylglucosamine 2-epimerase/N-acetylmannosamine kinase
GPI	Glycosylphosphatidylinositol
HCC	Hepatocellular carcinoma
HIF-1	Hypoxia-inducible factor-1
IFN- γ	Interferon gamma
IL-1β	Interleukin-1β
IL-6	Interleukin-6
ITAM	Immunoreceptor tyrosine-based activation motif
ITIM	Immunoreceptor tyrosine-based inhibitory motif
LGALS3BP	Lectin galactoside-binding soluble 3 binding protein
LILRB	Leukocyte immunoglobulin-like receptor subfamily B
LPS	Lipopolysaccharides
mAb	Monoclonal antibody
MDSC	Myeloid derived suppressor cell
MUC1	Mucin 1
NFκB	Nuclear factor kappa-light-chain-enhancer of activated B cells
NHL	Non-Hodgkin lymphoma
NK cell	Natural killer cell
PBMC	Peripheral blood mononuclear cell
PD-1	Programmed cell death protein 1
PD-L1	Programmed death-ligand 1
PKM2	Pyruvate kinase isozymes M2
PMN	Polymorphonuclear leukocytes
QPCTL	Glutaminyl-peptide cyclotransferase-like protein
ROS	Reactive oxygen species
SHP1/2	Src homology region 2 domain-containing phosphatase-1/2
Siglec	Sialic acid-binding immunoglobulin-like lectin
SIRPα	Signal regulatory protein α
SNAI1	Snail Family Transcriptional Repressor 1
SOCS3	Suppressor of cytokine signaling 3
ST6Gal-1	2,6-sialyltransferase 1
STAT3	Signal transducer and activator of transcription 3
TAA	Tumor associated antigen
TAM	Tumor-associated macrophages
TCF4	Transcription Factor 4TCL T-cell lymphoma
TME	Tumor microenvironment
TNF-α	Tumor necrosis factor α
ZEB1	Zinc Finger E-Box Binding Homeobox 1

frontiers | Frontiers in Immunology

PERSPECTIVE
published: 13 July 2022
doi: 10.3389/fimmu.2022.940674

Next Generation CD40 Agonistic Antibodies for Cancer Immunotherapy

Ran Salomon and Rony Dahan *

Department of Systems Immunology, Weizmann Institute of Science, Rehovot, Israel

The clinical use of anti-CD40 agonist monoclonal antibodies (mAbs) is aimed at recruiting the immune system to fight the tumor cells. This approach has been demonstrated to be effective in various preclinical models. However, human CD40 Abs displayed only modest antitumor activity in cancer patients, characterized by low efficacy and dose-limiting toxicity. While recent studies highlight the importance of engineering the Fc region of human CD40 mAbs to optimize their agonistic potency, toxicity remains the main limiting factor, restricting clinical application to suboptimal doses. Here, we discuss the current challenges in realizing the full potential of CD40 mAbs in clinical practice, and describe novel approaches designed to circumvent the systemic toxicity associated with CD40 agonism.

Keywords: CD40, fc receptor, agonistic antibody, therapeutic antibody, cancer immunotherapy, bispecific antibodies (BsAbs)

OPEN ACCESS

Edited by:
Peter Boross,
Genmab, Netherlands

Reviewed by:
Ramon Arens,
Leiden University Medical Center, Netherlands
Sara Mangsbo,
Uppsala University, Sweden
Fubin Li,
Shanghai Jiao Tong University, China

***Correspondence:**
Rony Dahan
rony.dahan@weizmann.ac.il

Specialty section:
This article was submitted to B Cell Biology, a section of the journal Frontiers in Immunology

Received: *10 May 2022*
Accepted: *21 June 2022*
Published: *13 July 2022*

Citation:
Salomon R and Dahan R (2022) Next Generation CD40 Agonistic Antibodies for Cancer Immunotherapy. Front. Immunol. 13:940674. doi: 10.3389/fimmu.2022.940674

INTRODUCTION

The field of immuno-oncology has progressed steadily over the last decade. Immunotherapy has joined the ranks of surgery, chemotherapy, radiation, and targeted therapy in the arsenal of cancer treatments (1, 2). An increasing number of immune checkpoint-targeted monoclonal antibodies (mAbs) have been developed with the aim of harnessing the immune system to eradicate tumor cells (3, 4). These efforts have resulted in successful clinical application of blocking mAbs against CTLA-4 and PD-1/PD-L1 checkpoints on T lymphocytes (T cells) to induce effective tumor-eliminating immunity. However, a remaining unmet clinical challenge is to stimulate immunity against "cold" tumors, which lack significant immune infiltration at treatment onset. Agonist mAbs targeting the cluster of differentiation 40 (CD40) immune receptor emerge as a potential approach to increase the number and quality of tumor-infiltrating T cells (TILs) and, thereby, response effectiveness, either as a monotherapy or to reverse resistance to checkpoint-blocking antibodies (5–9).

CD40 is a tumor necrosis factor receptor (TNFR) superfamily member. It is expressed on antigen-presenting cells (APCs) including dendritic cells (DCs), B cells, macrophages, classical and non-classical monocytes (10–12), on a variety of non-immune cells including platelets and endothelial cells (13, 14), and on several types of tumor cells (15). CD40 plays a central role in stimulating immune synapses, including during T cell priming by APCs, when its interaction with the CD40 ligand (CD40L) licenses DCs to activate antigen-specific T cells (5, 16). This is accomplished through the upregulation of major histocompatibility complex (MHC) molecules, increased expression of the costimulatory molecules CD86/CD80, and upregulation of TNF superfamily ligands on the DC surface, as well as by secretion of

interleukin-12 (IL-12), which fuels $CD8^+$ T cell activation. Likewise, the CD40/CD40L axis plays a central role in the B-T cell immune synapse, promoting B cell activation and proliferation as well as antigen presentation (5, 6, 11, 16).

Agonistic anti-CD40 Abs are designed to mimic CD40L by crosslinking CD40 and, thereby, promote the maturation of DCs and improve their antigen presentation capabilities. This results in expansion of tumor antigen-specific cytotoxic T cells, which can lead to the eradication of tumors (5, 17, 18). Motivated by promising results in a variety of cancer animal models, several human CD40 mAbs have been developed and evaluated in clinical trials over the last two decades (6, 19–22). However, the preclinical potency has not yet been recapitulated in clinical setting and none of these mAbs has advanced beyond early trial phases. Among the challenges that were encountered during these evaluations are low detected levels of immune activation and high toxicity levels associated with the treatment. The toxicity limited the use of CD40 mAbs to suboptimal doses, resulting in insufficient immune activation and antitumor efficacy (21, 23–26). Here, we highlight key factors and cellular pathways associated with effective agonism and the observed clinical toxicity. Furthermore, we describe recent antibody-engineering approaches and treatment regimens that we find the most advanced and promising in the quest to overcome the challenges preventing the clinical use of CD40 agonistic mAbs.

HARNESSING FCγRS TO POTENTIATE THE ACTIVITY OF CD40 mAbs

Fc-gamma receptors (FcγR) are central players in the *in vivo* agonistic activity of CD40 mAbs (25, 27–29). This Fc-mediated mechanism involves higher order crosslinking of the CD40 mAbs by FcγRIIB expressed in trans by cells neighboring the CD40-expressing cells. This results in enhanced clustering of CD40 on the target cell and, consequently, increased CD40 signaling. The relatively low clinical response elicited by different anti-human CD40 mAbs (15, 19) can be attribute to the structure of their IgG scaffold, which is not optimized for FcγRIIB binding. It was demonstrated that the *in vivo* activity of human CD40 mAbs is dependent on their affinity to FcγRIIB and, notably, this activity was significantly improved by Fc engineering (25) **(Figure 1)**. Following this preclinical observation, a second generation of Fc-engineered anti-human CD40 mAbs with enhanced FcγRIIB binding are now being tested in clinical trials (25, 30–32).

One such antibody is 2141-V11. Based on selicrelumab, the original IgG2 isotype was converted into IgG1 and the affinity to FcγRIIB was selectively enhance by Fc engineering. The Fc-engineered version of this mAb displayed a significantly enhanced *in vivo* antitumor response compared to the parental

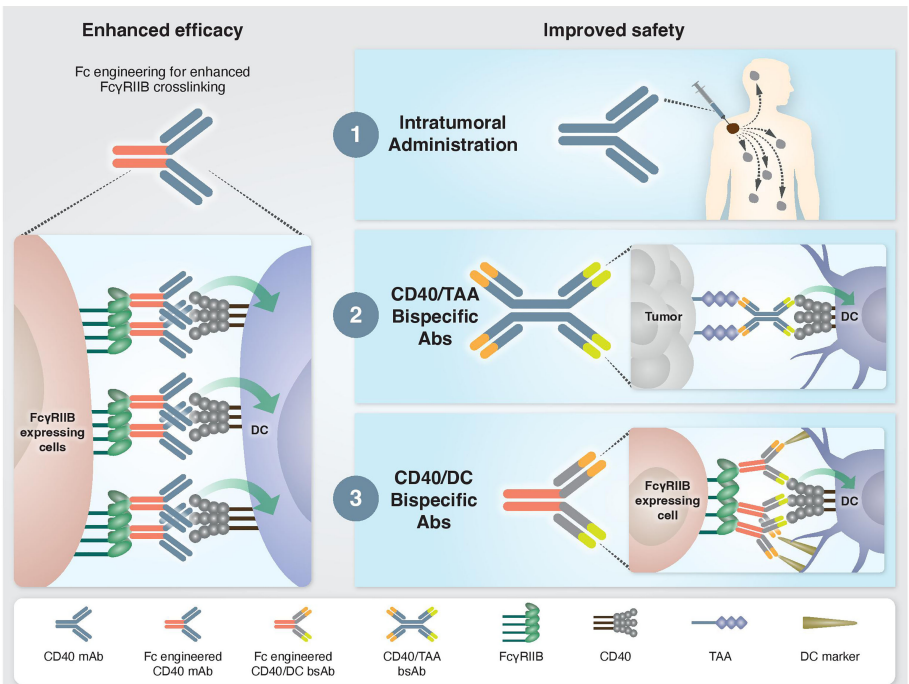

FIGURE 1 | Approaches to enhance the efficacy and safety of CD40 agonistic mAbs. Left: Enhanced CD40 agonism by Fc-engineered mAbs designed to increase FcγRIIB-mediated crosslinking. Right: Approaches to bypass treatment associated toxicities. 1) Intratumoral administration. Injection of low mAb dose directly into the tumor enables local antitumor immune activation without systemic side effects. 2) Tumor-targeted bispecific CD40 antibodies direct the agonistic antibody to the TME by targeting tumor-associated antigens, which are overexpressed and/or selectively expressed at the tumor site. 3) Dendritic cell-targeted bispecific CD40 antibodies direct the agonistic antibody to the cell types that drive treatment-associated antitumor activity but not toxicity.

IgG2 variant in multiple tumor models, includes melanoma, colon adenocarcinoma and bladder cancer (25, 30, 31). APX005M (sotigalimab) is another CD40 mAb that was Fc-engineered to increase the interaction with FcγRIIB, now evaluated in several early-phase studies (32, 33). Different Fc mutations were introduced to the IgG1-Fc scaffold of 2141-V11 and APX005M. While the binding of 2141-V11 is enhanced selectively to FcγRIIB and not to other FcγRs, APX005M engages both the inhibitory FcγRIIB and the activating FcγRIIA^{131R}. Preclinical studies showed increased *in vivo* agonistic activity for both Fc-engineered mAbs over their parental non-mutated IgG1 variant (25). However, due to the opposite effect of decreased mAb potency upon engagement with FcγRIIA, the FcγRIIB-selective enhanced Fc variant displayed superior agonistic activity.

Because crosslinking of CD40 on the membrane surface is key for the activity of CD40 agonists, various strategies to enhance CD40 receptor trimerization have been developed. These Fc-independent approaches include hinge engineering to the unique structural configuration of IgG2 subclass, which was reported to enhance CD40 agonistic activity. Mutations of specific cysteines in CD40 agonistic mAbs are used to prevent shuffling of disulfide bonds between the IgG2 hinge and CH1 regions, thus locking the hinge conformation that contributes to enhanced CD40 clustering (34, 35). Other approaches to promote CD40 receptor multimerization include the use of recombinant CD40L-based instead of antibody-based molecules (36), or utilizing Fc-docking scaffolds to multimerize anti-CD40 mAbs (37). A notable difference between these Fc-dependent and Fc-independent engineering approaches is the requirement for FcγRs engagement in addition to CD40 engagement in the former but not the latter, which may results in different biodistributions of these molecules. The consequences of these distinct properties for the mechanism and therapeutic index of these reagents should be clarified in future studies. A combination of different approaches to enhance agonism was also suggested in a study demonstrating synergistic agonist potency of a combined hinge and Fc-engineering strategy (38).

While these Fc and protein engineering strategies can improve the antitumor efficacy of CD40 agonists, the stronger potency of these next-generation agonists is accompanied by an increase in side effects and toxicity that characterize this type of immunotherapy (25, 30). Consequently, the systemic administration of these agonists is limited to suboptimal doses and their full potential could not be exploited.

SIDE EFFECTS AND TOXICITIES OF CD40 mAbs

As mentioned, human CD40 agonistic mAbs were reported to trigger severe adverse effects and toxicities. These include hepatotoxicity, cytokine release syndrome (CRS) (19, 20, 39), thrombocytopenia (19, 24, 25, 30), general hyperimmune stimulation (40), and tumor angiogenesis in response to endothelial cell activation (41). The broad expression of CD40 by various immune and non-immune cells types in the tumor and in other organs is likely to contribute to the occurrence of these side effects.

Recent studies highlighted the role of macrophages, Kupffer cells, platelets and neutrophils in mediating liver toxicity. Using a single-cell RNA sequencing approach, Siwicki et al. described a mechanistic interplay involving IFN-γ-secreting lymphocytes and IL-12-producing tissue-resident Kupffer cells, resulting in liver toxicity (42). This anti-CD40 mediated hepatotoxicity is associated with an IL-12-dependent accumulation of MHC II$^+$, CD14$^+$ and CD11b$^+$ macrophages in the liver (43). It was further shown that IL-12 and IFN-γ were not toxic by themselves and that neutrophils respond to these two cytokines by upregulation and secretion of TNF, the levels of which determine the severity of liver toxicity. Another player in the network that mediates the toxic effect of CD40 mAbs on the liver are platelets. In a recent study, we have demonstrated the causal role of macrophages and platelets in liver toxicity after CD40 treatment (44). Systemic cell depletion of macrophages or platelets completely abrogated the elevation in liver transaminases (ALT/AST) that was observed after anti-human CD40 treatment. While these findings highlight the involvement of macrophages, Kupffer cells, platelets and neutrophils, the full mechanistic interplay between these players driving liver toxicity following anti-CD40 treatment still needs to be elucidated.

In the clinic, CRS was evident within minutes to hours after CD40 mAb infusion and was associated in these patients with elevation in serum IL-6 (19). *In vivo* upregulation of intracellular IL-6 was detected by classical CD11c$^-$ monocytes in the blood, lymph nodes and spleen, after immunization with anti-human CD40 mAb in humanized CD40 mouse strain (44). This suggests monocytes as the major cell population driving IL-6 secretion.

DCs and, in particular, the conventional type-1 dendritic cells (cDC1s) are essential for CD40-targeted immunotherapy due to their key role in CD8$^+$ T cell priming and early CD4$^+$ T cell activation, which induce a strong and durable antitumor immunity (45). Unlike macrophages, monocytes and platelets that mediate hepatotoxicity, CRS and thrombocytopenia, respectively, cDC1 activation by CD40 agonist do not contribute to any of these dose-limiting toxicities.

Collectively, these findings suggest that different cellular pathways and locations are engaged by CD40 agonists, which determines the balance between antitumor immunity and side effects. Macrophages and, specifically, liver-resident Kupffer cells are the key population that is engaged by CD40 agonist to mediate hepatotoxicity, in which neutrophils and platelets have also been implicated. Other evidence suggests that IL-6 secretion by monocytes underlies CRS induced by CD40 mAbs.

APPROACHES TO INCREASE THE THERAPEUTIC WINDOW OF CD40 mAbs

Intratumoral Administration

Understanding the mechanisms driving the antitumor immunity of CD40-targeted immunotherapy, as well as those causing adverse effects, provides a rationale on how to improve the efficacy and safety profile of existing treatments. For example, the finding that

the location of immune activation is associated with distinct outcomes, i.e., antitumor activity vs. systemic toxicity, advanced approaches aiming to direct CD40 agonism selectively to the tumor microenvironment (TME) to avoid toxicity. One such strategy is an intratumoral route of mAb administration (30, 46) **(Figure 1)**. Indeed, preclinical studies demonstrated a safe profile and lack of hepatotoxicity and thrombocytopenia when anti-human CD40 mAb was administered intratumorally. Treatment resulted in T cell activation and was shown to induce abscopal effects characterized by systemic antitumor T cell activity and long-term memory response (30, 31, 46, 47). Comparison of biodistribution profiles after local or systemic anti-CD40 mAb administration in bladder cancer model revealed that local injection led to CD40 mAb accumulation in the draining lymph node and spleen, presumably because of the high density of $CD40^+$ immune cells, whereas systemic injection led to higher Ab concentration in the liver and blood circulation (47). In an early clinical study, intratumoral administration of anti-human CD40 mAb (ADC-1013) into superficial lesions was well tolerated and was accompanied by pharmacodynamic responses (48). Another advantage of local CD40 mAb administration is the avoidance of Ab sink effect by cells with high CD40 expression, mainly circulating B cells.

Tumor-Associated Antigen-Targeted Bispecific Antibodies

While intratumoral administration is a promising approach for some patients, it is not suitable for all tumors and may be limited to patients with primary or metastatic tumors near the skin, intravesical treatment of bladder cancers, and tumors that are accessible to radiographically directed therapy. This highlights the need to reduce the toxicity of CD40-targeted immunotherapy through systemic administration. One proposed solution is a bispecific antibody (bsAb) that contains a binding arm to tumor-associated antigens (TAA). The rationale behind this approach is that the anti-TAA arm will direct the antibody to the TME and activates APCs locally, thereby avoiding systemic immune stimulation and reducing toxicity **(Figure 1)**. The first developed CD40 bsAb is ABBV-428, which is constructed from a CD40 arm and a mesothelin TAA (49). This molecule was designed to engage the TME due to the overexpression of mesothelin by several types of tumor cells (50). Indeed, preclinical studies with ABBV-428 suggested less systemic toxicity with similar antitumor immunity compared to the parental monospecific CD40 mAb (49). In a phase 1 clinical trial, ABBV-428 showed a safe profile and the maximum tolerated dose was not reached. However, efficacy was very limited, with no signs of substantial response in patients (51). This outcome could be explained by low expression of mesothelin on tumor cells, that would limit bsAb accessibility to the tumor and thus its ability to crosslink the CD40 receptor, which is required for CD40 signaling (50). Indeed, it was shown in animal models that the expression levels of mesothelin on tumor cell lines dictates the antitumor activity of ABBV-428 (49).

The results of the ABBV-428 trial highlight the need for a bsAb targeting a more highly expressed TAA. 4224 is a CD40/EpCAM bsAb that displayed improved *in vivo* antitumor efficacy compared to the corresponding monospecific CD40 mAb (52). EpCAM is highly expressed on certain tumors and on tumor exosomes, which may induce cross-presentation of tumor-derived neoantigen (i.e., in exosomes or debris), resulting in better priming of tumor neoantigen-specific T cells (52). The toxic profile of 4224 compared to the parental monospecific CD40 mAb has not been reported to date.

A drawback of the CD40/TAA approach is its dependence on sufficient expression levels and density of a specific TAA, which may not be uniformly expressed across different tumor lesions and patients. This may result in variable clinical efficacy, potentially limiting the use of the compound to selective tumor types. In addition, TAA targeted by bsAbs may be required for CD40 crosslinking, similar to FcγRIIB role in neighboring cells. Therefore, their density, membrane fluidity and the binding affinity of the targeting bsAb can substantially affect the potency of these reagents. Because of these limitations, only a handful of tumor surface antigens have thus far been identified as suitable targets for CD40 bispecific antibodies.

Dendritic Cells-Targeted Bispecific Antibodies

An alternative approach that bypasses the dose-limiting toxicity is to induce CD40 agonism in a cell-specific rather than organ- or tissue-specific manner, by delivering the agonist to the cell population driving treatment efficacy but not toxicity **(Figure 1)**. As mentioned, cDC1s mediate the antitumor immunity of CD40 mAb without the toxic side effects. Harnessing this mechanistic understanding, our group recently developed Fc-engineered CD40/DC bsAbs, e.g. CD40/CD11c and CD40/CLEC9A, which exhibit preferred binding and selective activation towards cDC1 populations. This approach improved the therapeutic window of CD40-targeted immunotherapy significantly by increasing antitumor immunity and reducing systemic toxicity *in vivo* in an isogenic mouse model fully humanized for CD40 and FcγRs (44, 53). Importantly, these CD40/DC bsAbs displayed reduced binding and activation of B cells, macrophages and monocytes, the cell types that contribute to sink effect, liver toxicity and CRS. Comparing the mode of action in the TME of CD40/DC bsAb vs its parental monospecific CD40 mAb reveled similar activation of effector $CD4^+$ and $CD8^+$ T cell response, presumably the result of similar DC engagement by these two types of agonists, leading to DC maturation, expansion and subsequent T cell priming and activation (44). While the monospecific CD40 mAb induces remodeling of the cell state of non-DC $CD40^+$ myeloid and B cells in the TME, the DC-targeted bsAb lacks this activity. Despite the more restricted engagement of myeloid cell types in the tumor, the CD40/DC bsAb retains antitumor potency, further supporting the importance of activating the DC-T cell axis for the antitumor activity of CD40 agonists. While this effect was observed in multiple tests in transplantable syngeneic tumor models, further validation in additional tumor types and, eventually, in clinical settings is essential to evaluate the generalization and translational potential of this approach.

The monovalent nature of the CD40 arm in the CD40/DC bispecific format required special considerations in their design. First, these bsAbs exhibit increased sensitivity to FcγR-mediated

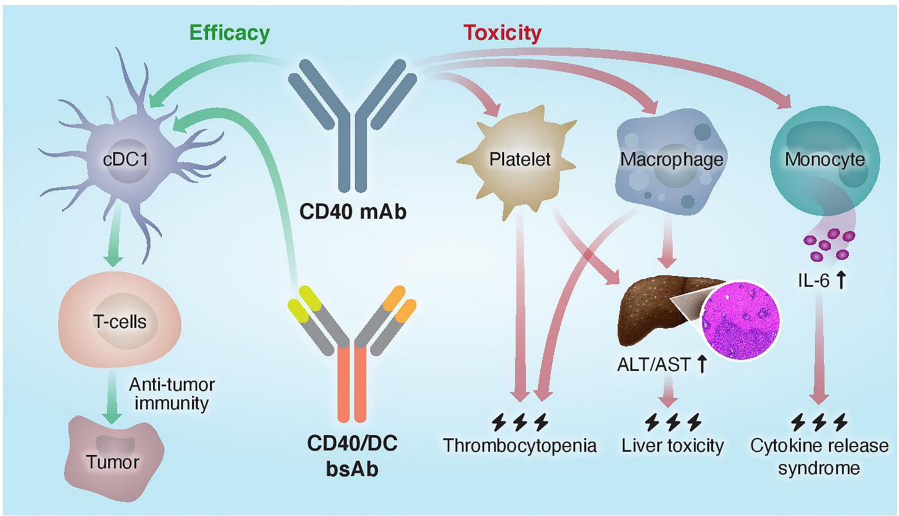

FIGURE 2 | Proposed mechanisms of mono- and bispecific CD40 agonistic antibody activity. Traditional monoclonal anti-CD40 Abs do not distinguish between different CD40$^+$ cells and activate both the efficacy arm, driven by cDC1s, and the toxicity arm, driven by macrophages, platelets, and monocytes. CD40/DC bsAbs, which display preferred binding to and selective activation of DC populations, improved the therapeutic window of CD40-targeted immunotherapy by increasing antitumor immunity and reducing systemic toxicity.

crosslinking as compared to bivalent IgG formats and Fc engineering was necessary to CD40 clustering and subsequent activation. Second, the monovalent CD40 targeting arm apparently reduces CD40 binding and agonism as compared to a bivalent parental CD40 mAb. However, fine-tuning the affinities of the Fab domains to optimize the DC selectivity of CD40 agonism allows to dose-up these bsAbs without compromising their safety profile, unlike with traditional CD40 mAbs. Thus, this new tri-functional antibody format requires efficient binding to FcγRIIB, CD40, and a DC marker to result in better safety profile and superior antitumor response compared to the parental monospecific CD40 mAb **(Figure 2)**.

DISCUSSION

Driven by recent mechanistic insights into the cellular pathways mediating efficacy and toxicity, as well as the latest developments in antibody and protein engineering, the next generation of Fc-engineered and multi-specific CD40 agonistic mAbs are being developed to bypass toxicity and optimize their potency. Multiple ongoing clinical trials evaluating the safety and potency of these new reagents, either as monotherapies or part of combination therapies, will soon reveal the potential of CD40 agonists as the next wave of immunotherapies. Besides CD40 agonists, the clinical translation of other types of agonistic mAbs has been restricted due to side effects associated with the broad expression profile of their targets on hematological and non-hematological cells. Lesson from pre-clinical and clinical studies of next-generation CD40 antibodies, together with mechanistic knowledge of the cellular pathways that mediate efficacy and toxicity, may enable the development of additional cell- and tumor-selective agonists with an improved therapeutic window.

DATA AVAILABILITY STATEMENT

The original contributions presented in the study are included in the article/supplementary material. Further inquiries can be directed to the corresponding author.

AUTHOR CONTRIBUTIONS

All authors listed have made a substantial, direct, and intellectual contribution to the work and approved it for publication.

REFERENCES

1. Hahn AW, Gill DM, Pal SK, Agarwal N. The Future of Immune Checkpoint Cancer Therapy After PD-1 and CTLA-4. *Immunotherapy* (2017) 9:681–92. doi: 10.2217/imt-2017-0024
2. Sharmea P. The Future of Immue Checkpoint Therapy. *Science* (2014) 348:56–61. doi: 10.1126/science.aaa8172
3. Ribas A, Wolchok JD. Cancer Immunotherapy Using Checkpoint Blockade. *Science* (2018). doi: 10.1126/science.aar4060
4. Topalian SL, Drake CG, Pardoll DM. Immune Checkpoint Blockade: A Common Denominator Approach to Cancer Therapy. *Cancer Cell* (2015) 27:451–61. doi: 10.1016/j.ccell.2015.03.001
5. Vonderheide RH. The Immune Revolution: A Case for Priming, Not Checkpoint. *Cancer Cell* (2018) 33:563–9. doi: 10.1016/j.ccell.2018.03.008

6. Vonderheide RH. CD40 Agonist Antibodies in Cancer Immunotherapy. *Annu Rev Med* (2020) 71:annurev-med-062518-045435. doi: 10.1146/annurev-med-062518-045435
7. Van Mierlo GJD, Den BAT, JP M, van der Voort EIH, Fransen MF, Offringa R, et al. CD40 Stimulation Leads to Effective Therapy of CD40- Tumors Through Induction of Strong Systemic Cytotoxic T Lymphocyte Immunity. *Proc Natl Acad Sci U.S.A.* (2002). doi: 10.1073/pnas.082107699
8. Luheshi NM, Coates-Ulrichsen J, Harper J, Mullins S, Sulikowski MG, Martin P, et al. Transformation of the Tumour Microenvironment by a CD40 Agonist Antibody Correlates With Improved Responses to PD-L1 Blockade in a Mouse Orthotopic Pancreatic Tumour Model. *Oncotarget* (2016). doi: 10.18632/oncotarget.7610
9. Byrne KT, Vonderheide RH. CD40 Stimulation Obviates Innate Sensors and Drives T Cell Immunity in Cancer. *Cell Rep* (2016) 15:2719–32. doi: 10.1016/j.celrep.2016.05.058
10. Caux BC, Massacrier C, Vanbervliet B, Dubois B, Van Kooten C, Durand I, et al. Sllmm~'y. CD40-CD40 Ligand. *J Leuk Biol* (2000) 67:2–17. doi: 10.1002/jlb.67.1.2
11. Clark EA. A Short History of the B-Cell-Associated Surface Molecule. *Front Immunol* (2014) 5:472. doi: 10.3389/fimmu.2014.00472
12. Alexandroff AB, Jackson AM, Paterson T, Haley JL, Ross JA, Longo DL, et al. Role for CD40-CD40 Ligand Interactions in the Immune Response to Solid Tumours. *Mol Immunol* (2000) 37:515–26. doi: 10.1016/S0161-5890(00)00079-1
13. Henn V, Steinbach S, Bu K, Presek P, Kroczek RA. The Inflammatory Action of CD40 Ligand (CD154) Expressed on Activated Human Platelets Is Temporally Limited by Coexpressed CD40. *Blood* (2001) 98:1047–54. doi: 10.1182/blood.v98.4.1047
14. Yellin BMJ, Brett J, Baum D, Matsushima A, Szabolcs M, Stern D, et al. Functional Interactions ofT Cells With Endothelial Cells : The Role of CD40L-CD40-Mediated Signals. *J. Exp Med* (1995) 182:1857–64. doi: 10.1084/jem.182.6.1857
15. Vonderheide RH, Glennie MJ. Agonistic CD40 Antibodies and Cancer Therapy. *Clin Cancer Res* (2013) 19:1035–43. doi: 10.1158/1078-0432.CCR-12-2064
16. Kooten CV, Banchereau J, Gene CDL. CD40-CD40 Ligand. *J Leuk Biol* (2000) 67:2–17.
17. Diehl L, den Boer AT, Schoenberger SP, van der Voort EI, Schumacher TN, Melief CJ, et al. CD40 Activation *In Vivo* Overcomes Peptide-Induced Peripheral Cytotoxic T-Lymphocyte Tolerance and Augments Anti-Tumor Vaccine Efficacy. *Nat Med* (1999) 5:1–6.
18. Uno T, Takeda K, Kojima Y, Yoshizawa H, Akiba H, Mittler RS, et al. Eradication of Established Tumors in Mice by a Combination Antibody-Based Therapy. *Nat Med* (2006) 12:693–8. doi: 10.1038/nm1405
19. Vonderheide RH, Flaherty KT, Khalil M, Stumacher MS, Bajor DL, Hutnick NA, et al. Clinical Activity and Immune Modulation in Cancer Patients Treated With CP-870,893, A Novel CD40 Agonist Monoclonal Antibody. *J Clin Oncol* (2007) 25:876–83. doi: 10.1200/JCO.2006.08.3311
20. Rüter J, Antonia SJ, Burris HA, Huhn RD, Vonderheide RH. Immune Modulation With Weekly Dosing of an Agonist CD40 Antibody in a Phase I Study of Patients With Advanced Solid Tumors. *Cancer Biol Ther* (2010) 10:983–93. doi: 10.4161/cbt.10.10.13251
21. Furman RR, Forero-Torres A, Shustov A, Drachman JG. A Phase I Study of Dacetuzumab (SGN-40, a Humanized Anti-CD40 Monoclonal Antibody) in Patients With Chronic Lymphocytic Leukemia. *Leuk Lymphoma* (2010). doi: 10.3109/10428190903440946
22. Johnson PW, Steven NM, Chowdhury F, Dobbyn J, Hall E, Ashton-Key M, et al. A Cancer Research UK Phase I Study Evaluating Safety, Tolerability, and Biological Effects of Chimeric Anti-CD40 Monoclonal Antibody (MAb), Chi Lob 7/4. *J Clin Oncol* (2010) 28:2507. doi: 10.1200/jco.2010.28.15_suppl.2507
23. Vonderheide RH, Bajor DL, Winograd R, Evans RA, Bayne LJ, Beatty GL. CD40 Immunotherapy for Pancreatic Cancer. *Cancer Immunol Immunother* (2013) 62:949–54. doi: 10.1007/s00262-013-1427-5
24. Vonderheide RH, Burg JM, Mick R, Trosko JA, Li D, Shaik MN, et al. Phase I Study of the CD40 Agonist Antibody CP-870,893 Combined With Carboplatin and Paclitaxel in Patients With Advanced Solid Tumors. *Oncoimmunology* (2013) 2:1–10. doi: 10.4161/onci.23033
25. Dahan R, Barnhart BC, Li F, Yamniuk AP, Korman AJ, Ravetch JV. Therapeutic Activity of Agonistic, Human Anti-CD40 Monoclonal Antibodies Requires Selective Fcγr Engagement. *Cancer Cell* (2016) 29:820–31. doi: 10.1016/j.ccell.2016.05.001
26. Chowdhury F, Johnson PW, Glennie MJ, Williams AP. Ex Vivo Assays of Dendritic Cell Activation and Cytokine Profiles as Predictors of *In Vivo* Effects in an Anti-Human CD40 Monoclonal Antibody ChiLob 7/4 Phase I Trial. *Cancer Immunol Res* (2014) 2:229–40. doi: 10.1158/2326-6066.CIR-13-0070
27. Li F, Ravetch JV. Inhibitory Fcγ Receptor Engagement Drives Adjuvant and Anti-Tumor Activities of Agonistic CD40 Antibodies. *Science* (2011) 333:1034–0. doi: 10.1126/science.1206954
28. White AL, Chan HTC, Roghanian A, French RR, Mockridge CI, Tutt AL, et al. Interaction With Fc RIIB Is Critical for the Agonistic Activity of Anti-CD40 Monoclonal Antibody. *J Immunol* (2011) 187:1754–63. doi: 10.4049/jimmunol.1101135
29. Li F, Ravetch JV. Antitumor Activities of Agonistic Anti-TNFR Antibodies Require Differential Fcγriib Coengagement. *vivo. Proc Natl Acad Sci USA* (2013) 110:19506–1. doi: 10.1073/pnas.1319502110
30. Knorr DA, Dahan R, Ravetch JV. Toxicity of an Fc-Engineered Anti-CD40 Antibody is Abrogated by Intratumoral Injection and Results in Durable Antitumor Immunity [Immunology and Inflammation]. *Proc Natl Acad Sci U.S.A.* (2018) 115:11053–48. doi: 10.1073/pnas.1810566115
31. Garris CS, Wong JL, Ravetch JV, Knorr DA. Dendritic Cell Targeting With Fc-Enhanced CD40 Antibody Agonists Induces Durable Antitumor Immunity in Humanized Mouse Models of Bladder Cancer. *Sci Transl Med* (2021) 13:eabd1346.
32. Hara MHO, Reilly EMO, Varadhachary G, Wolff RA, Wainberg ZA, Ko AH, et al. CD40 Agonistic Monoclonal Antibody APX005M (Sotigalimab) and Chemotherapy, With or Without Nivolumab, for the Treatment of Metastatic Pancreatic Adenocarcinoma: An Open-Label, Multicentre, Phase 1b Study. *Lancet Oncol* (2021) 22:131–18. doi: 10.1016/S1470-2045(20)30532-5
33. O'Hara M, Mick R, Lyman J, Xu J, Hosseini M, LaVallee T, et al. A Phase 1b/2 Study of CD40 Agonistic Monoclonal Antibody (APX005M) Together With Gemcitabine and Nab-Paclitaxel With or Without Nivolumab in Untreated Metastatic Pancreatic Adenocarcinoma Patients. *Cancer Res* (2019) 79:CT004. doi: 10.1158/1538-7445.AM2019-CT004
34. White AL, Chan HTC, French RR, Willoughby J, Mockridge CI, Roghanian A, et al. Conformation of the Human Immunoglobulin G2 Hinge Imparts Superagonistic Properties to Immunostimulatory Anticancer Antibodies. *Cancer Cell* (2015) 27:138–48. doi: 10.1016/j.ccell.2014.11.001
35. Yu X, Chan HTC, Fisher H, Tews I, Glennie MJ, Cragg MS, et al. Article Isotype Switching Converts Anti-CD40 Antagonism to Agonism to Elicit Potent Antitumor Activity Isotype Switching Converts Anti-CD40 Antagonism to Agonism to Elicit Potent Antitumor Activity. *Cancer Cell* (2020) 37:866–50. doi: 10.1016/j.ccell.2020.04.013
36. Vonderheide RH, Dutcher JP, Anderson JE, Eckhardt SG, Stephans KF, Razvillas B, et al. Phase I Study of Recombinant Human CD40 Ligand in Cancer Patients. *J Clin Oncol* (2001) 19:3280–7. doi: 10.1200/JCO.2001.19.13.3280
37. Divine R, Dang HV, Ueda G, Fallas JA, Vulovic I, Sheffler W, et al. Designed Proteins Assemble Antibodies Into Modular Nanocages. *Sci (80-)* (2021) 372:1–32. doi: 10.1126/science.abd9994
38. Liu X, Zhao Y, Shi H, Zhang Y, Yin X, He Y, et al. Antitumour Activities Through Biophysical Fl Exibility. *Nat Commun* (2019) 10:4206. doi: 10.1038/s41467-019-12097-6
39. Johnson P, Challis R, Chowdhury F, Gao Y, Harvey M, Geldart T, et al. Clinical and Biological Effects of an Agonist Anti-CD40 Antibody a Cancer Research UK Phase I Study. *Clin Cancer Res* (2015) 21:1328–21. doi: 10.1158/1078-0432.CCR-14-2355
40. Berner V, Liu H, Zhou Q, Alderson KL, Sun K, Weiss JM, et al. IFN-γ Mediates CD4+ T-Cell Loss and Impairs Secondary Antitumor Responses After Successful Initial Immunotherapy. *Nat Med* (2007) 13:3–6. doi: 10.1038/nm1554
41. Chiodoni C, Iezzi M, Guiducci C, Sangaletti S, Alessandrini I, Ratti C, et al. Triggering CD40 on Endothelial Cells Contributes to Tumor Growth. *J Exp Med* (2006) 203:2441–50. doi: 10.1084/jem.20060844

42. Siwicki M, Gort-freitas NA, Messemaker M, Bill R, Gungabeesoon J, Engblom C, et al. Resident Kupffer Cells and Neutrophils Drive Liver Toxicity in Cancer Immunotherapy. *Sci Immunol* (2021) 6:eabi7083. doi: 10.1126/sciimmunol.abi7083
43. Bonnans C, Thomas G, He W, Jung B, Chen W, Liao M, et al. CD40 Agonist-Induced IL- 12p40 Potentiates Hepatotoxicity. *J Immunother Cancer* (2020) 8: e000624. doi: 10.1136/jitc-2020-000624
44. Salomon R, Rotem H, Katzenelenbogen Y, Weiner A, Saban NC, Feferman T, et al. Bispecific Antibodies Increase the Therapeutic Window of CD40 Agonists Through Selective Dendritic Cell Targeting. *Nat Cancer* (2022) 3:287–302. doi: 10.1038/s43018-022-00329-6
45. Ferris ST, Durai V, Wu R, Theisen DJ, Ward JP, Bern MD, et al. Cdc1 Prime and are Licensed by CD4 + T Cells to Induce Anti-Tumour Immunity. *Nature* (2020) 584:629–4. doi: 10.1038/s41586-020-2611-3
46. Fransen MF, Sluijter M, Morreau H, Arens R, Melief CJM. Local Activation of CD8 T Cells and Systemic Tumor Eradication Without Toxicity *via* Slow Release and Local Delivery of Agonistic CD40 Antibody. *Clin Cancer Res* (2011) 17:2280–70. doi: 10.1158/1078-0432.CCR-10-2888
47. Sandin LC, Orlova A, Gustafsson E, Ellmark P, Tolmachev V, Tötterman TH, et al. Locally Delivered CD40 Agonist Antibody Accumulates in Secondary Lymphoid Organs and Eradicates Experimental Disseminated Bladder Cancer. *Cancer Immunol Res* (2014) 2:90–80. doi: 10.1158/2326-6066.CIR-13-0067
48. Irenaeus SMM, Nielsen D, Ellmark P, Yachnin J, Deronic A, Nilsson A, et al. First-In-Human Study With Intratumoral Administration of a CD40 Agonistic Antibody, ADC-1013, in Advanced Solid Malignancies. *Int J Cancer* (2019) 145:1189–99. doi: 10.1002/ijc.32141
49. Ye S, Cohen D, Belmar NA, Choi D, Tan SS, Sho M, et al. A Bispecific Molecule Targeting CD40 and Tumor Antigen Mesothelin Enhances Tumor-Specific Immunity. *Cancer Immunol Res* (2019) 7:1864–75. doi: 10.1158/2326-6066.CIR-18-0805
50. Bano JD, Florès-Florès R, Josselin E, Goubard A, Ganier L, Castellano R, et al. A Bispecific Antibody-Based Approach for Targeting Mesothelin in Triple Negative Breast Cancer. *Front Immunol* (2019) 10:1593. doi: 10.3389/fimmu.2019.01593
51. Luke JJ, Barlesi F, Chung K, Tolcher AW, Kelly K, Hollebecque A, et al. Phase I Study of ABBV-428, a Mesothelin-CD40 Bispecific, in Patients With Advanced Solid Tumors. *J Immunother Cancer* (2021) 9:1–10. doi: 10.1136/jitc-2020-002015
52. Ellmark P, Hägerbrand K, Levin M, Von Schantz L, Deronic A, Vara L, et al. A Bispecific Antibody Targeting CD40 and EPCAM Induces Superior Anti-Tumor Effects Compered to the Combination of the Monospecific Antibodies. *Nuevos Sist Comun e Inf* (2021) 8:A1–A559. doi: 10.1136/jitc-2020-SITC2020.0858
53. Hübner J, Nimmerjahn F. Zooming in on Dendritic Cells for CD40 Agonists. *Nat Cancer* (2022) 3:268–9. doi: 10.1038/s43018-022-00340-x

Conflict of Interest: RD is inventor in patents covering Fc-engineered CD40 mAbs. RS and RD are inventors in a PCT patent application covering CD40 bispecific antibodies discussed in this article.

Publisher's Note: All claims expressed in this article are solely those of the authors and do not necessarily represent those of their affiliated organizations, or those of the publisher, the editors and the reviewers. Any product that may be evaluated in this article, or claim that may be made by its manufacturer, is not guaranteed or endorsed by the publisher.

frontiers | Frontiers in Immunology

TYPE Original Research
PUBLISHED 29 July 2022
DOI 10.3389/fimmu.2022.933251

OPEN ACCESS

EDITED BY
Matthias Peipp,
University Medical Center Schleswig-Holstein, Germany

REVIEWED BY
Markus Biburger,
Friedrich-Alexander-University Erlangen-Nürnberg, Germany
Edwin Bremer,
University Medical Center Groningen, Netherlands

*CORRESPONDENCE
Michiel van der Flier
M.vanderFlier@umcutrecht.nl

†These authors share first authorship

‡These authors shared supervision of this study

SPECIALTY SECTION
This article was submitted to B Cell Biology, a section of the journal Frontiers in Immunology

RECEIVED 30 April 2022
ACCEPTED 29 June 2022
PUBLISHED 29 July 2022

CITATION
de Vor L, Beudeker CR, Flier A, Scheepmaker LM, Aerts PC, Vijlbrief DC, Bekker MN, Beurskens FJ, van Kessel KPM, de Haas CJC, Rooijakkers SHM and van der Flier M (2022) Monoclonal antibodies effectively potentiate complement activation and phagocytosis of *Staphylococcus epidermidis* in neonatal human plasma. *Front. Immunol.* 13:933251. doi: 10.3389/fimmu.2022.933251

Monoclonal antibodies effectively potentiate complement activation and phagocytosis of *Staphylococcus epidermidis* in neonatal human plasma

Lisanne de Vor[1†], Coco R. Beudeker[2†], Anne Flier[1], Lisette M. Scheepmaker[1], Piet C. Aerts[1], Daniel C. Vijlbrief[3], Mireille N. Bekker[4], Frank J. Beurskens[5], Kok P. M. van Kessel[1], Carla J. C. de Haas[1], Suzan H. M. Rooijakkers[1‡] and Michiel van der Flier[2*‡]

[1]Department of Medical Microbiology, University Medical Center Utrecht, Utrecht, Netherlands, [2]Department of Paediatric Infectious Diseases and Immunology, University Medical Center Utrecht, Utrecht, Netherlands, [3]Department of Neonatology, University Medical Center Utrecht, Utrecht, Netherlands, [4]Department of Obstetrics, University Medical Center Utrecht, Utrecht, Netherlands, [5]Genmab, Utrecht, Netherlands

Central line associated bloodstream infections (CLABSI) with *Staphylococcus epidermidis* are a major cause of morbidity in neonates, who have an increased risk of infection because of their immature immune system. As especially preterm neonates suffer from antibody deficiency, clinical studies into preventive therapies have thus far focused on antibody supplementation with pooled intravenous immunoglobulins from healthy donors (IVIG) but with little success. Here we study the potential of monoclonal antibodies (mAbs) against *S. epidermidis* to induce phagocytic killing by human neutrophils. Nine different mAbs recognizing Staphylococcal surface components were cloned and expressed as human IgG1s. In binding assays, clones rF1, CR5133 and CR6453 showed the strongest binding to *S. epidermidis* ATCC14990 and CR5133 and CR6453 bound the majority of clinical isolates from neonatal sepsis (19 out of 20). To study the immune-activating potential of rF1, CR5133 and CR6453, bacteria were opsonized with mAbs in the presence or absence of complement. We observed that activation of the complement system is essential to induce efficient phagocytosis of *S. epidermidis*. Complement activation and phagocytic killing could be enhanced by Fc-mutations that improve IgG1 hexamerization on cellular surfaces. Finally, we studied the ability of the mAbs to activate complement in r-Hirudin neonatal plasma conditions. We show that classical pathway complement activity in plasma isolated from neonatal cord blood is comparable to adult levels. Furthermore, mAbs could

10.3389/fimmu.2022.933251

greatly enhance phagocytosis of *S. epidermidis* in neonatal plasma. Altogether, our findings provide insights that are crucial for optimizing anti-*S. epidermidis* mAbs as prophylactic agents for neonatal CLABSI.

KEYWORDS

complement system, CLABSI, *Staphylococcus epidermidis*, monoclonal antibodies, phagocytosis, neonates

Introduction

Neonatal sepsis is a major cause of mortality and morbidity (1, 2). Due to the use of indwelling medical devices, more than half of all late-onset sepsis episodes (occurring after more than 7 days of age) are caused by central line associated bloodstream infections (CLABSI) (3). The incidence of CLABSI is highest in preterm neonates (gestational age (GA) < 37 weeks) compared to term neonates (≥ 37 weeks GA) and children admitted to pediatric intensive care units (4–6). The most common pathogens found in CLABSI are coagulase negative staphylococci, with *Staphylococcus epidermidis* being the predominant species (7, 8). Currently, no effective strategy exists to prevent late-onset sepsis in neonates.

The high risk of CLABSI in neonates compared to older children is likely related to transient immunodeficiency of immaturity (9–15). Three elements that are crucial for immune protection against Gram-positive bacteria, namely neutrophils (16), antibodies and the complement system, have been reported to be impaired in neonates. First, neonates have low levels of circulating neutrophils (14). Neutrophils are highly specialized immune cells that circulate in the blood and are attracted to the site of infection to phagocytose bacteria. Following uptake by neutrophils, bacteria are subjected to high levels of reactive oxygen species (ROS) and degranulation of antimicrobial products that are destructive to staphylococci, this makes phagocytosis an efficient way to eliminate *S. epidermidis* (17, 18). Second, neonates have low levels of circulating antibodies. Because endogenous antibody synthesis only begins at birth, neonates depend on passive transfer of maternal antibodies over the placenta which mainly occurs in the final trimester of pregnancy. As a result, preterm neonates have low IgG levels (19). IgM and IgA are not transported over the placenta, thus all neonates newborns are IgM/IgA deficient at birth (9, 10). Third, the complement system is less active in neonates when compared to adults, but it can be activated in the presence of infection (11–13, 15). Both antibodies and complement concentrations in neonatal plasma increase with gestational age, meaning that extremely preterm neonates are more at risk than term neonates. Antibodies and complement components are important opsonins that are needed to label bacteria for efficient phagocytosis. Antibodies consist of two functional domains: the fragment antigen binding (Fab) region confers antigen specificity, while the crystallizable fragment (Fc) region drives interaction with other components of the immune system (20). After binding to the bacterial surface, IgG and IgA antibodies can directly induce phagocytosis *via* interaction with Fc receptors on neutrophils. IgG and IgM antibodies are both able to activate the classical pathway of the complement system which leads to deposition of C3b on the bacterial surface. C3b is recognized by complement receptors on neutrophils and leads to phagocytosis of the pathogen (21). Thus, antibodies play a central role in the immune response against Gram-positive bacteria such as *S. epidermidis*.

Clinical trials have assessed if antibody supplementation therapy with pooled intravenous immunoglobulins from healthy donors (IVIG) can ameliorate neonatal antibody deficiency and prevent or treat neonatal sepsis. These studies show only a 3% reduction in sepsis incidence in neonates and no improvement in mortality (22). We hypothesize that the disappointing efficacy of IVIG therapy in neonatal infections could be caused by low concentration of antibodies specific to the relevant neonatal pathogens.

In this study, we wondered whether pathogen specific monoclonal antibodies (mAbs), which have a sole specificity for one target, can be more effective than IVIG. Therefore, we cloned and expressed nine different mAbs recognizing staphylococcal surface components as human IgG1s. Of the three best binders (rF1, CR5133 and CR6453), we tested the ability to recognize a panel of 20 clinical *S. epidermidis* isolates from neonatal sepsis and showed that CR5133 and CR6453 bound to the majority (19 out of 20) of isolates. We then studied the immune activating potential of rF1-, CR5133- and CR6453-IgG1 and found that activation of the complement system is essential to induce efficient phagocytosis of *S. epidermidis*. As shown before on *Staphylococcus aureus* (23) and *Streptococcus pneumoniae* (24), phagocytosis and killing of *S. epidermidis* could be further enhanced by Fc-mutations that improve IgG hexamerization, which is needed for efficient activation of the classical pathway (25–27). Finally, we collected human cord blood from neonates to study the ability of the mAbs to activate the neonatal complement system. In contrast to what is reported (11–13, 15, 28), plasma isolated from preterm and term neonatal

cord blood showed classical pathway complement activity comparable to adult levels. Furthermore, we demonstrate that pathogen specific monoclonal antibodies with hexamer enhancing mutations greatly enhanced phagocytosis of *S. epidermidis* in neonatal plasma by healthy donor neutrophils. Altogether, our findings provide insights that are crucial for optimizing anti-*S. epidermidis* mAbs as prophylactic or therapeutic agents for neonatal sepsis.

Materials and methods

Ethics statement

Human blood was obtained from healthy donors after informed consent was given by all subjects in accordance with the Declaration of Helsinki. Approval from the Medical Ethics Committee of the University Medical Center Utrecht was obtained (METC protocol 07-125/C approved on March 1, 2010). Cord blood (CB) was obtained from the umbilical cord after vaginal birth of neonates of different gestational age (GA); 32-37 weeks GA (n=2) and >37 weeks GA (n=3). Samples were collected at the obstetrics department and analyzed and stored anonymously. Written informed consent was obtained from the mother in accordance with the Declaration of Helsinki. The Ethics Committee for Biobanking of the University Medical Center Utrecht approved the collection protocol (TCBio 21/223, approved on June 14th, 2021).

IgG and IgM depletion from human serum

Normal human serum (NHS) from twenty healthy donors was depleted of IgG and IgM as previously described (29). Briefly, affinity chromatography was used to capture IgG by using HiTrap protein G High Performance column (Cytiva, GE Healthcare) and IgM with Capture Select IgM Affinity Matrix (Thermo Fischer Scientific) from NHS. Complement levels and activity were determined after depletion, using enzyme-linked immunosorbent serological assay (ELISA) and classical/alternative pathway hemolytic assays. Although C1q is partially co-depleted during the procedure, C1q was not supplemented in IgG/IgM depleted NHS (ΔNHS), because supplementation with 70 µg/ml C1q did not alter complement deposition on *S. epidermidis* (Figure S1), indicating that the amount of C1q left was sufficient.

Generation of human monoclonal antibodies

IgG1 mAbs A120, CR5133, CR6166 and CR6176 were produced by Genmab (Utrecht, the Netherlands) as described previously [WO 2017/198731 Al (30)]. IgG1 clones M130, CR5132, CR6171, CR6453, rF1 and G-2A2 (aDNP) and the subtypes of rF1, CR5133, CR6453 and G-2A2 (IgG3, IgG1 E345K, IgG3 E345K) were produced as described previously (23, 31). For mAb expression, variable heavy (VH) chain and variable light (VL) chain sequences were cloned in expression vectors pcDNA3.3 (Thermo Fisher Scientific) as described in Vink et al. (30) or pcDNA3.4 (Thermo Fisher Scientific) as described in de Vor et al. (31), containing human IgG1 heavy chain (HC) and light chain (LC) constant regions as indicated in Table S1. The E345K single mutation of Glu at position 345 into Lys was introduced in the heavy chain expression vectors by gene synthesis (IDT (Integrated DNA Technologies)). Variable heavy (VH) and light chain (VL) sequences from all antibodies were obtained from scientific publications or patents (Table S1). Antibodies were expressed as IgG1,κ except for CR6166 which was expressed as IgG1,λ. Plasmid DNA mixtures encoding both heavy and light chains of antibodies were transiently transfected in EXPI293F (Life technologies, USA) as described before (30) (31). IgG1 antibodies were isolated using HiTrap Protein A High Performance column (Cytiva, GE Healthcare) and IgG3 antibodies were collected using HiTrap Protein G High Performance column (Cytiva, GE Healthcare) in the Äkta Pure protein chromatography system (GE Healthcare). All antibody fractions were dialyzed overnight in PBS and filter-sterilized through 0.22 µm SpinX-filters. Size exclusion chromatography (SEC) (Cytiva, GE Healthcare) was performed to check for mAb homogeneity, and the monomeric fraction was separated when aggregation levels exceeded 5%. Final antibody concentration was determined by measuring the absorbance at 280 nm and antibodies were stored at -80°C or 4°C.

Bacterial strains and growth conditions

S. epidermidis type strain ATCC 14990 (32, 33) and twenty clinical bacteremia isolates from neonates admitted to the Wilhelmina Children's hospital (UMC Utrecht) were used in this study. Strains were grown overnight at 37°C on sheep blood agar (SBA) and were cultured overnight in Tryptic Soy Broth (TSB). Next, they were subcultured and grown to exponential phase for ± 2.5 hours. For flow cytometry, exponential phase bacteria were washed in PBS and incubated in 250 µg/ml fluorescein isothiocyanate (FITC) (Sigma Aldrich) in PBS for 30 minutes at 4°C. After washing, FITC labeled bacteria were diluted in RPMI (Gibco) supplemented with 0.05% human serum albumin (HSA) (Sanquin products) and the bacterial concentration was determined by flow cytometry using a MACSQuant analyzer (Miltenyi), counting bacterial events in a defined volume. Bacteria were aliquoted and stored at -20°C. When indicated, freshly grown exponential cultures were used of

which the concentration was determined based on optical density at 600 nm (OD_{600}) (OD 1.0 = 5 x 10^8 bact/ml).

Antibody binding to *S. epidermidis*

For the initial screening of mAb binding to *S. epidermidis*, freshly grown bacteria were washed and diluted in PBS supplemented with 0.1% bovine serum albumin (BSA) (Serva). For all other binding experiments, FITC labelled 14990 and N2297 were used. A total of 150,000 bacteria were incubated with a concentration range of mAbs or IVIG (Nanogam, Sanquin) in PBS-BSA in a round-bottom 96-wells plate for 30 minutes at 4°C, shaking (± 750 rpm). After washing, bacteria were further incubated for 30 minutes at 4°C, shaking (± 750 rpm) with 30 µl APC-conjugated goat anti-human IgG (H+L) F $(ab')_2$ antibody (Jackson Immunoresearch, 1 µg/ml) or APC-conjugated donkey anti-human IgG (H+L) $F(ab')_2$ antibody (Jackson Immunoresearch, 1:250) to detect both lambda and kappa chains or AlexaFluor647(AF647)-conjugated goat anti-human kappa $F('ab)_2$ antibody (Southern Biotech, 1 µg/ml) to compare binding of IgG1, IgG1 E345K, IgG3 and IgG3 E345K. After incubation with detection antibodies, bacteria were washed and fixed in 1% paraformaldehyde (PFA) (Polysciences) in PBS. Samples were measured by flow cytometry (BD FACSVerse), and data analyzed by FlowJo Software (Version 10). A control sample was used to set FSC-SSC gates to exclude debris and large aggregates of bacteria. In case we used FITC labelled bacteria, only FITC-positive events were analyzed. Data are presented as APC or AF647 geometric mean fluorescence intensity (GeoMFI ± SD).

Phagocytosis of *S. epidermidis* by neutrophils

Human neutrophils were isolated from blood of healthy donors by Ficoll-Histopaque gradient centrifugation and suspended in RPMI-HSA (34). For opsonization, 750,000 FITC labelled bacteria (20 µL) were incubated with 10 µL mAbs or IVIG supplemented with 10 µL ΔNHS or neonatal plasma (final concentration 1%) or buffer, to investigate complement- or Fc-receptor mediated phagocytosis, respectively. Bacteria were incubated in a round-bottom 96-wells plate for 15 minutes, at 37°C, shaking (± 750 rpm). Subsequently, 75,000 neutrophils (10 µL) were added, giving a 10:1 bacteria-to-cell ratio and samples were incubated for 15 minutes at 37°C, shaking (± 750 rpm). The reaction was stopped with 1% ice cold PFA in RPMI-HSA and FITC fluorescence was measured by flow cytometry (BD FACSVerse). To exclude debris, a neutrophil population incubated in RPMI-HSA alone was used to set FSC-SSC gates. Data were analyzed by FlowJo (version 10) and presented as FITC GeoMFI ± SD of the neutrophil population.

Killing of *S. epidermidis*

Freshly grown, exponential phase *S. epidermidis* was washed with Hanks Balanced Salt Solution (HBSS) (BioWitthaker) supplemented with 0.1% HSA. For opsonization, 850,000 bacteria were incubated with NHS or mAbs and ΔNHS in HBSS-HSA (concentrations indicated in figure legends) in a round bottom 96-deep-well plate for 30 minutes at 37°C, shaking (± 750 rpm) (final volume: 15 µl). After 30 minutes opsonization, 850,000 neutrophils were added (MOI 1:1) and further incubated for an additional 90 minutes at 37°C, 5% CO_2 with open cover, shaking (± 750 rpm) (final volume: 100 µl). The reaction was stopped by adding 900 µl of ice-cold, freshly prepared, 0.2 µm sterile filtered 0.3% saponin (w/v, Sigma) in Milli-Q water. Samples were incubated for 5-15 minutes at 4°C, shaking (± 750 rpm). Total viable bacterial counts were determined by serial dilution and plating. Data are presented as CFU ± SD. The following control conditions were always included: 10% NHS with neutrophils (positive control for killing), heat-inactivated-ΔNHS with neutrophils (negative control for killing), HBSS-HSA with neutrophils only (sterility control) and HBSS-HSA with bacteria only (reference control for the amount of bacteria added).

Production of anti-C3b AF647 conjugate

2000 µg/ml mouse IgG2a mAb against a neo-epitope C3b (clone Bh6) (35) was incubated with AF647 NHS ester (Life Technologies) (final concentration: 100 µg/ml) and sodium carbonate (pH 9.4, final concentration: 0.1 M) for 70 minutes, room temperature, rotating. The sample was separated from aggregates by spinning through 0.22 µm SpinX filter columns (Corning life Sciences BV) for 2 minutes at 1500x *g*. To remove free AF647 from the mixture, filtrate was transferred to a sterile PBS washed Zeba spin column (Thermo Scientific) and spun for 2 minutes at 1500x *g*. From OD_{280} and OD_{650} Nanodrop (Thermo Scientific) measurements, the degree of labelling (DOL) was determined at 4.14. The conjugate was checked for integrity by SDS-PAGE and fluorescence of antibody-conjugate was confirmed using ImageQuant LAS 4000.

Complement deposition on *S. epidermidis*

To determine C3b deposition on *S. epidermidis*, 150,000 FITC labeled bacteria were incubated with mAbs supplemented

with 1% ΔNHS in RPMI-HSA for 30 minutes at 37°C, shaking (± 750 rpm) (final volume: 30 µl). After washing twice with PBS-BSA, bacteria were further incubated for an additional 30 minutes at 4°C, shaking (± 750 rpm) with 15 µl anti-C3b AF647 detection antibody (3 µg/ml) in PBS-BSA. Bacteria were washed with PBS-BSA and fixed in 1% PFA in PBS-BSA for at least 30 minutes at 4°C, shaking (± 750 rpm) after which fluorescence was measured by flow cytometry (BD FACSVerse). To exclude debris and large aggregates of bacteria, control bacteria incubated in RPMI-HSA alone were used to set FSC-SSC gates, only FITC-positive events were analyzed. Data were analyzed by FlowJo Software (Version 10) and presented as AF647 GeoMFI ± SD.

Collection of plasma samples

Cord blood or peripheral venous blood of healthy human donors was collected in S-Monovette r-Hirudin tubes (Sarstedt) to preserve complement activity (36). The blood was centrifuged at 1000x g for 5 minutes and plasma was removed and stored immediately at -80°C. Plasma of 27 healthy donors was pooled before freezing and cord blood plasma was stored individually. For complement inactivation, the plasma was heat-inactivated for 30 minutes at 56°C.

Complement ELISAs

Complement ELISAs were performed as previously described (37) with minor modifications. Briefly, microtiter plates (Nunc maxisorp) were pre-coated with 3 µg/mL IgM (Sigma) for classical pathway (CP) ELISA, with 20 µg/ml LPS (from *Salmonella enteriditis*, Sigma) for alternative pathway (AP) ELISA and with 20 µg/mL mannan (from *Saccharomyces cerevisiae*, Sigma) for lectin pathway (LP) ELISA. All coatings were prepared in 0.1 M carbonate buffer (pH 9) and incubated overnight at room temp. Plasma samples were diluted in Veronal Buffered Saline (VBS) + 0.1% gelatin + 5 mM $MgCl_2$ + 10 mM EGTA for AP ELISA and in VBS + 0.1% gelatin + 0.5 mM $CaCl_2$ + 0.25 mM $MgCl_2$ for CP ELISA and LP ELISA. After washing the plates with PBS 0.05% Tween-20, wells were blocked with 4% BSA in PBS-Tween. Then, plasma samples were added for 1 hour at 37°C in the appropriate buffer and dilutions. After additional washing, deposited C3b was detected using DIG-labelled mouse anti C3 antibody (WM1, 0.1 µg/mL) followed by Peroxidase conjugated sheep anti-DIG-Fab fragments (1:8000, Roche 11207733910). Finally, the plates were washed and developed using 3,3',5,5'-tetramethylbenzidine (Thermo Fisher). The reaction was stopped by addition of 1 N H_2SO_4. Absorption at 450nm was measured using a microplate reader (Biorad).

Statistical analysis

Statistical analyses were performed in Prism software (version 8.3; Graphpad). The tests used to calculate P-values are indicated in the figure legends. The number of independent biological repeats per graph is indicated in the figure legends.

Results

Production and identification of human monoclonal antibodies against *S. epidermidis*

First, we produced a panel of nine mAbs by cloning the variable light chain (VL) and heavy chain (VH) sequences derived from scientific publications or patents (Table S1) into expression vectors to produce full-length human IgG1 antibodies. We selected clones rF1 (binding surface proteins of the SDR family (38)), M130 (binding peptidoglycan [US20030228322A]), A120 (binding LTA [WO-03059260-A3]), CR5132 (possible target LTA [2012/0141493 A1] or Wall Teichoic Acid (31), CR5133 (possible target LTA [2012/0141493 A1]) and CR6453 (possible target LTA [2012/0141493 A1]) that have already been described to bind and induce opsonophagocytic killing of different *S. epidermidis* strains, but not to our model strain ATCC 14990 (33). We also included clones CR6166, CR6171 and CR6176, that are related to CR6453 and were screened for cross-reactivity because they bind *S. aureus* [2012/0141493 A1]. As a negative control, we produced one antibody recognizing the hapten dinitrophenol (DNP) (G2a2-IgG1) (39).

Next, we compared the binding of the panel of IgG1 mAbs to the sequenced common laboratory strain *S. epidermidis* ATCC 14990 (33), using flow cytometry. Compared to the negative control antibody (aDNP-IgG1) which does not recognize a bacterial component, only three antibodies (CR5133-IgG1, CR6453-IgG1 and rF1-IgG1) significantly bound to ATCC 14990 (Figure 1A). Although binding to other *S. epidermidis* strains has been described, we could not detect significant binding of IgG1 mAbs M130 and A120 to ATCC 14990. Our results indicate that CR5132 also specifically binds ATCC14490, although not significant. As CR5132 has been described to bind the same target as CR5133, which does show stronger and significant binding, we selected CR5133 instead of CR5132 for further characterization. After titration, we detected a higher binding signal at lower concentrations for rF1-IgG1 compared to CR5133- and CR6453-IgG1 (Figure 1B), indicating that rF1-IgG1 is the best binding mAb in the panel.

We also compared the strength and broad specificity of mAb binding and IVIG binding to *S. epidermidis*. We could

10.3389/fimmu.2022.933251

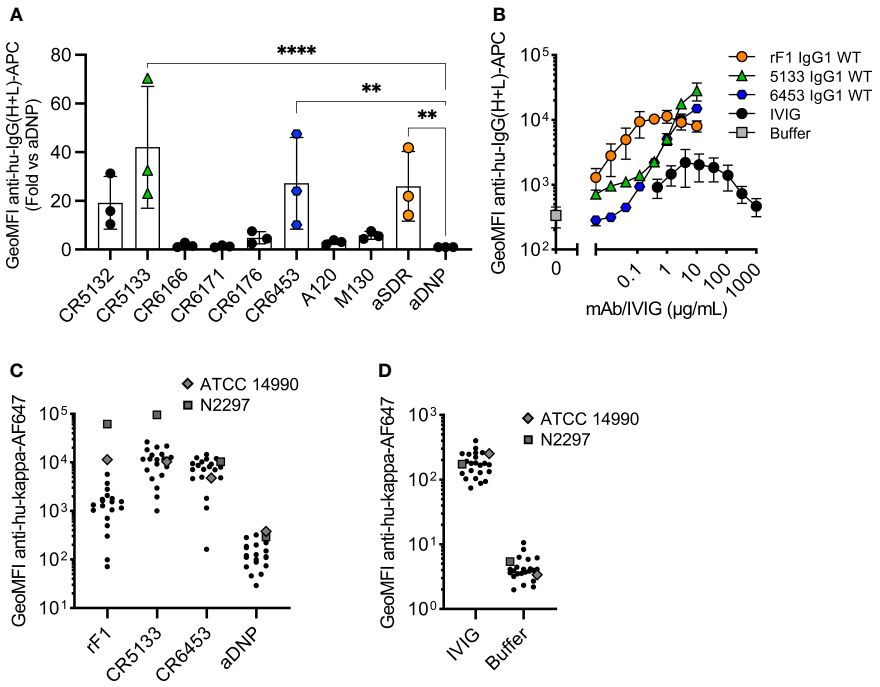

FIGURE 1
Identifying mAbs that bind *S. epidermidis* neonate isolates. **(A)** Screening mAb binding to *S. epidermidis* ATCC 14990. Bacteria were incubated with 2 µg/mL IgG1. MAb binding was detected using goat anti-hu-IgG(H+L)-APC and using flow cytometry. Data represent GeoMFI ± SD normalized to aDNP (ctrl)-IgG1 of three independent experiments. One-way ANOVA followed by Dunnett test was performed to test for differences in antibody binding versus aDNP and displayed only when significant as **P ≤ 0.01 and ****P ≤ 0.0001. **(B)** Titration of binding mAbs. FITC labelled ATCC 14990 were incubated in a 3-fold dilution range from 1000 µg/mL for IVIG and from 10 µg/mL for rF1-IgG1, CR5133-IgG1 or CR6453-IgG1. MAb binding detected with donkey anti-hu-IgG(H+L)-APC and analysed with flow cytometry. Data represent GeoMFI ± SD of three independent experiments. Histograms of flow cytometry analysis are included in Figure S2. **(C)** IVIG binding to clinical isolates. 20 clinical isolates and ATCC 14990, were incubated with 25 µg/mL IVIG. IVIG binding was detected with goat anti-hu-kappa-AF647. Data points are represented as mean AF647 GeoMFI of one experiment. **(D)** mAb binding to clinical isolates. 20 clinical isolates and ATCC 14990, were incubated with 2 µg/mL nM rF1-, CR5133-, CR6453- and aDNP-IgG1. mAb binding was detected with goat anti-hu-kappa-AF647. Data points are represented as mean AF647 GeoMFI of two independent experiments.

measure binding of IVIG antibodies to ATCC 14990, but this required higher concentrations (10 µg/mL IVIG *vs* 0.004 µg/mL rF1-IgG1 or 0.37 µg/mL CR5133- and CR6453-IgG1) to reach a similar binding level. One advantage of the polyclonal nature of IVIG is that it may be possible to target a broad range of isolates. As mAbs recognize one unique target, it is important that this target is present on the majority of *S. epidermidis* isolates found in the clinic. To test the broad specificity of rF1-, CR5133- and CR6453-IgG1 when compared to IVIG, we collected a set of twenty clinical *S. epidermidis* isolates from neonatal sepsis cases. Indeed, we could detect binding of IVIG to all clinical isolates in the panel (Figure 1C). CR5133- and CR6453-IgG1 bound 19/20 isolates and rF1 bound 11/20 isolates with good capacity (classified as at least 10x binding compared to ctrl-IgG1) (Figure 1D). Thus, although CR5133- and CR6453-IgG1 bind less well to ATCC 14990, overall they bind a larger fraction of clinical isolates compared to rF1-IgG1.

Activation of the complement system greatly enhances phagocytosis by mAbs

We then evaluated whether the selected IgG1 mAbs could induce phagocytosis of *S. epidermidis* by human neutrophils. First, we studied their capacity to directly engage Fc gamma receptors in the absence of the complement system. To study this, we incubated freshly isolated neutrophils together with *S. epidermidis* ATCC 14990 opsonized with mAb at a multiplicity of infection (MOI) of 10:1. CR5133-IgG1, CR6453-IgG1 and the negative control aDNP-IgG1 could not induce Fc gamma mediated phagocytosis after 15 minutes of co-incubation (Figure 2A). Only rF1-IgG1 was capable of inducing phagocytosis in absence of the complement system. When 1% normal human serum depleted of IgG and IgM (ΔNHS) as complement source was added, phagocytosis was enhanced (Figure 2B), with rF1-IgG1 reaching high phagocytosis levels from a concentration above 0.1 µg/mL. Phagocytosis induced by

10.3389/fimmu.2022.933251

CR5133-IgG1 and CR6453-IgG1 was also enhanced, but these antibodies were less efficient than rF1-IgG1 because higher concentrations were needed to reach similar phagocytosis levels as rF1-IgG1. This observation was very consistent with the ability of the mAbs to induce complement deposition on the bacterial surface, measured using a fluorescent mAb recognizing a neoepitope in C3b (35) and flow cytometry (Figure 2C). RF1-IgG1 was the most efficient, followed by CR5133-IgG1 and CR6453-IgG1. At a fixed concentration of 10 μg/mL, we observed large differences between phagocytosis induced in absence or presence of complement, showing that mAb binding and the complement system are essential for efficient phagocytosis (Figure 2D). Finally, we tested the ability of mAbs to induce phagocytic killing, measured as a reduction in colony forming units (CFU) after prolonged incubation (90 minutes) with neutrophils at an MOI of 1:1. Consistent with the phagocytosis data showing that only rF1-IgG1 can induce Fc-mediated phagocytosis (Figure 2A), we observed that rF1-IgG1, but not CR5133-IgG1 and CR6453-IgG1, could induce phagocytic killing in absence of complement (Figure 2E). Also, in the presence of complement, killing by rF1-IgG1 was more efficient than in the absence of complement. CR5133-IgG1 and CR6453-IgG1 seemed to perform better in the presence of complement, although no significant killing compared to buffer treated samples was observed (Figure 2E). Overall, there are potent mAbs (rF1-IgG1) and less potent mAbs (CR5133- and CR6453-IgG1), and complement enhances phagocytic uptake and killing.

Hexamer-enhancing mutations in CR5133- and CR6453-IgG1 enhance phagocytosis and killing of *S. epidermidis*

For optimal interaction with the six globular headpieces of C1q, target bound IgG molecules require organization into higher-order oligomers (IgG hexamers), which occurs *via* noncovalent Fc-Fc interactions (26, 27). Therefore, we hypothesized that hexamer-enhancing mutations can improve complement activation and phagocytosis of *S. epidermidis*. We introduced mutation E345K in the Fc backbone of rF1-IgG1, CR5133-IgG1, CR6453-IgG1. This mutation was selected based on previous results obtained with *Streptococcus pneumoniae* (24). After confirming that introduction of the E345K-mutations did not affect antibody binding to *S. epidermidis* (Figure S4), we tested their ability to induce C3b deposition (Figure 3A), phagocytosis (Figure 3B) and killing (Figure 3C). Introduction of the hexamer-enhancing mutation into the already potent rF1-IgG1 could only slightly improve complement deposition (Figure 3A). In contrast, hexamer-enhanced variants of CR5133-IgG1 and CR6453-IgG1 induced very potent complement deposition compared to the WT IgG1 mAbs. For CR5133-IgG1 and CR6453-IgG1, increased complement deposition by the IgG1-E345K variants translated into more efficient phagocytosis (Figure 3B), while for rF1-IgG1 we only measured a difference in phagocytosis at the lowest mAb concentrations. Interestingly, rF1-IgG1E E345K at higher concentrations induced less phagocytosis than rF1-IgG1, which did not correlate to C3b deposition. In general, more phagocytosis benefit was gained by alteration of CR5133- and CR6453-IgG1 than by alteration of the already potent rF1-IgG1, shifting the effectiveness to a lower mAb concentration. Finally, we determined the effect of the hexamer-enhancing mutation on killing. At the lowest concentration tested (0.147 μg/mL), no additive effects of rF1-IgG1 E345K compared to rF1-IgG1 were observed (Figure 3C), presumably because incubation with 0.147 μg/mL rF1-IgG1 already reached the maximum killing capacity of the assay. In line with this hypothesis, the use of higher concentrations rF1-IgG1 or rF1-IgG1 E345K did not increase killing (Figure S5A). However, we observed a striking increase in killing after introducing the hexamer-enhancing mutation in CR5133- and especially in CR6453-IgG1 (Figure 3C). Again, these data show that rF1-IgG1 is a potent mAb that could not be improved further by introducing a hexamer-enhancing mutation. Importantly, our data also shows that less potent IgG1 mAbs, such as CR5133 and CR6453, can be greatly improved by introducing hexamer-enhancing mutations.

Because antibodies of subclass IgG3 bind C1q more stable than IgG1 (40), we also studied the effect of subclass switching to IgG3. As the molecular weight of IgG3 is slightly different from the molecular weight of IgG1, we compared concentrations in nM instead of μg/mL. Subclass switching of rF1-IgG1 to IgG3 did not change its killing capacity (Figure S5A), again presumably because the maximum killing capacity was already reached by the IgG1 variant. For mAbs CR5133 and CR6453, the effect of subclass switching to IgG3 was only detectable at a concentration that was 10 times higher (100 nM) than the concentration at which the effect of hexamer-enhancing mutations was detectable (10 nM) (Figure S5BC). This indicates that introducing the E345K mutation is more effective than subclass switching to IgG3. Moreover, introduction of the hexamer-enhancing mutation in the IgG3 subclass (IgG3E) did not improve killing beyond its IgG1E counterpart.

Plasma isolated from human umbilical cord blood retains classical pathway activity

Previous studies have reported that the neonatal complement system is less active than in healthy adults (11–13, 15). To investigate if mAbs can also activate the neonatal complement system, we first compared neonatal cord blood plasma samples to adult pooled human plasma in complement activity ELISAs to measure classical (CP), lectin (LP) and

10.3389/fimmu.2022.933251

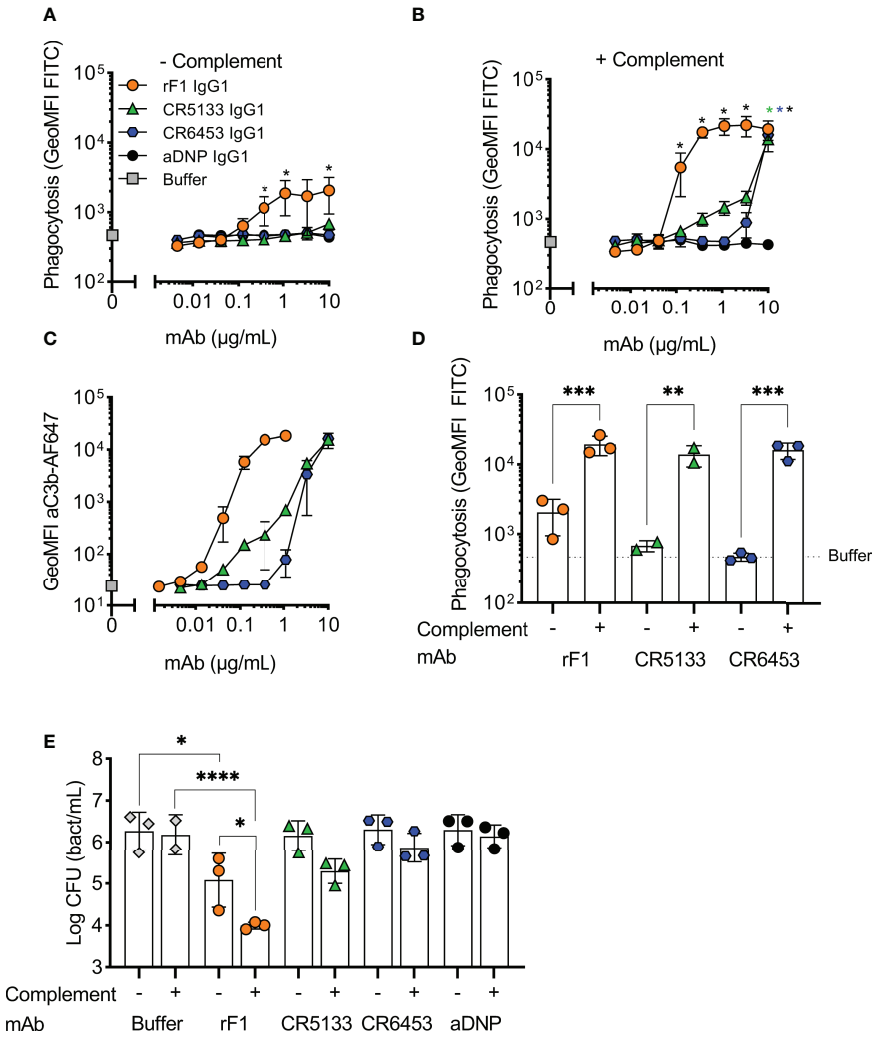

FIGURE 2
Activation of the complement system greatly enhances phagocytosis and killing with mAbs. **(A,B)** Phagocytosis of *S. epidermidis* ATCC 14990 by human neutrophils ((t=15 min), MOI 10:1) in **(A)** absence or **(B)** presence of complement. FITC labelled bacteria were incubated in **(A)** RPMI-HSA or **(B)** 1% IgG/IgM-depleted normal human serum (ΔNHS) supplemented with a concentration range of rF1, CR5133, CR6453, aDNP IgG1 or buffer. Phagocytosis was quantified by flow cytometry and plotted as FITC GeoMFI of the neutrophils population. The gating strategy at 1 µg/mL mAb is shown in Figure S3. Data represent mean ± SD of three independent experiments. One-way ANOVA followed by Bonferroni correction was used to test the effect of mAb addition compared to aDNP-IgG1. Test results were displayed only when significant as *P ≤ 0.05 (black for rF1, green for CR5133, blue for CR6453). **(C)** C3b deposition by mAbs. FITC labelled *S. epidermidis* ATCC 14990 were incubated in 1% ΔNHS supplemented with a concentration range of mAb. C3b deposition was detected by flow cytometry using an anti-neoC3b-AF647 antibody conjugate and plotted as AF647 GeoMFI of the FITC+ve bacterial population. Data represent mean ± SD of three independent experiments. **(D)** Comparison of mAb (10 µg/mL) induced phagocytosis in absence and presence of complement. One-way ANOVA was performed to test for the effect of complement addition on phagocytosis and displayed as *P ≤ 0.05, **P ≤ 0.01, ***P ≤ 0.001 and ****P ≤ 0.0001. **(E)** Killing of *S. epidermidis* ATCC 14990 by human neutrophils (t=90 min, MOI 1:1) in absence or presence of complement. Bacteria were incubated in 10% heat-inactivated (HI)-ΔNHS (–) or 10% ΔNHS (+) supplemented with buffer (dashed horizontal line) or 14.8 µg/mL (100 nM) rF1-, CR5133-, CR6453- or aDNP-IgG1. Data represent mean ± SD of three independent experiments. One-way ANOVA followed by Bonferroni correction was used to test the effect of mAb addition to HI-ΔNHS, mAb addition to ΔNHS and to test the effect of complement addition for each mAb specifically. Test results were displayed only when significant as *P ≤ 0.05, **P ≤ 0.01, ***P ≤ 0.001 and ****P ≤ 0.0001.

alternative (AP) pathway activity. We collected cord blood plasma from neonates (n=5) with a gestational age ranging from 32-42 weeks. Parallel, plasma from healthy adult volunteers was collected in the exact same procedure. To preserve complement activity, all samples were collected in r-Hirudin tubes. Hirudin is a direct thrombin inhibitor, which does not interfere with the complement system, in contrast to other anticoagulants such as heparin or sodium citrate (41, 42). We showed that in all neonatal samples the CP was equally active to adult pooled human plasma (Figure 4A). The LP was

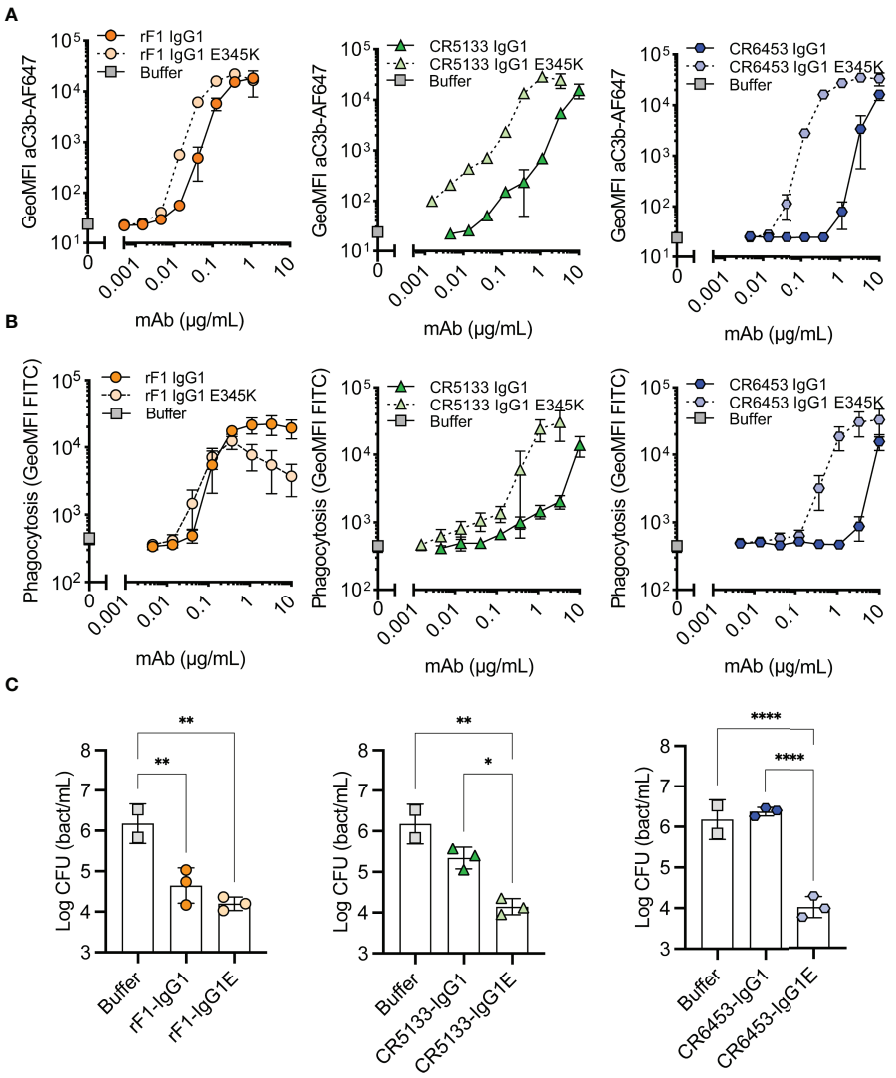

FIGURE 3
Hexamer enhancing mutations significantly improve effector functions against *S. epidermidis*. **(A)** Effect of introduced hexamer-enhancing mutations on deposition of C3b. FITC labelled *S. epidermidis* ATCC 14990 were incubated in 1% ΔNHS supplemented with a concentration range of mAb in IgG1 or IgG1-E345K variant. C3b deposition was detected by flow cytometry using an anti-neoC3b-AF647 antibody conjugate and plotted as AF647 GeoMFI of the FITC+ve bacterial population. Data represent mean ± SD of three independent experiments. **(B)** Phagocytosis of *S. epidermidis* ATCC 14990 by neutrophils (MOI 10:1) in the presence of complement. Bacteria were prepared as in **(A)**. Phagocytosis was assessed by flow cytometry and plotted as FITC GeoMFI of the neutrophils population. Data represent mean ± SD of three independent experiments. Data shown for IgG1 are identical to data shown in Figure 2B. **(C)** Killing of *S. epidermidis* ATCC 14990 by neutrophils (MOI 1:1) in presence of complement. Bacteria were incubated in 10% ΔNHS supplemented with 0.148µg/mL (1nM) rF1, 1.48µg/mL (10nM) CR5133 or CR6453. All concentrations tested can be viewed in Figure S5. Bacterial survival was quantified after neutrophils lysis by serial dilution and CFU counting. Data represent mean ± SD of three independent experiments. One-way ANOVA followed by Bonferroni correction was used to test the effect of mAb addition in ΔNHS, as well as the difference in bacterial survival of WT *vs* hexabody, *P ≤ 0.05, **P ≤ 0.01 and ****P ≤ 0.0001.

decreased in activity compared to pooled human plasma in only one neonatal donor (Figure 4B). On the other hand, the alternative pathway was decreased in all but one neonatal donor (Figure 4C). Thus, although not all complement pathways are equally active in neonatal plasma, we showed that the classical pathway, which is activated by mAbs, is not impaired.

Anti-*S. epidermidis* mAbs react with the neonatal complement system

Finally, we used the same assay to study if neonatal plasma could react with mAbs to opsonize bacteria for phagocytosis. Because umbilical cord blood was collected anonymously, there is a possibility that mothers received prophylaxis against group B

10.3389/fimmu.2022.933251

streptococci by Amoxicillin/Clavulanic acid (Augmentin®) during labor, which is transferred to the neonatal plasma. Unfortunately, ATCC 14990 was sensitive to this antibiotic. As this could interfere with our assays, we selected a clinical isolate (N2297) that was resistant to Amoxicillin/Clavulanic acid for use in the assays with neonatal plasma. First, we confirmed that all mAbs can bind N2297 and that introduction of the E-mutation did not affect mAb binding (Figure S6). We also compared mAb and IVIG binding and again observed that all mAbs showed increased binding compared to IVIG, even at very low concentrations.

As complement activity increases with gestational age (12, 13), we divided the donors in two groups of different gestational age; 32-37 weeks GA (n=2) (Figure 5A) and >37 weeks GA (n=3) (Figure 5B). Similar to the results on strain ATCC 14990 (Figure 3B), rF1-IgG1 could induce phagocytosis and introduction of the hexamer-enhancing mutation in rF1-IgG1 did not result in beneficial effects. CR5133-IgG1 was also capable of inducing phagocytosis in presence of neonatal plasma and CR5133-IgG1 E345K further enhanced phagocytosis. CR6453-IgG1 could not induce phagocytosis, but introduction of the hexamer-enhancing mutation greatly enhanced phagocytosis. For all mAbs, the phagocytosis was completely dependent on the neonatal complement system, because when heat inactivated plasma was used, there was no phagocytosis (Figure 5, S7). We also compared mAb efficacy to IVIG efficacy. To observe a response in presence of complement, we added a maximum of 1 mg/mL IVIG in 1% plasma. However, this dose is ~10 times higher than clinically relevant, as neonatal clinical trials reach maximum IVIG concentrations of 7-15 mg/mL in 100% plasma (22, 43), which corresponds to 70-150 µg/mL in 1% plasma. In absence of complement, IVIG could not induce phagocytosis (Figure S8). For CR5133-IgG1 E345K, a concentration of only 0.042 µg/mL was needed to reach a comparable level of phagocytosis as 1000 µg/mL IVIG. For the other mAbs, a concentration of ~1 µg/mL mAb was needed to reach comparable levels to 1000 µg/mL IVIG. We did not observe differences between the two donor groups, thus mAbs can react with the neonate complement system of term (>37 weeks GA) and pre-term (32-37 weeks) infants. Concluding, we show complement activity in term and preterm infant plasma is sufficient to enhance IgG1 mediated opsonophagocytosis by human neutrophils.

Discussion

Staphylococcus epidermidis is the most prevalent causative agent of late-onset sepsis in neonates, who are at high risk for infections because of transient immunodeficiency of immaturity (7–15, 44). In this study we show that monoclonal IgG1 antibodies against *S. epidermidis* can boost the neonatal complement system to opsonize bacteria for phagocytosis by

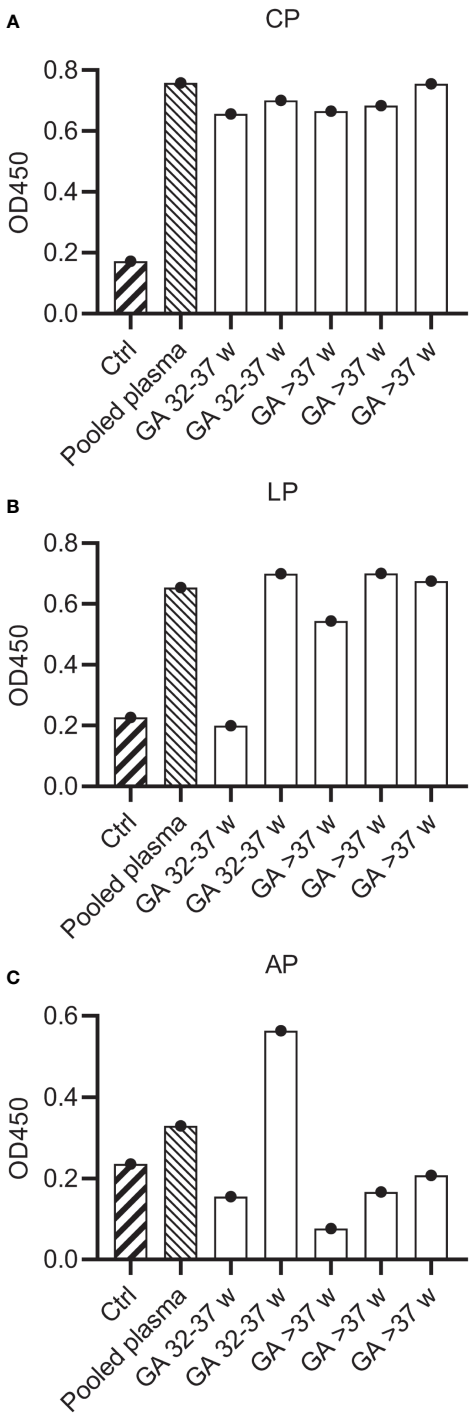

FIGURE 4
Complement activity of neonatal plasma. Complement activity in pooled human hiridun plasma and neonatal hirudin plasma (n=5) was determined in complement ELISAs, detecting deposition of C3b. Plates were coated with **(A)** IgM and 2% plasma to determine CP activity, **(B)** mannan and 2% plasma to determine LP activity and **(C)** LPS and 30% plasma to determine AP activity. Ctrl wells were uncoated and incubated with pooled adult plasma. CP, Classical pathway; LP, Lectin pathway; AP, Alternative pathway.

10.3389/fimmu.2022.933251

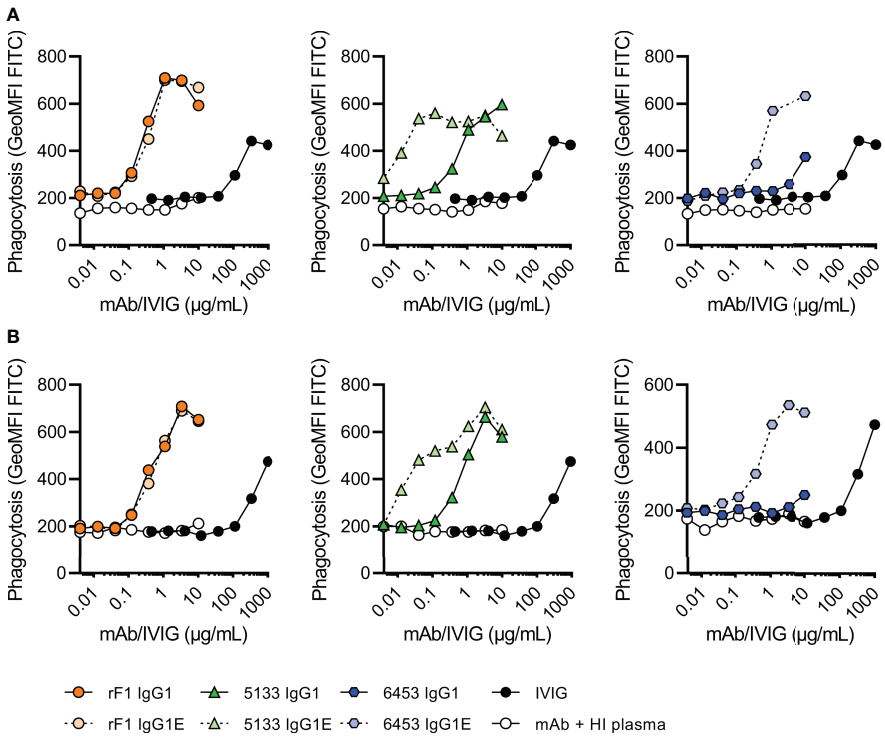

FIGURE 5
Phagocytosis of FITC labelled N2297 after incubation with mAbs or IVIG in 1% neonatal plasma. Phagocytosis of *S. epidermidis* N2297 by human neutrophils (MOI 10:1) in **(A)** a representative donor of 32-37 weeks GA and **(B)** a representative donor >37 weeks GA. FITC labelled bacteria were incubated in 1% neonatal plasma or 1% HI neonatal plasma supplemented with a concentration range of rF1, CR5133 or CR6453 IgG1 or IgG1 E345K or IVIG. Phagocytosis was quantified by flow cytometry and plotted as FITC GeoMFI of the neutrophils population. Data represent data of one independent experiment. Additional donors (n=5) can be viewed in Figure S5. GA, Gestational Age.

neutrophils, which is an efficient way for the immune system to eliminate Gram-positive bacteria such as *S. epidermidis* (18).

Our study highlights that complement is essential for antibody-mediated phagocytosis of *S. epidermidis*. For the different IgG1 mAbs we compared, Fc gamma receptor mediated phagocytosis was absent (CR5133 and CR6453) or low (rF1). In the presence of complement, uptake was greatly enhanced. This is in agreement with previous work on *Streptococcus pneumoniae*, where IgG1 mAbs directed against capsule polysaccharide CPS6 were completely dependent on complement deposition (24). In contrast, we previously observed that naturally occurring IgG, IVIG (45) and a monoclonal antibody against WTA (23) can induce Fc receptor mediated phagocytosis of *S. aureus* in absence of complement. However, also in these studies, phagocytosis could be improved when complement was added.

Recently, Fc mutations and subclass switching to modify the interaction of a mAbs Fc-part with C1q to increase antibody-mediated complement deposition are being explored (46). This is because for optimal interaction with the six globular headpieces of C1q, target bound IgG molecules require organization into hexamers, which occurs *via* noncovalent Fc-Fc interactions (26, 27). Hexamer enhancing mutations have already been shown to enhance complement mediated lysis of *Neisseria gonorrhoeae* (47) and tumor cells (26) *via* the formation of membrane attack complex pores. Together with data on *S. aureus* (23) and *S. pneumoniae* (24), our study provides an important proof of concept that hexamer enhancing mutations can also potentiate opsonization and phagocytic killing of Gram-positive bacteria. This indicates that hexamer enhancing mutations could be applied to a broad range of pathogens and diseases.

Our data also indicates that introducing the hexamer enhancing E345K mutation can enhance mAbs to a similar extent or more than switching to IgG3 subclass. This is an important insight because IgG1 is established to be safe for antibody therapy in other fields than infectious diseases such as oncology and auto-immune diseases (48), is easier to produce and purify than IgG3 (46) and has a longer half-life than IgG3 (49).

This study also sheds light on the role of mAb epitopes in efficacy of phagocytosis. We here compared mAbs with an identical Fc backbone but different Fab domains on the same bacterial strain. Our data shows that the use of different Fab

domains, which confers binding to epitopes, results in different efficacy between mAbs. This is novel compared to previous publications from our laboratory, in which we either compared mAbs recognizing different bacterial strains (*S. pneumoniae* (24)) or we studied one mAb (4497) with different Fc tails (*S. aureus* (23)). The direct comparison in this work is a strong indication that the epitope is crucial for the efficacy of mAbs to opsonize *S. epidermidis* for phagocytic killing. We hypothesize that the ideal epitope allows for IgG clustering, as literature describes that epitope density can influence hexamerization (26). Affinity for the epitope may also play a role, as binding with one Fab arm (instead of two) enhances hexamer formation (26, 50). In all, this stresses the importance of identifying the ideal epitope to target with mAb therapy.

Next to being able to trigger complement activation, for application of mAbs it is also important that they react with conserved antigens that are present on the majority of clinical isolates. This made rF1, although being the most potent mAb on our model strain, less ideal because it only bound ~50% of clinical isolates. Interestingly we showed that two mAbs (CR5133 and CR6453) could bind 19/20 clinical isolates. Even if CR5133- and CR6453-IgG1 were less potent in driving phagocytosis than rF1-IgG1, their functionality could be enhanced by hexamer enhancing mutations. The fact that we found two mAbs that bound 95% of clinical isolates indicates that mAb therapy for *S. epidermidis* holds potential, while for other pathogens, such as *S. pneumoniae*, the existence of many different serotypes will pose a challenge (51). The future of anti-bacterial preventive or therapeutic mAb therapies may well be in cocktails of multiple mAbs against different strains of a single species or against multiple species of interest (52).

Our study supports the presence of an effective complement system in neonates, enabling effective antibody induced opsonophagocytosis. Previous studies have reported a decreased complement activity and plasma concentrations of complement components in neonates, which is correlated with gestational age (11). Older studies described that most complement levels are at 50–70% of the adult values, rising to adult concentrations within 6 months after birth (11, 12, 15). Recent work describes significantly lower levels for approximately one third of the complement factors measured (28). We found lower complement activity compared to adults in the alternative pathway but not in the lectin and classical pathway. An explanation could be that we used r-Hirudin tubes to collect plasma in this study, which preserves complement activity the best (36). Even though alternative pathway activity, which is responsible for the complement amplification loop, was decreased, we showed that mAbs can greatly stimulate phagocytosis in the presence of neonatal complement. This confirms that neonatal complement can be activated by mAbs and that mAb therapy in neonates should be further explored.

As a proof of concept, we here show that mAbs (IgG1 and Fc : Fc enhanced IgG1) can react with the neonatal complement system to potentiate phagocytosis by healthy donor adult neutrophils. Others have shown neonatal neutrophils can efficiently phagocytose and kill *S. epidermidis* when opsonized with adult serum (44). Therefore, we expect that neonatal neutrophils will respond in the same manner as the adult neutrophils in our assay, although this will need further investigation.

In conclusion, we demonstrate that monoclonal antibodies against *S. epidermidis* can effectively induce opsonophagocytosis in the context of neonatal plasma. Opsonophagocytosis of *S. epidermidis* is dependent on complement activation and hexamer enhancing mutations in IgG effectuate more efficient opsonophagocytosis in neonatal plasma. Anti-*S. epidermidis* mAbs are a potential future preventive therapy that could be used in the neonatal setting to avoid *S. epidermidis* CLABSI in high-risk infants admitted to neonatal intensive care units.

Data availability statement

Datasets are available on request: The raw data supporting the conclusions of this article will be made available by the authors, without undue reservation.

Ethics statement

This study was reviewed and approved by Ethics Committee for Biobanking of the University Medical Center Utrecht. The patients/participants provided their written informed consent to participate in this study.

Author contributions

Conception and design: LV, CB, KK, SR, MF. Sample preparation and collection of data: AF, LS, CB, CH, PA, FB. Analysis and interpretation of data: LV, CB, AF, KK. Contribution of reagents and tools: CH, PA, FB. Supervision: SR, KK, MF. Preparation of figures and tables: LV, AF. Collection of neonatal samples: CB, MF, MB, DV. Manuscript preparation: LV, AF. Revision of manuscript: CB, SR and MF. All authors read and approved the submitted version.

Funding

This project was financially supported by a grant from the Wilhelmina Children's Hospital Fund (MvdF) and by a PPP Allowance made available by Health~Holland (LSHM17026), Top Sector Life Sciences & Health, to stimulate public-private partnerships.

Acknowledgments

The authors greatly thank J.T. van der Bruggen for providing *S. epidermidis* clinical isolates; prof. T. Mollnes and prof. P. Garred for providing clone Bh6 cells.

Conflict of interest

FB is affiliated with Genmab.

The remaining authors declare that the research was conducted in the absence of any commercial or financial relationships that could be construed as a potential conflict of interest.

Publisher's note

Supplementary material

The Supplementary Material for this article can be found online at: https://www.frontiersin.org/articles/10.3389/fimmu.2022.933251/full#supplementary-material

References

1. James SL, Abate D, Abate KH, Abay SM, Abbafati C, Abbasi N, et al. Global, regional, and national incidence, prevalence, and years lived with disability for 354 diseases and injuries for 195 countries and territories, 1990-2017: A systematic analysis for the global burden of disease study 2017. *Lancet* (2018) 392 (10159):1789–858. doi: 10.1016/S0140-6736(18)32279-7

2. Fleischmann C, Reichert F, Cassini A, Horner R, Harder T, Markwart R, et al. Global incidence and mortality of neonatal sepsis: A systematic review and meta-analysis. *Arch Dis Child* (2021) 106(8):745–52. doi: 10.1136/archdischild-2020-320217

3. Dong Y, Speer CP, Glaser K. Beyond sepsis: Staphylococcus epidermidis is an underestimated but significant contributor to neonatal morbidity. *Virulence* (2018) 9(1):621–33. doi: 10.1080/21505594.2017.1419117

4. Kollmann TR, Kampmann B, Mazmanian SK, Marchant A, Levy O. Protecting the newborn and young infant from infectious diseases: Lessons from immune ontogeny. *Immunity* (2017) 46(3):350–63. doi: 10.1016/j.immuni.2017.03.009

5. Hsu HE, Mathew R, Wang R, Broadwell C, Horan K, Jin R, et al. Health care-associated infections among critically ill children in the US, 2013-2018. *JAMA Pediatr* (2020) 174(12):1176. doi: 10.1001/jamapediatrics.2020.3223

6. Watson RS, Carcillo JA, Linde-Zwirble WT, Clermont G, Lidicker J, Angus DC. The epidemiology of severe sepsis in children in the united states. *Am J Respir Crit Care Med* (2003) 167(5):695–701. doi: 10.1164/rccm.200207-682OC

7. Claessens LC, Zonnenberg IA, Van Den Dungen FAM, Vermeulen RJ, Van Weissenbruch MM. Cerebral ultrasound abnormalities in preterm infants caused by late-onset sepsis. *PloS One* (2017) 12(3):1–10. doi: 10.1371/journal.pone.0173227

8. Isaacs D. A ten year, multicentre study of coagulase negative staphylococcal infections in Australasian neonatal units. *Arch Dis Child Fetal Neonatal Ed* (2003) 88(2):89–93. doi: 10.1136/fn.88.2.F89

9. Palmeira P, Quinello C, Silveira-Lessa AL, Zago CA, Carneiro-Sampaio M. IgG placental transfer in healthy and pathological pregnancies. *Clin Dev Immunol* (2012) 2012:1–13. doi: 10.1155/2012/985646

10. Malek A, Sager R, Kuhn P, Nicolaides KH, Schneider H. Evolution of maternofetal transport of immunoglobulins during human pregnancy. *Am J Reprod Immunol* (1996) 36(5):248–55. doi: 10.1111/j.1600-0897.1996.tb00172.x

11. McGreal EP, Hearne K, Spiller OB. Off to a slow start: Under-development of the complement system in term newborns is more substantial following premature birth. *Immunobiology* (2012) 217:176–86. doi: 10.1016/j.imbio.2011.07.027

12. Notarangelo LD, Chirico G, Chiara A, Colombo A, Rondini G, Plebani A, et al. Activity of classical and alternative pathways of complement in preterm and small for gestational age infants. *Pediatr Res* (1984) 18(3):281–5. doi: 10.1203/00006450-198403000-00014

13. Grumach AS, Ceccon ME, Rutz R, Fertig A, Kirschfink M. Complement profile in neonates of different gestational ages. *Scand J Immunol* (2014) 79(4):276–81. doi: 10.1111/sji.12154

14. Prosser A, Hibbert J, Strunk T, Kok CH, Simmer K, Richmond P, et al. Phagocytosis of neonatal pathogens by peripheral blood neutrophils and monocytes from newborn preterm and term infants. *Pediatr Res* (2013) 74 (5):503–10. doi: 10.1038/pr.2013.145

15. Høgåsen AKM, ØVerlie I, Hansen TWR, Abrahamsen TG, Finne PH, Høgåsen K. The analysis of the complement activation product SC5 b-9 is applicable in neonates in spite of their profound C9 deficiency. *J Perinat Med* (2000) 28(1). doi: 10.1515/JPM.2000.006

16. Lawrence SM, Corriden R, Nizet V. Age-appropriate functions and dysfunctions of the neonatal neutrophil. *Front Pediatr* (2017) 5. doi: 10.3389/fped.2017.00023

17. Rigby KM, DeLeo FR. Neutrophils in innate host defense against staphylococcus aureus infections. *Semin Immunopathol* (2012) 34(2):237–59. doi: 10.1007/s00281-011-0295-3

18. Segal AW. How neutrophils kill microbes. *Annu Rev Immunol* (2005) 23 (1):197–223. doi: 10.1146/annurev.immunol.23.021704.115653

19. Bayram RO, Özdemir H, Emsen A, Türk Dağı H, Artaç H. Reference ranges for serum immunoglobulin (Igg, iga, and igm) and igg subclass levels in healthy children. *Turkish J Med Sci* (2019) 49(2):497–505. doi: 10.3906/sag-1807-282

20. Lu LL, Suscovich TJ, Fortune SM, Alter G. Beyond binding: Antibody effector functions in infectious diseases. *Nat Rev Immunol* (2018) 18(1):46–61. doi: 10.1038/nri.2017.106

21. Dustin ML. Complement receptors in myeloid cell adhesion and phagocytosis. *Microbiol Spectr* (2016) 4(6). doi: 10.1128/microbiolspec.MCHD-0034-2016

22. Ohlsson A, Lacy JB. Intravenous immunoglobulin for suspected or proven infection in neonates. *Cochrane Database Syst Rev* (2020) 2020(1). doi: 10.1002/14651858.CD001239.pub6

23. Zwarthoff SA, Widmer K, Kuipers A, Strasser J, Ruyken M, Aerts PC, et al. C1q binding to surface-bound IgG is stabilized by C1r2s2 proteases. *Proc Natl Acad Sci.* (2021) 118(26). doi: 10.1073/pnas.2102787118

24. Aguinagalde L, den Boer MA, Castenmiller SM, Zwarthoff SA, Gosselaar-de Haas CJC, Aerts PC, et al. *Promoting fc-fc interactions between anti-capsular antibodies provides strong complement-dependent immune protection against streptococcus pneumoniae* (2022). Available at: http://biorxiv.org/content/early/2022/01/21/2022.01.21.477211.abstract.

25. Wang G, de Jong RN, van den Bremer ETJ, Beurskens FJ, Labrijn AF, Ugurlar D, et al. Molecular basis of assembly and activation of complement component C1 in complex with immunoglobulin G1 and antigen. *Mol Cell* (2016) 63(1):135–45. doi: 10.1016/j.molcel.2016.05.016

26. Diebolder CA, Beurskens FJ, De Jong RN, Koning RI, Strumane K, Lindorfer MA, et al. Complement is activated by IgG hexamers assembled at the cell surface. *Science* (2014) 343(6176):1260–63. doi: 10.1126/science.1248943

27. de Jong RN, Beurskens FJ, Verploegen S, Strumane K, van Kampen MD, Voorhorst M, et al. A novel platform for the potentiation of therapeutic antibodies based on antigen-dependent formation of IgG hexamers at the cell surface. *PloS Biol* (2016) 14(1):e1002344. doi: 10.1371/journal.pbio.1002344&type=printable

28. Willems E, Alkema W, Keizer-Garritsen J, Suppers A, van der Flier M, Philipsen RHLA, et al. Biosynthetic homeostasis and resilience of the complement system in health and infectious disease. *EBioMedicine* (2019) 45:303–13. doi: 10.1016/j.ebiom.2019.06.008

29. Zwarthoff SA, Magnoni S, Aerts PC, van Kessel KPM, Rooijakkers SHM. Method for depletion of IgG and IgM from human serum as naive complement source. In: *Methods in molecular biology (Clifton, N.J.)* (2021) 2227:21–32.

30. Vink T, Oudshoorn-Dickmann M, Roza M, Reitsma JJ, de Jong RN. A simple, robust and highly efficient transient expression system for producing antibodies. *Methods* (2014) 65(1):5–10. doi: 10.1016/j.ymeth.2013.07.018

31. de Vor L, van Dijk B, van Kessel K, Kavanaugh JS, de Haas C, Aerts PC, et al. Human monoclonal antibodies against staphylococcus aureus surface antigens recognize *In vitro* and *In vivo* biofilm. *Elife* (2022) 11:1–25.doi: 10.7554/eLife.67301

32. Hugh R, Ellis Ma. The neotype strain for staphylococcus epidermidis (Winslow and Winslow 1908) Evans 1916. *Int J Syst Bacteriol* (1968) 18(3):231–39. doi: 10.1099/00207713-18-3-231

33. Putonti C, Kalesinskas L, Cudone E, Engelbrecht KC, Koenig DW, Wolfe AJ. Draft genome sequence of staphylococcus epidermidis (Winslow and Winslow) Evans (ATCC 14990). *Genome Announc* (2017) 5(27). doi: 10.1128/genomeA.00619-17

34. Bestebroer J, Poppelier MJJG, Ulfman LH, Lenting PJ, Denis CV, Van Kessel KPM, et al. Staphylococcal superantigen-like 5 binds PSGL-1 and inhibits p-Selectin-Mediated neutrophil rolling. *Blood* (2007) 109(7):2936–43. doi: 10.1182/blood-2006-06-015461

35. Garred P, Mollnes TE, Lea T, Fischer E. Characterization of a monoclonal antibody MoAb Bh6 reacting with a neoepitope of human C3 expressed on C3b, Ic3b, and C3c. *Scand J Immunol* (1988) 27(3):319–27. doi: 10.1111/j.1365-3083.1988.tb02353.x

36. Bexborn F, Engberg AE, Sandholm K, Mollnes TE, Hong J, Ekdahl KN. Hirudin versus heparin for use in whole blood in vitro biocompatibility models. *J BioMed Mater Res - Part A* (2009) 89A(4):951–59. doi: 10.1002/jbm.a.32034

37. Seelen MA, Roos A, Wieslander J, Mollnes TE, Sjöholm AG, Wurzner R, et al. Functional analysis of the classical, alternative, and MBL pathways of the complement system: Standardization and validation of a simple ELISA. *J Immunol Methods* (2005) 296(1–2):187–98. doi: 10.1016/j.jim.2004.11.016

38. Hazenbos WLW, Kajihara KK, Vandlen R, Morisaki JH, Lehar SM, Kwakkenbos MJ, et al. Novel staphylococcal glycosyltransferases SdgA and SdgB mediate immunogenicity and protection of virulence-associated cell wall proteins. *PloS Pathog* (2013) 9(10):e1003653. doi: 10.1371/journal.ppat.1003653

39. Gonzalez ML, Frank MB, Ramsland PA, Hanas JS, Waxman FJ. Structural analysis of IgG2A monoclonal antibodies in relation to complement deposition and renal immune complex deposition. *Mol Immunol* (2003) 40(6):307–17. doi: 10.1016/S0161-5890(03)00167-6

40. Vidarsson G, Dekkers G, Rispens T. IgG subclasses and allotypes: From structure to effector functions. *Front Immunol* (2014) 5(October):520. doi: 10.3389/fimmu.2014.00520

41. Van Der Maten E, De Jonge MI, De Groot R, van der Flier M, Langereis JD. A versatile assay to determine bacterial and host factors contributing to opsonophagocytotic killing in hirudin-anticoagulated whole blood. *Sci Rep* (2017) 7(1):42137. doi: 10.1038/srep42137

42. Chang JY. The functional domain of hirudin, a thrombin-specific inhibitor. *FEBS Lett* (1983) 164(2):307–13. doi: 10.1016/0014-5793(83)80307-X

43. Ohlsson A, Lacy JB. Intravenous immunoglobulin for preventing infection in preterm and/or low birth weight infants. *Cochrane database of systematic reviews* (2020) 1(1):CD000361. doi: 10.1002/14651858.CD000361

44. Wolach B, Carmi D, Gilboa S, Satar M, Segal S, Dolfin T, et al. Some aspects of the humoral immunity and the phagocytic function in newborn infants. In: *Israel Journal of medical sciences* (1994) 30(5–6):331–5.

45. Boero E, Brinkman I, Juliet T, van Yperen E, van Strijp JAG, Rooijakkers SHM, et al. Use of flow cytometry to evaluate phagocytosis of staphylococcus aureus by human neutrophils. *Front Immunol* (2021) 12(February):1–15. doi: 10.3389/fimmu.2021.635825

46. Chu TH, Patz EF, Ackerman ME. Coming together at the hinges: Therapeutic prospects of Igg3. *mAbs* (2021) 13(1). doi: 10.1080/19420862.2021.1882028

47. Gulati S, Beurskens FJ, de Kreuk BJ, Roza M, Zheng B, Deoliveira RB, et al. Complement alone drives efficacy of a chimeric antigonococcal monoclonal antibody. *PloS Biol* (2019) 17(6):e3000323. doi: 10.1371/journal.pbio.3000323

48. Castelli MS, McGonigle P, Hornby PJ. The pharmacology and therapeutic applications of monoclonal antibodies. *Pharmacol Res Perspect* (2019) 7(6). doi: 10.1002/prp2.535

49. Morell A, Terry WD, Waldmann TA. Metabolic properties of IgG subclasses in man. *J Clin Invest* (1970) 49(4):673–80. doi: 10.1172/JCI106279

50. Wang B, Yang C, Jin X, Du Q, Wu H, Dall'Acqua W, et al. Regulation of antibody-mediated complement-dependent cytotoxicity by modulating the intrinsic affinity and binding valency of IgG for target antigen. *MAbs* (2020) 12 (1). doi: 10.1080/19420862.2019.1690959

51. Bentley SD, Aanensen DM, Mavroidi A, Saunders D, Rabbinowitsch E, Collins M, et al. Genetic analysis of the capsular biosynthetic locus from all 90 pneumococcal serotypes. *PloS Genet* (2006) 2(3):e31. doi: 10.1371/journal.pgen.0020031

52. Frandsen TP, Næsted H, Rasmussen SK, Hauptig P, Wiberg FC, Rasmussen LK, et al. Consistent manufacturing and quality control of a highly complex recombinant polyclonal antibody product for human therapeutic use. *Biotechnol Bioeng* (2011) 108(9):2171–81. doi: 10.1002/bit.23166

frontiers | Frontiers in Immunology

TYPE Original Research
PUBLISHED 16 August 2022
DOI 10.3389/fimmu.2022.949140

OPEN ACCESS

EDITED BY
Reiko Shinkura,
The University of Tokyo, Japan

REVIEWED BY
Adam Waickman,
Upstate Medical University,
United States
Richard Tobin,
University of Colorado Anschutz
Medical Campus, United States

*CORRESPONDENCE
Thomas Valerius
t.valerius@med2.uni-kiel.de

†These authors have contributed
equally to this work

SPECIALTY SECTION
This article was submitted to
B Cell Biology,
a section of the journal
Frontiers in Immunology

RECEIVED 20 May 2022
ACCEPTED 26 July 2022
PUBLISHED 16 August 2022

CITATION
Baumann N, Arndt C, Petersen J,
Lustig M, Rösner T, Klausz K, Kellner C,
Bultmann M, Bastian L, Vogiatzi F,
Leusen JHW, Burger R, Schewe DM,
Peipp M and Valerius T (2022) Myeloid
checkpoint blockade improves killing
of T-acute lymphoblastic
leukemia cells by an IgA2 variant
of daratumumab.
Front. Immunol. 13:949140.
doi: 10.3389/fimmu.2022.949140

Myeloid checkpoint blockade improves killing of T-acute lymphoblastic leukemia cells by an IgA2 variant of daratumumab

Niklas Baumann[1†], Christian Arndt[1†], Judith Petersen[1], Marta Lustig[1], Thies Rösner[1], Katja Klausz[2], Christian Kellner[3], Miriam Bultmann[4], Lorenz Bastian[4], Fotini Vogiatzi[5], Jeanette H. W. Leusen[6], Renate Burger[1], Denis M. Schewe[7], Matthias Peipp[2] and Thomas Valerius[1*]

[1]Division of Stem Cell Transplantation and Immunotherapy, Department of Medicine II, Christian-Albrechts-University Kiel and University Medical Center Schleswig-Holstein, Kiel, Germany, [2]Division of Antibody-Based Immunotherapy, Department of Medicine II, Christian- Albrechts-University Kiel and University Medical Center Schleswig-Holstein, Kiel, Germany, [3]Division of Transfusion Medicine, Cell Therapeutics and Haemostaseology, University Hospital, LMU Munich, Munich, Germany, [4]Department of Medicine II, Christian-Albrechts-University Kiel and University Medical Center Schleswig-Holstein, Kiel, Germany, [5]Pediatric Hematology/Oncology, Christian-Albrechts-University Kiel and University Medical Center Schleswig-Holstein, Kiel, Germany, [6]Center for Translational Immunology, University Medical Center Utrecht, Utrecht, Netherlands, [7]Children's Hospital, University Medical Center Magdeburg, Magdeburg, Germany

Antibody-based immunotherapy is increasingly employed to treat acute lymphoblastic leukemia (ALL) patients. Many T-ALL cells express CD38 on their surface, which can be targeted by the CD38 antibody daratumumab (DARA), approved for the treatment of multiple myeloma. Tumor cell killing by myeloid cells is relevant for the efficacy of many therapeutic antibodies and can be more efficacious with human IgA than with IgG antibodies. This is demonstrated here by investigating antibody-dependent cellular phagocytosis (ADCP) by macrophages and antibody-dependent cell-mediated cytotoxicity (ADCC) by polymorphonuclear (PMN) cells using DARA (human IgG1) and an IgA2 isotype switch variant (DARA-IgA2) against T-ALL cell lines and primary patient-derived tumor cells. ADCP and ADCC are negatively regulated by interactions between CD47 on tumor cells and signal regulatory protein alpha (SIRPα) on effector cells. In order to investigate the impact of this myeloid checkpoint on T-ALL cell killing, CD47 and glutaminyl-peptide cyclotransferase like (QPCTL) knock-out T-ALL cells were employed. QPTCL is an enzymatic posttranslational modifier of CD47 activity, which can be targeted by small molecule inhibitors. Additionally, we used an IgG2σ variant of the CD47 blocking antibody magrolimab, which is in advanced clinical development. Moreover, treatment of T-ALL cells with all-*trans* retinoic acid

(ATRA) increased CD38 expression leading to further enhanced ADCP and ADCC, particularly when DARA-IgA2 was applied. These studies demonstrate that myeloid checkpoint blockade in combination with IgA2 variants of CD38 antibodies deserves further evaluation for T-ALL immunotherapy.

KEYWORDS

T-cell acute lymphoblastic leukemia (T-ALL), CD38, daratumumab, IgA, CD47, SIRPα, immunotherapy

Introduction

Antibody-based immunotherapy is a rapidly growing field with more than 100 antibody product approvals since 1986 and more than 50% of them during the last decade (1). The CD38 antibody daratumumab is an example of how individual antibodies can change the therapeutic landscape, in this case for multiple myeloma patients (2). For B cell precursor acute lymphoblastic leukemia (BCP-ALL), three antibody-based immunotherapeutics (rituximab, blinatumumab and inotuzumab-ozogamicin) have been approved so far (3). While antibody-based immunotherapy for patients with T cell (T)-ALL is not yet established, some monoclonal antibodies against T cell expressed antigens such as C-C chemokine receptor type 4 (mogamulizumab), CD52 (alemtuzumab), and CD30 (brentuximab-vetodine) have been approved in the treatment of other indications and are currently evaluated preclinically and clinically also in T-ALL (4, 5). The CD38 antigen is also expressed by many BCP- and T-ALL cells (6, 7), and both daratumumab and isatuximab, the second CD38 antibody approved for myeloma therapy, are being tested in clinical trials (5). Preclinical studies showed that both antibodies possess significant *in vitro* and *in vivo* activity against ALL cells with strong antibody-dependent cell-mediated cytotoxicity (ADCC) and antibody-dependent cellular phagocytosis (ADCP) effects (8–10).

Myeloid cell-mediated ADCC or ADCP can be increased by blocking myeloid checkpoint molecules – such as the CD47/signal regulatory protein alpha (SIRPα) axis (11). For example, daratumumab in combination with CD47 blockade was effective in T-ALL cell depletion *in vivo* in xenograft NSG mouse models (12), which was most likely caused by myeloid effector cells since these severely immunocompromised mice do not have T or NK cells and lack a functional complement system. The CD47 blocking antibody hu5F9-G4 (magrolimab) combined with the CD20 antibody rituximab showed promising clinical activity in advanced lymphoma patients (13). Another emerging strategy to impede CD47/SIRPα interactions is the pharmacological inhibition of glutaminyl cyclases, especially glutaminyl-peptide cyclotransferase like protein (QPCTL), which is highly expressed in tumor cells. QPCTL catalyzes the formation of pyro-glutamate, an amino acid derivative localized at the N-terminus of CD47, crucially involved in binding to SIRPα on myeloid cells (14, 15). Inhibition of glutaminyl cyclases in tumor cells by small molecules has been shown to inhibit binding of soluble SIRPα-Fc fusion proteins and to enhance myeloid cell activation against tumor cells (15–17). Antibody isotype switching from human IgG1 to IgA2 can further improve myeloid cell activation, in particular when neutrophils contribute to antibody efficacy (18). Here, we demonstrate the capacity of an IgA2 variant of daratumumab to trigger myeloid cell-mediated ADCP and ADCC against T-ALL cells when combined with CD47 blockade.

Materials and methods

All experiments with human material were approved by the Ethics Committee of the University Medical Center Schleswig-Holstein in accordance with the Declaration of Helsinki. Healthy volunteers and patients gave written informed consent before analyses.

Isolation of human effector cells

Polymorphonuclear granulocytes (PMN) and peripheral blood mononuclear cells (PBMC) were isolated from peripheral blood of healthy donors by density gradient centrifugation using either Polymorphprep® (Progen, Heidelberg, DE) or Ficoll Paque Plus (GE Healthcare, Chicago, IL, USA), respectively, as previously described (19, 20). PBMC were then used for generation of non-polarized (M0) macrophages as described (17). Briefly, after incubation in monocyte attachment medium (PromoCell, Heidelberg, DE) for 30 min at 37°C, cells were washed three times with PBS to dispose non-adherent cells and resuspended in X-VIVO 15 medium (Lonza, Basel, CH) supplemented with 0.5% v/v

penicillin/streptomycin (Gibco, Amarillo, TX, USA). After culturing for 24 h, 50 ng/ml M-CSF (PeproTech, Rocky Hill, CA, USA) were added and refreshed every 72 h at least twice before macrophages were used in ADCP experiments.

Cell lines and patient samples

Human T-ALL cell lines HSB-2, MOLT-13, and P12-ICHIKAWA (referred to as P12) as well as CHO-S and CHO-K1 were purchased from DSMZ (German Collection of Microorganisms and Cell Cultures, Braunschweig, DE). Generation and cultivation of human CD38 transgenic CHO-K1 cells (CHO-K1-CD38$^+$) was described previously (21). MOLT-13 QPCTL Knock-Out (KO) and MOLT-13 CD47 KO were generated using the CRISPR/Cas9 method. The gRNA sequences used for CD47 were $^{5'}$ATGCTTTGTTACT AATATGG$^{3'}$ & $^{5'}$AATAGTAGCTGAGCTGATCC$^{3'}$, and for QPCTL were $^{5'}$GCUUCCGAUCAAUGGGACCU$^{3'}$ & $^{5'}$UAAGUGCUCCAGAGACGCUG$^{3'}$. MOLT-13 control cells were transfected with Cas9 only (without gRNA). Primary T-ALL cells were from patients included in the ALL-BFM study 2000/2009 and described elsewhere (12).

Antibodies and reagents

The approved CD38 antibody daratumumab (human IgG1, DARA-IgG1, clone 005, DARZALEX®) was from Janssen Biotech (Horsham, PA, USA). An IgA2 variant of daratumumab (DARA-IgA2) was generated *de novo* (see below). Isotype control antibodies were the EGFR antibody cetuximab (human IgG1, clone 225; Erbitux®), which was obtained from Merck (Kenilworth, NJ, USA), and its IgA2 variant generated as described (22). The Fc silent CD47 antibody variant 5F9-IgG2σ with V234A/G237A/P238S/H268A/V309L/A330S/P331S substitutions and the soluble SIRPα-IgG2σ protein (referred to as SIRPα-Fc) were produced as described (17, 23). Murine antibodies against human CD38 (clone HB-7), CD47 (clone CC2C6) as well as the isotype control antibody (clone MOPC-21) were from BioLegend (San Diego, CA, USA). Murine antibody against CD47 (clone B6H12) was from Thermo Fisher Scientific (Waltham, MA, USA). All-*trans* retinoic acid (ATRA) was purchased from Sigma Aldrich (St. Louis, MO, USA).

Production and purification of DARA-IgA2

An IgA2 variant of daratumumab (DARA-IgA2) was produced based on the variable regions of daratumumab, which were *de novo* synthesized (Eurofins, Ebersberg, DE) according to the published sequences (patent WO 2017/079150 A1), and the constant region of an IgA2.0 variant of human IgA2 (22). The variable light chain (VL) sequence was cloned into the pSecTag2/Hygro C vector (coding for the kappa light chain), while the vector pCI Neo (coding for the IgA2.0 Fc heavy chain) was used for the variable heavy chain (VH). The vectors contained light chain (LC) and heavy chain (HC) secretion leaders of rituximab, respectively. For IgA2 antibody production, CHO-S cells were transiently transfected with both vectors at a VH : VL ratio of 1:1 by static electroporation using the MaxCyte STX electroporation system (MaxCyte, Gaithersburg, MD, USA) (24) according to the manufacturer's instructions. Antibodies were purified from the supernatant by affinity chromatography using human IgA-CH1 binding camelid-derived single domain (VHH) fragments (CaptureSelect Hu IgA-CH1 Affinity Matrix; Thermo Fisher Scientific, Waltham, MA, USA). After elution with 0.1 M glycine buffer at pH 2.5 and neutralization with 1 M TRIS at pH 8, antibodies were dialyzed in PBS and subsequently applied to a size exclusion chromatography (Superdex 200 26/600 in combination with the ÄKTAprime liquid chromatography system, both from GE Lifescience, Chicago, IL, USA). High performance size exclusion chromatography (HP-SEC) was performed in PBS as mobile phase. Monomeric IgA2 containing fractions were collected and concentrated with a 100 kDa spin column (Vivaspin 20, Sartorius, Göttingen, DE). All antibodies were sterile filtered using 0.22 µm filters.

Flow cytometric analyses

All flow cytometric analyses were performed by indirect immunofluorescence on a Navios flow cytometer (Beckman Coulter, Fullerton, CA, USA). Briefly, CD38 and CD47 specific antigen binding sites (SABC) on T-ALL cell lines and primary tumor samples were quantified using the QIFIKIT® (DAKO, Glostrup, DK) according to the manufacturer's instructions (25). The murine antibodies HB-7 for CD38 and B6H12 for CD47 were used. Antibody B6H12 detects overall cell surface levels of CD47 independent from the presence of pyro-glutamate. In contrast, expression of CD47 with N-terminal pyro-glutamate on MOLT-13 wildtype, CD47 KO and QPCTL KO cells was determined with the pyro-glutamate dependent CD47 antibody CC2C6, which recognizes the SIRPα binding site (15, 16). FITC conjugated anti-mouse IgG F(ab')$_2$ fragments were used for detection (Jackson ImmunoResearch Laboratories, West Grove, PA, USA). FITC labelled goat anti-human kappa light chain F(ab')$_2$ fragments (SouthernBiotech, Birmingham, AL, USA) were used for detection of DARA-IgG1 and –IgA2 bound on CHO-K1-CD38$^+$ cells. In order to confirm the purity of the daratumumab isotype preparations, CHO-K1-CD38$^+$ cells were incubated with 10 µg/ml DARA-IgG1 or DARA-IgA2

followed by FITC conjugated goat anti-human IgG or IgA F $(ab')_2$ fragments (Jackson ImmunoResearch Laboratories).

SDS-PAGE

Purified antibodies were separated by SDS-PAGE under non-reducing and reducing conditions using a 6% and 12% acrylamide gel, respectively (Rotiphorese® Gel 30, Carl Roth, Karlsruhe, DE). After a running time of 90 min at constant 120 V, gels were stained with Simply Blue Safe Stain Kit (Life Technologies, Carlsbad, CA, USA) according to the manufacturer's instructions.

Immunoblot

Cellular proteins were isolated by standard methods. Briefly, cells were homogenized in lysis buffer NP-40 containing PMSF and Protease Inhibitor Cocktail (all from Sigma-Aldrich, St. Louis, MO, USA). Protein amount was measured using Pierce BCA Protein Assay Kit (Thermo Fisher, Waltham, MA, USA). Proteins (60 µg per sample) were separated by SDS-PAGE under reducing conditions on a 10% acrylamide gel (Rotiphorese® Gel 30, Carl Roth, Karlsruhe, DE) and subsequently transferred to PVDF membrane (BioRad Laboratories, Hercules, CA, USA). After blocking the membrane with 5% BSA in 1x TBS buffer for 1 h at room temperature, a HRP-conjugated QPCTL antibody (Santa Cruz Biotechnologies, Dallas, TX, USA, 1:500 overnight at 4°C) was used for detection. Protein loading was monitored using a rabbit monoclonal antibody against human β tubulin (abcam, Cambridge, UK, 1:2000 overnight at 4°C), followed by HRP-conjugated goat anti-rabbit IgG (Jackson ImmunoResearch, West Grove, PA, USA, 1:5000 for 1 h at room temperature). Proteins were visualized by an enhanced chemiluminescence reagent (SuperSignal West Dura, Thermo Fisher, Waltham, MA, USA).

ADCP experiments

ADCP was measured by live-cell imaging (Incucyte®, Sartorius, Göttingen, DE) as previously described (23). Briefly, tumor cells were labelled with 0.5 µg/ml pHrodo for 1 h at room temperature. M0 macrophages were added at an effector-to-target cell (E:T) ratio of 1:1. ADCP in the presence of 10 µg/ml of the indicated antibodies was measured at 37°C every 40 min for 5 h. Phagocytosis was determined as red object counts per image (ROI) and analyzed using the Incucyte® software (v2019B) with Top-Hat segmentation, 2 red calibrated units (RCU) as threshold and a mean intensity of ≥ 17 calibrated units (CU).

ADCC experiments

PMN-mediated ADCC was analyzed in chromium-51 [^{51}Cr] release assays as previously described (22). DARA-IgG1 or DARA-IgA2 were added at varying concentrations. Cetuximab (CTX-IgG1) and its IgA2 variant (CTX-IgA2) served as isotype controls (22). The CD47 blocking antibody hu5F9-IgG2σ was applied at 20 µg/ml. Effector cells and ^{51}Cr-labelled target cells were added at a ratio of 80:1. After 3 h at 37°C, ^{51}Cr release was measured in counts per minute (cpm) in a MikroBetaTrilux 1450 liquid scintillation and luminescence counter (PerkinElmer, Rodgau Jügensheim, DE). Maximal ^{51}Cr release was achieved by addition of 2% v/v Triton-X 100 solution, while basal ^{51}Cr release was measured in the absence of antibodies. Specific tumor cell lysis in % was calculated as follows:

$$lysis\ [\%] = \frac{(experimental\ \ cpm - basal\ \ cpm)}{(maximal\ \ cpm - basal\ \ cpm)} \times 100$$

Data processing and statistical analyses

Graphical and statistical analyses were performed using GraphPad Prism 5.0 (GraphPad Prism Software, La Jolla, CA, USA). Dose-response curves were presented as means ± SEM. Statistical differences were calculated by one-way ANOVA and two-way ANOVA with Bonferroni's *post hoc* correction and multiple comparisons. The EC50 values were reported as mean values after calculation from dose-response curves. Grouped data were presented as means ± SEM or as values of individual samples. Statistical differences were calculated by two-way ANOVA with Bonferroni's *post hoc* correction and multiple comparisons. For primary samples, Wilcoxon matched-pairs signed rank test was used. Here, Shapiro-Wilk test showed non-normal distribution for the DARA-IgA2 group with CD47 blockade. Specifics regarding applied tests are given in the corresponding figure legend.

Results

The IgA2 variant of daratumumab recruits myeloid cells for T-ALL cell killing

An IgA2 variant of daratumumab (DARA-IgA2) was produced based on the variable regions of daratumumab and the constant region of an IgA2.0 variant (22). The binding capacity of DARA-IgA2 to CD38 positive cells is similar to the original IgG1 antibody (Figure S1). The functionality of DARA-IgA2 against the three T-ALL cell lines HSB-2, MOLT-13 and P12 was investigated in ADCP experiments using M0

macrophages and in ADCC experiments with GM-CSF stimulated PMN. All cell lines are positive for CD38 and CD47, but expression levels vary (Figure 1A). No phagocytosis or PMN-mediated cytotoxicity was seen with any of the two DARA isotypes against HSB-2 (Figure 1B, C). In contrast, DARA-IgA2 induced significant increased ADCP of MOLT-13 cells compared to DARA-IgG1 (ROI 869.3 ± 118.0 vs. 326.1 ± 19.42, respectively; Figure 1B). Opposite to MOLT-13, P12 cells were only weakly phagocytosed in the presence of DARA-IgA2, while DARA-IgG1 mediated ADCP was similarly low as against MOLT-13 (Figure 1B). In PMN-mediated ADCC against P12 cells, DARA-IgA2 induced higher tumor cell lysis (27.11 ± 1.75% with an EC_{50} value of 0.6 µg/ml/0.004 µM) than DARA-IgG1 (1.09 ± 1.12%), no significant tumor cell lysis was observed for HSB-2 and MOLT-13 (Figure 1C). DARA-IgG1 did not trigger significant ADCC with PMN against any of the cell lines (Figure 1C).

Genetic ablation of CD47 expression or pyro-glutamate formation increases myeloid cell mediated T-ALL killing by DARA-IgA2

Tumor cell killing by myeloid cells can be improved by disrupting CD47/SIRPα interactions, for example with CD47 blocking antibodies (11, 26). Pharmacological inhibition of glutaminyl cyclases that catalyze the formation of pyro-glutamate on CD47 in tumor cells, has been identified as another potential strategy (12, 15–17). As a more direct

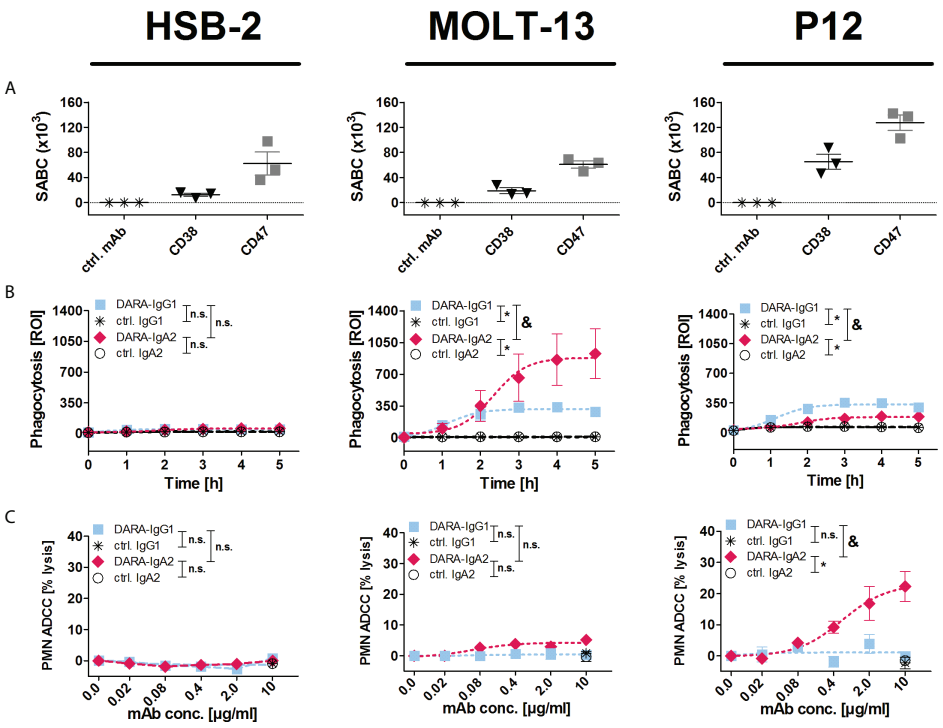

FIGURE 1
DARA-IgA2 mediates T-ALL cell killing by myeloid cells. **(A)** Expression of CD38 and CD47 on T-ALL cell lines HSB-2, MOLT-13 and P12-ICHIKAWA (P12) was quantified by indirect flow cytometry to determine the specific antigen-binding sites per cell (SABC). Mouse monoclonal antibodies against CD38 (clone HB-7) and CD47 (clone B6H12) were used at saturating concentrations (5 µg/ml) and detected with FITC-conjugated anti-mouse IgG $F(ab')_2$ fragments. The results from 3 independent experiments with means ± SEM are shown. The values of the control samples (ctrl. mAb) were subtracted from the values obtained with the antibodies. **(B)** Macrophage-mediated ADCP (E:T = 1:1) was analyzed by real-time fluorescence imaging over 5 h (300 min). Target cells were labelled with a pH-dependent red fluorescent dye (pHrodo), and phagocytosis was measured as red object counts per image (ROI) every 60 min. Antibodies were used at 10 µg/ml. Results are presented as means ± SEM of at least 3 experiments with effector cells from different donors. * indicates significant differences between DARA-IgG1 and IgG1 isotype control (ctrl. IgG1) or DARA-IgA2 and IgA2 isotype control (ctrl. IgA2) ($p < 0.05$ by two-way ANOVA), and & marks significant differences between DARA-IgG1 and DARA-IgA2 ($p < 0.05$ by two-way ANOVA). n. s., not significant. **(C)** PMN mediated ADCC (E:T = 80:1) was analyzed in 3 h ^{51}Cr release assays with the indicated antibody concentrations (0-10 µg/ml) using GM-CSF (50 U/ml) stimulated PMN. Results are presented as means ± SEM of at least 3 experiments with effector cells from different donors. * indicates significant differences between DARA and isotype control (ctrl.) antibodies at the highest concentration (10 µg/ml) ($p < 0.05$ by one-way ANOVA), & marks significant differences between IgG1 and IgA2 ($p < 0.05$ by two-way ANOVA). n. s., not significant.

approach to investigate the impact of both strategies on myeloid cell-mediated T-ALL killing, ADCP and ADCC experiments were performed with MOLT-13 cells, in which the CD47 or QPCTL genes were knocked-out by CRISPR/Cas technology. Loss of CD47 expression on cell surface in CD47 KO cells was confirmed by flow cytometry using the antibody B6H12 which detects overall cell surface levels of CD47, and knock-out of QPCTL in QPCTL KO cells was confirmed by Western blot analysis (Figure 2A). Importantly, the expression of CD38 remained unchanged compared to MOLT-13 control cells (Figure 2A left panel). QPCTL KO cells showed a 78% reduced binding of the pyro-glutamate dependent CD47 antibody CC2C6 which recognizes the SIRPα binding site (15, 16) (Figure 2B left), and reduced binding of soluble SIRPα-Fc (Figure 2B right) in comparison to control cells treated without guide RNA, confirming diminished N-terminal pyro-glutamate formation on CD47 in these cells. Neither the CD47 antibody nor soluble SIRPα-Fc showed binding to CD47 KO cells. In ADCP experiments, both QPCTL KO and CD47 KO MOLT-13 cells showed significantly enhanced phagocytosis compared to control cells, independent of the antibody isotype (Figure 2C left). In contrast, DARA-IgA2, but not DARA-IgG1 achieved significantly higher tumor cell lysis in ADCC experiments with CD47 KO and QPCTL KO cells compared to MOLT-13 control cells. In line with remaining SIRPα-Fc binding on QPCTL KO cells shown in Figure 2B, the lysis rates of QPCTL KO cells were lower compared to CD47 KO cells (Figure 2C right).

DARA-IgA2 in combination with CD47 blockade enhances myeloid cell mediated T-ALL cell killing

Direct targeting of CD47 by blocking antibodies is a clinically advanced strategy to improve antibody-based immunotherapy. Daratumumab in combination with the Fc-silent CD47 blocking antibody hu5F9-IgG2σ achieved statistically significantly increases in phagocytosis of T-ALL cell lines and primary tumor cells compared to CD38 antibodies alone (Figure 3). Here, both DARA-IgG1 and DARA-IgA2 were effective against T-ALL cell lines (Figure 3A upper panel). The mean ADCP values with and without CD47 blockade for HSB-2 were 38.9 ± 4.8 ROI vs. 27.6 ± 5.1 ROI (DARA-IgG1) and 42.0 ± 9.9 ROI vs. 16.0 ± 4.0 ROI (DARA-IgA2). For MOLT-13, it was 228.7 ± 67.2 ROI vs. 669.6 ± 193.5 ROI (DARA-IgG1) and 551.0 ± 245.3 ROI vs. 939.3 ± 210.8 ROI with DARA-IgA2. Improved ADCP against P12 cells was seen with ROI values of 876.8 ± 88.3 (DARA-IgG1) and 647.7 ± 66.5 (DARA-IgA2) in the presence of the CD47 antibody, and 352.3 ± 12.7 ROI (DARA-IgG1) and 164.2 ± 14.8 ROI (DARA-IgA2) without CD47 blockade. We already demonstrated earlier that combining DARA-IgG1 with CD47 blockade leads to effective phagocytosis of primary T-ALL cells *in vitro* (12). Here, daratumumab as IgA2 in combination with CD47 blockade is also able to enhance phagocytosis of primary T-ALL cells as shown in Figure 3B. The tested T-ALL primary patient-derived cells all expressed CD38 and CD47 (Figure 3B, table). ADCP with DARA-IgA2 achieved mean ROI values of 249.4 ± 84.8 with CD47 blockade vs. 69.5 ± 15.8 without CD47 blockade and thus could be enhanced more than 3.5-fold. Phagocytosis of primary patient cells is illustrated (red dots) in the microscopic images (Figure 3B, right). In PMN-mediated ADCC against T-ALL cell lines, significant cytotoxicity was seen with the IgA2 isotype of daratumumab when it was combined with the CD47 blocking antibody (Figure 3A, lower panel). The mean lysis rates were 14.2 ± 3.4% for HSB-2 and 31.1 ± 4.5% for MOLT-13 cells. CD47 blockade resulted in significant lysis of P12 cells with both isotypes: 25.8 ± 5.5% with DARA-IgG1 and an increase from 22.7 ± 3.9% to 49.4 ± 2.1% with DARA-IgA2. Importantly, the CD47 antibody alone did not trigger significant ADCP or ADCC.

Treatment of HSB-2 cells with ATRA enhances effector functions of daratumumab variants in combination with CD47 blockade

Both IgG1 and IgA2 variants of daratumumab had marginal, if any, effects on ADCP or ADCC against T-ALL cells with low CD38 expression, such as the HSB-2 cell line with less than 12.4 ± 2.6 x10^3 SABC (Figure 1). All-*trans* retinoic acid (ATRA) has been shown to increase the expression of CD38 on multiple myeloma and acute myeloid leukemia cells (27, 28). Treatment of HSB-2 cells with ATRA resulted in a dose- and time-dependent increase in CD38 antibody binding indicating an increase in CD38 expression, which reached its maximum with 1 µM ATRA after 48 h to 72 h (Figure 4A, left). The following experiments were performed with HSB-2 cells pre-treated with 1 µM ATRA for 72 h yielding a 25.1-fold increase of CD38 expression on the plasma membrane compared to DMSO treated control cells (Figure 4A, right; Figure 4B). In contrast to CD38, CD47 expression (as measured with CD47 antibody B6H12) and pyro-glutamate formation on CD47 (analyzed by CD47 antibody CC2C6) were not altered after ATRA treatment (Figure 4A). Additionally, binding of the CD47 blocking antibody 5F9-IgG2σ was also not influenced by ATRA treatment (data not shown). Combination of ATRA pre-treatment of HSB-2 cells and CD47 blockade resulted in significantly enhanced phagocytosis with both DARA-IgG1 and DARA-IgA2 compared to DMSO treated cells with CD47 blockade and ATRA treated cells. For DARA-IgG1, ROI values of 156.4 ± 41.4 with ATRA + CD47 blockade were achieved vs. 85.2 ± 32.2 with ATRA alone and 43.4 ± 11.7 DMSO with CD47

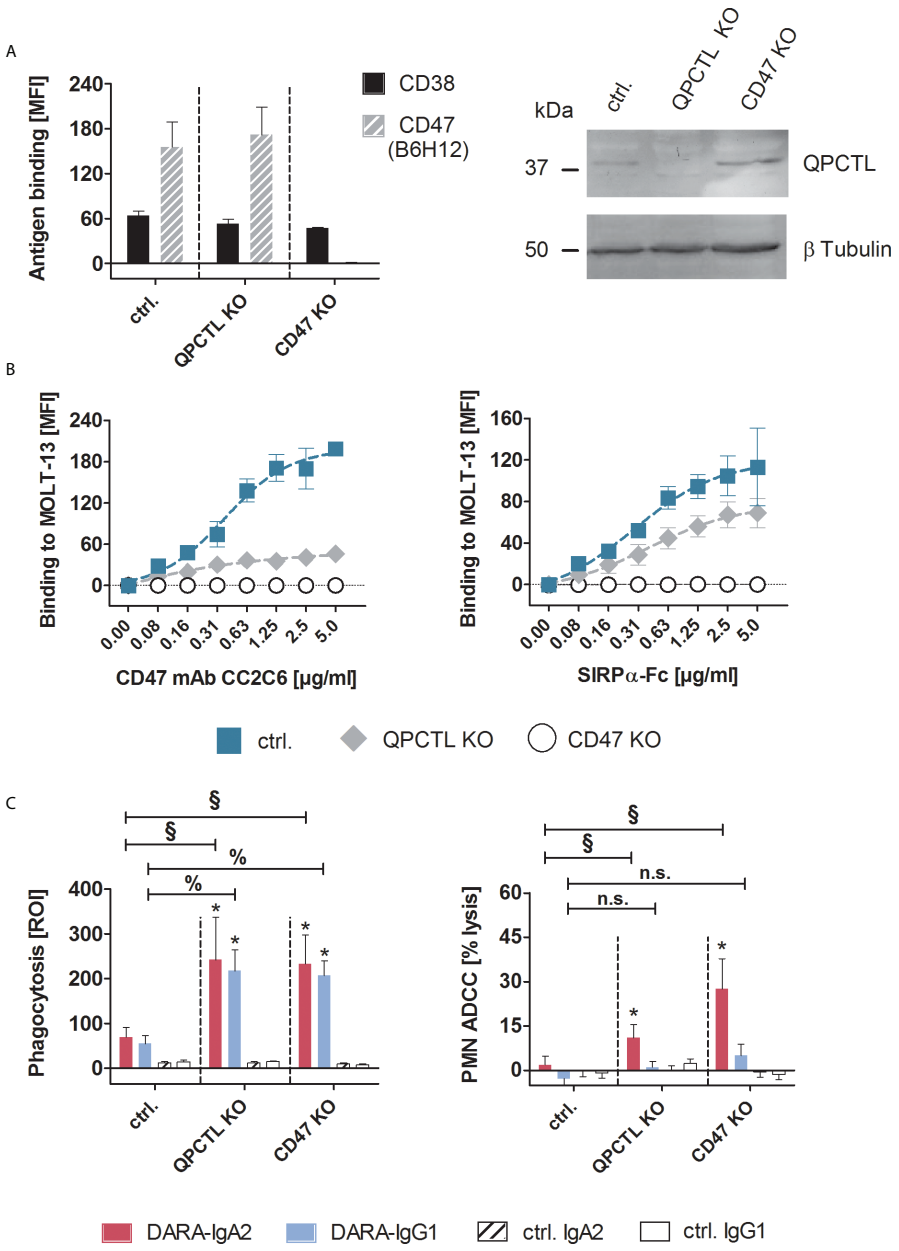

FIGURE 2
Genetic knock-out of CD47 or QPCTL improved myeloid cell-mediated T-ALL cell killing by IgG1 and IgA2 variants of daratumumab. **(A)** MOLT-13 QPCTL and CD47 knock-out (KO) cells were tested for the expression of CD38 and CD47 using antibody clones HB-7 and B6H12, respectively. The CD47 antibody B6H12 is pyro-glutamate independent and detects overall expression of the antigen. Control cells (ctrl.) were treated with Cas9 without QPCTL gRNA. Antibodies were used at saturating concentrations (5 µg/ml) and detected with FITC-conjugated goat anti-mouse Fcγ-specific F(ab)$_2$ fragments (left panel, n=3). Knock-out of QPCTL was confirmed by immunoblotting (right panel), β-tubulin was used for loading control. **(B)** Binding of the pyro-glutamate dependent CD47 antibody CC2C6 (left panel) and soluble SIRPα-Fc fusion protein (right panel) on MOLT-13 control and knock-out cells was measured by indirect immunofluorescence and staining with FITC-conjugated goat anti-mouse or goat anti-human Fcγ specific F(ab)$_2$ fragments. MFI values ± SEM of 3 independent experiments are shown. Background fluorescence of unlabeled cells was subtracted from each MFI value. **(C)** QPCTL KO and CD47 KO as well as control MOLT-13 cells were used as targets in macrophage-mediated ADCP (left panel) and in PMN-mediated ADCC (right panel) with DARA-IgA2 and DARA-IgG1 at 10 µg/ml. For ADCP, an E:T cell ratio of 1:1 was applied. Mean values ± SEM of the red object counts per image (ROI) after 4 h are shown (n=3 with different donors). PMN-mediated ADCC was determined by ^{51}Cr release assays with GM-CSF (50 U/ml) stimulated PMN at an E:T ratio of 80:1. Percentage of mean lysis ± SEM of 4 independent experiments with effector cells from different donors are shown. * indicates significant differences between DARA and isotype control ($p < 0.05$ by two-way ANOVA). Significant differences between the KO variants and the control cells are indicated by § for DARA-IgA2 and by % for DARA-IgG1 ($p < 0.05$ by two-way ANOVA). n.s., not significant. KO, knock-out; QPCTL, glutaminyl-peptide cyclotransferase like; MFI, mean fluorescence intensity; ROI, red object count per image.

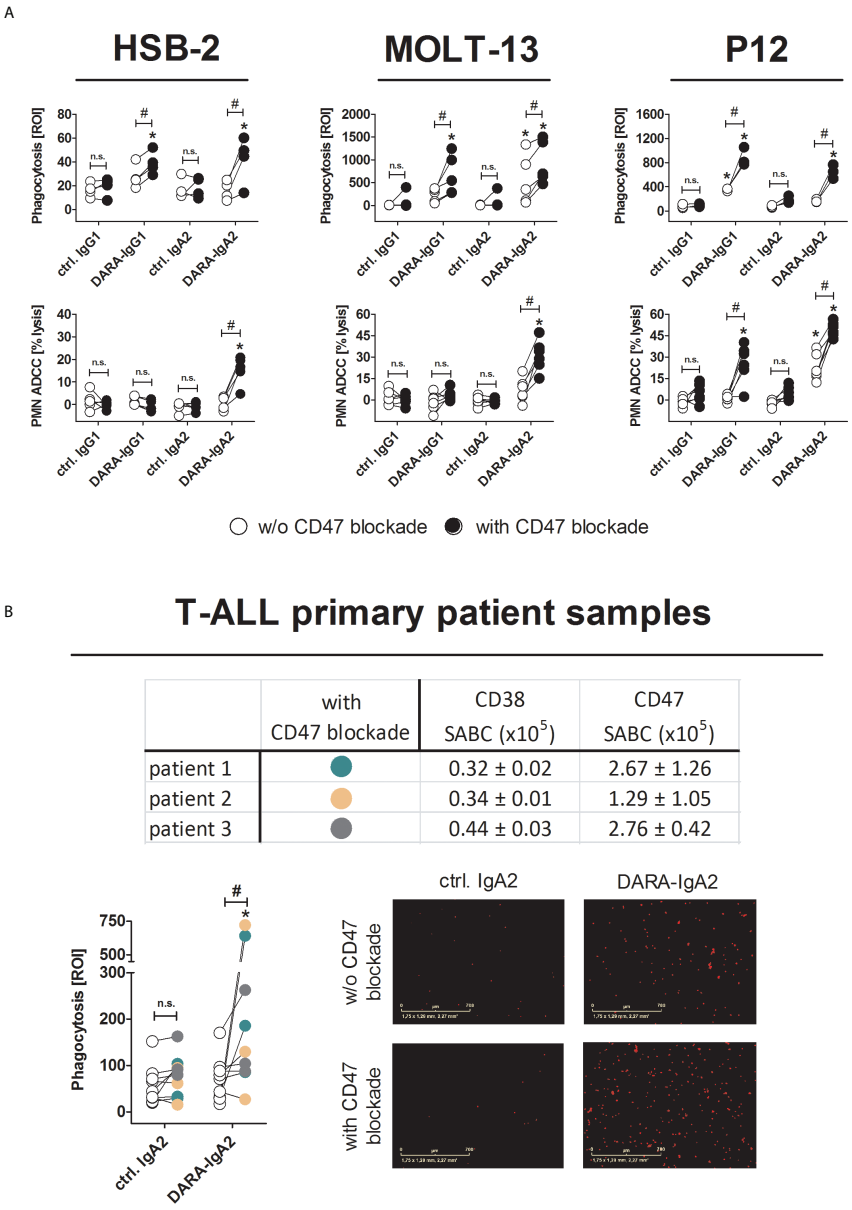

FIGURE 3
Blocking CD47/SIRPα interactions leads to efficient myeloid cell-mediated killing of T-ALL cell lines and patient samples by DARA-IgA2. **(A)** HSB-2, MOLT-13 and P12 cell lines were used as targets in ADCP (upper panel) and PMN-mediated ADCC (lower panel) assays in the absence (white circles) or presence (black circles) of the CD47 blocking antibody 5F9-IgG2σ (20 µg/ml). DARA and isotype controls were used at 10 µg/ml. For ADCP, an E:T ratio of 1:1 was applied while in ADCC assays the E:T ratio was 80:1. M0 macrophages were generated using 50 ng/ml M-CSF, PMN were activated with GM-CSF (50 U/ml). Values of at least three replicates using different donor effector cells are presented. * indicates significant differences between DARA and the respective isotype control ($p < 0.05$ by two-way ANOVA), # depicts significant differences between with and without CD47 blockade ($p < 0.05$ by two-way ANOVA). **(B)** T-ALL patient samples (n=3) were tested for expression of CD38 and CD47. Specific antigen-binding sites per cell (SABC) were quantified by CD38 antibody HB-7 and CD47 antibody B6H12 at saturating concentrations (5 µg/ml). FITC-conjugated anti-mouse IgG F(ab')$_2$ fragments were used for detection. Mean values ± SEM of three replicates are indicated in the table. ADCP assays (lower left panel) were performed in the absence or presence of the CD47 blocking antibody 5F9-IgG2σ (20 µg/ml). Patients were illustrated by different colors (color code included in table). DARA-IgA2 and isotype control were used at 10 µg/ml. An E:T cell ratio of 1:1 was applied. Shown are the red object counts per image (ROI) at maximal phagocytosis with macrophages from three different donors. Microscopic images (magnification 10x) show phagocytosed T-ALL patient cells (red dots) at the time of the highest phagocytosis rate. * indicates significant differences between DARA-IgA2 and isotype control ($p < 0.05$ by Wilcoxon matched-pairs signed rank test), # depicts significant differences between with and without CD47 blockade ($p < 0.05$ by Wilcoxon matched-pairs signed rank test. n. s., not significant.

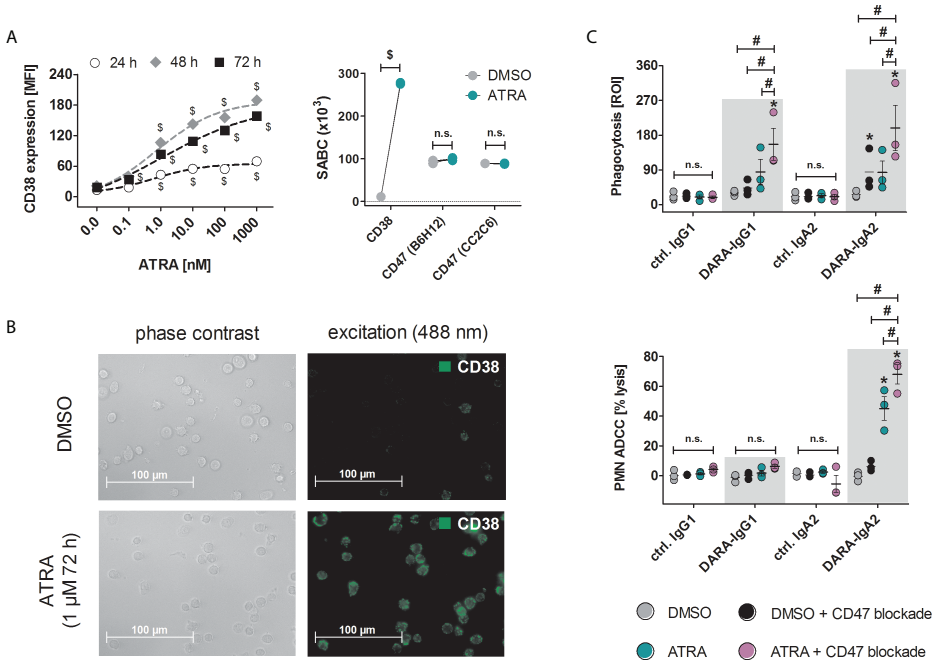

FIGURE 4
Treatment of HSB-2 cells with all-*trans* retinoic acid (ATRA) enhances CD38 expression and DARA-IgA2 mediated tumor cell killing by myeloid cells in combination with CD47 blockade. **(A)** Concentration and time dependent increase of CD38 expression on T-ALL cell line HSB-2 after treatment with ATRA at indicated concentrations for 24 h, 48 h and 72 h (left panel). CD38, CD47 expression and determination of the specific antigen-binding sites per cell (SABC, right panel) after treatment with 1 µM ATRA for 72 h were quantified using QIFIKIT. For both CD38 stainings, antibody HB-7 at saturating concentration (5 µg/ml) was used, while for CD47 staining, both B6H12 and CC2C6 antibodies were used. FITC-conjugated goat anti-mouse IgG F(ab')$_2$ fragments as secondary reagent was used. Values of three independent experiments are shown. $ depicts significant differences between ATRA and DMSO control ($p < 0.05$ by two-way ANOVA in both panels). **(B)** Microscopic images of HSB-2 cells stained for CD38 with antibody HB-7 and FITC-conjugated goat anti-mouse IgG F(ab')$_2$ fragments (40x magnification). **(C)** HSB-2 cells were treated with 1 µM ATRA or DMSO for 72 h and were then used in ADCP (upper panel) or PMN-mediated ADCC (lower panel) experiments. Daratumumab variants and ctrl. antibodies were applied at 10 µg/ml while CD47 blockade antibody 5F9-IgG2σ was used at 20 µg/ml. Values of three (ADCP and ADCC) different donors are depicted. * indicates significant differences between DARA and the respective isotype control ($p < 0.05$ by two-way ANOVA), # indicates significant differences between ATRA + CD47 blockade versus ATRA alone or CD47 blockade alone ($p < 0.05$ by two-way ANOVA). n. s., not significant.

blockade alone (Figure 4C, top). Similar results were obtained with DARA-IgA2: ROI values were 198.75 ± 58.9 with ATRA pre-treatment and CD47 blockade vs. 83.5 ± 29.8 for ATRA alone and 85.2 ± 30.6 with DMSO + CD47 blockade alone. In contrast, significant PMN-mediated cytotoxicity against ATRA pretreated HSB-2 cells was only achieved with the IgA2 isotype of daratumumab (up to 45.1 ± 7.9% specific tumor cell lysis vs 6.2 ± 1.9% lysis with CD47 blockade alone) and was increased to 68.0 ± 6.4% after combining ATRA treatment and CD47 blockade. Daratumumab as IgG1 was not able to induce ADCC by PMN under these conditions (Figure 4C, bottom).

Discussion

In this study, we investigated the efficiency of a novel human IgA2 variant of the CD38 antibody daratumumab to mediate T-ALL cell killing by myeloid cells. Interestingly, P12 cells were lysed efficiently by PMN, while in macrophage mediated ADCP experiments, tumor cell phagocytosis was rather weak. In contrast to P12 cells, MOLT-13 cells were efficiently phagocytosed by macrophages, but PMN mediated ADCC was not observed. Myeloid cells can express different inhibitory immune checkpoint molecules such as SIRPα, Siglecs, LILRBs (29) and additional ones are probably still undiscovered. Potentially, different expression levels of immune checkpoint ligands on tumor cells and concomitantly differential expression patterns of inhibitory receptors on myeloid cells impact tumor cell killing by different effector cell populations. Moreover, also the ratio between activating and inhibitory signals can influence the tumor cell killing (30). However, our results demonstrate that DARA-IgA2 is more efficient in activating PMN for T-ALL cell killing compared to the clinically available IgG1 antibody, especially in combination with CD47 blockade. Similar

observations have been reported comparing IgG1 and IgA antibodies against other target antigens such as EpCAM, EGFR, HER2, GD2, HLA class II, CD20, CD30 and carcinoembryonic antigen (18). Neutrophils can express all three classes of IgG receptors – FcγRI (CD64), FcγRIIa (CD32a) and FcγRIIIb (CD16b) – and the IgA binding receptor FcαRI (CD89). Activation of FcαRI by clustered IgA as its natural ligand or by bispecific antibodies has been demonstrated to effectively trigger intracellular signaling (e.g. ERK activation), leading to high ADCC activity of PMN (31).

IgA2-mediated ADCP against T-ALL cell lines HSB-2, MOLT-13 and P12 and primary patient samples was significantly enhanced blocking the CD47/SIRPα axis through the genetic ablation of either CD47 or QPCTL, or by the use of a CD47 blocking antibody. However, in contrast to CD47 knock-out cells, the genetic ablation of QPCTL did not cause complete binding reduction of soluble SIRPα-Fc. The SIRPα-Fc fusion protein used here is a truncated version and the higher avidity compared to wildtype SIRPα-Fc has to be considered (32).

Notably, phagocytosis of primary T-ALL cells was quite heterogeneous, which was not due to differences in the levels of CD38 or CD47 expression, since they were similar. However, activity of the macrophages seemed to be donor-related (Figure S2), which e. g. may be related to alloreactivity (33) since primary T-ALL cells and macrophages were not from the same donors.

Myeloid checkpoint inhibition by blockade of CD47/SIRPα interactions is a clinically advanced approach to improve antibody-based cancer immunotherapy (11). A phase I/II study with the CD47 antibody magrolimab (hu5F9-G4) in combination with the CD20 antibody rituximab revealed mild toxicities and demonstrated encouraging clinical responses in patients with advanced non-Hodgkin's lymphomas (13). Pre-clinical studies already showed that combining daratumumab and CD47/SIRPα blockade could be a promising therapeutic approach for T-ALL and multiple myeloma (12, 34). In our study, we used an Fc-silent IgG2σ variant of hu5F9 to investigate the impact of myeloid checkpoint blockade on CD38 antibody mediated T-ALL cell cytotoxicity. The ability to enhance myeloid cell activation by addition of the CD47 blocking antibody was observed with both, macrophages and neutrophils, and with both isotypes, DARA-IgG1 and DARA-IgA2.

Overall, the extent of antibody-dependent cytotoxicity seems to correlate with the CD38 expression, at least partially. We observed elevated CD38 expression and increased killing of HSB-2 cells upon treatment with ATRA, especially when combined with CD47 blockade. Similarly, treatment of myeloma cells with ATRA has been shown before to increase CD38 expression and improve efficacy of daratumumab *in vitro* and *in vivo* (27). The addition of ATRA to daratumumab in the treatment of patients with daratumumab-refractory multiple myeloma was safe and had some but limited activity (35). ATRA in combination with daratumumab, preferably as an IgA2 antibody, and CD47 blockade is an interesting approach for T-ALL treatment and deserves further evaluation. However, the clinical development of IgA antibodies is currently hampered by difficulties in establishing relevant *in vivo* models. Since mice do not express a functional IgA receptor (18), approaches using human CD89 transgenic mice (36, 37) and patient-derived ALL xenograft (PDX) models (38) may be valuable to make relevant progress. Myeloid cells constitute an important part of the immune cell infiltrate in ALL patients (39), suggesting that improved myeloid cell recruitment by CD38 antibodies of the IgA isotype may enhance the efficacy of antibody-based therapeutic approaches in these patients.

Data availability statement

The original contributions presented in the study are included in the article/Supplementary Material. Further inquiries can be directed to the corresponding author.

Ethics statement

The studies involving human participants were reviewed and approved by Ethik-Kommision Medizinische Fakultät der Christian-Albrechts-Universität zu Kiel. The patients/participants provided their written informed consent to participate in this study.

Author contributions

NB, CA, JP, and ML performed the experiments and data/graph presentation. NB, CA, ML, and TR analysed the data. KK, CK, and MB, LB, FV provided essential reagents/tools. NB, RB, and TV wrote the manuscript; JL, DS, MP and TV conceived and designed the research. TV supervised the study. All authors critically revised the manuscript and approved submission.

Funding

These studies were supported by an intramural grant from the University of Kiel to TR, by research grants from the Stiftung Deutsche Krebshilfe to CK and DMS (70113524, 70113533) and by research grants from the Deutsche Forschungsgemeinschaft (KFO 5010) to TV and DMS.

Conflict of interest

The authors declare that the research was conducted in the absence of any commercial or financial relationships that could be construed as a potential conflict of interest.

Publisher's note

Supplementary material

The Supplementary Material for this article can be found online at: https://www.frontiersin.org/articles/10.3389/fimmu.2022.949140/full#supplementary-material

SUPPLEMENTARY FIGURE S1

Biochemical characterization of an IgA2 version of daratumumab (DARA-IgA2). **(A)** HP-SEC profile of the IgA2 variant of DARA showing the purity of the IgA2 antibody preparation after production in CHO-S cells and purification via affinity chromatography. **(B)** DARA-IgA2 antibody preparations were separated by SDS-PAGE and gels were stained with Coomassie blue. One specific band at approx. 150 kDa was detected under non-reducing conditions (left panel) representing the complete IgA2 antibody. Under reducing conditions (right panel), two specific bands representing the heavy chain (HC) at 50 kDa and the light chain (LC) at 25 kDa. **(C)** Binding of saturating concentrations (10 µg/ml) of IgG1 and IgA2 variants of DARA to human CD38 transfected CHO-K1 cells was detected by flow cytometry using FITC-labelled anti-human IgG or IgA heavy chain-specific secondary antibodies. The MFI values ± SEM of three experiments are shown. **(D)** Dose-dependent binding to CD38 transfected CHO-K1 cells of DARA-IgG1 and DARA-IgA2 variants at increasing concentrations was analyzed by indirect immunofluorescence using an anti-human kappa light chain-directed FITC-labelled secondary antibody. Results are presented as MFI ± SEM from 3 independent experiments. MFI, mean fluorescence intensity; mAU, milli absorbance units; ctrl., control; mAb, monoclonal antibody.

SUPPLEMENTARY FIGURE S2

M0 donor dependency on ADCP of primary T-ALL cells. ADCP of primary T-ALL cells was performed in the absence or presence of the CD47 blocking antibody 5F9-IgG2σ (20 µg/ml). Patients were illustrated by different colors. DARA-IgA2 and isotype control were used at 10 µg/ml. An E:T cell ratio of 1:1 was applied. Shown are the red object counts per image (ROI) at maximal phagocytosis. * indicates significant differences between DARA-IgA2 and isotype control, # depicts significant differences between with and without CD47 blockade ($p < 0.05$ by two-way ANOVA). n.s., not significant.

References

1. Mullard A. FDA Approves 100th monoclonal antibody product. *Nat Rev Drug Discov* (2021) 20(7):491–5. doi: 10.1038/d41573-021-00079-7

2. Plesner T, Krejcik J. Daratumumab for the treatment of multiple myeloma. *Front Immunol* (2018) 9:1228. doi: 10.3389/fimmu.2018.01228

3. Dinner S, Liedtke M. Antibody-based therapies in patients with acute lymphoblastic leukemia. *Hematol Am Soc Hematol Educ Program* (2018) 2018 (1):9–15. doi: 10.1182/asheducation-2018.1.9

4. Izykowska K, Rassek K, Korsak D, Przybylski GK. Novel targeted therapies of T cell lymphomas. *J Hematol Oncol* (2020) 13(1):176. doi: 10.1186/s13045-020-01006-w

5. Bayon-Calderon F, Toribio ML, Gonzalez-Garcia S. Facts and challenges in immunotherapy for T-cell acute lymphoblastic leukemia. *Int J Mol Sci* (2020) 21 (20):7685. doi: 10.3390/ijms21207685

6. Karawajew L, Dworzak M, Ratei R, Rhein P, Gaipa G, Buldini B, et al. Minimal residual disease analysis by eight-color flow cytometry in relapsed childhood acute lymphoblastic leukemia. *Haematologica* (2015) 100(7):935–44. doi: 10.3324/haematol.2014.116707

7. Leong S, Inglott S, Papaleonidopoulou F, Orfinada K, Ancliff P, Bartram J, et al. CD1a is rarely expressed in pediatric or adult relapsed/refractory T-ALL: implications for immunotherapy. *Blood Adv* (2020) 4(19):4665–8. doi: 10.1182/bloodadvances.2020002502

8. Bride KL, Vincent TL, Im SY, Aplenc R, Barrett DM, Carroll WL, et al. Preclinical efficacy of daratumumab in T-cell acute lymphoblastic leukemia. *Blood* (2018) 131(9):995–9. doi: 10.1182/blood-2017-07-794214

9. Vogiatzi F, Winterberg D, Lenk L, Buchmann S, Cario G, Schrappe M, et al. Daratumumab eradicates minimal residual disease in a preclinical model of pediatric T-cell acute lymphoblastic leukemia. *Blood* (2019) 134(8):713–6. doi: 10.1182/blood.2019000904

10. Wang A, Song Z, Zheng G, Nicolazzi C, Fromm JR, Shehu E, et al. Evaluation of preclinical activity of isatuximab in patients with acute lymphoblastic leukemia. *Mol Cancer Ther* (2021) 20(10):1916–25. doi: 10.1158/1535-7163.MCT-21-0058

11. Feng M, Jiang W, Kim BYS, Zhang CC, Fu YX, Weissman IL. Phagocytosis checkpoints as new targets for cancer immunotherapy. *Nat Rev Cancer* (2019) 19 (10):568–86. doi: 10.1038/s41568-019-0183-z

12. Müller K, Vogiatzi F, Winterberg D, Rösner T, Lenk L, Bastian L, et al. Combining daratumumab with CD47 blockade prolongs survival in preclinical models of pediatric T-ALL. *Blood* (2022) 140(1):45–57. doi: 10.1182/blood.2021014485

13. Advani R, Flinn I, Popplewell L, Forero A, Bartlett NL, Ghosh N, et al. CD47 blockade by Hu5F9-G4 and rituximab in non-hodgkin's lymphoma. *N Engl J Med* (2018) 379(18):1711–21. doi: 10.1056/NEJMoa1807315

14. Hatherley D, Graham SC, Turner J, Harlos K, Stuart DI, Barclay AN. Paired receptor specificity explained by structures of signal regulatory proteins alone and complexed with CD47. *Mol Cell* (2008) 31(2):266–77. doi: 10.1016/j.molcel.2008.05.026

15. Logtenberg MEW, Jansen JHM, Raaben M, Toebes M, Franke K, Brandsma AM, et al. Glutaminyl cyclase is an enzymatic modifier of the CD47- SIRPa axis and a target for cancer immunotherapy. *Nat Med* (2019) 25(4):612–9. doi: 10.1038/s41591-019-0356-z

16. Wu Z, Weng L, Zhang T, Tian H, Fang L, Teng H, et al. Identification of glutaminyl cyclase isoenzyme isoQC as a regulator of SIRPa-CD47 axis. *Cell Res* (2019) 29(6):502–5. doi: 10.1038/s41422-019-0177-0

17. Baumann N, Rösner T, Jansen JHM, Chan C, Marie Eichholz K, Klausz K, et al. Enhancement of epidermal growth factor receptor antibody tumor immunotherapy by glutaminyl cyclase inhibition to interfere with CD47/signal regulatory protein alpha interactions. *Cancer Sci* (2021) 112(8):3029–40. doi: 10.1111/cas.14999

18. van Tetering G, Evers M, Chan C, Stip M, Leusen J. Fc engineering strategies to advance IgA antibodies as therapeutic agents. *Antibodies (Basel)* (2020) 9(4):70. doi: 10.3390/antib9040070

19. Derer S, Glorius P, Schlaeth M, Lohse S, Klausz K, Muchhal U, et al. Increasing FcgRIIa affinity of an FcgRIII-optimized anti-EGFR antibody restores neutrophil-mediated cytotoxicity. *MAbs* (2014) 6(2):409–21. doi: 10.4161/mabs.27457

20. Oberg HH, Kellner C, Gonnermann D, Sebens S, Bauerschlag D, Gramatzki M, et al. Tribody [(HER2)2xCD16] is more effective than trastuzumab in enhancing gd T cell and natural killer cell cytotoxicity against HER2-expressing cancer cells. *Front Immunol* (2018) 9:814. doi: 10.3389/fimmu.2018.00814

21. Klausz K, Cieker M, Kellner C, Oberg HH, Kabelitz D, Valerius T, et al. A novel fc-engineered human ICAM-1/CD54 antibody with potent anti-myeloma activity developed by cellular panning of phage display libraries. *Oncotarget* (2017) 8(44):77552–66. doi: 10.18632/oncotarget.20641

22. Lohse S, Meyer S, Meulenbroek LA, Jansen JH, Nederend M, Kretschmer A, et al. An anti-EGFR IgA that displays improved pharmacokinetics and myeloid effector cell engagement *in vivo*. *Cancer Res* (2016) 76(2):403–17. doi: 10.1158/0008-5472.CAN-15-1232

23. Evers M, Rösner T, Dünkel A, Jansen J, Baumann N, Ten Broeke T, et al. The selection of variable regions affects effector mechanisms of IgA antibodies against CD20. *Blood Adv* (2021) 5(19):3807–20. doi: 10.1182/bloodadvances.2021004598

24. Steger K, Brady J, Wang W, Duskin M, Donato K, Peshwa M. CHO-s antibody titers >1 gram/liter using flow electroporation-mediated transient gene expression followed by rapid migration to high-yield stable cell lines. *J Biomol Screen* (2015) 20(4):545–51. doi: 10.1177/1087057114563494

25. Lenkei R, Gratama JW, Rothe G, Schmitz G, D'Hautcourt JL, Arekrans A, et al. Performance of calibration standards for antigen quantitation with flow cytometry. *Cytometry* (1998) 33(2):188–96. doi: 10.1002/(SICI)1097-0320(19981001)33:2<188::AID-CYTO13>3.0.CO;2-Q

26. Zhang W, Huang Q, Xiao W, Zhao Y, Pi J, Xu H, et al. Advances in anti-tumor treatments targeting the CD47/SIRPa axis. *Front Immunol* (2020) 11:18. doi: 10.3389/fimmu.2020.00018

27. Nijhof IS, Groen RW, Lokhorst HM, van Kessel B, Bloem AC, van Velzen J, et al. Upregulation of CD38 expression on multiple myeloma cells by all-trans retinoic acid improves the efficacy of daratumumab. *Leukemia* (2015) 29(10):2039–49. doi: 10.1038/leu.2015.123

28. Buteyn NJ, Fatehchand K, Santhanam R, Fang H, Dettorre GM, Gautam S, et al. Anti-leukemic effects of all-trans retinoic acid in combination with daratumumab in acute myeloid leukemia. *Int Immunol* (2018) 30(8):375–83. doi: 10.1093/intimm/dxy040

29. Nakamura K, Smyth MJ. Myeloid immunosuppression and immune checkpoints in the tumor microenvironment. *Cell Mol Immunol* (2020) 17(1):1–12. doi: 10.1038/s41423-019-0306-1

30. Suter EC, Schmid EM, Harris AR, Voets E, Francica B, Fletcher DA. Antibody:CD47 ratio regulates macrophage phagocytosis through competitive receptor phosphorylation. *Cell Rep* (2021) 36(8):109587. doi: 10.1016/j.celrep.2021.109587

31. Brandsma AM, Bondza S, Evers M, Koutstaal R, Nederend M, Jansen JHM, et al. Potent fc receptor signaling by IgA leads to superior killing of cancer cells by neutrophils compared to IgG. *Front Immunol* (2019) 10:704. doi: 10.3389/fimmu.2019.00704

32. Uger RA S-PP, Pang X. *Treatment of CD47+ disease cells with SIRPa-fc fusions. U.S.* Toronto, CA, USA: Trillium Therapeutics Inc (2015).

33. Liu W, Xiao X, Demirci G, Madsen J, Li XC. Innate NK cells and macrophages recognize and reject allogeneic nonself *in vivo via* different mechanisms. *J Immunol* (2012) 188(6):2703–11. doi: 10.4049/jimmunol.1102997

34. Storti P, Vescovini R, Costa F, Marchica V, Toscani D, Dalla Palma B, et al. CD14(+) CD16(+) monocytes are involved in daratumumab-mediated myeloma cells killing and in anti-CD47 therapeutic strategy. *Br J Haematol* (2020) 190(3):430–6. doi: 10.1111/bjh.16548

35. Frerichs KA, Minnema MC, Levin MD, Broijl A, Bos GMJ, Kersten MJ, et al. Efficacy and safety of daratumumab combined with all-trans retinoic acid in relapsed/refractory multiple myeloma. *Blood Adv* (2021) 5(23):5128–39. doi: 10.1182/bloodadvances.2021005220

36. Boross P, Lohse S, Nederend M, Jansen JH, van Tetering G, Dechant M, et al. IgA EGFR antibodies mediate tumour killing *in vivo*. *EMBO Mol Med* (2013) 5(8):1213–26. doi: 10.1002/emmm.201201929

37. van Egmond M, van Vuuren AJ, Morton HC, van Spriel AB, Shen L, Hofhuis FM, et al. Human immunoglobulin a receptor (FcaRI, CD89) function in transgenic mice requires both FcR g chain and CR3 (CD11b/CD18). *Blood* (1999) 93(12):4387–94. doi: 10.1182/blood.V93.12.4387

38. Olson B, Li Y, Lin Y, Liu ET, Patnaik A. Mouse models for cancer immunotherapy research. *Cancer Discovery* (2018) 8(11):1358–65. doi: 10.1158/2159-8290.CD-18-0044

39. Witkowski MT, Dolgalev I, Evensen NA, Ma C, Chambers T, Roberts KG, et al. Extensive remodeling of the immune microenvironment in b cell acute lymphoblastic leukemia. *Cancer Cell* (2020) 37(6):867–82 e12. doi: 10.1016/j.ccell.2020.04.015

frontiers | Frontiers in Immunology

TYPE Original Research
PUBLISHED 31 August 2022
DOI 10.3389/fimmu.2022.957874

OPEN ACCESS

EDITED BY
Christian Kosan,
Friedrich Schiller University Jena,
Germany

REVIEWED BY
Paul W.H.I. Parren,
Lava Therapeutics B.V., Netherlands
Mark S. Cragg,
University of Southampton,
United Kingdom

*CORRESPONDENCE
Matthias Peipp
m.peipp@med2.uni-kiel.de

†PRESENT ADDRESS
Pegah Rahmati,
Institute of Transfusion Medicine and Transplant Engineering, Hannover Medical School, Hannover, Germany

‡These authors have contributed equally to this work and share first authorship

SPECIALTY SECTION
This article was submitted to B Cell Biology, a section of the journal Frontiers in Immunology

RECEIVED 31 May 2022
ACCEPTED 12 August 2022
PUBLISHED 31 August 2022

CITATION
Gehlert CL, Rahmati P, Boje AS, Winterberg D, Krohn S, Theocharis T, Cappuzzello E, Lux A, Nimmerjahn F, Ludwig RJ, Lustig M, Rösner T, Valerius T, Schewe DM, Kellner C, Klausz K and Peipp M (2022) Dual Fc optimization to increase the cytotoxic activity of a CD19-targeting antibody. *Front. Immunol.* 13:957874. doi: 10.3389/fimmu.2022.957874

Dual Fc optimization to increase the cytotoxic activity of a CD19-targeting antibody

Carina Lynn Gehlert[1‡], Pegah Rahmati[1‡†], Ammelie Svea Boje[1], Dorothee Winterberg[2], Steffen Krohn[1], Thomas Theocharis[1], Elisa Cappuzzello[3], Anja Lux[4], Falk Nimmerjahn[4], Ralf J. Ludwig[5], Marta Lustig[6], Thies Rösner[6], Thomas Valerius[6], Denis Martin Schewe[7], Christian Kellner[8], Katja Klausz[1] and Matthias Peipp[1*]

[1]Division of Antibody-Based Immunotherapy, Department of Medicine II, Christian Albrechts University Kiel and University Medical Center Schleswig-Holstein, Kiel, Germany, [2]Department of Pediatrics I, University Hospital Schleswig-Holstein and Christian-Albrechts-University Kiel, Kiel, Germany, [3]Oncology and Immunology Section, Department of Surgery Oncology and Gastroenterology, University of Padova, Padova, Italy, [4]Division of Genetics, Department of Biology, Friedrich-Alexander-Universität Erlangen-Nürnberg, Erlangen, Germany, [5]Lübeck Institute of Experimental Dermatology, University of Lübeck, Lübeck, Germany, [6]Division of Stem Cell Transplantation and Immunotherapy Department of Medicine II, Christian Albrechts University Kiel and University Medical Center Schleswig-Holstein, Kiel, Germany, [7]Department of Pediatrics, Otto-von-Guericke University Magdeburg, Magdeburg, Germany, [8]Division of Transfusion Medicine, Cell Therapeutics and Haemostaseology, Ludwig-Maximilians-University (LMU) University Hospital Munich, Munich, Germany

Targeting CD19 represents a promising strategy for the therapy of B-cell malignancies. Although non-engineered CD19 antibodies are poorly effective in mediating complement-dependent cytotoxicity (CDC), antibody-dependent cell-mediated cytotoxicity (ADCC) or antibody-dependent cellular phagocytosis (ADCP), these effector functions can be enhanced by Fc-engineering. Here, we engineered a CD19 antibody with the aim to improve effector cell-mediated killing and CDC activity by exchanging selected amino acid residues in the Fc domain. Based on the clinically approved Fc-optimized antibody tafasitamab, which triggers enhanced ADCC and ADCP due to two amino acid exchanges in the Fc domain (S239D/I332E), we additionally added the E345K amino acid exchange to favor antibody hexamerization on the target cell surface resulting in improved CDC. The dual engineered CD19-DEK antibody bound CD19 and Fcγ receptors with similar characteristics as the parental CD19-DE antibody. Both antibodies were similarly efficient in mediating ADCC and ADCP but only the dual optimized antibody was able to trigger complement deposition on target cells and effective CDC. Our data provide evidence that from a technical perspective selected Fc-enhancing mutations can be combined (S239D/I332E and E345K) allowing the enhancement of ADCC, ADCP and CDC with isolated effector populations. Interestingly, under more physiological conditions when the complement system and FcR-positive effector cells are available as effector source, strong complement deposition negatively impacts FcR engagement. Both effector functions were simultaneously active only at selected antibody concentrations.

Dual Fc-optimized antibodies may represent a strategy to further improve CD19-directed cancer immunotherapy. In general, our results can help in guiding optimal antibody engineering strategies to optimize antibodies' effector functions.

KEYWORDS

antibody therapy, Fc engineering, CD19, antibody hexamerization, CDC, ADCC, ADCP

Introduction

Monoclonal antibodies and antibody-based immunotherapies represent an efficient treatment option in cancer therapy and have remarkably improved the therapeutic outcomes in hematological malignancies (1, 2). For the treatment of B-cell lymphomas and leukemias several monoclonal antibodies (e.g. rituximab, tafasitamab) and other antibody-based therapies (e.g. bispecific T-cell engager (BiTE), antibody drug conjugates) as well as chimeric antigen receptor (CAR) T cells, are approved for clinical use (3–5).

An attractive target antigen in B-lineage lymphoid malignancies is represented by the cluster of differentiation (CD) 19, a type I membrane protein of the immunoglobin superfamily (4, 6, 7). CD19 shows a restricted expression profile on B cells and is expressed from early to mature stages of B-cell differentiation. Non-engineered CD19-IgG1 antibodies have shown low therapeutic efficiency in preclinical models in contrast to CD20 antibodies. Canonical CD19 antibodies only inefficiently mediate programmed cell death or growth arrest and are not potent in mediating complement-dependent cytotoxicity (CDC), antibody-dependent cell-mediated cytotoxicity (ADCC) or antibody-dependent cellular phagocytosis (ADCP) (4, 8–10). To date different immunotherapeutic strategies for targeting CD19 like the [CD3xCD19] BiTE blinatumumab, CAR T cells (tisagenlecleucel, axicabtagen-ciloleucel and lisocabtagene maraleucel) or loncastuximab tesirine, an antibody drug conjugate, are clinically approved for the therapy of B-cell malignancies (11–13).

In murine syngenic and xenograft models the relevance of effector cell recruitment for the *in vivo* activity of antibodies was demonstrated and also in patients the importance of efficient Fcγ receptor (FcγR) engagement was suggested in earlier clinical observations (14–22), but also a series of studies was not able to find this correlation in patients (19, 21). Based on these findings, various strategies have been pursued to improve the therapeutic efficacy of IgG1 antibodies, by engineering the fragment crystallizable (Fc) domain. Fc glyco-engineering, by modifying the glycosylation profile, represents an established strategy to enhance antibody-dependent cell-mediated cytotoxicity (ADCC) of therapeutic antibodies. This technology is used in the clinically approved CD20 antibody obinutuzumab, the antibody drug conjugate belantamab mafodotin as well as the bispecific antibody amivantamab (23–25). Fc protein-engineering, by exchanging selected amino acids in the CH2 and CH3 region, is an efficient alternative approach to increase the affinity to FcγR expressed on effector cells leading to an improved effector cell activation (26, 27). We previously showed that an Fc protein-engineered CD19 antibody carrying the amino acid substitutions S239D/I332E (DE-modification) in the CH2 region displayed enhanced NK-cell mediated ADCC and likewise enhanced ADCP by macrophages (28, 29). Recently, tafasitamab, a DE-modified CD19 antibody (MOR208 or Xmab®5574), was approved in combination with lenalidomide for the treatment of relapsed and refractory DLBCL (5, 30). Although this Fc-modified antibody showed increased tumor cell cytotoxicity *via* ADCC and ADCP, it is not capable of triggering complement activation (5, 28). The role of complement in antibody therapy is still controversial (31). An important role of the complement system has been suggested in selected preclinical mouse models and clinical studies of CD20 antibody therapy (32). E.g. patients receiving rituximab show a consumption of complement proteins and individual patients benefit from plasma application as a source of complement (33, 34). Furthermore, an increased expression level of inhibitory membrane-bound complement regulatory protein (mCRP) CD59 has been associated with rituximab resistance in chronic lymphocytic leukemia (CLL) patients (35). In contrast, several mouse models demonstrated strong FcR dependence for the B cell-depleting activity of CD19 or CD20 antibodies and full activity in complement deficient mice (7, 22). Furthermore, clinical trials with CD20 antibodies with augmented CDC activity, such as ofatumumab have not shown superior therapeutic activity compared to rituximab (36).

In summary, these observations may suggest that depending on the respective clinical setting, specific disease biology and target antigen characteristics both complement, and effector cell recruitment could represent important effector functions in antibody therapy. Therefore, enhancing these Fc-mediated effector functions may be advantageous.

The ability and efficacy of antibodies to activate the complement system and to induce CDC is dependent on various parameters, e.g. the antibody isotype, the characteristics of the antigen and the epitope, the antigen density as well as the intrinsic capacity of an antibody to form hexamers on the cell surface of target cells (37, 38). Therefore, only a minority of therapeutic antibodies directed against selected target antigens, e.g. CD20 (e.g. rituximab or ofatumumab), CD38 (e.g. daratumumab) and CD52 (e.g. alemtuzumab) show potent complement activating capacity as single agents (32, 39–42). Different Fc engineering strategies have been described to improve C1q binding of monoclonal antibodies to enhance CDC (26). For example, mixed-isotype IgG1/IgG3 rituximab variants exhibit enhanced CDC activity (43, 44). Also the exchange of selected amino acids in the Fc domain (e.g. S267E, H268F, S324T) leads to improved CDC activity by enhancing C1q binding, other amino acid exchanges such as E345R or the addition of a C-terminal IgM tail piece promotes on-target antibody hexamer assembly on the cell surface which augmented CDC (43, 45, 46). De Jong and colleagues showed that the amino acid exchanges E345K or E340G (HexaBody mutations) in the CH3-domain lead to enhanced on-target hexamer formation of antibodies on the cell surface and hence efficient CDC of target cells (37). These antibody variants exhibit no hexamerization or aggregation in solution at physiological concentrations which prevents target-independent complement activation and retain the regular pharmacokinetics of IgG antibodies (37). Besides antibodies directed against surface antigens on hematological tumors such as CD19 or CD38, also an EGFR-directed antibody with the HexaBody mutation (E345K or E340G) demonstrated improved C1q fixation which leads to activation of the classical complement pathway as monitored by C4b deposition on the cell surface (47). Complement activation *via* the classical pathway, besides the formation of the membrane-attack complex which mediates direct target cell lysis, also may increase the sensitivity of opsonized tumor cells (C3b and C4b) for phagocytosis by myeloid cells (48, 49).

The simultaneous enhancement of FcγR-mediated effector functions (like ADCC and ADCP) and complement-dependent cytotoxicity (CDC) by amino acid alteration in the FC domain of IgG antibodies is challenging, presumptively because the binding site for C1q and the binding site for Fcγ receptors overlap (50–52). We recently showed that ADCC and CDC can be improved simultaneously by combining Fc protein- and Fc glyco-engineering. The double Fc-engineered CD19 and CD20 antibodies were generated by introducing the EFTAE modification for enhancement of CDC, while ADCC was enhanced by reducing the fucosylation level (53, 54).

Here, we were able to improve the activity of three effector functions ADCC, ADCP and CDC of a CD19 antibody by dual Fc-protein engineering. To achieve this, DE-mutations described to increase ADCC and ADCP activity were combined with the E345K mutation favoring on-target antibody hexamerization resulting in improved CDC activity. Our data provide evidence that from a technical perspective selected Fc-enhancing mutations can be combined (S239D/I332E and E345K) allowing the enhancement of ADCC, ADCP and CDC when isolated effector sources are analyzed. Interestingly, under physiological conditions in whole blood when the complement system and FcR-positive effector cells are available as effector source, strong complement deposition negatively impacts FcR engagement. Both effector functions were simultaneously active only at selected antibody concentrations. Dual Fc-optimized antibodies may represent a strategy to further improve CD19-directed cancer immunotherapy and our results may help in guiding optimal antibody engineering strategies to optimize antibodies' effector functions.

Material and methods

Cell culture/lines

SEM (55), Jurkat, CEM, MOLT-16 and Nalm-6 cells (DSMZ) were cultured in RPMI 1640 Glutamax-I medium (Thermo Fisher Scientific) supplemented with 10% fetal calf serum (FCS; Thermo Fisher Scientific), 100 U/mL penicillin and 100 µg/mL streptomycin (Thermo Fisher Scientific) (R10+). BHK-CD16a (FcγRIIIa V158) cells were cultured in R10+ medium supplemented with 10 µmol/l methotrexate (Sigma-Aldrich) and 500 µg/ml geneticin (Thermo Fisher Scientific) as described before (53, 54, 56). CHO-CD32a (FcγRIIa H131) cells were cultivated in DMEM medium (Thermo Fisher Scientific) supplemented with 10% FCS, 100 U/ml penicillin and 100 µg/ml streptomycin (57). Medium was supplemented with 1% NEAA (Thermo Fisher Scientific), 1% sodiumpyruvat (Thermo Fisher Scientific) and 500 µg/ml geneticin. Chinese hamster ovary cells (CHO-S, Thermo Fisher Scientific) were cultured in serum-free CD-CHO medium (Thermo Fisher Scientific) containing 1% HT supplement (Thermo Fisher Scientific) and 2 mM GlutaMax (Thermo Fisher Scientific). After transfection CHO-S cells were cultured in CD OptiCHO medium (Thermo Fisher Scientific) containing 1% HT supplement, 2 mM GlutaMax and 0.1% Pluronic F-68 (Thermo Fisher Scientific).

Preparation of human effector cells and source of complement

Human Serum and PBMC (peripheral blood mononuclear cells) were prepared as described previously (53). Monocytes were isolated through adherence of PBMC in monocyte attachment medium (PromoCell) for 30 min at 37°C. Monocytes were differentiated into macrophages in serum-free X-vivo medium (Lonza) containing 50 U/mL penicillin and

50 µg/mL streptomycin and 50 ng/mL recombinant macrophage colony stimulating factor (MCSF; PeproTech) for 11 to 14 days. Experiments were approved by the Ethics Committee of the Christian-Albrechts-University of Kiel (Kiel, Germany), in accordance with the Declaration of Helsinki.

Antibody generation

For generation of the dual engineered CD19 antibody (CD19-DEK), the variable regions of the antibody tafasitamab (MOR208) were used (58). The VH was excised from vector pSectag2-CD19-HC-DE and was cloned into the vector pSecTag2-HC-DEK, which contained the S239D/I332E and the E345K amino acid exchanges (unpublished). The generation of the expression vectors of the CD19-DE heavy chain (HC) and the tafasitamab-based light chain (LC) has been described previously (28, 59). Plasmid DNA was purified endotoxin-free by Nucleo Bond 2000 EF (Macherey-Nagel) and correct sequences were confirmed by Sanger sequencing. Antibodies were produced in CHO-S cells by electroporation using the MaxCyte (STX) large scale electroporation system, following the manufacturer's recommendations. For purification, Capture Select IgG-CH1-XL affinity matrix (ThermoFisher) were used, followed by size exclusion chromatography (ÄKTA pure, GE Healthcare/Cytiva).

SDS-PAGE analysis

One µg of the respective purified recombinant protein was loaded on 12% Tris–acrylamide gels under reducing or on 4-15% precast polyacrylamide gels (Mini-PROTEAN® TGX™, BioRad) under non-reducing conditions and were stained with Coomassie brilliant blue staining solution (Carl Roth GmbH).

Flow cytometry

Flow cytometry analysis was performed on a Navios flow cytometer (Beckman Coulter) and analyzed with Kaluza Analysis software (Beckman Coulter). 3-5 x 10^5 cells were washed in PBS containing 1% BSA and 0.1% sodium azide (PBA buffer). To analyze the binding of the antibodies, cells were incubated on ice for 60 min with 50 µg/ml of the indicated antibodies. For concentration dependent binding, cells were treated with antibodies at varying concentrations for 1 h on ice and then washed three times with 1 ml PBA buffer and subsequently stained with a secondary anti-human-kappa-FITC antibody (SouthernBiotech) on ice for 30 min.

Antigen expression levels were quantified by determination of antigen binding capacities of CD19-specific mouse Antibody (#392502, Biolegend) using the QIFIKIT (Agilent DAKO) according to the manufacturers' protocols.

To analyze complement deposition, target cells were incubated on ice with 10 µg/ml of the indicated antibodies for 15 min and subsequently incubated at 37°C with 25% v/v human serum of healthy donors supplemented with 800 µg/ml eculizumab for 10 min to prevent target cell lysis. Deposition was measured with 50 µg/ml FITC conjugated rabbit anti-human C1q, C3b/c and C4b/c antibodies (Agilent DAKO).

Cytotoxicity assays

Cytotoxicity assays were performed as described (53, 60). To prevent target cell lysis *via* the complement system human serum was supplemented with 50 µg/ml eculizumab. Increasing concentrations of recombinant C1q protein (Complement Technologies) was added to analyze if binding of C1q may diminish the interaction of the Fc part of the antibodies with Fcγ receptors on effector cells. To inhibit FcγR-mediated cytotoxicity 100 µg/ml of CD16 (FcγRIII) or CD32a (FcγRIIa) specific blocking antibodies (recombinant versions of clones 3G8 and IV.3) with silenced Fc domains (L234A/L235A/G237A/P238S/H268A/A330S/P331S) were added to the assays (61). ^{51}Cr-release from triplicates was measured in counts per minute (cpm). Percentage of cellular cytotoxicity was calculated using the formula: % specific lysis = (experimental cpm – basal cpm)/(maximal cpm – basal cpm) × 100. The maximal ^{51}Cr release was determined by adding Triton X-100 (1% final concentration) to target cells and basal release was measured in the absence of antibodies and effector cells.

Phagocytosis assays/live cell imaging

For the analysis of ADCP, 10^4 macrophages were seeded in a 96-well flat-bottom plate and allowed to adhere for 1 h at RT. Target cells were labeled with the pH-sensitive red fluorescence dye pHrodo (Thermo Fisher Scientific) following the manufacturer's protocols. 10^4 labelled cells were added to the macrophages per well, resulting in an E:T ratio of 1:1, and antibodies were applied to a final concentration of 10 µg/mL. The assay was incubated for 4 h at 37°C in the IncuCyte high-throughput fluorescence microscope system (Sartorius) and fluorescence pictures of each well were created every 20 minutes. Phagocytosis was determined as the red object counts per image (represent the phagocytosed B-ALL cells) over time (62).

Graphical and statistical analysis

Graphical and statistical analyses were performed using GraphPad Prism 5 Software (GraphPad). *P*-values were calculated with One- or Two-way ANOVA with Bonferroni post-tests or with a two-tailed Mann-Whitney T-test and significance (*) was accepted with $P<0.05\%$.

Results

Generation of a dual Fc-optimized CD19 antibody

To generate the dual Fc-optimized CD19-specific antibody (CD19-DEK), the VL and VH sequences of the approved CD19 antibody tafasitamab were used. For enhanced Fcγ receptor (FcγRIIa and FcγRIIIa) binding and improved effector cell recruitment, two amino acid exchanges (S239D and I332E) were introduced in the CH2 domain of the Fc part (Figure 1A) (64). The amino acid substitution E345K in the CH3 domain has been described to favor Fc hexamerization of the IgG antibodies on the target cell surface resulting in effective C1q binding and complement activation (Figure 1A) (37). The antibody was produced in CHO-S cells and purified by affinity chromatography followed by size exclusion chromatography (SEC). The SEC re-analysis of the purified protein showed a single protein peak at the expected elution volume (Figure 1B). To confirm the purity of CD19-DEK, SDS-PAGE followed by Coomassie blue staining was performed. The two expected bands of the HC and the LC at the calculated molecular masses of approx. 50 kDa and 25 kDa using reducing conditions and a molecular mass of approx. 150 kDa, comparable with CD19-DE, were detected under non-reducing conditions (Figure 1C). CD19-DEK showed a similar binding capacity on target antigen positive cell lines SEM and Nalm-6 compared to CD19-DE, while no binding to CD19-negative cells was detected (Figure 1D). Of note, similar target binding capacity of a non-engineered CD19 antibody vs a CD19 antibody carrying the DE Fc mutation has been demonstrated previously (8). Analysis of dose dependent binding on CD19-positive Nalm-6 cells showed half-maximal binding in the low nanomolar (nM) range (CD19-DEK: 0.32 nM; CD19-DE: 0.19 nM) (Figure 1E). The two Fc-optimized CD19 antibodies also demonstrated comparable binding abilities to FcγRIIa and FcγRIIIa (Figures 1D, F). As expected, no binding was observed for a control antibody with a silent Fc part (Figure 1F).

In conclusion, combining the different Fc modifications of CD19-DEK did not alter target antigen binding on CD19-positive cell lines and introduction of the E345K amino acid exchange has no negative impact on the optimized FcγR binding ability (due to the DE-mutation).

CD19-DEK induces effective ADCC and ADCP of BCP-ALL cell lines

To examine if the dual-engineered CD19-DEK was able to trigger Fc-mediated effector functions, like ADCC and ADCP, similar effective as CD19-DE, we performed chromium release assays and phagocytosis assays with the B-ALL cell lines Nalm-6 and SEM. Efficient tumor cell lysis was mediated in a concentration dependent manner by CD19-DEK with PBMC as effector cells (Figure 2A). The calculated EC_{50}-values obtained with CD19-DEK (SEM: 0.008 nM, Nalm-6: 0.005 nM) and CD19-DE (SEM: 0.01 nM, Nalm-6: 0.007 nM) were comparable. None of the control antibodies (ctrl-DE and ctrl-DEK) induced ADCC, demonstrating antigen-specific tumor cell lysis of the two Fc-engineered CD19 antibodies. The ADCP activity of CD19-DEK was analyzed with SEM and Nalm-6 cells as target cell lines and monocyte derived macrophages from healthy donors (Figure 2B). The antibody variant carrying the on-target hexamerization-enhancing mutation was able to trigger efficient ADCP of different B-ALL cell lines to a similar extent as CD19-DE (Figure 2B). As expected, this effect was antigen specific because no phagocytosis could be detected with the control antibodies (ctrl-DE and ctrl-DEK) (Figure 2B). The tumor cell lysis and the phagocytosis rate were higher for the SEM cell line compared to the Nalm-6 cells. This effect could be explained by the CD19 expression levels on these cell lines. The quantification of the target antigen on the two B-ALL cell lines showed a higher CD19-specific antibody binding capacity (SABC) on SEM cells (SABC= 66494) compared to Nalm-6 cells (SABC= 27208) and B cells of healthy donors (SABC=14071) (Supplementary Figure S1).

In conclusion, the CD19-DEK variant was able to mediate ADCC and ADCP of B-ALL cell lines with different CD19 expression levels comparable to CD19-DE, which suggests that introduction of the E345K amino acid exchange has no significant negative impact on enhanced effector cell-mediated killing of antibodies carrying the ADCC and ADCP enhancing DE-mutations.

Dual engineered CD19 antibody triggers complement deposition and complement-dependent cytotoxicity of CD19-positive cell lines

To analyze whether introduction of the E345K amino acid exchange in the Fc domain already harboring the DE-mutations results in improved complement activation, binding of C1q and deposition of C3b/c and C4b/c on target cells was analyzed. SEM cells were incubated with the respective antibodies and human serum supplemented with the C5-specific antibody eculizumab

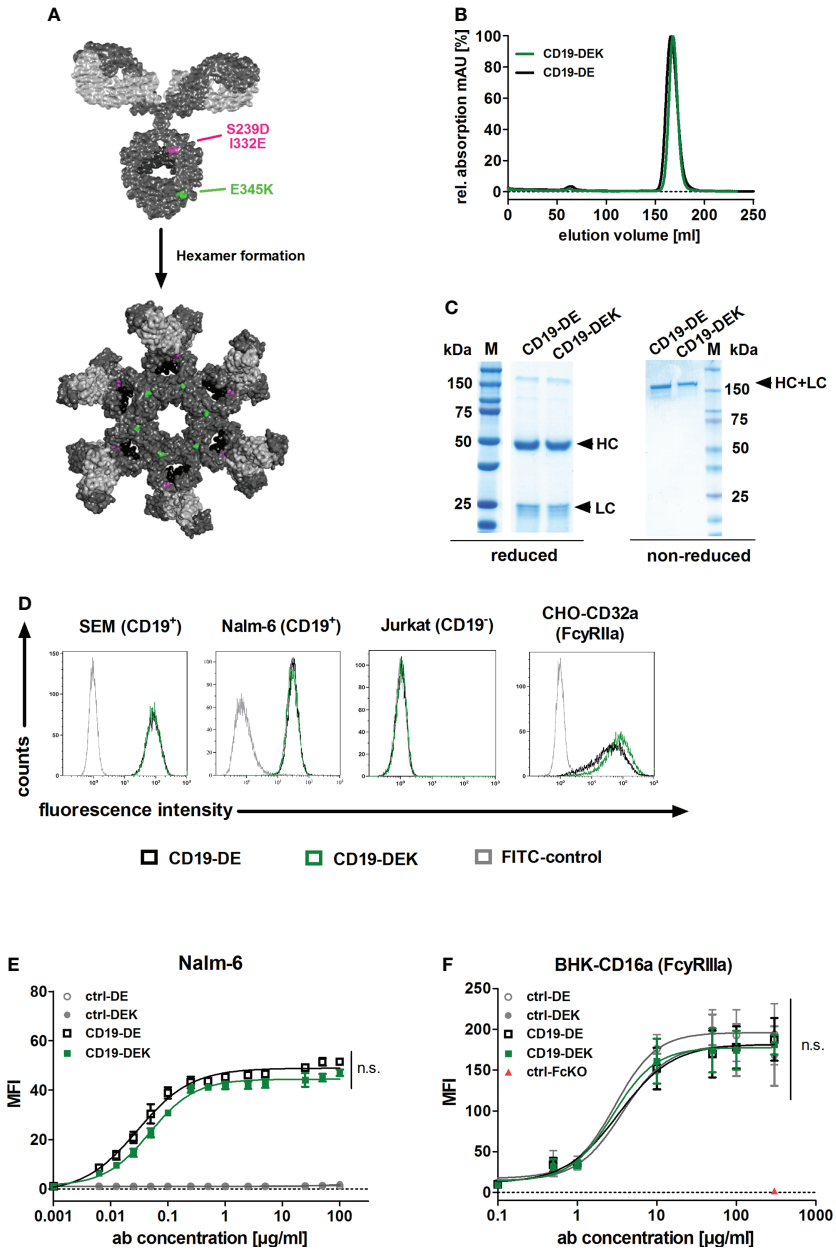

FIGURE 1
Generation and binding characteristics of CD19-DEK. **(A)** Schematic illustration of a CD19-antibody with a dual engineered Fc part for improved FcγR binding and effector cell recruitment (DE-variant: S239D/I332E, pink) and efficient recruitment of the complement system (C1q) *via* E345K amino acid substitution (green) to favor antibody hexamerization on the target cell surface resulting in improved CDC. IgG model structure based on pdb file provided by Dr. Mike Clark (63) and Hexamer model structure based on crystal structure of IgG1-b12 (1HZH) provided by Dr. Rob de Jong was modified using Discovery Studio Visualizer (Biovia). **(B)** CD19-DEK and CD19-DE were analyzed by size exclusion chromatography. **(C)** SDS-PAGE under reducing and non-reducing conditions and Coomassie blue staining validated the purity and molecular mass of the dual-engineered CD19 antibody compared to CD19-DE. **(D)** Binding specificity of CD19-DEK and CD19-DE was tested *via* flow cytometry on CD19-positive cell lines SEM and Nalm-6. The CD19-negative T-ALL cell line Jurkat was used as control. The binding capacity of the optimized Fc part to FcγRIIa was investigated by flow cytometry on stably transfected cells. Data show representative results of three independent experiments. **(E)** Concentration dependent binding of CD19-DEK and CD19-DE compared to isotype control antibodies (ctrl-DE and crtl-DEK) was tested with the CD19-positive BCP-ALL cell line Nalm-6 *via* flow cytometry. **(F)** Concentration dependent binding of the optimized Fc part of CD19-DEK and CD19-DE to FcγRIIIa was analyzed by flow cytometry on stably transfected BHK cell line (BHK-CD16a). A control antibody with a silent Fc domain lacking FcγR binding (ctrl-FcKO) was used as a negative control. Mean values ± SEM of three independent experiments, **P*<0.05%, ns, not significant. Two-way ANOVA with Bonferroni post-test.

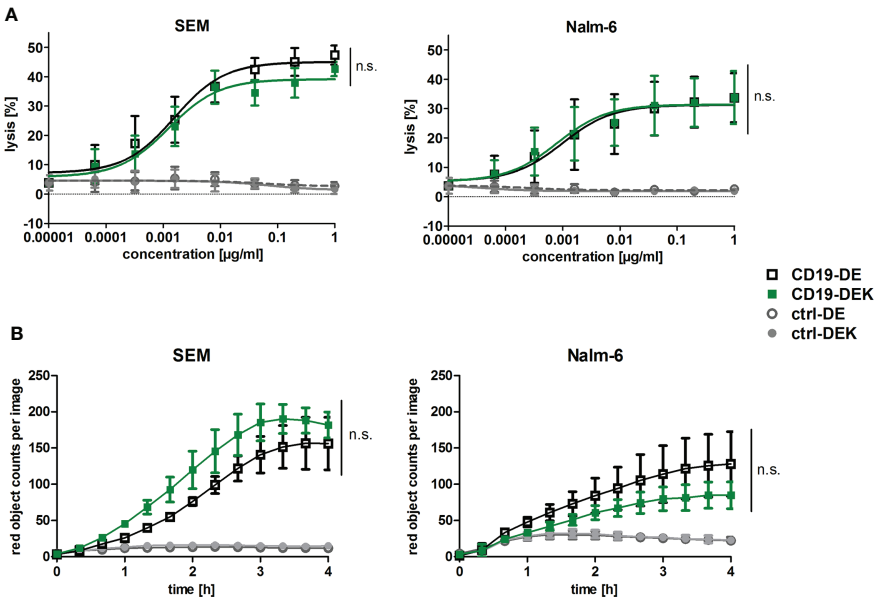

FIGURE 2
The dual Fc-optimized antibody CD19-DEK triggers FcγR-mediated effector functions comparable to CD19-DE. **(A)** Chromium release assays were performed to analyze ADCC. CD19-positive tumor cell lines SEM and Nalm-6 were used as target cells and PBMC of healthy donors at an Effector : Target (E:T) ratio of 40:1 were applied. The tumor cell lysis triggered by CD19-DEK and CD19-DE was compared to control antibodies (ctrl-DEK and ctrl-DE). **(B)** The antibody-dependent cell-mediated phagocytosis (ADCP) was measured for 4 h by high-throughput fluorescence microscopy. CD19-positive cell lines were labelled with a pH-sensitive red-fluorescent dye and were incubated at an E:T ratio of 1:1 with polarized M0 macrophages and 10 µg/ml of the indicated antibodies. Phagocytosis is depicted as the relative red object counts per image. Data represent mean values ± SEM of three independent experiments, *P<0.05%, ns, not significant. CD19-DEK vs. CD19-DE, Two-way ANOVA with Bonferroni post-test.

to inhibit lysis of target cells (Figure 3A). Targeting with CD19-DEK resulted in C1q binding and C3b/c and C4b/c deposition on the target cell surface, whereas CD19-DE was not able to trigger complement deposition on SEM cells (Figure 3A). To evaluate induction of CDC triggered by the CD19 antibodies we performed chromium release assays with human serum of healthy donors and SEM or Nalm-6 cells as target cells. As depicted in Figure 3B, CD19-DEK was able to mediate effective CDC in both CD19-positive cell lines, while CD19-DE was incapable of triggering complement-dependent cytotoxicity. The concentration dependent tumor cell lysis of CD19-DEK showed EC_{50} values in the nanomolar range with both CD19-positive cell lines (SEM: 0.18 nM and Nalm-6: 0.14 nM). No tumor cell lysis was detected with the control antibodies indicating that CDC was induced in a strict target antigen-dependent manner (Figure 3B). No CDC of CD19-negative cell lines was triggered by CD19-DEK (Figure 3C).

To analyze Fc-mediated effector functions under more physiological conditions, we analyzed the cytolytic capacity of CD19-DEK using whole blood of healthy donors as effector source. The dual-optimized CD19 antibody showed a significant higher tumor cell lysis of the B-ALL cell line SEM compared to CD19-DE, when FcγR-positive effector cells (ADCC) and the complement system (CDC) were present as effector components (Figure 4A). The same tendency could be detected for the BCP-ALL cell line Nalm-6 although statistical significance was not reached (Figure 4A). The lysis of tumor cells mediated by CD19-DE was reduced to background with an FcγRIII (CD16) blocking antibody whereas the blockade of the FcγRIIa (CD32a) or of the complement system by eculizumab had no significant effect on the tumor cell killing of CD19-DE (Figure 4B). This suggested that the killing triggered by CD19-DE was most likely due to engagement of FcγRIIIa-positive effector cells such as NK cells. Interestingly, in contrast the CD19-DEK-mediated tumor cell lysis was almost completely blocked by addition of eculizumab (Figure 4A). These data suggest a fully complement-dependent effect of the dual-engineered CD19-antibody. To analyze if binding of C1q may diminish the interaction of the Fc part of CD19-DEK with Fcγ receptors on effector cells, we performed assays with increasing concentrations of recombinant C1q protein and PBMC as effector cells. No significant impact of C1q on the ADCC activity was found (Supplementary Figure S2). These data suggest that binding of C1q to the Fc part of CD19-DEK is not sufficient to block FcR engagement and that probably deposition of other complement factors such as C3b/c and C4b/c on the target cell surface may play a dominant role in the reduction of tumor cell lysis mediated by CD19-DEK in whole blood assays supplemented with eculizumab.

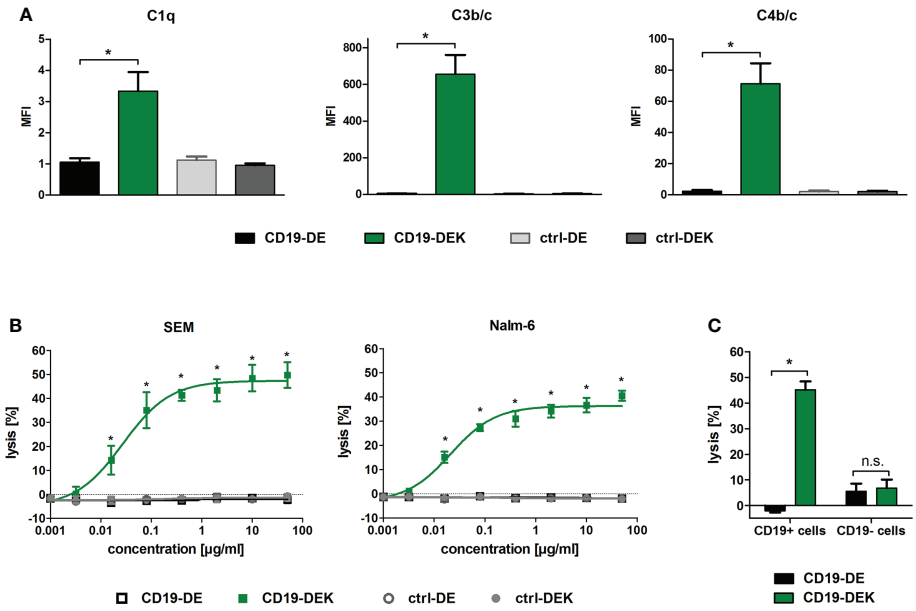

FIGURE 3
CD19-DEK efficiently triggers antibody-dependent complement deposition on target cells and CDC. **(A)** Antibody-dependent complement deposition on CD19-positive B-ALL cell line SEM was analyzed *via* flow cytometry. Target cells were incubated with the respective antibodies (10 µg/ml) and 25% v/v human serum of healthy donors supplemented with eculizumab. Mean values ± SEM of three independent experiments are presented, **P*<0.05% CD19-DEK vs. CD19-DE, One-way ANOVA with Bonferroni post-test. **(B)** CDC of the tumor cell lines SEM and Nalm-6 was performed in chromium release assays with increasing antibody concentrations and 25% v/v human serum of healthy donors. The tumor cell lysis was tested for CD19-DEK and CD19-DE and was compared to the control antibodies ctrl-DEK and ctrl-DE. Mean values ± SEM of three independent experiments are presented, **P*<0.05% CD19-DEK vs. CD19-DE, Two-way ANOVA with Bonferroni post-test. **(C)** Target antigen specific CDC was tested in chromium release assays with CD19-positive (Nalm-6, SEM) and CD19-negative (MOLT-16, CEM) tumor cells at an antibody concentration of 50 µg/ml and 25% v/v human serum of healthy donors. The tumor cell lysis mediated by CD19-DEK was compared to CD19-DE. Mean values ± SEM of three independent experiments are presented, * *P*<0.05%, ns, not significant. CD19-DEK vs. CD19-DE, two-tailed t-Test with Mann-Whitney test.

To investigate the relative contribution of CDC and ADCC in whole blood in more detail, we performed chromium release assays with increasing concentrations of the respective antibodies using the B-ALL cell line SEM as target cells and whole blood of healthy donors as effector source. Complement-mediated killing was blocked with the C5-specific inhibitory antibody eculizumab. As expected, efficient tumor cell lysis was mediated in a concentration dependent manner by CD19-DEK without the addition of eculizumab (Figure 4C). The tumor cell lysis was completely blocked at a CD19-DEK concentration of 2µg/ml in the presence of eculizumab (Figures 4C, D). This suggested a fully complement-dependent activity of the dual-engineered CD19-antibody at high antibody concentrations. At lower CD19-DEK concentrations (e.g. 0.016 µg/ml) tumor cell lysis was not fully blocked by the addition of eculizumab. The extent of tumor cell lysis of CD19-DEK in the presence or absence eculizumab is significantly different at an antibody concentration of 2 µg/ml, whereas no significant difference in tumor cell lysis is observed at an antibody concentration of 0.016 µg/ml (Figure 4D). In addition, the extent of tumor cell lysis of CD19-DEK and the parental CD19-DE antibody at a concentration of 0.016 µg/ml were comparable (Figure 4D). These data suggest that at lower concentrations of CD19-DEK, receptor occupancy is probably low and not sufficient to trigger significant complement deposition. In this situation engagement of Fc receptors is possible to trigger ADCC. Overall, the effector cell killing capacity in these experiments was low and differed between donors, most likely due to varying contents of NK cells. Together, these data suggest that at high antibody concentrations CDC is the dominant effector mechanism and complement deposition completely prevents effector cell killing. At very low antibody concentrations (0.016 µg/ml) tumor cell lysis is mediated by ADCC only. In between, there are dose levels allowing both ADCC and CDC to be active (Figure 4D). As shown in Figure 4B, the tumor cell lysis of CD19-DE in whole blood is most likely mediated by NK cells (FcγRIIIa).

Together our data showed that the dual-engineered CD19 antibody was able to trigger efficient ADCC and ADCP to the same extent as CD19-DE and in addition triggers CDC when isolated effector populations were applied. Our data from whole blood show that optimizing several effector functions is more complex and suggest that only selected effector functions may be active at the same time depending on antibody concentration and the availability of different effector sources.

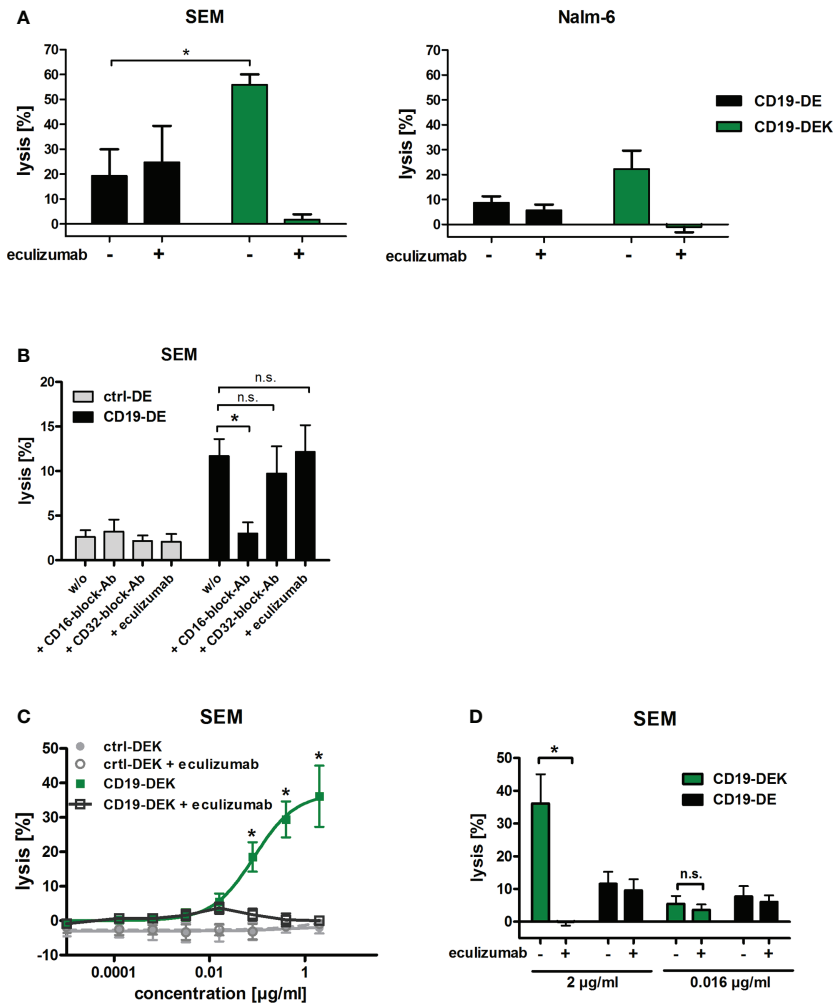

FIGURE 4
The dual-engineered antibody CD19-DEK showed improved cytotoxic activity compared to CD19-DE using whole blood as effector source. **(A, B)** Chromium release assays with a concentration of 2 µg/ml of the respective antibodies and 25% v/v whole blood of healthy donors was performed to analyze the combined anti-tumor effect of CD19-DEK *via* the complement system (CDC) and *via* recruitment of effector cells (ADCC). For inhibition of tumor cell lysis *via* the complement system the blood was supplemented with 50µg/ml eculizumab. Mean values ± SEM of three (SEM cells) or seven (Nalm-6 cells) independent experiments, *P<0.05% CD19-DEK vs. CD19-DE, One-way ANOVA with Bonferroni post-test. **(B)** For inhibition of tumor cell lysis *via* FcγRIII (CD16) or FcγRIIa (CD32a) expressing effector cells the blood was preincubated with 100µg/ml specific blockade antibodies with an silenced Fc-part, lacking FcγR binding. **(C, D)** Chromium release assays with the B-ALL cell line SEM and increasing concentrations of the respective antibodies and 25% v/v whole blood of healthy donors was performed. For inhibition of tumor cell lysis *via* the complement system the blood was supplemented with 50µg/ml eculizumab. Mean values ± SEM of three independent experiments, *P<0.05%, ns, not significant. One- or Two-way ANOVA with Bonferroni post-test.

Discussion

In the current study we successfully generated a dual Fc-engineered antibody CD19-DEK by combining the DE-modification with the HexaBody mutation E345K. This led to an enhancement of all Fc-mediated effector functions (ADCC, ADCP and CDC) when isolated effector sources were analyzed. Interestingly, the relative contribution of ADCC and CDC to the tumor cell killing activity in whole blood depended on antibody concentration.

CD19 is an attractive target antigen for antibody therapy of B-cell leukemias and lymphomas, as reflected by CD19's position among the top 10 targets of the first 100 approved antibodies (2). Nevertheless, non-engineered CD19-IgG1 antibodies are poorly effective in mediating Fc-effector functions like ADCC, ADCP and CDC. Reasons why CD19

antibodies are not as potent as for example non-engineered type I CD20 antibodies are not fully understood and probably not referable to antigen density on malignant B cells. Possible reasons could be antibody characteristics like epitope location and specificity or antigen characteristics like structure and size, antigen membrane fluidity or the antigen's plasma membrane microdomain localization (65–68). Despite the fact that CD19 antibodies show poor effector functions, they can be converted into efficient therapeutic agents through Fc engineering and the associated improvement of antibody-mediated effector functions (26, 69). The clinically approved antibody tafasitamab is an Fc-protein engineered CD19 antibody with amino acid substitutions S239D/I332E (DE-modification). The optimized FcγR binding characteristics result in increased ADCC and ADCP. Since tafasitamab is lacking CDC activity (28–30), its therapeutic activity may be further enhanced by adding CDC as an additional effector function.

To date, six Fc-optimized antibodies are approved for clinical use in cancer. The afucosylated antibodies obinutuzumab and mogamulizumab, the afucosylated bispecific antibody amivantamab, the antibody drug conjugate belantamab mafodotin and the Fc-protein engineered antibodies tafasitamab and margetuximab are optimized for improved FcγR binding resulting in enhanced ADCC and/or ADCP activity (24, 25, 27). Whereas to our knowledge no antibodies optimized for complement activation are clinically approved to date, currently two HexaBody molecules are in phase I and II clinical trials. The HexaBody-CD38 derived from the clinically approved antibody daratumumab showed potent anti-tumor activity in preclinical models of hematological diseases such as multiple myeloma (MM), B-cell malignancies and acute lymphoblastic leukemia (ALL), and the DuoHexaBody-CD37 may represent a potential therapeutic antibody for the treatment of certain B-cell malignancies (70, 71). The two HexaBodies carry the E430G amino acid alteration, which leads to an enhanced Fc-Fc interaction after antigen binding on the cell surface and these IgG hexamer formations increase the binding of hexavalent complement component C1q and leads to a potent CDC activity (37, 46, 70, 71). To our knowledge, dual optimized antibody variants as described here are not in clinical development to date.

Several *in vivo* observations suggested that both complement activation and effector cell recruitment represent important effector functions in antibody therapy of different hematological malignancies. This has led to the presumption that simultaneous enhancement of effector cell activation and complement activation may be advantageous. For CD20 antibodies, it was shown that depending on the murine tumor model the therapeutic efficiency of the antibodies exclusively depends on complement activity or on FcγR-mediated effector functions (14, 15, 32). Besides the variation in the relative contribution of CDC and effector cell mediated functions in murine models, also the tumor burden and the anatomic location, as well as the tumor microenvironment and the immune status of patients can affect the therapeutic effect of monoclonal antibodies (72, 73). In patients the responsiveness of tumor cells to CDC or ADCC and ADCP may be regulated by different tumor cell characteristics like target antigen density and expression of regulatory antigens on the cell surface and may ascertain which effector mechanism is available to the antibody. Thus, the expression of inhibitory antigens on the cell surface such as CD47 or human leukocyte antigens (HLA) restricted effector mechanism like ADCC and ADCP, whereas an increased expression of NK cell-activating danger signals like NKG2D ligands can improve cellular cytotoxicity (74–76). The expression of inhibitory mCRPs like CD46, CD55 and CD59 can protect tumor cells from CDC (77, 78). Accordingly, in certain situations different Fc-mediated effector mechanisms such as CDC, ADCC and ADCP may be necessary for an effective tumor cell depletion, which suggests that dual Fc-engineered antibodies, like the CD19-DEK in the current study, may be beneficial.

We recently demonstrated that dual Fc-engineered CD19 and CD20 antibodies (glyco- and protein-engineered) are able to enhance both ADCC and CDC activity (53, 54), but the applied technologies compared to the approach described here differ significantly. Glyco-engineering by producing afucosylated antibody variants as applied in our previous studies exclusively enhances FcγRIIIa affinity which mediates improved ADCC by NK cells, while Fc protein-engineering such as DE-modification increases the affinity of antibodies to different FcγR (FcγRIIIa, FcγRIIa, FcγRI) which leads to enhanced ADCC by NK cells and improved ADCP by macrophages (26). In addition, the affinity to FcγRIIIa is significantly higher for DE-modified antibodies compared to non-fucosylated variants (79). The EFTAE amino acid modifications used in our previous studies led to a higher binding affinity to the C1q molecule, resulting in antibodies with potent CDC activity (45). The optimized C1q binding of EFTAE-modified antibodies is independent of target antigen binding which could potentially lead to target cell independent complement activation in solution. Contrary to this, the E345K or E430G amino acid substitutions do not result in enhanced binding affinity to C1q but lead to enhanced Fc-Fc interaction of IgGs only after antigen binding on the cell surface. These IgG hexameric structures improve the binding of the hexavalent complement component C1q and trigger efficient CDC (37, 46). Therefore, the approach described here may be advantageous compared to previously described approaches to improve ADCC, ADCP and CDC simultaneously.

The simultaneous enhancement of Fc-mediated effector functions like ADCC, ADCP and CDC by amino acid substitutions of IgG antibodies is challenging, because the binding sites for Fcγ receptors and the complement component C1q overlap (50–52) and C1q binding may enhance the hexamerization of antibodies by stabilizing the hexamer (80, 81). Therefore, introducing amino acid

substitutions in the Fc domain may not necessarily improve both effector functions. In the current study, we showed that by introducing an amino acid exchange in the CH3 domain of the dual Fc-engineered CD19-DEK antibody ADCC and ADCP activity was not compromised and comparable to CD19-DE and that the dual engineered antibody additionally mediated CDC of target antigen positive tumor cells *in vitro*. From our data we cannot exclude that the DE mutation may impact on-target hexamerization. Further studies are needed to figure out whether the DEK combination of amino acid exchanges is as efficient to trigger CDC as a K amino acid exchange only variant. Interestingly, at high CD19-DEK antibody concentrations tumor cell lysis in whole blood, when both complement and effector cells are available, was completely complement dependent. At low antibody concentrations tumor cell killing was strictly FcR-dependent. Only at selected antibody concentrations both effector functions contributed to tumor cell killing. Since addition of isolated C1q did not significantly inhibit the ADCC activity of CD19-DEK, these data suggest that strong complement deposition reduce the capacity of an antibody to recruit Fc receptors. Wang and colleges described that NK-cell mediated ADCC of rituximab-coated target cells was inhibited by C3b deposition and the depletion of C3 complement component enhances the ability of antibody-coated target cells to activate human NK cells (82, 83). On the other hand, C3b or C4b opsonized tumor cells may be sensitized for phagocytic activity of macrophages and myeloid cells by engagement of complement receptors (49). Furthermore, complement activation and thereby release of anaphylatoxins may attract FcR-positive effector cells, enlarging the pool of available effector cells. This may further boost complex adaptive immune responses mediated by antibody variants optimized for FcγRIIa and FcγRIIIa binding (84).

In comparison to these types of *in vitro* observations, the *in vivo* situation may even be more complex. In this situation compartment effects and availability of effector cell populations and bioavailability of complement factors in selected tissues may have a significant impact which effector mechanism is available at a defined anatomical site (85, 86). Therefore, the competition of FcγR mediated effector functions and the complement system may not be as relevant in the *in vivo* situation compared to our *in vitro* observations in whole blood depending on the biological features and location of the respective tumor (78). Addressing these complex aspects *in vivo* is challenging because murine models may not perfectly reflect the human situation in terms of Fc receptor binding especially when dealing with engineered human Fc domains. Although, meanwhile complex transgenic mouse models engineered to express all human FcγR on the respective effector cell populations or stem cell humanized mouse models are available (87, 88), in particular the contribution of the complement system and CDC may be difficult to investigate in small animal models (43, 89). A variety of parameters, such as target antigen density, expression of complement inhibitory molecules, target cell location and other factors affect susceptibility of target cells to complement lysis. Therefore, it might not be surprising that for example the *in vivo* activity of rituximab in different mouse models has been demonstrated to be strictly dependent on complement activation or absolutely independent (14, 32, 43, 89). Accordingly, the complex therapeutic effects of dual Fc-engineered antibodies, like CD19-DEK, could probably best evaluated in clinical trials or non-human primates.

In conclusion, our data provide evidence that from a technical perspective selected Fc-enhancing mutations can be combined (S239D/I332E and E345K) allowing the enhancement of ADCC, ADCP and CDC activity when isolated effector populations are analyzed. In situations where the complement system and FcR-positive effector cells are available as effector source, strong complement deposition may negatively impact FcR engagement. Both effector functions may be simultaneously active only at selected antibody concentrations. Nevertheless, this dual Fc engineering approach may display a new strategy to improve antibody therapy of various tumor types but further carefully designed *in vivo* studies are necessary to support this concept. As a perspective, our results may help in guiding optimal antibody engineering strategies to optimize antibodies' effector functions.

Data availability statement

The raw data supporting the conclusions of this article will be made available by the authors, without undue reservation.

Ethics statement

The studies involving human participants were reviewed and approved by Ethics Committee of the Christian-Albrechts-University of Kiel (Kiel, Germany). The patients/participants provided their written informed consent to participate in this study.

Author contributions

CG and PR designed and performed the experiments and analyzed data. CG and MP wrote the manuscript. AL, AB, DW, SK, TT, FN, RL, ML, TR, TV, DS, KK performed research,

provided essential reagents and contributed to writing the manuscript. CK and MP initiated and designed experiments and supervised the study. All authors discussed the manuscript. All authors have read and agreed to the published version of the manuscript.

Funding

The work was supported by research funds within the clinical research unit CATCH-ALL funded by the Deutsche Forschungsgemeinschaft (DFG, German Research Foundation) - 444949889 to MP, DMS and TV, the DFG Excellence Cluster Precision Medicine in Inflammation (TI-4) (MP, RL) and the Deutsche José Carreras Leukämie Stiftung (MP, CK).

Acknowledgments

We thank Anja Muskulus and Britta von Below for excellent technical assistance.

Conflict of interest

The authors declare that the research was conducted in the absence of any commercial or financial relationships that could be construed as a potential conflict of interest.

Publisher's note

Supplementary material

The Supplementary Material for this article can be found online at: https://www.frontiersin.org/articles/10.3389/fimmu.2022.957874/full#supplementary-material

References

1. Carter PJ, Lazar GA. Next generation antibody drugs: Pursuit of the 'High-hanging fruit'. *Nat Rev Drug Discov* (2018) 17(3):197–223. doi: 10.1038/nrd.2017.227

2. Mullard A. FDA Approves 100th monoclonal antibody product. *Nat Rev Drug Discovery* (2021) 20(7):491–5. doi: 10.1038/d41573-021-00079-7

3. Advani AS. New immune strategies for the treatment of acute lymphoblastic leukemia: Antibodies and chimeric antigen receptors. *Hematol Am Soc Hematol Educ Program* (2013) 2013:131–7. doi: 10.1182/asheducation-2013.1.131

4. Hammer O. CD19 as an attractive target for antibody-based therapy. *MAbs* (2012) 4(5):571–7. doi: 10.4161/mabs.21338

5. Salles G, Dlugosz-Danecka M, Ghesquieres H, Jurczak W. Tafasitamab for the treatment of relapsed or refractory diffuse Large b-cell lymphoma. *Expert Opin Biol Ther* (2021) 21(4):455–63. doi: 10.1080/14712598.2021.1884677

6. Hoelzer D. Novel antibody-based therapies for acute lymphoblastic leukemia. *Hematol Am Soc Hematol Educ Program* (2011) 2011:243–9. doi: 10.1182/asheducation-2011.1.243

7. Yazawa N, Hamaguchi Y, Poe JC, Tedder TF. Immunotherapy using unconjugated CD19 monoclonal antibodies in animal models for b lymphocyte malignancies and autoimmune disease. *Proc Natl Acad Sci U.S.A.* (2005) 102 (42):15178–83. doi: 10.1073/pnas.0505539102

8. Horton HM, Bernett MJ, Pong E, Peipp M, Karki S, Chu SY, et al. Potent in vitro and in vivo activity of an fc-engineered anti-CD19 monoclonal antibody against lymphoma and leukemia. *Cancer Res* (2008) 68(19):8049–57. doi: 10.1158/0008-5472.CAN-08-2268

9. Hekman A, Honselaar A, Vuist WM, Sein JJ, Rodenhuis S, ten Bokkel Huinink WW, et al. Initial experience with treatment of human b cell lymphoma with anti-CD19 monoclonal antibody. *Cancer Immunol Immunother* (1991) 32 (6):364–72. doi: 10.1007/BF01741331

10. Kellner C, Peipp M, Gramatzki M, Schrappe M, Schewe DM. Perspectives of fc engineered antibodies in CD19 targeting immunotherapies in pediatric b-cell precursor acute lymphoblastic leukemia. *Oncoimmunology* (2018) 7(8):e1448331. doi: 10.1080/2162402X.2018.1448331

11. Frigault MJ, Maus MV. State of the art in car T cell therapy for CD19+ b cell malignancies. *J Clin Invest* (2020) 130(4):1586–94. doi: 10.1172/JCI129208

12. Kantarjian H, Stein A, Gokbuget N, Fielding AK, Schuh AC, Ribera JM, et al. Blinatumomab versus chemotherapy for advanced acute lymphoblastic leukemia. *N Engl J Med* (2017) 376(9):836–47. doi: 10.1056/NEJMoa1609783

13. Caimi PF, Ai W, Alderuccio JP, Ardeshna KM, Hamadani M, Hess B, et al. Loncastuximab tesirine in relapsed or refractory diffuse Large b-cell lymphoma (Lotis-2): A multicentre, open-label, single-arm, phase 2 trial. *Lancet Oncol* (2021) 22(6):790–800. doi: 10.1016/S1470-2045(21)00139-X

14. Clynes RA, Towers TL, Presta LG, Ravetch JV. Inhibitory fc receptors modulate in vivo cytotoxicity against tumor targets. *Nat Med* (2000) 6(4):443–6. doi: 10.1038/74704

15. de Haij S, Jansen JH, Boross P, Beurskens FJ, Bakema JE, Bos DL, et al. *In vivo* cytotoxicity of type I CD20 antibodies critically depends on fc receptor itam signaling. *Cancer Res* (2010) 70(8):3209–17. doi: 10.1158/0008-5472.CAN-09-4109

16. Cartron G, Dacheux L, Salles G, Solal-Celigny P, Bardos P, Colombat P, et al. Therapeutic activity of humanized anti-CD20 monoclonal antibody and polymorphism in IgG fc receptor fcgammariiia gene. *Blood* (2002) 99(3):754–8. doi: 10.1182/blood.v99.3.754

17. Weng WK, Levy R. Two immunoglobulin G fragment c receptor polymorphisms independently predict response to rituximab in patients with follicular lymphoma. *J Clin Oncol* (2003) 21(21):3940–7. doi: 10.1200/JCO.2003.05.013

18. Persky DO, Dornan D, Goldman BH, Braziel RM, Fisher RI, Leblanc M, et al. Fcγ receptor 3a genotype predicts overall survival in follicular lymphoma patients treated on swog trials with combined monoclonal antibody plus chemotherapy but not chemotherapy alone. *Haematologica* (2012) 97(6):937–42. doi: 10.3324/haematol.2011.050419

19. Strefford JC, Nowicka M, Hargreaves CE, Burton C, Davies A, Ganderton R, et al. Single-nucleotide fcγ receptor polymorphisms do not impact Obinutuzumab/Rituximab outcome in patients with lymphoma. *Blood Adv* (2021) 5(15):2935–44. doi: 10.1182/bloodadvances.2020003985

20. Burkhardt B, Yavuz D, Zimmermann M, Schieferstein J, Kabickova E, Attarbaschi A, et al. Impact of fcγ-receptor polymorphisms on the response to rituximab treatment in children and adolescents with mature b cell Lymphoma/Leukemia. *Ann Hematol* (2016) 95(9):1503–12. doi: 10.1007/s00277-016-2731-x

21. Mellor JD, Brown MP, Irving HR, Zalcberg JR, Dobrovic A. A critical review of the role of fcγ receptor polymorphisms in the response to monoclonal antibodies in cancer. *J Hematol Oncol* (2013) 6:1. doi: 10.1186/1756-8722-6-1

22. Uchida J, Hamaguchi Y, Oliver JA, Ravetch JV, Poe JC, Haas KM, et al. The innate mononuclear phagocyte network depletes b lymphocytes through fc receptor-dependent mechanisms during anti-CD20 antibody immunotherapy. *J Exp Med* (2004) 199(12):1659–69. doi: 10.1084/jem.20040119

23. Mossner E, Brunker P, Moser S, Puntener U, Schmidt C, Herter S, et al. Increasing the efficacy of CD20 antibody therapy through the engineering of a new type II anti-CD20 antibody with enhanced direct and immune effector cell-mediated b-cell cytotoxicity. *Blood* (2010) 115(22):4393–402. doi: 10.1182/blood-2009-06-225979

24. Markham A. Belantamab mafodotin: First approval. *Drugs* (2020) 80 (15):1607–13. doi: 10.1007/s40265-020-01404-x

25. Syed YY. Amivantamab: First approval. *Drugs* (2021) 81(11):1349–53. doi: 10.1007/s40265-021-01561-7

26. Kellner C, Otte A, Cappuzzello E, Klausz K, Peipp M. Modulating cytotoxic effector functions by fc engineering to improve cancer therapy. *Transfus Med Hemother* (2017) 44(5):327–36. doi: 10.1159/000479980

27. Liu R, Oldham RJ, Teal E, Beers SA, Cragg MS. Fc-engineering for modulated effector functions-improving antibodies for cancer treatment. *Antibodies (Basel)* (2020) 9(4):64. doi: 10.3390/antib9040064

28. Schewe DM, Alsadeq A, Sattler C, Lenk L, Vogiatzi F, Cario G, et al. An fc-engineered CD19 antibody eradicates mrd in patient-derived mll-rearranged acute lymphoblastic leukemia xenografts. *Blood* (2017) 130(13):1543–52. doi: 10.1182/blood-2017-01-764316

29. Kellner C, Zhukovsky EA, Potzke A, Bruggemann M, Schrauder A, Schrappe M, et al. The fc-engineered CD19 antibody Mor208 (Xmab5574) induces natural killer cell-mediated lysis of acute lymphoblastic leukemia cells from pediatric and adult patients. *Leukemia* (2013) 27(7):1595–8. doi: 10.1038/leu.2012.373

30. Salles G, Duell J, Gonzalez Barca E, Tournilhac O, Jurczak W, Liberati AM, et al. Tafasitamab plus lenalidomide in relapsed or refractory diffuse Large b-cell lymphoma (L-mind): A multicentre, prospective, single-arm, phase 2 study. *Lancet Oncol* (2020) 21(7):978–88. doi: 10.1016/S1470-2045(20)30225-4

31. Golay J, Taylor RP. The role of complement in the mechanism of action of therapeutic anti-cancer mabs. *Antibodies (Basel)* (2020) 9(4):58. doi: 10.3390/antib9040058

32. Di Gaetano N, Cittera E, Nota R, Vecchi A, Grieco V, Scanziani E, et al. Complement activation determines the therapeutic activity of rituximab in vivo. *J Immunol* (2003) 171(3):1581–7. doi: 10.4049/jimmunol.171.3.1581

33. Kennedy AD, Beum PV, Solga MD, DiLillo DJ, Lindorfer MA, Hess CE, et al. Rituximab infusion promotes rapid complement depletion and acute CD20 loss in chronic lymphocytic leukemia. *J Immunol* (2004) 172(5):3280–8. doi: 10.4049/jimmunol.172.5.3280

34. Klepfish A, Schattner A, Ghoti H, Rachmilewitz EA. Addition of fresh frozen plasma as a source of complement to rituximab in advanced chronic lymphocytic leukaemia. *Lancet Oncol* (2007) 8(4):361–2. doi: 10.1016/S1470-2045(07)70106-7

35. Bannerji R, Kitada S, Flinn IW, Pearson M, Young D, Reed JC, et al. Apoptotic-regulatory and complement-protecting protein expression in chronic lymphocytic leukemia: Relationship to in vivo rituximab resistance. *J Clin Oncol* (2003) 21(8):1466–71. doi: 10.1200/JCO.2003.06.012

36. Maloney DG, Ogura M, Fukuhara N, Davis J, Lasher J, Izquierdo M, et al. A phase 3 randomized study (Homer) of ofatumumab vs rituximab in inhl relapsed after rituximab-containing therapy. *Blood Adv* (2020) 4(16):3886–93. doi: 10.1182/bloodadvances.2020001942

37. de Jong RN, Beurskens FJ, Verploegen S, Strumane K, van Kampen MD, Voorhorst M, et al. A novel platform for the potentiation of therapeutic antibodies based on antigen-dependent formation of IgG hexamers at the cell surface. *PloS Biol* (2016) 14(1):e1002344. doi: 10.1371/journal.pbio.1002344

38. Bondza S, Marosan A, Kara S, Losing J, Peipp M, Nimmerjahn F, et al. Complement-dependent activity of CD20-specific IgG correlates with bivalent antigen binding and C1q binding strength. *Front Immunol* (2020) 11:609941. doi: 10.3389/fimmu.2020.609941

39. de Weers M, Tai YT, van der Veer MS, Bakker JM, Vink T, Jacobs DC, et al. Daratumumab, a novel therapeutic human CD38 monoclonal antibody, induces killing of multiple myeloma and other hematological tumors. *J Immunol* (2011) 186(3):1840–8. doi: 10.4049/jimmunol.1003032

40. Nijhof IS, Casneuf T, van Velzen J, van Kessel B, Axel AE, Syed K, et al. CD38 expression and complement inhibitors affect response and resistance to daratumumab therapy in myeloma. *Blood* (2016) 128(7):959–70. doi: 10.1182/blood-2016-03-703439

41. Xia MQ, Hale G, Waldmann H. Efficient complement-mediated lysis of cells containing the campath-1 (Cdw52) antigen. *Mol Immunol* (1993) 30(12):1089–96. doi: 10.1016/0161-5890(93)90155-5

42. Pawluczkowycz AW, Beurskens FJ, Beum PV, Lindorfer MA, van de Winkel JG, Parren PW, et al. Binding of submaximal C1q promotes complement-dependent cytotoxicity (CDC) of b cells opsonized with anti-CD20 mabs ofatumumab (Ofa) or rituximab (Rtx): Considerably higher levels of CDC are induced by ofa than by rtx. *J Immunol* (2009) 183(1):749–58. doi: 10.4049/jimmunol.0900632

43. Sopp JM, Peters SJ, Rowley TF, Oldham RJ, James S, Mockridge I, et al. On-target igg hexamerisation driven by a c-terminal IgM tail-piece fusion variant confers augmented complement activation. *Commun Biol* (2021) 4(1):1031. doi: 10.1038/s42003-021-02513-3

44. Natsume A, In M, Takamura H, Nakagawa T, Shimizu Y, Kitajima K, et al. Engineered antibodies of IgG1/IgG3 mixed isotype with enhanced cytotoxic activities. *Cancer Res* (2008) 68(10):3863–72. doi: 10.1158/0008-5472.CAN-07-6297

45. Moore GL, Chen H, Karki S, Lazar GA. Engineered fc variant antibodies with enhanced ability to recruit complement and mediate effector functions. *MAbs* (2010) 2(2):181–9. doi: 10.4161/mabs.2.2.11158

46. Diebolder CA, Beurskens FJ, de Jong RN, Koning RI, Strumane K, Lindorfer MA, et al. Complement is activated by IgG hexamers assembled at the cell surface. *Science* (2014) 343(6176):1260–3. doi: 10.1126/science.1248943

47. Tammen A, Derer S, Schwanbeck R, Rosner T, Kretschmer A, Beurskens FJ, et al. Monoclonal antibodies against epidermal growth factor receptor acquire an ability to kill tumor cells through complement activation by mutations that selectively facilitate the hexamerization of IgG on opsonized cells. *J Immunol* (2017) 198(4):1585–94. doi: 10.4049/jimmunol.1601268

48. Stasilojc G, Osterborg A, Blom AM, Okroj M. New perspectives on complement mediated immunotherapy. *Cancer Treat Rev* (2016) 45:68–75. doi: 10.1016/j.ctrv.2016.02.009

49. Lee CH, Romain G, Yan W, Watanabe M, Charab W, Todorova B, et al. IgG fc domains that bind C1q but not effector fcγ receptors delineate the importance of complement-mediated effector functions. *Nat Immunol* (2017) 18(8):889–98. doi: 10.1038/ni.3770

50. Schneider S, Zacharias M. Atomic resolution model of the antibody fc interaction with the complement C1q component. *Mol Immunol* (2012) 51(1):66–72. doi: 10.1016/j.molimm.2012.02.111

51. Radaev S, Motyka S, Fridman WH, Sautes-Fridman C, Sun PD. The structure of a human type III fcγ receptor in complex with fc. *J Biol Chem* (2001) 276(19):16469–77. doi: 10.1074/jbc.M100350200

52. Sondermann P, Huber R, Oosthuizen V, Jacob U. The 3.2-a crystal structure of the human IgG1 fc fragment-fc gammariii complex. *Nature* (2000) 406 (6793):267–73. doi: 10.1038/35018508

53. Rosskopf S, Eichholz KM, Winterberg D, Diemer KJ, Lutz S, Munnich IA, et al. Enhancing CDC and ADCC of CD19 antibodies by combining fc protein-engineering with fc glyco-engineering. *Antibodies (Basel)* (2020) 9(4):63. doi: 10.3390/antib9040063

54. Wirt T, Rosskopf S, Rosner T, Eichholz KM, Kahrs A, Lutz S, et al. An fc double-engineered CD20 antibody with enhanced ability to trigger complement-dependent cytotoxicity and antibody-dependent cell-mediated cytotoxicity. *Transfus Med Hemother* (2017) 44(5):292–300. doi: 10.1159/000479978

55. Greil J, Gramatzki M, Burger R, Marschalek R, Peltner M, Trautmann U, et al. The acute lymphoblastic leukaemia cell line sem with T (4,11) Chromosomal rearrangement is biphenotypic and responsive to interleukin-7. *Br J Haematol* (1994) 86(2):275–83. doi: 10.1111/j.1365-2141.1994.tb04726.x

56. Glorius P, Baerenwaldt A, Kellner C, Staudinger M, Dechant M, Stauch M, et al. The novel tribody [(CD20)(2)xCD16] efficiently triggers effector cell-mediated lysis of malignant b cells. *Leukemia* (2013) 27(1):190–201. doi: 10.1038/leu.2012.150

57. Lux A, Yu X, Scanlan CN, Nimmerjahn F. Impact of immune complex size and glycosylation on IgG binding to human fcγs. *J Immunol* (2013) 190(8):4315–23. doi: 10.4049/jimmunol.1200501

58. Amersdorffer J, Steidl S, Winderlich M, Krohn S, Rojkjaer L. Combination therapy with an anti-CD19 antibody and a purine analog. *US Patent* (2012) 14:20140227277.

59. Winterberg D, Lenk L, Osswald M, Vogiatzi F, Gehlert CL, Frielitz FS, et al. Engineering of CD19 antibodies: A CD19-trail fusion construct specifically induces apoptosis in b-cell precursor acute lymphoblastic leukemia (BCP-ALL) cells in vivo. *J Clin Med* (2021) 10(12):2634. doi: 10.3390/jcm10122634

60. Peipp M, Lammerts van Bueren JJ, Schneider-Merck T, Bleeker WW, Dechant M, Beyer T, et al. Antibody fucosylation differentially impacts cytotoxicity mediated by NK and PMN effector cells. *Blood* (2008) 112(6):2390–9. doi: 10.1182/blood-2008-03-144600

61. Tam SH, McCarthy SG, Armstrong AA, Somani S, Wu SJ, Liu X, et al. Functional, biophysical, and structural characterization of human IgG1 and IgG4 fc variants with ablated immune functionality. *Antibodies (Basel)* (2017) 6(3):12. doi: 10.3390/antib6030012

62. Baumann N, Rosner T, Jansen JHM, Chan C, Marie Eichholz K, Klausz K, et al. Enhancement of epidermal growth factor receptor antibody tumor immunotherapy by glutaminyl cyclase inhibition to interfere with CD47/Signal regulatory protein alpha interactions. *Cancer Sci* (2021) 112(8):3029–40. doi: 10.1111/cas.14999

63. Clark MR. IgG effector mechanisms. *Chem Immunol* (1997) 65:88–110.

64. Lazar GA, Dang W, Karki S, Vafa O, Peng JS, Hyun L, et al. Engineered antibody fc variants with enhanced effector function. *Proc Natl Acad Sci U.S.A.* (2006) 103(11):4005–10. doi: 10.1073/pnas.0508123103

65. Cleary KLS, Chan HTC, James S, Glennie MJ, Cragg MS. Antibody distance from the cell membrane regulates antibody effector mechanisms. *J Immunol* (2017) 198(10):3999–4011. doi: 10.4049/jimmunol.1601473

66. Tiroch K, Stockmeyer B, Frank C, Valerius T. Intracellular domains of target antigens influence their capacity to trigger antibody-dependent cell-mediated cytotoxicity. *J Immunol* (2002) 168(7):3275–82. doi: 10.4049/jimmunol.168.7.3275

67. Kumar A, Planchais C, Fronzes R, Mouquet H, Reyes N. Binding mechanisms of therapeutic antibodies to human CD20. *Science* (2020) 369 (6505):793–9. doi: 10.1126/science.abb8008

68. Rouge L, Chiang N, Steffek M, Kugel C, Croll TI, Tam C, et al. Structure of CD20 in complex with the therapeutic monoclonal antibody rituximab. *Science* (2020) 367(6483):1224–30. doi: 10.1126/science.aaz9356

69. Dalziel M, Beers SA, Cragg MS, Crispin M. Through the barricades: Overcoming the barriers to effective antibody-based cancer therapeutics. *Glycobiology* (2018) 28(9):697–712. doi: 10.1093/glycob/cwy043

70. De Goeij BE, Janmaat ML, Andringa G, Kil L, Van Kessel B, Frerichs KA, et al. Hexabody-CD38, a novel CD38 antibody with a hexamerization enhancing mutation, demonstrates enhanced complement-dependent cytotoxicity and shows potent anti-tumor activity in preclinical models of hematological malignancies. *Blood* (2019) 134(Supplement_1):3106–. doi: 10.1182/blood-2019-125788

71. Oostindie SC, van der Horst HJ, Kil LP, Strumane K, Overdijk MB, van den Brink EN, et al. Duohexabody-CD37((R)), a novel biparatopic CD37 antibody with enhanced fc-mediated hexamerization as a potential therapy for b-cell malignancies. *Blood Cancer J* (2020) 10(3):30. doi: 10.1038/s41408-020-0292-7

72. Boross P, Jansen JH, de Haij S, Beurskens FJ, van der Poel CE, Bevaart L, et al. The in vivo mechanism of action of CD20 monoclonal antibodies depends on local tumor burden. *Haematologica* (2011) 96(12):1822–30. doi: 10.3324/haematol.2011.047159

73. Gong Q, Ou Q, Ye S, Lee WP, Cornelius J, Diehl L, et al. Importance of cellular microenvironment and circulatory dynamics in b cell immunotherapy. *J Immunol* (2005) 174(2):817–26. doi: 10.4049/jimmunol.174.2.817

74. Ferris RL, Jaffee EM, Ferrone S. Tumor antigen-targeted, monoclonal antibody-based immunotherapy: Clinical response, cellular immunity, and immunoescape. *J Clin Oncol* (2010) 28(28):4390–9. doi: 10.1200/JCO.2009.27.6360

75. Chao MP, Alizadeh AA, Tang C, Myklebust JH, Varghese B, Gill S, et al. Anti-CD47 antibody synergizes with rituximab to promote phagocytosis and eradicate non-Hodgkin lymphoma. *Cell* (2010) 142(5):699–713. doi: 10.1016/j.cell.2010.07.044

76. Inagaki A, Ishida T, Yano H, Ishii T, Kusumoto S, Ito A, et al. Expression of the ulbp ligands for NKG2D by b-nhl cells plays an important role in determining their susceptibility to rituximab-induced adcc. *Int J Cancer* (2009) 125(1):212–21. doi: 10.1002/ijc.24351

77. Meyer S, Leusen JH, Boross P. Regulation of complement and modulation of its activity in monoclonal antibody therapy of cancer. *MAbs* (2014) 6(5):1133–44. doi: 10.4161/mabs.29670

78. Derer S, Beurskens FJ, Rosner T, Peipp M, Valerius T. Complement in antibody-based tumor therapy. *Crit Rev Immunol* (2014) 34(3):199–214. doi: 10.1615/critrevimmunol.2014009761

79. Repp R, Kellner C, Muskulus A, Staudinger M, Nodehi SM, Glorius P, et al. Combined fc-protein- and fc-Glyco-Engineering of ScFv-fc fusion proteins synergistically enhances CD16a binding but does not further enhance NK-cell mediated ADCC. *J Immunol Methods* (2011) 373(1-2):67–78. doi: 10.1016/j.jim.2011.08.003

80. Wang G, de Jong RN, van den Bremer ET, Beurskens FJ, Labrijn AF, Ugurlar D, et al. Molecular basis of assembly and activation of complement component C1 in complex with immunoglobulin G1 and antigen. *Mol Cell* (2016) 63(1):135–45. doi: 10.1016/j.molcel.2016.05.016

81. Overdijk MB, Strumane K, Beurskens FJ, Ortiz Buijsse A, Vermot-Desroches C, Vuillermoz BS, et al. Dual epitope targeting and enhanced hexamerization by Dr5 antibodies as a novel approach to induce potent antitumor activity through Dr5 agonism. *Mol Cancer Ther* (2020) 19(10):2126–38. doi: 10.1158/1535-7163.MCT-20-0044

82. Wang SY, Racila E, Taylor RP, Weiner GJ. Nk-cell activation and antibody-dependent cellular cytotoxicity induced by rituximab-coated target cells is inhibited by the C3b component of complement. *Blood* (2008) 111(3):1456–63. doi: 10.1182/blood-2007-02-074716

83. Wang SY, Veeramani S, Racila E, Cagley J, Fritzinger DC, Vogel CW, et al. Depletion of the C3 component of complement enhances the ability of rituximab-coated target cells to activate human NK cells and improves the efficacy of monoclonal antibody therapy in an in vivo model. *Blood* (2009) 114(26):5322–30. doi: 10.1182/blood-2009-01-200469

84. DiLillo DJ, Ravetch JV. Differential fc-receptor engagement drives an anti-tumor vaccinal effect. *Cell* (2015) 161(5):1035–45. doi: 10.1016/j.cell.2015.04.016

85. Gordan S, Albert H, Danzer H, Lux A, Biburger M, Nimmerjahn F. The immunological organ environment dictates the molecular and cellular pathways of cytotoxic antibody activity. *Cell Rep* (2019) 29(10):3033–46e4. doi: 10.1016/j.celrep.2019.10.111

86. Lux A, Seeling M, Baerenwaldt A, Lehmann B, Schwab I, Repp R, et al. A humanized mouse identifies the bone marrow as a niche with low therapeutic IgG activity. *Cell Rep* (2014) 7(1):236–48. doi: 10.1016/j.celrep.2014.02.041

87. Nimmerjahn F, Ravetch JV. Antibodies, fc receptors and cancer. *Curr Opin Immunol* (2007) 19(2):239–45. doi: 10.1016/j.coi.2007.01.005

88. Casey E, Bournazos S, Mo G, Mondello P, Tan KS, Ravetch JV, et al. A new mouse expressing human fcγ receptors to better predict therapeutic efficacy of human anti-cancer antibodies. *Leukemia* (2018) 32(2):547–9. doi: 10.1038/leu.2017.293

89. Beers SA, French RR, Chan HT, Lim SH, Jarrett TC, Vidal RM, et al. Antigenic modulation limits the efficacy of anti-CD20 antibodies: Implications for antibody selection. *Blood* (2010) 115(25):5191–201. doi: 10.1182/blood-2010-01-263533

frontiers | Frontiers in Immunology

TYPE Original Research
PUBLISHED 09 September 2022
DOI 10.3389/fimmu.2022.987151

OPEN ACCESS

EDITED BY
Falk Nimmerjahn,
University of Erlangen
Nuremberg, Germany

REVIEWED BY
Dapeng Zhou,
Tongji University, China
Eric J. Sundberg,
Emory University, United States
Friedrich Altmann,
University of Natural Resources and
Life Sciences Vienna, Austria

*CORRESPONDENCE
Zhang Yang
yang@sund.ku.dk
Gestur Vidarsson
g.vidarsson@sanquin.nl
Henrik Clausen
hclau@sund.ku.dk

†PRESENT ADDRESS
Zhang Yang,
Department of Cell Therapy Discovery,
Novo Nordisk A/S, Måløv, Denmark

SPECIALTY SECTION
This article was submitted to
B Cell Biology,
a section of the journal
Frontiers in Immunology

RECEIVED 05 July 2022
ACCEPTED 16 August 2022
PUBLISHED 09 September 2022

CITATION
Van Coillie J, Schulz MA,
Bentlage AEH, de Haan N, Ye Z,
Geerdes DM, van Esch WJE,
Hafkenscheid L, Miller RL, Narimatsu Y,
Vakhrushev SY, Yang Z, Vidarsson G
and Clausen H (2022) Role of *N*-
Glycosylation in FcγRIIIa Interaction
With IgG.
Front. Immunol. 13:987151.
doi: 10.3389/fimmu.2022.987151

Role of *N*-Glycosylation in FcγRIIIa interaction with IgG

Julie Van Coillie[1,2,3], Morten A. Schulz[1], Arthur E. H. Bentlage[2,3], Noortje de Haan[1], Zilu Ye[1], Dionne M. Geerdes[4], Wim J. E. van Esch[4], Lise Hafkenscheid[1], Rebecca L. Miller[1], Yoshiki Narimatsu[1,5], Sergey Y. Vakhrushev[1], Zhang Yang[1,5*†], Gestur Vidarsson[2,3*] and Henrik Clausen[1*]

[1]Copenhagen Center for Glycomics, Department of Cellular and Molecular Medicine, Faculty of Health Sciences, University of Copenhagen, Copenhagen, Denmark, [2]Department of Experimental Immunohematology, Sanquin Research, Amsterdam, Netherlands, [3]Department of Biomolecular Mass Spectrometry and Proteomics, Utrecht Institute for Pharmaceutical Sciences and Bijvoet Center for Biomolecular Research, Utrecht University, Utrecht, Netherlands, [4]Sanquin Reagents, Amsterdam, Netherlands, [5]GlycoDisplay ApS, Copenhagen, Denmark

Immunoglobulins G (IgG) and their Fc gamma receptors (FcγRs) play important roles in our immune system. The conserved *N*-glycan in the Fc region of IgG1 impacts interaction of IgG with FcγRs and the resulting effector functions, which has led to the design of antibody therapeutics with greatly improved antibody-dependent cell cytotoxicity (ADCC) activities. Studies have suggested that also *N*-glycosylation of the FcγRIII affects receptor interactions with IgG, but detailed studies of the interaction of IgG1 and FcγRIIIa with distinct *N*-glycans have been hindered by the natural heterogeneity in *N*-glycosylation. In this study, we employed comprehensive genetic engineering of the *N*-glycosylation capacities in mammalian cell lines to express IgG1 and FcγRIIIa with different *N*-glycan structures to more generally explore the role of *N*-glycosylation in IgG1:FcγRIIIa binding interactions. We included FcγRIIIa variants of both the 158F and 158V allotypes and investigated the key *N*-glycan features that affected binding affinity. Our study confirms that afucosylated IgG1 has the highest binding affinity to oligomannose FcγRIIIa, a glycan structure commonly found on Asn162 on FcγRIIIa expressed by NK cells but not monocytes or recombinantly expressed FcγRIIIa.

KEYWORDS

Fc gamma receptors, CD16a, mAbs, IgG, glycoengineering, *N*-glycosylation, glycosyltransferases, surface plasmon resonance

Introduction

Immunoglobulin G (IgG) consists of both an antigen-binding variable Fab region and an Fc region which allows antibodies to activate the complement system through C1q binding or activate effector cells through Fc gamma Receptor (FcγR) or CD16a binding. This interaction is influenced by both the IgG subclass and the IgG-Fc

N-glycan composition at the conserved Asn297 site. The IgG1-Fc Asn297 *N*-glycan site is partially masked from the *N*-glycan glycosyltransferases and together with the glycosyltransferase substrate specificity and glycan-peptide backbone interactions, this results in a complex-type, biantennary, core-fucosylated *N*-glycan with partially incomplete galactosylation and α2-6 sialylation (1–5). The IgG1-Fc core fucose interferes with binding to FcγRIII and IgG1 lacking this core fucose, hereafter called afucosylated IgG1, has an increased affinity up to 40 times to FcγRIII (6–8). Interestingly, afucosylated IgG1 is generally low abundant in circulating IgG, but high levels of antigen-specific afucosylated IgG1 have been observed in several conditions against membrane-embedded epitopes, such as alloimmune responses to blood cells, malaria and enveloped viruses including; HIV, Dengue, and SARS-CoV-2 (9–15). In addition to core fucosylation, IgG-Fc galactosylation further enhances the affinity to FcγRIII (8, 16, 17).

The FcγRIIIa receptor is an activating IgG receptor of medium-high affinity (K_D≈10-400 nM), mainly expressed on NK cells, macrophages, and monocytes (18–20). It has been shown that the binding strength of IgG1 and IgG3 to FcγRIIIa directly correlates with antibody-dependent cellular cytotoxicity (ADCC) and therapeutic outcome (21–25). There are two common allotypes: FcγRIIIa-158V and -158F. FcγRIIIa-158V has a 5-fold increased affinity to IgG1 in comparison to the 158F allotype (8), the latter being the dominant allele in humans (26–28). This glycoprotein has five *N*-glycan sites (Asn38, Asn45, Asn74, Asn162, and Asn169) of which mainly Asn162 influences IgG1 binding (29, 30). Site-specific *N*-glycan analysis of FcγRIIIa from different sources shows extensive compositional heterogeneity ranging from oligomannose structures to complex sialylated tetra-antennary glycans with LacNAc extensions. These site-specific differences in *N*-glycan processing depend on cell type and individual (31–36). Similar to the unique restricted *N*-glycan processing seen for IgG-Fc Asn297, the Asn162 and Asn45 in FcγRIIIa also appear to exhibit restricted *N*-glycans processing. Furthermore, FcγRIIIa expressed on NK cells shows the highest level of oligomanosylated Asn162 and Asn45, followed by FcγRIIIa on monocytes and finally recombinantly expressed FcγRIIIa (37). Recombinantly expressed FcγRIIIa obtains almost exclusively complex-type *N*-glycans that correlate with the repertoire of glycosyltransferases expressed in these respective cell lines (37).

While the influence of glycosylation of IgG is well studied, few studies have addressed the influence of FcγRIIIa *N*-glycans on IgG binding and subsequent immune cell activation. Several limitations complicate FcγRIIIa glycan studies, such as the number of *N*-glycan sites with their inherent heterogeneity, the scarcity of endogenous FcγRIIIa material, and the fact that recombinantly expressed FcγRIIIa in HEK293 (33, 38), CHO (33, 39), NS0 (40), and BHK (41) appears to have *N*-glycan structures dissimilar to those found on endogenously expressed FcγRIIIa (32, 37). However, recent studies of IgG : FcγRIIIa interactions revealed that FcγRIIIa with an oligomannose structure at Asn162 has increased binding capacity to IgG1 (35, 42, 43). Furthermore, FcγRIIIa with hybrid-type and truncated *N*-glycan, which existed of only the innermost GlcNAc at Asn162, also has an increased IgG1 affinity, whereas sialic acid (Sia) had a negative influence on IgG1 binding and was shown to induce increased dissociation (32, 38, 43, 44). Furthermore, several limitations, such as the experimental surface plasmon resonance (SPR) setup, antibody and FcγR allotype and glycosylation heterogeneity, make comparing affinity measurements across studies challenging. Due to the recent wide availability of gene editing, the heterogeneity of these *N*-glycans can now be limited and defined glycan structures of interest can be expressed on IgG and Fc Receptors, among many other glycoproteins (45–47).

Here, we aimed to systematically study the impact of *N*-glycosylation features on both IgG1 and FcγRIIIa in their interaction. For this, we produced a library of defined glycoengineered IgG1 and FcγRIIIa (158F and 158V allotypes) glycoproteins and tested these in binding by SPR. The results show that the interaction between afucosylated IgG and FcγRIIIa with oligomannose *N*-glycans produces the highest achievable affinity in our setup. Our study supports previous findings (32, 38, 43, 44) and demonstrates that *N*-glycosylation of not only IgG but also FcγRIIIa affects binding interactions. Furthermore, FcγR glycosylation studies in both health and disease should be performed to discover how the immune system regulates this glycosylation interplay to drive pro- or anti-inflammatory responses.

Results

Glycoengineering and production of recombinant IgG1 glycoforms

A panel of glycoengineered IgG1 (mAb SO57) (48, 49) with different *N*-glycoforms using stably glycoengineered CHO cells was previously generated (45). In brief, we first established a CHO wildtype clone stably expressing IgG1 (IgG1-CHO^{WT}) and used IgG1-CHO^{WT} to generate a library of *N*-glycoengineered clones by knockout (KO) using CRISPR/Cas9 and stable knock-in (KI) of key glycosyltransferases in the *N*-glycosylation pathway using Zinc finger nucleases and the ObLiGaRe Strategy (50) (Figure 1, Supplementary Table S1). To obtain afucosylated IgG1, a *Fut8* and *B4galt1* KO was created, resulting in the IgG1-G0 clone. An *Mgat1* KO was created (IgG1-Oligomannose) to obtain oligomannosylated IgG1 and KO of *Mgat2* and *Man2a1/2* resulted in hybrid (IgG1-Hybrid) and monoantennary (IgG1-Monoantennae) IgG1-expressing clone, respectively. To increase galactosylation compared to IgG1-CHO^{WT}, the IgG1-G2F clone was created by KI of *B4GALT1*. To further increase linkage-specific sialylated IgG1, KI of

ST3GAL4 or *ST6GAL1* was introduced on top of the *B4GALT1* KI clone, resulting in α2-3 linked (IgG1-G2FS(2-3)) or α2-6 linked Sia (IgG1-G2FS(2-6)), respectively, as previously described (45) (Figure 1, Supplementary Table S1).

The isolated glycoengineered IgG1 glycoforms were validated by SDS-PAGE for correct protein expression and purity, and to confirm concentration determination. All IgG1 glycoforms resulted in a heavy chain (HC) and low chain (LC) band of 50 and 25 kDa, respectively (Figure 2A). Further validation of glycosylation patterns was done by MALDI-TOF-MS employing linkage-specific sialic acid derivatization to differentiate between α2-3 and α2-6 linked Sia (Supplementary Figure S1) (52, 53). IgG1-CHO^{WT} showed a heterogeneous profile including dominant G0F glycans with small amounts of G1F (Supplementary Figure S1A) (45). Homogenous afucosylated, agalactosylated IgG1 was produced by IgG1-G0 (Supplementary Figure S1B) and homogenous Man5 IgG1 by IgG1-Oligomannose (Supplementary Figure S1C). The dominant glycoform for IgG1-Monoantennae was the galactosylated monoantennary IgG1 with small amounts being agalactosylated and minor amounts being galactosylated and α2-3 sialylated (Supplementary Figure S1D). The same galactosylation and sialylation trend was seen for IgG1-Hybrid (Supplementary Figure S1E). IgG1-G2F produced homogenous G2F, which is a significant galactosylation increase in comparison to IgG1-CHO^{WT} (Supplementary Figure S1F). For both sialyltransferase KI clones (IgG1-G2FS(2-3) and IgG1-G2FS (2-6)), the dominant glycoforms remained G2F, with a minority of species being sialylated (Supplementary Figures S1G, H). Sialylation in IgG1-G2FS(2-6) was lower compared to our previous study (45), and this may be due to differences in cell density and viability during cell culturing. However, sialylation was increased compared to IgG1-CHO^{WT} and IgG1-G2F (Supplementary Figures S1A, F–H).

Glycoengineering and production of recombinant FcγRIIIa-158F/V glycoforms

FcγRIIIa has five consensus *N*-glycosites occupied by heterogeneous *N*-glycans. These display site-specific *N*-glycan structures and variation hereof in different cell types and individuals (54). We generated a library of glycoengineered HEK293 cells with different *N*-glycosylation capacities by combinatorial KO and KI of glycosyltransferase genes as previously reported (47). For afucosylated FcγRIIIa, *FUT8* was knocked out. To obtain oligomannose, monoantennae, and hybrid FcγRIIIa-158F/V we used KO of *MGAT1*, *MGAT2/3*, or *MAN2A1/2*, respectively. KO of *B4GALN3/4* and *MGAT3/4A/4B/5* in combination with *ST3GAL3/4/6* or *ST6GAL1*, resulted in clones expressing complex-type biantennary α2-3 or α2-6 linked sialylated *N*-glycans without LacNAc repeats, respectively. Recombinant FcγRIIIa-158F and 158V were transiently expressed in CHO^{WT} and HEK293^{WT}, resulting in FcγRIIIa-CHO^{WT} and FcγRIIIa- HEK^{WT}, respectively (Figure 1, Supplementary Figure S2, Supplementary Table S1). Transfection of the above-mentioned glycoengineered HEK cells resulted in FcγRIIIa-Afucosylated, FcγRIIIa-Hybrid, FcγRIIIa-Oligomannose, FcγRIIIa-Monoantennae, FcγRIIIa-G2FS(2-3), and FcγRIIIa-G2FS(2-6) (Figure 1, Supplementary Figure S2, Supplementary Table S1).

The produced FcγRIIIa-158F/V were validated by SDS-PAGE and mass spectrometry to confirm *N*-glycan structures and evaluate glycan heterogeneity (Figures 2, 3, Supplementary Figures S3, 4). Glycoengineered FcγRIIIa resulted in a heterogeneous glycoprofile migrating as a broad band with an apparent molecular weight ranging from 40 to 50 kDa depending on clone, highlighting the *N*-glycan heterogeneity and mass contribution of the five *N*-glycans per FcγRIIIa molecule.

For glycoprofiling, PNGaseF-released esterified *N*-glycans of FcγRIIIa-158F/V were analyzed by MALDI-TOF-MS (Supplementary Figures S3, 4) (52). Since the Asn162 glycosite of FcγRIIIa has shown to influence IgG1 binding (29), site-specific analysis of Asn162 by LC-MS/MS was performed. For this, FcγRIIIa was digested by chymotrypsin and Glu-C before subjection to LC-MS/MS and the top 90% most abundant glycan structures for the Asn162 glycosite are depicted (Figure 3). In general, the Asn162 *N*-glycan structures for both FcγRIIIa-158F/V confirm gene editing signatures and generally followed MALDI-TOF-MS data. However, underprocessed glycans were seen for Asn162 in comparison to the total *N*-glycan profiling, where more complex *N*-glycans were found for FcγRIIIa-HEK^{WT}, FcγRIIIa-CHO^{WT}, and FcγRIIIa-afucosylated (33, 35). The Asn162 of FcγRIIIa-CHO^{WT} was predominantly of the G2S type with overall high levels of galactosylation (G2S>G2S2>G2) and variable sialylation levels (G2S>G2S2) (Figure 3, Supplementary Figures S3A, 4A). The FcγRIIIa-HEK^{WT} Asn162 site had mainly biantennary *N*-glycans with GalNAc extensions and no sialylation. These were also the major glycan species found for the total FcγRIIIa-HEK^{WT} glycoprofiling data (Figure 3B). *N*-glycan profiling of FcγRIIIa-HEK^{WT} also showed minor sialylated, elongated, and branched glycospecies (Supplementary Figures S3A, 4A). Most complex *N*-glycans were seen for FcγRIIIa-afucosylated, supporting the higher molecular weight as seen on SDS-PAGE (Figures 2B, 3C, Supplementary Figures S3B, 4B). Confirmed by total protein glycoprofiling and Asn162 site-specific glycoanalysis, homogeneous Man5 was found for FcγRIIIa-Oligomannose (Figure 3D, Supplementary Figures S3C, 4C). The major Asn162 glycan structure for FcγRIIIa-Monoantennae is a sialylated monoantennary species (Figure 3E, Supplementary Figures S3D, 4D). However, a

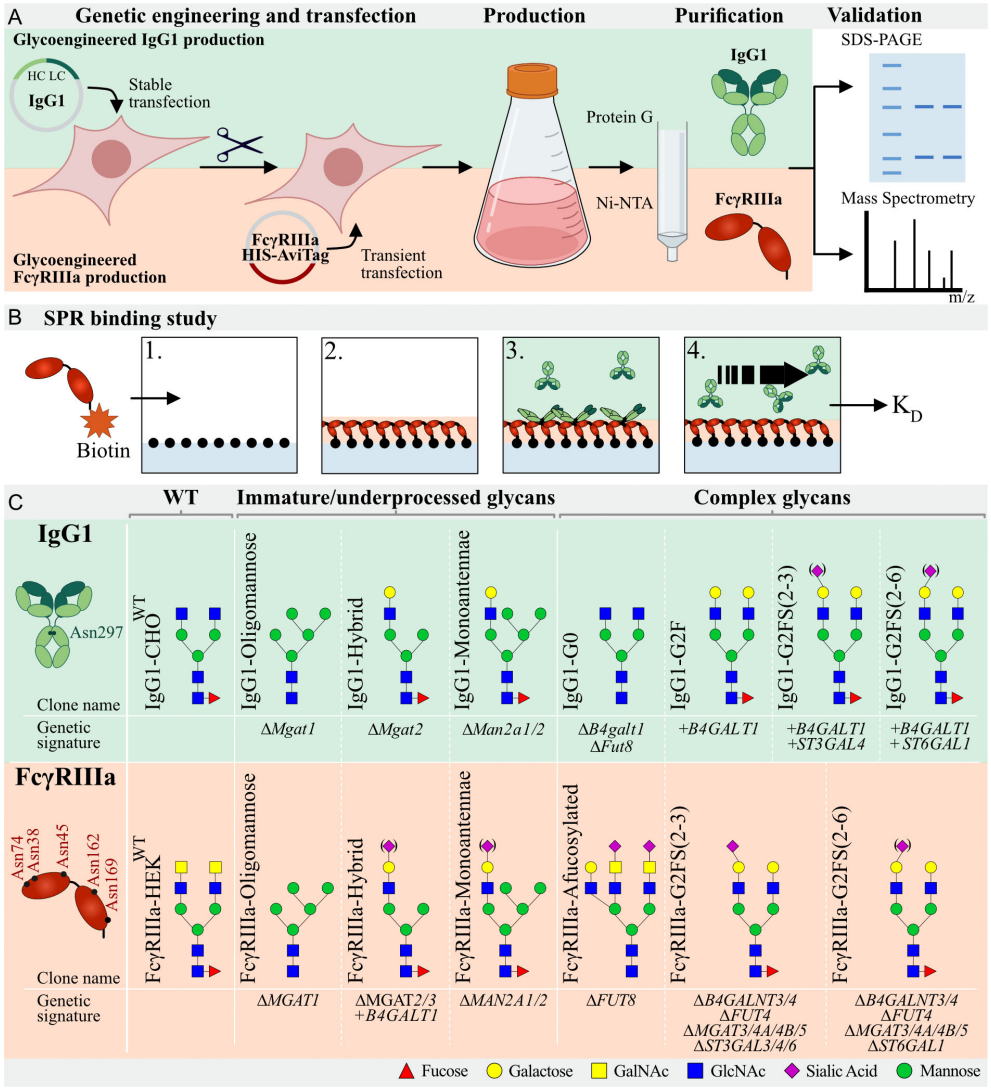

FIGURE 1
Graphic depiction of glycoengineered IgG1 and FcγRIIIa production, validation, and binding studies. **(A)** Top: Production of CHO^{WT} stably expressing IgG1. In this parental clone, KO and KI of glycosyltransferases resulted in a library of genetically glycoengineered CHO clones stably producing IgG1. Expressed IgG1 was purified by protein G and validated by SDS-PAGE and Mass Spectrometry (MS). Bottom, HEK293 cells were genetically engineered to display distinct *N*-glycan structures and this library of genetically engineered HEK clones were transiently transfected with soluble HIS- and AviTag-tagged FcγRIIIa-158F/V. Produced FcγRIIIa was purified by Ni-NTA columns and subjected to SDS-PAGE and MS for validation. **(B)** Schematic depiction of the IBIS MX96 SPR setup. 1) All glycoengineered FcγRIIIa glycoforms were enzymatically biotinylated by BirA and spotted at four different concentrations on a streptavidin-coated chip. 2) Glycoengineered IgG1 was injected at eight different dilutions, 3) allowing for binding affinity measurements of each antibody to all glycoengineered FcγRIIIa's simultaneously. 4) Regeneration after every sample was carried out after which the next IgG1 glycoform was injected. **(C)** Glycoengineered IgG1 and FcγRIIIa-158F/V expressing cell lines with clone name, gene editing background and expected *N*-glycan signature based on gene editing signature and literature. IgG1 has one *N*-glycan site (Asn297) per Fc domain and FcγRIIIa has 5 *N*-glycan sites (Asn38, Asn45, Asn74, Asn162, and Asn169). Designations for monosaccharides are according to the Consortium for Functional Glycomics (CFG) (51).

wider variety of other glycan structures were seen for both Asn162 and total FcγRIIIa glycoprofiling such as hybrid species and biantennary *N*-glycans and total *N*-glycoprofiling of FcγRIIIa-hybrid clone showed more complex N-glycans than expected. For both FcγRIIIa-G2FS (2-3) and FcγRIIIa-G2FS(2-6), biantennary *N*-glycans with variable sialylation levels were seen (Figures 3G, H, Supplementary Figures S3F, G, 4F, G). Furthermore, branching fucose was found in FcγRIIIa-G2FS(2-3) and -G2FS(2-6).

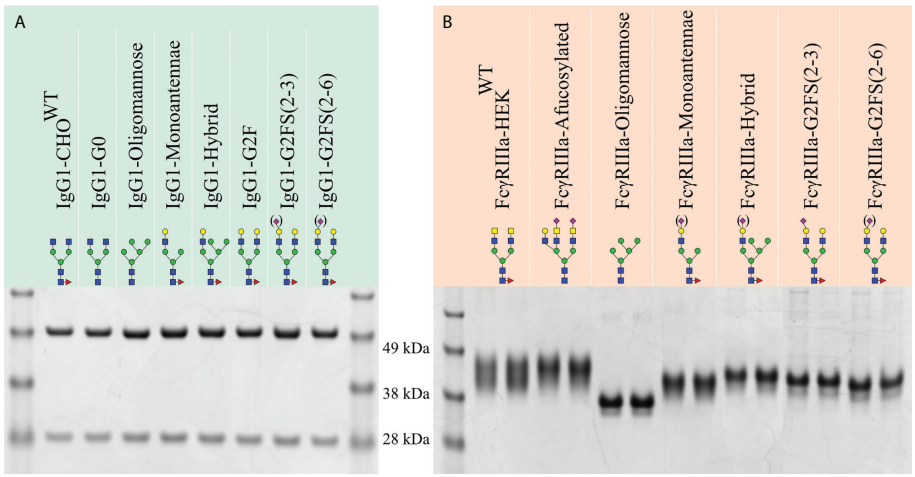

FIGURE 2
SDS-PAGE of purified recombinant IgG1 and FcγRIIIa-158F/V. Reducing SDS-PAGE of 1 µg purified **(A)** glycoengineered IgG1 produced in CHO cells with the heavy chain and light chain at ~50 and 30 kDa, respectively. **(B)** HEK293-expressed His- and AviTag-tagged FcγRIIIa-158F (left lane) and -158V (right lane) migrating as a broad band with a molecular weight ranging from 40 to 50 kDa. Designations for monosaccharides according to the CFG are indicated (51).

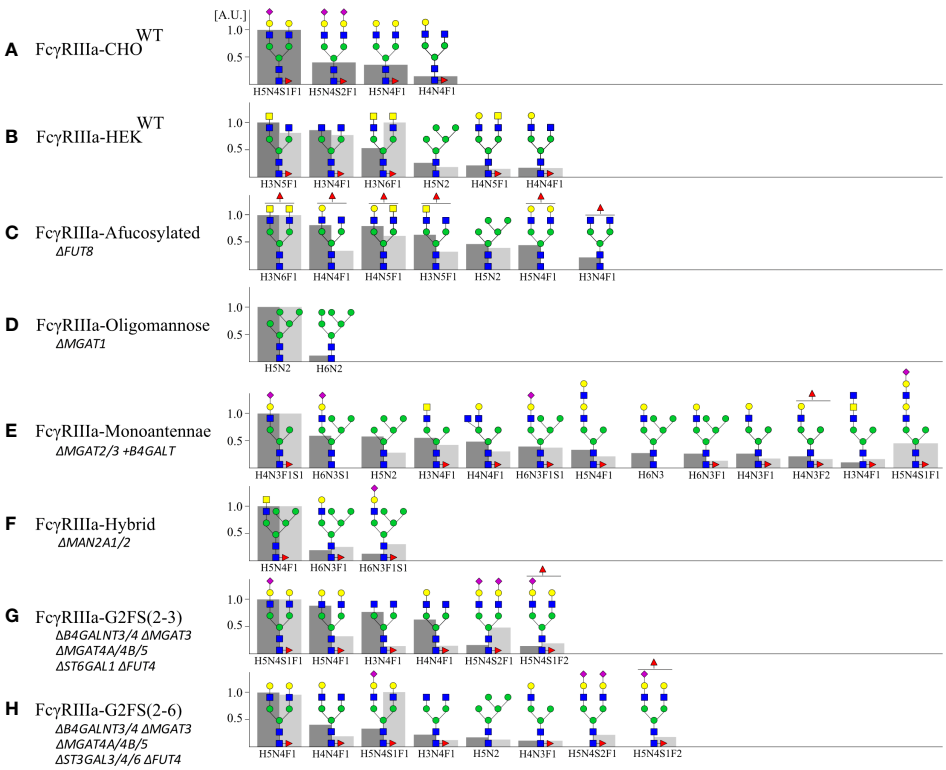

FIGURE 3
Site-specific *N*-glycan profiling of Asn162 FcγRIIIa-158F/V by LC-MS/MS. FcγRIIIa-158F and -158V expressed in **(A)** CHO and **(B–H)** HEK293 cells were digested by a combination of chymotrypsin and Glu-C and subjected to LC-MS/MS. Site-specific *N*-glycan profiling of Asn162 was carried out and the top 90% of the structures are represented relative to the most abundant structure (A.U. = 1) for FcγRIIIa-158F (dark grey, left) and -158V (light grey, right) with H: hexose, N: N-acetylhexosamine, F: fucose; S: Sialic acid. Proposed glycan structures are based on gene editing signatures and literature. Structures are depicted following the CFG notation (51).

N-glycan structures on both IgG1 and FcγRIIIa-158F/V influence their binding interaction

To study the role of *N*-glycoforms on the IgG1:FcγRIIIa interaction, we used the produced glycovariants for SPR analysis on the IBIS MX96 biosensor system, as described in Dekkers et al. (55). For this all FcγRIIIa-158F/V glycoforms were enzymatically biotinylated at the AviTag™ and immobilized on a sensor chip. Subsequently, all IgG1 variants were injected as analytes in a multi-cycle mode (Figure 1B). Humira, a recombinant human IgG1 monoclonal antibody with a G0F or G0NF glycan structure (56), and recombinant FcγRIIIa-158F/V purchased from SinoBiologicals, were used as controls (Supplementary Table S2). Binding was observed for all IgG1: FcγRIIIa combinations, however, the FcγRIIIa-158F binding to IgG1-Monoantennae and IgG1-Hybrid was weak and therefore K_D values could not be calculated from these interactions (Supplementary Figures S5, 2).

We could confirm that FcγRIIIa-158V exhibited on average a 3-6 fold increased affinity for IgG1 compared to FcγRIIIa-158F regardless of the IgG1 glycoform tested (Figure 4, Supplementary Table S2). The highest affinity for all IgG1 glycoforms was seen to FcγRIIIa-Oligomannose with a 2-3 fold increase compared to all other FcγRIIIa glycoforms (Figure 4, Supplementary Table S2). Surprisingly, FcγRIIIa-Monoantennae and FcγRIIIa-Hybrid, carrying immature *N*-glycan structures often found on Asn162 expressed by native immune cells (57), had a similar affinity to all IgG1 glycoforms when compared to FcγRIIIa-HEK^{WT} and FcγRIIIa-CHO^{WT}, with the exception of IgG1-hybrid (Figure 4, Supplementary Table S2). Sialylation of FcγRIIIa (FcγRIIIa-G2FS(2-3) and FcγRIIIa-G2FS(2-6)) influenced IgG1 binding to a certain degree, with FcγRIIIa-2FS (2-3) having approximately a 2-fold decrease in binding compared to FcγRIIIa-G2FS(2-6) and FcγRIIIa-HEK^{WT}. However, it needs to be taken into account that the sialylation levels for FcγRIIIa-G2FS(2-3) are much higher compared to G2FS(2-6), where G2F is the dominant glycoform on Asn162 (Supplementary Figures S3F, G). Surprisingly, FcγRIIIa-G2FS(2-3) has a lower affinity to most glycoengineered IgG1 compared to FcγRIIIa-CHO^{WT}, even though the Asn162 glycan pattern is similar.

As expected, the highest affinity of all FcγRIIIa receptors was observed to afucosylated IgG, both IgG1-G0 and the IgG1-Oligomannose (Figure 4, Supplementary Table S2) (29). Interestingly, the *N*-glycosylation state of the FcγRIIIa had minimal effect on the binding affinity when probed with afucosylated IgG, except for oligomannosylated FcγRIIIa where binding affinity is increased by a factor of two. All FcγRIIIa glycoforms bound equally to IgG1 capped by α2-3 or α2-6 Sia

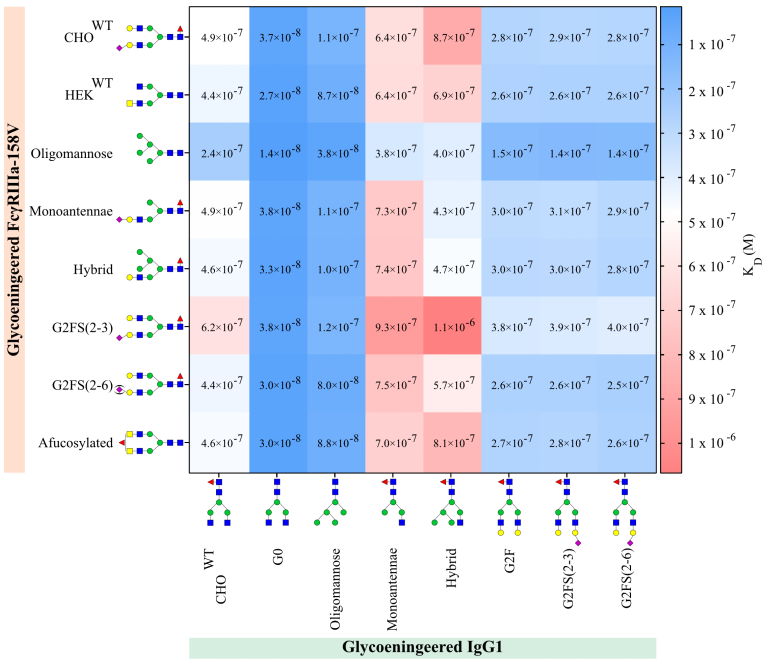

FIGURE 4
IgG1 and FcγRIIIa-158V binding. Surface plasmon resonance dissociation constant (K_D) was determined from SPR analysis after biotinylated glycoengineered FcγRIIIa-158V was spotted at 4 concentrations and bound to glycoengineered IgG1 at 8 times dilution series. Calculation of the dissociation constant was performed by equilibrium fitting to R_{max}= 500. Mean data is reported of three independent experiments for each IgG1:FcγRIIIa-158V pair.

(IgG1-G2FS(2-3) and IgG1-G2FS(2-6)), with minor differences that appear to be negligible (Figure 4, Supplementary Table S2). The highest K_D, and thus lowest affinity, was seen for IgG1-Hybrid and IgG1-Monoantennae to all FcγRIIIa. In contrast to IgG1-F0, for these suboptimal glycoengineered IgG1, the FcγRIIIa glycosylation influences binding (Figure 4, Supplementary Table S2). This combinatorial setup with glycoengineered IgG1 and FcγRIIIa-158F/V confirms that afucosylated IgG1 has the highest binding affinity to oligomannosylated FcγRIIIa-158V (FcγRIIIa-Oligomannose).

Discussion

Here, we systemically produced a library of defined *N*-glycoforms of FcγRIIIa (both 158F/V allotypes) and IgG1 to study *N*-glycosylation binding features and used combinations of these glycoforms with SPR to evaluate binding kinetics. Our study demonstrated that rather homogenous *N*-glycoforms of FcγRIIIa and IgG1 can be produced in genetically glycoengineered CHO and HEK293 mammalian cells as previously reported (45, 49). Importantly, the genetic engineering approach does not enable control of *N*-glycan structures at specific sites, but rather sets global restrictions on the repertoire of *N*-glycan structures on a given glycoprotein. Thus, the genetic engineering design will apply to all *N*-glycosites, except for those sites where *N*-glycan processing is naturally constrained by interaction with the protein backbone and glycosyltransferase substrate specificity, as for the Asn297 *N*-glycan of IgG1 (4). An IgG consists of two heavy chains, identical on the protein level, each having one *N*-glycosite, implying that one IgG molecule carries two glycan structures. The glycan composition of these two glycans might be different, referred to as an asymmetrically glycosylated antibody. Here, the obtained K_D measurements are an average of the IgG glycoforms population to a given population of FcγRIIIa glycoforms. However, as the antibody and receptor in this study are produced in the same cell with the same constrained glycoengineering background, we believe differences in glycan composition between these two glycans are minimal, and IgG1-Oligomannose, IgG1-G0 and IgG1-G2F are symmetrically glycosylated (45). While this conserved Fc *N*-glycan is unique by its restricted branching, galactosylation, and sialylation, many other *N*-glycoproteins are also known to have specific differentially processed *N*-glycosites, such as an oligomannose *N*-glycan on IgM or Man-6-phosphate tagging of lysosomal enzymes (46, 58–60). The Asn162 glycosite in FcγRIIIa and the adjacent 158F/V polymorphism are also interesting in this aspect, as this site is often occupied by oligomannose, monoantennae, and hybrid *N*-glycans in human leukocytes (31–34).

In our setup, a remarkable >300-fold difference in binding affinities was observed among the different IgG1 glycoforms and FcγRIIIa allotype and glycoforms tested. It is however important to note that these results are based on *in vitro* binding K_D values and may not fully translate into the *in vivo* properties of these interactions. *In vivo*, monovalent IgG competes with multivalent IgG-immunocomplexes or IgG-opsonized pathogens for FcR binding, of which only the latter results in FcγR-mediated cellular activation. Nevertheless, the reported relative binding affinities between FcγRIIIa and IgG1 are known to be reproducibly translated into relative differences in cellular effector functions as well as *in vivo* functional capacities (8, 24, 61). How these affinity changes translate into different activation potentials of NK cells or myeloid expressing cells, depends on many factors, such as epitope density of the target cell, antibody concentration, FcγR-polymorphisms of the patient/donor cells, and the antibody Fc-glycosylation, especially fucosylation, which can be highly variable in some immune response (11). These factors all impact avidity between the target and effector cell, which seems the principle component governing the FcγR-activation potential (24). Our results now suggest that FcγRIII-glycosylation itself can impact this as well, which has been reported to be differently glycosylated across cell types.

The FcγRIIIa-158V allotype has a higher binding affinity to IgG1 compared to the 158F allotype (62). This has recently been attributed to the formation of a less stable complex between the 158F allotype with IgG in comparison to the I58V allotype (63). This is also confirmed in our setup, where the FcγRIIIa-158V binding affinity is on average 4-6 times higher compared to FcγRIIIa-158F. Besides the different allelic variants, the FcγRIIIa *N*-glycosylation of both the 158F and V allotype also influences IgG1 binding (29, 30, 63). The Asn162 *N*-glycan site, and to a lesser extent Asn45, have shown to affect antibody-binding affinity (29, 30). For the remaining *N*-glycosites, specific functions remain unclear. Our findings showed that, even though all FcγRIIIa N-glycan forms are capable of binding IgG and subsequently activate the immune system, specific glycoforms are more capable of binding IgG. This is reflected by the 43- and 76-fold binding difference for the highest and lowest binding FcγRIIIa glycoforms for FcγRIIIa-158F and -158V, respectively (32). Interestingly, these stronger-binding oligomannose, hybrid, and monoantennae *N*-glycans, shown to have ~2.5-fold improved IgG1 binding compared to complex-type N-glycans, are often found on native FcγRIIIa expressed on human leukocytes (31–35, 37, 42, 43).

In this setup, the highest affinity to IgG1 was indeed seen for FcγRIIIa-Oligomannose, which was on average 2-3 fold better compared to all other FcγRIIIa glycoforms, in agreement with recent reports (35, 43). The FcγRIIIa-Oligomannose inherently also lacks the core fucose as the FUT8 α1-6 fucosyltransferase requires complex *N*-glycans as acceptor substrate (64). We could exclude that FcγRIIIa core fucose was solely responsible for the increased affinity to IgG1, since FcγRIIIa-Afucosylated did not have an increased binding affinity to IgG1 when compared to the fucosylated

complex-type FcγRIIIa. Interestingly, the *N*-glycoforms of FcγRIIIa-Afucosylated tended to have higher levels of complex structures with a higher degree of branching, which may affect the interpretation. Roberts et al. noted a ~2-fold increase for hybrid-type *N*-glycosylated FcγRIIIa (32). In contrast to the literature, in our setup, mono-antennae and hybrid *N*-glycosylated FcγRIIIa showed affinities to IgG1 similar to FcγRIIIa with complex *N*-glycan. The sialylation state of *N*-glycans on FcγRIIIa appeared to influence the IgG1 binding affinity with a decrease in binding affinity of α2-3 Sia capping compared to α2-6 Sia. Unfortunately, it was not possible to substantially increase sialylation, which is a well-known issue for IgG (45, 65–67). Furthermore, due to the differences in sialylation levels between the 158F and V allotype at the Asn162 glycosite, the comparison to asialylated FcγRIIIa is challenging and this conclusion should be treated with caution.

Our studies demonstrated that the combination of oligomannosylated FcγRIIIa had the highest binding affinity to afucosylated IgG1, which is in agreement with previous reports (6–8, 35, 43). In general, the FcγRIIIa *N*-glycosylation state had minimal influence on the binding affinity when probed with afucosylated IgG1. However, when FcγRIIIa was probed with IgG1 fucosylated glycoforms, the FcγRIIIa *N*-glycosylation state influenced the IgG1 binding affinity. Furthermore, IgG1 sialylation had a minimal effect on FcγRIIIa affinity, and differences in α2-3- and α2-6-linked Sia were negligible, as shown before (8, 68, 69). This, however, is in contrast with findings from other groups, which could be due to differences in sialylation levels (8, 70, 71). These findings likely translate into differential sensitivity of effector cells with its inherent FcγRIIIa glycosylation state to the IgG1 fucosylation state. A higher discriminatory power for the fucosylation state of IgG1 by oligomannosylated FcγRIIIa (~17-fold) was found, a glycan structure typically found on NK cells. For the hybrid and mono-antennary FcγRIIIa glycoforms, typically found on monocytes, this discrimination between fucosylation states of IgG1 was slightly less, or a ~13-fold increased preference for afucosylated IgG1. It remains unknown to which extent differential FcγRIII glycoprocessing on different cell types affects their activation state and future studies should address the biosynthetic and mechanistic basis for differential site-specific *N*-glycosylation of FcγRIIIa.

In summary, our study demonstrates that the *N*-glycosylation status of both FcγRIIIa and IgG1 influences binding affinity, highlighting the need to consider the *N*-glycosylation state of both IgG and Fc receptors in binding kinetics and effector function studies. The two most significant *N*-glycosylation features observed were the IgG1 core fucosylation state and FcγRIIIa oligomannose to complex *N*-glycosylation transition. We predict that the bilateral glycan interplay enables the immune system to fine-tune the FcγRIIIa and IgG interactions and modulate immune responses.

Methods

Cell culture

HEK293 were grown in suspension in serum-free F17 culture media (Invitrogen) supplemented with 0.1% Kolliphor P188 (SIGMA) and 4 mM GlutaMax as previously described (47). CHOZN GS-/- cells (Sigma) were maintained as suspension cultures in serum-free media (EX-CELL CHO CD Fusion). Cultures were grown at 37°C and 5% CO_2. HEK293 and CHO cultures were under constant agitation (120 rpm).

CRISPR/Cas9 targeted KO in HEK293 cells

KO was performed using a validated gRNA library for all human glycosyltransferases (GlycoCRISPR) (72), as previously described (73). In brief, HEK293 cells were seeded in 6-well plates (NUNC), transfected with 1 µg of gRNA and 1 µg of GFP-tagged Cas9-PBKS using Lipofectamine 3000 (Invitrogen) according to manufacturer's instructions. Cells were harvested after 24 hours, and bulk sorted for GFP expression by FACS (SONY SH800). After culturing, the sorted cell pool was further single-sorted into 96 well plates and screened by Indel Detection by Amplicon Analysis (IDAA) (74), and indels of selected clones were confirmed by Sanger sequencing.

CRISPR/Cas9-targeted KO in CHO cells

One day prior to transfection, cells were seeded in T25 flasks (NUNC). Electroporation was conducted with 2×10^6 cells with 1 µg of both endotoxin-free plasmid DNA of Cas9-GFP and gRNA in the U6GRNA plasmid (Addgene Plasmid #68370) using Amaxa Kit V and program U-24 with Amaxa Nucleofector 2B (Lonza). Electroporated cells were moved to a 6-well plate with 3 ml growth media. Forty-eight hours after nucleofection, the 10–15% highest GFP-labeled pool of cells was enriched by FACS, and after one week of culturing, cells were single-cell sorted by FACS (SONY SH800) into 96-well plates. KO clones were identified by IDAA, as mentioned above, as well as immunocytology with appropriate lectins or monoclonal antibodies, whenever possible. Selected clones were further verified by Sanger sequencing.

ZFN/CRISPR-mediated KI in CHO cells

Site-specific CHO Safe-Harbor locus KI was based on ObLiGaRe strategy (50) and performed with 2 µg of each ZFN (Merck/Sigma-Aldrich) tagged with GFP/Crimson (74), and 5 µg donor plasmid with full coding human genes, as described before (46).

IgG1 expression and purification

The anti-rabies human IgG1 SO57 (48) was used to establish stable expressing CHO clones as described by Schulz et al. (45). For IgG production, clones were seeded at 0.5 x 10^6 cells/ml without L-glutamine and cultured for three days. IgG was purified by HiTrap™ protein HP (CE Healthcare) as previously described (45). Protein purity and concentration were evaluated by SDS-PAGE and Coomassie staining.

Transient expression of soluble FcγRIIIa in HEK cells and protein purification

HEK293-6E cells were seeded at a cell density of 0.5 × 10^6 cells/ml and transfected with FcγRIIIa-158F/V with 10X his-tag and AviTag™ the next day with 1:3 µg DNA : PEI per 1 × 10^6 cells. Secreted protein was harvested after 72 hours and purified from culture medium by nickel affinity chromatography. For this, the culture medium was centrifuged, filtered (0.45 µm), mixed 3:1 (v/v) in 4X binding buffer (100 mM sodium phosphate, pH 7.4, 2 M NaCl) and applied to self-packed nickel-nitrilotriacetic acid (Ni-NTA) affinity resin column (Qiagen), which was pre-equilibrated in washing buffer (25 mM sodium phosphate, pH 7.4, 500 mM NaCl, 20 mM imidazole). After washing, bound protein was eluted with 250 mM imidazole in washing buffer. Purity and quantification were evaluated by SDS-PAGE and Coomassie staining. Purified protein was buffer-exchanged to approximately 1 mg/ml in 50mM AmBic buffer with 2 ml Zeba Spin Desalting Column 7K MWCO (ThermoFisher).

Stable expression of soluble FcγRIIIa in CHO cells and protein purification

Both FcγRIIIa-158F/V with 10X his-tag and AviTag™ constructs were both subcloned into a modified pCGS3 vector (Merck/Sigma-Aldrich) for glutamine selection in CHOZN GS −/− cells (Sigma). CHO cells were seeded at 0.5 X 10^6 cells/ml in T25 flasks (NUNC) one day prior to transfection. Two million cells were electroporated with 5 µg plasmids using Amaxa kit V and program U24 with Amaxa Nucleofector 2B (Lonza) and plated in 6-wells with 3 ml growth media. Three days after transfection, cells were plated in 96-wells at 1000 cells/well in 200 µl Minipool Plating Medium containing 80% EX-CELL® CHO Cloning Medium and EX-CELL CHO CD Fusion serum-free media without glutamine (Sigmaaldrich). High-expressing clones were selected by testing the medium using anti-HIS antibodies, and selected clones were scaled up in serum-free media without L-glutamine TPP TubeSpin® shaking Bioreactors (180 rpm, 37 °C, and 5% CO_2) for protein production. FcγRIIIa was purified as described above.

N-glycan profiling by MALDI-TOF

N-glycan protein profiling employing linkage-specific sialic acid esterification was obtained as described by Reiding et al. (52). In brief, 10 µg IgG1 and FcγRIIIa were denatured by incubating the samples 10 min at 60°C in 2% SDS. *N*-glycans were released by adding a release mixture containing 2% NP-40 and 0.5 mU PNGaseF at 37°C over night. Released *N*-glycans were esterified to obtain sialic acid linkage specificity. In brief, esterification reagent containing 0.5 M EDC and 0.5 M HOBt in ethanol were added to 1 µl glycan mixture and incubated for one hour at 37°C. After incubation, 25% NH_4OH and subsequently 100% ACN was added (52). Glycan enrichment was performed by cotton hydophilic interaction liquid chromatography (HILIC) (75). Briefly, pipet tips were packed with cotton thread which was conditioned by 85% ACN. The sample was loaded by pipetting 20 times into the reaction mixture. Tips were washed in 85% ACN 1% TFA, followed by 85% ACN and eluted in 10 µl MQ. For MALDI-TOF-MS analysis, 1µl HILIC purified glycan sample was spotted on an MTP AnchorChip™ 384 BC mixed on plate with 1µl sDHB (5mg/ml in 50% ACN) and left to air dry. The sample was recrystallized using 0.2µl ethanol. Measurement was performed on the Bruker Autoflex (Bruker Daltonik GmbH, Bremen, Germany) using the Bruker Flex Control 3.4 software. For each spectrum, 10 000 laser shots were accumulated at a laser frequency of 100 Hz. Spectra were recorded in the positive reflector mode (900-4500 Da) and the raw spectra were processed by the Flexanalysis 5.1.

Sample preparation for site-specific *N*-glycopeptide analysis

The purified protein was dissolved in 50mM ammonium bicarbonate buffer, reduced in 10 mM dithiothreitol (DTT), alkylated with 20 mM iodoacetamide (IAA), reduced again with 10 mM DTT, and digested with 1:20 chymotrypsin:protein followed by 1:20 GluC:protein (Roche). The proteolytic digest was desalted by in-house produced modified StageTip columns containing 3 layers of C18 membrane (3M Empore disks, Sigma Aldrich) (76). Samples were eluted with 50% methanol in 0.1%

formic acid (FA), dried down, and re-solubilized in 0.1% FA for LC-MS/MS analysis.

Site-specific FcγRIIIa *N*-glycopeptide analysis by LC-MS/MS

LC-MS/MS analysis was performed on EASY-nLC 1200 UHPLC (Thermo Scientific) interfaced *via* nanoSpray Flex ion source to an Orbitrap Fusion Lumos MS (Thermo Scientific). Briefly, the nLC was operated in a single analytical column set up using PicoFrit Emitters (New Objectives, 75 µm inner diameter) packed in-house with Reprosil-Pure-AQ C18 phase (Dr. Maisch, 1.9-µm particle size, 19-21 cm column length). Each sample was injected onto the column and eluted in gradients from 3 to 32% B in 75 min, and from 32% to 100% B in 10 min, and 100% B for 10 min at 200 nL/min (Solvent A, 100% H_2O; Solvent B, 80% acetonitrile; both containing 0.1% (v/v) formic acid). A precursor MS1 scan (m/z 350–2 000) of intact peptides was acquired in the Orbitrap at the nominal resolution setting of 120 000, followed by Orbitrap HCD-MS2 and at the nominal resolution setting of 60 000 of the five most abundant multiply charged precursors in the MS1 spectrum; a minimum MS1 signal threshold of 50 000 was used for triggering data-dependent fragmentation events. Targeted MS/MS analysis was performed by setting up a targeted MS^n (tMS^n) Scan Properties pane. A target list was composed of the top 30 most abundant glycans or glycopeptides from the proposed compositional list. The mass spectrometry proteomics data have been deposited to the ProteomeXchange Consortium *via* the PRIDE partner repository with the dataset identifier PXD035846.

Data analysis

Glycan and glycopeptide compositional analysis was performed from *m/z* features extracted from LC-MS data using in-house written SysBioWare software, as previously described (46, 77). Briefly, For *m/z* feature recognition from full MS scans LFQ Profiler Node of the Proteome discoverer 2.2 (Thermo Scientific) was used. The list of precursor ions (m/z, charge, peak area) was imported as ASCII data into SysBioWare and compositional assignment within 3 ppm mass tolerance was performed. The main building blocks used for the compositional analysis were: NeuAc, Hex, HexNAc, dHex and the theoretical mass increment of the most prominent peptide corresponding to each potential glycosites. The most prominent peptide sequence related to the *N*-glycosite of interest was determined experimentally by comparing the yield of deamidated peptides before and after PNGase F treatment. One or two phosphate groups were added as building blocks for assignment. To generate the potential glycopeptide list, all the glycoforms with an abundance higher than 10% of the most abundant glycoform were used for glycan feature analysis.

Surface plasmon resonance

Prior to SPR measurements, glycoengineered FcγRIIIa was site-specifically biotinylated on the BirA tag using BirA enzyme as described by Rodenko et al. (78). For biotinylation of 1 µM FcγRIIIa protein, 3.3 nM BirA ligase was used. After biotinylation overnight at 25°C, the biotinylated FcγRIIIa mixture was buffer-exchanged and subsequently concentrated in PBS pH 7.4 using Amicon Ultra centrifugal filter units (MWCO 3 kDa) (Merck, Millipore).

The biotinylated, recombinant, human FcγRIIIa-158F and 158V from SinoBiological (10389-H27H-B and 10389-H27H1-B, respectively) were used as an control for SPR. SPR measurements were performed on an IBIS MX96 (IBIS technologies) device as described previously by Dekkers *et al.* (8). All biotinylated FcγRIIIa were spotted using a Continuous Flow Microspotter (Wasatch Microfluidics) onto a SensEye G-streptavidin sensor (Senss, 1–08–04–008) allowing for binding affinity measurements of each glycoengineered antibody, and Humira®, to all glycoengineered FcγRIIIa simultaneously on the IBIS MX96.

The biotinylated FcγRIIIa were spotted in 4 concentrations with a 3-fold dilution ranging from 0.3 to 100nM, depending on the FcγRIIIa in PBS supplemented with 0.075% Tween-80 (VWR, M126–100ml), pH 7.4. Glycoengineered IgG1 was then injected over the IBIS at 8 times dilution series starting at 15.6 nM until 2000 nM in PBS + 0.075% Tween-80. Regeneration after every sample was carried out with 10 nM Gly-HCl, pH 2.4. Calculation of the dissociation constant (K_D) was performed by equilibrium fitting to R_{max}= 500. Analysis and calculation of all binding data were carried out with Scrubber software version 2 (Biologic Software) and Excel. Three independent experiments for each receptor/Fc pair were carried out on at least two different days and representative data are reported.

Data availability statement

The data presented in the study are deposited in the ProteomeXchange Consortium via the PRIDE partner repository, accession number PXD035846.

Author contributions

JVC, HC, and ZY conceived and designed the study. JVC, AB, NdH, MS, LH, ZY, SV, RM, DG and WvE contributed with experimental data and interpretation. JVC, HC, ZY, and GV

wrote the manuscript. All authors edited and approved the final version.

Funding

This work was supported by the Lundbeck Foundation, The Novo Nordisk Foundation, European Commission (GlycoImaging H2020-MSCA-ITN-721297, BioCapture H2020-MSCA-ITN-722171), the Danish National Research Foundation (DNRF107), the National Institutes of Health (AI114730 and R01AI41513, R01AI106987, U01OD024857), Kuang Hua Educational Foundation, The Carlsberg Foundation CF20-0412 and the Landsteiner foundation for Blood Transfusion Research (LSBR) grants 1721 and 1908, and ZonMW COVID-19 grants 1043001 201 0021. Noortje de Haan has received funding from the European Research Council (ERC) under the European Union's Horizon 2020 research and innovation programme (GlycoSkin H2020-ERC; 772735).

Conflict of interest

The University of Copenhagen has filed a patent application for the cell-based display platform. GlycoDisplay Aps, Copenhagen, Denmark, has obtained a license in the field of the patent application. Authors YN, ZY, and HC are co-founders of GlycoDisplay Aps and hold ownerships in the company.

The remaining authors declare that the research was conducted in the absence of any commercial or financial relationships that could be construed as a potential conflict of interest.

Publisher's note

Supplementary material

The Supplementary Material for this article can be found online at: https://www.frontiersin.org/articles/10.3389/fimmu.2022.987151/full#supplementary-material

References

1. Baković M, Selman H, Hoffmann H, Rudan I, Campbell H, Deelder A, et al. High-throughput IgG fc n-glycosylation profiling by mass spectrometry of glycopeptides. *J Proteome Res* (2013) 12:821–31. doi: 10.1021/PR300887Z

2. Stadlmann J, Pabst M, Kolarich D, Kunert R, Altmann F. Analysis of immunoglobulin glycosylation by LC-ESI-MS of glycopeptides and oligosaccharides. *Proteomics* (2008) 8:2858–71. doi: 10.1002/pmic.200700968

3. Barb AW, Brady EK, Prestegard JH. Branch specific sialylation of IgG-fc glycans by ST6Gal-I. *Biochemistry* (2009) 48:9705. doi: 10.1021/BI901430H

4. Guddat LW, Herron JN, Edmundson AB. Three-dimensional structure of a human immunoglobulin with a hinge deletion. *Proc Natl Acad Sci U.S.A.* (1993) 90:4271. doi: 10.1073/PNAS.90.9.4271

5. Barb AW, Prestegard JH. NMR analysis demonstrates immunoglobulin G n-glycans are accessible and dynamic. *Nat Chem Biol* (2011) 7:147–53. doi: 10.1038/NCHEMBIO.511

6. Shields RL, Lai J, Keck R, O'Connell LY, Hong K, Gloria Meng Y, et al. Lack of fucose on human IgG1 n-linked oligosaccharide improves binding to human FcγRIII and antibody-dependent cellular toxicity. *J Biol Chem* (2002) 277:26733–40. doi: 10.1074/jbc.M202069200

7. Shinkawa T, Nakamura K, Yamane N, Shoji-Hosaka E, Kanda Y, Sakurada M, et al. The absence of fucose but not the presence of galactose or bisecting n-acetylglucosamine of human IgG1 complex-type oligosaccharides shows the critical role of enhancing antibody-dependent cellular cytotoxicity. *J Biol Chem* (2003) 278:3466–73. doi: 10.1074/jbc.M210665200

8. Dekkers G, Treffers L, Plomp R, Bentlage AEH, de Boer M, Koeleman CAM, et al. Decoding the human immunoglobulin G-glycan repertoire reveals a spectrum of fc-receptor- and complement-mediated-effector activities. *Front Immunol* (2017) 8:877. doi: 10.3389/fimmu.2017.00877

9. Alter G, Ottenhoff THM, Joosten SA. Antibody glycosylation in inflammation, disease and vaccination. *Semin Immunol* (2018) 39:102–10. doi: 10.1016/j.smim.2018.05.003

10. Lofano G, Gorman MJ, Yousif AS, Yu W-H, Fox JM, Dugast A-S, et al. Antigen-specific antibody fc glycosylation enhances humoral immunity *via* the recruitment of complement. *Sci Immunol* (2018) 3:7796. doi: 10.1126/SCIIMMUNOL.AAT7796

11. Larsen MD, de Graaf EL, Sonneveld ME, Plomp HR, Nouta J, Hoepel W, et al. Afucosylated IgG characterizes enveloped viral responses and correlates with COVID-19 severity. *Sci (80-)* (2021) 371:eabc8378. doi: 10.1126/science.abc8378

12. Larsen MD, Lopez-Perez M, Dickson EK, Ampomah P, Tuikue Ndam N, Nouta J, et al. Afucosylated plasmodium falciparum-specific IgG is induced by infection but not by subunit vaccination. *Nat Commun* (2021) 12:5838. doi: 10.1101/2021.04.23.441082v1

13. Kapur R, Kustiawan I, Vestrheim A, Koeleman CAMM, Visser R, Einarsdottir HK, et al. A prominent lack of IgG1-fc fucosylation of platelet alloantibodies in pregnancy. *Blood* (2014) 123:471–80. doi: 10.1182/blood

14. Ackerman ME, Crispin M, Yu X, Baruah K, Boesch AW, Harvey DJ, et al. Natural variation in fc glycosylation of HIV-specific antibodies impacts antiviral activity. *J Clin Invest* (2013) 123:2183–92. doi: 10.1172/JCI65708

15. Bournazos AS, Thi H, Vo M, Duong V, Auerswald H, Bournazos S, et al. Antibody fucosylation predicts disease severity in secondary dengue infection. *Science* (2021) 372:1102–5. doi: 10.1126/science.abc7303

16. Lippold S, Nicolardi S, Wuhrer M, Falck D. Proteoform-resolved FcγRIIIa binding assay for fab glycosylated monoclonal antibodies achieved by affinity chromatography mass spectrometry of fc moieties. *Front Chem* (2019) 7:698. doi: 10.3389/fchem.2019.00698

17. Lippold S, Knaupp A, de Ru AH, Tjokrodirijo RTN, van Veelen PA, van Puijenbroek E, et al. Fc gamma receptor IIIb binding of individual antibody proteoforms resolved by affinity chromatography-mass spectrometry. *MAbs* (2021) 13:1982847. doi: 10.1080/19420862.2021.1982847

18. Vidarsson G, Dekkers G, Rispens T. IgG subclasses and allotypes: From structure to effector functions. *Front Immunol* (2014) 5:520. doi: 10.3389/fimmu.2014.00520

19. Golay J, Valgardsdottir R, Musaraj G, Giupponi D, Spinelli O, Introna M. Human neutrophils express low levels of FcγRIIIA, which plays a role in PMN activation. *Blood* (2019) 133:1395–405. doi: 10.1182/BLOOD-2018-07-864538

20. Nimmerjahn F, Gordan S, Lux A. FcγR dependent mechanisms of cytotoxic, agonistic, and neutralizing antibody activities. *Trends Immunol* (2015) 36:325–36. doi: 10.1016/J.IT.2015.04.005

21. Musolino A, Naldi N, Bortesi B, Pezzuolo D, Capelletti M, Missale G, et al. Immunoglobulin g fragment c receptor polymorphisms and clinical efficacy of trastuzumab-based therapy in patients with HER-2/neu-positive metastatic breast cancer. *J Clin Oncol* (2008) 26:1789–96. doi: 10.1200/JCO.2007.14.8957

22. Weng WK, Levy R. Two immunoglobulin G fragment c receptor polymorphisms independently predict response to rituximab in patients with follicular lymphoma. *J Clin Oncol* (2003) 21:3940–7. doi: 10.1200/JCO.2003.05.013

23. Yoon SR, Kim T-D, Choi I. Understanding of molecular mechanisms in natural killer cell therapy. *Exp Mol Med* (2015) 47:e141. doi: 10.1038/EMM.2014.114

24. Temming R, de Taeye S, de Graaf E, De Neef L, Dekkers G, Bruggeman CW, et al. Functional attributes of antibodies, effector cells, and target cells affecting NK cell–mediated antibody-dependent cellular cytotoxicity. *J Immunol* (2019) 203:3126–35. doi: 10.4049/jimmunol.1900985

25. Bruggeman CW, Dekkers G, Bentlage AEH, Treffers LW, Nagelkerke SQ, Lissenberg-Thunnissen S, et al. Enhanced effector functions due to antibody defucosylation depend on the effector cell fcγ receptor profile. *J Immunol* (2017) 199:204–11. doi: 10.4049/jimmunol.1700116

26. Hargreaves CE, Rose-Zerilli MJJ, Machado LR, Iriyama C, Hollox EJ, Cragg MS, et al. Fcγ receptors: Genetic variation, function, and disease. *Immunol Rev* (2015) 268:6–24. doi: 10.1111/imr.12341

27. Li X, Gibson AW, Kimberly RP. Human FcR polymorphism and disease. *Curr Top Microbiol Immunol* (2014) 382:275–302. doi: 10.1007/978-3-319-07911-0_13

28. Bruhns P, Iannascoli B, England P, Mancardi DA, Fernandez N, Jorieux S, et al. Specificity and affinity of human fcg receptors and their polymorphic variants for human IgG subclasses. *Blood* (2009) 113(16):3716–25. doi: 10.1182/blood-2008-09-179754

29. Ferrara C, Stuart F, Sondermann P, Brünker P, Umaña P. The carbohydrate at FcγRIIIa asn-162: An element required for high affinity binding to non-fucosylated IgG glycoforms. *J Biol Chem* (2006) 281:5032–6. doi: 10.1074/jbc.M510171200

30. Shibata-Koyama M, Iida S, Okazaki A, Mori K, Kitajima-Miyama K, Saitou S, et al. The n-linked oligosaccharide at FcγRIIIa asn-45: An inhibitory element for high FcγRIIIa binding affinity to IgG glycoforms lacking core fucosylation. *Glycobiology* (2009) 19:126–34. doi: 10.1093/glycob/cwn110

31. Patel KR, Roberts JT, Barb AW. Allotype-specific processing of the CD16a N45-glycan from primary human natural killer cells and monocytes. *Glycobiology* (2020) 30:427–32. doi: 10.1093/glycob/cwaa002

32. Roberts JT, Patel KR, Barb AW. Site-specific n-glycan analysis of antibody-binding fc γ receptors from primary human monocytes. *Mol Cell Proteomics* (2020) 19:362–74. doi: 10.1074/mcp.RA119.001733

33. Zeck A, Pohlentz G, Schlothauer T, Peter-Katalinić J, Regula JT. Cell type-specific and site directed n-glycosylation pattern of fc RIIIa. *J Proteome Res* (2011) 10:3031–9. doi: 10.1021/pr1012653

34. Patel KR, Nott JD, Barb AW. Primary human natural killer cells retain proinflammatory IgG1 at the cell surface and express CD16a glycoforms with donor-dependent variability. *Mol Cell Proteomics* (2019) 18:2178–90. doi: 10.1074/mcp.RA119.001607. mcp.RA119.001607.

35. Patel KR, Roberts JT, Subedi GP, Barb AW. Restricted processing of CD16a/Fc receptor IIIa n-glycans from primary human NK cells impacts structure and function. *J Biol Chem* (2018) 293:3477–89. doi: 10.1074/jbc.RA117.001207

36. Edberg JC, Barinsky M, Redecha PB, Salmon JE, Kimberly RP. Fc gamma RIII expressed on cultured monocytes is a n-glycosylated transmembrane protein distinct from fc gamma RIII expressed on natural killer cells. *J Immunol* (1990) 144:4729–34.

37. Patel KR, Rodriguez Benavente MC, Lorenz WW, Mace EM, Barb A. Fc γ receptor IIIa / CD16a processing correlates with the expression of glycan-related genes in human natural killer cells. *JBC* (2021) 296:100183. doi: 10.1074/jbc.RA120.015516

38. Hayes JM, Frostell A, Karlsson R, Müller S, Martín SM, Pauers M, et al. Identification of fc gamma receptor glycoforms that produce differential binding kinetics for rituximab. *Mol Cell Proteomics* (2017) 16:1770–88. doi: 10.1074/mcp.M117.066944

39. Washburn N, Meccariello R, Duffner J, Getchell K, Holte K, Prod'homme T, et al. Characterization of endogenous human FcRIII by mass spectrometry reveals site, allele and sequence specific glycosylation. *Mol Cell Proteomics* (2019) 18:534–45. doi: 10.1074/mcp.RA118.001142

40. Cosgrave EFJ, Struwe WB, Hayes JM, Harvey DJ, Wormald MR, Rudd PM. N -linked glycan structures of the human fcγ receptors produced in NS0 cells. *J Proteome Res* (2013) 12:3721–37. doi: 10.1021/pr400344h

41. Takahashi N, Cohen-solal J, Galinha A, Fridman WH, Sautès-Fridman C, Kato K. N-glycosylation profile of recombinant human soluble fcg receptor III. *Glycobiology* (2002) 12:507–15. doi: 10.1093/glycob/cwf063

42. Subedi GP, Barb AW. N-glycan composition impacts CD16a binding. *J Biol Chem* (2018) 293:16842–50. doi: 10.1074/jbc.RA118.004998

43. Falconer DJ, Subedi GP, Marcella AM, Barb AW. Antibody fucosylation lowers the FcγRIIIa/CD16a affinity by limiting the conformations sampled by the N162-glycan. *ACS Chem Biol* (2018) 13:2179–89. doi: 10.1021/acschembio.8b00342

44. Hayes JM, Frostell A, Cosgrave EFJ, Struwe WB, Potter O, Davey GP, et al. Fc gamma receptor glycosylation modulates the binding of IgG glycoforms: A requirement for stable antibody interactions. *J Proteome Res* (2014) 13:5471–85. doi: 10.1021/pr500414q

45. Schulz MA, Tian W, Mao Y, Van Coillie J, Sun L, Larsen JS, et al. Glycoengineering design options for IgG1 in CHO cells using precise gene editing. *Glycobiology* (2018) 28:542–9. doi: 10.1093/glycob/cwy022

46. Tian W, Ye Z, Wang S, Schulz MA, Van Coillie J, Sun L, et al. The glycosylation design space for recombinant lysosomal replacement enzymes produced in CHO cells. *Nat Commun* (2019) 10:1785. doi: 10.1038/s41467-019-09809-3

47. Narimatsu Y, Joshi HJ, Nason R, Van Coillie J, Karlsson R, Sun L, et al. An atlas of human glycosylation pathways enables display of the human glycome by gene engineered cells. *Mol Cell* (2019) 75:394–407.e5. doi: 10.1016/j.molcel.2019.05.017

48. Sealover NR, Davis AM, Brooks JK, George HJ, Kayser KJ, Lin N. Engineering Chinese hamster ovary (CHO) cells for producing recombinant proteins with simple glycoforms by zinc-finger nuclease (ZFN)-mediated gene knockout of mannosyl (alpha-1,3-)-glycoprotein beta-1,2-N-acetylglucosaminyltransferase (Mgat1). *J Biotechnol* (2013) 167:24–32. doi: 10.1016/j.jbiotec.2013.06.006

49. Yang Z, Wang S, Halim A, Schulz MA, Frodin M, Rahman SH, et al. Engineered CHO cells for production of diverse , homogeneous glycoproteins. *Nat Biotechnol* (2015) 33:842–4. doi: 10.1038/nbt.3280

50. Maresca M, Lin VG, Guo N, Yang Y. Obligate ligation-gated recombination (ObLiGaRe): Custom-designed nuclease-mediated targeted integration through nonhomologous end joining. *Genome Res* (2013) 23:539–46. doi: 10.1101/gr.145441.112

51. Varki A, Cummings RD, Aebi M, Packer NH, Seeberger PH, Esko JD, et al. Symbol nomenclature for graphical representations of glycans. *Glycobiology* (2015) 25:1323–4. doi: 10.1093/glycob/cwv091

52. Reiding KR, Blank D, Kuijper DM, Deelder AM, Wuhrer M. High-throughput profiling of protein n-glycosylation by MALDI-TOF-MS employing linkage-specific sialic acid esterification. *Anal Chem* (2014) 86:5784–93. doi: 10.1021/ac500335t

53. Lageveen-Kammeijer G, de Haan N, Mohaupt P, Wagt S, Filius M, Nouta J, et al. Highly sensitive CE-ESI-MS analysis of n-glycans from complex biological samples. *Nat Commun* (2019) 10:2137. doi: 10.1038/S41467-019-09910-7

54. Barb AW. Fc γ receptor compositional heterogeneity: Considerations for immunotherapy development. *J Biol Chem* (2021) 296:100057. doi: 10.1074/jbc.rev120.013168

55. Dekkers G, Bentlage AEH, Stegmann TC, Howie HL, Lissenberg-Thunnissen S, Zimring J, et al. Affinity of human IgG subclasses to mouse fc gamma receptors. *MAbs* (2017) 9:767–73. doi: 10.1080/19420862.2017.1323159

56. Tebbey PW, Varga A, Naill M, Clewell J, Venema J. Consistency of quality attributes for the glycosylated monoclonal antibody humira® (adalimumab). *MAbs* (2015) 7:805–11. doi: 10.1080/19420862.2015.1073429

57. Patel KR, Roberts JT, Barb AW. Multiple variables at the leukocyte cell surface impact fc γ receptor-dependent mechanisms. *Front Immunol* (2019) 10:223. doi: 10.3389/fimmu.2019.00223

58. Čaval T, Heck AJR, Reiding KR. Meta-heterogeneity: Evaluating and describing the diversity in glycosylation between sites on the same glycoprotein. *Mol Cell Proteomics* (2021) 20:100010. doi: 10.1074/MCP.R120.002093

59. Watanabe Y, Allen JD, Wrapp D, McLellan JS, Crispin M. Site-specific glycan analysis of the SARS-CoV-2 spike. *Science* (2020) 369:330–3. doi: 10.1126/SCIENCE.ABB9983

60. Cao L, Diedrich JK, Ma Y, Wang N, Pauthner M, Park SKR, et al. Global site-specific analysis of glycoprotein n-glycan processing. *Nat Protoc* (2018) 13:1196–212. doi: 10.1038/NPROT.2018.024

61. Braster R, Bögels M, Benonisson H, Wuhrer M, Plomp R, Bentlage AEH, et al. Afucosylated IgG targets FcγRIV for enhanced tumor therapy in mice. *Cancers (Basel)* (2021) 13:2372. doi: 10.3390/CANCERS13102372

62. Cartron G, Dacheux L, Salles G, Solal-Celigny P, Bardos P, Colombat P, et al. *Response: Implication for how the single nucleotide polymorphism (SNP) of fc receptor FcRIIIa alters the interaction with anti-CD20 monoclonal antibody* (2001).

Available at: http://ashpublications.org/blood/article-pdf/99/12/4649/1686199/h81202004642d.pdf (Accessed March 3, 2021).

63. Kremer PG, Barb AW. The weaker-binding fc gamma receptor IIIa F158 allotype retains sensitivity to the n-glycan composition and exhibits a destabilized antibody-binding interface. *J Biol Chem* (2022) 298(9):102329. doi: 10.1016/j.jbc.2022.102329

64. García-García A, Serna S, Yang Z, Delso I, Taleb V, Hicks T, et al. FUT8-directed core fucosylation of n-glycans is regulated by the glycan structure and protein environment. *ACS Catal* (2021) 11:9052–65. doi: 10.1021/ACSCATAL.1C01698

65. Dekkers G, Plomp R, Koeleman CAM, Visser R, Von Horsten HH, Sandig V, et al. Multi-level glyco-engineering techniques to generate IgG with defined fc-glycans. *Sci Rep* (2016) 6:1–12. doi: 10.1038/srep36964

66. Lalonde ME, Durocher Y. Therapeutic glycoprotein production in mammalian cells. *J Biotechnol* (2017) 251:128–40. doi: 10.1016/j.jbiotec.2017.04.028

67. Castilho A, Strasser R, Stadlmann J, Grass J, Jez J, Gattinger P, et al. In planta protein sialylation through overexpression of the respective mammalian pathway. *J Biol Chem* (2010) 285:15923–30. doi: 10.1074/JBC.M109.088401

68. Subedi GP, Barb AW. *The immunoglobulin G1 n-glycan composition affects binding to each low affinity fc γ receptor*. MAbs: Taylor and Francis Inc (2016). doi: 10.1080/19420862.2016.1218586

69. Yu X, Baruah K, Harvey DJ, Vasiljevic S, Alonzi DS, Song BD, et al. Engineering hydrophobic protein-carbohydrate interactions to fine-tune monoclonal antibodies. *J Am Chem Soc* (2013) 135:9723–32. doi: 10.1021/ja4014375

70. Anthony RM, Nimmerjahn F, Ashline DJ, Reinhold VN, Paulson JC, Ravetch JV. Recapitulation of IVIG anti-inflammatory activity with a recombinant IgG fc. *Sci (80-)* (2008) 320:373–6. doi: 10.1126/science.1154315

71. Kaneko Y, Nimmerjahn F, Ravetch JV. Anti-inflammatory activity of immunoglobulin G resulting from fc sialylation. *Sci (80-)* (2006) 313:670–3. doi: 10.1126/science.1129594

72. Narimatsu Y, Joshi HJ, Yang Z, Gomes C, Chen Y-H, Lorenzetti FC, et al. A validated gRNA library for CRISPR/Cas9 targeting of the human glycosyltransferase genome. *Glycobiology* (2018) 28:295–305. doi: 10.1093/glycob/cwx101

73. Lonowski LA, Narimatsu Y, Riaz A, Delay CE, Yang Z, Niola F, et al. Genome editing using FACS enrichment of nuclease-expressing cells and indel detection by amplicon analysis. *Nat Publ Gr* (2017) 12:581–603. doi: 10.1038/nprot.2016.165

74. Yang Z, Steentoft C, Hauge C, Hansen L, Thomsen L, Niola F, et al. Fast and sensitive detection of indels induced by precise gene targeting. *Nucleic Acids Res.* (2015) 43:e59. doi: 10.1093/nar/gkv126

75. Selman MHJ, Hemayatkar M, Deelder AM, Wuhrer M. Cotton HILIC SPE microtips for microscale purification and enrichment of glycans and glycopeptides. *Anal Chem* (2011) 83:2492–9. doi: 10.1021/AC1027116

76. Rappsilber J, Mann M, Ishihama Y. Protocol for micro-purification, enrichment, pre-fractionation and storage of peptides for proteomics using StageTips. *Nat Protoc* (2007) 2:1896–906. doi: 10.1038/nprot.2007.261

77. Vakhrushev SY, Dadimov D, Peter-Katalinić J. Software platform for high-throughput glycomics. *Anal Chem* (2009) 81:3252–60. doi: 10.1021/AC802408F

78. Rodenko B, Toebes M, Hadrup SR, van Esch WJE, Molenaar AM, Schumacher TNM, et al. Generation of peptide-MHC class I complexes through UV-mediated ligand exchange. *Nat Protoc* (2006) 1:1120–32. doi: 10.1038/nprot.2006.121

frontiers | Frontiers in Immunology

TYPE Review
PUBLISHED 12 September 2022
DOI 10.3389/fimmu.2022.953649

OPEN ACCESS

EDITED BY
Falk Nimmerjahn,
University of Erlangen Nuremberg, Germany

REVIEWED BY
Johann Sellner,
Landesklinikum Mistelbach-Gänserndorf, Austria
Anja Lux,
University of Erlangen Nuremberg, Germany

*CORRESPONDENCE
Jan D. Lünemann
jan.luenemann@ukmuenster.de

†These authors have contributed equally to this work and share senior authorship

SPECIALTY SECTION
This article was submitted to B Cell Biology, a section of the journal Frontiers in Immunology

RECEIVED 26 May 2022
ACCEPTED 29 July 2022
PUBLISHED 12 September 2022

CITATION
Mariottini A, Muraro PA and Lünemann JD (2022) Antibody-mediated cell depletion therapies in multiple sclerosis.
Front. Immunol. 13:953649.
doi: 10.3389/fimmu.2022.953649

Antibody-mediated cell depletion therapies in multiple sclerosis

Alice Mariottini[1,2], Paolo A. Muraro[1†] and Jan D. Lünemann[3*†]

[1]Department of Brain Sciences, Imperial College London, London, United Kingdom, [2]Department of Neurosciences, Drug and Child Health, University of Florence, Florence, Italy, [3]Department of Neurology with Institute of Translational Neurology, University Hospital Münster, Münster, Germany

Development of disease-modifying therapies including monoclonal antibody (mAb)-based therapeutics for the treatment of multiple sclerosis (MS) has been extremely successful over the past decades. Most of the mAb-based therapies approved for MS deplete immune cell subsets and act through activation of cellular Fc-gamma receptors expressed by cytotoxic lymphocytes and phagocytes, resulting in antibody-dependent cellular cytotoxicity or by initiation of complement-mediated cytotoxicity. The therapeutic goal is to eliminate pathogenic immune cell components and to potentially foster the reconstitution of a new and healthy immune system. Ab-mediated immune cell depletion therapies include the CD52-targeting mAb alemtuzumab, CD20-specific therapeutics, and new Ab-based treatments which are currently being developed and tested in clinical trials. Here, we review recent developments in effector mechanisms and clinical applications of Ab-based cell depletion therapies, compare their immunological and clinical effects with the prototypic immune reconstitution treatment strategy, autologous hematopoietic stem cell transplantation, and discuss their potential to restore immunological tolerance and to achieve durable remission in people with MS.

KEYWORDS

antibody, therapy, multiple scleorsis (MS), immunotherapy, immune reconstitution

Multiple sclerosis (MS) is the most common chronic inflammatory, demyelinating disease of the central nervous system (CNS), afflicting more than 2.5 million people worldwide (1). MS develops in young adults with a complex predisposing genetic trait and probably requires inciting environmental insults to trigger the disease. Both experimental and clinical evidence suggest that MS is an autoimmune disease with dysregulated adaptive immunity at its core. Genome-wide association studies have revealed multiple associations with immune-system-related gene variants, most importantly the HLA-DR15 haplotype (2); focal MS lesions are thought to be caused by the infiltration of immune cells, including T cells, B cells and myeloid cells, into CNS parenchyma (3); a substantial fraction of T and B cells isolated from CNS lesional tissue

and the cerebrospinal fluid (CSF) from MS patients are derived from clonal expansion (4, 5); intrathecally produced oligoclonal antibodies present in the CSF show evidence for antigen-dependent affinity maturation (6); various immunotherapies targeting lymphocyte survival, function or migration show beneficial treatment effects (7); and some facets of MS can be mimicked in experimental animal models largely driven by autoimmune T cells and collectively termed experimental autoimmune encephalomyelitis (EAE) (8). Long considered a variant of MS, Neuromyelitis optica (NMO) is a separate, rare disease entity characterized, in most cases, by selective but not exclusive involvement of the optic nerve and spinal cord, also evolving with a relapsing-remitting clinical course. Pathogenic immunoglobulin G (IgG) antibodies binding to aquaporin-4 (AQP4), a water channel located at the terminal feet of astrocytes in the blood–brain barrier, are detectable with high specificity in patients with NMO, but not in MS. The term NMO spectrum disorders (NMOSD) was coined to include rare CNS syndromes with predominant optic nerve and spinal cord involvement even in absence of AQP4-specific IgG. While patients with NMOSD benefit from immunosuppressive therapy, not all treatment modalities effective in MS are equally effective in NMOSD, indicating that underlying disease mechanisms are different (9).

Although there is still no curative treatment for (MS), disease-modifying medications have developed enormously during the last 30 years. Interferon-β and glatiramer acetate were the first modalities approved for the therapy of MS three decades ago. The introduction of oral medications including sphingosine 1-phosphate receptor modulators, fumarates, dihydroorotate dehydrogenase inhibitors, and purine nucleoside analogues was a second important milestone (10), followed by the development of recombinantly produced monoclonal antibodies (mAbs) for MS therapy. Natalizumab, a recombinant humanised anti-α4-integrin antibody marketed as Tysabri®, was the first mAb to be approved in the USA and Europe for the treatment of MS in 2004 (11). Natalizumab blocks the interaction of α4 integrins with their ligands, thereby inhibiting migration and trafficking of leukocytes through the blood-brain barrier and the extracellular matrix within the central nervous system. Most of the mAbs currently approved for the treatment of MS employ a different, immunosuppressive mechanism of action: they deplete pathogenic immune cells through pro-inflammatory Fc receptor-mediated effector mechanisms. In addition to immune cell-depletion, some of these therapies might re-establish immune tolerance through short-term immunosuppression followed by rebuilding of a new and healthy immune system. This review illustrates recent developments in the design and effector mechanisms of Ab-based cell deletion therapies in MS, evaluates clinical benefits and risks of currently approved treatment modalities and provides an outlook on emerging and future developments. To examine immune reconstitution effects as well as measures of efficacy, we compare Ab-based therapies with autologous haematopoietic stem cell transplantation (AHSCT), a treatment strategy involving mobilization and storage of haematopoietic stem/progenitor cells and intensive immune ablation followed by re-infusion of the autologous stem/progenitor cells and repopulation of the lympho- and haematopoietic systems (12).

Effector mechanisms of cell-depleting therapeutic Abs in MS

Cell-depleting therapeutic IgG antibodies in MS lyse target cells through at least three mechanisms (Figure 1): I.) antibody-dependent cellular cytotoxicity (ADCC) triggered by signaling through activating Fc receptors (FcγRs) expressed by natural killer cells; II.) complement-dependent cytotoxicity (CDC) through binding of C1q, which initiates activation of the classical complement pathway; and III.) antibody-dependent cellular phagocytosis (ADCP) mediated by phagocytes recognizing opsonized target cells. Membrane-bound complement cleavage products such as C3b or C4b also function as opsonins by interacting with complement receptors on effector cells which can result in complement-dependent cellular phagocytosis (CDCP) (Figure 1).

Immune cell-depleting Abs currently approved for MS therapy include alemtuzumab and CD20-targeting Abs. Alemtuzumab is a humanized monoclonal IgG1 kappa antibody that selectively targets CD52, an antigen highly expressed on T and B cells, to a lesser extent on innate immune cells, but not on haematopoietic stem cells (HSCs) (13). It is currently approved by the FDA and EMA for highly active relapsing-remitting (RR) MS, and data from initial treatment cohorts as well as extension studies of phase III clinical trials provided evidence that alemtuzumab can induce prolonged disease remission with no evidence for disease activity in more than 50% of treated patients (14, 15).

$CD20^+$ B cell-depleting therapy is highly effective against relapsing forms of the disease, and is also the first treatment approach proven to prevent disability worsening in primary progressive MS (PP-MS). Rituximab, initially developed and approved for the therapy of B cell-lymphomas, is effective in the treatment of several autoimmune diseases including MS (16). Ocrelizumab (Ocrevus ®), a second-generation humanized anti-CD20 antibody, is approved by the FDA, the EMA and other regulatory agencies for the treatment of relapsing MS and PP-MS. Ofatumumab (Kesimpta ®) is a fully humanized CD20-specifc Ab approved by the FDA and EMA for the treatment of active relapse-onset MS.

All of the three aforementioned Abs are of the human IgG1 subclass and target the CD20 antigen, expressed by a broad range (immature, transitional, naïve and memory) of B cells but not by plasma blasts/cells, and by approximately 5% of circulating T cells (17). Therapeutic anti-CD20 mAbs differ,

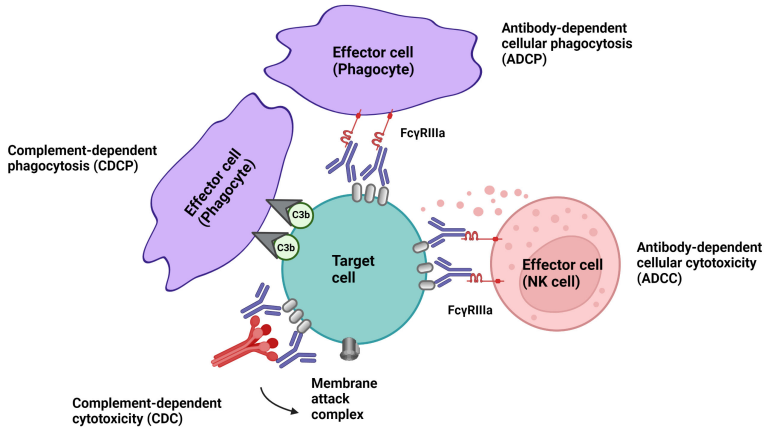

FIGURE 1
Effector mechanism of cell-depleting therapeutic IgG antibodies in MS. Complement-dependent cytotoxicity (CDC) is triggered through binding of C1q, which initiates activation of the classical complement pathway. Signalling through activating Fc receptors (FcγRs) expressed by innate immune cells such as natural killer cells and phagocytes initiates antibody-dependent cellular cytotoxicity (ADCC) and antibody-dependent phagocytosis (ADCP). Membrane-bound complement cleavage products such as C3b can additionally function as opsonins by interacting with complement receptors on effector cells which can result in complement-dependent cellular phagocytosis (CDCP).

however, from each other in their structure, epitopes targeted within the CD20 molecule, binding affinity to cell-surface CD20, and their mechanisms of action of B cell depletion (Figure 2). Depending on their capacity to cluster CD20 on the cell surface, anti-CD20 antibodies are grouped into type I and type II, the latter not having this ability (18, 19). Type I antibodies like rituximab, ocrelizumab and ofatumumab have been shown to efficiently activate complement, presumably because clustering facilitates the formation of hexameric IgG-Fc platforms suitable for C1q binding (20, 21). While both type I and type II antibodies are able to induce ADCC as well as ADCP (19), type II antibodies appear to be superior in inducing direct cell death (22, 23). *In vitro* data indicates that rituximab depletes through both FcγRs as well as complement dependent effector mechanisms. Ocrelizumab, equipped with humanized Ab backbone, exhibits greater ADCC compared to CDC than

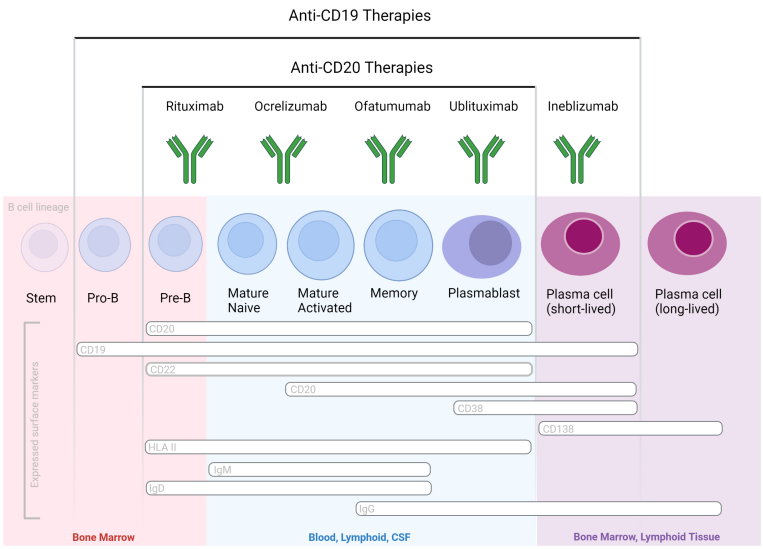

FIGURE 2
B cell-depleting mAbs with proven efficacy in MS and NMOSD, based on phase 3 randomized controlled clinical trials. Therapeutic Abs differ in their molecular design and targeted epitopes.

rituximab, but also depletes B cells through antibody-dependent cellular phagocytosis. Ofatumumab, a fully human monoclonal antibody was designed for greater CDC than ADCC activity (24–27) and is currently the only anti-CD20 mAb administered in a subcutaneous, rather than intravenous, dosing regimen. To what extent these different effector mechanisms contribute to cell-depleting or, in general, therapeutic Ab activity *in vivo* is less well understood and might depend on the disease condition treated and on the organ environment in which the antibody mediates its activity (28). It has become clear across many pre-clinical animal model systems that cytotoxic antibody binding to cellular FcγRs is critical for their therapeutic activity *in vivo* (29, 30).

Ab effector functions are regulated by a single biantennary glycan of the heavy chain, which resides just below the hinge region, and the presence of specific sugar moieties on the glycan has profound implications on IgG effector functions. The majority of circulating IgG antibodies are fucosylated which, compared to afucosylated isotypes, reduces IgG´s binding affinity for the activating FcγRIII (CD16) and thereby its potential to induce ADCC (31, 32). Fucosylation also appears to impair ADCP (33, 34). Consequently, afucosylation of therapeutic cell-depleting mAbs results in improved target cell elimination.

Ublituximab is a novel type I chimeric, (IgG1) anti-CD20 mAb glycoengineered with a low fucose content in its fragment crystallizable (Fc) region to enhance affinity for all variants of FcγRIIIa receptors, thereby producing potent ADCC (35). Ublituximab targets a unique epitope on CD20 not targeted by other anti-CD20 mAbs and exhibits 100 times greater natural killer cell–mediated ADCC *in vitro* than rituximab in cells from patient donors with chronic lymphocytic leukemia (CLL) (36). The potent ADCC activity allow for administering lower doses and shorter infusions times versus other presently available anti-CD20s mAbs. Two identical Phase 3, randomized, multi-center, double-blinded, active-controlled studies, ULTIMATE-I (NCT03277261) and ULTIMATE-II (NCT03277248), are reported to show clinical efficacy in patients with relapsing forms of MS (37).

Inebilizumab is an afucosylated type 1 humanized IgG1 mAb specific for CD19 and depletes a wide range of B lineage cells, including plasmablasts and some plasma cells (38). Targeting of the latter two populations could have a therapeutic merit particularly in antibody-mediated neurological disease such as NMOSD. Efficacy and safety of inebilizumab in individuals with (NMOSD) and detection of pathogenic antibodies specific for aquaporin 4 were demonstrated in the randomized, double-blind, phase 3 placebo-controlled study (ClinicalTrials.gov identifier: NCT02200770) (Clinicaltrials.gov) (39). Due to its efficacy for targeting a broader range of B cells, including Ab-secreting cells unrecognized by anti-CD20 agents, inebilizumab may have a greater therapeutic impact than the aforementioned CD20-specific agents. The aforementioned RCTs reported an acceptable safety profile of inebilizumab in neurological patients. However, longer-term safety profiles of CD19-immunotherapies in neurological patients remain to be determined, specifically related to IgG depletion and risks for infectious diseases. Inebilizumab is currently undergoing clinical evaluation for kidney transplant desensitization, myasthenia gravis, and IgG4-related disease. Safety and tolerability of inebilizumab in MS has been tested in a phase 1 trial (40), but the clinical program to develop the drug for MS has been discontinued. (Table 1)

Effect of cell depleting-Abs on adaptive immune signatures in MS

Immunological studies on cell-depleting Abs, as well as those on AHSCT, provided important insights into mechanisms responsible for their clinical efficacy and safety profiles. We can distinguish for both on- and off-target (or unanticipated) effects, desirable and unwanted side effects (Table 2).

Alemtuzumab

Alemtuzumab induces the reduction of circulating lymphocyte counts with little effect on monocytes, NK cells and granulocytes, promoting a rapid (within 1 month) and marked depletion of B (up to 85%) and T lymphocytes (up to 95% for CD4+ and 85% for CD8+ T cells), with similar dynamics following each course of treatment (42). After depletion, immune cell repopulation occurs with different rates across lymphocytes subsets.The median time to recover the lower limit of normal was shorter for B cells (7.1 months) compared with T cells (median of 20 and 35 months for CD8+ and CD4+ T cells, respectively), and values after 1 year of treatment were still reduced by 70% for CD4+ cells and by 50% for CD8+ cells (94, 95) Furthermore, over a median follow-up of 12 years (range 0.5 – 16) the recovery to baseline levels for CD8+ and CD4+ counts was reported in only 30% and 21% of the patients, respectively (44).

Alemtuzumab depletes both naïve and memory phenotypes, and the subsequent repopulation occurs according to differential patterns for T and B cells, inducing changes in the relative proportions of subsets compared to pre-treatment. In the T cell compartment, the immune cell repopulation is mainly driven by homeostatic proliferation of residual clones, inducing a relative decrease in naïve and increase in effector memory cells, especially in the T CD8+ pool, with a predominance of terminally differentiated memory CD45RA+ (TEMRA) cells for at least 24 months (45, 51). Consistent with the sustained peripheral proliferation of T cells, CD4 and CD8 Ki67 expression was increased for up to 2 years after alemtuzumab,

TABLE 1 Abbreviations used in the manuscript.

Ab: antibody
AHSCT: autologous haematopoietic stem cell transplantation
ARR: annualized relapse rate
AQP4: aquaporin 4
Breg: regulatory B cells
CDI: confirmed disability improvement
CDI-FS: confirmed disability improvement-free survival
CDW: confirmed disability worsening
CDW-FS: confirmed disability worsening-free survival
CI: confidence interval
CNS: central nervous system
CSF: Cerebrospinal fluid
DMT: disease-modifying treatment
EDSS: Expanded disability status scale
IFN: interferon beta
Ig: immunoglobulin
mAb: monoclonal antibody
MRI: magnetic resonance imaging
NEDA: no evidence of clinical and radiological disease activity, defined as the absence of all the following: relapses, disability worsening and signs of inflammatory activity (new T2 lesions and/or gadolinium-enhancing lesions) at brain magnetic resonance imaging
NEDA-S: NEDA survival, i.e. proportion of cases who had not yet experienced any clinical or radiological disease activity
OLE: open-label extension phase of a randomized clinical trial
OR: odds ratio
PP-MS: primary-progressive multiple sclerosis
R-FS: relapse-free survival
R-MS: relapsing multiple sclerosis
RR-MS: relapsing-remitting multiple sclerosis
RCT: randomized clinical trial
SD: standard deviation
SP-MS: secondary-progressive multiple sclerosis
Th: T helper cell
Treg: regulatory T cells

as were markers of increased activation (HLA-DR) and susceptibility to Fas-mediated apoptosis (CD95), with evidence in both CD4+ and CD8+ cells of chronic activation and repeated cell division (51). CD4 expression of programmed death-1 (PD-1) and lymphocyte activation gene-3 (LAG-3) were increased 6–9 months after treatment (51). The lack of a relevant contribution of thymic reactivation is suggested by: (i) a reduced number of cells recently generated from the thymus identified by T cell receptor (TCR) excision circles (TRECs); (ii) the observation that up to month 12 following treatment T cells exhibit reduced clonality in the TCR repertoire, being the baseline high-frequency clones expanded post-treatment (51). Similar findings were reported also within the regulatory T (Treg) cell compartment (48).

As for B cells, a rapid and early hyper-repopulation is observed, achieving absolute values above baseline by 35.3% in CARE-MS I and by 26.8% in CARE-MS II (42), being higher increments (up to 165% of the baseline count) also reported (96). Opposite to the T cell pool, the repopulated B cell pool is dominated by immature phenotypes associated with an increase in B-Cell Activating Factor (BAFF) levels (96) The depletion of total memory B cells is sustained up to month 36 compared with baseline, and it is associated with a significant elevation of total naïve B cells from month 5 to 48, up to a 180% increase compared with pre-treatment levels (42, 49). Plasma cells express little or no CD52 and seem not to be affected by alemtuzumab (97, 98).

As an on-target effect, the lymphocyte depletion induced by alemtuzumab promotes a long-term abrogation of MS disease activity, which is thought to be mediated, at least in part, by the ablation of disease-mediating T and B cells. Compared with untreated MS patients and healthy controls, an increase in proliferative responses of T cells to self-antigens was observed following alemtuzumab treatment (41). However, this was associated with a marked increase in T cell apoptosis persisting for at least 18 months, with increased expression of caspase-3 in T cells and monocytes compared with untreated MS (41). More recently, the antigen-specific immune response to different CNS self-antigens and control non-self-antigens was evaluated in five patients by ELISpot, showing that both the cumulative number of IFN-γ secreting cells and the ratio of IFN-γ secreting cells/CD4+ T cell counts were reduced following treatment compared to baseline (43). Although Th1 counts were not assessed, the Authors speculated that these data might suggest that alemtuzumab induces functional changes in the immune cell repertoire.

Correlations between the kinetics of immune cell repopulation and disease activity were not consistently detected across studies, suggesting that subtle qualitative changes in immune cell subsets might be relevant to the

TABLE 2 Summary of on- and off-target effects on the immune system of therapeutic cell-depleting mAbs and relationship with benefits and risks of adverse events.

	On-target beneficial effect	On-target detrimental effect	Off-target (or unanticipated) beneficial effect	Off-target (or unanticipated)detrimental effect
Alemtuzumab	Ablation of disease-mediating B and T cells (41–43)	Prolonged T cell depletion, particularly CD4+ (42, 44)	Increase in regulatory T and B cell phenotypes (45–50) Changes in cytokine patterns: reduced production of pro-inflammatory (e.g. IL-6, IL-17, IL-21, IL-22, IFN- γ) and increase of anti-inflammatory cytokines (e.g. IL-7, IL-4, IL-10, TGF-β) (43, 45, 46, 50, 51)	Early B cell hyper-population (increased risk of antibody-mediated secondary autoimmunity) (45, 52–55) T cell repopulation driven by homeostatic proliferation (increased risk of T cell-mediated secondary autoimmunity) (51, 56)
CD-20 depleting mAbs: Ocrelizumab Ofatumumab* Rituximab Ublituximab*	Ablation of CD20+ B cells contributing with pleiotropic functions to disease pathogenesis (e.g. antigen presentation and activation of pathogenetic T cell clones) (16, 57–62). Ablation of potentially disease-mediating CD20+ T cells (5, 63–66)	Reduced humoral immunity (e.g. response to vaccination, increased risk of infections) (16, 57–59, 67–71)	Changes in B cell subsets after immune repopulation: skewing towards naïve and regulatory phenotypes (5, 65, 72) Modifications in the pattern of cytokine secretion (e.g. increase in IL-10; reduction in IL-6 and lymphotoxin) (65, 72–74) Reduced percentage and activation/ proliferation of pro-inflammatory T cell phenotypes (Th17 and Th1) (64–66, 73, 75)	
Inebilizumab	Depletion of putative disease-mediating CD19+ B cell clones (40, 76)	Reduced humoral immunity (40, 76)		
AHSCT	Ablation of disease-mediating T cells (77–79) Ablation of B cells contributing to disease pathogenesis (79)	Transient reduction in cell mediated and innate immunity (increased risk of infections) (79–81). Transient reduction in myeloid-derived blood cells (79–81).	Immune cell reconstitution promoted by thymic reactivation with regeneration of T cell receptor repertoire diversity (80, 82, 83) Increase in regulatory function of B and T cells (79, 84–86) Reduced percentage and activation/ proliferation of pro-inflammatory T cell phenotypes (Th17, Th1, MAIT) (79, 86–88) Reduced production of pro-inflammatory cytokines, with shift towards anti-inflammatory profile (77, 84, 86, 87, 89) Down-regulation of pro-inflammatory genes in adaptive and innate immunity cells (90–92)	Secondary autoimmunity (93)

*Most of the evidence on the effects of Ab-mediated cell depletion therapies were provided by studies on ocrelizumab and rituximab.

therapeutic effects (99–101). Aligned with this observation, CD4+CD25+CD127+foxP3-Teff cells were recently suggested as a possible marker for monitoring disease activity, as patients with stable disease showed a trend for reduced levels of such population, with reduced Teff: Treg ratios (49). Furthermore, exploratory analyses using a random generalized estimating equation Poisson model suggested that the relative balance of several key potentially pathogenic and regulatory subsets might be associated with the risk for gadolinium-enhancing lesions, with an association between the risk for T2 lesions and CD3+CD8+CXCR3+ T cells (49).

A modification in the balance between cell subsets and in patterns of cytokine secretion following immune cell repopulation may therefore be considered as an unexpected off-target beneficial effect of alemtuzumab that may contribute to the abrogation of disease activity.

An increase in regulatory populations was described following alemtuzumab treatment, both in the T and B cell

compartments (49). Briefly, an expansion in Treg compared with baseline was observed starting at month 1, with a more modest although significant elevation up to year 2 (45, 46). Treg predominantly exhibited a mature/activated phenotype and performed an effective suppression of induced proliferation of patients' peripheral blood mononuclear cells at months 5 and 17 of treatment compared with CD25-depleted peripheral blood mononuclear cells with effective reduction in the IL-17 and IFN-γ responses upon myelin-basic protein (MBP) stimulation (49). These observations suggest that Tregs are functional and may exhibit enhanced suppressive activity in the early phase of repopulation after each course of alemtuzumab treatment (49). In another study, the suppressive function of post-depletion Treg from MS patients remained constantly increased compared to baseline over 24 months after alemtuzumab start, nearly reaching levels comparable to those seen in Treg obtained from healthy donors (48). The restoration of deficient counts of B cells expressing a "regulatory" phenotype (CD19+CD24^{hi}CD38^{hi} and CD19+PD-L1^{hi}) in the peripheral blood of relapsing MS patients was observed during the first year following alemtuzumab (47) Values of the naïve B "regulatory" phenotype CD19+CD20+CD27-CD24^{hi}CD38^{hi} were significantly increased compared with baseline up to month 36 following treatment in another study, with a marked decrease in the ratio of total memory B cells to naïve "regulatory" cells (49). In a cross-sectional study, B cells collected from patients who had received alemtuzumab secreted significantly higher levels of IL-10 and brain-derived neurotrophic factor (BDNF) up to month 24 compared to a cohort of pre-treated MS patients (50). Furthermore, B cells from post-treatment cohorts showed a greater inhibition of the proliferation of autologous CD4+CD25- T cells as compared to the pre-treated cohort, suggesting enhanced regulatory ability of B cells up to month 24 after treatment commencement.

Changes in the relative proportion of CD4+ and CD8+ T cell subsets were demonstrated by the observation of an incremental increase in the percentage of TGF- β1, and IL-10–producing CD4+ and CD8+ T cells within 12 months from treatment, as well as of IL-4–producing Th2 and CD8+ T cells, whereas the percentages of IL-17A–producing Th17 cells and IFN-γ–producing Th1 and CD8+ T cells were significantly decreased (45, 51). A transient increase in the percentage of CD4+IFN-γ+ Th1 cells at month 5 compared with baseline was observed in another study (49). Consistent with Treg and Th2 expansion, gradually increasing serum levels of IL-7 and IL-4 were observed over the first 6 months after treatment compared with baseline, whereas cytokines produced by or polarizing towards Th17 and Th1 phenotypes (IL-17A, IL-17F, IL-21, IL-22, and IFN- γ; IL-11, IL-1β, IL-6, and IL-23, IL-27 and IL-12) were reduced (45)A significant reduction in concentrations of IL-2, IFN-γ and IL-17A compared to baseline was reported up to month 23 after treatment (49). Accordingly, mRNA levels of the anti-inflammatory cytokines IL-10, IL-27, and TGF-β significantly increased after alemtuzumab treatment compared with baseline (46). On the other hand, levels of proinflammatory cytokines and transcriptional factors related to the Th17 and Th1 subset, and of proinflammatory chemokines or chemokine receptors (CCR3, CCR4, CCR5, CCR6, CXCR3, CXCL10, CCL20, VLA4) significantly decreased. These modifications occurred during the first 12 months, and remained at values similar to month 12 over the subsequent year of follow-up (46). After alemtuzumab treatment, an increase of CD4+ and CD8+ T cells that express CXCR3 and CCR5 and of CD8+ T cells that express CDR3 and CCR4 was reported the majority of these cells expressed VLA-4, suggesting heightened trafficking potential in activated T cells (49).

Few data are available on the impact on the CSF compartment, and CSF oligoclonal bands (i.e. two or more oligoclonal IgG bands detected by separation of CSF proteins while not demonstrable in corresponding serum) (102) were still present in all the 15 cases tested before and after 3 to 28 months following alemtuzumab administration in one study (44). More recently, a decreased intrathecal IgG production was reported in association with reduced peripheral blood IgG levels, and oligoclonal bands disappeared in two cases at month 24 of follow-up (103).

Increased risk of infections might be considered as an unwanted on-target effect, that may be attributed at least in part to prolonged T cell depletion, particularly CD4+ (42). A progressive reduction in the concentrations of all (Ig)subgroups, that was described over 36 months after initiation of alemtuzumab therapy in one study, might also contribute to this adverse event, as reduced IgG concentrations were associated with an increased incidence of pneumonia, otitis, and sinusitis (103).

Secondary autoimmunity may be considered as an unexpected off-target detrimental effect of alemtuzumab, promoted by "unbalances" between cell subsets that take place during immune cell repopulation Both antibody-mediated and T-cell mediated autoimmune diseases have been described following alemtuzumab treatment (56).

Rapid hyper-population of B cells, which might not be adequately counterbalanced by Tregs (absolute number of CD4 Tregs reduced by 81% in CARE-MS I and 86.3% in CARE-MS compared with baseline) (45, 52), and homeostatic proliferation of T cells are supposed to contribute to this category of adverse events. Patients developing autoimmunity showed, compared to those who did not, reduced thymopoiesis at month 12 (51), and higher rates of T cell cycling, with increased proliferation and apoptosis but without differences in lymphopenia between groups (41) Occurrence of autoimmunity was associated with increased production of IL-21 in one study, possibly driven by a genetical susceptibility (41). Furthermore, a greater T cell clonal restriction following alemtuzumab treatment by both sequencing (increased high-frequency clones) and TCR CDR-3 length spectratyping (more

undetectable BV families and reduced complexity of the remaining families) was associated with the development of autoimmunity (51). Serial TCR sequencing showed that T-cell pool remained oligoclonal at month 12 in one patient who developed autoimmunity, whereas TCR diversity had recovered by month 6 and was higher than pre-treatment at month 12 in another who did not (51). B cell hyper-population was suggested to drive also B cell-mediated tumefactive CNS demyelination reported in a few cases after alemtuzumab treatment (53–55) This event was associated with a decrease in B regulatory cells with CD19+CD24^{hi}CD38^{hi} phenotype at the time of disease reactivation in one case (104).

Ocrelizumab, ofatumumab and rituximab

Ocrelizumab induced a reduction of CD19+ cells to negligible levels by week 2 from treatment, whereas CD4+ T cells remained stable throughout the treatment period in the pivotal trials (59, 60). An initial 2–6% mean decrease from baseline in peripheral-blood counts of CD3+ or CD8+ cells was observed at week 2, followed by an additional 2-6% decrease for CD8+ cells from week 2 to the end of the trials (week 96 or 120) (59, 60).

In the phase 2 dose-finding trial MIRROR, ofatumumab (from 3 to 60-mg doses every 12 weeks, or 60 mg every 4 weeks) induced a dose-dependent depletion of B cells, being greater for the 60-mg dose every 4 weeks (to <2% of baseline levels at maximum depletion) and the 30- and 60-mg dose every 12 weeks (to ≈5% of baseline) than for the 3-mg dose every 12 weeks (to ≈25% of baseline) (61). Similar rates of B-cell repopulation were observed across groups, being B-cell repletion achieved by 64% to 74% of patients by week 24 after the last administration, but repopulation was slower for the higher-dose groups. After the loading dose of 60 mg, ofatumumab leads to B-cell depletion in the peripheral blood, which is sustained following subsequently monthly 20 mg dosing (69). By day 14 (i.e. after having received 40 mg-ofatumumab), B-cell counts were below the lower limit of normal in all the treated patients, with a median depletion by 99.1% of baseline values. A bioequivalent rapid B-cell depletion was observed with ofatumumab 20 mg every 4 weeks self-administered subcutaneously *via* autoinjector compared with the pre-filled syringe, independent of body weight quartiles (105). In ofatumumab-treated patients, a significant relationship between weighted mean B-cell count and new gadolinium-enhancing lesions was reported by *post-hoc* analyses, but moderate B-cell depletion (with circulating B-cell levels to ≈25% of baseline) was surprisingly effective in significantly reducing new gadolinium-enhancing lesions (relative reduction: 71%) (61). Partially explaining this finding, the observation from animal models that subcutaneous administration of antibodies allows more direct access to the lymph nodes compared with intravenous infusion, promoted by the absorption into the lymphatic system (106, 107). This may allow targeting B cells in the lymph nodes directly while sparing those in the spleen, a phenomenon that could help preserve the immunosurveillance (105).

Two doses of rituximab 1000 mg induced a rapid and near-complete depletion of CD19+ B lymphocytes (>95% reduction from baseline) starting from week 2 until week 24 and followed by gradual replenishment with a return to 31% of the baseline value by week 48 (16). Following two additional doses administered six months after the first course, one-third of the patients recovered B cell count at week 122 (57). Similar reductions compared with baseline were observed after subsequent courses of treatment, without a significant effect of the dose (< or ≥2 g each course) of rituximab administered, suggesting a possible ceiling effect (108) however, time to recovery of B cell count was faster for lower doses (250 mg) compared with higher doses (500 – 2000 mg) (109). Rituximab induced a similar pattern of depletion in NMOSD patients, followed by a repopulation promoted mainly by CD27- naïve B cells, that represented on average 86.2% of the B cell poo (58).

As an on-target effect, anti-CD20 mAbs promote the depletion of CD20 expressing cells, including subsets that may plausibly contribute to MS pathogenesis. Most of the CD20 bearing cells are represented by B cells, but the mechanisms underlying B cell role in disease pathogenesis are not fully understood: these might include pleiotropic functions involved in the interaction with the T cell compartment, such as cytokine secretion, antigen presentation, and driving of auto-proliferation of Th1 brain-homing CD4+ T cells by memory B cells (110). The beneficial effects of B cell depletion may be mediated, at least in part, by phenotypic and functional changes occurring in the re-populated B cell pool. This latter is characterized by a skewing towards naïve phenotypes after both ocrelizumab or rituximab administration, with an early decrease in naïve and memory B-cell numbers associated with an increase in percentages of plasmablasts and transitional B cells (5, 65). The subsequent replenishment is dominated by IgD+CD27- naïve and transitional B cell subsets, whereas memory B cell populations and IgD-CD27- B cells remained depleted for significantly longer, up to weeks 37–52 after rituximab administration (5, 65).

Modifications in the pattern of cytokine secretion towards an anti-inflammatory balance were also described, and they could contribute to reducing the state of activation and proliferation of pathogenetic T cells.

Relative to the total CD19+ B cell number, ocrelizumab induced a decrease in the percentage of B cells producing TNF-α, and an increase in the proportion of regulatory B cells producing IL-10 (65). However, the relative increase in the production of GM-CSF and frequency of IL-6 producing B cells suggest that complete restoration of immune tolerance was not achieved (65).

Opposite to this latter finding, repopulated B cells from MS patients treated with rituximab secreted reduced levels of IL-6, achieving values comparable with healthy controls (73). In another study, the secretion of IL-10 increased, whereas the frequencies of circulating GM-CSF+ B cells and secretion of GM-CSF decreased after treatment with rituximab (at a time when B cells were reconstituted to pre-treatment levels) compared to baseline, therefore resulting in an essentially normalized GM-CSF/IL-10 ratio (74). These changes were associated with decreased myeloid cell proinflammatory responses that persisted even after B cells reconstitution, in keeping with the diminished proinflammatory response profile of the reconstituted B cells. Similarly, rituximab promoted an enhancement of regulatory B cell function in NMOSD patients, as newly developed B cells secreted higher levels of IL-10 and decreased levels of lymphotoxin following depletion compared to baseline, consistent with the predominance of naïve B cells over memory phenotypes in the repopulated pool (72).

As an off-target unexpected effect plausibly mediated by enhanced regulatory function of B cells, modifications in T cell activation were also observed. A decrease in the percentages of CD4+ and CD8+ T cells producing IFN-γ to total CD4+ and CD8+ T cells, respectively, was reported following ocrelizumab treatment (65). Th1 (IFN-γ) and Th17 (IL-17) responses and proliferative responses of CD4+ and CD8+ T cells were reduced in MS patients treated with rituximab compared with baseline these modifications were suggested to be mediated by a reduced production of the pro-inflammatory cytokines lymphotoxin and TNF-α by the repopulated B cells (75).

In another study, IL-17 production in peripheral blood mononuclear cells from RR-MS patients treated with rituximab was lower than pre-treatment (without differences in IFN-γ), suggesting that this could be mediated by a reduced IL-6 production after B cell depletion (73).

Although the CD20+ pool is mostly constituted by B cells, CD20 is expressed also by a minor subset of T cells exhibiting an activated phenotype with increased production of proinflammatory cytokines (111). CD20+ T cells can be detected in peripheral blood, CSF and CNS lesions from MS patients and are considered possibly relevant to disease pathogenesis (112). The depletion of CD20+ T cells might therefore contribute to the therapeutic effectiveness of anti-CD20 mAbs, and its occurrence was independently reported following the administration of ocrelizumab or rituximab.

Two weeks after the first administration of 300 mg ocrelizumab, CD3+CD20+ T cells (representing at baseline almost 20% of the CD20+ cells) were rapidly and efficiently depleted from peripheral blood of MS patients (63) These findings were confirmed by another study showing a marked decrease in both absolute numbers and percentages of CD20+ T cells relative to CD3+ T cells six months after ocrelizumab start, being the relative reduction significant in both CD4+ and CD8+ subsets (65).

Similarly, a near-complete depletion of CD3+CD20+ T cells during weeks 1–12 after rituximab administration was reported, from a mean frequency of 7.8% to 0.36%, lasting for at least one year and followed by partial repletion (2.7%) starting from weeks 25–36 (5).

Mild and transient changes were observed after ocrelizumab administration also in the CD20- T cell population, with a decline in the proportion of effector T cells associated with a relative increase of CD8+ naïve T cells and the ratio of naïve/effector subsets for both CD4+ and CD8+ T cells, suggesting the redistribution of the T-cell compartment favoring naïve vs effector phenotypes (65).

Different effects on the T cell pool were observed after rituximab administration. No significant changes were reported in the whole CD3+ T cell counts in three studies on MS patients (5, 16, 57), whereas an early and transient reduction in CD3+ cells (by on average 25%) was observed in the first three months after treatment in a mixed cohort of MS and NMOSD patients, without significant changes compared to baseline following subsequent courses of treatment (108). Different factors, such as concomitant treatment, previous exposure to immunosuppressive drugs and presence of lymphopenia at baseline in a subset of cases, could contribute, at least in part, to this latter finding No significant changes in the numbers of CD4+, CD8+ cells nor in the CD4+/CD8+ ratio over long-term follow-up were observed in another study on MS and NMOSD patients (109).

Cell depletion was evident also in the CSF, where, at week 24 after 4 weekly doses of rituximab 375 mg/m^2, the number of CD19+ B cells and CD3+ T cells were reduced by 90% and 55% compared with baseline, respectively (113). In the same study, no significant differences in IgG concentration, IgG index, IgG synthesis rate or number of oligoclonal bands were observed . A significant decline of CSF levels of CXCL13 (a chemoattractant factor for B cells and activated T cells) was reported following treatment with rituximab, with a positive correlation between CXCL13 and the degrees of reduction of T cell counts in the CSF (114). Based on these observations, the Authors speculated that B cells may indirectly promote reduced T cell trafficking across the blood-brain barrier involving the reduced CNS production of chemoattractant factors, such as CXCL13, by non-B cells.

As an on-target detrimental effect, serum Ig levels were reduced by CD-20 depleting mAbs, with potential implications for long-term safety.

At week 96 of the pivotal trials of ocrelizumab in R-MS, proportions of treated patients with Ig levels below the lower limit of normal were 1.5% and 2.4% for IgG and IgA, respectively, and 16.5% for IgM; no impact on existing antibody titers for mumps, rubella, varicella, or pneumococcus was reported (59). After five years of treatment, serum Ig levels were further reduced, being below the lower limit of normal in 5.4% and 5.1% of the cases for IgG and IgA, respectively, and in 29.5% for IgM, compared to 0.5% for IgG and IgM and 1.2% for

IgG at baseline (70). Similar proportions were observed in ocrelizumab-treated PP-MS patients, being cases with IgM levels below the lower limit of normal 15.5% at week 120, compared with 1.2% of those in the placebo group (60). These proportions increased to 29% for IgM and 5% for both IgG and IgA at 6.5 study years of follow-up (71). In a pooled population of R-MS and PP-MS patients who received ocrelizumab in the pivotal trials, serious infections following episodes of a drop in Ig concentrations below the lower limit of normal were rare (67). Most of the infections (mainly represented by urinary tract infections, cellulitis, and pneumonia) resolved with standard treatment, without requiring ocrelizumab withdrawal.

Similar rates of patients with Ig deficiency were observed during ofatumumab treatment, being the proportion of cases with IgM levels below the lower limit of normal 14.3% (69).

A reduction of IgM levels below the lower limit of normal was reported in 22% and 32% of MS patients who had received 2 or 4 1000 mg-administrations of rituximab, respectively, with higher rates reported for longer exposures to treatment (16, 57), IgM were reduced in 37% of the NMOSD patients at year 5 of treatment, and IgA and IgG were reduced in 30% and 13% of the cases, respectively (58).

As a consequence of the impairment in antibody production, B cell-depleting therapies might interfere with the generation of an effective response to vaccination, as suggested by the observation that MS patients receiving ocrelizumab showed an attenuated humoral response compared to those receiving interferon or no treatment to clinically relevant non-live vaccines (tetanus toxoid, pneumococcal polysaccharide, pneumococcal conjugate vaccine, seasonal inactivated influenza) administered 12 weeks after treatment initiation (68). However, recent evidence suggests that cell-mediated immune response may preserve vaccine efficacy in B-cell depleted MS patients, although differential effects depending on the specific vaccination strategy adopted cannot be excluded (115, 116).

Ublituximab

CD19+ B cells were efficiently depleted in most patients within 24 hours of receiving the initial 150 mg dose of ublituximab within 2 weeks after the second infusion, B-cell count was reduced by at least 95% from baseline, being the reduction sustained without significant recovery both at week 24 (pre-dose) and at week 48 of follow-up (62). Similarly, an immediate B cell depletion after a single 450 mg-dose of ublituximab was observed in five NMOSD patients treated in a pilot study, with a sustained depletion in B cell count ≤0.2% for two months in 4/5 cases, being 0.9% in the remaining one (117).

A transient but significant reduction in the percentage of T cells with respect to the total peripheral blood mononuclear cells count (from 43% of baseline to 29% of day 2) was observed about 24 hours after ublituximab administration, reverting to baseline by week 2. This phenomenon could be interpreted as a relative decrease of T cells in the peripheral blood due to efflux of myeloid cells from the bone marrow in response to the rapid depletion of B cells, as suggested by the observation, in the same timeframe, of a significant increase in the percentage of myeloid cells (64).

As for T cell subsets, a relative increase in the proportions of naïve CD4+ and CD8+ T cells with a reciprocal decrease in effector and central memory CD4+ and CD8+ T cells, without changes in the CD4+/CD8+ ratio, was observed during the first 24 weeks of ublituximab treatment (64). These modifications were significant starting from week 12 for the CD4+ T cells, whereas for CD8+ T cells the change in naïve/memory ratio occurred immediately on day 2, suggesting that some CD8+ T cells bearing the CD20+ marker may have been deleted by ublituximab. The depletion of CD20+ T cells by ublituximab was confirmed in MS patients by a subsequent study, showing an early (within 24 hours from the first administration) and long-term depletion of the vast majority of CD20+ T cells, being these latter naïve cells (as determined by CD45RA) in >95% of the cases (66). The modifications in the T cell subset persisted after the third ublituximab infusion performed at 24 weeks, up to week 48 (66).

A significant decline in the percentage of Th1, but not in IL-17+ and GM-CSF+ CD4+ T cells, and an increase in the percentage of Tregs ($CD4+CD25^{hi}Foxp3+$ T cells) was observed over time in MS patients treated with ublituximab (64), and the proportion of Tregs doubled baseline values at week 48 (66). Furthermore, there was a significant decrease in the ratio of Th1:Tregs, Th17:Tregs, and CD4+GM-CSF+:Tregs, suggesting a shift in the T cell profile towards anti-inflammatory phenotypes, plausibly able to effectively regulate potentially pathogenic CD4+ T cells in MS (66).

Inebilizumab

Inebilizumab treatment in NMOSD patients induced a robust depletion of CD20-positive B cells, that was maintained for at least 4 years (76). In a phase I study on 21 MS patients treated with different doses of inebilizumab, rapid B-cell depletion was observed at all dosing regimens except the 60-mg subcutaneously dose; the extent and duration of the B-cell depletion were dose-dependent, with most dose groups maintaining 90% depletion throughout the 24-week follow-up period (40). To our knowledge, no data are available so far on the effect of inebilizumab on T and B cell phenotypes or activation status in MS or NMOSD.

As an unwanted on-target effect, concentrations of IgG, IgM, IgA, and IgE decreased over time during treatment with inebilizumab. Most participants (76%) maintained normal IgG levels, and no significant associations were observed between the

lowest reported IgG categories and severe infections, although the relatively small number of the participants could have prevented from finding significant correlations (76). In a phase I study on MS patients, total Ig levels at week 24 showed a mean percentage decrease of 10.5% from baseline, rising to 15.0% at the 18-month follow-up (40). The reduction was greatest for IgM, but was observed in all the Ig subtypes, although the total Ig levels remained within the normal range in all the study patients, and no reduction in the tetanus titer was observed.

AHSCT

Substantial immunological changes, particularly affecting adaptive immunity, have been reported in patients undergoing AHSCT for autoimmune disorders, including major contributions from studies in people with MS. The topic of immune reconstitution following AHSCT in MS has been recently reviewed in detail (118). Among the most relevant effects that support the notion of "immune resetting" we highlight: the demonstration of thymic reactivation with regeneration of T cell receptor repertoire diversity (80); the demonstration of ablation of pre-treatment T cell repertoire in blood and CSF, and replacement with new T cells (83); and enhanced immune cell regulation (85). There is some evidence of regeneration of the B cell pool, with expansion of naïve B cell frequency after AHSCT (79), yet more research is needed to fill gaps in knowledge of the effects of AHSCT on the B cell compartment, which are potentially also relevant to the mechanism of action.

Clinical efficacy of immune-cell depleting Abs in MS

Relapses, disability and signs of focal inflammation at brain MRI are used, alone or in combination, to assess the effectiveness of DMTs in MS.

Clinical outcomes focus on relapses and disability. Relapses are defined as acute or sub-acute episodes of new or increasing neurological dysfunction followed by full or partial recovery, in the absence of fever or infection (119). The impact of a DMT on relapses is usually estimated using the following outcome measures: relapse-free survival (R-FS), i.e. cumulative proportion of subjects who have not yet experienced a relapse at a definite timepoint (120); and/or annualized relapse rate (ARR), defined as the number of relapses that occur during a specific timeframe, adjusted to a one-year period.

Disability is measured with the expanded disability status scale (EDSS), a non-linear scale ranging from 0 (absence of neurological signs and symptoms) to 10 (death due to MS) (121). Disability milestones are EDSS scores of 4.0 (limited walking ability, being the patient able to walk without aid or rest for more than 500 m), 6.0 (need for unilateral aid to walk for about 100 m without rest) and 7.0 (essential restriction to wheelchair). Confirmed disability worsening (CDW) is usually defined as an increase of at least 1.0 or 0.5 points if baseline EDSS was <5.5 or ≥5.5, respectively (or of 1.5 points if baseline EDSS was 0), confirmed at a subsequent neurological evaluation performed after 12 or 24 weeks. Disability outcomes are usually expressed as CDW-free survival (CDW-FS), and/or EDSS changes over a definite period of observation. More recently, confirmed improvement of disability (CDI) has been included as disability outcome in clinical trials. CDI is usually defined as a confirmed decrease in EDSS score of at least 1.0 or 0.5 points if baseline EDSS was <5.5 or ≥5.5, respectively.

MRI inflammatory activity is defined as the presence at brain MRI of gadolinium-enhancing lesions and/or new or enlarging T2 focal lesions compared with a reference scan (122). More complex radiological measures, such as brain atrophy, are also evaluated in recent trials, but are not yet routinely adopted in clinical setting due to the complexity of post-processing analyses required for their estimation (123).

No evidence of disease activity (NEDA-3) is a combined clinical and radiological outcome measure referring to the absence of all the following: relapses, EDSS worsening and MRI activity (as defined above) (124).

Figure 3 summarizes clinical efficacy of Ab-mediated cell depletion therapies and AHSCT on relapses (panel A), EDSS worsening (panel B) and clinical-radiological disease activity (NEDA-3; panel C) in patients affected by MS (data from randomized clinical trials -RCTs - and prospective randomized studies for Ab-mediated cell depletion therapies, and from prospective and retrospective cohort studies for AHSCT). The group DMTs represents the control arm of AHSCT in the MIST trial, and includes patients who received different treatments (interferons, glatiramer-acetate, dimethyl-fumarate, teriflunomide, fingolimod, natalizumab, rituximab, mitoxantrone, cyclophosphamide) "of higher efficacy or a different class than the therapy they were taking at the time of randomization" (125).

Reducing MS relapses

Alemtuzumab

In two (RCTs) the efficacy and safety of alemtuzumab were compared with interferon beta 1a (IFN) in people with RR-MS who were naïve to treatments (CARE-MS I) or had relapsed while taking IFN or glatiramer acetate (CARE-MS II) (94, 95). In both the trials, the patients were randomized, in a 2:1 ratio, to receive alemtuzumab (12 mg per day) infused intravenously on 5 days at baseline and 3 days at 12 months, or IFN (44 μg) given

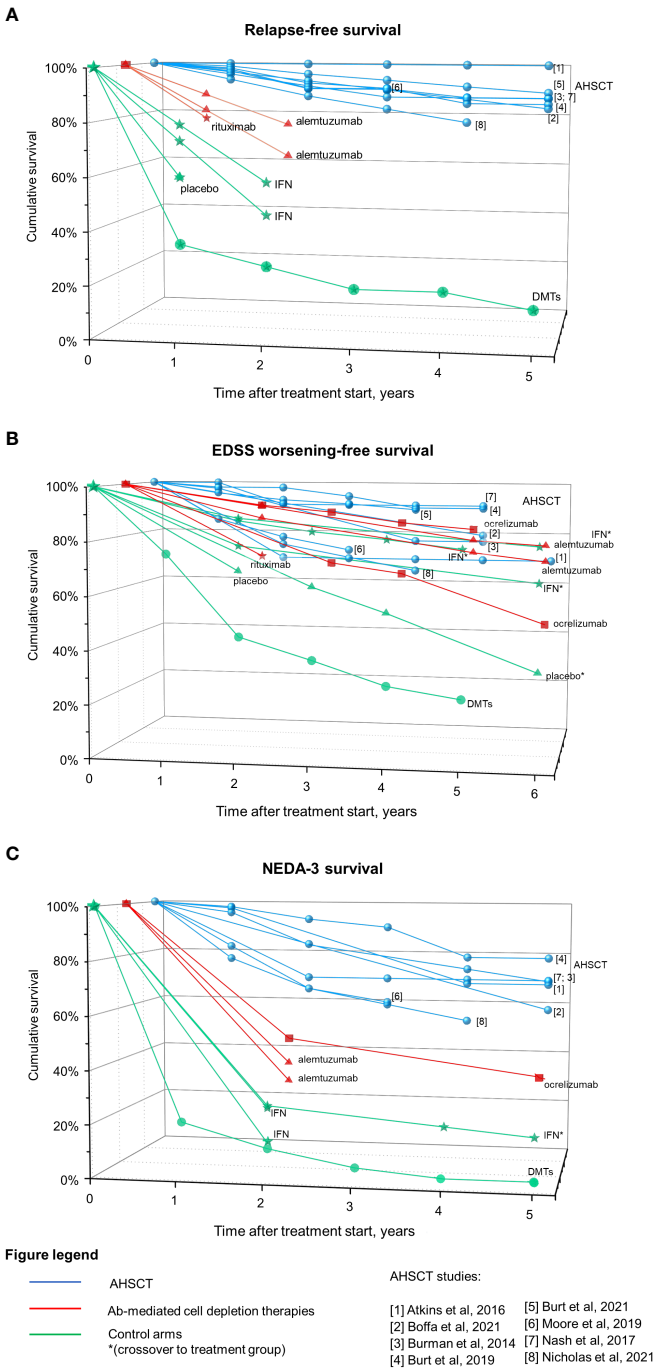

FIGURE 3
Efficacy on Ab-mediated cell depletion therapies and AHSCT on clinical and radiological measures of disease activity in MS. Data derived from AHSCT studies (blue), treatment arm of RCTs on Ab-mediated cell depletion therapies (red) and corresponding control arms (green) are reported as cumulative rates of survival free from relapses **(A)**, EDSS worsening **(B)**, and combined clinical-radiological disease activity (NEDA-3, **(C)**. Patients originally randomized to the control arm who were switched to the treatment under investigation during the OLE phase are marked with *. The control arm of the MIST trial on AHSCT is also depicted (DMTs), including patients who had failed DMTs prior to inclusion and received DMTs of higher efficacy or a different class than the therapy they were taking at the time of randomization. Differences in the characteristics of the patient populations included across trials (such as the selection of patients with highly active disease while on treatment and the lack of escalation in a subset of the cases for the DMTs group) could explain, at least in part, the fact that the DMTs group from the MIST trial performed lower than the placebo group of other trials.

subcutaneously three times per week after dose titration. CARE-MS II originally included an additional arm (alemtuzumab 24 mg) in which recruitment was prematurely closed after a protocol amendment, and the cases treated in this arm were excluded from primary analyses. Patients in the CARE-MS I were affected by early MS (inclusion criteria: naïve, disease duration up to 5 years and Expanded Disability Status Scale - EDSS - score up to 3.0), whereas those enrolled in the CARE-MS II were affected by a more advanced disease (inclusion criteria: disease duration up to 10 years and EDSS score up to 5.0). Occurrence of at least one relapse in the year before enrollment was required in both the studies. Primary analyses included 187 IFN-treated and 376 alemtuzumab-treated patients in the CARE-MS I, and 202 IFN-treated and 426 alemtuzumab-treated patients in the CARE-MS II trial. The mean EDSS score at baseline was 2.0 in CARE-MS I and 2.7 in CARE-MS II; the mean disease duration and age were 2.0 years and 33 years in CARE-MS I, 4.5 years and 35 years in CARE-MS II, respectively. At year 2, R-FS was significantly higher in the alemtuzumab group compared with the IFN group in both the trials ($p<0.0001$). For alemtuzumab-treated patients, R-FS was 77.6% (95% confidence interval, CI, 72.9 – 81.6) in CARE-MS I and 65.4% (95% CI 60.7 – 69.7) in CARE-MS II, compared with 58.7% (95% CI 51.1 – 65.5) and 46.7% (95% CI 39.5 – 53.5) for the IFN-treated patients in the two trials, respectively. Alemtuzumab reduced the risk of relapses compared to IFN by 54.9% in CARE-MS I and by 49.4% in CARE-MS II, being the yearly relapse rate on alemtuzumab treatment of 0.18 (95% CI 0.13 – 0.23) and 0.26 (95% CI 0.21 – 0.33), respectively.

Most of the alemtuzumab treated patients from the CARE-MS I and II trials were enrolled in a 4-year open-label extension (OLE) study. The results were provided as 3-year interim analyses for alemtuzumab treated patients in the core studies (defined as alemtuzumab-only group) (15, 126), and as a final 6-year report including also the outcomes of originally IFN-treated patients who switched to alemtuzumab at enrollment in the OLE (defined as IFN-alemtuzumab group) (127). During the OLE, alemtuzumab re-treatment due to disease activity (up to six courses in 0.3 – 1% of the cases) was received by 35.5% and 45.7% of MS patients enrolled in the core studies CARE-MS I and II, respectively treatment with other DMTs was administered in 2.6% of the patients from CARE-MS I and in 10.1% of those from CARE-MS II (127).

(ARR)remained low during the OLE, with a cumulative ARR over years 0-6 of 0.16 and 0.24 for the alemtuzumab-only groups from the core CARE-MS I and II, respectively (127). The proportion of MS patients free from relapses annually over years 3-6 was 84-89% in naïve (from CARE-MS I) and 79-87% in previously treated patients (from CARE-MS II) . As expected, a significant reduction in ARR compared to the core study was observed in the IFN-alemtuzumab groups, with a cumulative ARR in years 3-6 of 0.12 and 0.15 for patients from CARE-MS I and II, respectively.

Ocrelizumab

In two identical RCTs (OPERA I and OPERA II), people affected by relapsing MS (R-MS; PP-MS excluded) with active disease (defined as the presence of relapses over the previous 2 years) were randomized, in a 1:1 ratio, to receive intravenous ocrelizumab at a dose of 600 mg every 24 weeks or subcutaneous IFN at a dose of 44 μg three times weekly for 96 weeks (59). MS patients included in the analyses were 827 and 829 for the ocrelizumab and IFN arms, respectively. The mean age at enrolment was 37 years; the mean EDSS score at baseline was 2.8, and patients were naïve to treatment in most of the cases (71 – 75% across groups). The ARR on ocrelizumab treatment was 0.16 compared with 0.29 for IFN-treated patients, with a 46% and 47% lower rate with ocrelizumab in the OPERA I and II trials, respectively ($p<0.001$).

More than 94% of MS patients who completed the core OPERA I and II trials were enrolled in an OLE phase of 3 years, during which patients previously treated with ocrelizumab continued the treatment, whereas those treated with IFN switched to ocrelizumab 600 mg every 24 weeks (70). Through years 1-5, ARR remained low in MS patients receiving continuous ocrelizumab (ranging from 0.07 in year 5 to 0.14 over year 1), whereas in previously IFN-treated patients it was significantly reduced by 52% after switching to ocrelizumab (ARR 0.10 in year 3, and 0.07 in year 5). The difference in ARR was not significant between the two groups over years 3 to 5 ($p=0.8$, 0.97, and 0.7, respectively).

Ofatumumab

In the two identical RCTs ASCLEPIOS I and II, 1882 patients with active R-MS (PP-MS excluded) were randomized, in a 1:1 ratio, to receive ofatumumab at a dose of 20 mg subcutaneously every 4 weeks (after 20-mg loading doses at days 1, 7, and 14), or oral teriflunomide at a dose of 14 mg once daily, for up to 30 months (69). Patients were affected mostly by RR-MS (94% of the cases), with a mean age of 38 years and baseline EDSS of 3.0; on average, and 38-40% of the cases were naïve to treatment. Over a median follow-up of 1.6 years, ARR was 0.11 (95% CI 0.09 – 0.14) and 0.10 (95% CI 0.08 – 0.13) in the ofatumumab groups compared with 0.22 (95% CI 0.18 – 0.26) and 0.25 (95% CI 0.21 – 0.30) in the teriflunomide groups The relapse rate ratio was 0.49 (95% CI 0.37 – 0.65; $p<0.001$) and 0.42 (95% CI 0.31 – 0.56; $p<0.001$) for the ASCLEPIOS I and II trials, respectively. Analyzing pooled data from the two trials, R-FS at year 2 was 82.3% in ofatumumab-treated vs 69.2% in teriflunomide treated patients (128).

Long-term data on the safety (primary objectives) and effectiveness (secondary objectives) of ofatumumab will be provided by the ongoing open-label umbrella OLE study ALITHIOS, that enrolled 1701 R-MS patients who had previously participated in ofatumumab trials (phase 3 ASCLEPIOS, and phase 2 APOLITOS and APLIOS) (129).

Rituximab

In the phase 2 RCT HERMES, 104 patients affected by active RR-MS (i.e. with relapses over the previous year) were randomized in a 2:1 ratio to receive intravenous rituximab (1000 mg) or placebo on days 1 and 15, and followed up to week 48 (16). Mean age at inclusion was 39.6 (standard deviation - SD - 8.7) years in the rituximab and 41.5 (SD 8.5) years in the placebo arm, and median EDSS was 2.5 (range 0 -5) in both the arms; on average, 22% of the cases were naïve to treatment. The proportion of cases without gadolinium-enhancing lesions at baseline was unbalanced between groups, being 63.8% and 85.7% in the rituximab and placebo arms, respectively (p=0.02). The proportion of patients with relapses was reduced in the rituximab group compared with the placebo group both at weeks 24 (14.5% vs. 34.3%, p= 0.02) and 48 (20.3% vs. 40.0%, p=0.04), with an increased risk of relapse with placebo of 2.3 (90% CI 1.3 – 4.3) at week 24, and 1.9 (90% CI 1.1 - 3.2) at week 48. ARR was lower in the rituximab group compared with the placebo group at 24 weeks (0.37 vs. 0.84, p=0.04), but not at 48 weeks (0.37 vs. 0.72, p=0.08).

The efficacy of rituximab in PP-MS was explored in the phase 2/3 RCT OLYMPUS, where 439 people with PP-MS were randomized 2:1 to receive two doses (two weeks apart) of intravenous rituximab 1000 mg or placebo every 24 weeks through 96 weeks, for a total of 4 courses (57). The presence of active disease (i.e. relapses or MRI inflammatory activity) was not required as an inclusion criterion. The mean age at enrolment was 49.9 years (SD 8.9), the median EDSS score was 5.0 (range 2.0 – 6.5); 64.9% of the cases were naïve to treatment and gadolinium-enhancing lesions at baseline were observed in 24.5% of the cases. During the trial, relapses were observed in 2% of the patients in the rituximab group and 3.4% of those in the placebo group.

In an open label phase II trial, switching to rituximab from first line injectable therapies in clinically stable RR-MS patients induced a reduction in the number of gadolinium-enhancing lesion and in mean levels of CSF neurofilament light chains compared to the 3-months the run-in period (130), whereas another open label study randomizing 73 SP-MS patients to rituximab or glatiramer-acetate showed no differences between groups in relapse activity, nor in EDSS worsening (131).

The beneficial and adverse effects of rituximab as 'first choice' and as 'switching' therapy for adults with MS were recently explored in a Cochrane systematic review including 5 RCTs and 10 controlled non-randomized studies of interventions comparing rituximab with placebo or approved DMTs (132). Overall, 6,429 participants (13,143 affected by R-MS, and 3286 with progressive MS) were included; over one to two years study duration, rituximab was compared as 'first choice' with placebo (1 RCT) or other DMTs (1 non-randomized study of intervention), or as 'switching' against placebo (2 RCTs) or other DMTs (2 RCTs, 9 non-randomized studies of interventions. According to the Authors' conclusion, rituximab as 'first choice' and as 'switching' therapy may compare favourably with a wide range of approved DMTs for preventing relapses in R-MS, whereas its protective effect against disability worsening was uncertain. For progressive MS, the effect of rituximab could not be determined due to the limited information available.

Ublituximab

In a phase 2 study, 48 patient with active R-MS (i.e. with relapses in the previous 2 years) were randomized, in a 3:1 ratio, to receive intravenous ublituximab or placebo over a study period of 48 weeks (62). The administration of the drug was performed on days 1 (initial dose 150 mg), and 15, and then at week 24 (maintenance dose 450 or 600 mg). Patients were enrolled in six cohorts with different doses and rates of infusion, and those allocated in the placebo arm crossed over to receive ublituximab at day 28. The primary endpoint of the study was the proportion of ublituximab-treated patients with at least 95% peripheral CD19+ B cell depletion from baseline at week 4, whereas clinical and radiological outcomes of response to treatment were investigated as secondary or exploratory endpoints. The mean age at inclusion was 40 years (SD 10), mean EDSS was 2.44 (SD 1.36); 33% of the patients were naïve to treatment. R-FS (secondary endpoint) at week 48 was 93%, and the ARR on treatment (0.07) was reduced by 95% compared to the year prior to study entry (1.45).

Inebilizumab

In a phase 2/3 RCT trial (N-MOmentum), 230 people affected by (NMOSD) were randomized, in a 3:1 ratio, to receive intravenous inebilizumab (300 mg) or placebo on days 1 and 15 (38). After a randomized controlled period of 197 days, patients were offered participation in an OLE phase, where participants who were treated with inebilizumab during the core study received an additional dose of inebilizumab (300 mg on day 1), and those treated with placebo received two doses of inebilizumab (300 mg each) 15 days apart; subsequently, 300 mg inebilizumab was administered every 26 weeks. Enrolment in the N-MOmentum trial was prematurely halted in 2018 because of a clear demonstration of efficacy. History of NMOSD attack requiring rescue therapy in the previous two years was required for inclusion; at

enrolment, patients had on average 43 years and median EDSS was 3.5 (range 0 – 8.0) in the inebilizumab arm and 4.0 (range 1 – 8.0) in the placebo arm; 32-34% of the cases had not received any previous maintenance therapy. (AQP4) antibodies were positive in 92% - 93% of the cases. R-FS was higher in the inebilizumab group compared to the placebo group, being at day 197 86.7% and 59.9%, respectively (hazard ratio, HR 0.27, 95% CI 0.15 – 0.50; p<0.0001), and the treatment effect was similar in the AQP4-positive subgroup. At week 52 of the OLE, R-FS was 84% in the group receiving continuative treatment with inebilizumab and 51% in the placebo-inebilizumab group (133), and interim analyses of a subgroup of 75 AQP4-positive participants who had received inebilizumab for at least 4 years show an R-FS of 83%, and stabilization of the mean EDSS score in the overall cohort (76).

Inhibiting disability progression

Alemtuzumab

In treatment naïve RR-MS patients (CARE-MS I trial), 8.0% (95% CI 5.7 – 11.2) of MS patients in the alemtuzumab group showed 24-week (CDW) at year 2, being the difference not significant compared with the IFN arm (11.1%, 95% CI 7.3 – 16.7, p=0.22); accordingly, changes in EDSS score from baseline did not differ between the alemtuzumab and IFN groups (p=0.97) (94). At year 6 of the OLE, differences in disability outcomes were not significant, and (CDW-FS) compared with the core study baseline was 78% for the alemtuzumab-only group and 80% for the IFN-alemtuzumab group (127).

In previously treated RR-MS patients (CARE-MS II trial), the proportion of cases with CDW at year 2 was 12.7% (95% CI 9.9 – 16.3) in the alemtuzumab group, with a significant risk reduction of 42% compared with IFN (proportion with CDW: 21.1%, 95% CI 15.9 - 27.7, p=0.0084) (95 EDSS change from baseline was different between the two groups and EDSS score improved of mean -0.17 points in the alemtuzumab arm, whereas it worsened of mean 0.24 points in the IFN arm (p<0.0001). At year 6 of the OLE, CDW-FS was 72% in the alemtuzumab-only group and 67% in the IFN-alemtuzumab group, being the difference not significant (127).

At year 2 of the CARE-MS II trial, (CDI) was observed in 28.8% (95% CI 24.2 – 34.1) of the cases in the alemtuzumab group (mean change: -0.17 EDSS points) compared to 12.9% (95% CI 8.3 – 19.3) of those in the IFN group (mean change: +0.24 EDSS points), p=0.0002 (95). At year 6 of the OLE, EDSS improvement was detected in 24% of MS patients in the alemtuzumab-only group, and in 16% of those in the IFN-alemtuzumab group from CARE-MS II, being the cumulative proportion of patients with CDI significantly higher at each year from year 1 through year 6 (127). On the other hand, no significant differences were observed in CDI between the alemtuzumab-only and the IFN-alemtuzumab groups from the core CARE-MS I trial (21% vs 24%, respectively) (127).

Ocrelizumab

In the OPERA I and II trials, the cumulative proportion of patients with 24-week CDW at week 96 was 7.6% in MS patients treated with ocrelizumab compared to 12% in those receiving IFN, with HR of 0.60 (95% CI 0.43 – 0.84; p=0.003) (59). During the OLE, the proportion of patients with 24-week CDW from baseline remained significantly lower in MS patients receiving continuous ocrelizumab compared with those switching from IFN to ocrelizumab at the end of the core trials, being 16.1% vs 21.3% at the end of year 5 (p=0.014), with an HR for CDW during the OLE phase (i.e. with rebaselining at start of the OLE) of 1.06 (95% CI 0.8–1.41; p = 0.7) (Hauser et al., 2020).

Twelve-week CDI was reported in 20.7% and 15.6% of the pooled populations from OPERA I and II who received ocrelizumab and IFN, respectively, with a 33% higher rate of improvement with ocrelizumab, that was significant in the OPERA I trial only (p=0.02) (59). During the OLE, the proportion of MS patients with 24-week CDI was numerically higher in the continuous ocrelizumab-treated patients compared to switchers, although the difference reached significance only at year 5 (25.8% vs 20.6%; p = 0.046) (70). The HR for improvement was not significant in both the overall study period and the OLE only (i.e. after rebaselining at the start of the OLE period), being 1.31 (95% CI 0.96–1.78; p=0.06) and 0.89 (95% CI 0.61–1.31; p=0.6), respectively .

The effectiveness of ocrelizumab in PP-MS was explored in the RCT ORATORIO, where 732 PP-MS were randomized in a 2:1 ratio to receive intravenous ocrelizumab (600 mg) or placebo every 24 weeks for at least 120 weeks (60). The median age at inclusion was 46 years (range 18 – 56), and the median EDSS was 4.5 (range 2.5 – 7.0). Over a median trial duration of 2.9 years in the ocrelizumab group and 2.8 years in the placebo group, the proportion of patients with 24-week CDW was 29.6% and 35.7% in the ocrelizumab and placebo groups, respectively (HR 0.75; 95% CI 0.58 – 0.98, p=0.04; relative risk reduction: 25%). Ninety-five per cent of the participants who concluded the ORATORIO trial entered, after an extended controlled treatment period, the OLE phase where patients randomized to ocrelizumab during the core study continued to receive it (i.e. the continuous ocrelizumab group) and those who were randomly assigned to the placebo group were switched to ocrelizumab 600 mg every 24 weeks at the start of the OLE phase (i.e. the placebo to ocrelizumab group, equivalent to a delayed start cohort); interim results over at least 6.5 study years (48 weeks/year) of follow-up were provided as *post-hoc* analyses (71). The proportion of PP-MS patients showing 24-week CDW was lower in the continuous ocrelizumab group compared with the placebo to ocrelizumab group, being 51.7% vs 64.8% (difference 13.1%, 95% CI 4.9 – 21.3; p=0.0018) at 6.5 study

years of follow-up. Patients in the continuous ocrelizumab group had an HR for CDW of 0.72 (95% CI 0.58 – 0.89; p=0.0021) compared with the delayed start cohort, but there were no significant differences in EDSS accrual between the two groups when using the start of the OLE as baseline.

Ofatumumab

At year 2 in the ASCLEPIOS I and II trials, the cumulative proportion of cases with 24-week CDW was 8.1% in ofatumumab-treated patients compared with 12. 0% in teriflunomide-treated cases, with an HR of 0.68 (95% CI 0.50 to 0.92; p=0.01) (69). At the same timepoint, proportions of patients with CDI were similar between the two groups, being 11.0% in MS patients receiving ofatumumab and 8.1% in those receiving teriflunomide (HR 1.35; 95% CI 0.95 - 1.92; p=0.09).

Rituximab

In the OLYMPUS trial, the cumulative proportion of patients with 12-week CDW (primary endpoint) was 20.2% at week 48 and 30.2% at week 96 in rituximab-treated PP-MS, being similar to that observed in the placebo group (19.3% and 38.5% at the two time points, respectively, p=0.144) (57). Similarly, at week 96, the proportion of patients with 24-week CDW did not differ between the two arms (exploratory endpoint: 27.3% in the rituximab and 30.4% in the placebo group, p=0.59), nor did the mean EDSS change between baseline and last follow-up (0.33 and 0.45 in the rituximab and placebo arms, respectively, p=0.34). However, rituximab tended to delay the time to CDW compared with placebo, with HR of 0.77. Planned subgroup analyses of the primary endpoint according to baseline characteristics showed that age and presence of gadolinium-enhancing lesions were predictors for treatment effect: rituximab delayed time to CDW compared with placebo in treated patients aged <51 years (HR 0.52; p=0.010) or those with gadolinium-enhancing lesions at baseline MRI (HR 0.41; p=0.007); the presence of both these characteristics showed an additive predictive effect (HR 0.33, 95% CI 0.14 – 0.79; p=0.009).

Ublituximab

In a phase 2 study on patient with R-MS treated with ublituximab, 24-week CDW-FS (exploratory endpoint) was 92% at week 48, whereas 17% of the patients showed CDI at the same timepoint (62).

Inebilizumab

In the N-MOmentum trial, not confirmed EDSS score worsening from baseline at the last visit was observed in 16% of NMOSD patients treated with inebilizumab compared with 34% of those in the placebo arm, with OR 0.37 (95% CI 0.18 – 0.74; p=0.0049) (38). Prespecified subgroup analyses showed a consistently reduced risk of EDSS worsening in inebilizumab-treated participants compared with placebo regardless of the baseline EDSS score, number of previous attacks, or disease duration. Furthermore, *post-hoc* analyses confirmed a lower proportion of 12-week CDW in the inebilizumab group compared with the placebo group, being of 5.7% and 14.3%, respectively (HR 0.37; 95% CI 0.15 – 0.95; p=0.039) (134).

In the first year of the OLE, where all the patients received inebilizumab, the mean change in EDSS decreased in both originally placebo- and inebilizumab- treated cases (133).

Inhibiting MRI activity

Alemtuzumab

MRI inflammatory activity (new or enlarging T2 lesions and gadolinium-enhancing lesions) was lower in the alemtuzumab group compared to the IFN group in both the CARE-MS trials (94, 95). At year 2, the proportion of alemtuzumab-treated RR-MS patients who were free from new or enlarging T2 lesions ranged from 52% to 54% (vs 32 - 42% of IFN treated patients), being 91 to 93% of the patients free from gadolinium-enhancing lesions (vs 77 - 81% of IFN treated patients).

Cumulative MRI inflammatory activity-free survival (MRI-FS) over years 3-5 of the OLE was 53.8% and 48.6% in alemtuzumab-only patients from the CARE-MS I and II core trials, respectively (15, 126).

At year 6 of the OLE, MRI-FS was 66% - 70% in the alemtuzumab-only groups, and 67% - 71% in the IFN-alemtuzumab groups a significant reduction in MRI activity was observed in the IFN-alemtuzumab groups starting from year 3 of the OLE compared with the core studies (127).

Ocrelizumab

Ocrelizumab reduced the number of new or enlarging T2 lesions by 77% and 83% in the OPERA I and II trials, respectively (mean number of new or enlarging T2 lesions per T2-weighted MRI scan: 0.32 and 0.33 in the ocrelizumab groups compared with 1.41 and 1.90 in the IFN groups, p<0.001) (59). Most of the new or enlarging T2 lesions in the ocrelizumab groups were observed between baseline and week 24, with a reduction compared with IFN by 94-96% during the weeks 24 – 48, and by 97-98% during the weeks 48 to 96. The total mean number of gadolinium-enhancing lesions per T1-weighted MRI scan was 0.02 with ocrelizumab compared with 0.29 and 0.42 for IFN in the OPERA I and II trials, respectively, corresponding to a reduction in the ocrelizumab group by 94% and 95% (59). The proportion of R-MS patients without new or enlarging T2 lesions was 61.7% and 60.9% in the ocrelizumab groups, and 38.7% and 38% in the IFN groups (p<0.001), whereas the proportion of cases without gadolinium-enhancing lesions was 91.7% and 90.2% in the ocrelizumab groups and 69.8% and 63.9% in the IFN groups (p<0.001) (59).

In R-MS, continuous administration of ocrelizumab during the OLE maintained the near-complete suppression of MRI

disease activity seen in the core phase, with an unadjusted rate of total T1 gadolinium-enhancing lesions and of new or newly enlarged T2 lesions of 0.006 and 0.031 over year 5, respectively (70). Switching from IFN to ocrelizumab induced an almost complete and sustained suppression of MRI lesion disease activity from year 3 to 5, MRI lesion counts were similar to those observed in continuous ocrelizumab-treated patients during the OLE, except for new T2 lesions at year 3 (higher number in switcher compared with continuous ocrelizumab-treated).

Similar results were observed in PP-MS during the OLE phase of the ORATORIO trial, with persistent suppression of MRI inflammatory activity in patients receiving continuous ocrelizumab, and almost complete and sustained suppression of new MRI lesion disease activity throughout the OLE in those switching from IFN to ocrelizumab. No differences were observed in T1 gadolinium-enhancing and new or enlarging T2 lesion counts between the two groups, except for new or enlarging T2 lesions at two timepoints where lesion numbers were already very low (71).

Ofatumumab

The mean number of gadolinium-enhancing lesions per T1-weighted MRI scan was 0.01 and 0.03 with ofatumumab compared to 0.45 and 0.51 with teriflunomide in ASCLEPIOS I and II, respectively, corresponding to a relative reduction with ofatumumab by 97% and 94%, respectively (69). The mean numbers of new or enlarging lesions per year on T2-weighted MRI scans were 0.72 and 0.64 with ofatumumab, compared with 4.00 and 4.15 with teriflunomide in the two trials, corresponding to a reduction with ofatumumab by 82% and 85% ($p<0.001$) in ASCLEPIOS I and II trials, respectively.

In a *post-hoc* analysis of pooled data from the two trials, survival free from gadolinium-enhancing lesion activity over two years was 54.1% in ofatumumab compared with 27.5% in teriflunomide treated patients (128).

Rituximab

In RR-MS patients from the HERMES trial, rituximab reduced by 91% total gadolinium-enhancing lesion counts compared with placebo at each study week analysed, beginning at week 12 (primary endpoint), with a mean of 0.5 and 5.5 gadolinium-enhancing lesions in the rituximab and placebo groups, respectively ($p<0.001$) (16). The proportion of cases without new gadolinium-enhancing lesions was 84.8% with rituximab and 54.3% with placebo ($p<0.001$). As for T2 lesions, the reduction in the volume of T2 lesion load from baseline to weeks 24 and 36 was greater in MS patients who received rituximab than in those who received placebo ($p=0.008$ and 0.004, respectively).

In the OLYMPUS trial, rituximab significantly reduced the median increase in T2 lesion volume compared with placebo from baseline to week 96, being 302 mm^3 and 809 mm^3 in the two groups, respectively (57).

Ublituximab

In R-MS, ublituximab suppressed the occurrence of gadolinium-enhancing lesions at weeks 24 and 48 of a phase 2 study (secondary endpoint), with a 100% reduction from baseline (mean number of gadolinium-enhancing lesions: 3.63, SD 7.80; $p=0.003$) (62). Occurrence of new or enlarging T2 lesions was observed in 15% of the cases between baseline and week 24, and in 2% of the cases between weeks 24 and 48, with a mean number of 0.20 (SD 0.43) and 0.04 (SD 0.29) new lesions, respectively. The MRI-FS was 83% at week 48.

Inebilizumab

In patients with NMOSD, inebilizumab significantly reduced compared with placebo the cumulative number of active MRI lesions (i.e. gadolinium-enhancing, or new or enlarging T2 lesions), being the mean number 1.6 (SD 1.0) and 2.3 (SD 1.3), respectively (relative ratio: 0.57, 95% CI 0.39 – 0.83) (38).

Reaching status of "no evidence of clinical and radiological disease activity"

Alemtuzumab

At year 2, the proportion of RR-MS patients showing NEDA (NEDA survival, NEDA-S) was 39% and 32% in alemtuzumab-treated patients from the CARE-MS I and II trials, respectively, compared with 27% and 14% of the IFN treated patients from the same trials (94, 95). These differences corresponded to an odds ratio (OR) favouring alemtuzumab over IFN of 1.75 (95% CI 1.17 – 2.61) for the CARE-MS I and of 3.03 (95% CI 1.89 – 4.86) for the CARE-MS II trial

Cumulative NEDA-S over years 3-5 of the extension was 39.5% and 27% in alemtuzumab-only patients from the CARE-MS I and II core trials, respectively (15, 126).

Ocrelizumab

In R-MS patients treated with ocrelizumab, NEDA-S was 47.9% and 47.5% compared with 29.2% and 25.1% of IFN-treated patients for the two OPERA trials ($p<0.001$), but these findings were considered to be nonconfirmatory as a result of failure of the hierarchical analysis (59). Data from the OLE showed a higher proportion of patients with NEDA in the ocrelizumab compared with the IFN group during both the core OPERA I-II studies (at year 2: 48.5% vs 27.8%; $p < 0.001$) and the overall observation period (at year 5: 35.7% vs 19.0%; $p < 0.001$; relative increase with ocrelizumab: 88%); the difference between groups was significant also considering the OLE phase only (65.4% vs 55.1%; $p<0.001$) (70).

Ofatumumab

In a *post-hoc* analysis of pooled data from the ASCLEPIOS I-II trials, the proportion of R-MS patients achieving NEDA at month 12 was 47% in the ofatumumab group compared with 24.5% in the teriflunomide group (OR 3.36, 95% CI 2.67 - 4.21; p<0.001) (128). From month 12 to 24, proportions of patients with NEDA were 87.8% and 48.2% in the ofatumumab and teriflunomide groups, respectively (OR 8.09, 95% CI 6.26 - 10.45; p<0.001).

Ublituximab

At week 48, 74% of the R-MS patients treated with ublituximab achieved NEDA (exploratory endpoint) (62).

Adverse events of Ab-mediated cell depletion therapies

Administration-associated reactions (most commonly headache, rash, pruritus, throat irritation nausea and pyrexia) were the most frequent adverse events in MS patients receiving Ab-mediated cell depletion therapies, and were reported in 90% of the alemtuzumab-treated patients (being serious in 3% of the cases) (94, 95), in 34 - 40% of ocrelizumab-treated patients (being mild to moderate in 98% of the cases) (59, 60), and 67-78% MS patients treated with rituximab (mild-moderate in 93% of the cases) (16, 57), with decreasing rate and severity over subsequent administrations. Systemic and injection-site associated reactions were reported in 20% and 11%, respectively, of R-MS patients treated with ofatumumab in the ASCLEPIOS I-II trials, mostly occurring at the first injection and being severe in 0.2% of the cases (69). Fifty per cent of R-MS patients receiving ublituximab experienced infusion-related adverse events, mostly on the first infusion day and all mild to moderate in severity (62). The incidence of infusion-associated reactions was similar in NMOSD patients receiving inebilizumab or placebo (9% and 11%, respectively) in the N-MOmentum trial (38).

Infections (most commonly upper respiratory, urinary tract and herpetic) were reported in 67% and 77% of the patients treated in the CARE-MS I and II trials, respectively, and were serious in 2-4% of the cases, but no life-threatening or fatal events were observed nor events requiring treatment discontinuation (94, 95). Incidence of infections peaked at year 1 after initiating treatment (60%), with a cumulative exposure-adjusted incidence rate of 8 and 10 events per 100 patients-years during years 0-2 and 3-6, respectively; serious infection incidence did not exceed 1.8% throughout the OLE up to year 6 (127).

Infections were observed in 57-60% of R-MS and 70% of PP-MS patients treated in the OPERA I-II and ORATORIO trials, respectively (59, 60). Upper respiratory and urinary tract infection and nasopharyngitis were the most common, with severe events in 1.3% of the RR-MS and 6% of the PP-MS treated patients; herpesvirus-associated infections were reported in 5-6% of the cases, mostly mild to moderate in severity. During the OLE of the OPERA trials, the rate of infections in R-MS per 100 patient-years was 75, and serious events occurred at a rate of 1.5 per 100 patient-years over the 5-year period (70). In PP-MS patients from the ORATORIO OLE, the rate of infections per 100 patient-years was 73, consistent with the rate observed in both the ocrelizumab-treated and placebo groups from the core trial the rate of serious infection was 4.13 per 100 patient-years, similar to that of the placebo group in the core trial (71).

A reduction in serum Ig levels was observed over the OLE in ocrelizumab-treated patients, and the proportion of MS patients showing levels below the lower limit of normalranged from 5% for IgG and IgA to 30% for IgM (70, 71). Serious infections following episodes of a drop in Ig concentrations below normal limits were rare and most resolved with standard treatment (67).

Infections were reported in 52% of MS patients receiving ofatumumab (mostly nasopharyngitis, upper respiratory and urinary tract infection) and were serious in 2.5% of the cases; herpesvirus associated infections were observed in 4-9% of the patients, being all mild or moderate (69).

The incidence rate of infections was similar between rituximab (68-70%) and placebo-treated (65-71%) patients from the HERMES and OLYMPUS trials, but urinary tract infections and sinusitis were more frequent among rituximab recipients; infection-associated serious adverse events were reported in 3-4.5% of the cases (16, 57).

A recently published Cochrane systematic review reported uncertain about the effect of rituximab on serious adverse events, as these were relatively rare in patients with MS, and they were not well reported in studies; an increased risk of common infections with rituximab was reported, but absolute risk was considered to be small (132).

The incidence of infection was reported to be similar in inebilizumab-treated compared with placebo-treated participants in the N-MOmentum trial, being urinary tract infection (11 vs 9%), more frequent with inebilizumab (38).

Secondary autoimmunity was observed following alemtuzumab treatment, and the more frequent events observed were thyroiditis (peak of incidence at year 3: 16%; incidence of serious events <3.5%/year), autoimmune blood and lymphatic system disorders (16-18%, serious in 1-3%; mostly represented by autoimmune thrombocytopenia with annual incidence from 0.1% to 1.1%) and immune-mediated nephropathy (94, 95, 127).

Malignancies were reported in 0.5 – 2% of mAbs-treated patients across core studies (60, 69, 70, 127), and no evidence of

increased risk compared to demographically matched epidemiological studies was provided by OLE phases (71).

Future developments

Ab-mediated immune cell depletion is now standard in the therapeutic armamentarium to treat people with MS, and the number and variety of clinically applicable Ab-based cell depleting treatment platforms continues to grow. New developments include approaches that allow Abs to pass the blood brain barrier for more effective depletion of pathogenic immune cells within the central nervous system. The transferrin receptor and the insulin receptor expressed by endothelial cells facilitate receptor-mediated transport through the blood brain barrier and treatment platforms that shuttle immune-cell depleting Abs through these natural brain portals are currently being developed (135, 136).

While rare but serious side effects restricted the use of alemtuzumab, the first immune cell-depleting Ab approved for MS therapy, CD20-targeting B cell-depletion therapies are generally well tolerated and show a favorable safety profile. These therapies were originally developed as a method of eliminating cancerous B cells, and new and emerging cell-depletion approaches in MS have been adopted from protocols used to treat cancer patients. These approaches include targeting of CD19 to affect a wider array of B cells including plasma blasts or CD38, additionally expressed on antibody-producing short- and long-lived plasma cells. Daratumumab, an anti-CD38 mAb initially developed to target tumoral plasma cells in multiple myeloma (137) is also effective in inhibiting clinical activity of antibody-mediated autoimmune diseases, such as autoimmune cytopenia following hematopoietic stem cell transplantation (138) or systemic lupus erythematosus (SLE) (139). The B cell maturation antigen (BCMA) or CD269 is preferentially by mature B lymphocytes, with minimal expression in hematopoietic stem cells or nonhematopoietic tissue, and is essential for the survival of long-lived bone marrow plasma cells, but not overall B-cell homeostasis (140). Anti-BCMA therapies currently being evaluated in clinical trials in patients with multiple myeloma include bispecific Ab constructs, which facilitate cell-to-cell interactions between malignant plasma cells and cytotoxic T cells. Whether plasma cell-depleting therapies show beneficial effects for patients with MS remains to be demonstrated. However, both of the aforementioned molecules, CD38 and BCMA, are attractive targets to deplete long-lived plasma cells in antibody-driven neurological diseases such as NMOSD or antibody-mediated autoimmune encephalitides. T cells genetically engineered to express Ab-based chimeric antigen receptors (CARs) can induce impressive immune responses and achieve remarkable clinical efficacy in patients with certain haematological malignancies. Adoptive transfer of autologous CD19-targeted CAR T cells was among the earliest CAR T cell therapies used in successful clinical trials and the first to gain FDA approval (141). CD19-Targeted CAR T Cells were also reported to induce rapid clinical diseases remission in a patient with difficult to treat SLE (142). The success of Ab-based B cell-depleting therapies in MS suggest that CAR T-cell therapies targeting B-cell antigens should be explored for their potential therapeutic benefit in patients with MS who otherwise have limited treatment options due to high disease activity or poor response to standard treatments. A proportion of MS patients estimated in 4-14% (according to the definition used) can be considered affected by “aggressive MS”, bearing high risk of unfavorable outcomes (143). Although disease activity is controlled by high efficacy DMTs in most of the patients, a not negligible proportion of the cases fails to respond to treatment: as an example, 35% of patients treated with alemtuzumab relapsed by year 2 in the CARE-MS II trial, and 16% of the ocrelizumab-treated patients from the OPERA I-II trials progressed by year 5. The proportion of treatment failure achieves more than 50% of the treated cases when considering NEDA-3 (e.g. 52% for ocrelizumab and 68% for alemtuzumab at year 2) (59, 95). Whether the potential of these new treatment platforms for changing adaptive immune features is superior to currently approved cell-depleting therapies remains to be demonstrated.

During the last two decades the clinical potential of Ab-mediated cell depletion therapy has materialized into therapies that benefit people with MS. With dedicated attention to basic, translational, and clinical research, even more effective, and safe cell-depletion treatment strategies will be developed and likely soon be translated into the clinic.

Author contributions

AM, PM, and JL contributed to the conception or design of the work, data analysis and interpretation, drafting and critical revision of the article. All authors contributed to the article and approved the submitted version.

Funding

Work was supported by the German Research Foundation (DFG, SFB-TRR129, to JL)

Conflict of interest

The handling editor FN declared past co-authorships with the author JL.

The remaining authors declare that the research was conducted in the absence of any commercial or financial relationships that could be construed as a potential conflict of interest.

Publisher's note

References

1. Koch-Henriksen N, Magyari M. Apparent changes in the epidemiology and severity of multiple sclerosis. Nature reviews. *Neurology* (2021) 17(11):676–88. doi: 10.1038/s41582-021-00556-y

2. Moutsianas L, Agarwala V, Fuchsberger C, Flannick J, Rivas MA, Gaulton KJ, et al. The power of gene-based rare variant methods to detect disease-associated variation and test hypotheses about complex disease. *PloS Genet* (2015) 11(4): e1005165. doi: 10.1371/journal.pgen.1005165

3. Lucchinetti C, Bruck W, Parisi J, Scheithauer B, Rodriguez M, Lassmann H. Heterogeneity of multiple sclerosis lesions: Implications for the pathogenesis of demyelination. *Ann Neurol* (2000) 47(6):707–17. doi: 10.1002/1531-8249(200006)47:6<707::AID-ANA3>3.0.CO;2-Q

4. Babbe H, Roers A, Waisman A, Lassmann H, Goebels N, Hohlfeld R, et al. Clonal expansions of CD8+ T cells dominate the T cell infiltrate in active multiple sclerosis lesions as shown by micromanipulation and single cell polymerase chain reaction. *J Exp Med* (2000) 192(3):393–404. doi: 10.1084/jem.192.3.393

5. Palanichamy A, Jahn S, Nickles D, Derstine M, Abounasr A, Hauser SL, et al. Rituximab efficiently depletes increased CD20-expressing T cells in multiple sclerosis patients. *J Immunol* (2014) 193(2):580–6. doi: 10.4049/jimmunol.1400118

6. Obermeier B, Mentele R, Malotka J, Kellermann J, Kümpfel T, Wekerle H, et al. Matching of oligoclonal immunoglobulin transcriptomes and proteomes of cerebrospinal fluid in multiple sclerosis. *Nat Med* (2008) 14(6):688–93. doi: 10.1038/nm1714

7. Attfield KE, Jensen LT, Kaufmann M, Friese MA, Fugger L. The immunology of multiple sclerosis. *Nat Rev Immunol* (2022), 1–17. doi: 10.1038/s41577-022-00718-z

8. Wekerle H, Flügel A, Fugger L, Schett G, Serreze D. Autoimmunity's next top models. *Nat Med* (2012) 18(1):66–70. doi: 10.1038/nm.2635

9. Jarius S, Paul F, Weinshenker BG, Levy M, Kim HJ, Wildemann B. Neuromyelitis optica. *Nat Rev Dis Primers* (2020) 6(1):1–32. doi: 10.1038/s41572-020-0214-9

10. Faissner S, Gold R. Oral therapies for multiple sclerosis. *Cold Spring Harb Perspect Med* (2019) 9(1). doi: 10.1101/cshperspect.a032011

11. Rudick R, Polman C, Clifford D, Miller D, Steinman L. Natalizumab: bench to bedside and beyond. *JAMA Neurol* (2013) 70(2):172–82. doi: 10.1001/jamaneurol.2013.598

12. Muraro PA, Martin R, Mancardi GL, Nicholas R, Sormani MP, Saccardi R. Autologous haematopoietic stem cell transplantation for treatment of multiple sclerosis. *Nat Rev Neurol* (2017) 13(7):391–405. doi: 10.1038/nrneurol.2017.81

13. Rodig SJ, Abramson JS, Pinkus GS, Treon SP, Dorfman DM, Dong HY, et al. Heterogeneous CD52 expression among hematologic neoplasms: Implications for the use of alemtuzumab (CAMPATH-1H). *Clin Cancer Res* (2006) 12(23):7174–9. doi: 10.1158/1078-0432.CCR-06-1275

14. Tuohy O, Costelloe L, Hill-Cawthorne G, Bjornson I, Harding K, Robertson N, et al. Alemtuzumab treatment of multiple sclerosis: Long-term safety and efficacy. *J Neurolo Neurosurg Psychiatry* (2015) 86(2):208–15. doi: 10.1136/jnnp-2014-307721

15. Havrdova E, Arnold DL, Cohen JA, Hartung HP, Fox EJ, Giovannoni G, et al. Alemtuzumab CARE-MS I 5-year follow-up: Durable efficacy in the absence of continuous MS therapy. *Neurology* (2017) 89(11):1107–16. doi: 10.1212/WNL.0000000000004313

16. Hauser SL, Waubant E, Arnold DL, Vollmer T, Antel J, Fox RJ, et al. B-cell depletion with rituximab in relapsing-remitting multiple sclerosis. *N Engl J Med* (2008) 358(7):676–88. doi: 10.1056/NEJMoa0706383

17. von Essen MR, Ammitzbøll C, Hansen RH, Petersen ER, McWilliam O, Marquart HV, et al. Proinflammatory CD20+ T cells in the pathogenesis of multiple sclerosis. *Brain* (2019) 142(1):120–32. doi: 10.1093/brain/awy301

18. Cragg MS, Morgan SM, Chan HC, Morgan BP, Filatov A, Johnson PW, et al. Complement-mediated lysis by anti-CD20 mAb correlates with segregation into lipid rafts. *Blood J Am Soc Hematol* (2003) 101(3):1045–52. doi: 10.1182/blood-2002-06-1761

19. Herter S, Herting F, Mundigl O, Waldhauer I, Weinzierl T, Fauti T, et al. Preclinical activity of the type II CD20 antibody GA101 (obinutuzumab) compared with rituximab and ofatumumab *in vitro* and in xenograft models. *Mol Cancer Ther* (2013) 12(10):2031–42. doi: 10.1158/1535-7163.MCT-12-1182

20. Diebolder CA, Beurskens FJ, De Jong RN, Koning RI, Strumane K, Lindorfer MA, et al. Complement is activated by IgG hexamers assembled at the cell surface. *Science* (2014) 343(6176):1260–3. doi: 10.1126/science.1248943

21. Ugurlar D, Howes SC, de Kreuk B-J, Koning RI, de Jong RN, Beurskens FJ, et al. Structures of C1-IgG1 provide insights into how danger pattern recognition activates complement. *Science* (2018) 359(6377:794–7. doi: 10.1126/science.aao4988

22. Alduaij W, Ivanov A, Honeychurch J, Cheadle EJ, Potluri S, Lim SH, et al. Novel type II anti-CD20 monoclonal antibody (GA101) evokes homotypic adhesion and actin-dependent, lysosome-mediated cell death in b-cell malignancies. *Blood J Am Soc Hematol* (2011) 117(17):4519–29. doi: 10.1182/blood-2010-07-296913

23. Reddy V, Klein C, Isenberg DA, Glennie MJ, Cambridge G, Cragg MS, et al. Obinutuzumab induces superior b-cell cytotoxicity to rituximab in rheumatoid arthritis and systemic lupus erythematosus patient samples. *Rheumatology* (2017) 56(7):1227–37. doi: 10.1093/rheumatology/kex067

24. Teeling JL, French RR, Cragg MS, van den Brakel J, Pluyter M, Huang H, et al. Characterization of new human CD20 monoclonal antibodies with potent cytolytic activity against non-Hodgkin lymphomas. *Blood* (2004) 104(6):1793–800. doi: 10.1182/blood-2004-01-0039

25. Teeling JL, Mackus WJ, Wiegman LJ, van den Brakel JH, Beers SA, French RR, et al. The biological activity of human CD20 monoclonal antibodies is linked to unique epitopes on CD20. *J Immunol* (2006) 177(1):362–71. doi: 10.4049/jimmunol.177.1.362

26. Li B, Shi S, Qian W, Zhao L, Zhang D, Hou S, et al. Development of novel tetravalent anti-CD20 antibodies with potent antitumor activity. *Cancer Res* (2008) 68(7):2400–8. doi: 10.1158/0008-5472.CAN-07-6663

27. Bondza S, Marosan A, Kara S, Lösing J, Peipp M, Nimmerjahn F, et al. Complement-dependent activity of CD20-specific IgG correlates with bivalent antigen binding and C1q binding strength. *Front Immunol* (2021) 11:3343. doi: 10.3389/fimmu.2020.609941

28. Lux A, Seeling M, Baerenwaldt A, Lehmann B, Schwab I, Repp R, et al. A humanized mouse identifies the bone marrow as a niche with low therapeutic IgG activity. *Cell Rep* (2014) 7(1):236–48. doi: 10.1016/j.celrep.2014.02.041

29. Biburger M, Lux A, Nimmerjahn F. How immunoglobulin G antibodies kill target cells: revisiting an old paradigm. *Adv Immunol* (2014) 124:67–94. doi: 10.1016/B978-0-12-800147-9.00003-0

30. Gordan S, Albert H, Danzer H, Lux A, Biburger M, Nimmerjahn F. The immunological organ environment dictates the molecular and cellular pathways of cytotoxic antibody activity. *Cell Rep* (2019) 29(10):3033–3046. e3034. doi: 10.1016/j.celrep.2019.10.111

31. Shields RL, Lai J, Keck R, O'Connell LY, Hong K, Meng YG, et al. Lack of fucose on human IgG1 n-linked oligosaccharide improves binding to human FcγRIII and antibody-dependent cellular toxicity. *J Biol Chem* (2002) 277(30):26733–40. doi: 10.1074/jbc.M202069200

32. Li T, DiLillo DJ, Bournazos S, Giddens JP, Ravetch JV, Wang LX. Modulating IgG effector function by fc glycan engineering. *Proc Natl Acad Sci U.S.A.* (2017) 114(13):3485–90. doi: 10.1073/pnas.1702173114

33. Golay J, Da Roit F, Bologna L, Ferrara C, Leusen JH, Rambaldi A, et al. Glycoengineered CD20 antibody obinutuzumab activates neutrophils and mediates phagocytosis through CD16B more efficiently than rituximab. *Blood J Am Soc Hematol* (2013) 122(20):3482–91. doi: 10.1182/blood-2013-05-504043

34. Herter S, Birk MC, Klein C, Gerdes C, Umana P, Bacac M. Glycoengineering of therapeutic antibodies enhances monocyte/macrophage-mediated phagocytosis and cytotoxicity. *J Immunol* (2014) 192(5):2252–60. doi: 10.4049/jimmunol.1301249

35. Babiker HM, Glode AE, Cooke LS, Mahadevan D. Ublituximab for the treatment of CD20 positive b-cell malignancies. *Expert Opin Investig Drugs* (2018) 27(4):407–12. doi: 10.1080/13543784.2018.1459560

36. Garff-Tavernier L, Herbi L, De Romeuf C, Nguyen-Khac F, Davi F, Grelier A, et al. Antibody-dependent cellular cytotoxicity of the optimized anti-CD20 monoclonal antibody ublituximab on chronic lymphocytic

leukemia cells with the 17p deletion. *Leukemia* (2014) 28(1):230–3. doi: 10.1038/leu.2013.240

37. Steinman L, Fox E, Hartung H-P, Alvarez E, Qian P, Wray S, et al. Efficacy and safety of ublituximab versus teriflunomide in relapsing multiple sclerosis: Results of the phase 3 ULTIMATE I and II trial, (4494). *Neurology*, AAN enterprises. (2021) 96 (15 Supplement):4494. doi: 10.55788/b70402f6

38. Cree BA, Bennett JL, Kim HJ, Weinshenker BG, Pittock SJ, Wingerchuk DM, et al. Inebilizumab for the treatment of neuromyelitis optica spectrum disorder (N-MOmentum): A double-blind, randomised placebo-controlled phase 2/3 trial. *Lancet* (2019) 394(10206):1352–63. doi: 10.1016/S0140-6736(19)31817-3

39. *Clinicaltrials.gov. n-MOmentum: A clinical research study of inebilizumab in neuromyelitis optica spectrum disorders*. Available at: https://www.clinicaltrials.gov/ct2/show/NCT02200770.

40. Common Terminology Criteria for Adverse Events (CTCAE), Agius MA, Klodowska-Duda G, Maciejowski M, Potemkowski A, Li J, et al. Safety and tolerability of inebilizumab (MEDI-551), an anti-CD19 monoclonal antibody, in patients with relapsing forms of multiple sclerosis: Results from a phase 1 randomised, placebo-controlled, escalating intravenous and subcutaneous dose study. *Multiple Scler J* (2019) 25(2):235–45. doi: 10.1177/1352458517740641

41. Jones JL, Phuah C-L, Cox AL, Thompson SA, Ban M, Shawcross J, et al. IL-21 drives secondary autoimmunity in patients with multiple sclerosis, following therapeutic lymphocyte depletion with alemtuzumab (Campath-1H). *J Clin Invest* (2009) 119(7):2052–61. doi: 10.1172/JCI37878

42. Baker D, Herrod SS, Alvarez-Gonzalez C, Giovannoni G, Schmierer K. Interpreting lymphocyte reconstitution data from the pivotal phase 3 trials of alemtuzumab. *JAMA Neurol* (2017) 74(8):961–9. doi: 10.1001/jamaneurol.2017.0676

43. Hilger C, Riedhammer C, Orsó E, Weissert R. Effects of alemtuzumab on (Auto)antigen-specific immune responses. *Front Immunol* (2020) 11. doi: 10.3389/fimmu.2020.563645

44. Hill-Cawthorne GA, Button T, Tuohy O, Jones JL, May K, Somerfield J, et al. Long term lymphocyte reconstitution after alemtuzumab treatment of multiple sclerosis. *J Neurolo Neurosurg Psychiatry* (2012) 83(3):298–304. doi: 10.1136/jnnp-2011-300826

45. Zhang X, Tao Y, Chopra M, Ahn M, Marcus KL, Choudhary N, et al. Differential reconstitution of T cell subsets following immunodepleting treatment with alemtuzumab (Anti-CD52 monoclonal antibody) in patients with relapsing–remitting multiple sclerosis. *J Immunol* (2013) 191(12):5867–74. doi: 10.4049/jimmunol.1301926

46. De Mercanti S, Rolla S, Cucci A, Bardina V, Cocco E, Vladic A, et al. Alemtuzumab long-term immunologic effect: Treg suppressor function increases up to 24 months. *Neurol Neuroimmunol Neuroinflamm* (2016) 3(1). doi: 10.1212/NXI.0000000000000194

47. Kim Y, Kim G, Shin H-J, Hyun J-W, Kim S-H, Lee E, et al. Restoration of regulatory b cell deficiency following alemtuzumab therapy in patients with relapsing multiple sclerosis. *J Neuroinflamm* (2018) 15(1):1–10. doi: 10.1186/s12974-018-1334-y

48. Haas J, Würthwein C, Korporal-Kuhnke M, Viehoever A, Jarius S, Ruck T, et al. Alemtuzumab in multiple sclerosis: Short- and long-term effects of immunodepletion on the peripheral treg compartment. *Front Immunol* (2019) 10. doi: 10.3389/fimmu.2019.01204

49. Gilmore W, Lund BT, Li P, Levy AM, Kelland EE, Akbari O, et al. Repopulation of T, b, and NK cells following alemtuzumab treatment in relapsing-remitting multiple sclerosis. *J Neuroinflamm* (2020) 17(1):1–21. doi: 10.1186/s12974-020-01847-9

50. Kashani N, Kelland EE, Vajdi B, Anderson LM, Gilmore W, Lund BT. Immune regulatory cell bias following alemtuzumab treatment in relapsing-remitting multiple sclerosis. *Front Immunol* (2021) 12. doi: 10.3389/fimmu.2021.706278

51. Jones JL, Thompson SA, Loh P, Davies JL, Tuohy OC, Curry AJ, et al. Human autoimmunity after lymphocyte depletion is caused by homeostatic T-cell proliferation. *Proc Natl Acad Sci* (2013) 110(50):20200–5. doi: 10.1073/pnas.1313654110

52. Cox AL, Thompson SA, Jones JL, Robertson VH, Hale G, Waldmann H, et al. Lymphocyte homeostasis following therapeutic lymphocyte depletion in multiple sclerosis. *Eur J Immunol* (2005) 35(11):3332–42. doi: 10.1002/eji.200535075

53. Barton J, Hardy TA, Riminton S, Reddel SW, Barnett Y, Coles A, et al. Tumefactive demyelination following treatment for relapsing multiple sclerosis with alemtuzumab. *Neurology* (2017) 88(10):1004–6. doi: 10.1212/WNL.0000000000003694

54. Haghikia A, Dendrou CA, Schneider R, Grüter T, Postert T, Matzke M, et al. Severe b-cell-mediated CNS disease secondary to alemtuzumab therapy. *Lancet Neurol* (2017) 16(2):104–6. doi: 10.1016/S1474-4422(16)30382-9

55. Wehrum T, Beume L-A, Stich O, Mader I, Mäurer M, Czaplinski A, et al. Activation of disease during therapy with alemtuzumab in 3 patients with multiple sclerosis. *Neurology* (2018) 90(7):e601–5. doi: 10.1212/WNL.0000000000004950

56. Ruck T, Pfeuffer S, Schulte-Mecklenbeck A, Gross CC, Lindner M, Metze D, et al. Vitiligo after alemtuzumab treatment: Secondary autoimmunity is not all about b cells. *Neurology* (2018) 91(24):e2233–7. doi: 10.1212/WNL.0000000000006648

57. Hawker K, O'Connor P, Freedman MS, Calabresi PA, Antel J, Simon J, et al. Rituximab in patients with primary progressive multiple sclerosis: Results of a randomized double-blind placebo-controlled multicenter trial. *Ann Neurol* (2009) 66(4):460–71. doi: 10.1002/ana.21867

58. Kim S-H, Huh S-Y, Lee SJ, Joung A, Kim HJ. A 5-year follow-up of rituximab treatment in patients with neuromyelitis optica spectrum disorder. *JAMA Neurol* (2013) 70(9):1110–7. doi: 10.1001/jamaneurol.2013.3071

59. Hauser SL, Bar-Or A, Comi G, Giovannoni G, Hartung HP, Hemmer B, et al. Ocrelizumab versus interferon beta-1a in relapsing multiple sclerosis. *N Engl J Med* (2017) 376(3):221–34. doi: 10.1056/NEJMoa1601277

60. Montalban X, Hauser SL, Kappos L, Arnold DL, Bar-Or A, Comi G, et al. Ocrelizumab versus placebo in primary progressive multiple sclerosis. *N Engl J Med* (2017) 376(3):209–20. doi: 10.1056/NEJMoa1606468

61. Bar-Or A, Grove RA, Austin DJ, Tolson JM, VanMeter SA, Lewis EW, et al. Subcutaneous ofatumumab in patients with relapsing-remitting multiple sclerosis: The MIRROR study. *Neurology* (2018) 90(20):e1805–14. doi: 10.1212/WNL.0000000000005516

62. Fox E, Lovett-Racke AE, Gormley M, Liu Y, Petracca M, Cocozza S, et al. A phase 2 multicenter study of ublituximab, a novel glycoengineered anti-CD20 monoclonal antibody, in patients with relapsing forms of multiple sclerosis. *Mult Scler* (2021) 27(3):420–9. doi: 10.1177/1352458520918375

63. Gingele S, Jacobus TL, Konen FF, Hümmert MW, Sühs K-W, Schwenkenbecher P, et al. Ocrelizumab depletes CD20+ T cells in multiple sclerosis patients. *Cells* (2019) 8(1):12. doi: 10.3390/cells8010012

64. Lovett-Racke AE, Gormley M, Liu Y, Yang Y, Graham C, Wray S, et al. B cell depletion with ublituximab reshapes the T cell profile in multiple sclerosis patients. *J Neuroimmunol* (2019) 332:187–97. doi: 10.1016/j.jneuroim.2019.04.017

65. Fernández-Velasco JI, Kuhle J, Monreal E, Meca-Lallana V, Meca-Lallana J, Izquierdo G, et al. Effect of ocrelizumab in blood leukocytes of patients with primary progressive MS. *Neurol Neuroimmunol Neuroinflamm* (2021) 8(2):e940. doi: 10.1212/NXI.0000000000000940

66. Lovett-Racke AE, Yang Y, Liu Y, Gormley M, Kraus E, Graham C, et al. B cell depletion changes the immune cell profile in multiple sclerosis patients: One-year report. *J Neuroimmunol* (2021) 359:577676. doi: 10.1016/j.jneuroim.2021.577676

67. Derfuss T, Weber M, Hughes R, Wang Q, Sauter A, Koendgen H, et al. Serum immunoglobulin levels and risk of serious infections in the pivotal phase III trials of ocrelizumab in multiple sclerosis and their open-label extensions. *Mult Scler* (2019) 25Suppl 2:20–1.

68. Bar-Or A, Calkwood JC, Chognot C, Evershed J, Fox EJ, Herman A, et al. Effect of ocrelizumab on vaccine responses in patients with multiple sclerosis: The VELOCE study. *Neurology* (2020) 95(14):e1999–2008. doi: 10.1212/WNL.0000000000010380

69. Hauser SL, Bar-Or A, Cohen JA, Comi G, Correale J, Coyle PK, et al. Ofatumumab versus teriflunomide in multiple sclerosis. *N Engl J Med* (2020a) 383(6):546–57. doi: 10.1056/NEJMoa1917246

70. Hauser SL, Kappos L, Arnold DL, Bar-Or A, Brochet B, Naismith RT, et al. Five years of ocrelizumab in relapsing multiple sclerosis: OPERA studies open-label extension. *Neurology* (2020c) 95(13):e1854–67. doi: 10.1212/WNL.0000000000010376

71. Wolinsky JS, Arnold DL, Brochet B, Hartung H-P, Montalban X, Naismith RT, et al. Long-term follow-up from the ORATORIO trial of ocrelizumab for primary progressive multiple sclerosis: a *post-hoc* analysis from the ongoing open-label extension of the randomised, placebo-controlled, phase 3 trial. *Lancet Neurol* (2020) 19(12):998–1009. doi: 10.1016/S1474-4422(20)30342-2

72. Duddy M, Niino M, Adatia F, Hebert S, Freedman M, Atkins H, et al. Distinct effector cytokine profiles of memory and naive human b cell subsets and implication in multiple sclerosis. *J Immunol* (2007) 178(10):6092–9. doi: 10.4049/jimmunol.178.10.6092

73. Barr TA, Shen P, Brown S, Lampropoulou V, Roch T, Lawrie S, et al. B cell depletion therapy ameliorates autoimmune disease through ablation of IL-6–producing b cells. *J Exp Med* (2012) 209(5):1001–10. doi: 10.1084/jem.20111675

74. Li R, Rezk A, Miyazaki Y, Hilgenberg E, Touil H, Shen P, et al. Proinflammatory GM-CSF–producing b cells in multiple sclerosis and b cell depletion therapy. *Sci Trans Med* (2015) 7(310):310ra166–310ra166. doi: 10.1126/scitranslmed.aab4176

75. Bar-Or A, Fawaz L, Fan B, Darlington PJ, Rieger A, Ghorayeb C, et al. Abnormal b-cell cytokine responses a trigger of t-cell–mediated disease in MS? *Ann Neurol* (2010) 67(4):452–61. doi: 10.1002/ana.21939

76. Rensel M, Zabeti A, Mealy MA, Cimbora D, She D, Drappa J, et al. Long-term efficacy and safety of inebilizumab in neuromyelitis optica spectrum disorder: Analysis of aquaporin-4–immunoglobulin G–seropositive participants taking inebilizumab for≥ 4 years in the n-MOmentum trial. *Multiple Scler J* (2021) 28:13524585211047223. doi: 10.1177/13524585211047223

77. Openshaw H, Lund BT, Kashyap A, Atkinson R, Sniecinski I, Weiner LP, et al. Peripheral blood stem cell transplantation in multiple sclerosis with busulfan and cyclophosphamide conditioning: report of toxicity and immunological monitoring. *Biol Blood Marrow Transplant* (2000) 6(5):563–75. doi: 10.1016/S1083-8791(00)70066-8

78. Sun W, Popat U, Hutton G, Zang YC, Krance R, Carrum G, et al. Characteristics of T-cell receptor repertoire and myelin-reactive T cells reconstituted from autologous haematopoietic stem-cell grafts in multiple sclerosis. *Brain* (2004) 127(5):996–1008. doi: 10.1093/brain/awh117

79. Karnell FG, Lin D, Motley S, Duhen T, Lim N, Campbell DJ, et al. Reconstitution of immune cell populations in multiple sclerosis patients after autologous stem cell transplantation. *Clin Exp Immunol* (2017) 189(3):268–78. doi: 10.1111/cei.12985

80. Muraro PA, Douek DC, Packer A, Chung K, Guenaga FJ, Cassiani-Ingoni R, et al. Thymic output generates a new and diverse TCR repertoire after autologous stem cell transplantation in multiple sclerosis patients. *J Exp Med* (2005) 201 (5):805–16. doi: 10.1084/jem.20041679

81. Saccardi R, Gualandi F. Hematopoietic stem cell transplantation procedures. *Autoimmunity* (2008) 41(8):570–6. doi: 10.1080/08916930802197776

82. Muraro PA, Robins H, Malhotra S, Howell M, Phippard D, Desmarais C, et al. T Cell repertoire following autologous stem cell transplantation for multiple sclerosis. *J Clin Invest* (2014) 124(3):1168–72. doi: 10.1172/JCI71691

83. Harris KM, Lim N, Lindau P, Robins H, Griffith LM, Nash RA, et al. Extensive intrathecal T cell renewal following hematopoietic transplantation for multiple sclerosis. *JCI Insight* (2020) 5(2):e127655. doi: 10.1172/jci.insight.127655

84. Burman J, Fransson M, Totterman TH, Fagius J, Mangsbo SM, Loskog AS. T-Cell responses after haematopoietic stem cell transplantation for aggressive relapsing-remitting multiple sclerosis. *Immunology* (2013) 140(2):211–9. doi: 10.1111/imm.12129

85. Darlington PJ, Stopnicki B, Touil T, Doucet JS, Fawaz L, Roberts ME, et al. Natural killer cells regulate Th17 cells after autologous hematopoietic stem cell transplantation for relapsing remitting multiple sclerosis. *Front Immunol* (2018) 9:834. doi: 10.3389/fimmu.2018.00834

86. Visweswaran M, Hendrawan K, Massey JC, Khoo ML, Ford CD, Withers B, et al. Sustained immunotolerance in multupe sclerosis after stem cell transplant. *Ann Clin Trans Neurol* (2022) 9(2):206–20. doi: 10.1002/acn3.51510

87. Darlington PJ, Touil T, Doucet JS, Gaucher D, Zeidan J, Gauchat D, et al. Diminished Th17 (not Th1) responses underlie multiple sclerosis disease abrogation after hematopoietic stem cell transplantation. *Ann Neurol* (2013) 73 (3):341–54. doi: 10.1002/ana.23784

88. Moore JJ, Massey JC, Ford CD, Khoo ML, Zaunders JJ, Hendrawan K, et al. Prospective phase II clinical trial of autologous haematopoietic stem cell transplant for treatment refractory multiple sclerosis. *J Neurol Neurosurg Psychiatry* (2019) 90 (5):514–21. doi: 10.1136/jnnp-2018-319446

89. Wiberg A, Olsson-Strömberg U, Herman S, Kultima K, Burman J. Profound but transient changes in the inflammatory milieu of the blood during autologous hematopoietic stem cell transplantation. *Biol Blood Marrow Transplant* (2020) 26 (1):50–7. doi: 10.1016/j.bbmt.2019.09.010

90. de Paula ASA, Malmegrim KC, Panepucci RA, Brum DS, Barreira AA, Carlos Dos Santos A, et al. Autologous haematopoietic stem cell transplantation reduces abnormalities in the expression of immune genes in multiple sclerosis. *Clin Sci (Lond)* (2015) 128(2):111–20. doi: 10.1042/CS20140095

91. Arruda LC, Lorenzi JC, Sousa AP, Zanette DL, Palma PV, Panepucci RA, et al. Autologous hematopoietic SCT normalizes miR-16, -155 and -142-3p expression in multiple sclerosis patients. *Bone Marrow Transplant* (2015) 50 (3):380–9. doi: 10.1038/bmt.2014.277

92. de Oliveira G, Ferreira A, Gasparotto E, Kashima S, Covas D, Guerreiro C, et al. Defective expression of apoptosis-related molecules in multiple sclerosis patients is normalized early after autologous haematopoietic stem cell transplantation. *Clin Exp Immunol* (2017) 187(3):383–98. doi: 10.1111/cei.12895

93. Burt RK, Muraro PA, Farge D, Oliveira MC, Snowden JA, Saccardi R, et al. New autoimmune diseases after autologous hematopoietic stem cell transplantation for multiple sclerosis. *Bone Marrow Transplant* (2021) 56 (7):1509–17. doi: 10.1038/s41409-021-01277-y

94. Cohen JA, Coles AJ, Arnold DL, Confavreux C, Fox EJ, Hartung HP, et al. Alemtuzumab versus interferon beta 1a as first-line treatment for patients with relapsing-remitting multiple sclerosis: a randomised controlled phase 3 trial. *Lancet* (2012) 380(9856:1819–28. doi: 10.1016/S0140-6736(12)61769-3

95. Coles AJ, Twyman CL, Arnold DL, Cohen JA, Confavreux C, Fox EJ, et al. Alemtuzumab for patients with relapsing multiple sclerosis after disease-modifying therapy: a randomised controlled phase 3 trial. *Lancet* (2012) 380(9856):1829–39. doi: 10.1016/S0140-6736(12)61768-1

96. Thompson SA, Jones JL, Cox AL, Compston DAS, Coles AJ. B-cell reconstitution and BAFF after alemtuzumab (Campath-1H) treatment of multiple sclerosis. *J Clin Immunol* (2010) 30(1):99–105. doi: 10.1007/s10875-009-9327-3

97. Magliocca JF, Knechtle SJ. The evolving role of alemtuzumab (Campath-1H) for immunosuppressive therapy in organ transplantation. *Transpl Int* (2006) 19(9):705–14. doi: 10.1111/j.1432-2277.2006.00343.x

98. Guilcher GMT, Shah R, Shenoy S. Principles of alemtuzumab immunoablation in hematopoietic cell transplantation for non-malignant diseases in children: A review. *Pediatr Transplant* (2018) 22(2):e13142. doi: 10.1111/petr.13142

99. Cossburn MD, Harding K, Ingram G, El-Shanawany T, Heaps A, Pickersgill TP, et al. Clinical relevance of differential lymphocyte recovery after alemtuzumab therapy for multiple sclerosis. *Neurology* (2013) 80(1):55–61. doi: 10.1212/WNL.0b013e31827b5927

100. Kousin-Ezewu O, Azzopardi L, Parker RA, Tuohy O, Compston A, Coles A, et al. Accelerated lymphocyte recovery after alemtuzumab does not predict multiple sclerosis activity. *Neurology* (2014) 82(24):2158–64. doi: 10.1212/WNL.0000000000000520

101. Wiendl H, Carraro M, Comi G, Izquierdo G, Kim HJ, Sharrack B, et al. Lymphocyte pharmacodynamics are not associated with autoimmunity or efficacy after alemtuzumab. *Neurol Neuroimmunol Neuroinflamm* (2020) 7(1):e635. doi: 10.1212/NXI.0000000000000635

102. Link H, Huang Y-M. Oligoclonal bands in multiple sclerosis cerebrospinal fluid: an update on methodology and clinical usefulness. *J Neuroimmunol* (2006) 180(1-2):17–28. doi: 10.1016/j.jneuroim.2006.07.006

103. Möhn N, Pfeuffer S, Ruck T, Gross CC, Skripuletz T, Klotz L, et al. Alemtuzumab therapy changes immunoglobulin levels in peripheral blood and CSF. *Neurol - Neuroimmunol Neuroinflamm* (2020) 7(2):e654. doi: 10.1212/NXI.0000000000000654

104. Hyun J-W, Kim Y, Kim G, Kim S-H, Kim HJ. Severe b cell–mediated disease activation despite two cycles of alemtuzumab in a patient with multiple sclerosis. *Multiple Scler J* (2019) 25(14):1942–5. doi: 10.1177/1352458518810261

105. Bar-Or A, Wiendl H, Montalban X, Alvarez E, Davydovskaya M, Delgado SR, et al. Rapid and sustained b-cell depletion with subcutaneous ofatumumab in relapsing multiple sclerosis: APLIOS, a randomized phase-2 study. *Mult Scler* (2022) 28(6):910–24. doi: 10.1177/13524585211044479

106. Kähäri L, Fair-Mäkelä R, Auvinen K, Rantakari P, Jalkanen S, Ivaska J, et al. Transcytosis route mediates rapid delivery of intact antibodies to draining lymph nodes. *J Clin Invest* (2019) 129(8):3086–102. doi: 10.1172/JCI125740

107. Theil D, Smith P, Huck C, Gilbart Y, Kakarieka A, Leppert D, et al. Imaging mass cytometry and single-cell genomics reveal differential depletion and repletion of b-cell populations following ofatumumab treatment in cynomolgus monkeys. *Front Immunol* (2019) 10:1340. doi: 10.3389/fimmu.2019.01340

108. Graves J, Vinayagasundaram U, Mowry EM, Matthews IR, Marino JA, Cheng J, et al. Effects of rituximab on lymphocytes in multiple sclerosis and neuromyelitis optica. *Mult Scler Relat Disord* (2014) 3(2):244–52. doi: 10.1016/j.msard.2013.10.003

109. Ellrichmann G, Bolz J, Peschke M, Duscha A, Hellwig K, Lee D-H, et al. Peripheral CD19+ b-cell counts and infusion intervals as a surrogate for long-term b-cell depleting therapy in multiple sclerosis and neuromyelitis optica/neuromyelitis optica spectrum disorders. *J Neurol* (2019) 266(1):57–67. doi: 10.1007/s00415-018-9092-4

110. Jelcic I, Al Nimer F, Wang J, Lentsch V, Planas R, Jelcic I, et al. Memory b cells activate brain-homing, autoreactive CD4+ T cells in multiple sclerosis. *Cell* (2018) 175(1):85–100. e123. doi: 10.1016/j.cell.2018.08.011

111. Hultin LE, Hausner MA, Hultin PM, Giorgi JV. CD20 (pan-b cell) antigen is expressed at a low level on a subpopulation of human T lymphocytes. *Cytom: J Int Soc Anal Cytol* (1993) 14(2):196–204. doi: 10.1002/cyto.990140212

112. Holley JE, Bremer E, Kendall AC, De Bruyn M, Helfrich W, Tarr JM, et al. CD20+ inflammatory T-cells are present in blood and brain of multiple sclerosis patients and can be selectively targeted for apoptotic elimination. *Multiple Scler Relat Disord* (2014) 3(5):650–8. doi: 10.1016/j.msard.2014.06.001

113. Cross AH, Stark JL, Lauber J, Ramsbottom MJ, Lyons J-A. Rituximab reduces b cells and T cells in cerebrospinal fluid of multiple sclerosis patients. *J Neuroimmunol* (2006) 180(1-2):63–70. doi: 10.1016/j.jneuroim.2006.06.029

114. Piccio L, Naismith RT, Trinkaus K, Klein RS, Parks BJ, Lyons JA, et al. Changes in b-and T-lymphocyte and chemokine levels with rituximab treatment in multiple sclerosis. *Arch Neurol* (2010) 67(6):707–14. doi: 10.1001/archneurol.2010.99

115. Apostolidis SA, Kakara M, Painter MM, Goel RR, Mathew D, Lenzi K, et al. Cellular and humoral immune responses following SARS-CoV-2 mRNA

vaccination in patients with multiple sclerosis on anti-CD20 therapy. *Nat Med* (2021) 27(11):1990–2001. doi: 10.1101/2021.06.23.21259389

116. Brill L, Rechtman A, Zveik O, Haham N, Oiknine-Djian E, Wolf DG, et al. Humoral and T-cell response to SARS-CoV-2 vaccination in patients with multiple sclerosis treated with ocrelizumab. *JAMA Neurol* (2021) 78(12):1510–4. doi: 10.1001/jamaneurol.2021.3599

117. Mealy MA, Levy M. A pilot safety study of ublituximab, a monoclonal antibody against CD20, in acute relapses of neuromyelitis optica spectrum disorder. *Medicine* (2019) 98(25):e15944. doi: 10.1097/MD.0000000000015944

118. Cencioni MT, Genchi A, Brittain G, de Silva TI, Sharrack B, Snowden JA, et al. Immune reconstitution following autologous hematopoietic stem cell transplantation for multiple sclerosis: a review on behalf of the EBMT autoimmune diseases working party. *Front Immunol* (2021) 12. doi: 10.3389/fimmu.2021.813957

119. Lublin FD, Reingold SC, Cohen JA, Cutter GR, Sørensen PS, Thompson AJ, et al. Defining the clinical course of multiple sclerosis: The 2013 revisions. *Neurology* (2014) 83(3):278–86. doi: 10.1212/WNL.0000000000000560

120. George B, Seals S, Aban I. Survival analysis and regression models. *J Nucl Cardiol* (2014) 21(4):686–94. doi: 10.1007/s12350-014-9908-2

121. Kurtzke JF. Rating neurologic impairment in multiple sclerosis: an expanded disability status scale (EDSS). *Neurology* (1983) 33(11):1444–52. doi: 10.1212/WNL.33.11.1444

122. Wattjes MP, Rovira À, Miller D, Yousry TA, Sormani MP, De Stefano N, et al. MAGNIMS consensus guidelines on the use of MRI in multiple sclerosis–establishing disease prognosis and monitoring patients. *Nat Rev Neurol* (2015) 11 (10):597–607. doi: 10.1038/nrneurol.2015.157

123. Andravizou A, Dardiotis E, Artemiadis A, Sokratous M, Siokas V, Tsouris Z, et al. Brain atrophy in multiple sclerosis: Mechanisms, clinical relevance and treatment options. *Autoimmun Highlights* (2019) 10(1):7. doi: 10.1186/s13317-019-0117-5

124. Lu G, Beadnall HN, Barton J, Hardy TA, Wang C, Barnett MH. The evolution of no evidence of disease activity in multiple sclerosis. *Multiple Scler Relat Disord* (2018) 20:231–8. doi: 10.1016/j.msard.2017.12.016

125. Burt RK, Balabanov R, Burman J, Sharrack B, Snowden JA, Oliveira MC, et al. Effect of nonmyeloablative hematopoietic stem cell transplantation vs continued disease-modifying therapy on disease progression in patients with relapsing-remitting multiple sclerosis: A randomized clinical trial. *Jama* (2019) 321(2):165–74. doi: 10.1001/jama.2018.18743

126. Coles AJ, Cohen JA, Fox EJ, Giovannoni G, Hartung HP, Havrdova E, et al. Alemtuzumab CARE-MS II 5-year follow-up: Efficacy and safety findings. *Neurology* (2017) 89(11):1117–26. doi: 10.1212/WNL.0000000000004354

127. Coles AJ, Arnold DL, Bass AD, Boster AL, Compston DAS, Fernández Ó, et al. Efficacy and safety of alemtuzumab over 6 years: Final results of the 4-year CARE-MS extension trial. *Ther Adv Neurol Disord* (2021) 14:1756286420982134. doi: 10.1177/1756286420982134

128. Hauser SL, Bar-Or A, Cohen JA, Comi G, Correale J, Coyle PK, et al. Ofatumumab versus teriflunomide in relapsing multiple sclerosis: Analysis of no evidence of disease activity (NEDA-3) from the ASCLEPIOS I and II trials. *Int J MS Care* (2020b) 22:85–6.

129. Fox E, Mayer L, Aungst A, Mancione L, Rennie N, Roustan A, et al. Long-term safety, compliance, and effectiveness of ofatumumab in patients with relapsing multiple sclerosis: The ALITHIOS phase 3b study. *Mult Scler J* (2020) 26:223–4.

130. de Flon P, Gunnarsson M, Laurell K, Söderström L, Birgander R, Lindqvist T, et al. Reduced inflammation in relapsing-remitting multiple sclerosis after therapy switch to rituximab. *Neurology* (2016) 87(2):141–7. doi: 10.1212/WNL.0000000000002832

131. Cheshmavar M, Mirmosayyeb O, Badihian N, Badihian S, Shaygannejad V. Rituximab and glatiramer acetate in secondary progressive multiple sclerosis: A randomized clinical trial. *Acta Neurol Scand* (2021) 143(2):178–87. doi: 10.1111/ane.13344

132. Filippini G, Kruja J, Del Giovane C. Rituximab for people with multiple sclerosis. *Cochrane Database Syst Rev* (2021) 11). doi: 10.1002/14651858.CD013874.pub2

133. Cree BAC, Bennett JL, Kim HJ, Weinshenker B, Pittock S, Wingerchuk D, et al. Long-term efficacy and safety of inebilizumab for neuromyelitis optica spectrum disorder in the randomized, double-blind n-MOmentum study and extension, (3998). *Neurology* (2020) 9415 Supplement:3998.

134. Marignier R, Bennett JL, Kim HJ, Weinshenker BG, Pittock SJ, Wingerchuk D, et al. Disability outcomes in the n-MOmentum trial of inebilizumab in neuromyelitis optica spectrum disorder. *Neurol - Neuroimmunol Neuroinflamm* (2021) 8(3):e978. doi: 10.1212/NXI.0000000000000978

135. Niewoehner J, Bohrmann B, Collin L, Urich E, Sade H, Maier P, et al. Increased brain penetration and potency of a therapeutic antibody using a monovalent molecular shuttle. *Neuron* (2014) 81(1):49–60. doi: 10.1016/j.neuron.2013.10.061

136. Yu Y, Atwal J, Zhang Y, Tong R, Wildsmith K, Tan C, et al. Therapeutic bispecific antibodies cross the blood-brain barrier in nonhuman primates. *Sci Transl Med* (2014) 6(261):261ra154. doi: 10.1126/scitranslmed.3009835

137. Lonial S, Weiss BM, Usmani SZ, Singhal S, Chari A, Bahlis NJ, et al. Daratumumab monotherapy in patients with treatment-refractory multiple myeloma (SIRIUS): an open-label, randomised, phase 2 trial. *Lancet* (2016) 387 (10027):1551–60. doi: 10.1016/S0140-6736(15)01120-4

138. Schuetz C, Hoenig M, Moshous D, Weinstock C, Castelle M, Bendavid M, et al. Daratumumab in life-threatening autoimmune hemolytic anemia following hematopoietic stem cell transplantation. *Blood Adv* (2018) 2(19):2550–3. doi: 10.1182/bloodadvances.2018020883

139. Ostendorf L, Burns M, Durek P, Heinz GA, Heinrich F, Garantziotis P, et al. Targeting CD38 with daratumumab in refractory systemic lupus erythematosus. *New Engl J Med* (2020) 383(12):1149–55. doi: 10.1056/NEJMoa2023325

140. O'Connor BP, Raman VS, Erickson LD, Cook WJ, Weaver LK, Ahonen C, et al. BCMA is essential for the survival of long-lived bone marrow plasma cells. *J Exp Med* (2004) 199(1):91–8. doi: 10.1084/jem.20031330

141. Park JH, Rivière I, Gonen M, Wang X, Sénéchal B, Curran KJ, et al. Long-term follow-up of CD19 CAR therapy in acute lymphoblastic leukemia. *New Engl J Med* (2018) 378(5):449–59. doi: 10.1056/NEJMoa1709919

142. Mougiakakos D, Krönke G, Völkl S, Kretschmann S, Aigner M, Kharboutli S, et al. CD19-targeted CAR T cells in refractory systemic lupus erythematosus. *New Engl J Med* (2021) 385(6):567–9. doi: 10.1056/NEJMc2107725

143. Menon S, Shirani A, Zhao Y, Oger J, Traboulsee A, Freedman MS, et al. Characterising aggressive multiple sclerosis. *J Neurolo Neurosurg Psychiatry* (2013) 84(11):1192–8. doi: 10.1136/jnnp-2013-304951

frontiers | Frontiers in Immunology

TYPE Original Research
PUBLISHED 29 September 2022
DOI 10.3389/fimmu.2022.970290

OPEN ACCESS

EDITED BY
Rudi W. Hendriks,
Erasmus University Rotterdam,
Netherlands

REVIEWED BY
Mark S. Cragg,
University of Southampton,
United Kingdom
Sean Lim,
University of Southampton,
United Kingdom

*CORRESPONDENCE
Falk Nimmerjahn
falk.nimmerjahn@fau.de

SPECIALTY SECTION
This article was submitted to
B Cell Biology,
a section of the journal
Frontiers in Immunology

RECEIVED 15 June 2022
ACCEPTED 30 August 2022
PUBLISHED 29 September 2022

CITATION
Reitinger C, Ipsen-Escobedo A, Hornung C, Heger L, Dudziak D, Lux A and Nimmerjahn F (2022) Modulation of urelumab glycosylation separates immune stimulatory activity from organ toxicity.
Front. Immunol. 13:970290.
doi: 10.3389/fimmu.2022.970290

Modulation of urelumab glycosylation separates immune stimulatory activity from organ toxicity

Carmen Reitinger[1], Andrea Ipsen-Escobedo[1], Chiara Hornung[1], Lukas Heger[2], Diana Dudziak[2,3,4,5], Anja Lux[1] and Falk Nimmerjahn[1,3]*

[1]Chair of Genetics, Department of Biology, Friedrich Alexander University of Erlangen-Nürnberg, Erlangen, Germany, [2]Laboratory of Dendritic Cell Biology, Department of Dermatology, University Hospital Erlangen, Erlangen, Germany, [3]Medical Immunology Campus Erlangen, Erlangen, Germany, [4]Deutsches Zentrum Immuntherapie (DZI), Erlangen, Germany, [5]Comprehensive Cancer Center Erlangen-European Metropolitan Area of Nuremberg (CCC ER-EMN), Erlangen, Germany

Checkpoint control and immunomodulatory antibodies have become important tools for modulating tumor or self-reactive immune responses. A major issue preventing to make full use of the potential of these immunomodulatory antibodies are the severe side-effects, ranging from systemic cytokine release syndrome to organ-specific toxicities. The IgG Fc-portion has been demonstrated to contribute to both, the desired as well as the undesired antibody activities of checkpoint control and immunomodulatory antibodies *via* binding to cellular Fcγ-receptors (FcγR). Thus, choosing IgG subclasses, such as human IgG4, with a low ability to interact with FcγRs has been identified as a potential strategy to limit FcγR or complement pathway dependent side-effects. However, even immunomodulatory antibodies on the human IgG4 background may interact with cellular FcγRs and show dose limiting toxicities. By using a humanized mouse model allowing to study the immunomodulatory activity of human checkpoint control antibodies *in vivo*, we demonstrate that deglycosylation of the CD137-specific IgG4 antibody urelumab results in an amelioration of liver toxicity, while maintaining T cell stimulatory activity. In addition, our results emphasize that antibody dosing impacts the separation of side-effects of urelumab from its therapeutic activity *via* IgG deglycosylation. Thus, glycoengineering of human IgG4 antibodies may be a possible approach to limit collateral damage by immunomodulatory antibodies and allow for a greater therapeutic window of opportunity.

KEYWORDS

CD137, Fc-receptors, glycosylation, therapeutic antibody, urelumab

Introduction

Monoclonal antibodies have become crucial therapeutic agents for the treatment of human cancer and autoimmune diseases and novel monoclonal antibodies are being developed continuously (1). In addition to cytotoxic antibodies, such as rituximab or herceptin, which recognize antigens expressed on tumor cells, antibodies aiming at harnessing tumor specific T cell responses have revolutionized the field of antibody-based cancer immunotherapy (2, 3). This class of antibodies is referred to as checkpoint blockade or immunomodulatory antibodies and contains antibodies specific for CTLA-4, PD-1, PD-L1, CD137, Ox40, GITR, or CD40 expressed on T cells or antigen presenting cells. Of note, some immunomodulatory antibodies directed against CTLA-4 or CD137 also show promise for modulating self-directed immune responses in pre-clinical model systems but also in patients with autoimmune diseases, broadening the therapeutic value of this class of molecules beyond the treatment of cancer (4–6).

A major factor restricting the therapeutic window of checkpoint control or immunomodulatory antibodies are the severe side-effects triggered upon antibody infusion, ranging from an acute cytokine storm to organ specific autoimmunity affecting the gut and liver, for example (7, 8). To circumvent systemic side-effects, an intra-tumoral injection of immunomodulatory antibodies may be a rescue strategy limited, however, to accessible tumor entities (9). To understand the activity of immunomodulatory antibodies in more detail, several groups have studied informative pre-clinical model systems. These studies have emphasized that the Fc-domain of various immunomodulatory antibodies can play a major role for antibody activity *in vivo*. For example, antibodies targeting molecules expressed on regulatory (T_{reg}) T cells, including CTLA-4, GITR, OX40, and CD137, have been shown to act as cytotoxic antibodies and deplete T_{reg} cells within the tumor microenvironment *via* binding to activating Fcγ-receptors (FcγRs) (10–14). Further along these lines, an optimal activity of CD40-specific antibodies required the *in vivo* cross-linking of these antibodies *via* the inhibitory FcγRIIb (15, 16). Alternatively, human IgG subclasses, such as IgG2, allowing for an optimal CD40 cross-linking through unique antibody isotype intrinsic features could circumvent the requirement for higher order cross-linking through neighbouring FcγRIIb expressing cells to achieve super-agonistic activity (17, 18). For immunomodulatory antibodies not requiring or not intended to have an IgG Fc-domain dependent enhancement of therapeutic activity, the use of Fc-domains, such as human IgG4, allowing to maintain a long antibody half-life while limiting the interaction with the complement or FcγR system have become the format of choice. This includes antibodies such as pembrolizumab or urelumab, targeting PD-1 or CD137 on T cells, respectively. Indeed, in mice a PD-1 antibody variant carrying an IgG2a Fc-domain allowing an optimal interaction with the FcγR system resulted in a reduced therapeutic activity *in vivo*, due to the elimination of intratumoral cytotoxic T cells (19). Further along these lines, CD137 (4-1BB)-specific antibodies on a mouse IgG2a backbone, efficiently depleted activated T cells and T_{reg} cells *via* activating FcγRs, while mouse IgG1 variants of the same antibody stimulated cytotoxic T cell responses *via* the inhibitory FcγRIIb (5, 10, 20, 21). However, several studies have shown that human IgG4 antibodies may productively interact with human FcγRs *in vitro* and *in vivo*, suggesting that human IgG4 Fc-domains are not inert and may contribute to wanted and unwanted effects of immunomodulatory antibodies *in vivo* (22–24). As a direct correlate to human IgG4 does not exist in the mouse, evaluating the impact of the human IgG4 Fc-domain on antibody activity has to rely on *in vitro* experimental settings. Thus, it remains largely unknown if the activity of human immunomodulatory antibodies using the IgG4 format relies on the Fc-portion and if modulating the interaction of human IgG4 to human FcγRs may be a valid strategy to optimize antibody activity or, more importantly, may allow to limit unwanted side-effects.

To allow studying human IgG subclass activity *in vivo*, we have developed a humanized mouse model in which a human immune system is transplanted into immunodeficient mice. Additionally, use of mice lacking the expression of mouse activating FcγRs (NSG-FcRγ-/- mice) focusses the interaction of human antibodies injected into these animals to human FcγRs (23, 25–27). By applying the CD137-specific IgG4 antibody urelumab in a glycosylated and non-glycosylated variant we now show that IgG4 deglycosylation maintains the immunostimulatory activity of the antibody, demonstrated by expansion of peripheral blood T cells, but limits the infiltration of T cells into the liver. Interestingly, in addition to glycosylation, the dose of the antibody played a very important role in triggering a systemic cytokine release and organ toxicity, with lower doses having a more pronounced effect on cytokine release and organ toxicity compared to higher doses. Thus, our study emphasizes that complex mechanisms underlie human immunomodulatory antibody activity *in vivo* and that glycoengineering of supposedly inert IgG subclasses may be a valid option to improve antibody safety in humans.

Results

Expression of CD137 in humanized mice

The human IgG4 CD137-specific antibody urelumab has shown promising results in pre-clinical and clinical settings. It has also become clear, however, that liver toxicity and a cytokine release syndrome are major dose limiting factors in many

patients (28). To allow studying human CD137-specific antibody activity *in vivo*, we made use of a modified humanized mouse model system allowing to study human antibody function in the context of a human immune system in the absence of mouse activating FcγRs through genetic ablation of the mouse common FcRγ-chain (NSG-FcRγ-/- mice) (23, 26, 27). We first analysed CD137 expression on human T cells, NK cells and monocytes present in these animals during the steady state. The gating strategy for human immune cells in humanized mice is depicted in Figure S1. As shown in Figures S2A-C low levels of CD137 were detectable on $CD4^+$ and $CD8^+$ T cells as well as on different NK and monocyte subsets in the peripheral blood, spleen, lymph node, bone marrow, and thymus of humanized mice and humans. The only immune cell subset expressing elevated levels of CD137 during the steady state, were small subsets of CD4 and CD8 double positive and double negative T cells in the peripheral blood of humanized mice and humans (Figure S2A). Thus, the humanized mouse model largely recapitulates CD137 expression patterns observed in humans.

Impact of targeting CD137 with glycosylated and deglycosylated urelumab on body weight and temperature of humanized mice

To assess how urelumab impacts general health parameters, such as body weight and body temperature, we intravenously injected humanized mice once with 3 or 6μg/g body weight of urelumab or a human IgG4 isotype control antibody. Although human IgG4 antibodies are largely considered to have a low capacity to interact with cellular FcγRs or the complement system, more recent data clearly demonstrates that IgG4 in its monomeric form can bind to the high affinity FcγRI and that IgG4 immune complexes may bind to several activating FcγRs (22, 24). Importantly, deglycosylation of IgG4 was able to diminish this interaction, suggesting that glycan engineering may be an option to modulate human IgG4 effector functions *in vivo* (24). Thus, we also generated a deglycosylated urelumab variant by treating the parental antibody with PNGase F to assess if and to what extend IgG4 Fc-dependent effects played a role for urelumab activity *in vivo* in humanized mice. As expected, PNGaseF treatment resulted in a reduced molecular weight of urelumab and a complete loss of lens culinaris agglutinin (LCA) binding, which detects the mannose core of the N297-linked sugar moiety (Figure S3A). Further in line with our previous study deglycoylsation of urelumab resulted in a strongly reduced binding of urelumab to CHO cells expressing the human high affinity FcγRI (Figure S3B) (24). As shown in Figure 1, urelumab injection was tolerated well in general. Mice injected with both, the 3 or 6μg/g dose of the glycosylated and deglycosylated urelumab variants only showed transient changes in body temperature and a slight delay in gaining body weight compared to IgG4 isotype treated mice over the observation period of three weeks (Figure 1A). Interestingly, a major drop in body temperature occurred at the 3 (but not at the 6) μg/g dose of urelumab, while the deglycosylated urelumab variant showed a much milder and delayed reduction in body temperature (Figure 1B). Thus, we conclude that treatment with urelumab, especially the deglycosylated variant, is well tolerated by humanized mice.

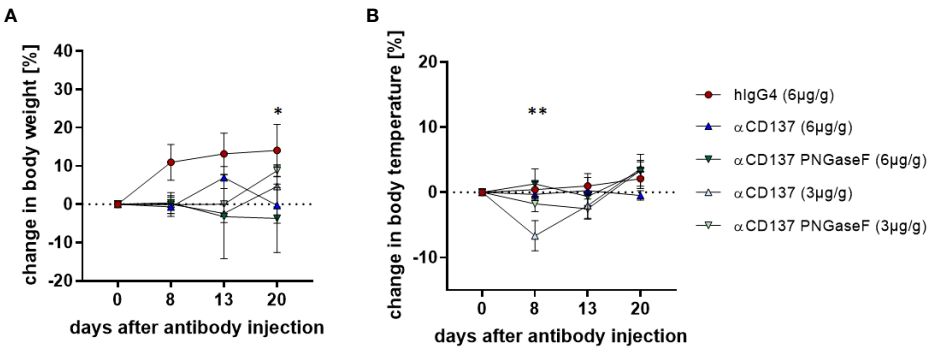

FIGURE 1
Effect of treatment with urelumab antibody variants on body weight and temperature in humanized mice. Shown are relative changes in body weight **(A)** and body temperature **(B)** of humanized mice after treatment with a human IgG4 isotype control (6μg/g) or 3μg/g or 6μg/g of urelumab (αCD137) or a deglycosylated urelumab variant (αCD137 PNGaseF) until twenty days after antibody injection (hIgG4: n=5, αCD137 6μg: n=7, αCD137 PNGaseF 6μg: n=3, αCD137 3μg: n=3, αCD137 PNGaseF 3μg: n=4). Shown is the mean+/-SEM of one representative out of two independent experiments. For assessment of statistical significance a Two Way ANOVA with Tukey's multiple comparison test was used. In **(A)** * indicates p<0.05 for hIgG4 (6μg/g) vs. αCD137 (6μg/g) and hIgG4 (6μg/g) vs. αCD137 PNGaseF (6μg/g). In **(B)** ** indicates p<0.01 for hIgG4 (6μg/g) vs. αCD137 (3μg/g), αCD137 (6μg/g) vs. αCD137 3(μg/g) and αCD137 PNGaseF (6μg/g) vs. αCD137 (3μg/g).

Effect of targeting CD137 with urelumab variants on human immune cells in humanized mice

In order to analyze the effect of urelumab variants on human T cell subsets in the peripheral blood of humanized mice, we performed flow cytometric analysis of immune cell subsets. We noted that both doses of urelumab triggered a strong expansion of both, $CD4^+$ and $CD8^+$ T cells (Figures 2A, B, S4). In line with observations in patients, urelumab injection triggered a faster and stronger expansion of $CD8^+$ T cells starting at one and peaking at two weeks after urelumab injection, followed by a decline thereafter (Figures 2A-F). In contrast, a significant expansion of $CD4^+$ T cells occurred roughly one week later and was preceded by a slow increase of $CD4^+$ T cell numbers until day 13. While the deglycosylated urelumab variant showed a slower expansion of $CD8^+$ T cells without the peak at day 13, the final number of $CD8^+$ T cells at three weeks after antibody injection was the same. This was also evident for the expansion of $CD4^+$ T cells at the 3μg/g dose, while the expansion of CD4+ T cells at the higher dose was diminished in animals receiving deglycosylated urelumab. With respect to relative changes in the different T cell subsets occurring after urelumab variant injection in humanized mice, $CD8^+$ T cells showed the strongest expansion, followed by an increase in a small subset of CD4/CD8 double positive T cells (Figures 2D, F). While CD137 expression is low on T cells in the steady state, CD137 becomes upregulated upon T cell activation. Indeed, we observed a strong upregulation of CD137 on T cells eight days after injection of 3 or 6μg/g urelumab (Figures 2G, H). Of note, while no change in CD137 upregulation was observed in animals receiving the deglycosylated urelumab variant (αCD137 PNGase F) at the 3μg/g dose, a delayed upregulation on both, $CD4^+$ and $CD8^+$ T cells was noted at the 6μg/g dose. With respect to monocytes and NK cells, urelumab injection did not trigger changes in cell abundance at either antibody dose (Figure 3). Interestingly, however, the deglycosylated urelumab variant resulted in a stronger and prolonged upregulation of CD137 on NK cell subsets and monocytes, respectively (Figures 3A-D, F). Within lymphoid organs, both urelumab variants triggered a strong expansion of T cells in lymph nodes, whereas the effect on splenic T cells was much milder (Figures 4A-C). While the 3μg/g dose resulted in a more pronounced effect on $CD4^+$ T cells in most organs, the 6μg/g dose induced a more dominant effect on $CD8^+$ T cells (Figures 4D, E). Interestingly, the parental as well as the deglycosylated urelumab variant induced an expansion of $CD8^+$ T cells in the thymus and lymph node at the 6μg/g dose (Figure 4E). Moreover, the deglycosylated variant of urelumab seemed to expand the small subset of CD4/CD8 double positive T cells in the lymph node and bone marrow of humanized mice (Figure 4C). In summary, our data indicate that deglycosylation of urelumab at most delays but does not impair T cell activation and expansion at both investigated antibody doses.

Effect of urelumab glycosylation on serum cytokine levels

Major side effects potentially associated with the injection of CD137-specific antibodies are a cytokine release syndrome and/or immune cell infiltrations in organs such as the liver (8, 28). To assess if injection of the parental or the deglycosylated variant of urelumab induces an increase in human serum cytokine levels we quantified the serum levels of human IL1β, IL6, IL8, IL10, IL12p40, IL17a, IFNα, IFNγ, and MCP-1 eight and thirteen days after injection of 3 or 6μg/g of the respective antibody preparations. As shown in Figures 5A, C, E, G, I, K, S5 we noted an increase of IL1β, IL6, IL8, MCP-1, IFNγ, and IL17a while IFNα, IL10 and IL12 levels increased only mildly or did not change upon injection of 3μg/g of urelumab. Deglycosylation of urelumab largely abrogated or greatly diminished serum cytokine levels, suggesting that IgG4 Fc-dependent effects were involved in triggering human cytokine release. Interestingly, injection of 6μg/g of urelumab trigger a much milder and transient cytokine release, which was fully abrogated upon deglycosylation of the antibody (Figures 5B, D, F, H, J, L, S5). In summary, urelumab triggered cytokine release showed a clear dependence on a functional IgG4 Fc-domain.

Effect of urelumab glycosylation on organ pathology

As deglycosylated urelumab induced reduced cytokine levels, we next assessed whether IgG4 deglycosylation would also impact urelumab induced organ pathology. With respect to immune cell infiltrates into organs we focused on the kidney and liver (Figures 6, 7). In the kidney, only mice receiving the 6μg/g dose showed slightly increased levels of blood urea nitrogen (BUN), indicative for a slightly impaired kidney functionality (Figure 6A, B). Deglycosylation of urelumab prevented this phenotype, again suggesting that IgG4 Fc-domain dependent effects played a role. With respect to kidney histology, no major immune cell infiltrates or major changes in glomerular structure were observed, further supporting the notion of a rather mild effect of urelumab on the kidney (Figure 6C). In contrast to the kidney, however, major immune cell infiltrates were noted in the liver at both antibody doses (Figures 7A-C). Whereas urelumab deglycosylation did not reduce the number of mice showing immune cell infiltrations (Figure 6C), injection of deglycosylated urelumab resulted in a greatly diminished size of immune cell infiltrations at the 6μg/g dose (Figure 6B). In contrast, no major effect of urelumab deglycosylation on immune cell infiltration into the liver became visible at the 3μg/g dose. A more detailed analysis of the immune cell infiltrations of animals receiving the 6μg/g urelumab dose by immunofluorescence analysis further revealed that T cells were a major component of the immune cell

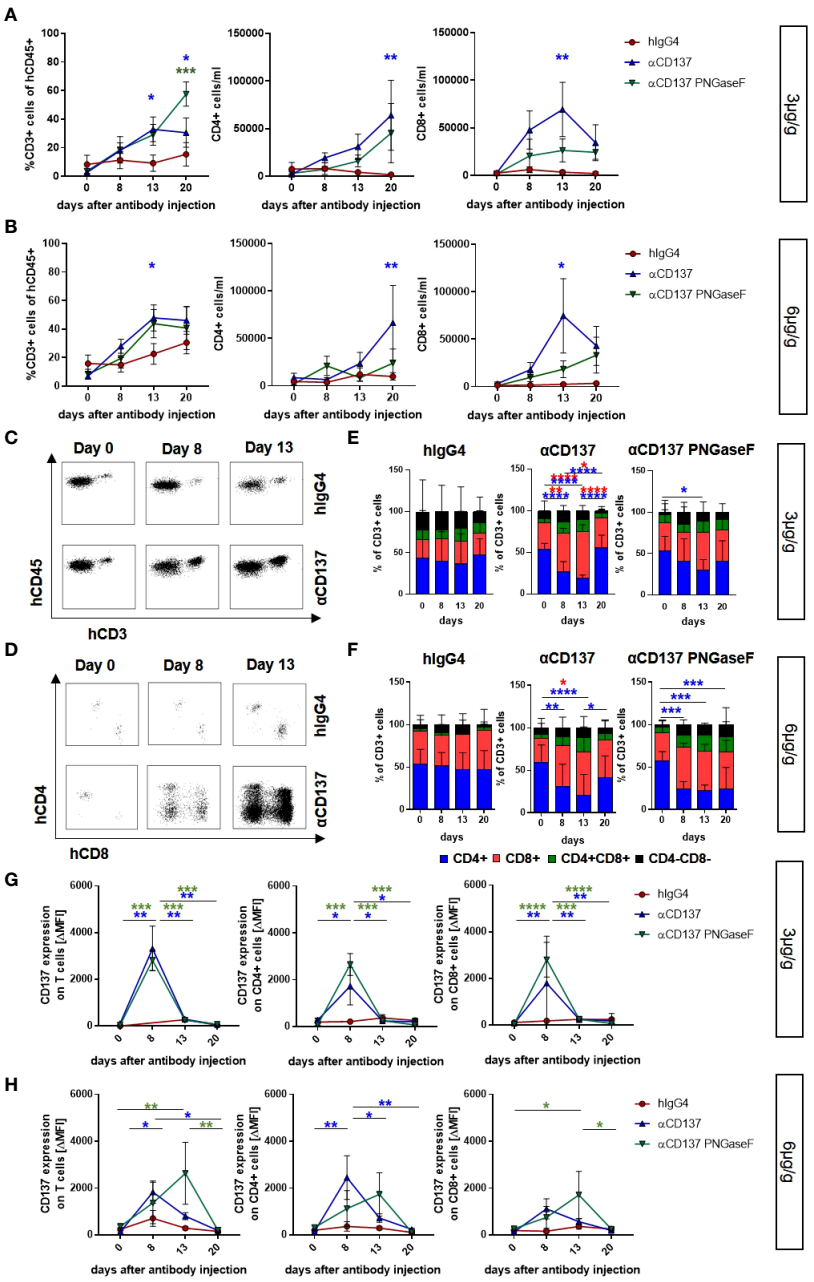

FIGURE 2
Impact of urelumab antibody dose and glycosylation on human T cells in the peripheral blood of humanized mice. Humanized mice received either 3 or 6µg/g of a human IgG4 isotype control, urelumab (αCD137) or deglycosylated urelumab (αCD137 PNGaseF) and were studied for the next twenty days after antibody injection. **(A, B)** Shown are the relative amounts of human CD3+ T cells (% of human CD45+ cells) and the absolute numbers of CD4+ or CD8+ T cells per ml blood of mice treated with 3µg/g (hIgG4: n= 5; αCD137: n=6; αCD137 PNGaseF: n=4) **(A)** or 6µg/g (hIgG4: n= 7-13; αCD137: n=10-11; αCD137 PNGaseF: n=6) **(B)** of the indicated antibody preparations. Coloured asterisks matching the respective colouring of the treatment group indicate significant differences at the indicated time-point of this group compared to the hIgG4 isotype control group. **(C-F)** Representative dot plots demonstrating the expansion of human CD3+ T cells **(C)** or CD4+ and CD8+ T cell subsets **(D)** in the peripheral blood of humanized mice before and at 8 or 13 days after injection of 6µg/g of the respective IgG4 antibodies; and quantification **(E, F)** of the relative abundance of human T cell subsets in mice receiving 3µg/g (hIgG4: n=6; αCD137: n=6 αCD137 PNGaseF: n=4) **(E)** or 6µg/g (hIgG4: n=11; αCD137: n=11 αCD137 PNGaseF: n=5) of the specified antibodies **(F)** at the indicated time points after injection. **(G, H)** CD137 expression (mean ΔMFI) on CD3+ (left panel), CD4+ (middle panel) and CD8+ (right panel) T cells in mice treated with 3µg/g **(G)** (hIgG4 n= 3; αCD137: n=6; αCD137 PNGaseF: n=4) or with 6µg/g **(H)** (hIgG4: n=7; αCD137: n=6-7; αCD137 PNGaseF: n=4-6) of the respective antibody preparations. Shown are pooled data from two to three independent experiments. Results are presented as mean +/-SEM. For statistical analysis 2-Way Anova with Tukey's multiple comparison test was used to assess significant differences between experimental groups. *p<0.05; **p<0.01; ***p<0.001; ****p<0.0001.

10.3389/fimmu.2022.970290

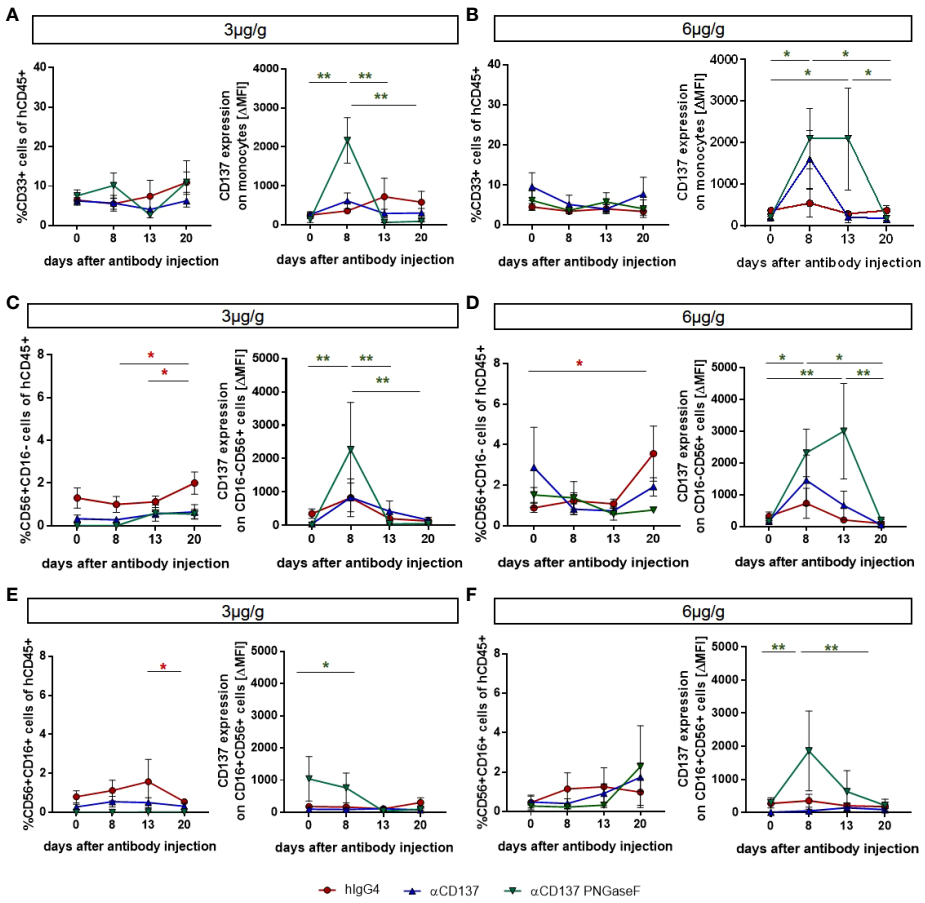

FIGURE 3
Effects of treatment with urelumab variants on human monocytes and NK cells in the peripheral blood of humanized mice. Humanized mice were injected with 3µg/g (hIgG4: n=3-4; αCD137: n=6; αCD137 PNGaseF: n=4) **(A, C, E)** or 6µg/g (hIgG4: n=7; αCD137: n=5; αCD137 PNGaseF: n=4) **(B, D, F)** of the human IgG4 isotype control, urelumab (αCD137), or deglycosylated urelumab (αCD137 PNGaseF) and studied for twenty days after antibody injection. **(A, B)** Shown are the relative changes in CD33+ monocyte numbers (left panel) as well as in CD137 expression (right panel, ΔMFI) on CD33+ monocytes at the indicated time-points after injection of 3 **(A)** or 6 **(B)** µg/g of the respective antibody preparations. **(C-F)** Shown are the relative changes in $CD56^{+}CD16^{-}$ **(C, D)** and $CD56^{+}CD16^{+}$ **(E, F)** NK cell subset abundance (left panel) as well as in CD137 expression (right panel) on the respective NK cell subsets at the indicated time-points after injection of 3 **(C, E)** or 6 **(D, F)** µg/g of the respective antibody preparations. Results are presented as mean +/-SEM. For statistical testing a 2-Way Anova with Tukey's multiple comparison test was used. *p<0.05; **p<0.01.

infiltrates and that urelumab deglycosylation reduced the number of cytotoxic T cells within the liver (Figures 7D, E). In summary, our results suggest that urelumab deglycosylation diminishes the release of pro-inflammatory cytokines at both antibody doses, while an infiltration of the liver by T cells could only be reduced at the 6µg/g dose.

Discussion

The introduction of checkpoint control and immunomodulatory antibodies in the therapy of cancer, autoimmune diseases or after solid organ transplantation marks a new era in immunotherapy. One agonistic antibody target that showed very promising results in pre-clinical studies in mouse models of cancer and autoimmunity is CD137, which is mainly expressed on activated T cells, monocytes, and NK cells (29–31). In humans two different CD137-specific antibodies, the IgG4 antibody urelumab or the IgG2 antibody utomilumab were tested in clinical trials (8, 28). Both antibody formats were chosen to limit unwanted side-effects *via* the interaction of the antibody Fc-domain with cellular FcγRs and the complement pathway. However, while the IgG4 antibody urelumab was characterized by a higher agonistic activity compared to utomilumab, it also triggered more severe side-effects, including a systemic cytokine release syndrome and hepatotoxicity requiring to readjust antibody dosing to levels at which clinical trials using urelumab as a monotherapy showed disappointing results (28). Despite the notion that IgG4 Fc-domains may not play a role in

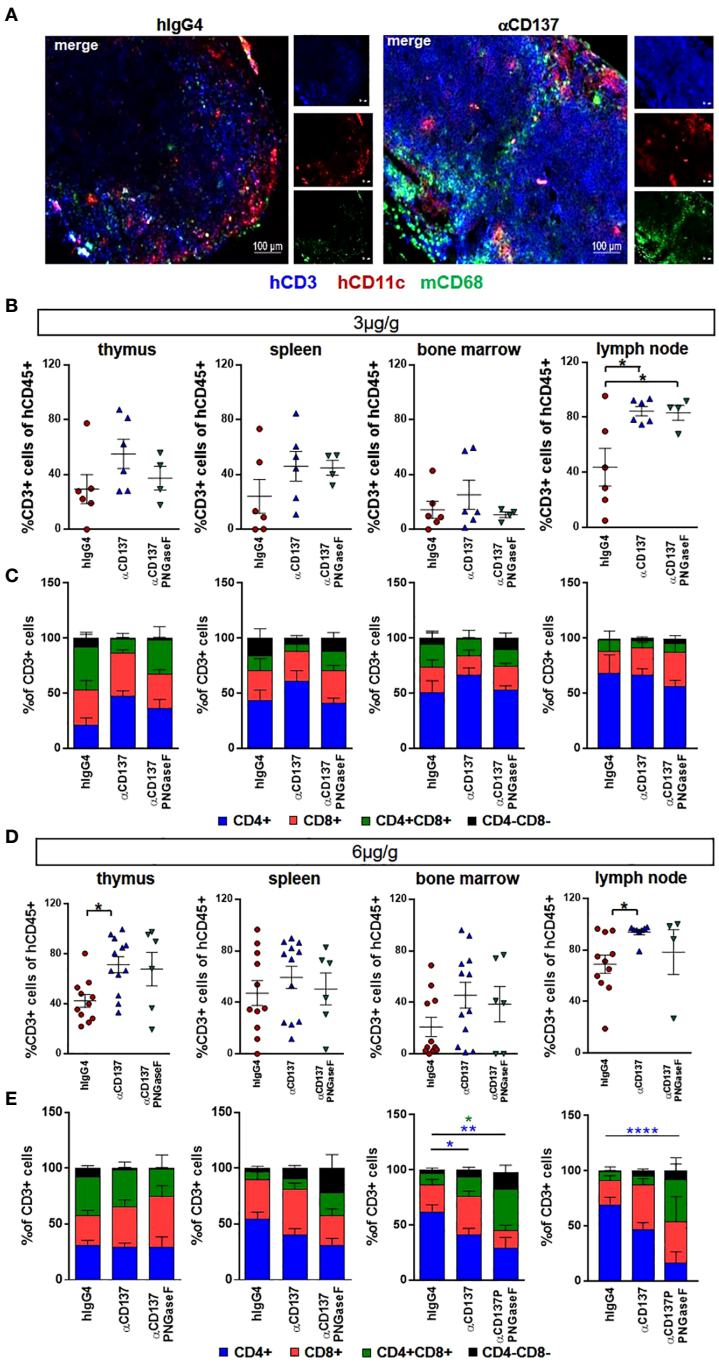

FIGURE 4
Effect of urelumab variant treatment on T cells in primary and secondary immunological organs. Humanized mice received either 3 or 6µg/g of a human IgG4 isotype control, urelumab (αCD137) or deglycosylated urelumab (αCD137 PNGaseF) and were studied for twenty days after antibody injection. **(A)** Shown are representative immunofluorescent stainings of lymph node sections of mice treated with 6µg/g hIgG4 as a control or with urelumab (αCD137) identifying human T cells (hCD3), human dendritic cells (hCD11c), as well as mouse macrophages (mCD68). **(B, C)** Depicted are relative amounts of human CD3+ cells **(B)** and of different T cell subsets **(C)** in thymus, spleen, bone marrow, and lymph nodes of mice treated with 3µg/g of the indicated antibodies (hIgG4: n= 6; αCD137: n=6; αCD137 PNGaseF: n=4). **(D, E)** Depicted are relative amounts of human CD3+ T cells **(D)** and of different T cell subsets **(E)** in thymus, spleen, bone marrow, and lymph nodes of mice treated with 6µg/g of the indicated antibody variants (hIgG4: n= 11; αCD137: n=8-12; αCD137-PNGaseF: n=4-6). Shown is the combined data from two to three independent experiments and results are represented as mean +/- SEM. Statistical analysis was done by Shapiro-Wilk normality test, Kruskal-Wallis with Dunn's multiple comparison test or 1-way ANOVA. For analysing T cell subsets a 2-Way ANOVA was performed. *p<0.05; **p<0.01; ****p<0.0001.

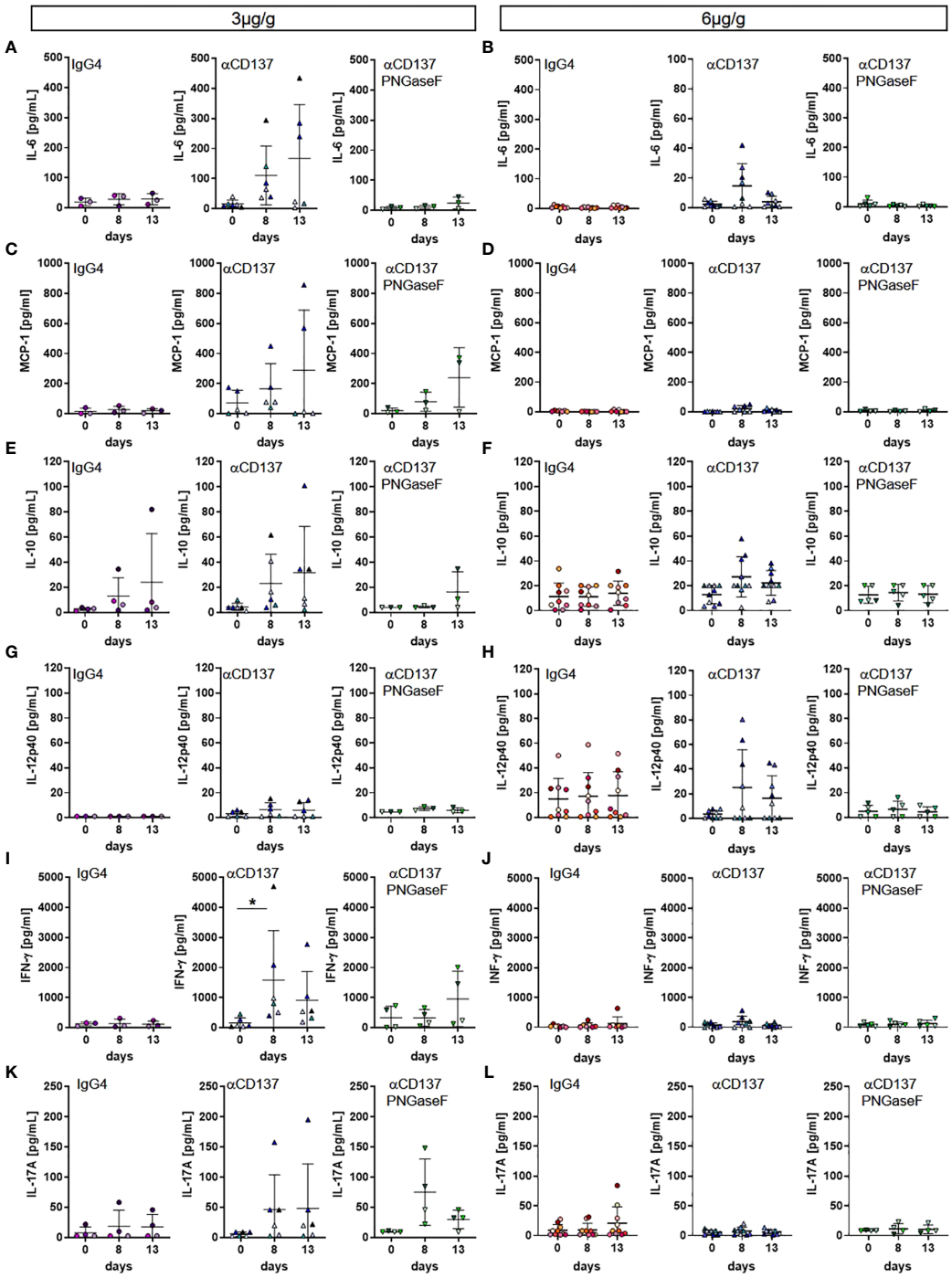

FIGURE 5
Effect of urelumab treatment dose and glycosylation on serum cytokine levels in humanized mice. Humanized mice received either 3 or 6µg/g of a human IgG4 isotype control, urelumab (αCD137) or deglycosylated urelumab (αCD137 PNGaseF) and serum samples were collected before and at 8 and 13 days after antibody injection. Shown are concentrations of serum cytokine levels before and at the indicated time-points after injection of 3 **(A, C, E, G, I, K)** or 6 **(B, D, F, H, J, L)** µg/g. Depicted are serum concentrations of IL-6 (hIgG4: n=3-8, αCD137: n=6-8, αCD137 PNGaseF: n=3-5) **(A, B)**, MCP-1 (hIgG4: n=3-7, αCD137: n=5-7, αCD137 PNGaseF: n=3-4) **(C, D)**, IL10 (hIgG4: n=4-9, αCD137: n=6-10, αCD137 PNGaseF: n=3-5) **(E, F)**, IL12p40 (hIgG4: n=3-9, αCD137: n=6-9, αCD137 PNGaseF: n=3-5) **(G, H)**, IFNγ (hIgG4: n=3-7, αCD137: n=6-8, αCD137 PNGaseF: n=4-5) **(I, J)**, and IL17A (hIgG4: n=4-8, αCD137: n=6-9, αCD137 PNGaseF: n=4) **(K, L)**. Results are expressed as mean +/-SD. Statistical analysis was done using ROUT outlier test (Q=1%) and Shapiro-Wilk normality test. For graphs showing serum concentration of cytokines either Friedman test with Dunn's multiple comparison test or RM-One-Way ANOVA with Tukey's multiple comparison test was performed. *p<0.05.

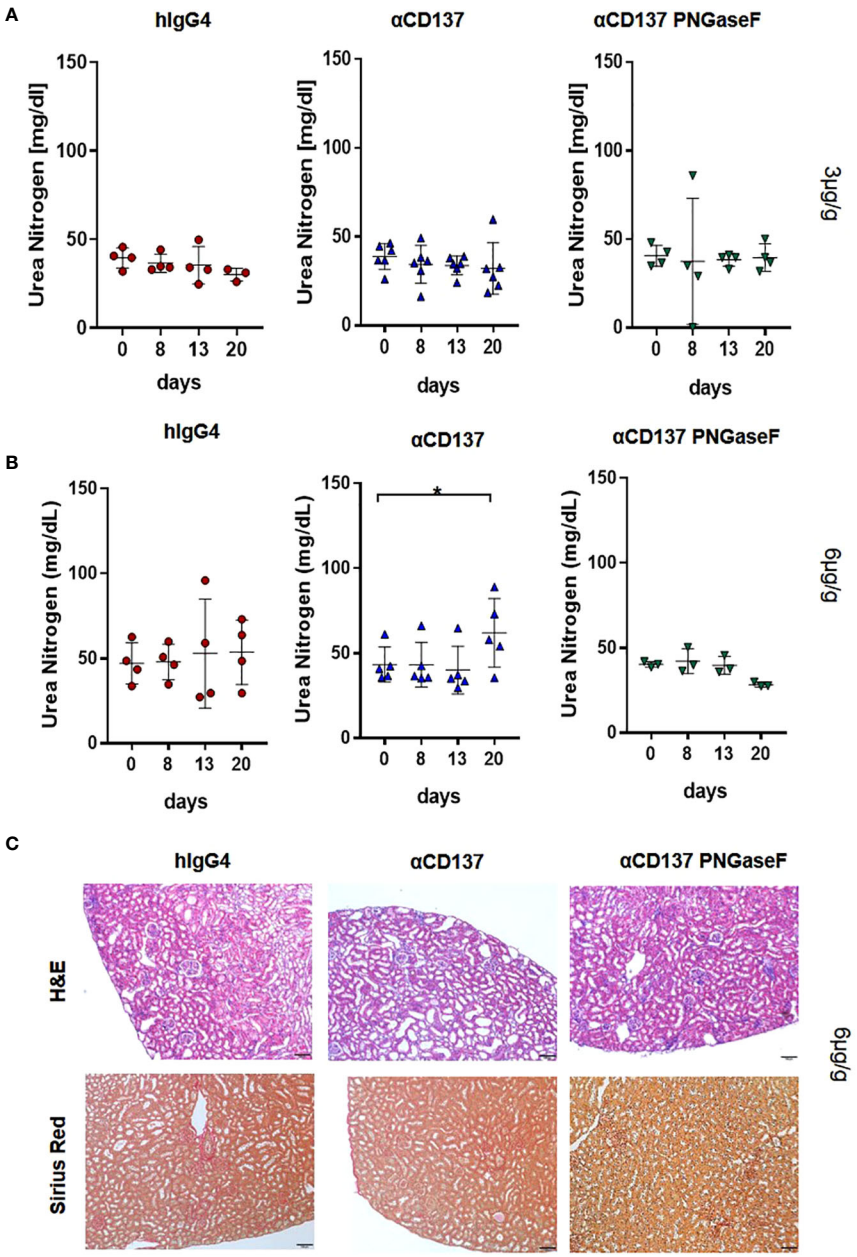

FIGURE 6
Impact of αCD137 treatment on kidney function. Humanized mice received either 3 or 6µg/g of a human IgG4 isotype control, urelumab (αCD137) or deglycosylated urelumab (αCD137 PNGaseF). **(A, B)** Shown are blood urea nitrogen (BUN) levels before (day 0) or at the indicated timepoints after treatment of humanized mice with 3 (hIgG4: n=4, αCD137: n=6, αCD137 PNGaseF: n=4) **(A)** or 6 (hIgG4: n=4, αCD137: n=5, αCD137 PNGaseF: n=3) **(B)** µg/g of the IgG4 antibody variants, as indicated. **(C)** Shown are hematoxylin-eosin (H–E) and Sirius red stainings of kidney sections of mice treated with 6µg/g of the indicated IgG4 antibody variants twenty days after antibody injection. Scale bars represent 100µm. Results are expressed as mean with SD. Statistical analysis was done by using Shapiro-Wilk normality test; p values were determined by using either Friedman test with Dunn's multiple comparison analysis or One-Way-Anova with Tukey's multiple comparison test. *p<0.05.

mediating urelumab activity, we reasoned that IgG4 immune complexes, formed *in vivo* upon CD137-specific antibody binding to T cells for example, may productively interact with human FcγRs and trigger Fc-dependent activities as suggested by several previous reports (22–24). Aiming to analyse this *in vivo* in the setting of a human immune system, we used deglycosylated IgG4, which has a strongly reduced capacity to bind to cellular FcγRs; and chose our well established NSG-FcRγ mouse model. This allows the transplantation

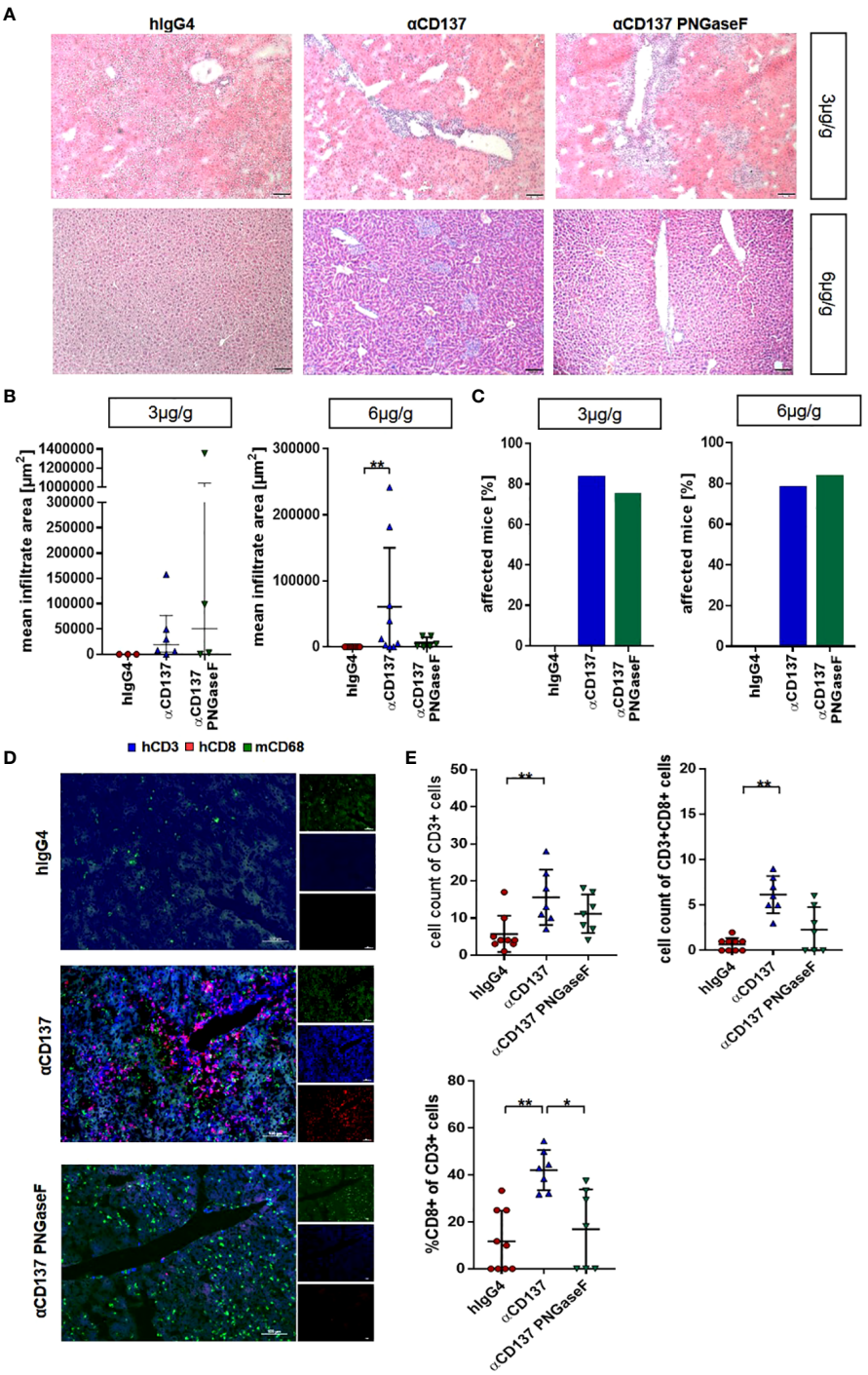

FIGURE 7
Impact of treatment with urelumab variants on liver pathology. Humanized mice received either 3 or 6µg/g of a human IgG4 isotype control, urelumab (αCD137) or deglycosylated urelumab (αCD137 PNGaseF) and liver pathology was studied twenty days after antibody injection. **(A, B)** Representative hematoxylin/eosin stained liver sections **(A)** of mice treated with 3 or 6µg/g of human IgG4 isotype control, urelumab and deglycosylated urelumab variants (scale bar 100µm) and quantification of the mean infiltrate area **(B)** of immune cell infiltrates (hIgG4: n=3, αCD137: n=6, αCD137 PNGaseF: n=4). **(C)** Shown is the percentage of mice with detectable immune cell infiltrates in the liver. **(D, E)** Immunofluorescent staining of liver sections (scale bar 100µm) **(D)** and quantification of the infiltration **(E)** of CD3+ T cells (upper panel) and the relative amount of CD3+CD8+ T cells within the CD3+ T cell population (lower panel) (hIgG4: n=9, αCD137: n=7, αCD137 PNGaseF: n=7, n represents the number of analysed images of two independent mice per group). Statistical testing was performed by using a Shapiro-Wilk and Kruskal Wallis test with a Dunn's multiple comparison test. *p<0.05; **p<0.01.

of a human immune system by injection of human hematopoietic stem cells into immunodeficient mice, lacking all mouse activating FcγRs, at the day of birth (23, 27, 32).

Consistent with a model in which the severe side effects triggered by urelumab injection are mediated by the interaction of the IgG4 Fc-domain with cellular FcγRs, our study demonstrates that a deglycosylated IgG4 variant of urelumab, which has a strongly reduced ability to bind cellular FcγRs, loses its ability to trigger a strong, systemic release of pro-inflammatory cytokines at both antibody doses. In addition, deglycosylated urelumab failed to recruit immune cell infiltrates into the liver at the high (but not at the low) antibody dose and did not trigger increased blood urea nitrogen levels. In contrast, only a mild reduction or delay in T cell proliferation was noted, suggesting that at least many of the beneficial immunomodulatory effects mediated by urelumab were maintained in the absence of urelumab glycosylation. Our study further suggests, that a much stronger and qualitatively different cytokine release was observed at the 3μg/g dosing scheme, which correlated with a drop in body temperature observed eight days after injection of urelumab. In contrast, deglycosylated urelumab injection resulted only in a minor and delayed reduction in body temperature. The observation that higher doses of urelumab may result in diminished release of pro-inflammatory cytokines is consistent with a recent study by Qi and colleagues demonstrating that human T cells secret less IFNγ when stimulated with 1 instead 0.3μg/ml of urelumab *in vitro* in the presence of FcγR expressing cells (21). The phenomenon that higher IgG doses may trigger less FcγR-dependent effects compared to lower antibody doses is well known as the Heidelberger-Kendall curve, although a more detailed titration would be necessary to demonstrate this more convincingly in our study (33, 34).

One surprising finding of our study was that urelumab deglycosylation strongly impairs immune cell infiltration into the liver at the 6μg/g dose but not at the 3μg/g antibody dose. Again, the Heidelberger-Kendall curve would predict that larger immune complexes could be formed at a lower antibody dose, which may retain binding to at least some activating FcγRs, such as FcγRI, even in an aglycosylated form as shown in this and our previous studies (24). As no FcγRI-specific antibody with highly efficient blocking activity for IgG binding is available, it is currently not possible to test this hypothesis directly. An alternative explanation may be afforded by the much more pronounced cytokine release syndrome observed at the lower antibody dose, which may trigger an infiltration of immune cells into the liver. However, urelumab deglycosylation largely blunted this cytokine release, yet the immune cell infiltration in the liver was maintained. Thus, this result rather suggests, that the cytokine release can be uncoupled from immune cell infiltration into the liver. More studies will be necessary to fully unravel the molecular and cellular basis for this result.

With respect to the need for a productive interaction of the Fc-domain of CD137-specific antibodies for stimulating T cell proliferation, several studies in mice demonstrated that different CD137-specific antibodies required a functional Fc-domain for maintaining their T cell stimulatory activity *in vivo* (10, 20, 21). The results of our study suggest that urelumab-dependent T cell proliferation may be maintained in the absence of an FcγR engaging Fc-domain, while unwanted side effects including the systemic cytokine release can be reduced. A major limitation of our study at present is that this humanized mouse model does not allow to assess the therapeutic activity of deglycosylated urelumab in the setting of tumor or autoimmune disease, for example. Without matching the tumor MHC haplotype to the human immune system it would be difficult to assign a reduction in tumor growth to the enhancement of tumor-specific immune reactions. Nonetheless, the maintenance of T cell proliferation upon injection of deglycosylated urelumab may indicate that the effect of T cell expansion can be uncoupled from the unwanted side-effects and hence may be less dependent on a functional Fc-domain.

Experimental procedures

Human material

Human material (blood, spleen, bone marrow and thymus samples) was provided by the University Hospital Erlangen. Leukocyte reduction cones were obtained from anonymous healthy adult donors, thymus samples were derived from cardiac surgeries of healthy children, spleen samples were collected from patients requiring therapeutic splenectomy, and bone marrow was obtained from biopsies performed to exclude bone marrow involvement in cancer. All samples were obtained under local ethical committee approvals (Ethikkommission der Friedrich-Alexander-Universität Erlangen-Nürnberg), and informed written consents were obtained in accordance with the Declaration of Helsinki. In brief, thymic and splenic tissues were chopped into small pieces using forceps and scalpel. The tissue was transferred into C-tubes (Miltenyi Biotec), filled with 5 ml RPMI1640, further mechanically disrupted using a Gentle MACS tissue dissociator (Miltenyi Biotec), and enzymatically digested with 400 U/ml collagenase D (Serva) and 100 μg (spleen) or 300 μg (thymus) deoxyribonuclease I (Sigma). After filtering the cell suspension twice, cell suspension of splenic and thymic tissue as well as the leukocyte enriched fraction of human blood was diluted with RPMI1640 and a density gradient centrifugation using Human Pancoll (ρ = 1.077 g/ml; Pan Biotech) was performed as described earlier. Bone marrow was filtered using a 100 μm cell strainer prior to the density gradient centrifugation. After the centrifugation, the interphase containing the mononuclear cells was collected, washed twice with RPMI1640, and used for experiments or resuspended in FCS + 10% DMSO at a final concentration of $5*10^7$ cells/ml and stored at -80 °C until analysis.

Mice

FcRγ-/- mice, deficient for the fcer1 gene, were provided by Jeffery Ravetch (Rockefeller University, New York, USA), whereas NOD-, SCID-, and γc-deficient mice were supplied by the Jackson Laboratories. For generating NOD-SCID/γc/FcRγ-/- (NSG-FcRγ-/-) mice the γc-/- as well as fcer1g-/- mouse strains were back-crossed to the NOD/Scid background for at least ten generations. Mice were kept according to the guidelines of the National Institutes of Health and the legal requirements of Germany.

Generation of humanized mice

The humanization of NSG-FcRγ-/- mice was performed as described before (35). In brief, hematopoietic stem cells were isolated from human umbilical cord blood using a 'Direct CD34 Progenitor Cell Isolation Kit, human' (Miltenyi Biotec) according to the manufacturer's instructions and frozen and stored in liquid nitrogen until further use. New-born NSG-FcRγ-/- mice were irradiated with a dose of 1.4 Gy within the first 24 hours after birth. 6-18 hours after irradiation, hematopoietic stem cells were injected intravenously into the facial vein (20,000-50,000 HSCs). Peripheral blood of transplanted mice was analyzed at 10-12 weeks of age and mice having greater than 5% hCD45+ cells in the peripheral blood were arbitrarily allocated to experimental groups and used for further experiments. As far as possible different humanized mice generated from one HSC donor received different treatments (isotype control, unmodified or aglycosylated urelumab) to allow a better comparison between control and experimental groups. With respect to comparison between 3 and 6μg/g treatment groups we aimed at including as many HSC donors as possible to limit batch effects of individual HSC donors. Thus, we included humanized mice generated from 22 different HSC donors in the experiments to mimic a diverse human clinical situation.

Antibody injection

Urelumab was injected intravenously at a dose of 3 or 6μg/g. As an isotype control, a human IgG4 antibody was administered. In addition, a deglycosylated variant of urelumab was generated by treating urelumab with 10 Units per μg IgG PNGase F (NEW ENGLAND BioLabs, Cat.#: P0704L) over night at 37°C. Urelumab deglycosylation was verified using lectin blot analysis with Lens culinaris agglutinin as described before (36)

Flow cytometric analysis

Peripheral blood (100μL) was collected by retro orbital puncture before and at select time points after antibody treatment. Single cell preparations from organs were generated by using a 70μm cell strainer. Erythrocytes were lysed using ddH_2O followed by adding 10x PBS to stop the lysis. After washing, cells were re-suspended in Fc-Block (0.5 μg/well, 2.4G2) and incubated for 15 min on ice, followed by another washing step and staining for 15 min at 4°C with fluorochrome-conjugated antibodies (see Table 1). Finally, DAPI was added (dilution 1:5,000) for identifying dead cells, cells were washed again, and re-suspended in 100 μl FACS buffer followed by analysis on a FACS Canto II. Data was evaluated using the BD Diva or FlowJo software.

Binding of urelumab variants to human FcγRI

100000 CHO cells or CHO cells expressing FcγRI were incubated with either 1μg of untreated urelumab (αCD137), 1μg of PNGase F treated urelumab (αCD137-PNGase F) or with PBS in 100μl FACS buffer for 1h on ice. After incubation, cells were washed and stained for 15 min on ice with either Protein L PE (1:10) in FACS buffer. Cells were washed again and resuspended in 50μL of FACS buffer and analysed at FACS CANTO II.

Cytokine release assay

For the determination of human cytokine levels, peripheral blood was obtained (as described above), incubated for 30min. at RT, and centrifuged at 10,000xg for 5 min. Serum was collected by taking off the supernatant, which was stored at -80°C until further use. To measure human cytokine levels in the serum, the human LEGENDplex™ Multi-Analyte Flow Assay Kit (Biolegend) was used according to the instructions of the manufacturer. Samples were analyzed by FACS analysis on a FACS Canto II and the data was analyzed by using Biolegend's LEGENDplex™ Data Analysis Software.

Determination of kidney dysfunction

For monitoring kidney dysfunction, blood urea nitrogen was measured using urea nitrogen colorimetric kit (Teco Diagnostics) using one tenth of the recommended volume. 0.5 μL serum was used and mixed with the BUN Enzyme Reagent. After 10 min of incubation at RT, Bun Color developer was added and again incubated 10 min at RT. The absorbance at 570nm was measured with 'VersaMax tunable microplate reader' (Molecular Devices).

TABLE 1 Key reagents used for the study.

Reagent type (species) or resource	Designation	Source reference	Catalogue number	Analysis and dilution
Antibody	Anti-human CD3 PerCP (mouse monoclonal) Clone UCHT1	BioLegend	Cat.#: 300428	Flow cytometry (1:200)
Antibody	Anti-human CD3 Brilliant Violet 510™ (mouse monoclonal) Clone SK7	BioLegend	Cat.#: 344828	Flow cytometry (1:100)
Antibody	Anti-human CD3 Alexa Fluor® 647 (mouse monoclonal) Clone UCHT1	BioLegend	Cat.#: 300416	Immuno-histochemistry (1:20)
Antibody	Anti-human CD4 FITC (mouse monoclonal) Clone IV T114	BioLegend	Cat.#: 300506	Flow cytometry (1:200)
Antibody	Anti-human CD8 PE (mouse monoclonal) Clone SK1	BioLegend	Cat.#: 344706	Immuno-histochemistry (1:20)
Antibody	Anti-human CD8 PE/Cy7 (mouse monoclonal) Clone SK1	BioLegend	Cat.#: 344712	Flow cytometry (1:200)
Antibody	Anti-human CD14 PE (mouse monoclonal) Clone M5E2	BioLegend	Cat.#: 301806	Flow cytometry (1:50)
Antibody	Anti-human CD16 FITC (mouse monoclonal) Clone 3G8	BioLegend	Cat.#: 302006	Flow cytometry (1:100)
Antibody	Anti-human CD33 Brilliant Violet 510™ (mouse monoclonal) Clone WM53	BioLegend	Cat.#: 303422	Flow cytometry (1:100)
Antibody	Anti-human CD45 APC/Fire™ 750 (monoclonal mouse) Clone HI30	BioLegend	Cat.#: 304062	Flow cytometry (1:200)
Antibody	Anti-mouse CD45.1 Brilliant Violet 421™ (mouse monoclonal) Clone A20	BioLegend	Cat.#: 110732	Flow cytometry (1:600)
Antibody	Anti-human CD56 PE/Cy7 (mouse monoclonal) Clone MEM-188	BioLegend	Cat.#: 304628	Flow cytometry (1:100)
Antibody	Anti-mouse CD68 Alexa Flour® 488 (rat monoclonal) Clone FA-11	BioLegend	Cat.#: 137011	Immuno-histochemistry (1:50)
Antibody	Anti-human CD137 APC (mouse monoclonal) Clone 4B4-1	BioLegend	Cat.#: 309810	FACS (1:100)
Antibody	Urelumab (αCD137)	In house (UK Erlangen)	—	i.v. injection
Antibody	Urelumab PNGase F digested	Digestion in house		i.v. injection
Antibody	IgG4 (S228P) isotype control	BioXcell	Cat.#: CP147	i.v. injection
Kit	LegendPlex™ Multi-Analyte Flow Assay Kit Custom Human Assay	BioLegend®	info@biolegend.com	Cytokine detection
Enzyme	PNGase F	NEW ENGLAND BioLabs	Cat.#: P0704L	Antibody digestion
Kit	Urea Nitrogen (BUN) Reagent Set (Colorimetric Method)	TECO DIAGNOSTICS	Cat.#: B551-132	Blood Urea Nitrogen
Kit	CD34 Micro Bead Kit, human	Miltenyi Biotec	Cat.#: 130-046-702	Stem cell isolation

Immunohistochemistry

Organ samples were frozen at -80°C in OCT and cut into 5 µM sections followed by fixation for 2.5 minutes with acetone. Unspecific antibody binding was prevented by incubation of the sections with blocking solution (5% goat serum in PBS) for 1 hour at RT. Blocking solution was removed and fluorochrome-conjugated antibodies were added for staining in 5% goat serum in PBS and incubated for 30 min at RT in the dark. Slides were rinsed 3 times with 1xPBS, mounted with a drop of mounting medium and dried for 30 minutes. Stained sections of liver and kidney were analyzed on an Axiovert 200M microscope.

For determination of liver and kidney pathology, Sirius Red collagen staining was performed to detect morphological abnormalities. H&E staining of liver and kidney samples was used for determination of cell-infiltrates. For both stainings, liver and kidney samples were embedded in paraffin and cut into 5 µM sections. Stainings were done using standard protocols beginning with paraffin removal using xylene, isopropanol and 96% ethanol. H&E staining was performed by incubating the

sections for 8 min in Mayer's hematoxylin solution (Merck 1:5), followed by washing steps and a 1 min incubation in eosin solution (Roth). After another washing step, slides were dipped into 96% ethanol, isopropanol and xylene. A drop of ROTI® Histokitt II ready-to use-solution (Roth) was placed over the tissue on each slide and a coverslip was added. For Sirius Red staining the slides were treated for 6 min with Weigert's iron hematoxylin (Roth), washed and then incubated in picro-sirius-red-solution for 5 min. Afterwards the sections were dipped in 100% ethanol and xylene. The sections were covered with a drop of ROTI® Histokitt II ready-to use-solution (Roth) and a coverslip was placed above the tissue.

For further examination of liver damage, H&E stained liver sections were examined and liver immune-cell-infiltrates measured using CellSens 1.14 Software (OLYMPUS). Cell-infiltrates were marked and their area was calculated automatically. To determine the mean infiltrate size, three images of a liver section were analyzed per mouse. For a more detailed examination of cell types infiltrating the liver, immunofluorescent staining of liver sections was performed. Human T cells were stained by CD3 and CD8 was used for human cytotoxic T cells (see Table 1). The overall T cell count and the $CD8^+$ T cell count was determined by counting the cells on 7-9 liver sections per group.

Statistical analysis

GraphPad Prism 7.03 software (GraphPad Software Inc, Sand Diego, CA) was used for graphs and statistical analysis. Data are given in means ± standard error of the mean (SEM) or standard deviation (SD). All samples were tested for Gaussian distribution. Dependent on the Shapiro-Wilk normality test and on the comparative data we used one-way or two-way analysis of variance (ANOVA), Friedman or Kruskal-Wallis-test followed by a multiple comparison test (Tukey or Dunn). Data was further evaluated by using ROUT's Outlier test (Q=1%). Detailed information of statistical test of individual results can be found in respective figure legends.

Data availability statement

The raw data supporting the conclusions of this article will be made available by the authors, without undue reservation.

Ethics statement

The animal study was reviewed and approved by Government of Lower Franconia.

Author contributions

CR, AI-E, AL, CH and LH performed experiments, analyzed the data, and wrote the manuscript. DD contributed essential reagents. FN wrote the manuscript. All authors contributed to the article and approved the submitted version.

Funding

This study was funded by the Deutsche Forschungsgemeinschaft (DFG, German Research Foundation - SFB TRR 305 - B02 to FN SFB TRR 305 - B05 to DD, and DU548/5-1 to DD), and by the Emerging Fields Initiative Big-Thera of the FAU (to FN and DD).

Acknowledgments

We are grateful to Heike Albert and Heike Danzer for expert technical assistance and to Robert Cesnjevar for providing human tissue samples.

Conflict of interest

The authors declare that the research was conducted in the absence of any commercial or financial relationships that could be construed as a potential conflict of interest.

Publisher's note

Supplementary material

The Supplementary Material for this article can be found online at: https://www.frontiersin.org/articles/10.3389/fimmu.2022.970290/full#supplementary-material

SUPPLEMENTARY FIGURE 1
Identification of human immune cell subsets in humanized mice *via* flow cytometry. Shown is an exemplary gating strategy separating mouse immune cells (mCD45+) from human immune cells (hCD45+) in splenic single cell preparations of humanized mice three months after HSC transplantation. Human immune cell subsets (hCD45+) were identified by expression of human immune cell lineage specific markers, such as CD3, CD4, and CD8 to detect human CD8+ and CD4+ T cell subsets or CD56 or CD33 to identify natural killer (NK) cells or monocytes, respectively. CD16 in

combination with CD56, as well as CD16/CD14 in combination with CD33 was used to identify further subsets of NK cells or monocytes.

SUPPLEMENTARY FIGURE 2
Comparison of CD137 expression on human T cells, NK cells and monocytes in humanized mice and humans. **(A)** Shown is CD137 expression on $CD3^+$ T cell subsets in humanized mice in blood (n=37), spleen, bone marrow, thymus and lymph node (n=8) samples. **(B)** Shown is CD137 expression on the indicated human $CD3^+$ T cell subsets in human peripheral blood, spleen, bone marrow as well as on thymic T cells (n=3). **(C, D)** Shown is CD137 expression on NK cell subsets in the respective organs in humanized mice (blood (n=33), spleen and bone marrow (n= 12)) **(C)** and humans (n=3) **(D)**. **(E, F)** Depicted is CD137 expression on $CD33^+$ monocyte subsets located within the indicated organs in humanized mice (blood: n=33, spleen and bone marrow: n= 12) **(E)**, as well as in the respective human organs **(F)** (n=3). Results are expressed as median of ΔMFI with interquartile range.

SUPPLEMENTARY FIGURE 3
Effect of urelumab deglycosylation on binding to human FcγRI. **(A)** Shown is a Coomassie stained PAA gel (left panel) and a western blot analysis (right panel) using lens culinaris agglutinin (LCA) to detect the effect of deglycosylation on urelumab size or the urelumab core sugar structure, respectively. **(B)** Depicted is the binding of untreated urelumab (αCD137) or of PNGaseF treated urelumab (αCD137 PNGaseF) to CHO cells (CHO-Blank) or CHO cells expressing human FcγRI (CHO-FcγRI) as the delta mean fluorescence intensity (ΔMFI) as determined by flow cytometry. Bound urelumab was detected with fluorescently labelled protein L. As a further control, CHO cells as well as CHO-FcγRI expressing cells were only stained with protein L in the absence of urelumab variants (Ø). Shown is the mean +/- SEM of two independent experiments.

SUPPLEMENTARY FIGURE 4
Effect of urelumab variants on T cells in the peripheral blood. Shown are the absolute numbers of CD3+ human T cells in the peripheral blood of humanized mice upon treatment with 3µg/g (hIgG4: n= 5; αCD137: n=6; αCD137 PNGaseF: n=4) or 6µg/g (hIgG4: n= 7-13; αCD137: n=10-11; αCD137 PNGaseF: n=6) of a human IgG4 isotype control antibody, urelumab (αCD137) or a PNGaseF treated urelumab variant (αCD137 PNGaseF). For each time point the mean+/-SEM is shown.

SUPPLEMENTARY FIGURE 5
Effect of urelumab variant injection on serum cytokine levels. Serum cytokine concentrations were determined before and at the indicated time-points after treating humanized mice with 3µg/g **(A, C, E)** or 6µg/g **(B, D, F)** of hIgG4, αCD137 or deglycosylated αCD137 PNGaseF variant. Depicted are serum concentrations of **(A)** IL-1β (hIgG4: n=3, aCD137: n=6, αCD137 PNGaseF: n=4), **(C)** IL-8 (hIgG4: n=3, αCD137: n=6, αCD137 PNGaseF: n=4), and **(E)** IFN-α (hIgG4: n=4, αCD137: n=6, aCD137 PNGaseF: n=4) in mice treated with 3µg/g of the indicated antibody variants. Concentration of **(B)** IL-1β (hIgG4: n=7, aCD137: n=9, aCD137 PNGaseF: n=5), **(D)** IL-8 (hIgG4: n=8, αCD137: n=8, αCD137 PNGaseF: n=4), and **(F)** IFN-α (hIgG4: n=9, αCD137: n=8, αCD137 PNGaseF: n=5), in mice treated with 6µg/g of antibody variants. Results are expressed as median of ΔMFI with interquartile range. A ROUT outlier test (Q=1%) and Shapiro-Wilk normality test were performed followed by either Friedman test with Dunn's multiple comparison test or RM-One-Way ANOVA with Tukey's multiple comparison test was performed.

References

1. Kaplon H, Reichert JM. Antibodies to watch in 2019. *MAbs* (2019) 11:219–38. doi: 10.1080/19420862.2018.1556465

2. Demaria O, Cornen S, Daeron M, Morel Y, Medzhitov R, Vivier E. Harnessing innate immunity in cancer therapy. *Nature* (2019) 574:45–56. doi: 10.1038/s41586-019-1593-5

3. Ribas A, Wolchok JD. Cancer immunotherapy using checkpoint blockade. *Science* (2018) 359:1350–5. doi: 10.1126/science.aar4060

4. Paluch C, Santos AM, Anzilotti C, Cornall RJ, Davis SJ. Immune checkpoints as therapeutic targets in autoimmunity. *Front Immunol* (2018) 9:2306. doi: 10.3389/fimmu.2018.02306

5. Sun Y, Chen JH, Fu Y. Immunotherapy with agonistic anti-CD137: two sides of a coin. *Cell Mol Immunol* (2004) 1:31–6.

6. Sun Y, Lin X, Chen HM, Wu Q, Subudhi SK, Chen L, et al. Administration of agonistic anti-4-1BB monoclonal antibody leads to the amelioration of experimental autoimmune encephalomyelitis. *J Immunol* (2002) 168:1457–65. doi: 10.4049/jimmunol.168.3.1457

7. Hassel JC, Heinzerling L, Aberle J, Bahr O, Eigentler TK, Grimm MO, et al. Combined immune checkpoint blockade (anti-PD-1/anti-CTLA-4): Evaluation and management of adverse drug reactions. *Cancer Treat Rev* (2017) 57:36–49. doi: 10.1016/j.ctrv.2017.05.003

8. Segal NH, Logan TF, Hodi FS, McDermott D, Melero I, Hamid O, et al. Results from an integrated safety analysis of urelumab, an agonist anti-CD137 monoclonal antibody. *Clin Cancer Res* (2017) 23:1929–36. doi: 10.1158/1078-0432.CCR-16-1272

9. Knorr DA, Dahan R, Ravetch JV. Toxicity of an fc-engineered anti-CD40 antibody is abrogated by intratumoral injection and results in durable antitumor immunity. *Proc Natl Acad Sci U.S.A.* (2018) 115:11048–53. doi: 10.1073/pnas.1810566115

10. Buchan SL, Dou L, Remer M, Booth SG, Dunn SN, Lai C, et al. Antibodies to costimulatory receptor 4-1BB enhance anti-tumor immunity *via* T regulatory cell depletion and promotion of CD8 T cell effector function. *Immunity* (2018) 49:958–970 e957. doi: 10.1016/j.immuni.2018.09.014

11. Bulliard Y, Jolicoeur R, Windman M, Rue SM, Ettenberg S, Knee DA, et al. Activating fc gamma receptors contribute to the antitumor activities of immunoregulatory receptor-targeting antibodies. *J Exp Med* (2013) 210:1685–93. doi: 10.1084/jem.20130573

12. Coe D, Begom S, Addey C, White M, Dyson J, Chai JG. Depletion of regulatory T cells by anti-GITR mAb as a novel mechanism for cancer immunotherapy. *Cancer Immunol Immunother* (2010) 59:1367–77. doi: 10.1007/s00262-010-0866-5

13. Marabelle A, Kohrt H, Sagiv-Barfi I, Ajami B, Axtell RC, Zhou G, et al. Depleting tumor-specific tregs at a single site eradicates disseminated tumors. *J Clin Invest* (2013) 123:2447–63. doi: 10.1172/JCI64859

14. Simpson TR, Li F, Montalvo-Ortiz W, Sepulveda MA, Bergerhoff K, Arce F, et al. Fc-dependent depletion of tumor-infiltrating regulatory T cells co-defines the efficacy of anti-CTLA-4 therapy against melanoma. *J Exp Med* (2013) 210:1695–710. doi: 10.1084/jem.20130579

15. Li F, Ravetch JV. Inhibitory fcgamma receptor engagement drives adjuvant and anti-tumor activities of agonistic CD40 antibodies. *Science* (2011) 333:1030–4. doi: 10.1126/science.1206954

16. White AL, Chan HT, Roghanian A, French RR, Mockridge CI, Tutt AL, et al. Interaction with FcgammaRIIB is critical for the agonistic activity of anti-CD40 monoclonal antibody. *J Immunol* (2011) 187:1754–63. doi: 10.4049/jimmunol.1101135

17. Lux A, Nimmerjahn F. No need for constant help: human IgG2 antibodies have an autonomous agonistic activity for immunotherapy of cancer. *Cancer Cell* (2015) 27:10–1. doi: 10.1016/j.ccell.2014.12.010

18. White AL, Chan HT, French RR, Willoughby J, Mockridge CI, Roghanian A, et al. Conformation of the human immunoglobulin g2 hinge imparts superagonistic properties to immunostimulatory anticancer antibodies. *Cancer Cell* (2015) 27:138–48. doi: 10.1016/j.ccell.2014.11.001

19. Dahan R, Sega E, Engelhardt J, Selby M, Korman AJ, Ravetch JV. FcgammaRs modulate the anti-tumor activity of antibodies targeting the PD-1/PD-L1 axis. *Cancer Cell* (2015) 28:543. doi: 10.1016/j.ccell.2015.09.011

20. Ho SK, Xu Z, Thakur A, Fox M, Tan SS, DiGiammarino E, et al. Epitope and fc-mediated cross-linking, but not high affinity, are critical for antitumor activity of CD137 agonist antibody with reduced liver toxicity. *Mol Cancer Ther* (2020) 19:1040–51. doi: 10.1158/1535-7163.MCT-19-0608

21. Qi X, Li F, Wu Y, Cheng C, Han P, Wang J, et al. Optimization of 4-1BB antibody for cancer immunotherapy by balancing agonistic strength with FcgammaR affinity. *Nat Commun* (2019) 10:2141. doi: 10.1038/s41467-019-10088-1

22. Bruhns P, Iannascoli B, England P, Mancardi DA, Fernandez N, Jorieux S, et al. Specificity and affinity of human fcgamma receptors and their polymorphic variants for human IgG subclasses. *Blood* (2009) 113:3716–25. doi: 10.1182/blood-2008-09-179754

23. Lux A, Seeling M, Baerenwaldt A, Lehmann B, Schwab I, Repp R, et al. A humanized mouse identifies the bone marrow as a niche with low therapeutic IgG activity. *Cell Rep* (2014) 7:236–48. doi: 10.1016/j.celrep.2014.02.041

24. Lux A, Yu X, Scanlan CN, Nimmerjahn F. Impact of immune complex size and glycosylation on IgG binding to human FcgammaRs. *J Immunol* (2013) 190:4315–23. doi: 10.4049/jimmunol.1200501

25. Brandsma AM, Hogarth PM, Nimmerjahn F, Leusen JH. Clarifying the confusion between cytokine and fc receptor "Common gamma chain". *Immunity* (2016) 45:225–6. doi: 10.1016/j.immuni.2016.07.006

26. Kao D, Danzer H, Collin M, Gross A, Eichler J, Stambuk J, et al. A monosaccharide residue is sufficient to maintain mouse and human IgG subclass activity and directs IgG effector functions to cellular fc receptors. *Cell Rep* (2015) 13:2376–85. doi: 10.1016/j.celrep.2015.11.027

27. Schwab I, Lux A, Nimmerjahn F. Pathways responsible for human autoantibody and therapeutic intravenous IgG activity in humanized mice. *Cell Rep* (2015) 13:610–20. doi: 10.1016/j.celrep.2015.09.013

28. Chester C, Sanmamed MF, Wang J, Melero I. Immunotherapy targeting 4-1BB: mechanistic rationale, clinical results, and future strategies. *Blood* (2018) 131:49–57. doi: 10.1182/blood-2017-06-741041

29. Hurtado JC, Kim SH, Pollok KE, Lee ZH, Kwon BS. Potential role of 4-1BB in T cell activation. comparison with the costimulatory molecule CD28. *J Immunol* (1995) 155:3360–7.

30. Hurtado JC, Kim YJ, Kwon BS. Signals through 4-1BB are costimulatory to previously activated splenic T cells and inhibit activation-induced cell death. *J Immunol* (1997) 158:2600–9.

31. Kwon BS, Weissman SM. cDNA sequences of two inducible T-cell genes. *Proc Natl Acad Sci U.S.A.* (1989) 86:1963–7. doi: 10.1073/pnas.86.6.1963

32. Lux A, Nimmerjahn F. Of mice and men: the need for humanized mouse models to study human IgG activity *in vivo*. *J Clin Immunol* (2013) 33Suppl 1:S4–8. doi: 10.1007/s10875-012-9782-0

33. Chen H, Maul-Pavicic A, Holzer M, Huber M, Salzer U, Chevalier N, et al. Detection and functional resolution of soluble immune complexes by an FcgammaR reporter cell panel. *EMBO Mol Med* (2022) 14:e14182. doi: 10.15252/emmm.202114182

34. Heidelberger M, Kendall FE. A quantitative study of the precipitin reaction between type iii pneumococcus polysaccharide and purified homologous antibody. *J Exp Med* (1929) 50:809–23. doi: 10.1084/jem.50.6.809

35. Baerenwaldt A, Lux A, Danzer H, Spriewald BM, Ullrich E, Heidkamp G, et al. Fcgamma receptor IIB (FcgammaRIIB) maintains humoral tolerance in the human immune system *in vivo*. *Proc Natl Acad Sci U.S.A.* (2011) 108:18772–7. doi: 10.1073/pnas.1111810108

36. Albert H, Collin M, Dudziak D, Ravetch JV, Nimmerjahn F. *In vivo* enzymatic modulation of IgG glycosylation inhibits autoimmune disease in an IgG subclass-dependent manner. *Proc Natl Acad Sci U.S.A.* (2008) 105:15005–9. doi: 10.1073/pnas.0808248105

frontiers | Frontiers in Immunology

TYPE Original Research
PUBLISHED 12 October 2022
DOI 10.3389/fimmu.2022.972168

OPEN ACCESS

EDITED BY
Falk Nimmerjahn,
University of Erlangen Nuremberg, Germany

REVIEWED BY
Dapeng Zhou,
Tongji University, China
Adam Barb,
University of Georgia, United States
Daron I. Freedberg,
United States Food and Drug Administration, United States

*CORRESPONDENCE
Roger Y. Tam
roger.tam@hc-sc.gc.ca

SPECIALTY SECTION
This article was submitted to B Cell Biology, a section of the journal Frontiers in Immunology

RECEIVED 17 June 2022
ACCEPTED 01 September 2022
PUBLISHED 12 October 2022

CITATION
Hatfield G, Tepliakova L, Gingras G, Stalker A, Li X, Aubin Y and Tam RY (2022) Specific location of galactosylation in an afucosylated antiviral monoclonal antibody affects its FcγRIIIA binding affinity. *Front. Immunol.* 13:972168. doi: 10.3389/fimmu.2022.972168

Specific location of galactosylation in an afucosylated antiviral monoclonal antibody affects its FcγRIIIA binding affinity

Grayson Hatfield, Lioudmila Tepliakova, Genevieve Gingras, Andrew Stalker, Xuguang Li, Yves Aubin and Roger Y. Tam*

Centre for Oncology, Radiopharmaceuticals and Research, Biologics and Radiopharmaceutical Drugs Directorate, Health Canada, Ottawa, ON, Canada

Monoclonal antibodies (mAbs) comprise an essential type of biologic therapeutics and are used to treat diseases because of their anti-cancer and anti-inflammatory properties, and their ability to protect against respiratory infections. Its production involves post-translational glycosylation, a biosynthetic process that conjugates glycans to proteins, which plays crucial roles in mAb bioactivities including effector functions and pharmacokinetics. These glycans are heterogeneous and have diverse chemical structures whose composition is sensitive to manufacturing conditions, rendering the understanding of how specific glycan structures affect mAb bioactivity challenging. There is a need to delineate the effects of specific glycans on mAb bioactivity to determine whether changes in certain glycosylation profiles (that can occur during manufacturing) will significantly affect product quality. Using enzymatic transglycosylation with chemically-defined *N*-glycans, we show that galactosylation at a specific location of *N*-glycans in an afucosylated anti-viral mAb is responsible for FcγRIIIA binding and antibody-dependent cell-mediated cytotoxicity (ADCC) activity. We report a facile method to obtain purified asymmetric mono-galactosylated biantennary complex *N*-glycans, and their influence on bioactivity upon incorporation into an afucosylated mAb. Using ELISA, surface plasmon resonance and flow cytometry, we show that galactosylation of the α6 antenna, but not the α3 antenna, consistently increases FcγRIIIA binding affinity. We confirm its relevance in an anti-viral model of respiratory syncytial virus (RSV) using an adapted ADCC reporter assay. We further correlate this structure-function relationship to the interaction of the galactose residue of the α6 antenna with the protein backbone using 2D-^{1}H-^{15}N-NMR, which showed that galactosylation of at this location exhibited chemical shift perturbations compared to glycoforms lacking this galactose residue. Our results highlight

10.3389/fimmu.2022.972168

the importance of identifying and quantifying specific glycan isomers to ensure adequate quality control in batch-to-batch and biosimilar comparisons.

KEYWORDS

monoclonal antibody, glycosylation, effector activity, 2D NMR, structure-function activity

Introduction

Monoclonal antibodies (mAbs) are an important class of glycoprotein-based biotherapeutics that are used to treat cancer, inflammation and viral disease, of which many marketed products are of the IgG1 class (1). IgG1 glycoproteins comprise heavy and light chains that form the variable (Fab) and constant (Fc) regions with an approximate molecular weight of 150 kDa, with each region having distinct biological activities (2). The Fab regions are typically designed to bind to a target molecule (some of which are receptors) to inhibit its function, while the Fc region can initiate downstream immunological responses by various immune cells to further affect the biological activity of mAbs such as antibody-dependent cellular cytotoxicity (ADCC). The Fc region is structurally similar amongst IgG1 molecules and has a single *N*-glycosylation site at N297 of each of the two heavy chains. Protein glycosylation is a post-translational modification that is dynamically regulated by numerous glycosyltransferase and glycosidase enzymes during protein synthesis in the endoplasmic reticulum and Golgi bodies, and by these enzymes that may be in the cell or in the extracellular matrix (3). As such, manufacturing and production of mAbs typically result in heterogeneous mixtures of glycan structures, whose composition is sensitive to numerous expression parameters such as pH, temperature and media composition (4).

Specific *N*-glycan structures can greatly influence mAb bioactivity by altering its binding affinity to Fc receptors (FcR) on the surface of immune cells. Amongst the most widely studied glycan structure is the core fucose residue in *N*-glycans, where its presence decreases ADCC activity (5, 6) by hindering binding to the FcγRIIIa (CD16A) receptor (7, 8). Galactose is another important terminal carbohydrate residue that is directly proportional to ADCC, with previous studies showing inconsistent results (9–16). Although these insightful studies highlight the overall effect of fucosylation and general galactosylation on the interaction between Fc and FcγRIIIa, the use of non-homogeneous or ambiguous galactosylated glycoforms limits its exact correlation to its biological activity. Recent advances in glycoengineering using enzymatic transglycosylation have enabled the synthesis of mAbs with chemically-defined glycans and perform more detailed structure function analyses (12, 17–21). A recent study has reported that in glycoengineered rituximab (a commercially-available anti-inflammatory mAb) comprising defined homogeneous glycoforms, the location of the galactose residue in fucosylated biantennary complex Fc *N*-glycans showed differing activity (21); a galactose residue on the α6-antenna showed greater FcR binding and ADCC activity compared to that in the absence of the α3 antenna. This difference in activity is important in the regulatory evaluation of mAb therapeutics, as different commercially-available mAbs have been shown to have varying degrees of each mono-galactosylated isomers (22). However, whether this difference in activity between mono-galactosylated isomers is also observed in non-fucosylated glycans and in other mAbs targeting other antigens has not been reported. Further, it is unclear how these changes using chemically-defined glycans affect the Fc protein structure at the molecular level. Understanding how these epitopes affect mAb bioactivity and correlation to their structural properties is important, as glycoengineering is emerging as a strategy in mAb drug design and glycan characterization is crucial to ensure mAb efficacy and safety (23, 24).

While several glycosylation structure-function studies have been performed on mAbs in the context of anti-cancer and anti-inflammatory diseases (12, 17–21), those that focus on anti-viral mAbs have remained limited (10, 25). With the increasing development of anti-viral mAbs, especially with mAbs targeting SARS-CoV2 (26), it is important to continue to increase the knowledge about how glycosylation affects mAbs targeting anti-viral diseases. To this end, we report how mAb glycosylation affects its activity towards Respiratory Syncytial Virus (RSV), a virus that causes respiratory illness primarily in children, the elderly, and immunocompromised individuals, and is often misdiagnosed as influenza (27). RSV infects bronchial epithelial cells and causes increased mucous production that restricts breathing. While RSV vaccines were first produced for over 30 years, they are ineffective and have even been shown to exacerbate the disease (28). Viral Infections occur *via* binding of RSV protein F (RSV-F) and RSV-G to host cell surfaces (29, 30) that permits viral entry into the cells. A monoclonal antibody (mAb) therapeutic, palivizumab (Synagis), is an RSV-F neutralizing mAb that is effective prophylactic treatment, especially in vulnerable patients such as premature and young

infants (31). Palivizumab functions by inhibiting the binding of RSV-F to its host cell surface receptor and therefore inhibits viral entry into the cell. Hiatt et al. previously reported that palivizumab produced in plant cells (*Nicotiana benthamiana*) yields afucosylated agalactosylated complex (G0, 76%) and high mannose glycans (Man7/9, 17%), which increased FcγRIIIa binding affinity and decreased viral titre in the lungs of Cotton Rats (25). However, a more detailed study on how glycosylation affects palivizumab has not been reported. Herein, we report that FcγRIIIa binding and ADCC activity is significantly increased by galactosylation of the α6 antenna (but not the α3 antenna) of afucosylated biantennary glycans in palivizumab. Using enzymatic transglycosylation to engineer afucosylated mAbs with chemically-defined glycans with varying degrees of galactosylation at specific locations, the changes in binding affinity to FcγRIIIa receptors were assessed using ELISA, surface plasmon resonance (SPR), flow cytometry and an ADCC assay. In order to support glycan-associated bioactivities measurements, we have characterized each glycoform using 2D-^{1}H-^{15}N-NMR fingerprints on isotopically labelled Fc domains to assess the location of the terminal galactose moieties.

Results

Synthesis of afucosylated palivizumab with defined glycoforms

The glycoprofile of commercially available palivizumab (Synagis) was first characterized using high pH anionic exchange chromatography-pulsed amperometric detection (HPAEC-PAD). Palivizumab was treated with the endoglycosidase PNGaseF to release free *N*-glycans that were measured directly *via* HPAEC-PAD. In our analysis, commercially-available palivizumab comprises predominantly G0F, G1F and G2F (25, 46 and 17% respectively) by HPAEC-PAD analysis (Supplementary Figures S1A, B). Surprisingly, HPAEC-PAD analysis revealed 4% of a high mannose (Man-5) glycan and pseudohybrid *N*-glycan structures, which were not detected by intact mass spectrometry analysis, nor reported previously. Intact mass spectrometry shows the presence of both symmetric and asymmetric glycosylation of the dimerized Fc heavy chains. Based on previous literature results (25) and our HPAEC-PAD analysis of PNGase F-released glycans (Supplementary Figures S1A, B), the peak at 147,958.813 Da corresponds to both glycans being of the agalactosylated G0F structure, while peaks at 148,118.953 and 148,440.328 Da indicate the asymmetric glycosylation comprising agalactosylated/monogalactosylated (G0F/G1F) and mono-/digalactosylated (G1F/G2F) structures, respectively (Supplementary Figures 1C, D).

With our goal to perform glycosylation-based structure-function studies on palivizumab, we used a glycoengineering strategy involving enzymatic transglycosylation (17, 32). Although several EndoS endoglycosidases have been reported with slightly varying substrate specificities (17, 19), we chose EndoS D233Q mutant, which does not affect mannose (Man5) glycans, and used this as an internal standard to further measure completeness of the transglycosylation reaction. Cleavage of the chitobiose core of complex *N*-glycans (*i.e.* between the two GlcNAc residues closest to the N297 position of the protein backbone) with EndoS D233Q leaves the palivizumab protein backbone with a single GlcNAc and a core-1,6-fucose residue, on each heavy chain (Pal-GlcNAc(Fuc), Figure 1A), as well as the aforementioned 4% uncleaved Man 5 glycans. Subsequent treatment with fucosidase GH29 cleaved the core fucose residue to afford the afucosylated analogue (Pal-GlcNAc) that could then undergo transglycosylation with purified glycan oxazoline compounds and EndoS D233Q. Of note, the three steps were performed sequentially in a one-pot reaction without the need for purification until the completion of the transglycosylation reaction steps.

To obtain biantennary glycan analogues with varying degrees of galactosylation, sialoglycoprotein (SGP) was first extracted from egg yolk (33) and treated with EndoS and α2-3,6,8 neuraminidase to cleave the glycans between the chitobiose core, and removal of the terminal sialic acid residues, respectively, Figure 1B. In addition to the production of the truncated digalactosylated (G2T) glycan, we observed the formation of a monogalactosylated glycan (18%) that was also previously reported, but the specific location of its terminal galactose residue was not identified (34). To this end, we purified the glycans by preparative porous graphitic carbon (PGC)-HPLC, a powerful technique that is able to separate glycan isomers as well as their respective anomers (35, 36), and confirmed glycan purity and structural identity by HPAEC-PAD and tandem mass spectrometry (Figure 1B, right panel, and Supplementary Figure S2A). A recent report showed that branch-specific glycan residue characterization can be achieved using positive mode CID MS/MS fragmentation, where the relative peak intensities of the MS/MS-fragmented glycan peaks are compared between two separate purified glycan biantennary branching isomers; MS/MS-induced cleavage of the α3 antenna between the GlcNAc-β1-2-Man linkage produces a relatively higher abundance of the cleaved and its complementary glycan fragments compared to cleavage of the α6 antenna (37). It is noteworthy that this fragmentation will occur at both α3 and α6 antennae, albeit at different rates, resulting in the presence of both cleaved peaks in the MS/MS spectra of a single compound; therefore MS/MS analysis of a single isomeric compound is insufficient for assigning antenna-specific glycan residues, and purified compounds of both isomers are required to enable antenna assignment. Thus, we required the synthesis of a glycan comprising monogalactosylation at a known antenna. It has been well characterized that LacZ β1-4 galactosidase can selectively cleave the Gal-β1-4-GlcNAc residue of the α3 antenna to yield monogalactosylation at the α6 antenna (38, 39), and thus we treated our purified G2T with LacZ β1-4 galactosidase, Figure 1C. Further extended reaction with this enzyme resulted in the

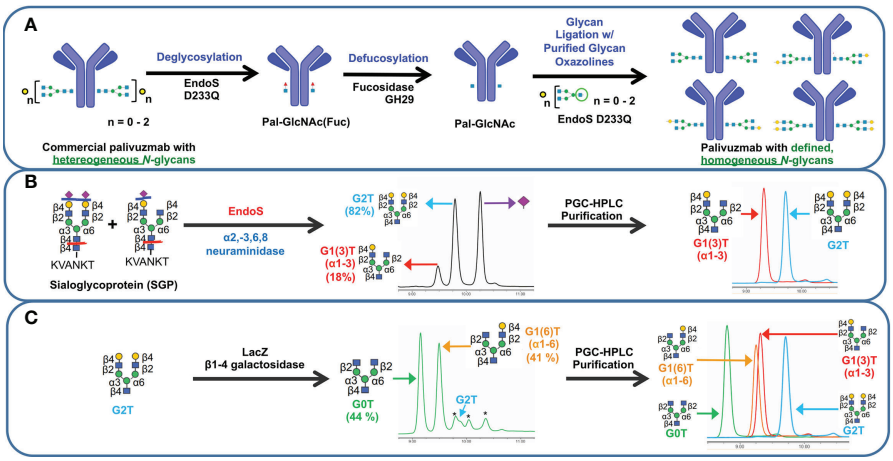

FIGURE 1
Schematic representation of transglycosylation of palivizumab to generate homogeneous glycoforms. **(A)** Deglycosylation of commercially-available palivizumab using EndoS D233Q generates the truncated GlcNAcFuc disaccharide (blue square = GlcNAc; red triangle = fucose) remaining on palivizumab. Defucosylation is achieved using fucosidase GH29, and subsequent glycan ligation of purified glycan oxazoline is achieved using EndoS 233Q. **(B)** Enzymatic reaction and purification of truncated glycans (mono-galactosylated at the α3 antenna (G1 (3)T) and digalactosylated (G2T)) using EndoS and α2-3,6,8 neuraminidase to cleave truncated glycans between the reducing end chitobiose core, followed by purification by porous graphitic carbon (PGC)-HPLC. **(C)** Synthesis of truncated agalactosylated (G0T) and monogalactosylated at the α6 antenna (G1 (6)T) glycans using LacZ β1-4 galactosidase (* indicates reaction byproduct peaks), followed by purification by PGC-HPLC. HPAEC-PAD trace of overlaid spectra of purified glycans are shown on the right in each of **(B, C)**.

formation of the truncated agalactosylated G0T glycan. PGC-HPLC purification of each glycan analogue following the LacZ reaction eluted the anomers of each glycan at different retention times (See Materials and Methods), which were also different than the previously unidentified monogalactosylated truncated glycan from the SGP isolation, indicating that the latter glycan was not monogalactosylated at the α6 antenna. The β- and α- anomers of SGP-derived monogalactosylated glycan eluted at approximately 23.0 and 28.0 min, while the anomers of G1 (6)T eluted at approximately 26.0 min and 31.5 min. As a further comparison, Figure 1C (right panel) shows the overlaid HPAEC-PAD chromatograms of the four PGC-HPLC-purified glycans with varying degrees of galactosylation; importantly, the two monogalactosylated glycans isolated using either the SGP isolation or LacZ β1-4 galactosidase treatment possessed different retention times. With the two purified monogalactosylated glycans in hand, comparative tandem MS/MS analysis revealed that the monogalactosylated product isolated from SGP had a higher relative abundance of the cleaved GalGlcNAc ($[GalGlcNAc+H]^+$, m/z 366.07) and its complementary fragment ($[M-GalGlcNAc+H]^+$, m/z 911.17, Supplementary Figure S2A, pink peaks) compared to the cleavage of the terminal GlcNAc of the opposite antenna ($[GlcNAc+H]^+$, m/z 204.02) and its complementary fragment ($[M-GlcNAc+H]^+$, m/z 1073.23, Supplementary Figure S2A, yellow peaks); conversely, an opposite relative abundance of these peaks are observed with the known α6-monogalactosylated product obtained following LacZ β1-4 galactosidase cleavage (Supplementary Figure S2B). Therefore, the previously unidentified monogalactosylated glycan isolated from SGP is assigned to be that of the α3 antenna.

Purified glycans were reacted with 2-chloro-1,3-dimethylimidazolinium chloride (DMC) and trimethylamine to obtain the glycan oxazoline precursors that were then used with EndoS D233Q for transglycosylation. Glycan-remodelled palivizumab were purified using Protein A resin, which included washing with 0.5 M sucrose solutions prior to mAb elution to remove unreacted glycan starting materials.

Completion of the reactions were monitored by SDS-PAGE and intact mass spectrometry, Supplementary Figure S3. Cleavage by PNGaseF further shows that the afucosylated glycans present in the remodelled palivizumab analogues are homogeneous and that the original chitobiose linkage to the asparagine residue (GlcNAc β1-4-GlcNAc-N297) was formed properly, Supplementary Figure S4. Importantly, the percentage of Man5 residues were between 2-3% compared to the ligated glycan for all four analogues, indicating that the degree of transglycosylation is between 97-98% for each glycoform.

Binding assays and biological activity to FcγRIIIA

To assess the role of varying glycan structures on palivizumab, we first examined whether changes in Fc glycosylation affects the binding of the Fab region to its targeted RSV F-protein, using RSV-F recombinant protein-

immobilized ELISA. Consistent with previous reports, varying galactosylation or fucosylation levels by enzymatic transglycosylation did not affect Fab binding, as EC50 values were not statistically significant between commercial (ie. most fucosylated), deglycosylated and afucosylated glycans with varying galactosylation (p=0.3184, Figure 2).

Next, we examined the influence of the terminal galactose residues of afucosylated Fc glycans on binding to the higher affinity isoform (V176) of FcγRIIIa (CD16A), a receptor primarily involved in ADCC. Using ELISA (Figure 3A), a significantly higher binding of all non-fucosylated glycans was observed compared to the commercially available palivizumab that comprises mostly fucosylated G0F and G1F glycans. Intriguingly, comparison amongst only afucosylated glycoforms revealed a higher binding activity in afucosylated glycans bearing a terminal galactose residue at the α6 antenna (i.e. G1 (6) and G2), compared to those that lack a galactose residue at this position (i.e. G0, G1 (3), Figure 3A). EC50 values of G0 and G1 (3) glycoforms were not determined, as they never reached maximum saturation compared to G1 (6) and G2 glycoforms. The presence of a single GlcNAc residue following EndoS and fucosidase treatment (i.e. Gn glycoform) exhibited minimal binding. We observe a similar trend for binding to the lower-affinity FcγRIIIA F176 variant, although the differences between the various galactosylation states are less pronounced compared to the high-affinity V176 isoform; statistical analysis of EC50 values reveals that the absence of a galactose residue on the α6 antenna was generally statistically different ($p < 0.0404$, with the exception of monogalactosylated G1 (3) vs G1 (6), $p = 0.059$, Figure 3B).

We further confirm these observations using surface plasmon resonance (SPR) by immobilizing the mAbs to Protein A-bound slides. With respect to binding to the higher-affinity V176 isoform, the dissociation constant (K_D) of glycoforms bearing the galactose at the α6 antenna is twice as low as glycans lacking a galactose at this position (approximately 6×10^{-9} M *vs.* 11×10^{-8} M, respectively, Figures 3C–F). Similar to the ELISA results, minimal binding was observed with the GlcNAc-only palivizumab. As with our ELISA results, this is drastically stronger than steady state binding of commercially available palivizumab (10^{-6} M). A similar case is observed with the binding affinity of the various galactosylated afucosylated glycoforms to the low-binding F176 isoform, albeit at an approximate five-fold decrease of each glycoform.

As coating recombinant proteins on to flat polystyrene surfaces can denature its conformation (40), and therefore skew binding affinity data, we next used more biologically-relevant model for FcγRIIIa binding, involving flow cytometry of a GFP-expressing natural killer T-cell line expressing the FcγRIIIa receptor (NK92-GFP-CD16A). NK92-GFP-CD16A cells bound with palivizumab at the Fc region was labeled with an AlexaFluor 647-conjugated anti-$F(ab`)_2$ antibody fragment, and the percentage of GFP^+AF647^+ NK92 cells were analyzed by flow cytometry, Figures 4A–C. Similarly, to the SPR results, an approximate 2-fold enhancement in binding or EC-50 is detected for the glycoforms containing a galactose at the α6 antenna of afucosylated glycans ($p < 0.05$). Surprisingly, when using the lower affinity NK92-GFP-CD16A F176 variant, we observed a more pronounced difference between the glycoforms, Figure 4D. The presence of a terminal galactose residue on the α6

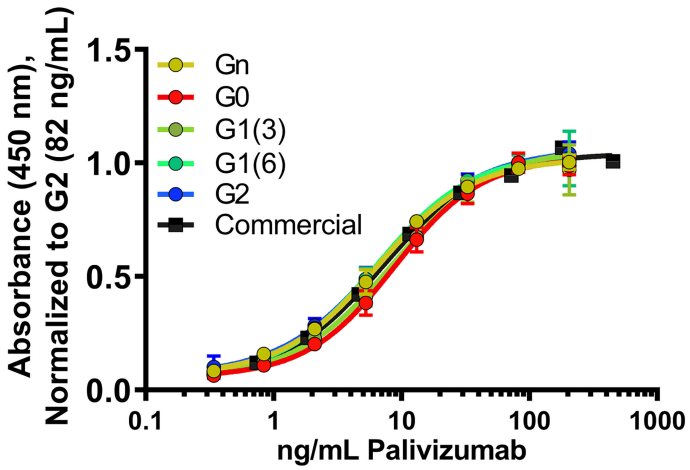

FIGURE 2
Fab binding of glycan-remodeled palivizumab to RSV-A2 F-protein is not affected by remodelled Fc-glycans. Comparable dose-response curves are obtained in the various glycoform analogues in an ELISA assay. RSV-A2 F-protein was coated at 0.25 μg/mL, followed by mAb binding. An anti-human Fc-HRP and Ultra-TMB were used for detection at 450 nm. Error bars show mean ± standard deviation (n=3 replicates); non-linear regression (4-PL) was used for curve-fitting in GraphPad. EC50 values generated and statistically analyzed (One-way Anova, Tukey *post-hoc* analysis) by GraphPad showed no significant differences between the various groups ($p = 0.3184$).

10.3389/fimmu.2022.972168

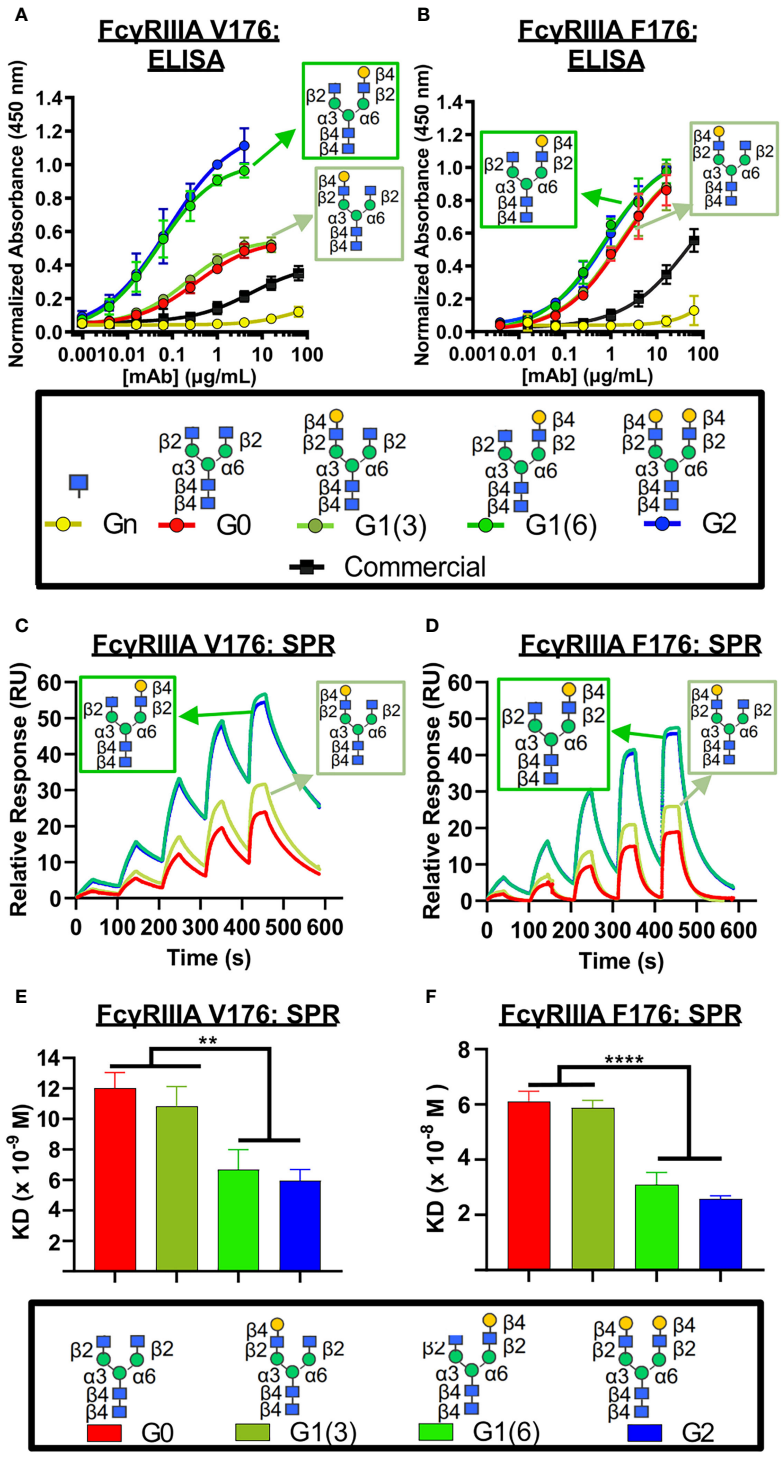

FIGURE 3
FcγRIIIa (CD16A) binding shows galactose on the α6 antenna significantly affects activity – 2D binding assays. **(A,B)** Dose response curves are obtained in the various glycoform analogues in an ELISA assay. **(A)** CD16A V 176 (high affinity) or **(B)** CD16A F176 (low affinity) were coated, followed by mAb binding. An anti-human Fab-HRP antibody, and Ultra-TMB were used for detection at 450 nm. Error bars show mean ± standard deviation (n=4 replicates); non-linear regression (variable slope, four parameters) was used for curve-fitting in GraphPad. **(C-F)** Surface Plasmon Resonance (SPR) of each palivizumab glycoform for either **(C, E)** CD16A V176 or **(D, F)** CD16A F176. **(C, D)** Overlaid sensograms and **(E, F)** dissociation constant (KD, M) are shown. For (**E, F**), error bars show mean KD ± standard deviation from 3 replicate binding experiments; **p < 0.01; ****p <0.0001, one-way ANOVA, Tukey *post-hoc* analysis.

antenna results in a binding of approximately 70% of cells at 16 μg/mL, whereas palivizumab lacking this galactose residue resulted in a maximum binding of approximately 30%. Furthermore, the Endo S- and fucosidase-treated deglycosylated palivizumab and the commercially available fucosylated showed similar minimal binding to the low affinity CD16A F176 variant.

Next, we measured the ADCC activity of the afucosylated palivizumab glycoforms using RSV-infected Hep2 cells with the Jurkat T-cell luciferase reporter system (Figures 4E, F). Hep2 cells were infected with RSV overnight prior to incubation with palivizumab glycoforms and then the reporter cells were added. Consistent with the bioactivity to those of the aforementioned FcγRIIIA binding assays, increased ADCC reporter activity is observed in glycoforms comprising a terminal galactose residue at the α6 antenna ($p < 0.05$). In contrast, the commercial palivizumab yielded low ADCC activity, even at a 50-fold increase in concentration (100 μg/mL), Figure 4E.

Characterization of glycan-Fc by NMR

The above observations points at the implication of the terminal galactose residue on the α6 antenna of the glycans. In order to ascertain the correctness of the glycoforms we prepared all four glycans on an isotopically labelled Fc fragment and applied NMR spectroscopy. As the NIST-mAb-Fc fragment shares the same amino acid sequence as the Fc fragment of palivizumab (41), we expressed this Fc fragment using *P. pastoris* yeast cells with $(^{15}NH_4)_2SO_4$ as the sole source of nitrogen, yielding a fragment that is over 98% labelled. Yeast expresses afucosylated high mannose glycans, and cleavage with Endo H produced the peptide bearing only a single GlcNAc residue at the N297 position. Treatment with EndoS D184M and the purified glycan oxazolines with variable galactosylation was performed, and completion was monitored by SDS PAGE (Figure 5A; Supplementary Figure S6).

Two dimensional (2D) ^{1}H-^{15}N-HSQC spectra were recorded for all four analogues along with its deglycosylated precursor (*i.e.* treated with EndoH). Since terminal galactose residues do not have proton-nitrogen pairs, chemical shift perturbations (CSPs) of the Fc protein backbone amides produced by the proximity of the galactose moiety were measured. The advantage of this approach is that the chemical shift of a single backbone amide pair is an absolute measurement of the magnetic environment surrounding this chemical group. In contrast, the intensity of a given NMR resonance can carry more variability due to many experimental factors (see Ghasriani et al. (42) for a more thorough discussion). In addition, binding or close proximity of a chemical entity such as a glycan perturbs the local magnetic environment of many amides. When the resonance assignment is known, this allows 2D-correlation spectra to identify binding sites, or presence and absence of nearby glycan moieties. The resonance assignments of the Fc fragment reported by Yagi et al. (43) were transposed onto the 2D-^{1}H-^{15}N-HSQC of ^{15}N-G0-NISTmAb-Fc; despite the NIST mAb-Fc having a primary sequence that differs at residues 356-358 compared to the Fc fragment assigned by Yagi and coworkers (*i.e.* ^{356}Asp-Glu-Leu^{358} *vs.* ^{356}Glu-Glu-Met^{358}, respectively), this difference in primary sequence is sufficiently distant from residues surrounding the glycans that assignment could be transposed.

We initially examined the 2D ^{1}H-^{15}N-HSQC NMR of the Endo H-deglycosylated ^{15}N-Gn-NISTmAb-Fc with the agalactosylated G0 glycoform (Supplementary Figure S7), and observed numerous CSPs, indicative of the large effect that entire glycans have on the solution conformation of the Fc protein backbone compared to a single GlcNAc residue. Spectral overlays of monogalactosylated ^{15}N-NISTmAb-Fc proteins with the agalactosylated ^{15}N-G0-NISTmAb-Fc further revealed interesting features that confirmed the identities of these glycans and provide insight into our observations with the remodeled afucosylated palivizumab glycoforms (Figures 5B, C). Relative to the agalactosylated ^{15}N-G0-NISTmAb-Fc, the presence of the terminal galactose in the α6 antenna (*i.e.* ^{15}N-G1 (6)-NISTmAb-Fc) induces greater CSPs of the peptide backbone (amongst them are L242, F243, K248, D249, T250, T260, C261, S304, L306, V308, L314, G316, A339, C367, A378) (Figure 5B) compared to its presence on the α3 antenna alone (*i.e.* ^{15}N-G1 (3)-NISTmAb-Fc, Figure 5C), indicating that galactosylation on the α6 antenna brings a galactose moiety in close proximity with the Fc protein. Next, we evaluated how galactosylation of each arm alone compared to digalactosylation on both arms (*i.e.* G2). Monogalactosylated ^{15}N-G1 (6)-NISTmAb-Fc shows significant overlap and few CSPs compared to the digalactosylated ^{15}N-G2-NISTmAb-Fc (Supplementary Figure S7A), whereas more CSPs are observed between the latter and the ^{15}N-G1 (3)-NISTmAb-Fc (Supplemental Figure S7B), demonstrating that galactosylation at the α6 antenna alone is sufficient to impart a glycan conformation comparable to the digalactosylated glycoform. This may result from an interaction between the galactose on the α6 antenna and the protein backbone. However, our data (Figure 5C) suggest that galactosylation at the α3 antenna does not have these galactose-protein backbone interactions. As a complementary method to compare differences in chemical shifts between Fc-glycoforms, we calculated the combined chemical shift difference (CCSD, in ppm), a weighted value of the differences in chemical shifts in a 2D spectrum (Supplemental Table 1). The aforementioned 15 amino acid residues with the greatest CSPs between glycoforms with or without the terminal α6 antenna galactose showed greater CCSD values, whereas CCSDs of the same amino acid residues between glycoforms with the terminal α6 antenna galactose (*i.e.* G1 (6) and G2) are less than 0.02 ppm (with the exception of L242 and C261, which are 0.06 and 0.04 ppm, respectively). As a control peak that showed minimal CSPs between samples, D312 was used, which had CCSDs of less than 0.01 ppm, regardless of the terminal galactose position.

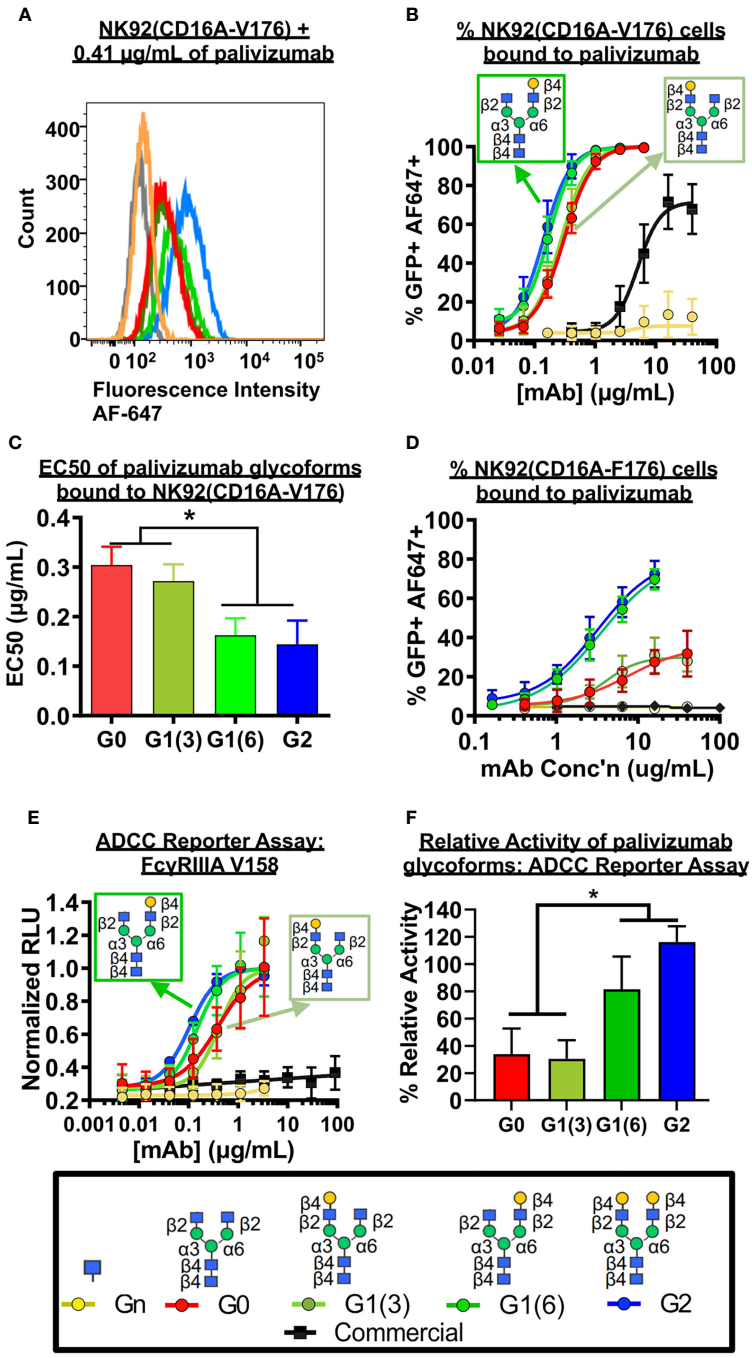

FIGURE 4
FcγRIIIa (CD16A) binding shows galactose on the α6 antenna significantly affects activity - Cell based assays. **(A-C)** NK92-CD16A expressing cells (V Variant) and **(D)** Jurkat T-cell luciferase reporter cell line (CD16A V Variant). **(A)** A representative flow cytometry histogram is shown of NK92-CD16A (V176) cells bound to 0.41 µg/mL of various palivizumab glycoforms that were detected using an anti-human IgG (F(ab') $_2$ –specific) conjugated to AlexaFluor(AF)-647. **(B)** Dose-response curve of % GFP+APC+ cells for each palivizumab glycoform analogue **(C)** EC 50 (µg/mL) shows that galactosylation in the α6 antenna result in approximately twice as low EC50 compared to glycoforms lacking galactosylation in this position. EC50s are calculated using GraphPad. *, p< 0.05, One-way ANOVA, Tukey *post-hoc* analysis. **(D)** Dose-response curve of % GFP+APC + cells for each palivizumab glycoform analogue to NK92-GFP cells expressing the low-affinity CD16A F176 variant. **(E)** Dose-response curve and **(F)** % relative activity of palivizumab glycoforms in the ADCC reporter assay, where % relative activity is the ratio of the EC50 of G2-palivizumab to the EC50 of each sample in each biological replicate. For **(B-F)**, error bars show mean ± standard deviation (n=3 biological replicates); for **(B, D, E)** non-linear regression (4-PL) was used for curve-fitting in GraphPad; for **(C, F)** EC50 values were calculated and statistical analyses were performed using GraphPad. *, p< 0.05, One-way ANOVA, Tukey *post-hoc* analysis.

10.3389/fimmu.2022.972168

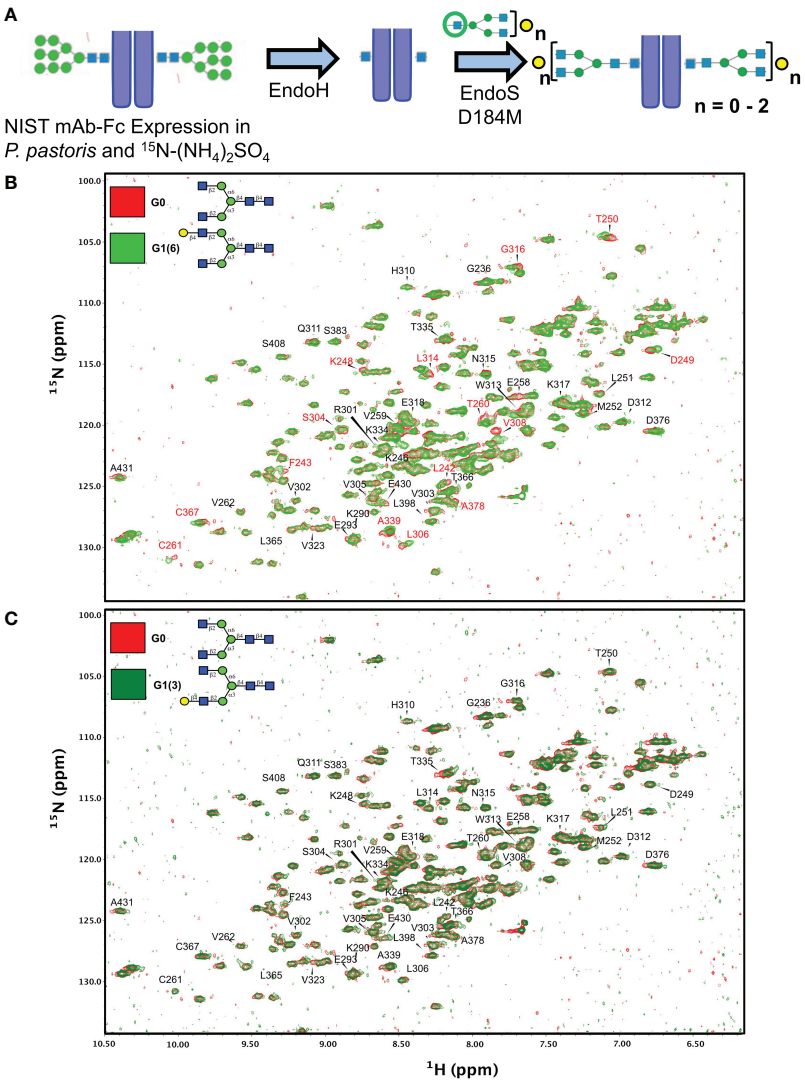

FIGURE 5
Synthetic scheme and NMR characterization of ^{15}N-isotopically labelled Fc subunits with homogenous monogalactosylated glycoforms. **(A)** Synthetic scheme showing the remodeling of ^{15}N-labelled Fc proteins expressed in *P. pastoris* and remodelled with sequential treatment with EndoH and EndoS D184M and purified glycan oxazolines. **(B, C)** Overlay of 2D-^{1}H-^{15}N NMR spectra of agalactosylated ^{15}N-G0-NISTmAb-Fc (red) with **(B)** ^{15}N-G1(6)-NISTmAb-Fc (bright green) and **(C)** ^{15}N-G1(3)-NISTmAb-Fc (dark green). Peptide backbone amino acid residues are labelled, and Combined Chemical Shift Differences (CCSDs) are calculated for those labeled in red and are shown in Table S1.

Mapping of twelve of these CSPs on the X-Ray structure (PDBID: 4byh) (44) highlight residues that are in close proximity with the galactose moiety of the α6 antenna (Figure 6A), which are located closer to the C_H3 domain, while the fewer and weaker CSPs for the G1 (3) are consistent with a galactose moiety more exposed to the solvent, away from the protein backbone (Figure 6B). In this case, the very small CSPs limited the calculation of CCSD. Previous reports have shown that the latter antenna experiences greater mobility in solution (45), which would also contribute to smaller perturbations of chemical shifts.

Discussion

Our method to generate asymmetrical mono-galactosylated glycans provides a facile alternative procedure to that previously reported (21, 39). Although monogalactosylated glycans at the α3 antenna only occurs at approximate 18% yield relative to digalactosylated glycans in sialoglycoprotein (SGP) extracted from inexpensive commercially available egg yolk, the ability to extract SGP at a relatively high yield enables its practicality. While the presence of a monogalactosylated species had been previously observed (34), it was neither further characterized nor

10.3389/fimmu.2022.972168

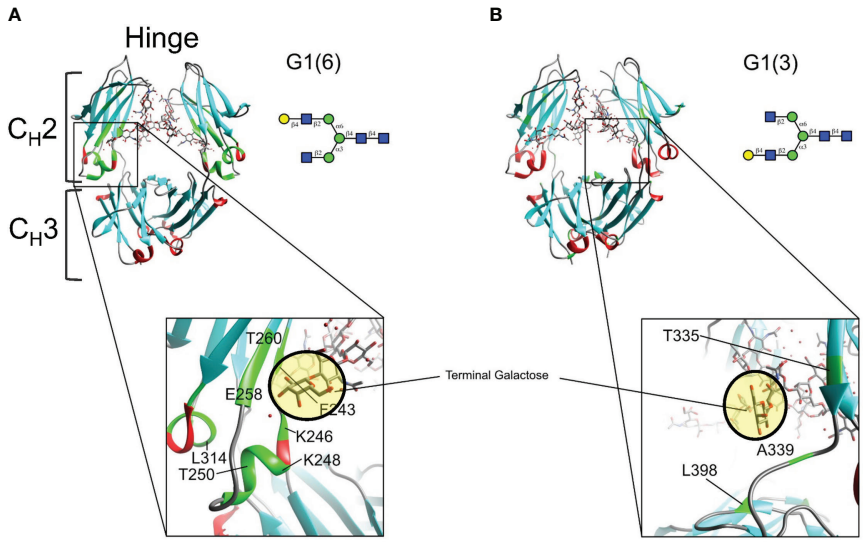

FIGURE 6
Mapping chemical shifts perturbations of Fc glycoproteins bearing a galactose residue at either the α3- or α6-antenna. **(A)** In the α6-antenna, the galactose is in close proximity with the protein backbone, whereas **(B)** in the α3-antenna, the galactose residue is exposed to the outer solvent. Residues that experiencing chemical shift perturbations are depicted in green. β-sheets are depicted in cyan, α-helix in red, and loops/turns are shown in gray. X-ray structure of glycosylated Fc (PDB ID: 4byh).

isolated, as focus was on obtaining either the digalactosylated or completely agalactosylated glycans (33, 34). Furthermore, the selectivity of LacZ β1-4-galactosidase to highly favour the cleavage of the Gal-β1-4-GlcNAc linkage in the α3 antenna of digalactosylated biantennary complex glycans (38, 39), coupled with the ability of PGC-HPLC to separate isomeric glycans (22), our results demonstrate a feasible method to isolate purified asymmetrically galactosylated biantennary glycans.

Our FcγRIIIa binding experiments show that galactosylation of both antennae of afucosylated glycans (*i.e.* G2) of the anti-viral mAb palivizumab increases binding, corroborating a recent report with polyclonal serum-derived IgG (IVIG) used for anti-inflammation (12). Using chemoenzymatic glycan remodeling with asymmetric galactosylated biantennary glycans, herein we further refined the structural requirements for this binding; data from our various binding experiments consistently demonstrate that only the terminal galactose residue on the α6 antenna (*i.e.* G1 (6)) is required to impart this increased binding affinity. In its absence (*i.e.* G0 and G1 (3)), the binding affinity is comparable to the agalactosylated afucosylated (G0) glycan. Our KD values for both high- (V176) and low- (F176) affinity FcγRIIIA obtained by SPR analysis are within the same magnitude as those previously reported; for example, our digalactosylated afucosylated (G2) palivizumab glycoform had KD values of 5.9 ± 0.8 nM and 25.6 ± 1.3 nM with the high- and low-affinity receptors respectively, compared to 2 nM and 25 nM for G2-rituximab (18). However, it is worth noting that these KD values are lower than those obtained for Fc fragments (*i.e.* lacking the Fab region) comprising G2 (64 nM) (16). Our observed decrease in binding affinity by two-fold upon removal of the galactose on the α3-antenna (KD = ~ 6 nM for G1 (6) and G2 *vs* ~ 11-12 nM for G0 and G1 (3) for high-affinity FcγRIIIA, and ~ 25-31 nM for G1 (6) and G2 *vs* ~ 60 nM for G0 and G1 (3) for low-affinity FcγRIIIA) is similar to the 1.5- to 1.7-fold decrease previously reported between agalactosylated and digalactosylated afucosylated glycoforms (i.e. G0 vs G2) (16, 46). However, Wada et al. had previously reported a decrease in relative binding affinity by 3.6-fold, although KD values were not reported (20). Interestingly, the cell-based binding assay using NK92 cells showed a difference between the commercially-available high- and low-affinity CD16A variants. A two-fold difference in EC50 was observed with the high-affinity NK92-GFP-CD16A V176 variant, while only glycoforms with a galactose in the α6 antenna (*i.e.* G1 (6) and G2) showed any appreciable binding to the low-affinity NK92-GFP-CD16A F176 variant.

While the increased FcγRIIIa binding in monogalactosylated at the α6 antenna was recently shown in fucosylated glycans (21) in the anti-inflammatory drug rituximab, we now demonstrate that this is also applicable to afucosylated glycans and in the context of an anti-viral mAb that binds different targets than rituximab. Commercial palivizumab (Synagis), which is predominantly core fucosylated, is generally considered to be a prophylactic mAb whose mechanism of action is acting as a neutralizing agent, rather than by actively destroying infected cells (47, 48), and has been shown to have relatively low ADCC

activity (48). Our ADCC reporter assay results using RSV-infected Hep2 cells corroborate the low activity of commercially-available palivizumab, even at 90 μg/mL (Figure 4E, black data points) (48). A previous report had shown that palivizumab expressed in *N. benthamiana* changed the glycoprofile from predominantly fucosylated glycans into one that comprised 79% agalactosylated, afucosylated (G0) glycans, and 17% of high mannosylated (Man 7/9) glycans (25). Our data here shows the synthesis of a higher purity of glycans with varying degrees of galactosylation (97%), with 3% high mannosylated (Man 5) glycan, and that upon galactosylation of the α6 antenna, we can further increase palivizumab binding to FcγRIIIa and ADCC activity by approximately two-fold compared to the agalactosylated afucosylated palivizumab (*i.e.* G0) glycoform. However, it is important to note that our comparison between the afucosylated glycoforms and commercial product (that is mostly fucosylated) is consistent with previous literature that removal of the core fucose residue remains a dominant feature to increase FcγRIIIA binding. Rather, our results provide further corroborating evidence with more recent studies that galactosylation further increases ADCC *via* FcγRIIIA binding (12, 21, 49) and is in contrast to previous studies that showed galactosylation had no effect (11, 13, 50). During the biosynthesis of complex *N*-glycans in glycoproteins, β-1,4-galactosyltransferase is involved in attaching the galactose residue to the terminal GlcNAc residue in complex *N*-glycans; Ramasamy et al. previously demonstrated that the human β-1,4 galactosytransferase exhibits selectivity towards the α6 antenna at lower glycan concentrations, while the α3 antenna is favoured at higher glycan concentrations (51). As this key enzyme can have opposing selectivity as a function of glycan concentration, this further emphasizes the need to carefully control conditions during manufacturing and production of glycoprotein-based biotherapeutics, and together with our data that shows the importance of galactose location within the Fc-glycan on FcγRIIIA binding, the proper characterization of glycan isomeric structures needs to be considered to properly evaluate the biological properties of monoclonal antibodies (51).

Previous data reported that soluble FcγRIIIA receptors bound to Fc proteins near the hinge region of the C_H2 domain (via hydrogen bonds at residues G236, G237, P238, S239, D265, Y296, as well as glycan-glycan interactions with the N162 glycan of sFcγRIIIA), and show that the terminal galactose moiety of the α6-antenna is far from any Fc- FcγRIIIa contacts (PDBIDs: A3Y4 (8), 3SGJ (7), 5D6D (52)). Therefore, the correlation between the enhancement of receptor affinity and biological activity with the presence of the terminal galactose residue at the α6-antenna of the glycan can be *a priori* puzzling. However, several reports suggest that glycan dynamics also play an important role in receptor affinity. Barb and Prestegard have shown using predominantly fucosylated and ^{13}C-labeled galactose on the α6 antenna, that this latter carbohydrate residue has broader resonance lines indicative of slower mobility, while the α3 antenna has increased mobility (45). Mutations to the Fc peptide backbone that increase galactose mobility of the α6 antenna are correlated to a 20- to 50-fold decrease of FcγRIIIA receptor affinity (53, 54). The chemoenzymatic strategy used herein to generate defined afucosylated, monogalactosylated glycans on a uniformly ^{15}N-labeled Fc fragment brings further support to the role of glycan dynamics. Two-dimensional NMR spectra of the ^{15}N-labeled Fc protein monogalactosylated at the α6 antenna show several chemical shift perturbations (CSPs) compared to the agalactosylated glycoform, indicating that the α6 antenna is in close proximity to the protein backbone and is consistent with reduced mobility; our use of ^{15}N-labeled Fc with defined monogalactosylation at the α6-antenna shows that this occurs independently of galactosylation at the α3 antenna. Conversely, the spectrum of ^{15}N-labeled Fc comprising monogalactosylation at the α3 antenna show small and weak CSPs which is consistent with a solvent-exposed galactose with greater mobility, and occurs independently of the presence of an α6-antennal galactose. It was not useful to measure CCSD for the perturbations observed in G1 (3) relative to G0 since the changes that are observed are either a change of peak shape (narrowing or broadening) or simply disappearance, depending of the frequency of the change in the local magnetic environment. The only residue that shows a clear CSP is T335 with a CCSD of 0.05 ppm where the peak shape has also changed (narrowing). The fact that the spectral overlay of G0 and G1 (3) is mainly showing changes in peak shape is consistent with a mobile galactose moiety that is mainly exposed to the solvent with little to no interactions with the protein backbone. The presence of the afucosylated α6-antennal galactose causes CSPs in a region closer to the C_H3 domain (*i.e.* F243, K248, D249, T250, T260, C261), and are in line with a previous study showing that residues F241 and F243 are in close proximity with this galactose in fucosylated digalactosylated glycans (G2F), and mutation of these residues increase glycan mobility and reduce FcγRIIIA receptor affinity (53). It is therefore plausible that the presence of an α6-antennal galactose (*i.e.* G1 (6) or G2) reduces mobility of afucosylated Fc-glycans by interacting with the Fc protein backbone, which enhances FcγRIIIA receptor affinity, similarly to previous reports with fucosylated glycans (53). However, the effect of glycan-glycan interactions involving the α6-antenna terminal galactose residue of a full mAb and the *N*-glycans of the FcγRIIIA receptor cannot be ruled out, although previous X-Ray work did not identify these interactions using truncated Fc proteins (8).

While afucosylation remains the predominant factor for FcγRIIIa binding and ADCC activity, this two-fold increase in activity based on the location of the terminal galactose residue highlights the importance to carefully characterize glycan structures in biotherapeutics. From a regulatory perspective, depending on the mechanism of action, this may warrant

attention when evaluating physicochemical data to assess batch-to-batch variability and comparing biosimilars to existing innovator mAb products.

Materials and methods

Glycan isolation, purification and oxazoline formation

Sialoglycoprotein (SGP) was isolated from commercially available egg yolk as previously described (33). Glycans were released from SGP using EndoS (New England Biolabs, Cat #P0741) containing a chitin-binding domain (CBD). EndoS-CBD was immobilized to chitin resin (New England Biolabs, Cat # S6651) by incubating 10 uL EndoS-CBD with 1.0 mL chitin resin slurry (0.5 mg/mL) overnight at 4°C. The slurry was mixed well using wide-bore pipette tips and transferred to a solution of SGP (10 mg/mL containing GlycoBuffer 1 (New England Biolabs, Cat # B1727S). 5 μL α2-3,6,8 neuraminidase (NEB, Cat #P0720) was then added to desialylate glycans. The reaction was incubated at 37°C with gentle agitation for 3 days, and monitored by HPAEC-PAD. For HPAEC-PAD analysis, a Dionex CarboPac PA200 IC column (3 mm x 250 mm, 5.5 μm particle size, Cat # 062896) was used, with a gradient of 20%/0%/80% to 60%/20%/20% of MP-A/MP-B/MP-C (MP-A: 200 mM NaOH; MP-B: 150 mM NaOAc in 200 mM NaOH; MP-C: MQ H_2O) over 10 min at 30°C was used to monitor glycan products. Following reaction completion, resin was removed by passing through a solid phase extraction tube and rinsed with MQ water. The reaction lyophilized, resuspended in MQ water and filtered through a 0.22 μm PVDF filter before it was purified by PGC-HPLC to isolate G1 (3)T and G2T glycans (HyperCarb PGC column (Thermo Fisher Cat # 35005-159070A, 10 cm x 150 cm, 5 μm particle size). Following an initial mobile phase composition of 1% MP-D: MP-E (MP-D: 95% acetonitrile in MQ H_2O containing 0.1% TFA; MP-E: MQ H_2O containing 0.1% TFA), a gradient of 6.0% to 13.7% MP-D: MP-E was used from 1.0 min to 42.0 min at 5 mL/min, at 40°C. Glycans were detected at 214 nm using a UV detector, collected using a fraction collector, analyzed by HPAEC-PAD prior to fraction combination, and lyophilized. Impure samples were re-purified as above. The β- and α- anomers of G1 (3)T eluted at approximately 23.0 and 28.0 min, while the anomers of G2T eluted at approximately 32.0 min and 37.0 min.

To prepare glycans containing zero or one terminal galactose residue (at the α6 antenna only) (G0T, G1 (6)T), G2T was diluted to 5 mg/mL (1.0 mL) with 150 μL of KCl (500 mM), 150 μL of a buffer containing 500 mM sodium acetate and 50 mM $CaCl_2$ (pH 5.7), and 4.55 mL MQ water. 150 uL β-1,4 galactosidase (Sigma, Cat# 10105031001) was then added, and the reaction was incubated at 30°C overnight. The reaction was monitored by HPAEC-PAD and purified by PGC-HPLC as above. The β- and α-anomers of G0T eluted at approximately 17.0 and 22.0 min, while the anomers of G1 (6)T eluted at approximately 26.0 min and 31.5 min.

With each purified glycan in hand, each was converted to their respective oxazoline intermediates by reaction with 2-chloro-1,3-dimethylimidazolinium chloride (DMC, Sigma, Cat# 529249-25G) and trimethylamine (TEA, Fisher, Cat #0484-100) at 4°C, and purified using 0.1% ammonium hydroxide in a column packed with G25 resin (Fisher, Cat # 45-002-048). Collected fractions were monitored by HPAEC-PAD, and those containing purified oxazolines were combined, lyophilized and stored at -80°C until use.

Monoclonal antibody transglycosylation

Methods were adapted from previously reported work (17, 32), with the following modifications. Palivizumab was purchased from McKesson Specialty Pharmacy (Cat #02438272), and the required amount of antibody was diluted to 10 mg/mL in PBS. For the scale of 1 mg (in 100 μL), palivizumab was first digested with EndoS D233Q (32) by adding 50 μL (2.0 mg/mL in PBS), followed by the addition of 100 μL fucosidase (GH29, CedarLane, Cat# CZ05662) that has been previously removed of glycerol. The reaction was incubated overnight at 37°C, and completion was monitored by SDS-PAGE. With the same EndoS D233Q remaining in the crude deglycosylated reaction mixture, deglycosylated palivizumab was passed through Amicon centrifugal filters (30 kDa MWCO, Sigma, Cat# UFC5030) to buffer exchange into cold transglycosylation buffer (50 mM Tris, pH 7.3) and concentrated back to 10 mg/mL. The solution was placed in a 30°C heating block, and glycan oxazoline (6 μL, 400 nM) was prepared and kept on ice. 1 μL of the oxazoline solution was added to the deglycosylated palivizumab containing EndoS D233Q every 5 minutes for a total of 6 additions. After a total reaction time of 30 mins, the reaction was quenched by dilution with 500μL of cold Protein A binding buffer buffer (100 mM Na_2PO_4, 100 mM NaCl, pH 8.0). To the solution, 250 μL rinsed Protein A resin slurry (ThermoFisher Scientific, Cat # 22810) was added and incubated at 4°C with gentle rocking for 5 min. The solution was then passed through a solid phase extraction tube and washed with cold Protein A binding buffer (0.75 mL x 2), followed by a 50 mM sucrose solution in PBS (1.0 mL x 2) and then cold Protein A binding buffer (0.75 mL x 2). Palivizumab was then eluted from the Protein A column using 50 mM sodium citrate buffer (pH 3.5), and neutralized with 200 μL of Protein A binding buffer. Eluted palivizumab was monitored using SDS PAGE and fractions were combined and

passed through Amicon centrifugal filters (30 kDa MWCO) to buffer exchange with Citrate Buffered Saline (130 mM NaCl, 20mM sodium citrate, pH 5.7) and concentrate palivizumab. Solutions were stored at 4°C at approximately 0.3 – 1.0 mg/mL, as quantified by nanodrop (at Absorbance of 280 nm).

Monoclonal antibody characterization

Reaction progress for glycan remodeling of palivizumab was monitored and characterized using reducing SDS PAGE and intact protein mass spectrometry. For reducing SDS PAGE, samples reduced in β-mercaptoethanol for 5 mins at 100°C, followed by loading onto 10% polyacrylamide gels which were then run at 200 V for 70 mins. To ensure accurate analysis of band migration at various glycosylation states, a lane was run comprising both starting material and final product within the same lane.

For mass spectrometry, samples were analyzed with an Orbitrap Fusion Lumos Tribrid Mass Spectrometer coupled to an Easy-nLC 1200 (Thermo Scientific) that was calibrated by infusion prior to analysis with a mixture of caffeine, MRFA, and Ultramark 1621. 0.5 µL of each sample was analyzed by loading onto a C4 Pepmap300 PS-DVB trap column (300A x 5µm x 5mm) and desalting with 0.1% formic acid in water (solvent A) before separating on a PepSwift Monolithic PS-DVB analytical column (200 µm x 25 cm) at 50°C. Chromatographic separation was achieved at a flow rate of 1 µl/min over 25 min in five linear steps as follows (solvent B was 0.1% formic acid in 80% acetonitrile): initial, 0% B; 5 min, 50% B; 10 min, 50% B; 20 min, 90% B; 25 min, 90% B. The eluting proteins were analyzed in Intact Protein mode with Orbitrap MS at 15000 resolutions, from 500-4000 m/z with auto maximum injection time, normalized AGC target of 50%, and 10 microscans. BiopharmaFinder3.0 (Thermo) was used to process the data. Protein deconvolution was performed with the ReSpect algorithm, using mass output of 130 – 160 kDa, Model Mass Range of 145000 – 150000, Charge State Range 40-80.

Following palivizumab transglycosylation reactions, remodelled glycans were characterized using PNGaseF (New England BIolabs, Cat # P0704) to release glycans, followed by HPAEC-PAD analysis. For HPAEC-PAD analysis, a Dionex IC-3000 instrument was used, equipped with a Dionex CarboPac PA200 IC column (3 mm x 250 mm, 5.5 µm particle size, Cat # 062896) and a Gold Standard PAD waveform with an AgCl electrode. For glycoprofile analyses, a flow rate of 0.4 mL/min, and the following gradient was used: 20%/0%/80% to 25%/5%/70% of MP-A/MP-B/MP-C over 25 mins at 30°C, followed by an increase to 0/80/20 over the next 3 mins, and then re-equilibration to 20/0/80 over the next 10 min.

FcγRIIIA binding assay by ELISA

Recombinant human FcγRIIIA proteins were immobilized onto MaxiSorp plates (ThermoFisher, Cat# 349454) overnight at 4°C, at 100 µL of 0.33 µg/mL for FcγRIIIA V176 (high affinity, R&D Systems, Cat# 4325-FC-050), or at 0.67 µg/mL for FcγRIIIA V176F (low affinity, R&D, Cat# 8894-FC-050). Following washing with 0.05% Tween 20 in PBS pH 7.4 (PBS-T) and blocking with 1% bovine serum albumin (Sigma, Cat # A3059-100G) in PBS-T, each palivizumab glycoform was serially diluted 2-fold in 1% BSA/PBS-T and 100 µL was added to each well. Plates were gently rocked for 20 min at room temperature, followed by incubation at 4°C overnight. The next day, wells were thoroughly washed with PBS-T, followed by addition of goat anti-Human IgG F(ab')2 Secondary Antibody-HRP (100 µL, 1/500 dilution in 1% BSA/PBS-T, ThermoFisher, Cat # PI31482). The plate was then gently rocked at room temperature in the dark for 45 mins, followed by thorough washing with PBS-T. 50 µL of Ultra-TMB (ThermoFisher, PI34028) was added, and the plate was gently rocked in the dark for 10 mins, before quenching with 50 µL of 2M H_2SO_4. Plates were immediately read on a BioTek Plate reader at 450 nm.

FcγRIIIA binding assay by surface plasmon resonance analysis

Samples were performed by the National Research Council Human Health Therapeutics Research Centre. Experiments were carried out using a Biacore T200 SPR instrument (Cytiva Inc., Marlborough, MA) at 25°C with a running buffer comprising PBS with 0.05% Tween 20 and 3.4 mM EDTA. Protein A (GenScript Inc., Piscataway, NJ) was immobilized onto two sequential CM-5 sensorchip surfaces at 2000 RUs each using standard amine coupling within the Biacore Immobilization Wizard. Palivizumab analogues were captured onto the second protein A surface at 2.5 µg/mL for 30 s, with the first protein A surface remaining as a blank control surface. FcγRIIIA CD16A isoforms (high binding (V) and low binding (F) variants) were produced and purified by the National Research Council (Canada), as described previously (55). Sensorgrams for FcγRIIIA binding to captured palivizumab were generated using a single-cycle kinetics method, which consist of five FcγRIIIA injections (25 µL/min injection time; 40 s contact time) of increasing concentrations between 2.3 nM and 0.56 µM were used, followed by a single dissociation phase of 120 s for each interaction. The protein A surfaces were regenerated with a 30 s pulse of 10 mM glycine pH 1.5 between each capture and injection cycle. The FcγRIIIa

sensorgrams were double referenced and fit to a 1:1 binding model for kinetic determination with affinity (KD) being based on the ratio of the calculated rate constants. Each binding experiment was repeated three times for each analogue.

FcγRIIIA binding assay by flow cytometry

NK92-GFP-CD16A cell lines were purchased from American Type Culture Collection (ATCC, V Variant: Cat # PTA-8836; F variant: Cat # PTA-8837) and cultured according to manufacturer protocols. 2.5-fold serial dilutions of palivizumab glycoforms were prepared (80 µL per well) in cold deep-well 96-well plates and kept at 4°C, using cold 1% bovine serum albumin (Sigma, Cat # A3059-100G) in PBS as the diluent. To prepare cells for palivizumab-FcγRIIIa binding experiments, NK92 were harvested, and washed with 1% BSA/PBS. Following re-suspension in 1% BSA/PBS with 2 mM EDTA, cells were counted using a haemocytometer. NK92 cells were mixed thoroughly, diluted to 0.625 x 10^6 cells/mL, and 40 µL was added into each well and mixed gently with a pipette, followed by gentle rocking at 4°C for 30 mins. Plates were then washed with 0.5 mL of cold 1% BSA/PBS, centrifuged at 1700 x rpm (7 min) and supernatant removed.

To each well, 150 µL of a 1/300 dilution of Alexa Fluor® 647-conjugated Goat Anti-Human IgG - F(ab')$_2$ specific (AffiniPure F(ab')$_2$ Fragment) (Jackson, Cat # 109-606-097) was then added, and incubated with gentle rocking at 4°C for 30 mins. As a positive control, APC-CD16 Ab, anti-human, REA423 (Miltenyi Biotec, Cat # 130-113-951) at 1/50 dilution was used. As a negative control, the aforementioned AlexaFluor-647 AffiniPure F(ab'')$_2$ Fragment was added, in the absence of any palivizumab. Then cells were washed with 1 mL of cold 1% BSA/PBS with 2 mM EDTA and centrifuged as above, followed by re-suspension in 135 µL of 1% BSA/PBS, and transferred into a shallow 96-well plate containing 45 µL of 4% PFA/PBS. Shallow plates were incubated with gentle rocking at room temperature for 30 min, followed by centrifugation at 100 xg (1 min) and removal of 140 µL of supernatant. Cell pellets were re-suspended in 80 µL of 0.4 M glycine (Sigma, Cat# G8898) in PBS. For each biological replicate (n=3 total), technical duplicates were performed.

Plates were then read using a BD LSR II Flow cytometer (FACS Diva, v 8.0.1), equipped with a multi-well plate reader and the following laser/filter sets: Blue laser 488nm (20mW) with GFP filter set: 505 Long Pass 525/50 Band Pass and SSC filter set: 488/10 Band Pass and FSC; Red Laser 640nm (40mW) with APC/AF647 filter set: 660/20 Band Pass. Voltages were optimized in initial experiments and saved as application settings. Application settings were used in FACS DIVA for all voltages in all subsequent experiments to keep measurements consistent between experiments. Data was analyzed using FlowJo (v 10.8.1), and the gating hierarchy is as follows: (i) FSC-A vs SSC-a, (ii) FSC-H vs HSC-W, (iii) SSC-H vs SSC-W, (iv) GFP+, (v) AF647+/-.

ADCC reporter assay with palivizumab glycoform analogues

ADCC assays were performed using the ADCC Reporter Bioassay, V Variant (Promega, Cat #G7010). To adapt it to the RSV model, Hep2 cells were first cultured in a 96-well plate at a cell density of 2.0 x 10^4 cells/well in 100 µL of DMEM media with 10% low IgG FBS (Fisher, Cat# SH3089802), and incubated at 37°C for 24 h. The next day, cells were infected with 100µL/well of RSV in DMEM containing 10% low IgG FBS, at a MOI of 5, with followed by incubation at 37°C for 24 h. RSV was removed, and wells were washed with PBS (200 µL). 25 µL of RPMI 1640 containing 10% low IgG FBS was immediately added to each well. Solutions of palivizumab glycoforms were diluted in RPMI 1640 with 10% low IgG FBS and 25 µL were added into each well, and incubated for 37°C for 30 min. A vial of effector cells was thawed according to manufacturer protocols, and 25 µL were added into each well and incubated for 37°C for 4 h 45 min. 75 µL Bio-Glo luciferase reagent was then added to each well and the plate was immediately read on a BioTek plate reader.

Synthesis of ^{15}N-isotopically-labeled Fc

A starting culture in 50 mL yeast nitrogen based (YNB) media, containing 3.4 g/L of YNB powder without amino acids (Sigma), 100 mM KH_2PO_4 at pH 6.0, 10 g/L of ^{15}N-ammonium sulfate, 10 g/L D-glucose, 20 µg/L of biotin, was inoculated with a single colony of Pichia X33-NIST-mAb-Fc and incubated at 29°C until an optical dispersion (OD_{600}) of 0.4 is obtained. An aliquot of 22 mL of this culture was used to inoculate a 450 mL of YNB growth media and incubated at 29°C until an optical dispersion (OD_{600}) of 6.6 is obtained. Optical density is accurately measured with a 1:10 dilution of an aliquot from the culture with water. In order to remove unspent glucose that would inhibit protein synthesis, cells were harvested by centrifugation @ 3000 X g for 10 minutes then re-suspended in i-wash media (same composition to YNB, but without glucose) and incubated at 25°C for 1 h. Cells were then centrifuged and re-suspended in 25 mL in wash media, and sufficient amount of the slurry (18 mL) to obtain an OD_{600} of 1.0 was used to inoculate 2 X 1 L of induction media (same composition to YNB growth media with the glucose replaced by 10 mL/L of methanol). Protein induction was carried out for 72 hours at 29°C and 10 mL of methanol 5% were added per liter at 24 h and 48 h post-induction. Cells were separated from media containing ^{15}N-NIST-mAb-Fc by centrifugation at 3000 X g for 10 minutes at 4 °C. To inhibit proteolytic cleavage of the

target protein, benzamidine (5mM) and EDTA (0.5 mM) were added, then the pH of the media at 5.84 was adjusted to 7.3 with the addition of potassium hydroxide (10 N). After pH adjustment, a white precipitate formed. After 30 minutes, the precipitate was separated by centrifugation.

The target protein was purified by affinity chromatography by loading the solution on a 15 mL protein A column at 1 mL/min. Elution of the protein was carried out with 0.1 M glycine-HCl at pH 3.0 after a wash of the resin with 1x PBS (with protease inhibitors). Fractions containing the ^{15}N-NIST-mAb-Fc were dialysed against 50 mM sodium citrate pH 5.5 prior to glycan removal. The high mannose rich glycan was cleaved using 20000 units of Endo H (New England Biolabs, Cat # P0702S) per 5 mg of protein for 2 hours at 37°C. The reaction mixture was then purified using the Protein A affinity chromatography, then fractions containing the target protein were dialyzed against 50 mM sodium acetate pH 5.0.

NMR spectroscopy

Data acquisition was acquired as previously reported (56). All NMR samples contained the appropriate fragments at approximately 15 µM protein concentration in 20 mM sodium phosphate at pH 6.0 and 5% v/v deuterium oxide for field frequency lock purposes. Spectra were recorded on Bruker AVANCE III-HD 700 MHz spectrometers equipped with a 1.7 mm TCI cryoprobe. All NMR data were collected at 50 °C in 1.7 mm capillary tubes containing 40 µL of sample. Proton-nitrogen correlation spectra were collected using the phase-sensitive sofast-hmqc pulse sequence from the Bruker library (sfhmqcf3gpph) with the following parameters: the pc9 pulse with a 120 ° excitation was increased to 2210 µs, corresponding to a 3400 Hz bandwidth, (the pc9 pulse has bandwidth factor of 7.512) and centered at 8.4 ppm, 8096 transients per FID were collected to produce a data matrix of 512 × 64 complex points for a total acquisition time of 108 h. The nitrogen dimension used a spectral window of 35 ppm that was centered at 117 ppm (corresponding to a 26 ms acquisition time for the nitrogen dimension). The inter scan delays was 0.3 s. All NMR spectra were processed with NMRPipe and viewed using NMRView (57, 58). Structural models were visualized using chimera (59). Combined Chemical Shift Difference (CCSD) was calculated based on the following equation:

where α=0.1 and δH and δN are differences in chemical shifts in ppm for ^{1}H and ^{15}N with respect to a reference cross peak (42).

$$CCSD = \sqrt{(0.5 * [(\delta H)2 + (\alpha * \delta N)2])}$$

Statistical analysis

All statistical analyses were performed using GraphPad Prism version 9.0.0 (GraphPad Software, San Diego, CA, USA). Non-linear regression (variable slope, four parameters) was used for curve-fitting, and differences amongst two treatments were assessed using one-way ANOVA with Tukey *post hoc* tests to identify statistical differences. An α level of 0.05 was set as the criterion for statistical significance. Graphs are annotated with p values represented as *p ≤ 0.05, **p ≤ 0.01, ***p ≤ 0.001, ****p ≤ 0.0001. All data are presented as mean + standard deviation.

Data availability statement

Mass Spectrometry data presented in the study are deposited in the FigShare repository, doi: 10.6084/m9.figshare.20171174.v1

Author contributions

GH synthesized glycans, performed glycan remodeling on monoclonal antibodies/^{15}N-NISTmAb-Fc proteins, and data analysis. LT performed binding and cell-based assays. GG expressed ^{15}N-NISTmAb-Fc proteins. AS performed flow cytometry experiments and analyzed data. XL conceptualized experiments provided resources for cell culture experiments and edited manuscript. YA performed NMR experiments, experimental conceptualization, data interpretation, wrote and edited manuscript. RT conceptualized experiments, synthesized glycans, performed cell-based assays, data analysis and interpretation, wrote and edited manuscript. All authors contributed to the article and approved the submitted version.

Funding

This work was funded by the Government of Canada.

Acknowledgments

We thank Yi-Min She, Lisa Walrond and Marybeth Creskey of the Mass Spectrometry lab at the Regulatory Research Division at Health Canada for performing mass spectrometry sample analyses. We thank Drs. Jessie Lavoie, Michael Johnston, Simon Sauvé and Michael Rosu-Myles for critical review of this manuscript and thoughtful comments.

Conflict of interest

The authors declare that the research was conducted in the absence of any commercial or financial relationships that could be construed as a potential conflict of interest.

Publisher's note

Supplementary material

The Supplementary Material for this article can be found online at: https://www.frontiersin.org/articles/10.3389/fimmu.2022.972168/full#supplementary-material

SUPPLEMENTARY FIGURE 1
N-glycan characterization of palivizumab. **(A)** HPAEC-PAD chromatogram of commercially-available palivziumab and **(B)** glycan analysis of palivizumab obtained commercially, compared to those reported in literature (25) **(C)** Intact mass spectrometry analysis of commercially available palivizumab shows the presence of various glycoforms on the same mAb (*i.e.* on each heavy chain of the mAb dimer). **(D)** Theoretical and observed intact mass values (Da) and mass error (ppm) of various glycoforms in commercial palivizumab.

SUPPLEMENTARY FIGURE 2
Mass spectrometry characterization of branch-specific truncated monogalactosylated isomers **(A)** G1(3)T and **(B)** G1(6)T, obtained following purification by PGC-LC-HPLC. MS/MS spectra are shown at the doubly charged ions of m/z 638.7374 and 638.7375 for **(A)** and **(B)**, respectively. Cleavage of the α3 antenna between the GlcNAc-β1-2-Man linkage produces a relatively higher abundance of the cleaved and its complementary glycan fragment compared to cleavage of the α6 antenna.

SUPPLEMENTARY FIGURE 3
Characterization of defucosylated palivizumab analogues with varying degrees of galactosylation. **(A)** SDS-PAGE analysis shows the shift in bands between starting material (deglycosylated) and completed reaction (glycosylated). **(B-G)** Deconvoluted intact mass spectrometry spectra shows the presence of palivizumab **(B)** following deglycosylation with EndoS, **(C)** Fucosidase GH29, then transglycosylation with EndoS D233Q and purified oxazoline glycans to form homogeneous palivizumabs comprising **(D)** agalactosylated G0, **(E)** monogalactosylation at the α3 antenna (G1(3)), **(F)** monogalactosylation at the α6 antenna (G1(6)), or**(G)** digalactosylated G2. **(H)** Theoretical and observed intact mass values (Da) and mass error (ppm) of various palivizumab glycoform intermediates and final products following enzymatic transglycosylation.

SUPPLEMENTARY FIGURE 4
HPAEC-PAD chromatogram of PNGase-F-released *N*-glycans from remodeled palivizumab. Un-remodelled Man5 glycans were 3% for each analogue, indicating that enzymatic glycosylation is consistent for all remodelled analogues.

SUPPLEMENTARY FIGURE 5
Characterization of transglycosylated ^{15}N-NISTmAb-Fc with homogeneous glycoforms. Reducing SDS-PAGE gels show the shift in band migration of transglycosylated isotopically ^{15}N-NISTmAb-Fc (with G0, G1(3), G1(6), or G2) compared to starting material comprising only a single GlcNAc residue on each monomer. Lanes showing two bands contain both starting material and the transglycosylated Fc product to ensure these are two discreet bands.

SUPPLEMENTARY FIGURE 6
Overlay of 2D ^{1}H-^{15}N NMR spectra of EndoH-treated ^{15}N-Gn-NISTmAb-Fc (orange) and remodelled ^{15}N-G0-NISTmAb-Fc (red).

SUPPLEMENTARY FIGURE 7
Overlay of 2D ^{1}H-^{15}N NMR spectra of digalactosylated ^{15}N-G2-NISTmAb-Fc (blue) with **(A)**. monogalactosylated remodelled ^{15}N-G1(6)-NISTmAb-Fc (green), and **(B)** ^{15}N-G1(3)-NISTmAb-Fc (dark green). Peptide backbone amino acid residues that show chemical shift perturbations (CSPs) are labelled and highlighted with a red box, while examples of other residues that show little to no CSPs are labelled as black text only without a red box. Compared to the digalactosylated protein, more chemical shift perturbations are observed with the monogalactosylation at the α3 antenna **(B)** compared to the α6 antenna **(A)**.

SUPPLEMENTARY TABLE 1
^{1}H and ^{15}N chemical shifts (in ppm) and Combined Chemical Shift Difference (CCSD, in ppm) of amino acid residues that show Chemical Shift Perturbations (CSPs) between agalactosylated afucosylated Fc glycoform (G0) with glycoforms bearing a terminal galactose residue at the α6 antenna. Low CCSD values are observed amongst afucosylated glycoforms with a terminal galactose residue at the α6 antenna (i.e. G1(6) vs G2). D312 is used as a reference for a residue that showed low CCSD in all analogues.

References

1. Leader B, Baca QJ, Golan DE. Protein therapeutics: a summary and pharmacological classification. *Nat Rev Drug Discov* (2008) 7(1):21–39. doi: 10.1038/nrd2399

2. Chiu ML, Goulet DR, Teplyakov A, Gilliland GL. Antibody structure and function: The basis for engineering therapeutics. *Antibodies (Basel)* (2019) 8(4):55. doi: 10.3390/antib8040055

3. Spiro RG. Protein glycosylation: nature, distribution, enzymatic formation, and disease implications of glycopeptide bonds. *Glycobiology* (2002) 12(4):43R–56R. doi: 10.1093/glycob/12.4.43R

4. Zhang P, Woen S, Wang T, Liau B, Zhao S, Chen C, et al. Challenges of glycosylation analysis and control: an integrated approach to producing optimal and consistent therapeutic drugs. *Drug Discov Today* (2016) 21(5):740–65. doi: 10.1016/j.drudis.2016.01.006

5. Shields RL, Lai J, Keck R, O'Connell LY, Hong K, Meng YG, et al. Lack of fucose on human IgG1 n-linked oligosaccharide improves binding to human fcgamma RIII and antibody-dependent cellular toxicity. *J Biol Chem* (2002) 277 (30):26733–40. doi: 10.1074/jbc.M202069200

6. Niwa R, Shoji-Hosaka E, Sakurada M, Shinkawa T, Uchida K, Nakamura K, et al. Defucosylated chimeric anti-CC chemokine receptor 4 IgG1 with enhanced antibody-dependent cellular cytotoxicity shows potent therapeutic activity to T-cell leukemia and lymphoma. *Cancer Res* (2004) 64(6):2127–33. doi: 10.1158/0008-5472.CAN-03-2068

7. Ferrara C, Grau S, Jager C, Sondermann P, Brunker P, Waldhauer I, et al. Unique carbohydrate-carbohydrate interactions are required for high affinity binding between FcgammaRIII and antibodies lacking core fucose. *Proc Natl Acad Sci USA* (2011) 108(31):12669–74. doi: 10.1073/pnas.1108455108

8. Mizushima T, Yagi H, Takemoto E, Shibata-Koyama M, Isoda Y, Iida S, et al. Structural basis for improved efficacy of therapeutic antibodies on defucosylation of their fc glycans. *Genes Cells* (2011) 16(11):1071–80. doi: 10.1111/j.1365-2443.2011.01552.x

9. Houde D, Peng Y, Berkowitz SA, Engen JR. Post-translational modifications differentially affect IgG1 conformation and receptor binding. *Mol Cell Proteomics* (2010) 9(8):1716–28. doi: 10.1074/mcp.M900540-MCP200

10. Chung AW, Crispin M, Pritchard L, Robinson H, Gorny MK, Yu X, et al. Identification of antibody glycosylation structures that predict monoclonal antibody fc-effector function. *AIDS* (2014) 28(17):2523–30. doi: 10.1097/QAD.0000000000000444

11. Shinkawa T, Nakamura K, Yamane N, Shoji-Hosaka E, Kanda Y, Sakurada M, et al. The absence of fucose but not the presence of galactose or bisecting n-acetylglucosamine of human IgG1 complex-type oligosaccharides shows the critical role of enhancing antibody-dependent cellular cytotoxicity. *J Biol Chem* (2003) 278 (5):3466–73. doi: 10.1074/jbc.M210665200

12. Mimura Y, Mimura-Kimura Y, Saldova R, Rudd PM, Jefferis R. Enhanced immunomodulatory effect of intravenous immunoglobulin by fc galactosylation and nonfucosylation. *Front Immunol* (2022) 13:818382. doi: 10.3389/fimmu.2022.818382

13. Hodoniczky J, Zheng YZ, James DC. Control of recombinant monoclonal antibody effector functions by fc n-glycan remodeling *in vitro*. *Biotechnol Prog* (2005) 21(6):1644–52. doi: 10.1021/bp050228w

14. Peschke B, Keller CW, Weber P, Quast I, Lunemann JD. Fc-galactosylation of human immunoglobulin gamma isotypes improves C1q binding and enhances complement-dependent cytotoxicity. *Front Immunol* (2017) 8:646. doi: 10.3389/fimmu.2017.00646

15. Dekkers G, Treffers L, Plomp R, Bentlage AEH, de Boer M, Koeleman CAM, et al. Decoding the human immunoglobulin G-glycan repertoire reveals a spectrum of fc-receptor- and complement-Mediated-Effector activities. *Front Immunol* (2017) 8:877. doi: 10.3389/fimmu.2017.00877

16. Subedi GP, Barb AW. The immunoglobulin G1 n-glycan composition affects binding to each low affinity fc gamma receptor. *MAbs* (2016) 8(8):1512–24. doi: 10.1080/19420862.2016.1218586

17. Parsons TB, Struwe WB, Gault J, Yamamoto K, Taylor TA, Raj R, et al. Optimal synthetic glycosylation of a therapeutic antibody. *Angew Chem Weinheim Bergstr Ger* (2016) 128(7):2407–13. doi: doi : 10.1002/ange.201508723

18. Li T, DiLillo DJ, Bournazos S, Giddens JP, Ravetch JV, Wang LX. Modulating IgG effector function by fc glycan engineering. *Proc Natl Acad Sci USA* (2017) 114(13):3485–90. doi: 10.1073/pnas.1702173114

19. Giddens JP, Lomino JV, DiLillo DJ, Ravetch JV, Wang LX. Site-selective chemoenzymatic glycoengineering of fab and fc glycans of a therapeutic antibody. *Proc Natl Acad Sci USA* (2018) 115(47):12023–7. doi: 10.1073/pnas.1812833115

20. Wada R, Matsui M, Kawasaki N. Influence of n-glycosylation on effector functions and thermal stability of glycoengineered IgG1 monoclonal antibody with homogeneous glycoforms. *MAbs* (2019) 11(2):350–72. doi: 10.1080/19420862.2018.1551044

21. Aoyama M, Hashii N, Tsukimura W, Osumi K, Harazono A, Tada M, et al. Effects of terminal galactose residues in mannose alpha1-6 arm of fc-glycan on the effector functions of therapeutic monoclonal antibodies. *MAbs* (2019) 11(5):826–36. doi: 10.1080/19420862.2019.1608143

22. Song T, Ozcan S, Becker A, Lebrilla CB. In-depth method for the characterization of glycosylation in manufactured recombinant monoclonal antibody drugs. *Anal Chem* (2014) 86(12):5661–6. doi: 10.1021/ac501102t

23. Reusch D, Tejada ML. Fc glycans of therapeutic antibodies as critical quality attributes. *Glycobiology* (2015) 25(12):1325–34. doi: 10.1093/glycob/cwv065

24. Sjogren J, Lood R, Nageli A. On enzymatic remodeling of IgG glycosylation; unique tools with broad applications. *Glycobiology* (2020) 30(4):254–67. doi: 10.1093/glycob/cwz085

25. Hiatt A, Bohorova N, Bohorov O, Goodman C, Kim D, Pauly MH, et al. Glycan variants of a respiratory syncytial virus antibody with enhanced effector function and *in vivo* efficacy. *Proc Natl Acad Sci USA* (2014) 111(16):5992–7. doi: 10.1073/pnas.1402458111

26. Takashita E, Kinoshita N, Yamayoshi S, Sakai-Tagawa Y, Fujisaki S, Ito M, et al. Efficacy of antibodies and antiviral drugs against covid-19 omicron variant. *N Engl J Med* (2022) 386:995–8. doi: 10.1056/NEJMc2119407

27. Nair H, Nokes DJ, Gessner BD, Dherani M, Madhi SA, Singleton RJ, et al. Global burden of acute lower respiratory infections due to respiratory syncytial virus in young children: a systematic review and meta-analysis. *Lancet* (2010) 375 (9725):1545–55. doi: 10.1016/S0140-6736(10)60206-1

28. Acosta PL, Caballero MT, Polack FP. Brief history and characterization of enhanced respiratory syncytial virus disease. *Clin Vaccine Immunol* (2015) 23 (3):189–95. doi: 10.1128/CVI.00609-15

29. Levine S, Klaiber-Franco R, Paradiso PR. Demonstration that glycoprotein G is the attachment protein of respiratory syncytial virus. *J Gen Virol* (1987) 68(Pt 9):2521–4. doi: 10.1099/0022-1317-68-9-2521

30. Feldman SA, Audet S, Beeler JA. The fusion glycoprotein of human respiratory syncytial virus facilitates virus attachment and infectivity *via* an interaction with cellular heparan sulfate. *J Virol* (2000) 74(14):6442–7. doi: 10.1128/JVI.74.14.6442-6447.2000

31. Johnson S, Oliver C, Prince GA, Hemming VG, Pfarr DS, Wang SC, et al. Development of a humanized monoclonal antibody (MEDI-493) with potent *in vitro* and *in vivo* activity against respiratory syncytial virus. *J Infect Dis* (1997) 176 (5):1215–24. doi: 10.1086/514115

32. Tang F, Wang LX, Huang W. Chemoenzymatic synthesis of glycoengineered IgG antibodies and glycosite-specific antibody-drug conjugates. *Nat Protoc* (2017) 12(8):1702–21. doi: 10.1038/nprot.2017.058

33. Sun B, Bao W, Tian X, Li M, Liu H, Dong J, et al. A simplified procedure for gram-scale production of sialylglycopeptide (SGP) from egg yolks and subsequent semi-synthesis of Man3GlcNAc oxazoline. *Carbohydr Res* (2014) 396:62–9. doi: 10.1016/j.carres.2014.07.013

34. Liu L, Prudden AR, Bosman GP, Boons GJ. Improved isolation and characterization procedure of sialylglycopeptide from egg yolk powder. *Carbohydr Res* (2017) 452:122–8. doi: 10.1016/j.carres.2017.10.001

35. Koizumi K, Okada Y, Fukuda M. High-performance liquid chromatography of mono- and oligo-saccharides on a graphitized carbon column. *Carbohydr Res* (1991) 215(1):67–80. doi: 10.1016/0008-6215(91)84008-3

36. She YM, Tam RY, Li X, Rosu-Myles M, Sauve S. Resolving isomeric structures of native glycans by nanoflow porous graphitized carbon chromatography-mass spectrometry. *Anal Chem* (2020) 92(20):14038–46. doi: 10.1021/acs.analchem.0c02951

37. Helm J, Grunwald-Gruber C, Thader A, Urteil J, Fuhrer J, Stenitzer D, et al. Bisecting Lewis X in hybrid-type n-glycans of human brain revealed by deep structural glycomics. *Anal Chem* (2021) 93(45):15175–82. doi: 10.1021/acs.analchem.1c03793

38. van den Eijnden DH, Blanken WM, van Vliet A. Branch specificity of β-d-galactosidase from escherichia coli. *Carbohydr Res* (1986) 151:329–35. doi: 10.1016/S0008-6215(00)90352-5

39. Calderon AD, Zhou J, Guan W, Wu Z, Guo Y, Bai J, et al. An enzymatic strategy to asymmetrically branched n-glycans. *Org Biomol Chem* (2017) 15 (35):7258–62. doi: 10.1039/C7OB01765K

40. Schwab C, Bosshard HR. Caveats for the use of surface-adsorbed protein antigen to test the specificity of antibodies. *J Immunol Methods* (1992) 147(1):125–34. doi: 10.1016/S0022-1759(12)80037-8

41. Johnson LS, Braden B, investors. *Crystals and structure of Synagis Fab*. MedImmune Inc., Bowie State University, assignees. United States patent US 6955717B2 (2005).

42. Ghasriani H, Hodgson DJ, Brinson RG, McEwen I, Buhse LF, Kozlowski S, et al. Precision and robustness of 2D-NMR for structure assessment of filgrastim biosimilars. *Nat Biotechnol* (2016) 34(2):139–41. doi: 10.1038/nbt.3474

43. Yagi H, Zhang Y, Yagi-Utsumi M, Yamaguchi T, Iida S, Yamaguchi Y, et al. Backbone (1)H, (13)C, and (15)N resonance assignments of the fc fragment of human immunoglobulin G glycoprotein. *Biomol NMR Assign* (2015) 9(2):257–60. doi: 10.1007/s12104-014-9586-7

44. Crispin M, Yu X, Bowden TA. Crystal structure of sialylated IgG fc: implications for the mechanism of intravenous immunoglobulin therapy. *Proc Natl Acad Sci USA* (2013) 110(38):E3544–6. doi: 10.1073/pnas.1310657110

45. Barb AW, Prestegard JH. NMR analysis demonstrates immunoglobulin G n-glycans are accessible and dynamic. *Nat Chem Biol* (2011) 7(3):147–53. doi: 10.1038/nchembio.511

46. Yamaguchi Y, Nishimura M, Nagano M, Yagi H, Sasakawa H, Uchida K, et al. Glycoform-dependent conformational alteration of the fc region of human immunoglobulin G1 as revealed by NMR spectroscopy. *Biochim Biophys Acta* (2006) 1760(4):693–700. doi: 10.1016/j.bbagen.2005.10.002

47. Jiang XR, Song A, Bergelson S, Arroll T, Parekh B, May K, et al. Advances in the assessment and control of the effector functions of therapeutic antibodies. *Nat Rev Drug Discovery* (2011) 10(2):101–11. doi: 10.1038/nrd3365

48. Gupta N, LeGoff J, Chamat S, Mercier-Delarue S, Touzelet O, Power UF, et al. Affinity-purified respiratory syncytial virus antibodies from intravenous immunoglobulin exert potent antibody-dependent cellular cytotoxicity. *PloS One* (2013) 8(7):e69390. doi: 10.1371/journal.pone.0069390

49. Thomann M, Schlothauer T, Dashivets T, Malik S, Avenal C, Bulau P, et al. *In vitro* glycoengineering of IgG1 and its effect on fc receptor binding and ADCC activity. *PloS One* (2015) 10(8):e0134949. doi: 10.1371/journal.pone.0134949

50. Boyd PN, Lines AC, Patel AK. The effect of the removal of sialic acid, galactose and total carbohydrate on the functional activity of campath-1H. *Mol Immunol* (1995) 32(17-18):1311–8. doi: 10.1016/0161-5890(95)00118-2

51. Ramasamy V, Ramakrishnan B, Boeggeman E, Ratner DM, Seeberger PH, Qasba PK. Oligosaccharide preferences of beta1,4-galactosyltransferase-I: crystal structures of Met340His mutant of human beta1,4-galactosyltransferase-I with a pentasaccharide and trisaccharides of the n-glycan moiety. *J Mol Biol* (2005) 353 (1):53–67. doi: 10.1016/j.jmb.2005.07.050

52. Ahmed AA, Keremane SR, Vielmetter J, Bjorkman PJ. Structural characterization of GASDALIE fc bound to the activating fc receptor FcgammaRIIIa. *J Struct Biol* (2016) 194(1):78–89. doi: 10.1016/j.jsb.2016.02.001

53. Subedi GP, Hanson QM, Barb AW. Restricted motion of the conserved immunoglobulin G1 n-glycan is essential for efficient FcgammaRIIIa binding. *Structure* (2014) 22(10):1478–88. doi: 10.1016/j.str.2014.08.002

54. Hanson QM, Barb AW. A perspective on the structure and receptor binding properties of immunoglobulin G fc. *Biochemistry* (2015) 54(19):2931–42. doi: 10.1021/acs.biochem.5b00299

55. Dorion-Thibaudeau J, Raymond C, Lattova E, Perreault H, Durocher Y, De Crescenzo G. Towards the development of a surface plasmon resonance assay to evaluate the glycosylation pattern of monoclonal antibodies using the extracellular domains of CD16a and CD64. *J Immunol Methods* (2014) 408:24–34. doi: 10.1016/j.jim.2014.04.010

56. Hodgson DJ, Ghasriani H, Aubin Y. Assessment of the higher order structure of Humira(R), Remicade(R), Avastin(R), Rituxan(R), Herceptin(R), and Enbrel(R) by 2D-NMR fingerprinting. *J Pharm BioMed Anal* (2019) 163:144–52. doi: 10.1016/j.jpba.2018.09.056

57. Delaglio F, Grzesiek S, Vuister GW, Zhu G, Pfeifer J, Bax A. NMRPipe: a multidimensional spectral processing system based on UNIX pipes. *J Biomol NMR* (1995) 6(3):277–93. doi: 10.1007/BF00197809

58. Johnson BA. Using NMRView to visualize and analyze the NMR spectra of macromolecules. *Methods Mol Biol* (2004) 278:313–52. doi: 10.1385/1-59259-809-9:313

59. Pettersen EF, Goddard TD, Huang CC, Couch GS, Greenblatt DM, Meng EC, et al. UCSF chimera–a visualization system for exploratory research and analysis. *J Comput Chem* (2004) 25(13):1605–12. doi: 10.1002/jcc.20084

frontiers | Frontiers in Immunology

TYPE Original Research
PUBLISHED 27 October 2022
DOI 10.3389/fimmu.2022.929339

OPEN ACCESS

EDITED BY
Pablo Engel,
University of Barcelona, Spain

REVIEWED BY
Mark S Cragg,
University of Southampton, United Kingdom
Robin Van Bruggen,
Sanquin Diagnostic Services, Netherlands

*CORRESPONDENCE
Christian Kellner
christian.kellner@med.uni-muenchen.de

†These authors have contributed equally to this work and share first authorship

SPECIALTY SECTION
This article was submitted to B Cell Biology, a section of the journal Frontiers in Immunology

RECEIVED 26 April 2022
ACCEPTED 12 October 2022
PUBLISHED 27 October 2022

CITATION
Zeller T, Lutz S, Münnich IA, Windisch R, Hilger P, Herold T, Tahiri N, Banck JC, Weigert O, Moosmann A, von Bergwelt-Baildon M, Flamann C, Bruns H, Wichmann C, Baumann N, Valerius T, Schewe DM, Peipp M, Rösner T, Humpe A and Kellner C (2022) Dual checkpoint blockade of CD47 and LILRB1 enhances CD20 antibody-dependent phagocytosis of lymphoma cells by macrophages.
Front. Immunol. 13:929339.
doi: 10.3389/fimmu.2022.929339

Dual checkpoint blockade of CD47 and LILRB1 enhances CD20 antibody-dependent phagocytosis of lymphoma cells by macrophages

Tobias Zeller[1†], Sebastian Lutz[1†], Ira A. Münnich[1], Roland Windisch[1], Patricia Hilger[1], Tobias Herold[2,3,4], Natyra Tahiri[2], Jan C. Banck[2], Oliver Weigert[2,3,4], Andreas Moosmann[2,5,6], Michael von Bergwelt-Baildon[2,3,4], Cindy Flamann[7], Heiko Bruns[7], Christian Wichmann[1], Niklas Baumann[8], Thomas Valerius[8], Denis M. Schewe[9], Matthias Peipp[10], Thies Rösner[8], Andreas Humpe[1] and Christian Kellner[1*]

[1]Division of Transfusion Medicine, Cell Therapeutics and Haemostaseology, University Hospital, LMU Munich, Munich, Germany, [2]Department of Medicine III, University Hospital, LMU Munich, Munich, Germany, [3]German Cancer Consortium (DKTK), Partner Site Munich, Munich, Germany, [4]German Cancer Research Center (DKFZ), Heidelberg, Germany, [5]DZIF – German Center for Infection Research, Munich, Germany, [6]Helmholtz Zentrum München, Munich, Germany, [7]Department of Internal Medicine 5, University Hospital Erlangen, Erlangen, Germany, [8]Division of Stem Cell Transplantation and Immunotherapy, Department of Internal Medicine II, Christian Albrechts University and University Hospital Schleswig-Holstein, Kiel, Germany, [9]Department of Pediatrics, Otto-von-Guericke University Magdeburg, Magdeburg, Germany, [10]Division of Antibody-Based Immunotherapy, Department of Internal Medicine II, Christian Albrechts University and University Hospital Schleswig-Holstein, Kiel, Germany

Antibody-dependent cellular phagocytosis (ADCP) by macrophages, an important effector function of tumor targeting antibodies, is hampered by 'Don´t Eat Me!' signals such as CD47 expressed by cancer cells. Yet, human leukocyte antigen (HLA) class I expression may also impair ADCP by engaging leukocyte immunoglobulin-like receptor subfamily B (LILRB) member 1 (LILRB1) or LILRB2. Analysis of different lymphoma cell lines revealed that the ratio of CD20 to HLA class I cell surface molecules determined the sensitivity to ADCP by the combination of rituximab and an Fc-silent variant of the CD47 antibody magrolimab (CD47-IgGσ). To boost ADCP, Fc-silent antibodies against LILRB1 and LILRB2 were generated (LILRB1-IgGσ and LILRB2-IgGσ, respectively). While LILRB2-IgGσ was not effective, LILRB1-IgGσ significantly enhanced ADCP of lymphoma cell lines when combined with both rituximab and CD47-IgGσ. LILRB1-IgGσ promoted serial engulfment of lymphoma cells and potentiated ADCP by non-polarized M0 as well as polarized M1 and M2 macrophages, but required CD47 co-blockade and the presence of the CD20 antibody. Importantly, complementing rituximab and CD47-IgGσ, LILRB1-IgGσ

increased ADCP of chronic lymphocytic leukemia (CLL) or lymphoma cells isolated from patients. Thus, dual checkpoint blockade of CD47 and LILRB1 may be promising to improve antibody therapy of CLL and lymphomas through enhancing ADCP by macrophages.

KEYWORDS

antibody therapy, macrophages, phagocytosis, CD20, CD47, LILRB1 (ILT2), innate immune checkpoint blockade, lymphoma

Introduction

Therapeutic antibodies are well established in the treatment of cancer (1). In B-cell Non-Hodgkin lymphomas (B-NHL), tumor targeting CD20 antibodies such as rituximab and obinutuzumab have considerably improved the patient outcome (2). However, individual patients fail to respond and relapsed or refractory disease remains challenging. Progress was made by the approval of chimeric antigen receptor T cell therapies, tailor-made fragment crystallizable (Fc)-engineered antibodies, bispecific antibodies and T cell immune checkpoint inhibitors (1, 3–6). Besides, antibodies targeting checkpoints in innate immune cells such as natural killer (NK) cells or myeloid cells have gained increasing attention (7). In particular, they may hold the potential to boost key functions of typical tumor targeting antibodies such as antibody dependent cell-mediated cytotoxicity (ADCC) or phagocytosis (ADCP) (1, 7, 8).

Several studies highlighted that macrophages, which in humans express the activating immunoglobulin γ Fc region receptors (FcγR) FcγRI, FcγRIIA and FcγRIIIA as well as inhibitory FcγRIIB, represent major effector cells for rituximab and other therapeutic antibodies (2, 9, 10). According to their functional polarization, macrophages were roughly categorized into classically activated, pro-inflammatory M1 macrophages and alternatively activated, anti-inflammatory M2 macrophages. This classification was later refined by grouping the latter into M2a, M2b, M2c and M2d subtypes to take account of distinct stimuli and diverse functional properties (11, 12). However, macrophages exert a high level of plasticity and M1 and the different M2 states represent the extreme ends in a broad spectrum of different functional states. Also, subsets with intermediate phenotypes exist (12). Macrophages are among the most frequent normal cells in the tumor microenvironment (9). High numbers of tumor-associated macrophages (TAM), which often become tumor-edited into a pro-tumorigenic M2-like state, correlated with tumor progression and poor prognosis (13–16). Yet, during antibody therapy, macrophages may contribute to tumor eradication by eliminating malignant cells directly by ADCC and ADCP or by promoting adaptive immune responses by presenting tumor antigens to T cells (8, 10). Thus, studies in B-NHL patients receiving rituximab suggested that a high content of TAM correlated with improved survival and that rituximab therapy abrogated the correlation between high numbers of TAM and poor prognosis (15, 17, 18). The anti-tumoral functions of macrophages during antibody therapy may be further promoted by certain chemotherapeutic agents, as demonstrated for example for cyclophosphamide in a murine model of B cell leukemia (19).

In regard of the important role of macrophages, strategies were developed to improve their recruitment and ADCP function. These approaches include Fc engineering to enhance the antibody`s affinity to activating FcγR (20, 21) as well as the blockade of inhibitory checkpoints that interfere with FcγR signaling (10). Signal-regulatory protein (SIRP) α is one of the best characterized myeloid inhibitory receptors. SIRPα recognizes the ubiquitously expressed 'Don`t Eat Me!' signal molecule CD47, and antibody blockade of either CD47 or SIRPα strongly enhanced ADCP by macrophages (22, 23). For example, the combination of rituximab with a CD47 antibody increased ADCP of lymphoma cells by macrophages *in vitro* and improved the therapeutic efficacy in xenograft models of B-NHL (24). Moreover, accompanying CD38 antibody therapy with CD47 checkpoint blockade demonstrated efficacy in patient-derived T cell acute lymphoblastic leukemia xenograft models (25). At present, monoclonal CD47 antibodies, anti-SIRPα antibodies and SIRPα-Fc fusion proteins, as well as small molecule inhibitors are in different stages of pre-clinical or clinical development (23, 26–30). Promising results were obtained with the combination of rituximab plus the CD47 antibody hu5F9-G4 (magrolimab) in a clinical phase Ib study in B-NHL patients (28). Although the IgG4 antibody magrolimab was well tolerated by the patients, safety of CD47 targeting remains a serious concern due to the ubiquitous CD47 expression by normal cells, which may cause on-target toxicity. In particular, CD47 expressing red blood cells (RBC), which display cell surface "Eat Me!" signals and downregulate CD47 during their lifespan, are vulnerable to CD47 antibody therapy. This may result in enhanced RBC clearance during CD47 antibody therapy, even when antibody formats with diminished Fc-mediated functions such as IgG4 isotypes are employed (10, 28).

Leukocyte immunoglobulin-like receptor (LILR) B 1 may represent another target for immune checkpoint blockade in monocytes and macrophages (10, 31). LILRB1 and other members of the inhibitory subfamily B of LILR share structural similarities with human killer cell immunoglobulin-like receptors (KIR) and are characterized by cytoplasmic immunoreceptor tyrosine-based inhibition motifs (ITIM) (32). In addition to several pathogen-derived ligands, LILRB1 binds classical human leukocyte antigen (HLA) class I as well as non-classical HLA-G and HLA-F molecules by interaction with the α3 domain and β2-microglobulin (33–35). Recently, it has been shown that antibody blockade of either LILRB1 or HLA-class I promotes phagocytosis of solid tumor cells, that genetic ablation of cell surface expression of HLA class I and CD47 augmented ADCP by anti-EpCAM or anti-EGFR antibodies and that MHC class I expression confers protection from macrophages in a murine tumor model (36). In addition, macrophages express LILRB2, another inhibitory receptor for HLA class I molecules that interferes with FcγR signaling (37, 38). Interestingly, LILRB2 antagonism was suggested to reprogram tumor-associated myeloid cells, to enhance pro-inflammatory responses and to promote antitumor effects of T cell immune checkpoint inhibitors (39). However, whether LILRB2 directly impairs phagocytosis is currently not known (10).

Here, the impact of HLA class I expression on macrophage-mediated ADCP of lymphoma cells and the potential of antibodies blocking the cognate inhibitory receptors LILRB1 and LILRB2 was analyzed. To prevent the induction of any Fc-mediated effects by these blocking antibodies, which may cause difficulties in unraveling effects mediated by FcγR engagement or receptor blockade, Fc-silent IgGσ variants were used, in which both FcγR and complement binding was abrogated by Fc engineering (40, 41). Clinically, such Fc-silent immune checkpoint blocking antibodies may cause less on-target side effects, as they do not induce ADCC, ADCP or CDC on their own and avoid cross-linkage of antibody bound receptors by effector cells through Fc-FcγR interactions. The anti-LILRB1 antibody was found to significantly enhance ADCP when combined with CD20 and CD47 antibodies by analyzing different B-NHL cell lines and tumor cells from chronic lymphocytic leukemia (CLL) or mantle cell lymphoma (MCL) patients.

Materials and methods

Antibodies and reagents

The antibodies rituximab, obinutuzumab and trastuzumab (Hoffmann-La Roche AG, Basel, Switzerland) were provided by the institutional pharmacy. The allophycocyanin (APC)-labeled CD11b antibody (clone M1/70) as well as phycoerythrin (PE)-conjugated antibodies specific for CD80 (clone REA661), CD163 (clone REA812), LILRB1 (clone REA998) or LILRB2 (clone REA184) and the corresponding isotype antibody (clone REA293) were from Miltenyi Biotec (Bergisch Gladbach, Germany). The APC-conjugate of the anti-LILRB1 antibody clone GHI/75 as well as Brilliant Violet 421-conjugated CD163 (GHI/61) and Brilliant Violet 510-coupled CD15 (W6D3) antibodies were purchased from BioLegend (San Diego, CA, USA). Murine antibodies against cell surface antigens CD20 (clone S1815E), HLA-A,-B,-C (clone W6/32), HLA-G (clone 87G), SIRPα (clone 15-414), LILRB1 (clone GHI/75), CD47 (clone B6H12) and an IgG2a isotype (clone MOPC-173) were purchased from BioLegend. The anti-LILRB2 antibody (clone 287219) and an IgG1 istotype antibody (clone 11711) were obtained from R&D systems, Inc. (Minneapolis, MN, USA). Secondary PE-conjugated $F(ab')_2$ fragments of goat anti-human Fcγ region antibodies were purchased from Jackson ImmunoResearch Laboratories, Inc. (West Grove, PA, USA). Human recombinant macrophage colony stimulating factor (M-CSF), granulocyte macrophage-colony stimulating factor (GM-CSF), interferon (IFN)-γ and interleukin-10 (IL-10) were purchased from PeproTech (Cranbury, NJ, USA). Lipopolysaccharide (LPS) O127:B8 was obtained from Sigma-Aldrich (St. Louis, MO, USA).

Cell culture

Carnaval, DG-75 and SU-DHL-4 (German Collection of Microorganisms and Cell Cultures GmbH, DSMZ, Braunschweig, Germany) cells were cultured in Roswell Park Memorial Institute 1640 medium (Thermo Fisher Scientific, Waltham, MA, USA) supplemented with 10% fetal calf serum (FCS, Thermo Fisher Scientific) and 1% penicillin (Pen)/streptomycin (Strep) solution (Lonza, Basel, Switzerland). Granta 519 (DSMZ), Chinese hamster ovary (CHO)-K1 (DSMZ) and Lenti-X^{TM} 293T cells (Clontech, Saint-Germain-en-Laye, France) were kept in Dulbecco's Modified Eagle's Medium (Thermo Fisher Scientific) containing 10% FCS and 1% Pen/Strep. MEC2 cells (DSMZ) were maintained in Iscove's Modified Dulbecco's Medium (Thermo Fisher Scientific) supplemented with 20% FCS and 1% Pen/Strep. Cells were cultured in a humidified atmosphere at 37°C and 6% CO_2.

Isolation of mononuclear cells and generation of macrophages

Experiments were approved by the Ethics Committee of the faculty of medicine, LMU Munich (18-821 and 21-0816), in accordance with the Declaration of Helsinki. Blood samples were collected after receiving the donors` written informed consents. MNC were isolated from peripheral blood or leukoreduction system chambers by density gradient centrifugation using

Ficoll® Paque Plus (Cytiva, Marlborough, MA, USA). Monocytes were isolated by plastic adherence using monocyte attachment medium (PromoCell GmbH, Heidelberg, Germany) following the manufacturer`s protocols. To generate non-polarized M0 macrophages adherent monocytes were cultivated in X-Vivo™ 15 (Lonza) medium supplemented with 0.5% Pen/Strep and, unless otherwise indicated, M-CSF at a concentration of 50 ng/ml for 7 days. In individual experiments, M-CSF was replaced by GM-CSF (10 ng/ml). If not specified, polarized M1 macrophages were obtained by culturing cells in the presence of GM-CSF (10 ng/ml) for 6 days to drive macrophage differentiation towards an M1 phenotype, before stimulation with IFN-γ (10 ng/ml) and LPS (100 ng/ml) for additional 48 h. M2 macrophages (M2c subtype) were polarized with M-CSF (50 ng/ml) for 6 days, before IL-10 was added at a concentration of 10 ng/ml for additional 48 h. Macrophages were harvested by accutase (Thermo Fisher Scientific) treatment following the manufacturer`s recommendations.

Isolation of bone marrow macrophages from lymphoma patients

Macrophages, defined as CD163-positive and CD15-negative cells, were isolated from cryo-preserved BM-derived samples from diffuse large B cell lymphoma (DLBCL) patients by density-gradient centrifugation and fluorescence activated cell sorting as described previously (42). Bone marrow samples from DLBCL patients with BM infiltration served as a source for lymphoma associated macrophages (LAM). The purity was greater than 95%. Each patient gave informed consent prior to surgery or bone marrow biopsy, and the institutional ethics committee approved the study (Erlangen: Ref. number 21-403-Br).

Cloning, expression and purification of recombinant antibodies

Anti-LILRB1 and anti-LILRB2 antibodies were derived from the sequences from the antibody clones GHI/75 and 19.h1, respectively (43, 44). As a murine IgG1 antibody GHI/75 has been demonstrated to block HLA class I/β2M binding to LILRB1, thereby promoting phagocytosis of cancer cells (36). The antibody clone 19.h1 is a humanized version of antibody 19.1, which had been selected for its abilities to block interactions between HLA class I and LILRB2 and to shift macrophage polarization towards an M1 phenotype (44). For construction of the Fc-silent anti-LILRB1 antibody (LILRB1-IgGσ), DNA fragments encoding the variable light (VL) and heavy (VH) chains of antibody GHI/75 as well as the constant human κ light (LC) and IgG2σ heavy chain (HC) regions (amino acid substitutions: V234A/G237A/P238S/H268A/V309L/A330S/P331S) were synthesized *de novo* (Thermo Fisher Scientific) according to published sequences (40, 45). LC and HC sequences were cloned into vector pSecTag2/Hygro C (Thermo Fisher Scientific) using NheI/PmeI restriction sites. To generate an IgG1σ (amino acid substitutions L234A/L235A/G237A/P238S/H268A/A330S/P331S) variant (41) of the anti-LILRB2 antibody 19.h1 (LILRB2-IgGσ), VL and VH sequences were synthesized *de novo* (Thermo Fisher Scientific) conforming to published sequences (44) and ligated into vectors pSecTag2-LC (20) and pSecTag2-HC-IgG1σ (C Kellner, unpublished) as NheI/HindIII and NheI/PpuMI cassettes, respectively. For generation of antibody CD47-IgGσ, VL and VH regions of antibody hu5F9 (46) were synthesized *de novo* and cloned into vectors pSec-CD3-HC-IgG2σ (M. Peipp, unpublished) and pSecTag2-LC (20) as NheI/HindIII and NheI/PpuMI cassettes, respectively. The expression vector for the HC of an Fc-engineered version of rituximab (RTX-DE; amino acid substitutions S239D/I332E) was generated by excising rituximab VH regions from vector pSecTag2-CD20-HC (47) and ligation into vector pSecTag2-HC-DE (20) using NheI/PpuMI restriction sites. The vectors encoding rituximab LC, trastuzumab LC or an Fc-engineered HC of trastuzumab (HER2-DE; amino acid substitutions S239D/I332E) have been described previously (20, 47). The vector encoding an Fc-silent IgG2σ HC variant of trastuzumab (HER2-IgGσ) was obtained by ligation of trastuzumab VH chain sequences in vector pSec-CD3-HC-IgG2σ using NheI/PpuMI restriction sites. For expression, Lenti-X™ 293T cells were co-transfected with HC and LC expression vectors by calcium phosphate transfection with chloroquine following standard protocols. Cell culture supernatants were collected for six days. Antibodies were purified by affinity chromatography using CaptureSelect™ IgG-CH1 affinity matrix (Thermo Fisher Scientific) as described earlier (47) and dialyzed against PBS (Thermo Fisher Scientific). The IgA2 isotype variants of rituximab (RTX-IgA2) and the anti-epidermal growth factor receptor (EGFR) antibody cetuximab have been described previously and were expressed in CHO-S cells (Thermo Fisher Scientific) by transient transfection following published procedures (48–50).

Microfluidic chip electrophoresis

Purity, integrity and concentrations of the purified antibodies were determined by microfluidic chip electrophoresis under reducing and non-reducing conditions. Four microliters of antibody preparations were analyzed using the Agilent Protein 230 Kit and the Agilent 2100 Bioanalyzer system (Agilent Technologies, Santa Clara, CA, USA) following the manufacturer's recommendations.

Sodium dodecyl sulfate polyacrylamide gel electrophoresis (SDS PAGE) and Western Transfer experiments

SDS-PAGE and Western Transfer experiments were performed using standard procedures as described elsewhere (47). Antibody LC and HC were detected with horseradish peroxidase (HRP)-conjugated goat anti human κ light chain (Bio-Rad Laboratories, Inc.) and goat anti-human IgG/Fc specific (Merck, Darmstadt, Germany) antibodies, respectively.

Gel filtration

Gel filtration was performed using the ÄKTApure protein purification system (Cytiva). For analysis, 100 - 300 µg of antibodies were loaded on a Superdex™ 200 Increase 10/300 GL column (Cytiva) and analyzed at a flow speed of 0.75 ml/min using PBS as running buffer.

Expression of cell surface antigens by transient transfection

DNA sequences encoding human full-length LILRB1 and LILRB2 proteins (UniProtKB accession numbers Q8NHL6 and Q8N423, respectively) were synthesized *de novo* (Thermo Fisher Scientific) and cloned into expression vector pcDNA 3.1 (+) (Thermo Fisher Scientific). CHO-K1 cells were transfected using Lipofectamine® LTX and Plus™ Reagent (Thermo Fisher Scientific) according to the manufacturer's recommendation. After 48 h, the transfected cells (i.e. CHO-LILRB1 and CHO-LILRB2, respectively) were used in functional analysis.

Flow cytometry

Flow cytometry experiments were performed on a FACSCalibur™ flow cytometer (BD Biosciences, Franklin Lakes, NJ, USA) with the exception of multi-colour analysis, which were performed on a FACSCanto II cytometer (BD Biosciences). Three hundred thousand cells were washed once with 2 ml PBS containing 1% bovine serum albumin (FACS buffer). In direct immunofluorescence assays, cells were incubated with fluorescent dye-conjugated antibodies at dilutions recommended by the manufacturer in FACS buffer at 4°C for 60 min. Expression of cell surface antigens was quantified by calibrated indirect flow cytometry using Qifikit® (Dako, Glostrup, Denmark) according to the manufacturer's recommendations. Murine antibodies were applied at a concentration of 20 µg/ml in FACS buffer supplemented with 1 mg/ml pooled human immunoglobulin (Gamunex® 10%; Grifols, Barcelona, Spain) to block FcγR. Binding of chimeric or humanized antibodies was analyzed by incubation of cells with antibodies at a concentration of 50 µg/ml at 4°C for 60 min. Cells were washed once with 2 ml of FACS buffer. $F(ab')_2$ fragments of goat anti-human IgG, Fcγ fragment specific antibodies were used for detection. To analyze the ability of anti-LILRB1 and anti-LILRB2 antibodies to block receptor binding by HLA class I molecules, 0.3×10^6 CHO-LILRB1 or CHO-LILRB2 cells were incubated with the antibodies at a concentration of 50 µg/ml in 20 µl FACS buffer for 1 h at 4°C. Then, 3 µl of PE-conjugated MHC I Dextramer® of CMV pp65 peptide (NLVPMVATV)-loaded HLA-A*0201 (Immudex, Kopenhagen, Denmark) were added. Cells were incubated for 30 min, washed with FACS buffer, and analyzed. Mean fluorescence intensity (MFI) values were normalized to the control reaction and residual binding of HLA molecules was calculated. In all experiments, appropriate scatter gates were applied to exclude debris or dead cells and 10,000 events were counted. Data were analyzed using FlowJo v10.7.2 software (Becton Dickinson).

Analysis of ADCP by fluorescence microscopy

Twenty thousand macrophages per well were plated in M0, M1 or M2c macrophage differentiation media on 8 well µ-slides (Ibidi GmbH, Graefelfing, Germany) and incubated overnight. Lymphoma cells were labeled using carboxyfluorescein succinimidyl ester (CFSE) Cell Division Tracker Kit (BioLegend) according to the manufacturer's recommendations. Forty thousand lymphoma cells were added to each well in a final volume of 300 µl. Antibodies were applied and cells were incubated at 37°C with 6% CO_2 for 2 h. Non-phagocytosed target cells were removed by exchanging the supernatant by fresh medium. ADCP was determined by counting the number of phagocytosed tumor cells per individual macrophages using the fluorescence microscope Axio Observer D1 (Carl Zeiss AG, Oberkochen, Germany), unless otherwise indicated. Fifty to 100 macrophages were analyzed. The phagocytic index was calculated by the equation: Phagocytic index = (number of engulfed target cells/number of macrophages) × 100. In individual experiments, cytoplasmic membranes of macrophages and nuclei were stained with CellBrite™ Orange Cytoplasmic Membrane Labeling Dye (Biotium, Inc., Fremont, CA, USA) and NucBlue™ Live ReadyProbes™ (Thermo Fisher Scientific), respectively, according to the manufacturer's recommendations.

The phagocytic activity of LAM was analyzed by plating purified LAM in 8-chamber slides (Thermo Fisher Scientific). LAM were co-incubated for 2 h with Cytolight Rapid Green (Sartorius, Göttingen, Germany) labeled Carnaval cells (E:T cell ratio: 1:1) in the presence of the indicated antibodies at a

concentration of 1 µg/ml. The adherent cells were washed with PBS, stained with an APC-conjugated CD11b antibody, and were fixed with 4% paraformaldehyde in PBS. The slide was then overlaid with DAPI medium and covered with a glass cover slide. Slides were analyzed using a confocal microscope (LSM700, Carl Zeiss AG).

Live cell imaging

To analyze the phagocytic uptake of target cells, 4×10^4 macrophages were plated in 50 µl of M0, M1 or M2c macrophage differentiation media in 96-well cell culture plates (Greiner Bio-One GmbH, Frickenhausen, Germany) and allowed to settle at 37°C with 6% CO_2 for at least 1 h. Antibodies were added at the indicated concentrations. Target cells were labeled with the pH-sensitive labeling dye pHrodo® (Sartorius AG) at 500 ng/ml according to the manufacturer's recommendations. Per well, 8×10^4 target cells were added in 50 µl X-Vivo™ 15 medium and live cell imaging was initiated using the IncuCyte® system (Sartorious AG). Four images per well were recorded every 30 minutes and red object counts per image were determined.

To analyze the depletion of target cells, CFSE-labeled target cells were co-cultured with macrophages in the presence of antibodies in 8 well µ-slides (Ibidi GmbH) as described above for ADCP analysis by fluorescence microscopy. After 2 h, the supernatant was carefully resuspended without disturbing adherent macrophages. For quantitation, 100 µl were transferred to a 96-well plate, pelleted by centrifugation and green fluorescent cells were counted using the Incucyte® system by analyzing nine images per well. Relative residual numbers of target cells were determined by normalizing data to the control reaction performed in the absence of antibodies and the percentage of target cell depletion was calculated.

Data processing and statistical analyses

Statistical and graphical analyses were performed using the GraphPad Prism 8.0.2 software (GraphPad Software, La Jolla, CA, USA). Statistically significant differences between treatment groups were assessed using two-sided Student´s t-test, one-way or two-way ANOVA and Šidàk´s, Tukey´s or Fisher´s LSD post-tests, as indicated. The correlation between the ratio of CD20 to HLA class I molecules per cell and susceptibility to ADCP was calculated using the Pearson correlation test. P-values ≤ 0.05 were considered statistically significant.

Results

In an effort to define critical determinants of ADCP of lymphoma cells, we analyzed the sensitivity of the lymphoma cell lines Granta 519 (MCL), Carnaval (DLBCL), DG-75 (Burkitt lymphoma), MEC2 (CLL) and SU-DHL-4 (DLBCL) using human, non-polarized M0 macrophages. To induce ADCP, cells were treated with the CD20 antibody rituximab or a combination of rituximab and a variant of the CD47 antibody magrolimab with abrogated FcγR binding (referred to as CD47-IgGσ; Supplementary Figure 1). Each antibody was analyzed at the saturating concentration of 10 µg/ml. The analysis by fluorescence microscopy revealed that the extent of ADCP induced by rituximab or by the combination of rituximab plus CD47-IgGσ differed considerably between the cell lines. The CD47 antibody, which was unable to trigger ADCP on its own due to abrogated FcγR binding, enhanced ADCP by rituximab in Carnaval, MEC2 and Granta 519 cells significantly. Minor add-on effects from the CD47 antibody were observed with DG-75 cells, which were hardly engulfed even in the presence of both antibodies, and SU-DHL-4 cells, which were extraordinarily sensitive to rituximab-mediated ADCP (Figure 1A). Regarding the 'Don´t Eat Me!' function described for HLA class I molecules by interaction with the inhibitory receptor LILRB1, we hypothesized that their expression interfered with ADCP of lymphoma cells and contributed to the observed differences. Therefore, the cell surface expression levels of HLA class I molecules, the rituximab target antigen CD20 and CD47 were determined (Figure 1B). The cell lines showed diverging expression of these antigens, with high variation in the expression of classical HLA class I molecules (HLA-A,-B,-C) and CD20, while moderate differences in CD47 expression were observed. HLA-G expression was not detectable with the exception of Granta 519 cells. Although a correlation between the expression of either HLA class I or CD20 and ADCP by combination treatment with rituximab and the CD47 antibody was not found (Supplementary Figure 2), a correlation between ADCP and the expression ratio of CD20 to HLA class I molecules was observed (Figure 1C; Supplementary Table 1). Thus, the number of displayed binding sites for rituximab and inhibitory HLA class I molecules contributed to determining the sensitivity to ADCP.

MCSF-generated M0 macrophages expressed significant amounts of the HLA class I receptors LILRB1 and LILRB2 (Figure 1D). In an attempt to further enhance ADCP by blocking the anticipated inhibitory function of HLA class I receptors, Fc-silent antibodies against LILRB1 and LILRB2 (LILRB1-IgGσ and LILRB2-IgGσ, respectively) were generated

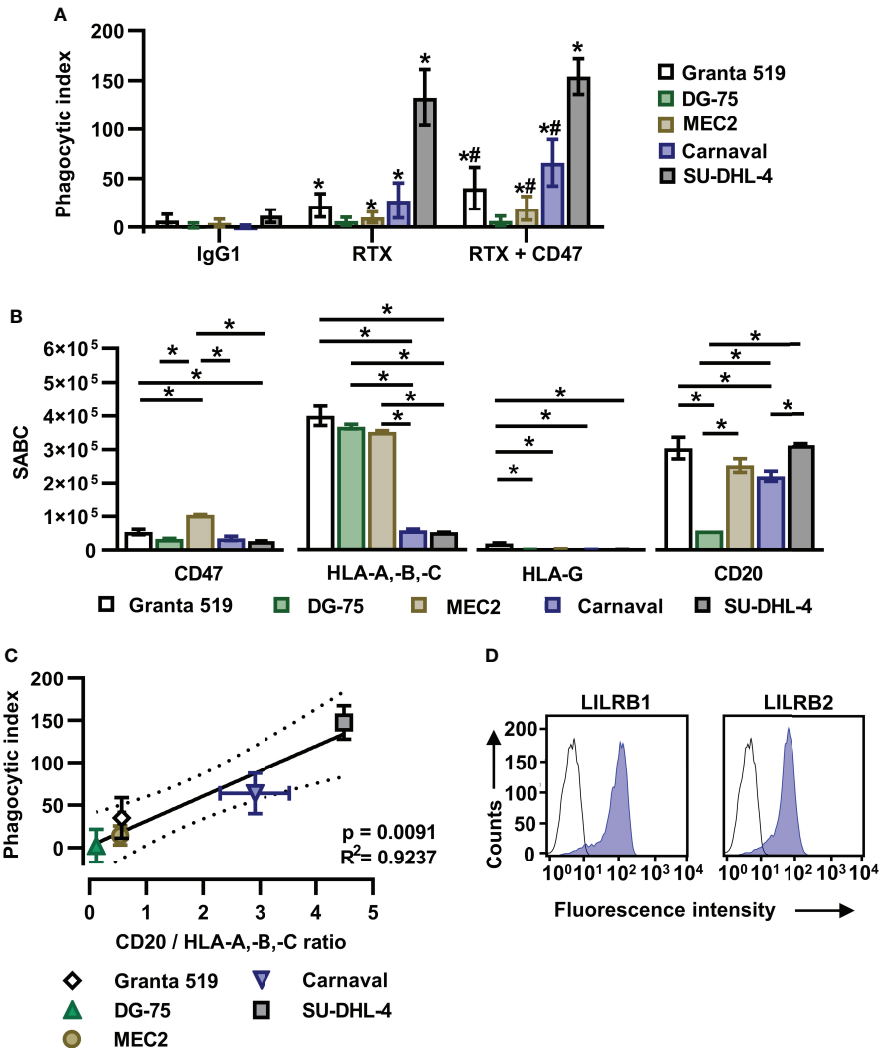

FIGURE 1
The ratio of CD20 to HLA-A,-B,-C antigen expression determines the efficacy of the combination of rituximab and a CD47 blocking antibody in initiating ADCP. **(A)** Human M0 macrophages were incubated with CFSE-labeled Granta 519 (*n* = 8), DG-75 (*n* = 6), MEC2 (*n* = 10), Carnaval (*n* = 11) or SU-DHL-4 (*n* = 4) lymphoma cells (E:T cell ratio: 1:2) in the presence of either rituximab (RTX) or a combination of RTX plus CD47-IgGσ (CD47) for 2 h. ADCP was analyzed by fluorescence microscopy and the phagocytic index was calculated. Trastuzumab (IgG1) was used as control. Antibodies were applied at 10 µg/ml. Bars represent mean values ± SD. Statistically significant differences ($P \leq 0.05$) in ADCP compared to treatment with IgG1 (*) or RTX (#) are indicated (Two-way ANOVA with Tukey's multiple comparisons test). **(B)** Lymphoma cells were stained with antibodies specific for CD20, CD47, HLA-A,-B,-C or HLA-G and specific antibody binding capacities (SABC) were determined by calibrated flow cytometry. Bars indicate mean values ± SEM (*n* = 3). Statistically significant differences between individual lymphoma cell lines are indicated (*$P \leq 0.05$; one-way ANOVA with Tukey's *post hoc* test). **(C)** For each lymphoma cell line the ratio of CD20 to HLA-A,-B,-C expression was determined and plotted against the calculated mean phagocytic index values for treatment with RTX plus CD47-IgGσ. The solid line represents the best-fit curve, dotted lines indicate the 95% confidence interval. Error bars indicate SD. **(D)** M0 macrophages were stained with murine antibodies against LILRB1 or LILRB2 (blue shaded peaks) or an isotype control antibody (black outlined peaks). Secondary FITC-conjugated goat anti-mouse immunoglobulins (DAKO) were used for detection. Cell surface expression was analyzed by flow cytometry. One representative experiment is shown (*n* = 7).

(Supplementary Figures 1A, B). Gel filtration revealed that the antibodies were monomeric and no significant multimers or higher molecular weight aggregates were detectable (Supplementary Figure 1C). The antigen specific binding of both antibodies was confirmed by flow cytometry using CHO-K1 cells transiently transfected with either LILRB1 or LILRB2 cDNA expression constructs, showing that the two antibodies exerted the expected binding profile (Supplementary Figure 3). Moreover, both LILRB1-IgGσ and LILRB2-IgGσ were able to block binding of soluble HLA class I molecules to LILRB1 and LILRB2 transfected CHO cells, respectively (Figure 2A). To analyze, whether the antibody blockade of LILRB1 and

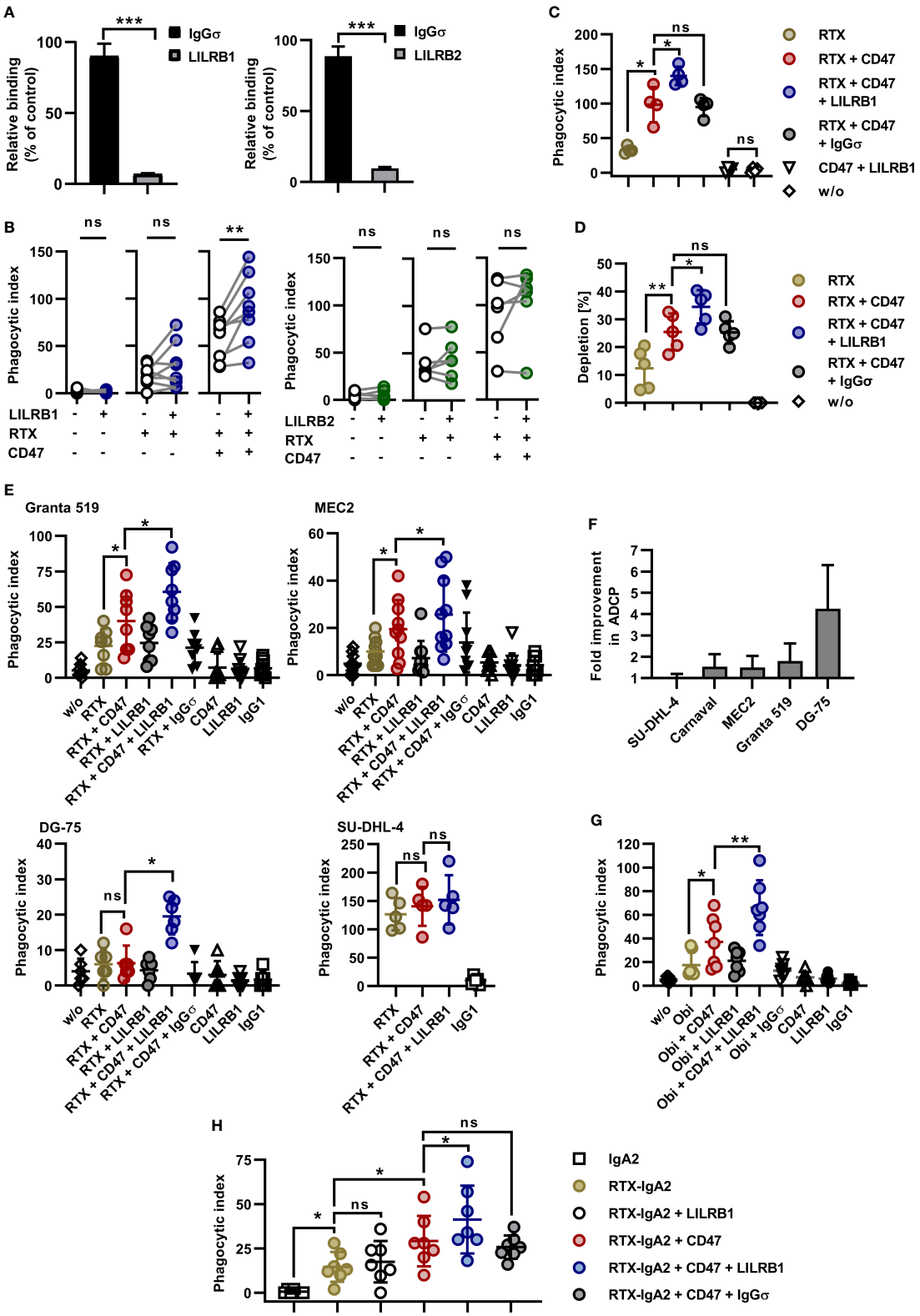

FIGURE 2 (Continued)

FIGURE 2 (Continued)
Dual checkpoint blockade of LILRB1 and CD47 enhances ADCP of lymphoma cells. **(A)** CHO-K1 cells transiently transfected with LILRB1 (*left graph*) or LILRB2 expression vectors (*right graph*) were incubated with antibodies LILRB1-IgGσ (LILRB1) and LILRB2-IgGσ (LILRB2), respectively, at a concentration of 50 µg/ml to mask LILRB receptors. Antibody HER2-IgGσ (IgGσ) was used as a control. Cells were then reacted with PE-conjugated MHC I Dextramer® of NLVPMVATV-peptide-loaded HLA-A*0201 molecules. Mean fluorescence intensity was determined by flow cytometry and residual binding of HLA molecules relative to the control was calculated. Bars represent mean values ± SEM (n = 3; ***P ≤ 0.001; Student's t test). **(B)** LILRB1-IgGσ (LILRB1; *left*, n = 8) and LILRB2-IgGσ (LILRB2; *right*, n = 6) were analyzed in ADCP reactions using human M0 macrophages and CFSE-labeled Carnaval cells (E:T cell ratio: 1:2). The antibodies (concentration: 10 µg/ml) were tested alone, together with rituximab (RTX) or in combination with RTX plus CD47-IgGσ (CD47). After 2 h, the phagocytic index was determined by fluorescence microscopy. Data points represent results obtained with individual preparations of macrophages from different donors (**P ≤ 0.01; ns, not significant; one-way ANOVA with Šidák´s multiple comparisons test). **(C)** To verify antigen specific mode of action, LILRB1-IgGσ was compared with antibody HER2-IgGσ (IgGσ) in ADCP reactions. CFSE-labeled Carnaval cells were incubated in the absence (w/o) or in the presence of the indicated antibodies. Each antibody was applied at a concentration of 10 µg/ml. After 2 h, ADCP was analyzed by fluorescence microscopy. Data points represent phagocytic index values for individual preparations of macrophages from different donors (n = 4). Horizontal lines indicate mean values ± SD (*P ≤ 0.05; ns, not significant; one-way ANOVA with Šidák´s multiple comparisons test). **(D)** Carnaval cells were labeled with CFSE and incubated with human M0 macrophages in the presence of the indicated antibodies (10 µg/ml). After 2 h, the supernatant was analyzed for residual lymphoma cells by live cell imaging and the percentage of residual lymphoma cells relative to the control reaction without added antibodies was calculated. Horizontal lines indicate mean values ± SD. (**P ≤ 0.01; *P ≤ 0.05; ns, not significant; one-way ANOVA and Šidák´s multiple comparisons test; n = 5). **(E)** Granta 519 (n = 8), MEC2 (n = 10), DG-75 (n = 6), and SU-DHL-4 (n = 5) lymphoma cells were analyzed as target cells for RTX and anti-LILRB1 and CD47 antibodies. Target cells were labeled with CFSE and co-cultured with human M0 macrophages (E:T cell ratio: 1:2) in the absence (w/o) or in the presence of the indicated antibodies (10 µg/ml) for 2 h prior to analysis by fluorescence microscopy. In individual experiments, HER2-IgGσ (IgGσ) and trastuzumab (IgG1) were analyzed as controls. Data points represent phagocytic index values for macrophages from individual donors. Horizontal lines indicate mean values ± SD (*P ≤ 0.05; ns, not significant; one-way ANOVA with Šidák´s multiple comparisons test). **(F)** The relative fold improvement in the extent of ADCP achieved by addition of LILRB1-IgGσ to RTX plus CD47-IgGσ over ADCP induced by the combination of RTX plus CD47-IgGσ only was calculated using phagocytic index values for different target cell lines as determined in **(B)**, **(C)** and **(E)**. Bars represent mean values ± SD. **(G)** Obinutuzumab (Obi) was analyzed in combination with LILRB1-IgGσ and CD47-IgGσ for induction of ADCP using a fluorescence microscopy based assay as described above. Granta 519 cells were used as target cells and human M0 macrophages were effector cells. Data points represent phagocytic index values for individual macrophage preparations from seven different donors. Horizontal lines represent mean values ± SD. (*P ≤ 0.05; **P ≤ 0.01; one-way ANOVA with Šidák´s multiple comparisons test). **(H)** An IgA2 variant of rituximab (RTX-IgA2) was analyzed alone or in combination with CD47-IgGσ and/or LILRB1-IgGσ antibodies in ADCP assays with Carnaval cells. ADCP was analyzed as described above by fluorescence microscopy. As a control, an IgA2 version of cetuximab was employed (IgA2). *P ≤ 0.05; ns, not significant; one-way ANOVA with Šidák´s multiple comparisons test (n = 7).

LILRB2 translated in enhanced ADCP, initial experiments with M0 macrophages and Carnaval target cells were performed. As a result, although not being effective alone or when combined with rituximab only, the LILRB1-IgGσ antibody significantly enhanced ADCP when applied together with both rituximab and CD47-IgGσ (Figure 2B). In contrast, no improvements in ADCP were observed by LILRB2 blockade, neither when LILRB2-IgGσ was applied alone nor in combination (Figure 2B). To demonstrate the antigen-specific mode of action of LILRB1-IgGσ, an Fc-silent control antibody, HER2-IgGσ, was combined with rituximab and CD47-IgGσ in ADCP reactions (Figure 2C). Whereas again LILRB1-IgGσ significantly improved ADCP, the HER2-IgGσ control antibody did not mediate any effects. Phagocytosis was also not observed when the LILRB1-IgGσ and CD47-IgGσ antibodies were applied in the absence of rituximab (Figure 2C), indicating that disruption of both signaling pathways was not sufficient in the absence of an activating signal. In addition, the direct comparison of the two triple combinations consisting of rituximab and CD47-IgGσ plus either LILRB1-IgGσ or LILRB2-IgGσ revealed significant differences between the two treatment groups, further demonstrating the benefits of the antigen-specific blockade of LILRB1 (Supplementary Figure 4A). In agreement with these findings, the application of the triple antibody combination consisting of rituximab, CD47-IgGσ plus LILRB1-IgGσ resulted in an enhanced depletion of Carnaval target cells, as analyzed by determining the residual remaining target cells using the IncuCyte® live cell imaging system (Figure 2D).

LILRB1-IgGσ revealed the potential also to enhance ADCP of other lymphoma cell lines. In experiments with both Granta 519 and MEC2 cells LILRB1-IgGσ was effective when applied in a triple combination with rituximab and CD47-IgGσ (Figure 2E). Remarkably, rituximab plus the dual checkpoint blockade of LILRB1 and CD47 resulted in profound phagocytosis of DG-75 cells, which hardly responded to the treatment with rituximab plus CD47-IgGσ. Yet, ADCP of SU-DHL-4 cells was not significantly improved further, which might be explained by their high susceptibility to ADCP (Figure 2E). Thus, among the analyzed cell lines, the highest fold improvement in ADCP by inclusion of LILRB1-IgGσ was achieved with DG-75 cells (Figure 2F), which had the lowest CD20 expression levels (Figure 1B). In contrast, LILRB2 blockade was not effective in enhancing ADCP of MEC2 and DG-75 cells (Supplementary Figure 4B). Using DG-75 target cells, the potency of LILRB1 blockade relative to LILRB2 blockade was further demonstrated in a direct comparison of the two respective antibodies in combination with rituximab and CD47-IgGσ (Supplementary Figure 4C). Therefore, we focused on the LILRB1-IgGσ antibody in subsequent experiments. To analyze the effects of the dual checkpoint blockade with a different CD20 antibody, ADCP was investigated in combinations with the Fc glyco-engineered CD20 antibody obinutuzumab using Granta 519 target cells. As observed in experiments with rituximab, LILRB1-IgGσ demonstrated efficacy and enhanced ADCP when applied together with obinutuzumab and CD47-IgGσ (Figure 2G). Next, the efficacy

of LILRB1 blockade was analyzed in combinations with an IgA2 isotype switch variant of rituximab (RTX-IgA2; Figure 2H). Using Carnaval target cells, RTX-IgA2 induced ADCP, and its efficacy was enhanced by combination with CD47-IgGσ. Importantly, LILRB1-IgGσ further potentiated ADCP when added to the RTX-IgA2 and CD47-IgGσ combination.

Individual macrophages are able to engulf multiple tumor target cells. Indeed, the analysis by fluorescence microscopy demonstrated that serial ADCP of Carnaval cells by M0 macrophages occurred in particular when rituximab was combined with CD47 and anti-LILRB1 antibodies (Figure 3A). To quantify the relative contribution, phagocytic events were assigned to uptake of the first lymphoma cell (initial phagocytosis) or to engulfment of subsequent cells (serial phagocytosis; Figure 3B). Serial phagocytosis was observed with Carnaval, Granta 519, MEC2 and, to a lesser extent, with DG-75 cells, and was promoted by co-treatment with CD47-IgGσ and LILRB1-IgGσ antibodies. Especially with more ADCP sensitive Carnaval and Granta 519 cells, increases in extent of ADCP by co-blockade of LILRB1 and CD47 were attributed to enhanced phagocytic activities of individual macrophages engulfing multiple target cells. The differences in the occurrence of serial phagocytosis of Carnaval and DG-75 cells was further evidenced by grouping macrophages according to the numbers of engulfed target cells (Supplementary Figure 5).

To analyze kinetics of ADCP induction, live cell imaging experiments were performed using DG-75 cells as targets (Figures 3C, D). Again, ADCP by rituximab was enhanced by dual checkpoint blockade of CD47 and LILRB1. ADCP occurred rapidly and reached a peak after 2 h. To analyze the dose dependent mode of action of LILRB1-IgGσ, rituximab and CD47-IgGσ were complemented with varying concentrations of either LILRB1-IgGσ or the control antibody HER2-IgGσ (Figure 3E). As a result, ADCP augmented with increasing concentrations of LILRB1-IgGσ while HER2-IgGσ was not effective.

Improving FcγR engagement by Fc engineering has been shown to enhance ADCP (21). To analyze, whether ADCP could be further potentiated, an Fc-engineered variant of rituximab (RTX-DE) was generated by introducing the amino acid substitutions S239D/I332E (Supplementary Figure 1). This modification enhances the antibody`s affinity to activating FcγRI, FcγRIIA and FcγIIIA and improves ADCP and ADCC (51). RTX-DE was compared with rituximab in the absence or presence of immune checkpoint inhibitors in ADCP assays using DG-75 cells by live cell imaging (Figure 3F). As a result, rituximab and RTX-DE were only marginally effective, in agreement with previous findings for this cell line. By combination of both antibodies with CD47-IgGσ ADCP was enhanced. Importantly, the triple antibody combination consisting of RTX-DE, LILRB1-IgGσ and CD47-IgGσ was more effective than the triple antibody combination containing rituximab. This demonstrates the impact of efficient FcγR engagement and indicates that ADCP can be promoted further by improving the affinity of the tumor targeting antibody to activating FcγR.

To analyze the impact of HLA class I receptors on ADCP by polarized macrophages, macrophages were differentiated towards M1 and M2c phenotypes using GM-CSF, LPS and IFN-γ or M-CSF and IL-10, respectively. Macrophage polarization was verified by determining expression levels of the M1 and M2 marker antigens CD80 and CD163, respectively (Figure 4A) The analysis of LILRB1 and LILRB2 cell surface expression revealed that M1 and M2c macrophages expressed both receptors at similar levels as M0 macrophages (Figure 4A). However, the expression of SIRPα was reduced in M1 macrophages. M1 and M2c macrophages were then analyzed as effector cells for combinations of rituximab, CD47-IgGσ and LILRB1-IgGσ in ADCP assays with Carnaval cells and compared to non-polarized, M-CSF differentiated M0 macrophages from the same donors (Figure 4B). As a result, rituximab was effective in inducing ADCP with different macrophage populations (Figure 4B). In experiments with M0 and M2c macrophages, CD47-IgGσ augmented rituximab-mediated ADCP significantly. With M1 macrophages a similar trend was observed, but statistical significance was not reached. Importantly, LILRB1-IgGσ enhanced ADCP not only by M0 macrophages, but also by polarized M1 or M2c macrophages when applied in addition to rituximab and CD47-IgGσ. As observed with M0 macrophages, LILRB1 blockade alone was not sufficient to enhance ADCP by rituximab with both M1 and M2c macrophages (Figure 4B). Moreover, ADCP by differentially polarized macrophages was analyzed by live cell imaging using DG-75 as target cells (Figure 4C). These experiments demonstrated improved ADCP of DG-75 cells by rituximab when combined with both LILRB1-IgGσ and CD47-IgGσ antibodies irrespective of the macrophage polarization status. In agreement with results obtained with M0 macrophages, LILRB2-IgGσ was not effective when M1 or M2c macrophages were analyzed (Supplementary Figures 4D, E). Furthermore, M0 macrophages were differentiated from monocytes in the presence of either M-CSF or GM-CSF and then polarized to M1 macrophages using LPS and IFN-γ. Interestingly, cell surface expression of both LILRB1 and LILRB2 was upregulated upon polarization with LPS and IFN-γ, while SIRPα expression was reduced (Figure 4D). In ADCP experiments using fluorescence microscopy, non-activated M0 macrophages differentiated with GM-CSF were not effective in comparison with macrophages differentiated with M-CSF (Figure 4E). Pre-treatment with LPS/IFN-γ improved ADCP by GM-CSF macrophages, in particular when the triple combination consisting of RTX, CD47-IgGσ and LILRB1-IgGσ was applied. LPS/IFN-γ stimulation also slightly enhanced the ADCP activity of M-CSF macrophages, which were superior to GM-CSF macrophages for each antibody treatment also upon M1 polarization with LPS/IFN-γ. Of note, the triple combination consisting of RTX, LILRB1-IgGσ and

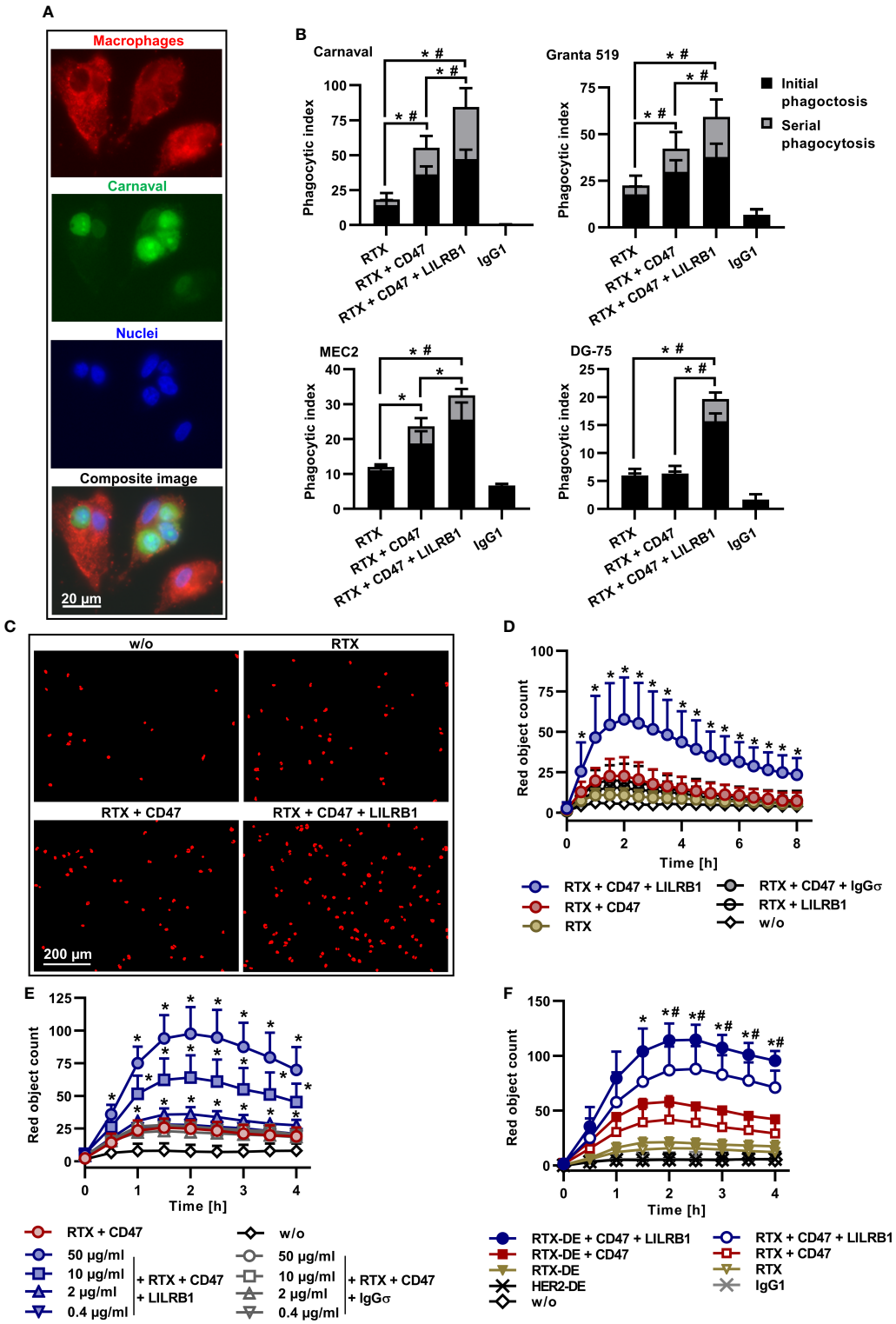

FIGURE 3 (Continued)

FIGURE 3 (Continued)
Serial ADCP, kinetics, dose-dependency and further enhanced ADCP by improved FcγR engagement. **(A)** CFSE-labeled Carnaval cells were incubated with Cell Brite™ Orange labeled human M0 macrophages in the presence of rituximab (RTX), CD47-IgGσ and LILRB1-IgGσ (E:T cell ratio: 1:2). Shown are three macrophages, having engulfed one or three Carnaval cells, or none. Nuclei were stained with NucBlue™. The bottom image represents a microscope composite image of the same cells viewed separately with the red, green and blue channels as indicated. **(B)** LILRB1-IgGσ (LILRB1) and CD47-IgGσ (CD47) antibodies promote serial ADCP of Carnaval (n = 9), Granta 519 (n = 8), MEC2 (n = 6) and DG-75 (n = 6) B-NHL cells. Phagocytic events by treatment with RTX, RTX + CD47-IgGσ, the triple combination of RTX + CD47-IgGσ + LILRB1-IgGσ or trastuzumab (IgG1) were assigned to uptake of the first lymphoma cell (initial phagocytosis) or to engulfment of subsequent cells (serial phagocytosis) and are presented as a proportion of phagocytic index values. Bars indicate mean values ± SEM. Statistically significant differences between treatment groups in initial (*) and serial (#) phagocytosis event values are indicated ($P \leq 0.05$, two-way ANOVA with Tukey`s *post hoc* test). **(C)** ADCP induced by treatment with different antibodies (10 µg/ml) alone or in combination was analyzed by live cell imaging using pHrodo® labeled DG-75 cells and human M0 macrophages (E:T cell ratio: 1:2). For analysis, cells were imaged at different time points and red fluorescent objects were counted. Shown are representative results for the control reaction without added antibodies (w/o), treatment with RTX, RTX + CD47-IgGσ (CD47) and RTX + CD47-IgGσ + LILRB1-IgGσ (LILRB1). The images were taken after 1.5 h (n = 9). **(D)** The kinetics of ADCP was analyzed by live cell imaging as described before. M0 macrophages from different donors were used as effector cells and DG-75 cells were applied as targets. Data points represent means ± SD of red object counts per image (n = 9; w/o, without added antibody). Statistically significant ($P \leq 0.05$) differences between treatment groups RTX + CD47-IgGσ vs. RTX + CD47-IgGσ + LILRB1-IgGσ are indicated (*$P \leq 0.05$; two-way ANOVA with Fisher´s LSD test). **(E)** PHrodo® labeled DG-75 lymphoma cells were incubated with human M0 macrophages from different donors (n = 4) in the presence of RTX and CD47-IgGσ (each at a constant concentration of 10 µg/ml) plus LILRB1-IgGσ at varying concentrations. HER2-IgG2σ (IgGσ) was used as an isotype control. ADCP was analyzed over 4 h by live cell imaging. Data points represent means ± SD of red object count per image. Statistically significant differences between LILRB1-IgGσ and HER2-IgGσ treatments are indicated (*$P \leq 0.05$, two-way ANOVA with Fisher´s LSD test). **(F)** RTX and an Fc-engineered RTX variant with enhanced FcγR binding (RTX-DE) were analyzed either alone or in combination with CD47-IgGσ and LILRB1-IgGσ as indicated using pHrodo® labeled DG-75 cells and human M0 macrophages. Trastuzumab (IgG1) and its Fc-engineered version HER2-DE served as controls. ADCP was determined by live cell imaging analysis. Data points represent means of red object counts per image ± SD (n = 4). *, statistically significant differences between RTX-DE + CD47-IgGσ + LILRB1-IgGσ vs. RTX-DE + CD47-IgGσ; #, statistically significant differences between RTX-DE + CD47-IgGσ + LILRB1-IgGσ vs. RTX + CD47-IgGσ + LILRB1-IgGσ; $P \leq 0.05$, two-way ANOVA with Fisher´s LSD test.

CD47-IgGσ was most efficacious in experiments with both macrophage populations.

In an effort to analyze the potential of LILRB1 and CD47 co-blockade to enhance the ADCP activity also of lymphoma-associated macrophages (LAM), MNC were prepared from BM samples from DLBCL patients with BM infiltration (Figure 5). Of note, flow cytometry analysis revealed a strong expression of LILRB1 by LAM, which were defined as CD163-positive/CD15-negative cells (Figures 5A, B). For comparison, also LILRB1 expression by BM macrophages from DLBCL patients without BM infiltration was assessed (Figures 5A, B). A trend towards a higher LILRB1 expression in the mean was found in LAM, although the observed differences were not statistically significant. For subsequent ADCP analysis, CD163-positive/CD15-negative LAM were purified by fluorescence activated cell sorting and analyzed without further manipulation as effector cells for rituximab and the antibody combinations using Carnaval target cells (Figures 5C, D). Importantly, a considerable further improvement in ADCP was observed when the antibody triple combination consisting of rituximab, CD47-IGgσ and LILRB1-IgGσ was applied relative to the combination treatment with RTX and CD47-IgGσ only.

Because cell lines do not reflect the clinical heterogeneity of patients, the dual checkpoint blockade of CD47 and LILRB1 was investigated using tumor cells from patients. CLL cells were enriched from the peripheral blood of twelve patients. The analysis of cell surface antigen expression levels revealed pronounced expression of CD20, CD47 and classical HLA class I molecules in all CLL patient samples, in contrast to HLA-G, which was hardly detected (Figure 6A). Patient cells were then analyzed in ADCP experiments using M0 macrophages from healthy donors and fluorescence microscopy (Figure 6B). CD47-IgGσ enhanced ADCP by rituximab in the majority of individual patient samples, with exception of samples CLL_04 and CLL_10, in which CD47 blockade did not improve ADCP despite considerable CD20 and CD47 expression (Supplementary Figure 6). Of note, dual checkpoint blockade of CD47 and LILRB1 enhanced ADCP by rituximab further and LILRB1-IgGσ amplified the degree of ADCP when combined with rituximab and CD47-IgGσ. Thus, in all cases analyzed the triple antibody combination of rituximab, LILRB1-IgGσ and CD47-IgGσ was more efficacious than the double antibody combination consisting of rituximab and CD47-IgGσ (Figure 6C; Supplementary Figure 6). Sample group analysis revealed statistical significance of the observed differences between different treatment groups (Figure 6D). The application of LILRB1-IgGσ with rituximab in the absence of the CD47 antibody did not translate into higher ADCP (Figure 6D). With all CLL cell samples tested, LILRB2 blockade was not effective (unpublished data). Further analysis revealed that, as also observed with cell line experiments, serial ADCP events occurred and were observed more frequently upon treatment with the antibody triple combination (Figure 6E). Finally, dual checkpoint blockade of CD47 and LILRB1 was tested with MCL tumor cells isolated from two patients (Figure 6F). Similar to CLL cells, rituximab-mediated ADCP was augmented by co-blockade of CD47 and LILRB1 with LILRB1-IgGσ providing an amplifying effect.

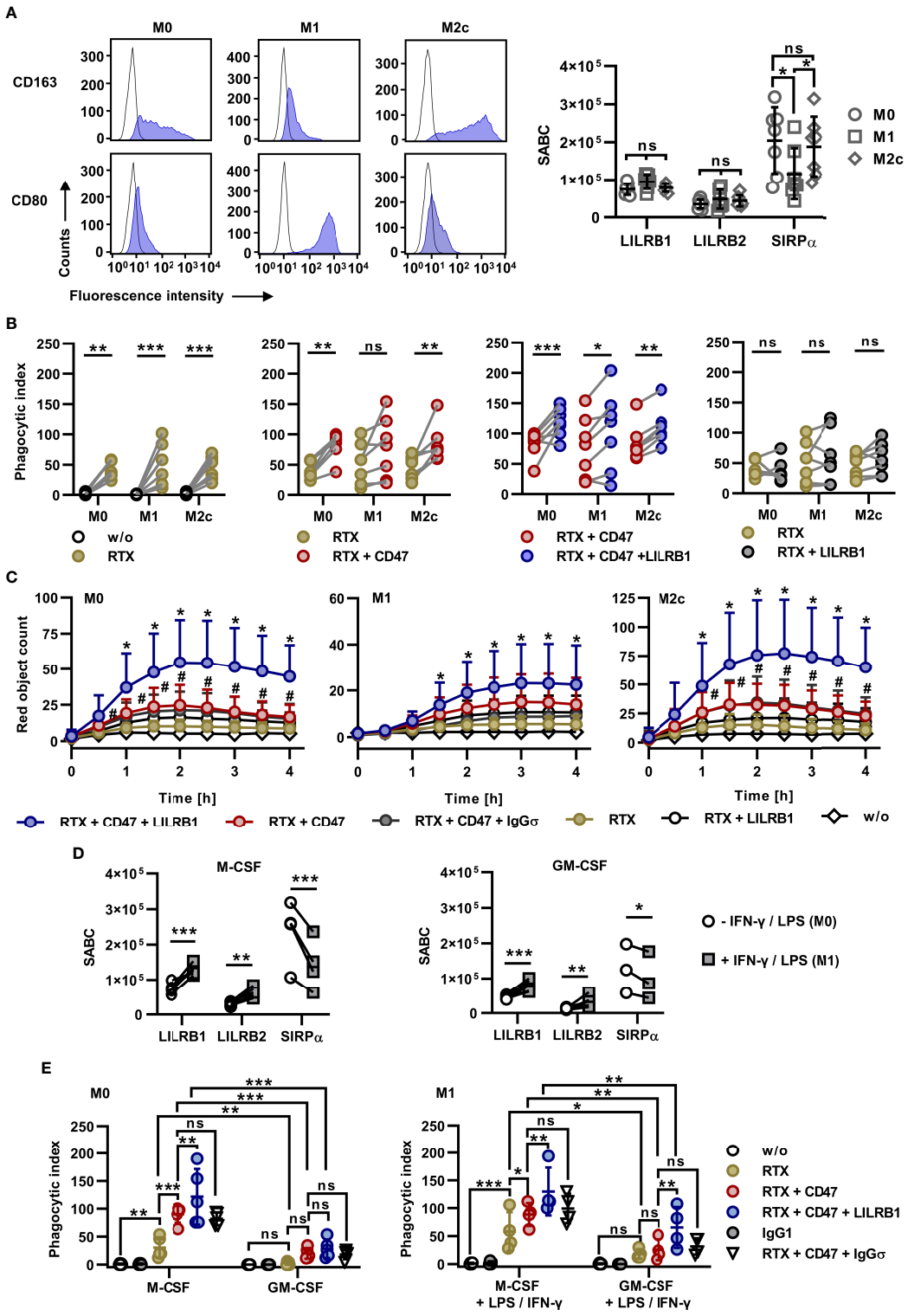

FIGURE 4 (Continued)

FIGURE 4 (Continued)
Efficacy of dual checkpoint blockade of CD47 and LILRB1 with differentially polarized macrophages. **(A)** *Left panel:* Monocytes were differentiated with M-CSF (M0 macrophages), GM-CSF, LPS and IFN-γ (M1 macrophages) or M-CSF and IL-10 (M2c macrophages) and stained with PE-conjugated antibodies against CD163, CD80 (blue shaded peaks) or an isotype control antibody (black outlined peaks). Cell surface expression was analyzed by flow cytometry. One representative experiment is shown (n = 3). *Right panel:* Cell surface expression of LILRB1, LILRB2 and SIRPα by M0, M1 and M2c macrophages was analyzed by calibrated flow cytometry. Data points indicate specific antibody binding capacity (SABC) for macrophage preparations from individual donors. Horizontal lines represent mean values ± SD (n = 7). *P ≤ 0.05; ns, not significant; two way ANOVA and Tukey`s *post hoc* test. **(B)** Macrophages were differentiated in parallel from monocytes from seven donors towards M0, M1 or M2c phenotypes and analyzed in fluorescence microscopy-based ADCP assays using CFSE-labeled Carnaval cells (E:T cell ratio: 1:2). Efficacy was determined for rituximab (RTX) vs. phagocytosis in the absence of an antibody (w/o, *first graph*), RTX + CD47-IgGσ (CD47) vs. RTX (*second graph*), and RTX + CD47-IgGσ + LILRB1-IgGσ (LILRB1) vs. RTX + CD47-IgGσ (*third graph*) and RTX + LILRB1-IgGσ vs. RTX (*fourth graph*). Antibodies were applied at a concentration of 10 µg/ml. Statistically significant differences are indicated (*P ≤ 0.05; **P ≤ 0.01; ***P ≤ 0.001; ns, not significant; two-way ANOVA with Šidàk´s multiple comparisons test). **(C)** Live-cell imaging analysis of ADCP by M0, M1 and M2c macrophages in the presence of the indicated antibodies (each at a concentration of 10 µg/ml). HER2-IgGσ (IgGσ) was used in control reactions. Target cells were pHrodo® labeled DG-75 cells (E:T cell ratio: 1:2). Data points represent means ± SD of the red object count per image of independent experiments using macrophages from six different donors that were polarized in parallel towards M0, M1 or M2c phenotypes (w/o, without antibody; #, statistically significant differences between RTX + CD47-IgGσ vs. RTX; *, statistically significant differences between RTX + CD47-IgGσ + LILRB1-IgGσ vs. RTX + CD47-IgGσ, two-way ANOVA and Fisher´s LSD test; P ≤ 0.05). **(D)** Macrophages were differentiated from peripheral monocytes in the presence of either M-CSF (*left graph*) or GM-CSF (*right graph*) for six days. Cells were left untreated or stimulated with IFN-γ and LPS for additional 48 h and analyzed for cell surface expression of LILRB1, LILRB2 and SIRPα by calibrated flow cytometry. Data points represent the specific antibody binding capacities (SABC) that were determined for individual macrophage preparations. Statistically significant differences between groups treated with IFN-γ and LPS and the control groups are indicated (*P ≤ 0.05; **P ≤ 0.01; ***P ≤ 0.001; two-way ANOVA with Fisher´s LSD test). **(E)** Macrophages were differentiated with M-CSF or GM-CSF and analyzed without further stimulation (M0 macrophages; *left graph*; n = 5) or after polarization with LPS and IFN-γ (M1 macrophages; *right graph*; n = 4) in 2 h ADCP assays using CFSE-labeled Carnaval cells and the different antibodies as indicated. ADCP was analyzed by fluorescence microscopy. Data points indicate phagocytic index values for macrophages from individual donors. Horizontal lines represent mean values ± SD (*P ≤ 0.05; **P ≤ 0.01; ***P ≤ 0.001; ns, not significant; two-way ANOVA and Fisher´s LSD test).

Discussion

Analysis of different B-NHL cell lines revealed that the expression ratio of CD20 to HLA class I molecules determined the sensitivity to ADCP by the combination of rituximab and a CD47 blocking antibody. We thus investigated the impact of blocking the HLA class I receptors LILRB1 and LILRB2 on CD20 antibody-mediated ADCP with or without concomitant masking of CD47 using Fc-silent antibodies. While the anti-LILRB2 antibody was not effective, the anti-LILRB1 antibody enhanced ADCP considerably, but strictly required simultaneous CD47 blockade and the presence of a tumor targeting CD20 antibody to become effective. Thus, the dual checkpoint blockade of CD47 and LILRB1 enhanced ADCP by rituximab, obinutuzumab, an Fc-engineered variant of rituximab and an IgA2 version of rituximab. The LILRB1 co-blockade promoted serial uptake of lymphoma cells, and demonstrated efficacy in both B-NHL cell lines and freshly isolated MCL or CLL cells from patients.

In recent years, impressive clinical results were obtained with the application of adaptive immune checkpoint inhibitors to establish T cell tumor immunity (6, 52). Regarding B cell lymphomas, promising results were observed with immune checkpoint inhibitors targeting the PD-1/PD-L1 axis in the treatment of classical Hodgkin lymphoma with response rates exceeding 70% (53). Yet, response rates with immune checkpoint monotherapies in the majority of B-NHL types including DLBCL, follicular lymphoma and CLL were unsatisfactory (53, 54). For example, a phase II trial with the anti-PD-1 antibody nivolumab in patients with relapsed or refractory DLBCL revealed response rates of only 10%, and no objective responses were observed in relapsed CLL patients upon treatment with the anti-PD-1 antibody pembrolizumab (55, 56). The application of immune checkpoint inhibitors in combination with other therapies such as R-CHOP chemo-immunotherapy may hold promise (53, 57), but will require further investigation. Limitations arise when tumors create an immune hostile microenvironment and exert insufficient immunogenicity. In this situation, the recruitment of innate immune cells, which in the tumor microenvironment contribute to tumor immunity, may be an alternative (7, 58). Particularly the immune checkpoint blockade in myeloid cells has gained increasing attention and encouraging clinical results were obtained by the combination treatment with rituximab and the CD47 antibody magrolimab in B-NHL patients (28).

As demonstrated here, the blockade of LILRB1 in addition to CD47 may offer a possibility further enhancing rituximab-mediated ADCP of lymphoma cells. However, even when both antigens were blocked, a considerable variation between different target cells in susceptibility to ADCP was observed. This may reflect the complex regulation of phagocytosis, which is governed by an interplay between activating and inhibitory receptors. Thus, 'Don´t Eat Me!' functions have been demonstrated for several antigens including programmed death ligand 1, CD24, adipocyte plasma membrane-associated protein, and signaling lymphocyte activation molecule (SLAM) family members (10, 59–61). Cognate receptors may cooperate with LILRB1 and SIRPα, and the expression of ligands for such receptors may contribute to less ADCP sensitive phenotypes of for example DG-75 cells or CLL cells from certain patients in our

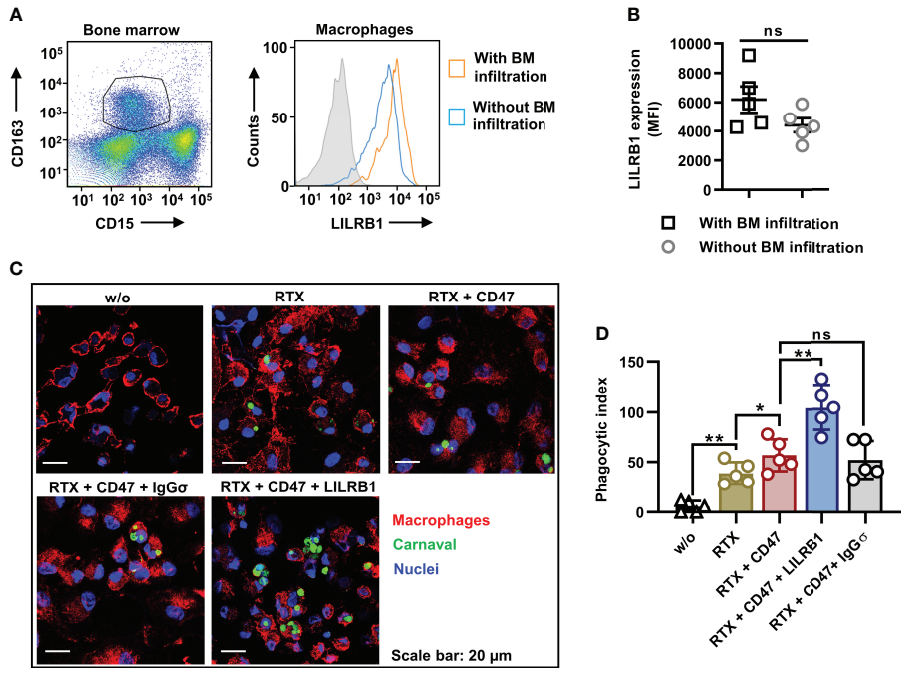

FIGURE 5
Dual checkpoint blockade of CD47 and LILRB1 enhances ADCP by LAM from DLBCL patients. **(A)** Lymphoma associated macrophages (LAM) in the MNC fraction from bone marrow (BM) samples of DLBCL patients with BM infiltration (*n* = 5) were defined as CD163-positive/CD15-negative cells by staining with Brilliant Violet 421-conjugated CD163 and Brilliant Violet 510-labeled CD15 antibodies and flow cytometry analysis (*left histogram*). Macrophages were gated, and analyzed for the cell surface expression of LILRB1, which was detected using an APC-antibody-conjugate (*right histogram*). For comparison, BM macrophages from DLBCL patients without BM infiltration were analyzed in parallel. The gray histogram indicates the isotype control. **(B)** The graph summarizes results for the LILRB1 expression according to median fluorescent intensities for BM macrophages from individual patients with (LAM) or without BM infiltration. Horizontal lines show mean values, error bars indicate SD (ns, not significant; P = 0.129). **(C)** CD163-positive/CD15-negative LAM were purified by fluorescence activated cell sorting. In ADCP reactions, LAM were plated and incubated with Carnaval cells labeled with Cytolight Rapid Green (E:T cell ratio: 1:1) in the absence (w/o) or in the presence of the antibodies rituximab (RTX), LILRB1-IgGσ (LILRB1), CD47-IgGσ (CD47) or HER-IgGσ (IgGσ; each at a concentration of 1 µg/ml), as indicated. After 2 h, cells were stained with an APC-conjugated CD11b antibody, fixed and stained with DAPI. ADCP was analyzed using a confocal microscope at x630 magnification. Images from one representative experiment are shown (*n* = 5). **(D)** The graph summarizes the phagocytic index values for ADCP of Carnaval cells by LAM upon treatment with different antibodies as indicated. Data points represent the phagocytic index values for LAM isolated from individual patients (*n* = 5). Bars indicate mean values ± SD (*P ≤ 0.05; **P ≤ 0.01; ns, not significant; one way ANOVA with Šidák´s multiple comparisons test).

study. In addition, the engagement of pro-phagocytic receptors such as prolow-density lipoprotein receptor-related protein 1, CD137, CD11b and the currently discussed SLAMF7, as well as additional target cell characteristics such cell size, shape or rigidity may be important (10, 62–65).

The observation that the anti-LILRB1 antibody required simultaneous blockade of the CD47-SIRPα axis suggests that SIRPα exerts a dominant inhibitory role in the regulation of ADCP. Whether differences between receptors in signaling pathways exist, leading to impairment of phagocytosis at different stages of phagocytosis initiation, still needs to be investigated. Both receptors signal *via* ITIM in their intracellular domains. Initiation of SIRPα signaling suppresses phagocytosis by reducing contacts between macrophages and target cells through inhibition of integrin activation, inhibition of cytoskeleton rearrangement by dephosphorylation of myosin IIA, and inactivation of neighboring FcγR through dephosphorylation of ITAM (66–68). The molecular pathways by which LILRB1 regulates phagocytosis by macrophages have not been clarified, yet impaired tyrosine phosphorylation of FcγR chain and inhibition of intracellular calcium mobilization was demonstrated upon co-ligation of FcγRI and LILRB1 (38). Of note, the dual checkpoint blockade of CD47 and LILRB1 alone was not sufficient to trigger phagocytosis and the presence of an FcR engaging CD20 antibody was required. Thus, in this approach, the specificity for phagocytic target cell elimination is maintained and is pre-defined by the tumor targeting antibody bearing a functional Fc domain to provide an activating signal.

In contrast to LILRB1, no benefits were obtained by blockade of LILRB2 - though the receptor was expressed by monocyte-derived macrophages at similar levels as LILRB1, the antibody used in this study blocked receptor binding of HLA molecules in agreement with previous findings (44), and interference with FcγR signaling by LILRB2 signaling has been demonstrated

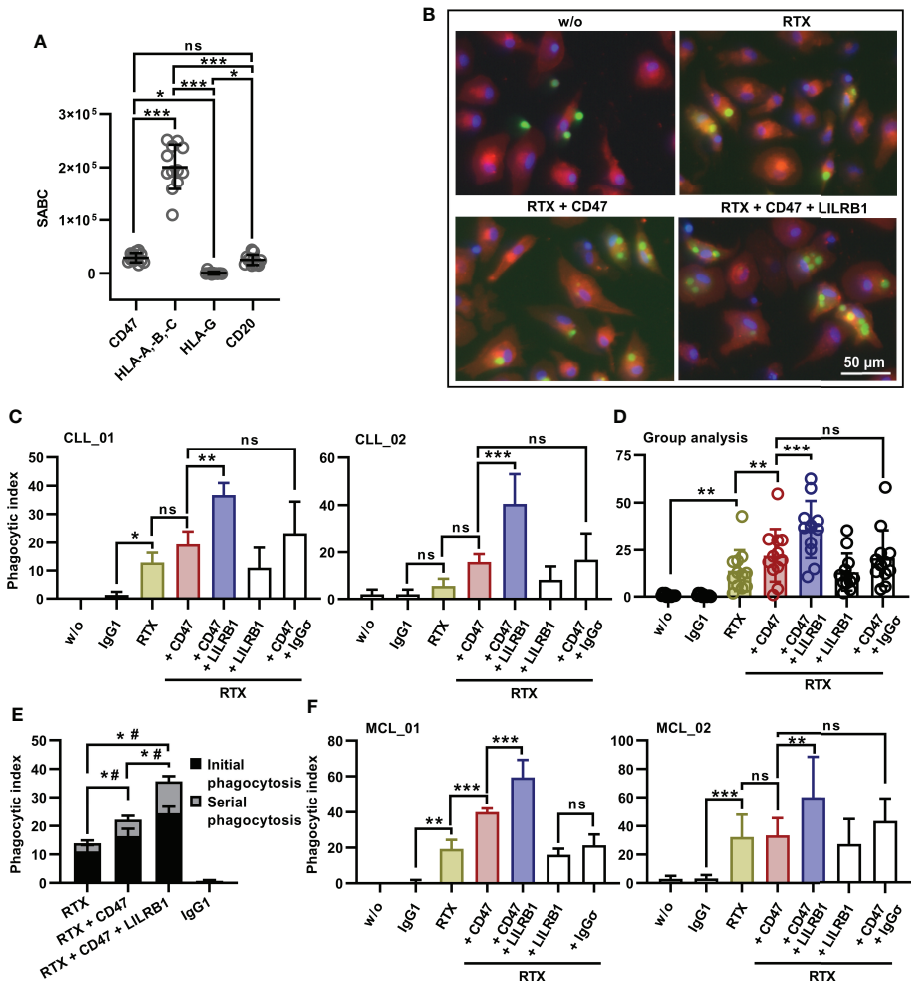

FIGURE 6
Enhanced ADCP of patient-derived CLL or MCL cells by dual checkpoint blockade of CD47 and LILRB1. **(A)** Cell surface expression levels of CD20, CD47, HLA-A,-B,-C and HLA-G by patient CLL cells was analyzed by calibrated flow cytometry. Data points represent specific antibody binding capacity (SABC) for individual patient samples. The horizontal lines indicate mean values ± SD (*P ≤ 0.05; ***P ≤ 0.001; ns, not significant; one-way ANOVA with Tukey's multiple comparison test. **(B)** CFSE-labeled CLL cells (patient CLL_05) were incubated with M0 macrophages (labeled with Cell Brite™ Orange cytoplasmic membrane dye, E:T cell ratio: 1:2) in the absence (w/o) or in the presence of the antibodies rituximab (RTX), CD47-IgGσ (CD47) and LILRB1-IgGσ (LILRB1; each at a concentration of 10 µg/ml) as indicated for 2 h. Nuclei were stained with NucBlue™. ADCP was analyzed by fluorescence microscopy. **(C)** CLL cells from patients CLL_01 and CLL_02 were labeled with CFSE and incubated with M0 macrophages without (w/o) or with antibodies trastuzumab (IgG1), rituximab (RTX), LILRB1-IgGσ (LILRB1), CD47-IgGσ (CD47) or HER2-IgGσ (IgGσ) as indicated (each at a concentration of 10 µg/ml) for 2 h. ADCP was analyzed by fluorescence microscopy. Bars represent mean phagocytic index values ± SD from three independent experiments using macrophages from different donors (*P ≤0.05; **P ≤ 0.01; ***P ≤ 0.001; ns, not significant; one-way ANOVA with Fisher`s LSD test). **(D)** Group analysis of ADCP summarizing results obtained with CLL cells from 12 different patients as target cells. ADCP was determined for the indicated antibodies or their combinations as described in **(C)**. Data points represent mean phagocytic index values for individual patient samples as determined in independent experiments using macrophages from different donors, as illustrated in Suppl. Figure 6. Bars indicate overall mean phagocytic index values ± SD (**P ≤ 0.01; ***P ≤ 0.001; ns, not significant; one-way ANOVA with Šidàk´s multiple comparisons test). **(E)** LILRB1 and CD47 immune checkpoint blockade promotes serial ADCP of patient CLL cells by human M0 macrophages. Phagocytic events were assigned to phagocytosis of the first CLL cell (initial phagocytosis) or to engulfment of subsequent CLL cells (serial phagocytosis) and are presented as a proportion of phagocytic index values. Bars represent mean values ± SEM. Statistically significant differences between treatment groups in initial phagocytosis (*) and serial phagocytosis (#) are indicated (P ≤ 0.05; two-way ANOVA and Tukey`s multiple comparison test; *n* = 12). **(F)** MCL cells were isolated from two patients, labeled with CFSE and analyzed as target cells for M0 macrophages in the presence of the indicated antibodies (each at a concentration of 10 µg/ml) by fluorescence microscopy as described in **(C)**. Data points represent mean phagocytic index values ± SD from three (MCL_01) or six (MCL_02) independent experiments using macrophages from different donors (**P ≤0.01; ***P ≤ 0.001; ns, not significant; one-way ANOVA with Fisher`s LSD test).

previously (38). However, structural differences in binding exist in that LILRB1 binds only β2-microglobulin associated HLA molecules, while LILRB2 also binds free forms (35, 69). In addition, the receptors differ in their affinity to individual HLA alleles (69). We assume that the quality of receptor engagement, the affinity to HLA molecules or the initiation and strength of the individual receptor's intracellular signaling pathway may contribute to the observed differences. In addition, it cannot be fully excluded that the particular antibody clone employed in these experiments exerted agonistic functions and activated LILRB2 signaling in parallel to inhibition of ligand binding.

Enhanced ADCP by co-blockade of LILRB1 and CD47 was demonstrated for combinations with CD20-specific IgG antibodies. Improved ADCP was observed not only in combinations with the native IgG1 molecule rituximab, but also with the Fc glyco-engineered antibody obinutuzumab and the Fc-protein engineered rituximab variant RTX-DE. Moreover, co-inhibition of LILRB1 and CD47 was effective, when the antibodies were combined with an IgA2 variant of rituximab. IgA antibodies may hold potential for cancer immunotherapy. They are able to trigger myeloid effector cells including neutrophils, monocytes and macrophages by engagement of the IgA Fc receptor FcαRI. Previously it has been demonstrated that CD47 blockade enhances macrophage-mediated ADCP by CD20 IgA antibodies (49). As demonstrated in the present study, the efficacy can be further improved by co-blockade of LILRB1, suggesting that LILRB1 also regulates signaling by FcαRI.

Besides promoting ADCP, anti-LILRB1 antibodies may exert additional effector functions. Both antibody blockade of LILRB2 and genetic deletion of LILRB1 were shown to drive macrophage polarization towards an inflammatory M1 phenotype (36, 39). Therefore, the blockade of these receptors may facilitate to relieve immune suppression in the tumor microenvironment by shaping TAM or myeloid derived suppressor cells (58). In addition, enhanced engulfment of tumor cells may increase antigen presentation and promote T cell responses (10). In a murine tumor model, adaptive T cell responses were observed after treatment with CD47 antibodies (70). However, to unravel a role for LILRB1 in this context will require further investigation. In addition, LILRB1 and LILRB2 are expressed by other immune cell populations. For example, LILRB1 is expressed by T cells and a subpopulation of NK cells (32). Therefore, manipulation of LILRB1 may also promote cytotoxic functions by lymphocytes (71, 72). Regarding that NK cells may express SIRPα in certain situations even co-blockade of LILRB1 and CD47 may be effective in enhancing NK cell-mediated ADCC (73). In neutrophils, conflicting results on the expression of LILRB1 were published, but LILRB2 is displayed (32, 74). Albeit LILRB2-IgGσ lacked efficacy in enhancing ADCP by macrophages, it may be worth testing this antibody with neutrophils, in which blockade of the CD47-SIRPα axis was shown to enhance ADCC and trogoptosis (75).

To further advance the proposed concept animal studies will be required. However, this is a challenging issue, because LILRB1 is not expressed in mice and the murine receptor orthologue paired immunoglobulin-like receptor B does not react with HLA/β2M complexes (36). The generation of LILRB1 transgenic mice could offer an opportunity to study this. In a previous study, LILRB1 knock-in mice were established in the background of immune competent mice (76), but here immune deficient mice will be required to facilitate the engraftment of human lymphoma cells. Humanized mice in which human immune cells are established by transplantation of human CD34-positive progenitor cells could offer another option (77). However, the presence of human immune cells may hamper the co-engraftment of tumor cells and partial HLA matching may be required. In addition, co-existing murine macrophages, which respond to CD47 but not to anti-LILRB1 antibody blockade (36), may distort results, and an accompanying depletion of murine macrophages may be necessary. Yet, our *in vitro* results provide a rationale to undertake these efforts to realize such xenograft *in vivo* studies.

In conclusion, our preclinical *in vitro* results suggest potential of combining CD20, CD47 and anti- LIRB1 antibodies. LILRB1 blockade complemented CD47 inhibition and thus a dual checkpoint blockade of CD47-SIRPα and LILRB1-HLA class I interactions may have the potential to improve antibody therapy of lymphomas further by enhancing ADCP by macrophages. Therefore, combinations of tumor targeting antibodies with LILRB1 and either CD47 or SIRPα immune checkpoint inhibitors deserve further evaluation in animal models towards clinical application.

Data availability statement

The original contributions presented in the study are included in the article/Supplementary Material. Further inquiries can be directed to the corresponding author.

Ethics statement

The studies involving human participants were reviewed and approved by Ethics Committee of the faculty of medicine, LMU Munich. The patients/participants provided their written informed consent to participate in this study.

Author contributions

Conceptualization, CK. Methodology, TZ, SL, MP, HB, AM and CK. Validation, TZ, SL and CK. Formal analysis, TZ, SL, IM,

AM and CK. Investigation, TZ, SL, IM, RW, PH, TR, NB, CF, HB and CK. Resources, NT, JB, TH, OW, CW, MB-B, MP, HB, DS and AH. Writing - original draft preparation, TZ and CK. Writing - review and editing, SL, RW, TH, OW, MB-B, CW, TV, DS, HB and AH. Visualization, TZ, SL, HB and CK. Supervision, CK. All authors have read and agreed to the published version of the manuscript.

Funding

This work was funded by research grants by the Deutsche Krebshilfe (70113524 and 70113533, to DS and CK), the Verein zur Förderung von Wissenschaft und Forschung an der Medizinischen Fakultät der Ludwig-Maximilians-Universität München (to CK) and the Deutsche José Carreras Leukämie-Stiftung to TH (DJCLS 10 R/2021).

Acknowledgments

Irene Pauls, Lena Halang, and Fiona E. Rosmus are kindly acknowledged for expert technical assistance. The Deutsche José Carreras Leukämie-Stifung and the Deutsche Gesellschaft für Hämatologie und Medizinische Onkologie are gratefully acknowledged for the José Carreras-DGHO scholarship for doctoral research to TZ (05 PSD/2021). We also kindly thank the study participants.

Conflict of interest

The authors declare that the research was conducted in the absence of any commercial or financial relationships that could be construed as a potential conflict of interest.

Publisher's note

Supplementary material

The Supplementary Material for this article can be found online at: https://www.frontiersin.org/articles/10.3389/fimmu.2022.929339/full#supplementary-material

References

1. Carter PJ, Lazar GA. Next generation antibody drugs: pursuit of the 'high-hanging fruit'. *Nat Rev Drug Discovery* (2018) 17(3):197–223. doi: 10.1038/nrd.2017.227

2. Marshall MJE, Stopforth RJ, Cragg MS. Therapeutic antibodies: What have we learnt from targeting CD20 and where are we going? *Front Immunol* (2017) 8:1245. doi: 10.3389/fimmu.2017.01245

3. Larson RC, Maus MV. Recent advances and discoveries in the mechanisms and functions of CAR T cells. *Nat Rev Cancer* (2021) 21(3):145–61. doi: 10.1038/s41568-020-00323-z

4. Liu R, Oldham RJ, Teal E, Beers SA, Cragg MS. Fc-engineering for modulated effector functions-improving antibodies for cancer treatment. *Antibodies (Basel)* (2020) 9(4):64. doi: 10.3390/antib9040064

5. Goebeler ME, Bargou RC. T Cell-engaging therapies - BiTEs and beyond. *Nat Rev Clin Oncol* (2020) 17(7):418–34. doi: 10.1038/s41571-020-0347-5

6. Wei SC, Duffy CR, Allison JP. Fundamental mechanisms of immune checkpoint blockade therapy. *Cancer Discovery* (2018) 8(9):1069–86. doi: 10.1158/2159-8290.CD-18-0367

7. Lentz RW, Colton MD, Mitra SS, Messersmith WA. Innate immune checkpoint inhibitors: The next breakthrough in medical oncology? *Mol Cancer Ther* (2021) 20(6):961–74. doi: 10.1158/1535-7163.MCT-21-0041

8. Gul N, van Egmond M. Antibody-dependent phagocytosis of tumor cells by macrophages: A potent effector mechanism of monoclonal antibody therapy of cancer. *Cancer Res* (2015) 75(23):5008–13. doi: 10.1158/0008-5472.CAN-15-1330

9. Wynn TA, Chawla A, Pollard JW. Macrophage biology in development, homeostasis and disease. *Nature* (2013) 496(7446):445–55. doi: 10.1038/nature12034

10. Feng M, Jiang W, Kim BYS, Zhang CC, Fu YX, Weissman IL. Phagocytosis checkpoints as new targets for cancer immunotherapy. *Nat Rev Cancer* (2019) 19(10):568–86. doi: 10.1038/s41568-019-0183-z

11. Mantovani A, Sica A, Sozzani S, Allavena P, Vecchi A, Locati M. The chemokine system in diverse forms of macrophage activation and polarization. *Trends Immunol* (2004) 25(12):677–86. doi: 10.1016/j.it.2004.09.015

12. Hourani T, Holden JA, Li W, Lenzo JC, Hadjigol S, O'Brien-Simpson NM. Tumor associated macrophages: Origin, recruitment, phenotypic diversity, and targeting. *Front Oncol* (2021) 11:788365. doi: 10.3389/fonc.2021.788365

13. Chittezhath M, Dhillon MK, Lim JY, Laoui D, Shalova IN, Teo YL, et al. Molecular profiling reveals a tumor-promoting phenotype of monocytes and macrophages in human cancer progression. *Immunity* (2014) 41(5):815–29. doi: 10.1016/j.immuni.2014.09.014

14. Farinha P, Masoudi H, Skinnider BF, Shumansky K, Spinelli JJ, Gill K, et al. Analysis of multiple biomarkers shows that lymphoma-associated macrophage (LAM) content is an independent predictor of survival in follicular lymphoma (FL). *Blood* (2005) 106(6):2169–74. doi: 10.1182/blood-2005-04-1565

15. Canioni D, Salles G, Mounier N, Brousse N, Keuppens M, Morchhauser F, et al. High numbers of tumor-associated macrophages have an adverse prognostic value that can be circumvented by rituximab in patients with follicular lymphoma enrolled onto the GELA-GOELAMS FL-2000 trial. *J Clin Oncol* (2008) 26(3):440–6. doi: 10.1200/JCO.2007.12.8298

16. Shen L, Li H, Shi Y, Wang D, Gong J, Xun J, et al. M2 tumour-associated macrophages contribute to tumour progression *via* legumain remodelling the extracellular matrix in diffuse large b cell lymphoma. *Sci Rep* (2016) 6:30347. doi: 10.1038/srep30347

17. Taskinen M, Karjalainen-Lindsberg ML, Nyman H, Eerola LM, Leppa S. A high tumor-associated macrophage content predicts favorable outcome in follicular lymphoma patients treated with rituximab and cyclophosphamide-doxorubicin-vincristine-prednisone. *Clin Cancer Res* (2007) 13(19):5784–9. doi: 10.1158/1078-0432.CCR-07-0778

18. Riihijarvi S, Fiskvik I, Taskinen M, Vajavaara H, Tikkala M, Yri O, et al. Prognostic influence of macrophages in patients with diffuse large b-cell

lymphoma: a correlative study from a Nordic phase II trial. *Haematologica* (2015) 100(2):238–45. doi: 10.3324/haematol.2014.113472

19. Pallasch CP, Leskov I, Braun CJ, Vorholt D, Drake A, Soto-Feliciano YM, et al. Sensitizing protective tumor microenvironments to antibody-mediated therapy. *Cell* (2014) 156(3):590–602. doi: 10.1016/j.cell.2013.12.041

20. Schewe DM, Alsadeq A, Sattler C, Lenk L, Vogiatzi F, Cario G, et al. An fc-engineered CD19 antibody eradicates MRD in patient-derived MLL-rearranged acute lymphoblastic leukemia xenografts. *Blood* (2017) 130(13):1543–52. doi: 10.1182/blood-2017-01-764316

21. Lazar GA, Dang W, Karki S, Vafa O, Peng JS, Hyun L, et al. Engineered antibody fc variants with enhanced effector function. *Proc Natl Acad Sci U.S.A.* (2006) 103(11):4005–10. doi: 10.1073/pnas.0508123103

22. Barclay AN, Van den Berg TK. The interaction between signal regulatory protein alpha (SIRPalpha) and CD47: structure, function, and therapeutic target. *Annu Rev Immunol* (2014) 32:25–50. doi: 10.1146/annurev-immunol-032713-120142

23. Logtenberg MEW, Scheeren FA, Schumacher TN. The CD47-SIRPalpha immune checkpoint. *Immunity* (2020) 52(5):742–52. doi: 10.1016/j.immuni.2020.04.011

24. Chao MP, Alizadeh AA, Tang C, Myklebust JH, Varghese B, Gill S, et al. Anti-CD47 antibody synergizes with rituximab to promote phagocytosis and eradicate non-Hodgkin lymphoma. *Cell* (2010) 142(5):699–713. doi: 10.1016/j.cell.2010.07.044

25. Muller K, Vogiatzi F, Winterberg D, Rosner T, Lenk L, Bastian L, et al. Combining daratumumab with CD47 blockade prolongs survival in preclinical models of pediatric T-ALL. *Blood* (2022) 140(1):45–57. doi: 10.1182/blood.2021014485

26. Yu WB, Ye ZH, Chen X, Shi JJ, Lu JJ. The development of small-molecule inhibitors targeting CD47. *Drug Discovery Today* (2021) 26(2):561–8. doi: 10.1016/j.drudis.2020.11.003

27. Sikic BI, Lakhani N, Patnaik A, Shah SA, Chandana SR, Rasco D, et al. First-in-Human, first-in-Class phase I trial of the anti-CD47 antibody Hu5F9-G4 in patients with advanced cancers. *J Clin Oncol* (2019) 37(12):946–53. doi: 10.1200/JCO.18.02018

28. Advani R, Flinn I, Popplewell L, Forero A, Bartlett NL, Ghosh N, et al. CD47 blockade by Hu5F9-G4 and rituximab in non-hodgkin's lymphoma. *N Engl J Med* (2018) 379(18):1711–21. doi: 10.1056/NEJMoa1807315

29. Ansell SM, Maris MB, Lesokhin AM, Chen RW, Flinn IW, Sawas A, et al. Phase I study of the CD47 blocker TTI-621 in patients with relapsed or refractory hematologic malignancies. *Clin Cancer Res* (2021) 27(8):2190–9. doi: 10.1158/1078-0432.CCR-20-3706

30. Yang Y, Yang Z, Yang Y. Potential role of CD47-directed bispecific antibodies in cancer immunotherapy. *Front Immunol* (2021) 12:686031. doi: 10.3389/fimmu.2021.686031

31. Colonna M, Navarro F, Bellon T, Llano M, Garcia P, Samaridis J, et al. A common inhibitory receptor for major histocompatibility complex class I molecules on human lymphoid and myelomonocytic cells. *J Exp Med* (1997) 186 (11):1809–18. doi: 10.1084/jem.186.11.1809

32. De Louche CD, Roghanian A. Human inhibitory leukocyte ig-like receptors: from immunotolerance to immunotherapy. *JCI Insight* (2022) 7(2):e151553. doi: 10.1172/jci.insight.151553

33. Willcox BE, Thomas LM, Bjorkman PJ. Crystal structure of HLA-A2 bound to LIR-1, a host and viral major histocompatibility complex receptor. *Nat Immunol* (2003) 4(9):913–9. doi: 10.1038/ni961

34. Shiroishi M, Tsumoto K, Amano K, Shirakihara Y, Colonna M, Braud VM, et al. Human inhibitory receptors ig-like transcript 2 (ILT2) and ILT4 compete with CD8 for MHC class I binding and bind preferentially to HLA-G. *Proc Natl Acad Sci U.S.A.* (2003) 100(15):8856–61. doi: 10.1073/pnas.1431057100

35. Jones DC, Kosmoliaptsis V, Apps R, Lapaque N, Smith I, Kono A, et al. HLA class I allelic sequence and conformation regulate leukocyte ig-like receptor binding. *J Immunol* (2011) 186(5):2990–7. doi: 10.4049/jimmunol.1003078

36. Barkal AA, Weiskopf K, Kao KS, Gordon SR, Rosental B, Yiu YY, et al. Engagement of MHC class I by the inhibitory receptor LILRB1 suppresses macrophages and is a target of cancer immunotherapy. *Nat Immunol* (2018) 19 (1):76–84. doi: 10.1038/s41590-017-0004-z

37. Abdallah F, Coindre S, Gardet M, Meurisse F, Naji A, Suganuma N, et al. Leukocyte immunoglobulin-like receptors in regulating the immune response in infectious diseases: A window of opportunity to pathogen persistence and a sound target in therapeutics. *Front Immunol* (2021) 12:717998. doi: 10.3389/fimmu.2021.717998

38. Fanger NA, Cosman D, Peterson L, Braddy SC, Maliszewski CR , Borges L. The MHC class I binding proteins LIR-1 and LIR-2 inhibit fc receptor-mediated signaling in monocytes. *Eur J Immunol* (1998) 28(11):3423–34. doi: 10.1002/(SICI)1521-4141(199811)28:11<3423::AID-IMMU3423>3.0.CO;2-2

39. Chen HM, van der Touw W, Wang YS, Kang K, Mai S, Zhang J, et al. Blocking immunoinhibitory receptor LILRB2 reprograms tumor-associated myeloid cells and promotes antitumor immunity. *J Clin Invest* (2018) 128 (12):5647–62. doi: 10.1172/JCI97570

40. Vafa O, Gilliland GL, Brezski RJ, Strake B, Wilkinson T, Lacy ER, et al. An engineered fc variant of an IgG eliminates all immune effector functions *via* structural perturbations. *Methods* (2014) 65(1):114–26. doi: 10.1016/j.ymeth.2013.06.035

41. Tam SH, McCarthy SG, Armstrong AA, Somani S, Wu SJ, Liu X, et al. Functional, biophysical, and structural characterization of human IgG1 and IgG4 fc variants with ablated immune functionality. *Antibodies (Basel)* (2017) 6(3):12. doi: 10.3390/antib6030012

42. Hofbauer D, Mougiakakos D, Broggini L, Zaiss M, Buttner-Herold M, Bach C, et al. beta2-microglobulin triggers NLRP3 inflammasome activation in tumor-associated macrophages to promote multiple myeloma progression. *Immunity* (2021) 54(8):1772–87 e9. doi: 10.1016/j.immuni.2021.07.002

43. Pulford K, Micklem K, Thomas J, Jones M, Mason DY. A 72-kD b cell-associated surface glycoprotein expressed at high levels in hairy cell leukaemia and plasma cell neoplasms. *Clin Exp Immunol* (1991) 85(3):429–35. doi: 10.1111/j.1365-2249.1991.tb05744.x

44. Cohen HB, Mackenzie LP, Shaffer DR, Smith JY, O'Malley KSF. *Antibodies to LILRB2*. U.S. Patent No 11,359,019. Washington, DC: U.S. Patent and Trademark Office

45. Maute RL, Weiskopf KA, Ring AM, Weissman IL. *Composition and methods for inducing phagocytosis of MHC class I positive cells and counteracting anti-CD47/SIRPA resistance*. U.S. Patent No 11,459,388. Washington, DC: U.S. Patent and Trademark Office 10,889,649. U.S (2021).

46. Liu J, Wang L, Zhao F, Tseng S, Narayanan C, Shura L, et al. Pre-clinical development of a humanized anti-CD47 antibody with anti-cancer therapeutic potential. *PloS One* (2015) 10(9):e0137345. doi: 10.1371/journal.pone.0137345

47. Wirt T, Rosskopf S, Rosner T, Eichholz KM, Kahrs A, Lutz S, et al. An fc double-engineered CD20 antibody with enhanced ability to trigger complement-dependent cytotoxicity and antibody-dependent cell-mediated cytotoxicity. *Transfus Med Hemother* (2017) 44(5):292–300. doi: 10.1159/000479978

48. Lohse S, Meyer S, Meulenbroek LA, Jansen JH, Nederend M, Kretschmer A, et al. An anti-EGFR IgA that displays improved pharmacokinetics and myeloid effector cell engagement. *In Vivo Cancer Res* (2016) 76(2):403–17. doi: 10.1158/0008-5472.CAN-15-1232

49. Evers M, Rosner T, Dunkel A, Jansen JHM, Baumann N, Ten Broeke T, et al. The selection of variable regions affects effector mechanisms of IgA antibodies against CD20. *Blood Adv* (2021) 5(19):3807–20. doi: 10.1182/bloodadvances.2021004598

50. Baumann N, Arndt C, Petersen J, Lustig M, Rosner T, Klausz K, et al. Myeloid checkpoint blockade improves killing of T-acute lymphoblastic leukemia cells by an IgA2 variant of daratumumab. *Front Immunol* (2022) 13:949140. doi: 10.3389/fimmu.2022.949140

51. Richards JO, Karki S, Lazar GA, Chen H, Dang W, Desjarlais JR. Optimization of antibody binding to FcgammaRIIa enhances macrophage phagocytosis of tumor cells. *Mol Cancer Ther* (2008) 7(8):2517–27. doi: 10.1158/1535-7163.MCT-08-0201

52. Chen DS, Mellman I. Oncology meets immunology: the cancer-immunity cycle. *Immunity* (2013) 39(1):1–10. doi: 10.1016/j.immuni.2013.07.012

53. Ansell SM. Checkpoint blockade in lymphoma. *J Clin Oncol* (2021) 10 (39):525–33. doi: 10.1200/JCO.20.01522

54. Armand P, Janssens A, Gritti G, Radford J, Timmerman J, Pinto A, et al. Efficacy and safety results from CheckMate 140, a phase 2 study of nivolumab for relapsed/refractory follicular lymphoma. *Blood* (2021) 137(5):637–45. doi: 10.1182/blood.2019004753

55. Ansell SM, Minnema MC, Johnson P, Timmerman JM, Armand P, Shipp MA, et al. Nivolumab for Relapsed/Refractory diffuse Large b-cell lymphoma in patients ineligible for or having failed autologous transplantation: A single-arm, phase II study. *J Clin Oncol* (2019) 37(6):481–9. doi: 10.1200/JCO.18.00766

56. Ding W, LaPlant BR, Call TG, Parikh SA, Leis JF, He R, et al. Pembrolizumab in patients with CLL and Richter transformation or with relapsed CLL. *Blood* (2017) 129(26):3419–27. doi: 10.1182/blood-2017-02-765685

57. Smith SD, Till BG, Shadman MS, Lynch RC, Cowan AJ, Wu QV, et al. Pembrolizumab with r-CHOP in previously untreated diffuse large b-cell lymphoma: potential for biomarker driven therapy. *Br J Haematol* (2020) 189 (6):1119–26. doi: 10.1111/bjh.16494

58. Demaria O, Cornen S, Daeron M, Morel Y, Medzhitov R, Vivier E. Harnessing innate immunity in cancer therapy. *Nature* (2019) 574(7776):45–56. doi: 10.1038/s41586-019-1593-5

59. Barkal AA, Brewer RE, Markovic M, Kowarsky M, Barkal SA, Zaro BW, et al. CD24 signalling through macrophage siglec-10 is a target for cancer immunotherapy. *Nature* (2019) 572(7769):392–6. doi: 10.1038/s41586-019-1456-0

60. Kamber RA, Nishiga Y, Morton B, Banuelos AM, Barkal AA, Vences-Catalan F, et al. Inter-cellular CRISPR screens reveal regulators of cancer cell phagocytosis. *Nature* (2021) 597(7877):549–54. doi: 10.1038/s41586-021-03879-4

61. Li D, Xiong W, Wang Y, Feng J, He Y, Du J, et al. SLAMF3 and SLAMF4 are immune checkpoints that constrain macrophage phagocytosis of hematopoietic tumors. *Sci Immunol* (2022) 7(67):eabj5501. doi: 10.1126/sciimmunol.abj5501

62. Stoll A, Bruns H, Fuchs M, Volkl S, Nimmerjahn F, Kunz M, et al. CD137 (4-1BB) stimulation leads to metabolic and functional reprogramming of human monocytes/macrophages enhancing their tumoricidal activity. *Leukemia* (2021) 35 (12):3482–96. doi: 10.1038/s41375-021-01287-1

63. Chen J, Zhong MC, Guo H, Davidson D, Mishel S, Lu Y, et al. SLAMF7 is critical for phagocytosis of haematopoietic tumour cells *via* mac-1 integrin. *Nature* (2017) 544(7651):493–7. doi: 10.1038/nature22076

64. He Y, Bouwstra R, Wiersma VR, de Jong M, Jan Lourens H, Fehrmann R, et al. Cancer cell-expressed SLAMF7 is not required for CD47-mediated phagocytosis. *Nat Commun* (2019) 10(1):533. doi: 10.1038/s41467-018-08013-z

65. Sosale NG, Rouhiparkouhi T, Bradshaw AM, Dimova R, Lipowsky R, Discher DE. Cell rigidity and shape override CD47's "self"-signaling in phagocytosis by hyperactivating myosin-II. *Blood* (2015) 125(3):542–52. doi: 10.1182/blood-2014-06-585299

66. Morrissey MA, Kern N, Vale RD. CD47 ligation repositions the inhibitory receptor SIRPA to suppress integrin activation and phagocytosis. *Immunity* (2020) 53(2):290–302.e6. doi: 10.1016/j.immuni.2020.07.008

67. Tsai RK, Discher DE. Inhibition of "self" engulfment through deactivation of myosin-II at the phagocytic synapse between human cells. *J Cell Biol* (2008) 180 (5):989–1003. doi: 10.1083/jcb.200708043

68. Suter EC, Schmid EM, Harris AR, Voets E, Francica B, Fletcher DA. Antibody : CD47 ratio regulates macrophage phagocytosis through competitive receptor phosphorylation. *Cell Rep* (2021) 36(8):109587. doi: 10.1016/j.celrep.2021.109587

69. Shiroishi M, Kuroki K, Rasubala L, Tsumoto K, Kumagai I, Kurimoto E, et al. Structural basis for recognition of the nonclassical MHC molecule HLA-G by the leukocyte ig-like receptor B2 (LILRB2/LIR2/ILT4/CD85d). *Proc Natl Acad Sci U.S.A.* (2006) 103(44):16412–7. doi: 10.1073/pnas.0605228103

70. Liu X, Pu Y, Cron K, Deng L, Kline J, Frazier WA, et al. CD47 blockade triggers T cell-mediated destruction of immunogenic tumors. *Nat Med* (2015) 21 (10):1209–15. doi: 10.1038/nm.3931

71. Villa-Alvarez M, Lorenzo-Herrero S, Gonzalez-Rodriguez AP, Lopez-Soto A, Payer AR, Gonzalez-Garcia E, et al. Ig-like transcript 2 (ILT2) suppresses T cell function in chronic lymphocytic leukemia. *Oncoimmunology* (2017) 6(10): e1353856. doi: 10.1080/2162402X.2017.1353856

72. Villa-Alvarez M, Sordo-Bahamonde C, Lorenzo-Herrero S, Gonzalez-Rodriguez AP, Payer AR, Gonzalez-Garcia E, et al. Ig-like transcript 2 (ILT2) blockade and lenalidomide restore NK cell function in chronic lymphocytic leukemia. *Front Immunol* (2018) 9:2917. doi: 10.3389/fimmu.2018.02917

73. Deuse T, Hu X, Agbor-Enoh S, Jang MK, Alawi M, Saygi C, et al. The SIRPalpha-CD47 immune checkpoint in NK cells. *J Exp Med* (2021) 218(3): e20200839. doi: 10.1084/jem.20200839

74. Lewis Marffy AL, McCarthy AJ. Leukocyte immunoglobulin-like receptors (LILRs) on human neutrophils: Modulators of infection and immunity. *Front Immunol* (2020) 11:857. doi: 10.3389/fimmu.2020.00857

75. Matlung HL, Babes L, Zhao XW, van Houdt M, Treffers LW, van Rees DJ, et al. Neutrophils kill antibody-opsonized cancer cells by trogoptosis. *Cell Rep* (2018) 23(13):3946–59.e6. doi: 10.1016/j.celrep.2018.05.082

76. Belkin D, Torkar M, Chang C, Barten R, Tolaini M, Haude A, et al. Killer cell ig-like receptor and leukocyte ig-like receptor transgenic mice exhibit tissue- and cell-specific transgene expression. *J Immunol* (2003) 171(6):3056–63. doi: 10.4049/jimmunol.171.6.3056

77. Stripecke R, Munz C, Schuringa JJ, Bissig KD, Soper B, Meeham T, et al. Innovations, challenges, and minimal information for standardization of humanized mice. *EMBO Mol Med* (2020) 12(7):e8662. doi: 10.15252/emmm.201708662

Frontiers in Immunology

Explores novel approaches and diagnoses to treat immune disorders. The official journal of the International Union of Immunological Societies (IUIS) and the most cited in its field, leading the way for research across basic, translational and clinical immunology.

Discover the latest Research Topics

See more →

Frontiers

Avenue du Tribunal-Fédéral 34
1005 Lausanne, Switzerland
frontiersin.org

Contact us

+41 (0)21 510 17 00
frontiersin.org/about/contact